Université de Montréal

Vers des assemblages de complexes métalliques oligonucléaires, servant d'antenne solaire au niveau moléculaire

par
Daniel Chartrand

Département de chimie
Faculté des arts et des sciences

Thèse présentée à la Faculté des études supérieures et postdoctorales
en vue de l'obtention du grade de Philosophiae Doctor (Ph.D.)
en chimie

décembre, 2013

Université de Montréal
Faculté des études supérieures et postdoctorales

Cette thèse intitulée :

Vers des assemblages de complexes métalliques oligonucléaires, servant d'antenne solaire au niveau moléculaire

Présentée par :
Daniel Chartrand

A été évaluée par un jury composé des personnes suivantes :

Christian Reber, Président-rapporteur et représentant du doyen de la FAS
Garry S. Hanan, directeur de recherche
Davit Zargarian, membre du jury
Stefan Bernhard, examinateur externe

Résumé

Ce projet de recherche vise l'élaboration de systèmes métallosupramoléculaires artificiels imitant le processus naturel de la photosynthèse. Idéalement, ces systèmes seraient capables de fournir l'énergie et la séparation de charge nécessaire pour catalyser des réactions à transfert multiélectroniques, tel que l'hydrolyse de l'eau ou la réduction du gaz carbonique. La réalisation d'un tel système catalytique créerait une source d'énergie renouvelable, sous forme d'énergie chimique, crée directement à partir de l'énergie solaire.

Le système envisagé, schématisé sous la forme d'une antenne, possède trois parties distinctes. Tout d'abord, des chromophores forment un état excité en captant l'énergie de la lumière visible du soleil. Vient ensuite un centre de liaison qui lie tous les chromophores et qui collecte l'énergie de cet état excité à travers un transfert d'électron. Cet électron est de nouveau transféré vers la dernière partie, un centre réactionnel catalytique. Cet assemblage permet de créer une séparation de charge entre le chromophore et le centre réactionnel qui sont séparés par le centre de liaison, évitant ainsi la recombinaison de charge.

Le projet se focalise sur la synthèse, la caractérisation et l'application en photocatalyse d'assemblages chromophore–centre-de-liaison–catalyseur. Tout d'abord, une étude de chromophores à base de fluorène et de rhénium a été effectuée dans le but d'évaluer le transfert électronique entre ces deux composants. Ensuite, des centres de liaisons à base de dimère de rhodium tétraamidinate ont été créés et étudiés afin d'établir leurs caractéristiques photophysiques et électrochimiques. Puis un d'entre eux a été assemblé avec des chromophores de rhénium, créant ainsi des espèces moléculaires discrètes contenant d'un à quatre chromophores. Et pour finir, ces assemblages ont été combinés avec un catalyseur à base de cobalt, puis ont été testés dans des expériences de photoproduction d'hydrogène. Cette dernière partie a requis l'élaboration d'un photoréacteur qui est aussi décrite en détail dans cet ouvrage.

Mots-clés : rhénium, chromophore, fulvène, transfert de charge, isomérisation, rhodium, couplage Suzuki, photophysique, électrochimie, théorie de la fonctionnelle de la densité, paramètre d'Hammett, paramètre de Taft, solvatochromisme, hydrogène, photocatalyse, cobalt, chromatographie en phase gazeuse.

Abstract

This research project involves synthetic metallosupramolecular systems developed to mimic the natural process of photosynthesis. Ideally, these systems would be able to provide the energy and the charge separation needed to catalyze multielectron-transfer reactions, such as water-splitting or carbon dioxide reduction. The realization of such a catalytic system would create a renewable energy source, in the form of chemical energy, created directly from solar energy.

The system envisioned has three distinct parts in the form of an antenna. First of all, chromophores go into an excited state, while capturing the visible light energy of the Sun. Then comes a hub which binds all the chromophores and collects this excited state energy through an electron transfer. This electron is then transferred again to the last part, a catalytic reaction center. This assembly creates a charge separation between the chromophore and the reaction center which are separated by the hub, thus avoiding the recombination of charge.

The project focuses on the synthesis, characterization and application in photocatalysis of chromophore-hub-catalyst assemblies. First of all, a study of fluorene and rhenium based chromophores was made to assess the electronic transfer between these two components. Then, tetraamidinate rhodium dimer based hubs have been created and studied in order to establish their photophysical and electrochemical characteristics. Then one of these assemblies was formed with chromophores of rhenium, thus creating discrete molecular species containing one to four chromophores. And finally, these assemblies were combined with a cobalt-based catalyst and were tested for hydrogen photoproduction. The latter required the development of a photoreactor which is also described in detail in this thesis.

Keywords: rhenium, chromophore, fulvene, charge transfer, isomerization, rhodium, Suzuki coupling, photophysics, electrochemistry, density functional theory, Hammett parameter, Taft parameters, solvatochromism, hydrogen, photocatalysis, cobalt, gas phase chromatography.

Table des matières

Liste des tableaux

Liste des figures

Liste des chartes et des schémas

Liste des abréviations

Å	Angström
ACN	Acétonitrile
AcOEt	Acétate d'éthyle
ATR	*Attenuated total reflectance*
B3LYP	*Becke, three-parameter, Lee-Yang-Parr exchange-correlation functional*
bpy	2,2'-bipyridine
br	*Broad*
CCD	*Charged-Coupled Device*
CIF	*Crystallographic information file*
CIS	Conversion intersystème
CPCM	*Polarizable conductor calculation model*
CV	*Cyclic voltammetry*
d	Doublet
dba	Dibenzylidèneacétone
DCM	Dichlorométhane
dd	Doublet de doublet
ddd	Doublet de doublet de doublet
DE	Donneur d'électron
deg	Degré
DFT	*Density functional theory*
DMF	*N*,*N*'-Dimethylformamide
DMSO	Diméthylsulfoxide
dpb	*N*,*N*'-diphénylbenzamidine ou *N*,*N*'-diphénylbenzamidinate
dpf	*N*,*N*'-diphénylformamidine ou *N*,*N*'-diphénylformamidinate
DRX	Diffraction de rayon X
ED	*Electron donor*
équiv.	Équivalent
éq.	cf. équiv.
ESI-MS	*Electrospray ionization mass spectrometry*

Et	Éthyle
FT-IR	Fourier transform infrared
fwhm	full-width at half-maximum
GC	*Gas chromatography*
GOF	Goodness of fit
GS	*Ground state*
HOMO	Highest occupied molecular orbital
I	Intensité lumineuse
IR	Infrarouge
ISC	*Intersystem crossing*
LANL2DZ	L*os Alamos National Laboratory 2 double ζ*
LMCT	*Ligand-to-metal; charge transfer*
LM_2CT	*Ligand-to-metal dimer; charge transfer*
LUMO	*Lowest occupied molecular orbital*
m	Multiplet
Me	Méthyle
MLCT	*Metal-to-ligand charge transfer*
M_2LCT	*Metal dimer-to-ligand charge transfer*
MLLCT	*Metal-ligand-to-ligand charge transfer*
m/z	ratio masse sur charge
NMR	*Nuclear magnetic resonance*
OAc	acétate
ORTEP	*Oak Ridge thermal ellipsoid program*
PCET	*Proton coupled electron transfer*
PCM	*Polarized continuum model*
Ph	Phényle
phen	1,10-henanthroline
ppm	Partie par million
PS	Photosensibilisateur
PTFE	Polytétrafluoroéhylène
py	Pyridine ou pyridyle

RMN	Résonnance magnétique nucléaire
SCE	*Standard calomel electrode*
sh	*shoulder*
SOMO	*Singly occupied molecular orbital*
S-PHOS	2-dicyclohexylphosphino-2',6'-diméthoxybiphényle
SWV	*Square-wave voltamperometry*
t	Triplet
TBAP	Tétrabutylammonium hexafluorophosphate
TCD	*Thermal conductivity detector*
TD-DFT	*Time-dependent Density Functional theory*
TEA	Triéthylamine
TEP	Transfert d'électron photoinduit
TEOA	Triéthanolamine
THF	Tétrahydrofurane
TLC	Thin layer chromatography
TOF	*Turnover Frequency*
TON	*Turnover Number*
v:v	volume:volume
UV	Ultraviolet
Z	Nombre de molécule dans la maille élémentaire

Schéma de référence des molécules

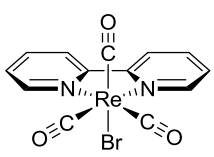

1-1 = 5-5

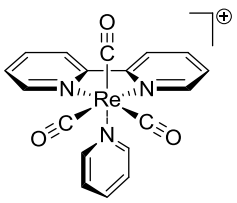

1-2 = 2-3 = 4-4

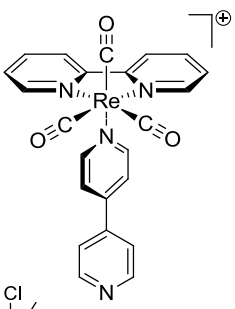

5-7

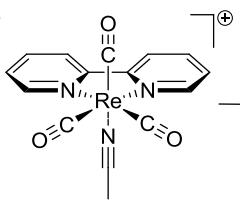

1-3 = 5-8

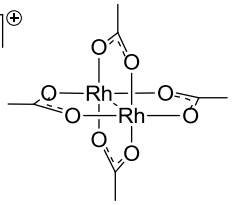

1-4

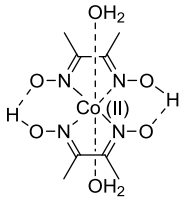

1-6 = 5-10

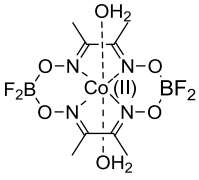

1-7 = 5-9

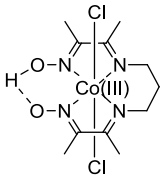

1-8

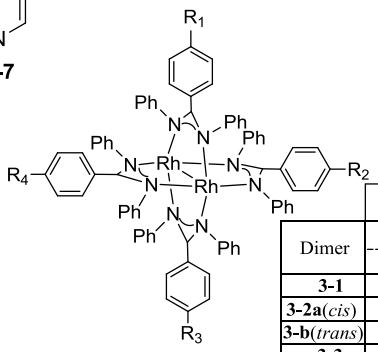

	R_n=	
Dimer	---Br	- - 
3-1	2,3,4	1
3-2a(*cis*)	3,4	1,2
3-b(*trans*)	2,4	1,3
3-3	4	1,2,3
3-4		1,2,3,4
3-5	1,2,3,4	

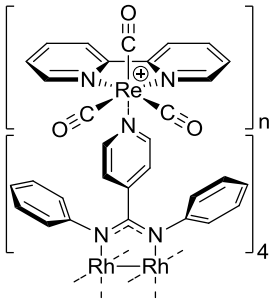

n = 1: **4-1 = 5-1**
n = 2: **4-2 = 5-2**
n = 3: **4-3 = 5-3**
n = 4: **4-4 = 5-4**

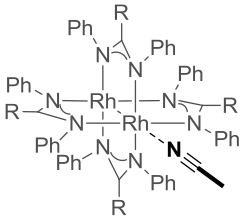

4-n+MeCN

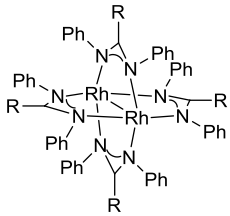

Dimer	R=
3-6 = 4-5 = 5-0	- - 
3-7	- -
3-8	- - 
1-5 = 3-9	- - -H

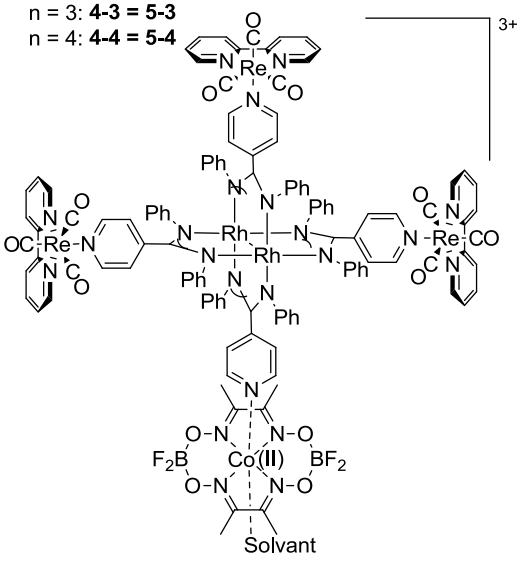

5-11

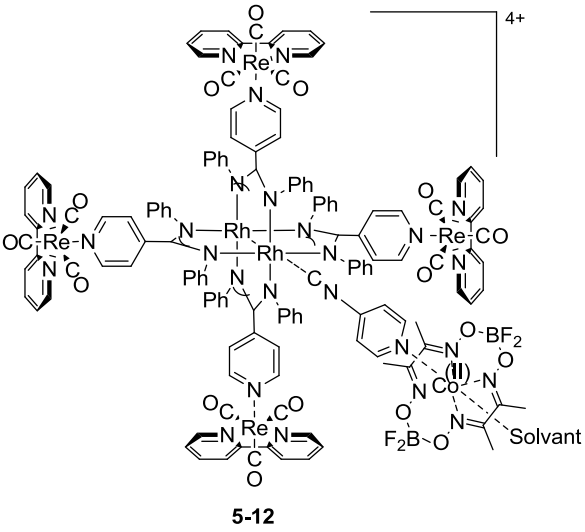

5-12

À mes trois enfants, Éliane, Cassandre et Nathaniel, mes petits projets parallèles. J'espère un jour vous être d'une aussi grande source de motivation que vous l'avez été pour moi pendant cette belle période de ma vie.

Remerciements

Je voudrais remercier tous ceux qui m'ont soutenu durant la thèse, plus particulièrement ma conjointe Chantal et nos trois enfants, Éliane, Cassandre et Nathaniel, qui ont été une source d'amour et d'inspiration inépuisable. Un chaleureux merci à mon directeur de thèse, Pr Garry Hanan, qui m'a permis de naviguer à travers d'innombrables défis et qui a permis mon plein épanouissement professionnel.

J'ai eu la chance de faire un stage outremer en Allemagne à Erlangen et je tiens à remercier le Pr Sven Rau et tout son groupe de recherche de l'époque pour leur chaleureuse réception, plus particulièrement à Evelyn Kastl et Nils Rockstroh.

Je voudrais remercier aussi toute les équipes de soutient de l'université de Montréal, qui m'ont appris tant de facettes de la chimie :

-Au groupe de DRX : Pr Frank Schaper, Dr Michel Simard, Françine Bélanger-Gariépy et Dr Thierry Maris. Ils m'ont permis de voir là où il n'y avait que désordre et maclage.

-Au groupe du service de spectrométrie de masse : Dr ALexandrea Furtos, Marie-christine Tang et Karine Venne. Ils m'ont permis d'identifier les arbres dans la forêt de masses.

-Au groupe RMN : Dr Minh Tan Phan Viet, Dr Cédric Malveau etSylvie Bilodeau. Ils m'ont permis d'entendre les couplages là où il n'avait que du bruit.

-Au service d'analyse élémentaire : Elena Nadezhina et Françine Bélanger-Gariépy. Elles m'ont permis de découvrir la pureté à travers la destruction de mes échantillons.

-Au personnel de l'atelier : Jean-François Myre, Yves Teasdale, Louis Beaumont, Cédric Ginart et Martin Lambert. Ils m'ont permis d'accoucher en ce monde de mes idées.

Je voudrais aussi remercier le Pr Matthias Ernzerhof et le Pr Radu Iftimie pour leur excellente formation qui m'a permis de me lancer et de lancer tant d'autres personnes dans l'univers virtuel de la chimie quantique.

Un gros merci aux étudiants séniors du groupe qui m'ont formé à mes débuts, Dr Michael Cooke, Dr Marie-Pierre Santoni et Dr Elaine Medlycott, ainsi qu'à tous les étudiants qui ont fait partie du groupe que j'ai côtoyés durant ces années (en ordre chronologique) : Pierre Ménard-Tremblay, François Laverdière, Isabelle Théobald, Mihaela Cibian, Amlan Pal, Dr Samik Nag, Carlos A Ruiz Castro, Dr Sophia Derossi, Dr Janaina Ferreira, André

Bessette, Nicholas Randell, Matthias Geist, Élodie Rousset, Brodie Reid et Mathieu Leblanc. Je voudrais particulièrement remercier Mihaela avec qui j'ai eu la chance de partager beaucoup plus qu'un bureau. Merci pour ton soutient.

Je voudrais aussi remercier les étudiants des autres groupes de recherche du Pr Schaper, du Pr Zargarian, du Pr Reber, du Pr Lafleur et du Pr Skene pour les milles et unes échanges. Plus particulièrement je voudrais remercier Dr Stéphane Dufresne et Dr Andréanne Bolduc pour avoir pris le temps de me montrer le fonctionnement de leurs appareils.

Je voudrais remercier de nouveau Élodie et Amlan qui m'ont beaucoup aidé dans la révision d'un article, ainsi que Chantal et Garry pour le temps considérable qu'ils ont investi pour la révision de cette thèse et de tant d'autres documents, en plein congé férié.

Finalement, je voudrais remercier mes parents, Gilles et Micheline, pour avoir toujours cru en moi, même dans les moments difficiles, ainsi que mon frère Alain pour sa grande amitié et son sens du devoir.

Chapitre 1 : Introduction

1.1. Contexte de la recherche

Le rayonnement solaire est sans aucun doute la source de toute vie sur notre planète. Il a permis aux organismes vivants de s'étendre sur toute la surface de la planète, de proliférer et de créer au fil du temps notre source d'énergie moderne : les énergies fossiles (pétrole, charbon et gaz naturel). Cette source moderne n'est cependant pas infinie. Sa consommation massive et incontrôlée risque d'entraîner des problèmes climatiques importants dus à l'accroissement de la concentration de gaz carbonique (CO_2) dans l'atmosphère.[1] Certains projets tentent de réduire le CO_2 atmosphérique, soit par séquestration, soit par transformation. D'autres se consacrent à la réduction de notre dépendance à cette ressource. La recherche dans ce domaine est très variée, passant de l'énergie marémotrice, des parcs d'éoliennes, de la culture de bactéries génétiquement modifiées produisant des biocarburants par photosynthèse vers de la création de réacteurs de fission ou de fusion nucléaire plus efficaces. Malgré la grande énergie emmagasinée dans l'atome, elle ne peut pas subvenir à notre demande énergétique à court ou moyen terme, tout simplement dû à l'effort colossal que chaque centrale nucléaire requiert en construction.[1] Le rayonnement solaire nous bombarde pourtant chaque jour de suffisamment d'énergie pour combler nos besoins énergétiques. Il nous suffit de transformer qu'une fraction de cette énergie en énergie électrique ou chimique.

Dans ce grand domaine, la chimie apporte plusieurs solutions en développant de nouveaux matériaux pour les cellules photovoltaïques, les piles électriques, la capture de CO_2, le stockage d'hydrogène (comme source alternative de carburant) ainsi que pour la photosynthèse artificielle. Cette photosynthèse artificielle accumule directement l'énergie solaire sous forme de lien chimique, i.e. sous forme de carburant. C'est vers cette dernière application que ce projet s'oriente.

Le but de la photosynthèse artificielle est d'imiter la nature qui transforme une molécule à basse énergie (le CO_2) en sucres à haute teneur énergétique grâce à l'énergie des photons capturés par les chromophores. L'approche naturelle est très complexe et les systèmes synthétiques ont des visées plus modestes : l'hydrolyse de l'eau pour la formation

d'hydrogène ou encore la conversion du CO_2 en produit plus énergétique, comme le monoxyde de carbone ou l'acide formique.

L'hydrolyse de l'eau effectuée par voie électrique (électrolyse) n'est pas rentable, trop énergivore, due au surpotentiel requis. La production industrielle d'hydrogène actuelle est effectuée à partir du gaz naturel, qui malgré sa grande efficacité, relâche toujours du CO_2. Beaucoup de recherches se penchent sur l'élaboration de matériaux pour catalyser la réduction et l'oxydation de l'eau en hydrogène et en oxygène.[2-4] Ces recherches permettraient de réduire le coût prohibitif pour l'électrolyse, mais la source d'électricité requise reste problématique, car seules les sources à base d'énergie renouvelable vont réellement permettre une production libre de carbone. L'approche photosynthétique a pour avantage de ne pas requérir une source d'électricité et pourrait être déployée loin du réseau électrique.

Notre recherche est beaucoup plus fondamentale. Elle consiste à créer et évaluer de nouveaux assemblages de chromophores pour leurs applications éventuelles dans de tels processus photocatalytiques. Elle comporte quatre thèmes distincts :

- l'étude de chromophores, plus particulièrement de chromophores à base de rhénium ;
- l'étude de centres de liaison pour des assemblages supramoléculaires, basés sur des dimères de rhodium ;
- l'étude d'assemblages supramoléculaires, composés de chromophores de rhénium et de dimères de rhodium ;
- l'étude de réactions de photocatalyse, à base des assemblages cités plus haut et de catalyseur de cobalt.

1.2. Les chromophores de rhénium et leurs applications en photocatalyse

Plusieurs molécules peuvent être considérées comme des chromophores. Pour une application en photocatalyse solaire, elles doivent posséder trois caractéristiques importantes. Tout d'abord, elles doivent absorber la lumière visible avec un bon rendement quantique, être photostables (ne pas se dégrader) et avoir un état excité d'assez longue durée pour permettre un transfert d'énergie ou d'électron.

La région d'absorption électronique de la molécule doit se situer dans le visible ou le proche ultra-violet (300 nm et plus). Ceci est dû simplement à la radiation solaire perçue au

niveau du sol, comme on peut le constater à la Figure 1.1. Le chromophore idéal aura donc une absorption molaire élevée dans le visible, afin de maximiser la capture des photons émis par le soleil

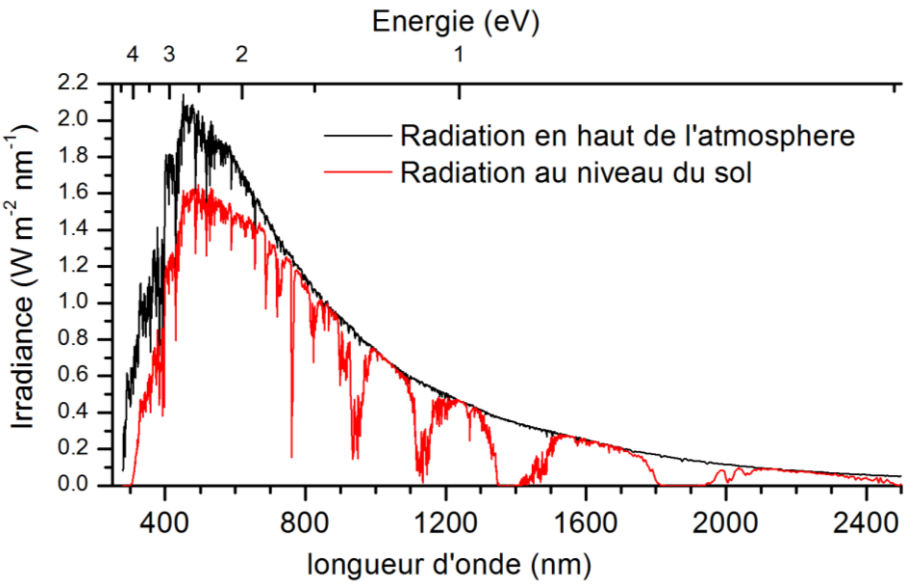

Figure 1.1. Spectre du rayonnement solaire reçu par la terre comme défini par ASTM G-173-03.[5]

Un chromophore ne peut pas non plus absorber trop loin dans le proche infrarouge, car le potentiel énergétique de la lumière diminue avec l'augmentation de la longueur d'onde (en bas d'un eV à 1300 nm). Selon la règle de Kasha, il n'y aura qu'une seule bande émissive de plus basse énergie ou égal à la plus basse bande d'absorption. Les transitions de plus hautes énergies vont généralement se dégrader vers l'état excité le plus bas en énergie avant de réémettre. En général, ces relaxations d'état plus énergétique sont trop rapides pour que ces états puissent être utilisés dans des réactions photocatalytiques. Seule l'énergie de l'état émissif sera disponible pour ces réactions en solution.

Dans le cas des chromophores de rhénium (voir Schéma 1.1), leurs maxima d'absorption se situent entre 350 et 380 nm avec une traînée qui s'étend jusqu'à environ 450 nm. Ils ont une absorptivité molaire d'environ 5000 $M^{-1}cm^{-1}$ ainsi que des rendements quantiques élevés, par exemple 41% pour le complexe **1-2.** Ils sont des chromophores de haute énergie, émettant dans le vert et le jaune, avec une émission se situant entre 530 et 620 nm.[6]

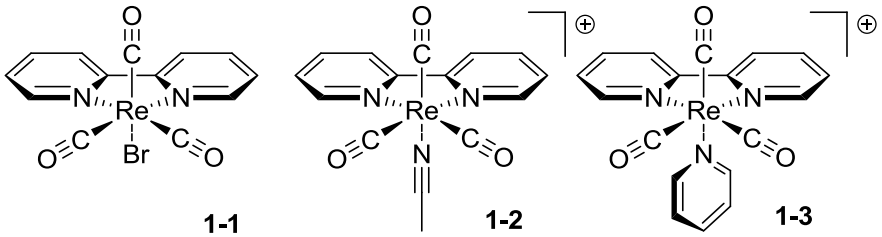

Schéma 1.1. Différents chromophores à base de rhénium

La stabilité sous irradiation va de soi, car si le chromophore se décompose directement par la lumière, il ne pourra pas jouer son rôle de médiateur d'énergie catalytique. Toutefois, les réactions de photocatalyse ont souvent besoin de plus qu'un transfert d'électron photoinduit (TEP) vers une autre molécule.

En général, le chromophore perd ou gagne un électron dans le processus. La stabilité de cet état radicalaire ou la durée de vie du chromophore dans cet état va devenir un élément très important lors de la catalyse. La plupart des chromophores vont se dégrader s'ils sont piégés dans un état réduit ou oxydé trop longtemps. Il est primordial d'optimiser la réaction pour éviter cette condition.

Le dernier point, la durée de l'état excité, est très subjectif. Tout d'abord, il ne s'agit pas nécessairement d'un état excité qui sera émissif. En général, les chromophores avec de longs temps de vie sont très efficaces, car ceux-ci génèrent un grand bassin de chromophores excités accessible pour réagir. Le chromophore **1-1**, contenant un brome, possède un temps de vie de l'état excité 24 fois inférieur (environ 50 ns) à **1-2** (environ 1200 ns) et un rendement quantique 80 fois inférieur. Il demeure malgré tout un très bon candidat employé pour la photocatalyse, et cela à cause de sa plus grande stabilité durant la réaction.[7-9]

Les chromophores de rhénium sont, quant à eux, très répandus, mais ne battent pas en popularité les chromophores à base de ruthénium, très utilisés dans les applications de cellules solaires à base de pigment.[10] Du point de vue de la fonctionnalisation, les chromophores de rhénium ne possèdent qu'un ligand diimine bidentate (versus trois pour le Ru), mais ont un site pour un ligand neutre ou anionique. Ce site rend les modifications faciles, le plus commun ligand utilisé est la pyridine (complexe **1-3**). C'est à travers ce groupement pyridyle que les chromophores de rhénium ont été modifiés dans cette recherche.

1.3. Étude d'assemblage supramoléculaire à base de rhodium-rhénium

Dans les systèmes photosynthétiques naturels, l'énergie de la lumière est récoltée par une multitude de chromophores et est canalisée vers un centre réactionnel situés dans les immenses protéines des photosystèmes (I et II).[11-14] Ces protéines, dont la plus petite, celle du photosystème II, est illustrée à la Figure 1.2, assemblent les chromophores de chlorophylle, de β-carotène et de phéophytine. C'est cet assemblage qui permet de récolter les photons sur une large surface et de les transférer vers un centre réactionnel au centre de la protéine. Dans le cas du photosystème II, ce centre réactionnel oxyde l'eau, source de protons et d'électrons qui seront utilisés dans les autres étapes de la photosynthèse.

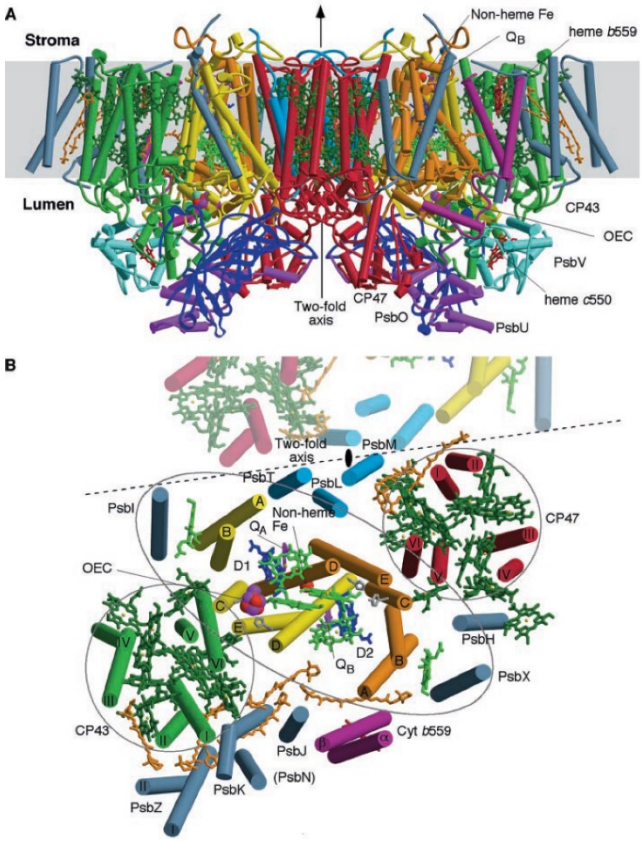

Figure 1.2. Structure du photosystème II. A) Vue du dimère photosystème II perpendiculaire à la normale de la membrane. B) Vue du monomère du photosystème II le long de la normale de la membrane. En vert : les unités chlorophylle; en bleu: les unités phéophytine; en orange : les unités β-carotène.

Ce système grandiose est trop complexe pour être reproduit, mais il est possible de s'en inspirer. L'approche envisagée est de lier plusieurs chromophores afin de former des molécules ou des supramolécules individuelles contenant plusieurs chromophores.[15]

L'utilisation de dimère de rhodium pour les assemblages d'antenne a été initiée par Michael Cooke durant ses études au sein du groupe du Pr Hanan.[16] Le concept est simple : utiliser la géométrie en moulin du dimère pour lier jusqu'à quatre chromophores (voir Schéma 1.2). Les premiers essais ont été réalisés avec des dimères à base d'acétate fonctionnalisés d'un chromophore, dans ce cas-ci un complexe de ruthénium bisterpyridine. Les espèces ont été synthétisées, mais les réactions étaient difficiles et le complexe final enclin à se décomposer en perdant des fragments acétates dans des solvants coordonnants. Une approche séquentielle a alors été développée à travers des ligands *N*,*N*-diaryl-amidinates. Ils sont analogues aux acétates du point de vue de la coordination au dimère, mais sont beaucoup plus stables et ne se dissocient pas aussi facilement. De plus, la présence de groupement sur les atomes d'azote de l'amidinate permet de fonctionnaliser davantage le ligand.

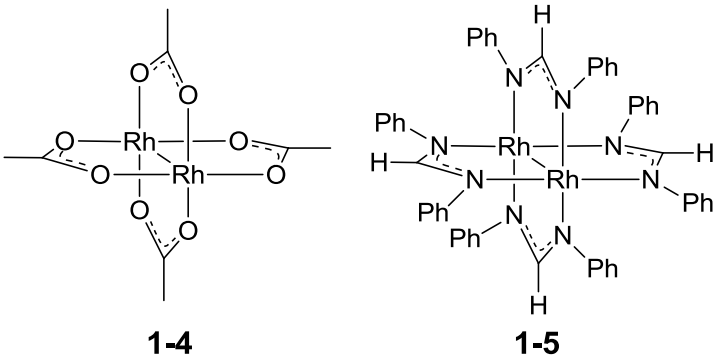

Schéma 1.2. La géométrie des dimères de rhodium : exemples de composés

Du point de vue synthétique, le dimère est formé par réaction directe avec le ligand amidine liquéfié à haute température et un dimère d'acétate de rhodium (Schéma 1.3). La gamme des ligands utilisables est limitée par deux facteurs : l'effet stérique des groupements aryles et la température de liquéfaction. L'effet stérique limite la formation du dimère à cause de la proximité des aryles dans le dimère. Les groupements en *ortho* de l'amidine vont rapidement empêcher la coordination. Toutefois, les autres positions sont accessibles et une grande série de *N*,*N*-diaryl-formamidinate a été déjà synthétisé.[17,18] Le point de liquéfaction est aussi important dû à la synthèse utilisée. La réaction directe doit se faire entre 100 et 210

°C, car à plus haute température le dimère d'acétate risque de se décomposer en oxyde de rhodium avant de réagir. Naturellement, il n'est pas possible d'utiliser un amidine qui ne se liquéfie pas, par exemple un amidine fonctionnalisé avec un complexe métallique. Donc la voie de synthèse utilisée précédemment pour les dimères d'acétate n'est pas utilisable pour greffer un chromophore inorganique directement.

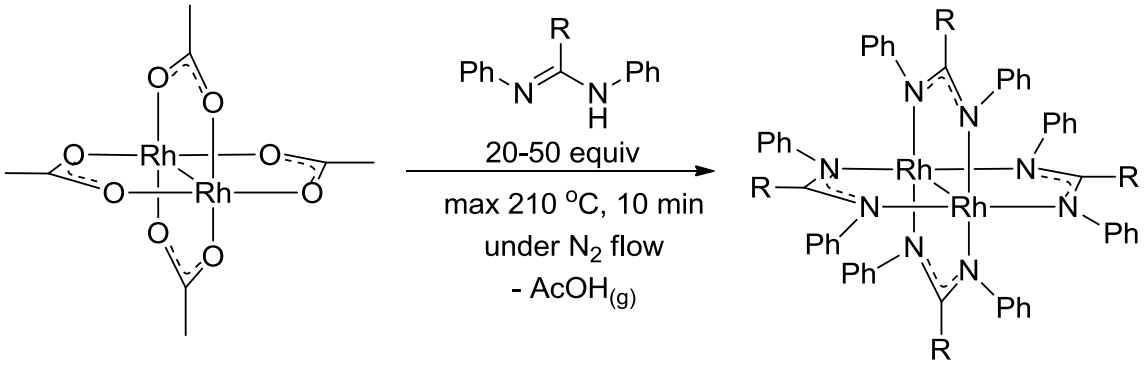

Schéma 1.3. Synthèse générale d'un dimère d'amidinate

Pour réaliser ces assemblages, il est nécessaire d'y aller par étape. L'amidinate du départ va soit être fonctionnalisé directement sur le dimère, soit il va déjà contenir un site de liaison pour lier un chromophore. Dr Cooke a démontré l'utilisation de groupements bromophényls sur le dimère pour faire un couplage de type Buchwald.[19] Il a ainsi pu mettre un groupement imine, qu'il a ensuite transformé en amine, pour en faire un couplage peptidique avec un chromophore ayant un groupement carboxylique. Cette approche fastidieuse permet de lier un chromophore par des liens covalents, mais n'est pas facilement réalisable.

Inspiré des assemblages utilisant un groupement pyridyle pour lier des chromophores de rhénium,[20-22] une voie synthétique plus simple a été envisagée pour fabriquer des assemblages de chromophores à partir des dimères de rhodium. Un ligand, contenant déjà une fonctionnalité pyridyle, a été utilisé pour former directement un dimère avec lequel des chromophores de rhénium peuvent être greffés aisément, sans réaction intermédiaire.[23] Le chemin synthétique devient très simple (Schéma 1.4) et l'assemblage peut être produit à plus grande échelle.

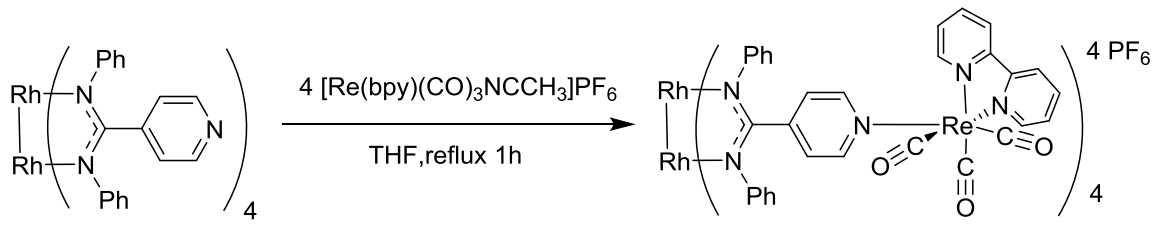

Schéma 1.4. Synthèse de l'assemblage rhodium-rhénium

1.4. Étude de réactions de photocatalyse avec un catalyseur de cobalt

Le dernier point abordé est l'application de ces chromophores lors des réactions photocatalytiques de production d'hydrogène. Ce domaine est en plein essor et plusieurs comptes rendus de qualité ont été publiés récemment sur la photocatalyse de l'hydrogène en solution.[24-32]

Ces travaux sont inspirés du Pr J.-M. Lehn qui fut l'un des pionniers dans ce type de réaction. Du point de vue expérimental, ces travaux sont inspirés de la recherche provenant du groupe du Pr R. Alberto qui se focalise sur les chromophores de rhénium et sur les catalyseurs de cobalt.[7,8,33-37]

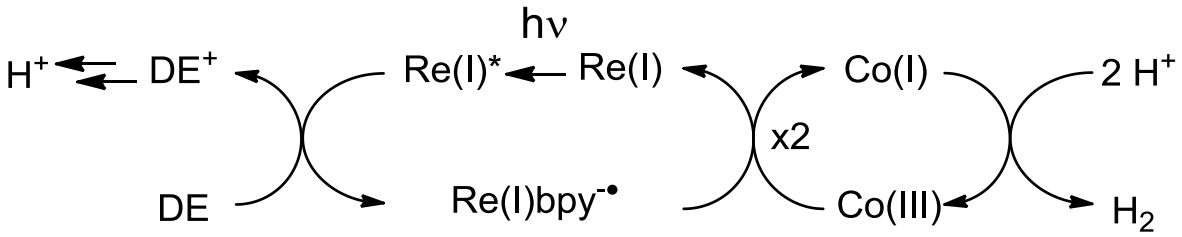

Schéma 1.5. Le cycle photocatalytique de la production d'hydrogène des systèmes Re-Co. (DE = donneur d'électrons)

Le processus typique de la photocatalyse est illustré dans le Schéma 1.5. Le chromophore de rhénium (le photosensibilisateur (PS)) à l'état excité réagit avec le donneur d'électron sacrificiel (DE) pour former une espèce radicalaire réduite qui va transférer son électron vers un catalyseur. Ce catalyseur, un complexe de cobalt, produira de l'hydrogène après que deux électrons aient été transférés. Ce processus, où le PS est tout d'abord réduit, est dit par voie réductrice. L'inverse, où le PS donne immédiatement un électron au catalyseur pour former l'espèce PS^+, se dit par voie oxydante. Le chemin pris dépend en premier lieu du chromophore et en deuxième lieu du donneur et de l'accepteur d'électron

(catalyseur ou médiateur rédox). Pour les chromophores de rhénium, il est établi qu'ils agissent par voie réductrice.[7,37]

Les catalyseurs de cobalt envisagés pour nos systèmes sont à base de diméthylglyoxime, souvent référés comme cobaloxime. Des exemples de ceux-ci sont illustrés sur le Schéma 1.6. Ces catalyseurs permettent une interaction axiale avec un groupement pyridyl, ce qui a été utilisé pour obtenir des assemblages de systèmes chromophore-catalyseur.[9,38-43] Le complexe **1-6** a été très étudié. Il peut être préparé *in situ* ou être isolé sous sa forme oxydée stable à l'air, et les molécules d'eau axiales peuvent être remplacées par des ligands pyridines, phosphines ou halogènes.[7,8,35,42,44]

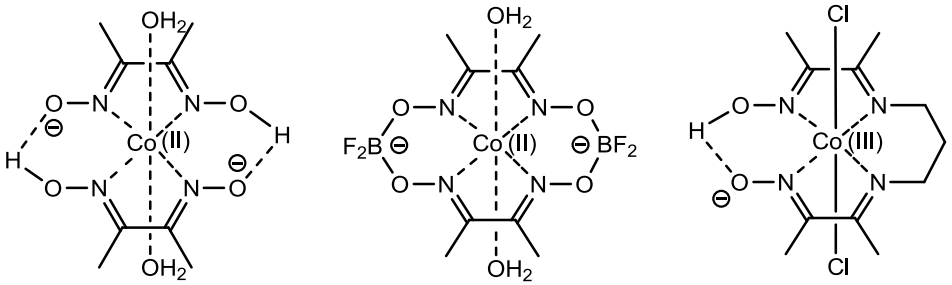

1-6 **1-7** **1-8**

Schéma 1.6. Différents catalyseurs à base de cobalt.

Deux dérivées sont aussi très employées. Le premier, le complexe **1-7**, où les deux ligands diméthylglyoxime sont fusionnés à travers un groupement BF_2, a été largement étudié en tant qu'électrocatalyseur et a également été étudié dans plusieurs systèmes photocatalytiques.[9,38,41,43,45-49] Ce catalyseur a été le point de départ des travaux présentés dans le Chapitre 5. Le second, le complexe **1-8**, n'est fusionné que d'un côté et a été étudié pour la photoproduction d'hydrogène. Il a été principalement étudié par le groupe du Pr Fontecave.[36,50-52]

Ces trois catalyseurs possèdent tous les mêmes cycles catalytiques, affinés et démontrés par plusieurs expériences et par des calculs théoriques.[44,45,50,53-56] La Schéma 1.7 illustre les deux grandes voies possibles : la voie homolytique et la voie hétérolytique.[24] La voie homolytique est observée pour les systèmes en milieu basique, où la concentration en proton défavorise la voie hétérolytique, qui s'applique seulement en milieu acide ou neutre. Le choix de la voie catalytique va dépendre surtout du pH, mais aussi de la nature du catalyseur.

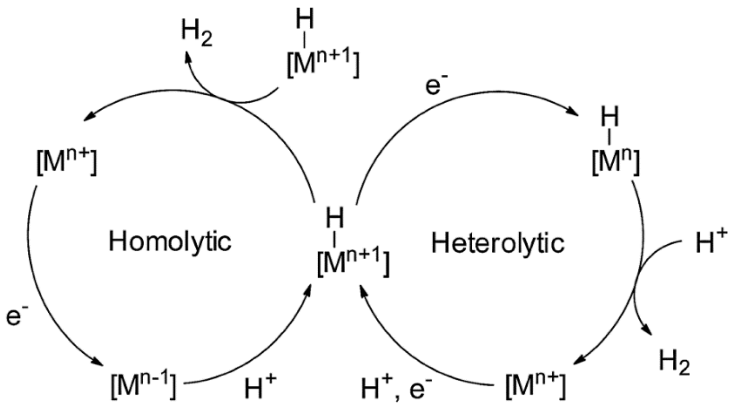

Schéma 1.7. Cycle catalytique général pour la production d'hydrogène. Reproduced from reference 24 by permission of The Royal Society of Chemistry, Copyright © 2012.

Un deuxième cycle,[50] présenté au Schéma 1.8, illustre un mécanisme homolytique avancé tenant compte d'un transfert d'électron concerté au transfert du proton (PCET : *Proton coupled electron transfer*). Ce transfert concerté est possible pour un catalyseur ayant un site avec un proton acide ou un site basique près du cobalt, ce qui est le cas pour le catalyseur **1-6** et **1-8**, mais qui n'est pas applicable pour **1-7**.

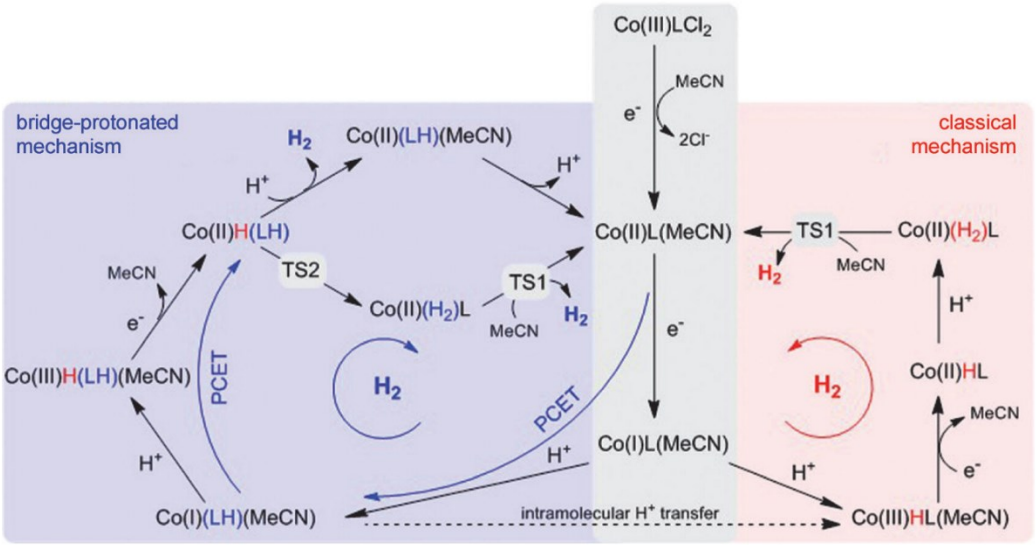

Schéma 1.8. Cycle catalytique proposé pour la production d'hydrogène avec le complexe de cobalt **1-8** passant par un PCET; TS1 et TS2 sont des états transitoires observés. Reproduced from reference 50 by permission of WILEY-VCH Verlag GmbH & Co. KGaA, Weinheim, Copyright © 2013.

Lorsque ces catalyseurs sont utilisés en photocatalyse, leurs cinétiques de réaction doivent être compatibles avec la cinétique de l'excitation du chromophore. Le Schéma 1.9

illustre ce problème pour un chromophore utilisant la voie réductrice. [30] Celui-ci se fait réduire et atteint une forme très active, généralement radicalaire. Il s'ensuit deux possibilités : soit le chromophore transfère l'électron vers le catalyseur, soit il se décompose. La cinétique des réactions k_1 et k_2 devient très importante, car il faut que la vitesse de réaction du transfert soit plus rapide que celle de la décomposition. En général, ceci implique que la concentration du catalyseur devra être très importante. Il faut aussi que la vitesse de réaction de la formation de l'hydrogène soit plus rapide que celle de la réduction du PS. Ceci est critique, car il ne faut pas que la concentration du catalyseur capable d'accepter des électrons chute pendant la photocatalyse. Si c'était le cas, le parcours de la décomposition sera favorisé.

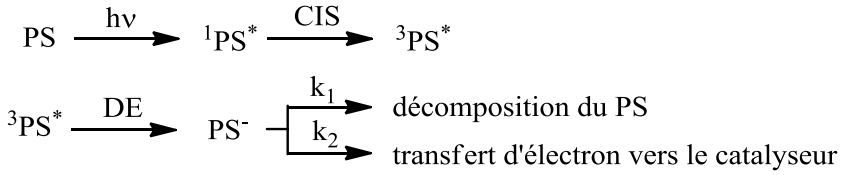

Schéma 1.9. Excitation du chromophore suivi par sa réduction menant au transfert d'électron ou menant à sa décomposition. Adapted from reference 30 by permission of The Royal Society of Chemistry, Copyright © 2012.

Un élément important dans cette catalyse est le donneur d'électron. Les plus populaires sont la triéthylamine (TEA), la triéthanolamine (TEOA) et l'acide ascorbique. Ces donneurs d'électrons ont leur propre chimie après leur réaction avec le PS. Celle de la TEOA est illustrée au Schéma 1.10. Il fournira, lors de sa décomposition, au total deux électrons et deux protons.[7] Ce deuxième électron provient d'une forme radicalaire beaucoup plus réductrice et pourra transférer l'électron directement au PS ou au catalyseur, sans apport de photon. Le TEA a le même type de parcours, tandis que l'acide ascorbique forme des espèces qui peuvent réoxyder le chromophore réduit, empoisonnant ainsi la réaction, mais prévenant la décomposition du chromophore.[33,36]

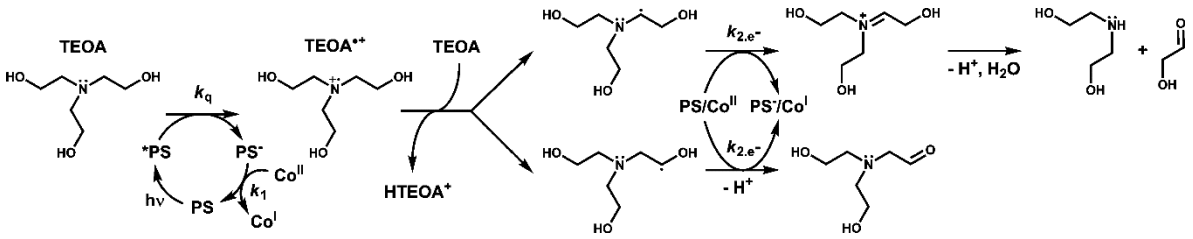

Schéma 1.10. Chemin de décomposition de la triéthanolamine. Reprinted with permission from reference 7. Copyright 2010 American Chemical Society

La production d'hydrogène se mesure en nombre de cycle catalytique ou TON (*Turnover Number*) et en fréquence de catalyse ou TOF (*Turnover frequency*). Le TOF se définit par le nombre de cycle de catalyse par unité de temps. Le TON se définit par le nombre de moles du produit formé divisé par le nombre de moles du catalyseur. Cependant, en photocatalyse, il y a deux composantes catalytiques, le PS et le catalyseur d'hydrogène. Dans la littérature, le TON du catalyseur se définit comme le nombre de moles de H_2 générées divisé par le nombre de moles du catalyseur. Cependant, le TON du PS est défini comme le double afin de tenir compte du fait que pour chaque molécule d'hydrogène formé deux électrons ont été transférés vers le catalyseur. Cette interprétation ne tient pas du tout compte de l'électron venant de la décomposition additionnelle du DE mentionné plus haut. Dans cette thèse, le TON du PS n'est pas doublé de cette façon.

1.5. Objectifs de recherche

L'objectif de la thèse est la synthèse d'un nouveau système photocatalytique composé de plusieurs chromophores liés à un centre de liaison et de tester ce système à des fins de production d'hydrogène. La thèse se divise en quatre chapitres, dont les grandes lignes ont déjà été énoncées à la fin de la section 1.1.

Chapitre 2 : Ce chapitre discute d'une fonctionnalisation du rhénium avec un autre groupement contenant un chromophore organique, le fluorène. Les caractéristiques photophysiques sont évaluées et une étude théorique de DFT (de l'anglais *Density functional theory*) et de TD-DFT (de l'anglais *time dependent* DFT) est effectuée, permettant de comprendre les phénomènes observés.

Chapitre 3 : Dans ce chapitre, un nouveau couplage est effectué à partir du dimère comprenant le groupement bromophényl. Un couplage de type Suzuki est utilisé pour greffer de un à quatre groupements pyridyles. Les caractéristiques intrinsèques de ces dimères de

rhodium sont étudiées en profondeur, utilisant les techniques computationnelles de DFT et TD-DFT pour approfondir la nature des transitions électroniques observées. De plus, une corrélation est effectuée entre la nature du groupement central de l'amidinate et les caractéristiques observables du dimère, à travers les paramètres empiriques d'Hammett et de Taft.

Chapitre 4 : Ce chapitre porte sur l'étude d'assemblages de dimère de rhodium tétra-*N*,*N*'-diphénylisonicotamidinate avec des chromophores de rhénium de type 2,2'-bipyridine tris carbonyle liés à travers le groupement pyridyle. Un effort considérable a été investi pour isoler les espèces partiellement saturées en chromophore de rhénium (contenant de 1 à 3 chromophores). Les caractéristiques de ces composés ont été étudiées par les mêmes méthodes que le chapitre 3. Le succès synthétique obtenu a permis d'ouvrir la voie vers l'étude photocatalytique de ces assemblages.

Chapitre 5 : Ce chapitre est divisé en deux parties : l'élaboration d'un photoréacteur pour effectuer des études photocatalytiques et les résultats de ces études pour les systèmes à base des assemblages présentés au chapitre 4. Ces assemblages ont été évalués avec différents catalyseurs à base de cobalt.

Chapitre VI : Une conclusion générale se concentrant plus particulièrement sur les perspectives des chapitres 2 à 4, non mentionnées dans les articles d'origines.

1.6. Références

(1) Lewis, N. S.; Nocera, D. G. *Proc. Natl. Acad. Sci. U. S. A.* **2006**, *103*, 15729.
(2) Teets, T. S.; Nocera, D. G. *Chem. Commun.* **2011**, *47*, 9268.
(3) Kanan, M. W.; Nocera, D. G. *Science* **2008**, *321*, 1072.
(4) Smith, R. D. L.; Prevot, M. S.; Fagan, R. D.; Zhang, Z.; Sedach, P. A.; Siu, M. K. J.; Trudel, S.; Berlinguette, C. P. *Science* **2013**, *340*, 60.
(5) ASTM Standard G-173-03, 2012, ASTM International, West Conshohocken, PA, **2013**, DOI: 10.1520/G0173-03R12, www.astm.org.
(6) Caspar, J. V.; Meyer, T. J. *J. Phys. Chem.* **1983**, *87*, 952.
(7) Probst, B.; Rodenberg, A.; Guttentag, M.; Hamm, P.; Alberto, R. *Inorg. Chem.* **2010**, *49*, 6453.
(8) Probst, B.; Kolano, C.; Hamm, P.; Alberto, R. *Inorg. Chem.* **2009**, *48*, 1836.
(9) Fihri, A.; Artero, V.; Pereira, A.; Fontecave, M. *Dalton Trans.* **2008**, 5567.
(10) Brugger, P. A.; Infelta, P. P.; Braun, A. M.; Gratzel, M. *J. Am. Chem. Soc.* **1981**, *103*, 320.

(11) McDermott, G.; Prince, S. M.; Freer, A. A.; Hawthornthwaite-Lawless, A. M.; Papiz, M. Z.; Cogdell, R. J.; Isaacs, N. W. *Nature* **1995**, *374*, 517.
(12) Ferreira, K. N.; Iverson, T. M.; Maghlaoui, K.; Barber, J.; Iwata, S. *Science* **2004**, *303*, 1831.
(13) Guskov, A.; Kern, J.; Gabdulkhakov, A.; Broser, M.; Zouni, A.; Saenger, W. *Nat Struct Mol Biol* **2009**, *16*, 334.
(14) Barber, J. *Philos. Trans. R. Soc., A* **2007**, *365*, 1007.
(15) Cooke, M. W.; Chartrand, D.; Hanan, G. S. *Coord. Chem. Rev.* **2008**, *252*, 903.
(16) Cooke, M. W., Université de Montréal, 2007.
(17) Ren, T.; Lin, C.; Valente, E. J.; Zubkowski, J. D. *Inorg. Chim. Acta* **2000**, *297*, 283.
(18) Ren, T. *Coord. Chem. Rev.* **1998**, *175*, 43.
(19) Cooke, M. W.; Santoni, M. P.; Hanan, G. S.; Proust, A.; Hasenknopf, B. *Dalton Trans.* **2009**, 3671.
(20) Casanova, M.; Zangrando, E.; Iengo, E.; Alessio, E.; Indelli, M. T.; Scandola, F.; Orlandi, M. *Inorg. Chem.* **2008**, *47*, 10407.
(21) Kuehn, F. E.; Zuo, J.-L.; Fabrizi de Biani, F.; Santos, A. M.; Zhang, Y.; Zhao, J.; Sandulache, A.; Herdtweck, E. *New J. Chem.* **2004**, *28*, 43.
(22) Xue, W. M.; Kuehn, F. E.; Herdtweck, E. *Polyhedron* **2001**, *20*, 791.
(23) Chartrand, D.; Hanan, G. S. *Chem. Commun.* **2008**, 727.
(24) Thoi, V. S.; Sun, Y.; Long, J. R.; Chang, C. J. *Chem. Soc. Rev.* **2013**, *42*, 2388.
(25) Mulfort, K. L.; Mukherjee, A.; Kokhan, O.; Du, P.; Tiede, D. M. *Chem. Soc. Rev.* **2013**, *42*, 2215.
(26) Manbeck, G. F.; Brewer, K. J. *Coord. Chem. Rev.* **2013**, *257*, 1660.
(27) Eckenhoff, W. T.; McNamara, W. R.; Du, P.; Eisenberg, R. *Biochim. Biophys. Acta, Bioenerg.* **2013**, *1827*, 958.
(28) Artero, V.; Fontecave, M. *Chem. Soc. Rev.* **2013**, *42*, 2338.
(29) Schulz, M.; Karnahl, M.; Schwalbe, M.; Vos, J. G. *Coord. Chem. Rev.* **2012**, *256*, 1682.
(30) Eckenhoff, W. T.; Eisenberg, R. *Dalton Trans.* **2012**, *41*, 13004.
(31) McDaniel, N. D.; Bernhard, S. *Dalton Trans.* **2010**, *39*, 10021.
(32) Rau, S.; Losse, S.; Vos, J. G. *Coord. Chem. Rev.* **2010**, *254*, 2492.
(33) Guttentag, M.; Rodenberg, A.; Bachmann, C.; Senn, A.; Hamm, P.; Alberto, R. *Dalton Trans.* **2013**, *42*, 334.
(34) Ziessel, R.; Hawecker, J.; Lehn, J. M. *Helv. Chim. Acta* **1986**, *69*, 1065.
(35) Hawecker, J.; Lehn, J. M.; Ziessel, R. *Nouv. J. Chim.* **1983**, *7*, 271.
(36) Guttentag, M.; Rodenberg, A.; Kopelent, R.; Probst, B.; Buchwalder, C.; Brandstaetter, M.; Hamm, P.; Alberto, R. *Eur. J. Inorg. Chem.* **2012**, *2012*, 59.
(37) Probst, B.; Guttentag, M.; Rodenberg, A.; Hamm, P.; Alberto, R. *Inorg. Chem.* **2011**, *50*, 3404.
(38) Fihri, A.; Artero, V.; Razavet, M.; Baffert, C.; Leibl, W.; Fontecave, M. *Angew. Chem. Int. Ed.* **2008**, *47*, 564.

(39) Mulfort, K. L.; Mukherjee, A.; Kokhan, O.; Du, P.; Tiede, D. M. *Chem. Soc. Rev.* **2013**, *42*, 2215.
(40) Mukherjee, A.; Kokhan, O.; Huang, J.; Niklas, J.; Chen, L. X.; Tiede, D. M.; Mulfort, K. L. *PCCP* **2013**.
(41) Cropek, D. M.; Metz, A.; Muller, A. M.; Gray, H. B.; Horne, T.; Horton, D. C.; Poluektov, O.; Tiede, D. M.; Weber, R. T.; Jarrett, W. L.; Phillips, J. D.; Holder, A. A. *Dalton Transactions* **2012**, *41*, 13060.
(42) Zhang, P.; Wang, M.; Li, X.; Cui, H.; Dong, J.; Sun, L. *Sci. China: Chem.* **2012**, *55*, 1274.
(43) Veldkamp, B. S.; Han, W.-S.; Dyar, S. M.; Eaton, S. W.; Ratner, M. A.; Wasielewski, M. R. *Energy Environ. Sci.* **2013**, *6*, 1917.
(44) Bhattacharjee, A.; Chavarot-Kerlidou, M.; Andreiadis, E. S.; Fontecave, M.; Field, M. J.; Artero, V. *Inorg. Chem.* **2012**, *51*, 7087.
(45) Muckerman, J. T.; Fujita, E. *Chem. Commun.* **2011**, *47*, 12456.
(46) Baffert, C.; Artero, V.; Fontecave, M. *Inorg. Chem.* **2007**, *46*, 1817.
(47) Bakac, A.; Brynildson, M. E.; Espenson, J. H. *Inorg. Chem.* **1986**, *25*, 4108.
(48) Bakac, A.; Espenson, J. H. *J. Am. Chem. Soc.* **1984**, *106*, 5197.
(49) Niklas, J.; Mardis, K. L.; Rakhimov, R. R.; Mulfort, K. L.; Tiede, D. M.; Poluektov, O. G. *J. Phys. Chem. B* **2012**, *116*, 2943.
(50) Bhattacharjee, A.; Andreiadis, E. S.; Chavarot-Kerlidou, M.; Fontecave, M.; Field, M. J.; Artero, V. *Chem. - Eur. J.* **2013**, *19*, 15166.
(51) Zhang, P.; Jacques, P.-A.; Chavarot-Kerlidou, M.; Wang, M.; Sun, L.; Fontecave, M.; Artero, V. *Inorg. Chem.* **2012**, *51*, 2115.
(52) Fourmond, V.; Jacques, P. A.; Fontecave, M.; Artero, V. *Inorg. Chem.* **2010**, *49*, 10338.
(53) Dempsey, J. L.; Winkler, J. R.; Gray, H. B. *J. Am. Chem. Soc.* **2010**, *132*, 1060.
(54) Solis, B. H.; Yu, Y.; Hammes-Schiffer, S. *Inorg. Chem.* **2013**, *52*, 6994.
(55) Smolentsev, G.; Guda, A.; Zhang, X.; Haldrup, K.; Andreiadis, E. S.; Chavarot-Kerlidou, M.; Canton, S. E.; Nachtegaal, M.; Artero, V.; Sundstrom, V. *J. Phys. Chem. C* **2013**, *117*, 17367.
(56) Shan, B.; Baine, T.; Ma, X. A. N.; Zhao, X.; Schmehl, R. H. *Inorg. Chem.* **2013**, *52*, 4853.

Chapitre 2 : Diimine Triscarbonyl Re(I) of Isomeric Pyridyl-fulvene Ligands: an Electrochemical, Spectroscopic and Computational Investigation

2.1. Résumé

Ce chapitre aborde l'étude d'un chromophore de rhénium (tris carbonyle 2,2'-bipiridine) fonctionnalisé avec un groupement (3 ou 4)-fluoren-9-ylidenemethyl-pyridine. Ce fragment comporte un groupement fluorène, un excellent chromophore organique. L'idée initiale était d'augmenter l'absorptivité du chromophore de rhénium, tout en gardant ses propriétés émissives. Cependant, le ligand comporte aussi un groupement fulvène. Celui-ci est aussi un excellent chromophore, mais il est de plus basse énergie et absorbe dans la même région que le MLCT du complexe. Son état triplet est de plus basse énergie, désactivant ainsi l'émission du rhénium. Ceci a été démontré par une étude photophysique accompagnée de calculs DFT et une étude TD-DFT ont permis d'établir la cause du phénomène de désactivation. La désactivation est causée par un état triplet centré sur le fulvène, ce qui cause une rotation de 90° de la liaison double de celui-ci. Ceci est similaire aux molécules de stilbène qui font une photoisomérisation *cis*/*trans*, mais dans ce cas-ci, la rotation de la liaison double n'est pas visible à cause de la symétrie du fluorène. La position de la pyridine (*para* ou *méta* au fulvène) joue un rôle important. La position *para* apporte une grande délocalisation, ce qui a pour effet d'augmenter l'absorptivité molaire et d'apporter un déplacement bathochromique de cette absorption du fulvène.

L'inverse de l'objectif a donc été réalisé : le chromophore de rhénium augmente l'absorption du fulvène et permet sa photoisomérisation à plus basse énergie. Il s'agit maintenant de tirer avantage de cela en fonctionnalisant le fluorène de départ pour observer cette photoisomérisation.

Contribution :

Carlos A. Castro Ruiz : Synthèse et caractérisation des ligands, première synthèse des complexes suivi par la caractérisation partielle de ceux-ci.

Daniel Chartrand : Synthèse optimisée des complexes et leurs caractérisations totales, résolution des structures cristallines, études photophysiques, modélisation des molécules par DFT et TD-DFT, rédaction de l'article.

Garry S. Hanan : Supervision, révision de l'article.

Diimine Triscarbonyl Re(I) of Isomeric Pyridyl-fulvene Ligands: an Electrochemical, Spectroscopic and Computational Investigation

*Daniel Chartrand, Carlos A. Castro Ruiz, Garry S. Hanan**

Department of Chemistry, Université de Montréal, Montréal, Québec, H3T 1J4 Canada

*: Tel: 1-514-340-5156. Fax: 1-514-343-7586.

Received: July 17, 2012; Published: November 15, 2012

dx.doi.org/10.1021/ic301559s

Reproduced with permission from *Inorg. Chem.* **2012**, 51, 12738−12747.

KEYWORDS: Rhenium, chromophore, fulvene, Charge Transfer, isomerization.

2.2. Table of Content Graphic

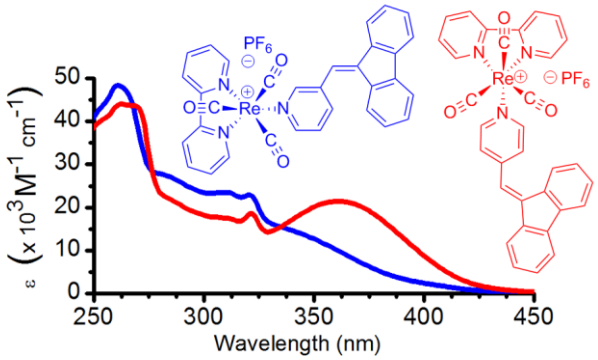

Two new dibenzofulvene functionalized rhenium chromophores of the form *fac*-[Re(bpy)(CO)3(**L**)]PF6 (bpy =2,2'-bipyridine) are reported, where **L** is a pyridine functionalized in *para* or *meta* position with a dibenzofulvene moiety. Results show interesting features of increased delocalization of the fulvene ligand into the rhenium core for one of the complexes. Neither complex emits, suggesting energy transfer toward the lowest energy triplet state of the fulvene.

2.3. Abstract

The synthesis and characterization of a novel family of positively charged *fac*-[Re(bpy)(CO)$_3$(**L**)]PF$_6$ (bpy = 2,2'-bipyridine) complexes are reported, where **L** is a pyridine functionalized in *para* or *meta* position with a fulvene moiety, namely, 4-fluoren-9-ylidenemethyl-pyridine (***p*Fpy**) and 3-fluoren-9-ylidenemethyl-pyridine (***m*Fpy**). The complexes were prepared in high yield (86%) by direct addition at room temperature of the corresponding pyridine to the tetrahydrofuran (THF) adduct *fac*-[Re(bpy)(CO)$_3$(THF)][PF$_6$] precursor. Both ligand and complex structures were fully characterized by a variety of techniques including X-ray crystallography. The complexes did not exhibit the expected triplet mixed metal—ligand-to-ligand charge transfer (MLLCT) emission, due to its deactivation by the non-emissive triplet excited state of fulvene. The absorption profile shows that the MLLCT is overshadowed by the fulvene centered π—π* transition of higher molar absorptivity as shown by time dependent density functional theory (TD-DFT) calculations. The position of the fulvene on the pyridyl ring has a large effect on this transition, the *para* position displaying a much higher absorption coefficient (21.3×10^3 $M^{-1}cm^{-1}$) at lower energy (364 nm) than the *meta* position (331 nm, 16.0×10^3 $M^{-1}cm^{-1}$)

2.4. Introduction

Rhenium triscarbonyl diimine chromophores have been studied extensively for the past 30 years; their unique characteristics (e.g., high stability, high energy excited states, capacity for reductive and oxidative electron transfer) make them ideal for photosensitizers.[1] They are found as photoactive components in various roles: chromophores supplying electrons to catalysts (e.g., hydrogen evolution);[2] photocatalysts reducing carbon dioxide to carbon monoxide;[3] photosensitizers permitting visible light photoisomerization;[4] and as chromophoric building-blocks for supramolecular assemblies.[5] One common variant involves a 2,2'-bipyridine (bpy) ligand and a secondary neutral ligand L in complexes of the type [Re(bpy)(CO)$_3$L]$^+$, with pyridine being the motif of choice for further functionalization of the rhenium chromophore through ligand L. To expand the utility of the rhenium-bpy unit, a *meta* and *para* fulvene functionalized pyridine was used as ligand L in this study, and the chemical and photophysical properties of its rhenium complexes were determined.

The properties of the fulvene ligands are similar to those of stilbene molecules in that they can undergo isomerization through their triplet excited state,[6] albeit the irradiation energy necessary for this isomerization is often found only in the UV region unless highly conjugated molecules are used. In addition, the quantum yield of isomerization is usually relatively low because of the triplet state of the molecule competing with the permitted fluorescence decay of the singlet excited-state. As such, grafting a rhenium onto the fulvene core may enhance both the absorption, by causing its red-shift with a concomitant increase in the coverage of a broader spectrum of light, and the efficiency, by quenching the fluorescence to a longer-lived, higher-energy triplet state centered on the rhenium bipyridine that will act as a reservoir for the triplet state centered on the fulvene. This process is well described for Ru(II) diimine complexes containing fused polycyclic moieties.[7]

Although energy transfer has been investigated using rhenium complexes displaying intramolecular charge transfer more than 25 years ago,[8] recent research has examined the addition of photoisomerizable ligands, containing stilbene analogues and other moieties, that once coordinated quench the luminescence of the rhenium in favor of their isomerization.[4a-i] Closer to our design is the 4-styrylpyridine motif, which upon coordination to rhenium was shown to undergo photoisomerization with lower energy light and at higher efficiency by spectroscopic and high level computational studies.[4k-m] In our case, no isomerization is observable because of the symmetry of the ligand, but energy transfer can still be observed because of the absence of emission of the rhenium complex, suggesting that the non-radiative decay of the excited state passes by the triplet state of the fulvene. Another interesting aspect of this study is the delocalization of the fulvene orbitals onto the rhenium core, which is seen in only one of the pyridyl isomers.

2.5. Experimental Section

2.5.1. General Considerations

All of the organic reagents were obtained from Sigma Aldrich, rhenium carbonyl from Pressure Chemical Co. and solvents from Fischer and Anachemia and were used as received without any further purification. IR spectra were recorded on solid samples using a diamond ATR Perkin-Elmer Spectrum 100 FT-IR. Nuclear magnetic resonance spectra were recorded using Bruker spectrometers (300 and 400 MHz) at room temperature, with ^{1}H and ^{13}C chemical shifts referenced to residual solvent resonances. Elemental analyses were

performed on the desolvated bulk samples by the university departmental service. Room temperature photophysical measurements were done in air-equilibrated and degassed freshly distilled dichloromethane (DCM), using a quartz cell. Low-temperature emission were recorded in degassed 1 MeOH: 4 EtOH (v:v) and 1 toluene: 1 DCM (v:v) glasses at 77 K in a borosilicate tube. Absorption and emission spectra were recorded using a Cary 500i UV—vis—NIR spectrophotometer and a Cary Eclipse 300 fluorimeter, respectively. Oscillator strengths and peak maxima are obtained from integrated fitted Gaussian curves of the molar absorptivity spectrum in function of wavenumber, following the following equation: $f = 1.44 \times 10^{-9} \int \varepsilon(\nu)\, d\nu$. The emission spectra used the maximum of absorption of the lowest energy band of the studied molecules as excitation wavelength. Electrochemical measurements were carried out in argon-purged DCM at room temperature with a BAS CV50W multipurpose equipment interfaced to a PC. The working electrode was a Pt electrode, the counter electrode was a Pt wire, and the pseudoreference electrode was a silver wire. The reference was set using an internal 1.0 mM ferrocene/ferrocinium sample with its redox couple adjusted to 460 mV vs SCE in dichloromethane.[9] The concentration of the compounds was around one mM. Tetrabutylammonium hexafluorophosphate (TBAP) was used as supporting electrolyte, and its concentration was 0.10 M. Cyclic voltammograms (CVs) were obtained at scan rates of 50 and 100 mV/s. For reversible processes, half-wave potentials (vs SCE) were measured with square wave voltammetry (SWV) experiments performed with a step rate of 4 mV, a square wave amplitude of 25 mV, and a frequency of 15 Hz. For irreversible oxidation processes, the cathodic peak was used as *E*, and the anodic peak was used for irreversible reduction processes. The criteria for reversibility were the separation of 60 mV between cathodic and anodic peaks, the close to unity ratio of the intensities of the cathodic and anodic currents, and the constancy of the peak potential on changing scan rate. Experimental uncertainties are as follows: absorption maxima, ± 2 nm; molar absorption coefficient, 10%; emission maxima, ± 5 nm; redox potentials, ± 10 mV.

2.5.2. Synthetic Methods

The rhenium complexes $Re(CO)_5Br$,[10] *fac*-[Re(bpy)$(CO)_3$Br],[11] *fac*-[Re(bpy)$(CO)_3$(MeCN)][PF_6],[12] *fac*-[Re(bpy)$(CO)_3$(pyridine)][PF_6] (**2-3**) and *fac*-[Re(bpy)$(CO)_3$(THF)][PF_6][13] were prepared following literature procedures. The ligands ***m*Fpy** and ***p*Fpy** were prepared by a modified literature method.[14] They have been synthesized by a similar route before, but with only basic characterization.[15] Herein, their

free base versions are fully characterized. See Supporting Information, Chart 2.S1 for the labeling of the proton peaks in NMR. Note that the hydrochloride salts were characterized more recently by proton NMR as well.[16]

3-((9*H*-fluoren-9-ylidene)methyl)pyridine (*m*Fpy). Fluorene (4.023 g, 24.2 mmol) and KOH (2.028 g, 36.1 mmol) were taken in ethylene glycol dimethyl ether (35 mL) in a round bottomed flask and stirred at reflux for 10 min. 3-Pyridinecarboxaldehyde (3.89 g, 36.3 mmol) was added dropwise, and the stirring was continued at the same temperature for 4 h, during which the initial red mixture turned dark green. After the mixture was cooled to room temperature, water (200 mL) was added, and the mixture stirred at ambient temperature for 45 min, resulting in a yellow-orange suspension. The suspension was isolated by filtration, and the resulting yellow precipitate was washed with hexane (4 × 40 mL) and purified by column chromatography (Al_2O_3, DCM/AcOEt (v:v) (1:1)) to afford a pale yellow pure compound. Yield: 70%.^{1}H NMR ($CDCl_3$ 300 MHz) δ ppm 8.85 (s, 1He), 8.65 (d, J = 4 Hz, 1Hf), 7.89 (d, J = 8 Hz, 1Hh), 7.78 (d, J = 7 Hz, 1Hj), 7.71 (d, J = 7 Hz, 2Hmm'), 7.57 (s, 1Hi), 7.45−7.37 (m, 3Hgj'k), 7.34 (ddt, J = 7, 3, 1 Hz, 2Hll'), 7.06 (dt, J = 8, 1 Hz, 1Hk'). ^{13}C{^{1}H} NMR (75 MHz, $CDCl_3$) δ ppm 150.2, 149.0, 141.5, 139.4, 138.9, 138.5, 136.5, 136.1, 133.9, 129.1, 128.7, 127.2, 126.9, 124.2, 123.3, 122.6, 120.4, 119.9, 119.7. HRMS (ESI, MeCN) (*m/z*): $[M+H]^+$ ($C_{19}H_{14}N$) calcd 256.11207; found 256.11255. Anal. Calcd for $C_{19}H_{13}N$: C, 89.38; H, 5.13; N, 5.49. Found: C, 88.85; H, 5.11; N, 5.28.

4-((9*H*-fluoren-9-ylidene)methyl)pyridine (*p*Fpy). Synthesized as the previous example, purification by crystallization from ethyl acetate/hexane (1:2 v:v) instead of column chromatography. Afforded pale yellow crystalline product. Yield: 38−50%. ^{1}H NMR (300 MHz, $CDCl_3$) δ ppm 8.71 (d, J = 6 Hz, 2He), 7.76 (d, J = 8 Hz, 1Hh), 7.70 (d, J = 8 Hz, 2Hmm'), 7.50 (s, 1Hi), 7.48 (d, J = 5 Hz, 2Hf), 7.44 (d, J = 8 Hz, 1Hj'), 7.41 (dt, J = 7, 1 Hz, 1Hk), 7.34 (dt, J = 7, 1 Hz, 2Hll'), 7.06 (dt, J = 7, 1 Hz, 1Hk'). ^{13}C{^{1}H} NMR (75 MHz, $CDCl_3$) δ ppm 150.2, 141.6, 140.3, 139.5, 138.8, 138.7, 135.9, 129.3, 129.0, 127.2, 126.9, 124.5, 123.8, 123.2, 120.5, 120.0, 119.7. HRMS (ESI, MeCN) (*m/z*): $[M+H]^+$ ($C_{19}H_{14}N$) calcd 256.11207; found 256.11240. Anal. Calcd for $C_{19}H_{13}N$: C, 89.38; H, 5.13; N, 5.49. Found: C, 89.35; H, 5.17; N, 5.50.

3-((9*H*-fluoren-9-ylidene)methyl)pyridine-2,2-bipyridine-tricarbonyl-rhenium(I) Hexafluorophosphate [Re(bpy)(CO)$_3$(*m*Fpy)][PF$_6$]. (2-1) Under an inert atmosphere, *fac*-[Re(bpy)(CO)$_3$(THF)][PF$_6$] (79.3 mg, 123 μmol) and ***m*Fpy** (32.2 mg, 126 μmol) were mixed

in THF (5 mL) and left to stir for 16 h at room temperature. The product was then precipitated by addition of hexane (50 mL), resulting in a yellow solid. The product was purified by dissolution in a minimum of dichloromethane (2 mL) with a few drops of toluene and followed by slow evaporation of DCM in a closed, toluene-containing jar, affording a pale yellow solid. Yield: 87.0 mg (105 μmol) (86%). ^{1}H NMR (400 MHz, $(CD_3)_2CO$**)** δ ppm 9.48 (ddd, *J* = 5, 2, 1 Hz, 2Ha), 8.76 (d, *J* = 8 Hz, 2Hd), 8.72 (dd, *J* = 2, 1 Hz, 1He), 8.66 (d, *J* = 5 Hz, 1Hf), 8.41 (dt, *J* = 8, 2 Hz, 2Hb), 8.22 (d, *J* = 8 Hz, 1Hh), 7.90 (ddd, *J* = 8, 5, 1 Hz, 2Hc), 7.83 (d, *J* = 8 Hz, 3Hjmm'), 7.66 (dd, *J* = 8, 5 Hz, 1Hg), 7.58 (s, 1Hi), 7.45 (dt, *J* = 8, 1 Hz, 1Hk), 7.37 (ddd, *J* = 13, 8, 1 Hz, 2Hll'), 6.97 (dt, *J* = 8, 1 Hz, 1Hk'), 6.77 (d, *J* = 8 Hz, 1Hj'). ^{13}C{^{1}H} NMR (75 MHz, $(CD_3)_2CO$) δ ppm 196.3, 156.8, 154.9, 152.8, 152.2, 142.4, 142.4, 141.2, 140.43, 140.35, 139.4, 137.3, 136.3, 130.43, 130.26, 129.96, 128.36, 128.23, 127.8, 125.8, 124.4, 121.84, 121.28, 121.19, 120.7. HRMS (ESI, MeCN) (*m/z*): $[M]^+$ ($C_{43}H_{21}N_3O_3{}^{187}Re$) calcd 682.11349; found 682.11275. IR (ATR, cm^{-1}) ν_{CO}: 2031s, 1944s, 1911s; ν_{PF} 837s. Anal. Calcd for $C_{32}H_{21}F_6N_3O_3PRe$ + 0.5 toluene: C, 48.85; H, 2.89; N, 4.81. Found: C, 48.53; H, 2.76; N, 4.81.

4-((9*H*-fluoren-9-ylidene)methyl)pyridine-2,2-bipyridine-tricarbonyl-rhenium(I) Hexafluorophosphate [Re(bpy)(CO)$_3$(*p*Fpy)][PF$_6$]. (2-2) Complex **2-2** was synthesized in the same manner as the previous example**.** The product was purified by dissolution in a minimum of chloroform (2 mL) with a few drops of ethyl acetate and crystallized by slow diffusion of ethyl acetate in a closed jar. Yield: 90.0 mg (108 μmol) (86%). ^{1}H NMR (400 MHz, $(CD_3)_2CO$**)** δ ppm 9.54 (ddd, *J* = 6, 2, 1 Hz, 2Ha), 8.79 (d, *J* = 8 Hz, 2Hd), 8.64 (dd, *J* = 5, 2 Hz, 2He), 8.51 (dt, *J* = 8, 2 Hz, 2Hc), 8.04 (ddd, *J* = 8, 3, 1 Hz, 2Hb), 7.83−7.79 (m, 3Hjmm'), 7.68 (dd, *J* = 7, 1 Hz, 2Hf), 7.60 (s, 1Hi), 7.42 (dt, *J* = 8, 1 Hz, 1Hk), 7.38 (dt, *J* = 8, 1 Hz, 1Hl'), 7.33 (dt, *J* = 8, 1.0 Hz, 1Hl), 7.25 (d, *J* = 8 Hz, 1Hj'), 7.01 (dt, *J* = 8, 1 Hz, 1Hk'). ^{13}C{^{1}H} NMR (75 MHz, $(CD_3)_2CO$) δ ppm 196.5, 156.8, 155.0, 153.1, 149.8, 142.88, 142.37, 141.2, 140.4, 139.5, 135.9, 130.97, 130.56, 130.07, 128.5, 127.89, 127.78, 125.76, 125.05, 122.62, 122.01, 121.2, 120.8. HRMS (ESI, MeCN) (*m/z*): $[M]^+$ ($C_{43}H_{21}N_3O_3{}^{187}Re$) calcd 682.11349; found 682.11374. IR (ATR, cm^{-1}) ν_{CO}: 2028s, 1925s, 1903s; ν_{PF} 832s. Anal. Calcd for $C_{32}H_{21}F_6N_3O_3PRe$: C, 46.49; H, 2.56; N, 5.08. Found: C, 46.56; H, 2.50; N, 4.99.

2.5.3. Computational Methods

All calculations were performed with the Gaussian 03 software.[17] All models used crystallographic structure data as starting point for ground-state geometry optimization (singlet and triplet). The geometry optimization was carried out with the density functional theory (DFT) method using the B3LYP functional in the gas phase.[18] The 6-31G** basis set was used for C, H, N, and O while the relativistic LANL2DZ with effective core potentials and one additional f-type polarization function was implemented for the Re atom (α_f = 0.890).[19] Energy levels and frequencies for both singlet and triplet optimized geometries were calculated using single-point energy calculation with a polarized continuum model (PCM) using dichloromethane as solvent.[20] The absorption spectra properties in DCM were calculated by the time-dependent DFT (TD-DFT) approach associated with the polarized continuum model (PCM).[20] GaussSum 2.2 was employed to draw absorption spectra (simulated with Gaussian distribution with a full-width at half-maximum (fwhm) set to 3000 cm^{-1}) and extract the atomic orbital population information from calculated data.[21]

2.5.4. Crystal Structure Determination

X-ray crystallographic data were collected from a single crystal sample, which was mounted on a loop fiber. For both ligands, data were collected with a Bruker Platform diffractometer, equipped with a Bruker SMART 4K Charged-Coupled Device (CCD) Area Detector and a Nonius FR591 rotating anode Cu Kα X-ray radiation source equipped with a Montel 200 optics at 200 (2) K. For the two complexes, data were collected with a Bruker Microstar diffractometer equipped with a Platinum 135 CCD Detector at 150 (2) K. The data was integrated with APEX2 software and corrected for absorption using the SADABS package.[22] Following analytical absorption corrections and solution by direct methods, the structures were refined against F^2 with full-matrix least-squares using the program SHELXL-97.[23] All H-atoms were added at calculated positions and refined by use of riding models with isotropic displacement parameters based on those of the parent atoms. Anisotropic displacement parameters were employed throughout for the non-hydrogen atoms. Images were generated using Ortep III and Pov-Ray.[24] X-ray quality crystals were obtained from slow evaporation of a chloroform solution for the ligands ***p*Fpy** and ***m*Fpy**. Crystals of **2-1** were obtained by slow diffusion of ethyl acetate into a chloroform solution of **2-1**. Complex **2-2** crystallized following the given purification procedure. Specific parameters of each

measurement are located in Table II-1. Note that ***p*Fpy** has been reported before but without any complete data set deposited in the Cambridge structural database.[15b]

Table II-1. Crystal Data and Structure Refinement Information for ***m*Fpy**, ***p*Fpy**, **2-1** and **2-2**

	***m*Fpy**	***p*Fpy**	**2-1**	**2-2**
Formula	$C_{19}H_{13}N$	$C_{19}H_{13}N$	$[C_{32}H_{21}N_3O_3Re][F_6P]\cdot 0.5(C_4H_8O_2)$	$[C_{32}H_{21}N_3O_3Re][F_6P]\cdot CH_2Cl_2$
Crystal System	triclinic	monoclinic	Orthorhombic	Triclinic
Space Group	P-1	$P2_1/c$	Pca21	P-1
a (Å)	6.2909(4)	9.2782(4)	29.1631(5)	8.1758(3)
b (Å)	11.8465(7)	21.8542(9)	12.2319(2)	14.2872(5)
c (Å)	18.5314(11)	6.9306(3)	18.7356(44)	14.8093(5)
α (deg)	90.475(3)	90	90	90.429(1)
β (deg)	96.308(3)	104.675(2)	90	90.852(2)
γ (deg)	105.025(3)	90	90	102.281(2)
V (Å^3)	1324.79(14)	1359.46(10)	6683.4(2)	1689.99(10)
Z	4	4	4	2
R1;wR2($I > 2\sigma$(I))	0.0472; 0.1151	0.0422; 0.1111	0.0263; 0.0730	0.0313; 0.0832
R1;wR2 (all data)	0.0685; 0.1227	0.0466; 0.1142	0.0258; 0.0735	0.0313; 0.0833
GoF(F^2)	0.985	1.035	1.065	1.089
Flack parameter	n.a.	n.a.	-0.002(6)	n.a.

2.6. Results and Discussion

The ligands were synthesized by a condensation reaction between fluorene and pyridinecarboxaldehyde, following a slightly modified protocol for benzylidene-fluorene synthesis.[14] Established procedures for the synthesis of 9-pyridylidenefluorene, studied mainly for their medicinal properties, are less accessible synthetically.[15a,16] Our first attempts to coordinate the ligands to the rhenium ion, using the precursor $[Re(bpy)(CO)_3(acetonitrile)][PF_6]$ and 10 equiv. of the ligand, following an established methodology, produced only moderate yields.[12] $[Re(bpy)(CO)_3(THF)][PF_6]$, first reported in 1985, was a better starting material as it is easily synthesized and is much more reactive, as the THF adduct exchanges neatly at room temperature with only 1 equivalent of the pyridyl ligand (Chart 2.1).[13] Near quantitative yields were obtained, and no purification was needed prior to crystallization.

Chart 2.1. Synthesis of the Rhenium Chromophores with the Labeling of the Species

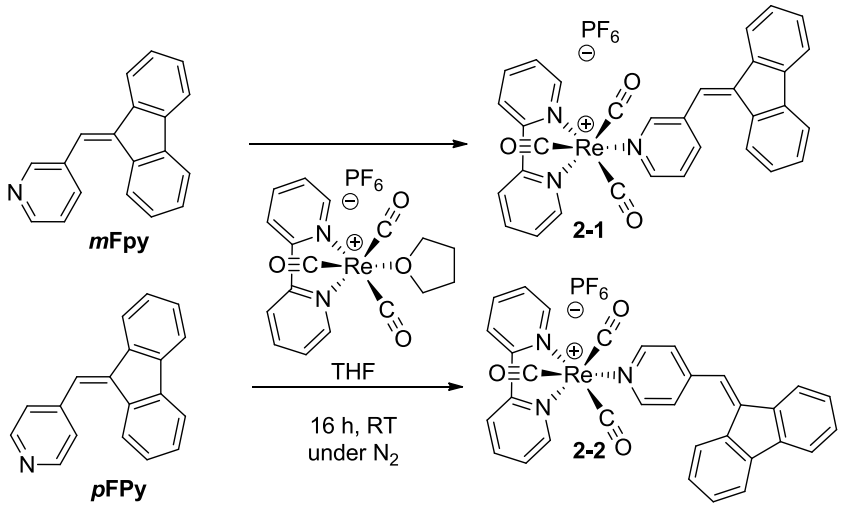

The IR spectra of both complexes are consistent with the facial configuration of the carbonyl ligands as indicated by three intense absorptions, which are observed in the 2031 to 1911 cm^{-1} region for **2-1** and the 2028 to 1903 region for **2-2**. These bands are similar to other rhenium complexes, for example, $[Re(bpy)(CO)_3(pyridine)][CF_3SO_3]$ (**2-3**), that has bands at 2026, 1921, and 1907 cm^{-1}.[25] No bands around 1600 cm^{-1} could be clearly identified as being part of the fulvene vinyl group, as they are masked by the other C=C stretches of the bipyridine and pyridine.

The proton chemical shifts remain essentially the same for both complexes, the biggest change is the downfield shift of the fluorene proton nearest to the vinyl proton of complex **2-1** (j' see Chart 2.S1 for labeling in Supporting Information). The chemical shift passes from 7.45 ppm to 6.77 ppm for **2-1** vs 7.25 ppm for **2-2**. This extra shielding comes from the $Re(bpy)(CO)_3$ fragment as it is nearer in the *meta* version because of the free rotation of the pyridyl group along its single bond to the fulvene core. The pyridine protons *ortho* to the nitrogen ligand shift by similar amounts upon coordination to the metal center (8.66 and 8.72 ppm for **2-1** vs 8.64 ppm for **2-2**), as expected.

Both ligand and complexes were fully characterized by X-ray crystallography and have excellent structure quality, with disorder present for the complexes only on the PF_6 counterion or cocrystallized solvent. It is noteworthy that complex **2-1** and ***m*Fpy** crystallized as two independent molecules in the asymmetric unit cell, which gives a good indication on

the precision of the bond lengths and inherent variability of the spatial arrangement of the atoms. Full unit-cell views of all molecules are found in the Supporting Information, Figure 2.S1 to Figure 2.S4.

The fulvene ligands are similar in structure, with the pyridyl ring being rotated out of the plane of the fluorene ring. The angle of rotation is more dependent on the packing itself, as there is a notable difference in the angle for the two crystallographically independent molecules of ***m*Fpy** (50.4° and 41.6°), while ***p*Fpy** has an angle is 60.8°. In the complexes these angles become 36.5° for complex **2-1** (both molecules have the same angle) and 45.9° for **2-2**.

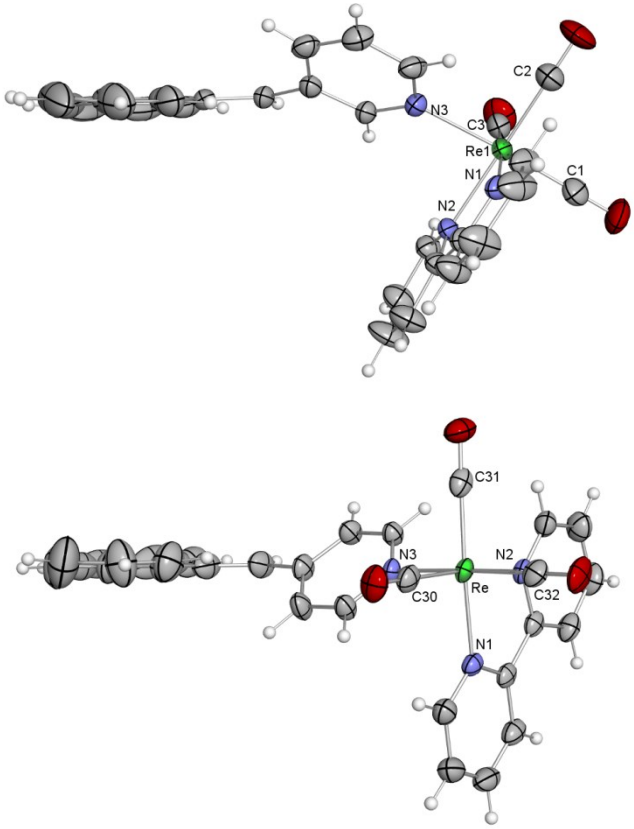

Figure 2.1. ORTEP view of the X-ray crystal structures of **2-1** (top) and **2-2** (bottom) along the fulvene plane (50% probability displacement ellipsoids; anion, solvent, and other chemically equivalent molecule removed).

The planarity of the fluorene is a good indication of its conjugation; it is measured by the angle of both planes formed by each fused phenyl ring. Both ligands and complexes show a similar planarity with no significant variations. The biggest angle change is seen for the two

crystallographically independent molecules of **2-1** at 4.5° and 2.8°, giving an almost 2° shift as a normal fluctuation because of crystal packing. The ***m*Fpy** ligand has distortion angles of 4.6° and 5.1°, the ***p*Fpy** ligand is at 3.9° (also reported at 4.1°)[15b] while in **2-2** it is at 4.4°. There is clearly no effect on the distortion angle from the coordination of rhenium to the ligand and no appreciable differences between the *meta* and *para* ligands.

A look at the length of the double bond bridging the pyridyl and the fluorene shows an average distance of 1.35 ± 0.01 Å (for both ligand and **2-1**); in the case of **2-2**, it is shorter at 1.318(8) Å. This could imply a stronger double bond and can be rationalized looking at the reduced torsion angle present in the vinyl bond of **2-2** (5 ± 1° for **2-2** versus 10 ± 2° for **2-1**). The increased planarity of the vinyl bond in **2-1** brings the twisted pyridine ring closer to the fulvene plane.

The rhenium centers have standard coordination geometry. The CO bonds are not significantly different, as can be shown in the case of the two distinct molecules present for **2-1**, where up to 0.02 Å variations can be observed for otherwise identical carbonyl environments. As shown in Figure 2.1, there is an observable coplanarity of the rhenium core (the plane formed by N3, N2, C32, and C30) and the fluorene moiety in the case of complex **2-2**; the rhenium atoms lying only 0.17 Å above the plane and there is an angle of only 2° between the fluorene and the rhenium cores. In the case of **2-1** the geometry of the rhenium core is completely twisted off the fluorene plane. The coplanarity of the rhenium core with the fulvene in **2-2** will be shown to have a role in its electronic properties despite the 45° rotation of the pyridine ring.

2.6.1. Electrochemistry

Electrochemistry reveals the energy of the highest occupied molecular orbital (HOMO) and lowest unoccupied molecular orbital (LUMO) and can give important information about the energy levels involved in electronic transitions.

On the oxidation side, a rhenium pyridyl complex should have a partially reversible oxidation around 1.85 V vs SCE in dichloromethane.[26] Also we can have oxidation of the fulvene ligand, measured as an irreversible oxidation at 1.72 V vs SCE (in CH_2Cl_2), very close to the reported 1.67 V for the closest analogue, 9-benzylidenefluorene.[27] As reported in Table II-2 and Supporting Information, Figure 2.S5, both complexes **2-1** and **2-2** have an oxidation at 1.84 V vs SCE in CH_2Cl_2. It is difficult to assign this redox couple as either the

expected Re(I)/Re(II) or as Fpy/Fpy$^{+\cdot}$ or both. A square-wave voltammetry suggests an electron count of at least two, implying both redox couples are occurring in the same region (Supporting Information, Figure 2.S6).

Table II-2. Electrochemical Data of the Complexes in CH_2Cl_2

	$E_{1/2}^{ox}$ (ΔE (mV))	$E_{1/2}^{red}$ (V) (ΔE (mV))			
	Re^{II}/Re^{I} ($Fluo^{+\cdot}$/Fluo)	bpy/$bpy^{-\cdot}$	Fluo/ $Fluo^{-\cdot}$	$Fluo^{-\cdot}/Fluo^{-2}$	$bpy^{-\cdot}/bpy^{-2}$
2-1	1.84 (250)	-1.11 (160)[a]		-1.45 (230)	-1.71 (irr)
2-2	1.84 (120)	-1.08 (66)	-1.23 (60)	-1.434 (230)	-1.74 (irr)
2-3[b]	1.85 (irr)	-1.2 (60)			-1.7 (irr)
Fpy[c]	1.72 (irr)		-1.55 (260)		

[a]Unresolved two one-electron reductions. [b]From literature, triflate salt with Bu_4NPF_6 (0.2 M) electrolyte.[26] [c]***m*Fpy** and ***p*Fpy** gave the same result.

On the reduction side, two redox couples are reported to be centered on the bipyridine ligand of complex **2-3**.[26] The first is reversible at −2 V and the other is irreversible and reported at −1.7 V. From the electrochemistry of the free **Fpy** ligand, we expect a semi-reversible reduction centered as low as −1.55 V, but because of the electron withdrawing effect of the rhenium, this reduction could occur at less negative potential.

Complexes **2-1** and **2-2** have four reduction processes. In the case of **2-1**, only three reduction waves are seen; in this case the first reduction wave is broad, at −1.10 V (160 mV width), and suggests a ratio of two-to-one electrons as compared to the second reduction wave observed at −1.45 V (Supporting Information, Figure 2.S6), suggesting that two unresolved reductions occur next to each other. This suggestion is sustained by the CV of **2-2**, showing two distinct and reversible peaks located at −1.08 and −1.23 V. The first reduction is without a doubt the bpy/$bpy^{-\bullet}$ redox couple, the second one has no choice to be centered on the fulvene ligand, since in **2-3** the second reduction of the bpy is at a much more negative potential (−1.7 V). Since a third wave is seen for both complexes around −1.45 V, two redox couples are centered on the fulvene ligand even if in the case of the free molecule only one was observable. The first one, in the case **2-1**, occurs at slightly more negative potential than the bpy reduction and overlaps with it. While for **2-2**, there is a clean separation between the peaks, this can be partly due to the higher delocalization of the fulvene, enabling

it to interact more with the singly reduced bpy and push its own reduction to a more negative potential; this delocalization will be further discussed with the spectral data. The second reduction of the fulvene is at more or less the same potential of **2-1** at −1.45 V. Finally, the second irreversible bpy reduction is seen in the expected range for both complexes.

Electrochemistry does not allow clear identification of the individual processes occurring on the oxidation side, but it is clear on the reduction side that the bpy is the first to reduce, then the **Fpy** ligand follows. In term of energy gap, all of the complexes have a HOMO LUMO gap around 2.94 (±0.02) V, suggesting again very little effect of the **Fpy** toward the rhenium core and that the oxidation potential of **Fpy** is very closely matched to that of its rhenium complex.

2.6.2. Photophysical Investigation and Comparison with Theoretical Models

The absorption spectra of the ligands as well as of the complexes were measured in dichloromethane solutions and are compared to the TD-DFT calculations, with a solvent dielectric potential to simulate solvation. It is noteworthy that these calculations only take into account the singlet-state transitions. In the case of rhenium complexes, there can be some absorption from triplet-state transitions due to the spin−orbit coupling induced by heavy atoms, but these effects are not modeled using Gaussian03.[28] Although the calculated electronic transitions do not correlate very well in terms of energy, usually being under-evaluated, the relative ratio of calculated oscillator strength matches very well with the relative ratios measured in experimental intensities between the *meta* and the *para* variants of both complexes and ligands.

In the case of the ligands, both show a very similar absorption spectrum (Figure 2.3 and Supporting Information, Figure 2.S7), characterized by a broad band around 320 nm and a sharper peak at 260 nm, very near fluorene's maximum intensity peak at 264 nm. Smaller maxima are seen near 300 and 290 nm corresponding to other fluorene transitions. The lowest energy transition is seen at 323 nm, very comparable to the nearest fulvene analogue, 9-benzylidenefluorene, with a band at 326 nm, implying very little effect of the heterocyclic ring on the overall electronic delocalization.[29] This transition implies a delocalized π−π* transition involving the pyridyl ring. This is confirmed by the TD-DFT calculation, in this case the lower energy transition is at 347 nm (a shift of +26 nm), and in both cases the transitions originate from HOMO and HOMO−1 states, localized on the diphenylfulvene and

the pyridine (Supporting Information, Figure 2.S8). For both ligands there is a strong red-shift in the position of the first calculated transition; however, all of the other measured values are in good accordance with the spectra. This is especially true of the relative oscillator strength between ligands; they always follow the same trend as the spectra even if they are far from the experimental absolute values (Table II-3). The other major transition at 260 nm only involves fluorene-based molecular orbitals and matches the energy of the calculated transition. It has a 2-fold increase in maximum absorbance vs fluorene molecule (~40000 vs 18000 $M^{-1}cm^{-1}$).

The low energy absorption and the complete delocalization of the HOMO and LUMO orbitals of both ligands suggest that the fulvene moiety will have an effect on the properties of the associated rhenium chromophores.

In the case of the rhenium complexes (Table II-3), the wavelength of the expected mixed singlet metal−ligand-to-ligand charge transfer (MLLCT) transition for pyridine adducts is found around 360 nm with a molar absorptivity of about 5000 M^{-1} cm^{-1}.[12] Note that the MLLCT term is used instead of metal-to-ligand charge transfer (MLCT) term because the implied molecular orbitals of the ground state possess a strong contribution from the carbonyl ligands.[30] Complex **2-1** only shows a decreasing band at that specific wavelength, but it has twice the molar absorptivity. As can be seen in both Table II-3 and Figure 2.2, the deconvoluted bands of **2-1** place the first peak maximum at 330 nm, which is the same position as the deconvoluted peak of the ligand. Only the larger width of the band suggests a buried MLLCT band. The MLLCT can be seen more clearly if we compare the spectrum of **2-1** with a superimposition of the spectra of **2-3** and ***m*Fpy** (Figure 2.3). They are almost identical in peak positions, indicating that the tailing in complex **2-1** above 375 nm is due to the MLLCT of the rhenium bipyridine chromophore.

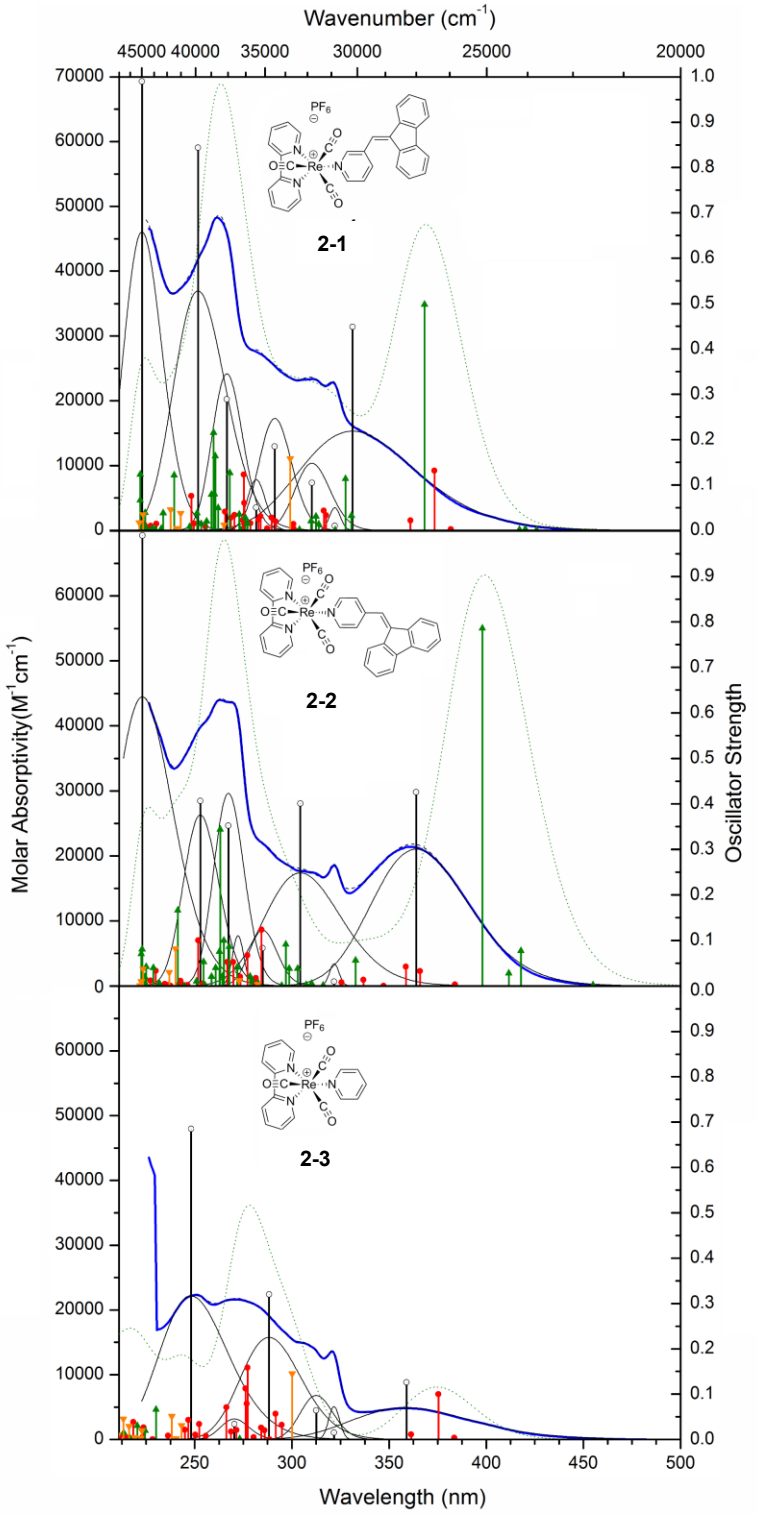

Figure 2.2. Absorption spectra in dichloromethane of the complexes (in blue; Top: **2-1**; middle: **2-2**; bottom: **2-3**.); Gaussian fits and sum of fits (black; full and dashed); Calculated curves from TD-DFT (dotted green); fitted oscillator strength (black circle); calculated from TD-DFT oscillator strength: Rhenium centered (red disk), Fulvene/pyridine centered (green triangle), bipyridine centered (orange triangle).

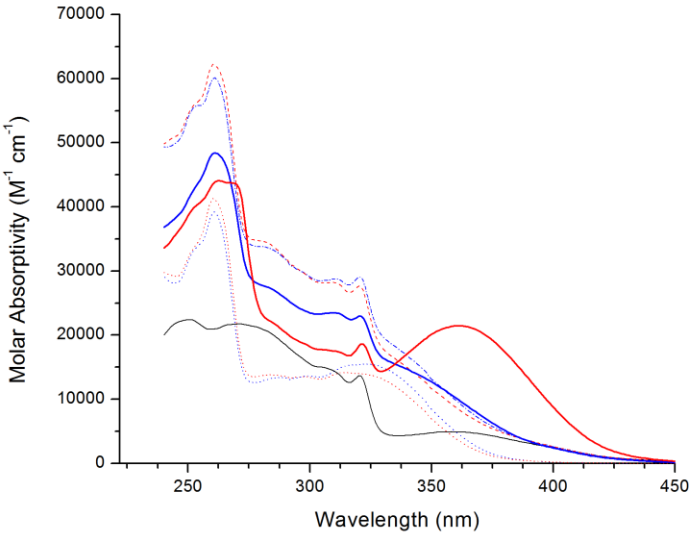

Figure 2.3. Comparison of the absorption spectra of **2-1** (blue line), **2-2** (red line), **2-3** (black line), ***m*Fpy** (dotted blue line), and ***p*Fpy** (dotted red line) with the additive spectra of **2-3** and their respective ligand ***m*Fpy** and ***p*Fpy** (dashed blue and red line).

In contrast, the spectrum of **2-2** does not superimpose well with the addition of the spectra of the ligand ***p*Fpy** and **2-3** (Figure 2.3). There is a new band at 270 nm (43000 $M^{-1}cm^{-1}$) of comparable intensity with the band at 260 nm (44000 $M^{-1}cm^{-1}$) and the expected band at 330 nm is shifted to 364 nm (22000 $M^{-1}cm^{-1}$). This molar absorptivity is four times greater than the pyridyl adduct and suggests a buried MLLCT (~5000 $M^{-1}cm^{-1}$), hidden beneath a red-shifted ligand-based absorption (~13000 $M^{-1}cm^{-1}$). A better comparison can be obtained by looking at the oscillator strengths of the implied transitions (Table II-3): MLLCT in **2-3** has a strength of 0.12, the ***p*Fpy**'s π–π* transition has 0.25 oscillator strength, for a total of 0.37 versus 0.43 for **2-2**, a net gain of 0.05 in oscillator strength. This is similar to **2-1**, for which we have 0.27 for the ligand first transition and 0.45 for the formed complex, again a gain of 0.06 in the oscillator strength. The small gain in both cases can be attributed to an increase in the absorbance cross section of the fulvene brought by the complexation of the rhenium, increasing its polarity.

Another characteristic band of $Re(bpy)(CO)_3L^+$ is the sharp peak at 321 nm; it is present in all of the pyridyl complexes, with a constant oscillator strength, suggesting again that the absorption transitions of the rhenium core are not affected by the fulvene moiety.

Table II-3. Measured and Calculated Electronic Absorption Properties of the Re Complexes and Ligand in DCM

	λ_{max} (nm); (ε ($cm^{-1}M^{-1}$)); [f (a.u.)]							
	Lowest energy transition			bpy transition		Fluorene transition		
	Expt.	Calc.		Expt.	Calc.	Expt.	Calc.	
		Fpy→ Fpy	Re→ bpy		bpy→ LUMO		Fluorene→LUMO	
***m*Fpy**	330 (15000) [0.27]	347 [0.65]				260 (39000) [0.22]	259 [0.48]	
***p*Fpy**	327 (13600) [0.25]	347 [0.60]				260 (41100) [0.25]	261 [0.61]	
2-1	331 (16000) [0.45]	367 [0.49]	360 [0.02] 373 [0.13]	321 (22800) [0.009]	299 [0.16]	261 (48300) [0.29]	260±1 [0.53][b]	
2-2	364 (21300) [0.43]	397 [0.79]	358 [0.04] 365 [0.03]	321 (18500) [0.010]	300±4 [0.16][a]	263 (44000) [0.35]	262±1 [0.44][b]	
2-3	359 (4800) [0.13]		361 [0.01] 375 [0.10]	321 (13500) [0.015]	300 [0.14]			

[a]Total oscillator strength of all stated transitions in a ±4 nm range. [b]In a ±1 nm range.

All theoretical transitions for the complexes are classified with their implied ground state orbitals as being rhenium-carbonyl, fulvene/pyridine or bipyridine based. This information is visualized in Figure 2.2 and the implied orbitals are visualized in Figure 2.4. The pyridyl complex (**2-3**) is the simplest to analyze, looking only at the major calculated oscillator strengths, we can see clearly three features: the MLLCT transition sitting around 375 nm (0.10), a bpy π−π* transition at 300 nm (0.14), and other MLLCT transitions at 275 nm (totaling 0.35 oscillator strength). The first two were assigned on the experimental spectra as the transition at 353 nm (0.13) (−22 nm shift) and the transition at 321 nm (0.15) (+21 nm shift). The last transition is not clearly assignable because of the quantity of peaks present at that wavelength, but fits well with the peak at 270 nm (- 5 nm) and the measured oscillator strength, 0.68, is a very rough estimate because of the quantity of peaks in the area and its proximity to the upper edge of the spectra.

Complex **2-1** shows the same transitions as the pyridyl complex: MLLCT at 373 nm (0.13 strength), bipyridine π−π* at 299 nm (0.16 strength) and MLLCT transitions centered at 275 nm (0.20 strength). Additional transitions from the fulvene ligand come into play. There is a group of fluorene-based transitions at 260 nm, matching very well with the measured 261 nm, en a fulvene to bpy Lastly, it has a fulvene π−π* transition (HOMO−1 to LUMO+1) at 367 nm (0.50 strength), a +20 nm shift from the calculated ligand absorption. This result does not compare well to the measured maximum of ***m*Fpy** and **2-1**, 330 and 331 nm, where there is no real shift of the fulvene π−π* transition, which suggests that the coordination of the metal has less influence on the delocalization of the fulvene orbital (HOMO−1) contrary to what the calculation indicates. Lastly, it is to note that the lowest

energy transition, HOMO to LUMO has near zero oscillator strength, because of lack of spatial overlap of the ground state and excited state: the HOMO being localized only on the fluorene moiety is disconnected from the bpy-centered LUMO (Figure 2.4).

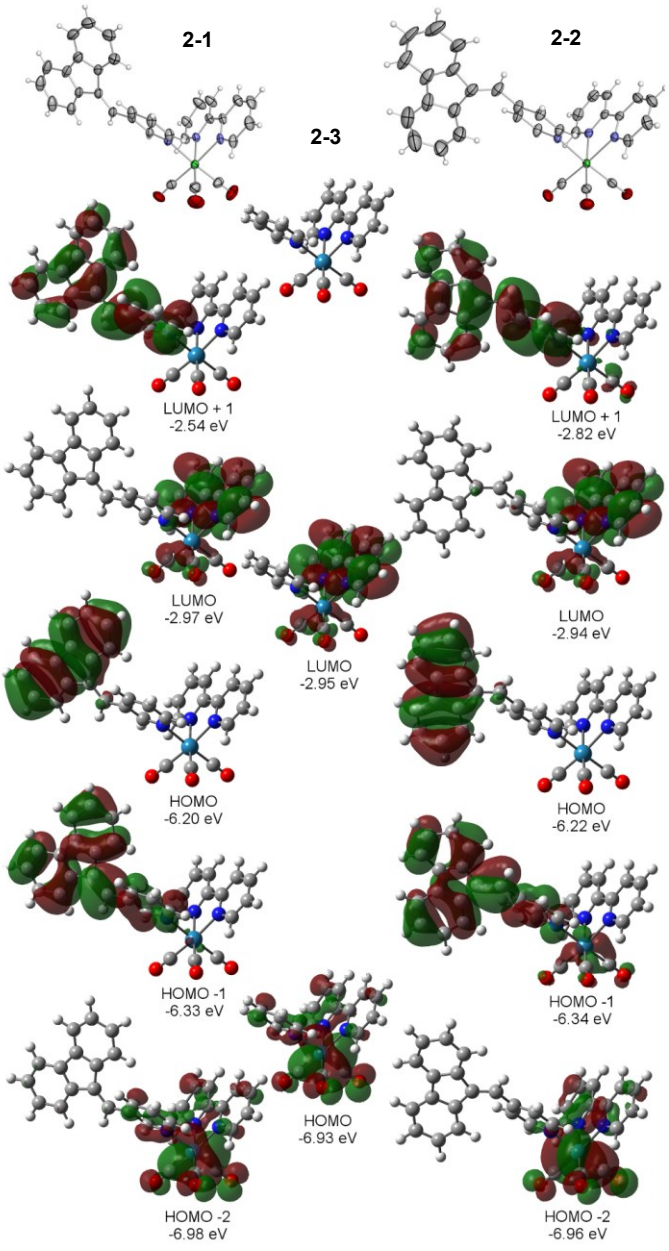

Figure 2.4. Topmost: ORTEP X-ray crystal structure of **2-1** (left) and **2-2** (right) used as starting point for the geometry optimization (% probability displacement ellipsoids, anion, solvent and other chemically equivalent molecule removed); Top center: optimized structure of **2-3** starting from crystallographic data.[31] Middle: Frontier molecular orbitals and orbital energies obtained from DFT (rb3lyp/LanL2DZ(f)[Re]6-31G**[C,H,N,O]) CPCM(CH_2Cl_2).

The calculated transitions of **2-2** differ from the two previous compounds; the lowest permitted transition is the HOMO−1 to LUMO+1 (π−π* fulvene centered) at 397 nm (0.87 strength), +50 nm shift from the free ligand. If we compare the measured value, 364 and 327 nm for **2-1** and ***p*Fpy**, respectively, we have a shift of +34 nm. In this case, the calculation models the extended delocalization in an error of about 20 nm, comparable to the deviation observed for **2-1**. A closer look of HOMO−1 reveals the origin of the lowering of the transition energy: the HOMO−1 delocalization now extends through the rhenium and the carbonyls; this is not the case for **2-1**. The extended delocalization also affects the LUMO +1 orbital (LUMO is centered on the bpy in all cases), where in **2-1** it is centered mainly on bpy and pyridine, and in **2-2** it is exclusively the delocalized antibonding orbital of ***p*Fpy**. This extended π−π* transition leads to a lower energy transition, as observed.

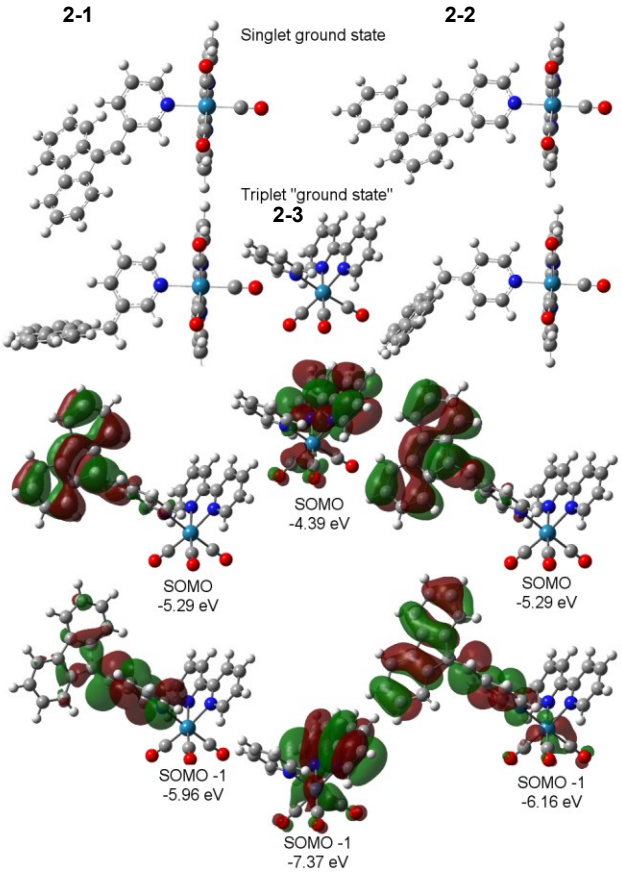

Figure 2.5. Top: Optimized singlet vs triplet ground state structure of **2-1** (left) and **2-2** (right); Top Center: optimized geometry of **2-3** triplet ground state; Bottom: SOMO and SOMO−1 molecular orbitals and orbital energies obtained from DFT (ub3lyp/LanL2DZ(f)[Re]6-31G**[C,H,N,O]), CPCM(CH_2Cl_2).

The rest of the calculated transitions of **2-2** are also affected by this interaction, as indicated by the splitting of the transitions and a greater part of fulvene orbitals being present in the various expected transitions of the Re core. The MLLCT splits to 368 and 358 nm (0.07 total strength); the bpy transition is mixed with a fulvene-based transition at 298 and 302 nm (0.08 total strength). Other noteworthy transitions are the metal-based transition seen at 276 nm (0.07) and finally the fluorene transition, seen at its expected position at 263 nm (0.4 total strength).

2.6.3. Emission and Excited State Theoretical Studies

Neither the ligands nor the complexes emit at room temperature or at 77 K. The closest relative to the pyridylfulvene ligands, 9-benzylidenefluorene, is also reported to have no fluorescence at room temperature or at 77 K.[32] From fluorescence and laser flash photolysis studies, it was reported that the deactivation pathway lies through the triplet state. The transient absorption signal, seen at 450 nm, had a decay of approximately 100 ns. We propose that both ***m*Fpy** and ***p*Fpy** follow this pathway, passing from $^1\pi-\pi^*$ to $^3\pi-\pi^*$ efficiently by intersystem crossing.

As previously mentioned neither complex **2-1** or **2-2** emits, in contrast to the pyridyl analog **2-3**, which has a very strong emission at 540 nm (500 nm at 77 K). Solutions of the complexes did have very weak emission, centered at 545 nm (512 nm at 77 K), but these were proven to be dissociation products attributable to trace $Re(bpy)(CO)_3(solvent)^+$, as seen from the 77 K emission spectra. Note that this dissociation is very small and not perceptible by UV−vis or ^{1}H NMR spectroscopy.

The general absence of a strong emission at low temperature suggests a rapid quenching mechanism of the normally emissive ^{3}MLLCT, suggesting it is no longer the lowest excited energy state. This can be readily rationalized by examining the HOMO and LUMO orbital of the singlet ground state (^{1}GS), the LUMO being a good approximation of the SOMO in the singlet excited state (^{1}ES) and by identifying the singly occupied molecular orbital (SOMO) orbital from the lowest energy triplet excited state (^{3}ES) of the molecule, obtained with a DFT optimization of the triplet "ground state". In the case of **2-3**, the calculated LUMO orbitals suggest a ^{1}ES centered on the bpy (Figure 2.4, center). This excited state is very similar to the ^{3}ES, assigned to the ^{3}MLLCT transition state, where the SOMO is also centered on the bpy (Figure 2.5, center). However, the DFT calculation obtained for **2-1** and **2-2** shows

a HOMO ^{1}GS centered on the fluorene, not the rhenium core (Figure 2.4, left and right), while the LUMO, representing the ^{1}ES lies on the expected bipyridine moiety. The Re based orbitals are located at lower levels: HOMO−2, −3 and −5 for both complexes. The SOMO and SOMO−1 of the ^{3}ES of both complexes are not centered on the expected bpy, they are instead on the fulvene and the optimized geometry showed a 90° rotation of the fluorene around the vinyl double bond (Figure 2.5). This twist in the ^{3}ES is reminiscent of 4-styrylpyridine, bound to a rhenium chromophore, which has been extensively studied by high-level calculations.[4k-m] Fulvene's ability to twist is also known and has been studied in detail as well.[6c-f] The measured triplet energy of unsubstituted pentafulvene is around 2.34 eV (530 nm), and the dibenzofulvene is expected to be lower because of its extended delocalization.[6b] By the difference of total energy calculated from triplet and singlet ground states, the following estimated triplet energy can be made for our complexes: 1.52 eV (814 nm) and 1.49 eV (835 nm) for **2-1** and **2-2**, while **2-3** is estimated at 2.76 eV (450 nm) (Supporting Information Table II-S1). Although these estimates are approximate (with 50 nm error from the measured emission of **2-3** at 77 K), they nonetheless suggests an important driving force for the observed quenching of the ^{3}MLLCT emission.

The ^{1}MLLCT state, centered on the bpy ligand, $^1\pi$–π^*(fulvene) state, and the whole **Fpy** ligand (including the pyridyl) are very close in energy to each other, the ^{1}MLLCT state being slightly lower energy for **2-1** and of similar energy for **2-2**. Furthermore, these two states are very close spatially, being separated only by the rhenium ion. As such, it is expected that singlet−singlet Dexter energy transfer can occur easily between these states. Both of these excited singlet states can undergo intersystem crossing to their respective triplet state, the MLLCT ISC is very fast, in the order of 200 fs as reported for similar rhenium complexes.[33] The next step is a fast triplet–triplet Dexter energy transfer between ^{3}MLLCT and the $^3\pi$–π^*(fulvene) states, again as described for 4-styrylpyridine containing rhenium complexes.[33] The non-radiative $^3\pi$–π^*(fulvene) state acts as the sink for the system, since it is of lower energy than the ^{3}MLLCT state. It thus only needs a shorter lifetime than the ^{3}MLLCT to quench completely the emission coming from that state. From literature data, the lifetime of the ^{3}MLLCT of **2-3**, 669 ns, is longer-lived than the transient lifetime of the closest analogue to our ligand, 9-benzylidenefluorene, at around 100 ns. We propose that the life-time of the $^3\pi$–π^*(fulvene) state of our **Fpy** ligands is similar and leads to the observed quenching. [12,32] Chart 2.1 illustrate the pathways for non-radiative relaxation.

Chart 2.1. Possible Relaxation Pathways for Complexes **2-1** and **2-2**

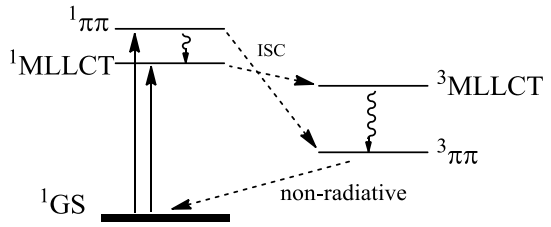

2.7. Conclusions

Incorporating a pyridyl-dibenzofulvene moiety in the coordination sphere of the rhenium(I) complex significantly increases its absorptivity, especially in the case of **2-2** where the red-shifting of the permitted $^1\pi-\pi^*$ transition of the fulvene ligand is at the same level as the ^{1}MLLCT of the rhenium chromophore. In the case of **2-1**, the rhenium core has low impact on the fulvene ligand electronic state, as it only increases the absorption of the ligand marginally. From the absence of any fluorescence or phosphorescence of the complex, we can postulate that the fulvene ligand has a non-emissive triplet state of lower energy then the ^{3}MLLCT of the rhenium core, and a fast energy transfer occurs between these two states. This non-emissive triplet state of the fulvene can lead to isomerization. Of course, in this case, no net structural change has occurred, but a small modification on either side of the fluorene would confirm if the implied fulvene triplet non-radiative deactivation pathway occurs through the expected photoisomerization. With the break in symmetry, electronic spectroscopy or NMR can monitor the isomerization. Further studies of this quenching would prove interesting, since the addition of the rhenium complex can lead to an increased isomerization quantum yield to the fulvene class of photoisomers.

2.8. Acknowledgements

We are grateful to the Natural Sciences and Engineering Research Council of Canada, the Ministère de l'Éducation du Québec, and the Université de Montréal for financial support and for the Université de Montréal's Altix super computer supported by le Réseau Québécois de Calculs de Haute Performances (RQCHP) for computer calculations.

2.9. Supporting Information

X-ray crystallographic data in CIF format, extra figures, and computational data. This material is available free of charge via the Internet at http://pubs.acs.org.

2.10. References

(1) (a) Wrighton, M.; Morse, D. L. *J. Am. Chem. Soc.* **1974**, *96*, 998. (b) Caspar, J. V.; Sullivan, B. P.; Meyer, T. J. *Inorg. Chem.* **1984**, *23*, 2104. (c) Kalyanasundaram, K. *J. Chem. Soc., Faraday Trans. 2* **1986**, *82*, 2401.(d) Lees, A. J. *Chem. Rev.* **1987**, *87*, 711. (e) Sacksteder, L.; Zipp, A. P.; Brown, E. A.; Streich, J.; Demas, J. N.; DeGraff, B. A. *Inorg. Chem.* **1990**, *29*, 4335. (f) Stufkens, D. J.; Vlcek, A., Jr. *Coord. Chem. Rev.* **1998**, *177*, 127. (g) Kirgan, R. A.; Sullivan, B. P.; Rillema, D. P. *Top. Curr. Chem.* **2007**, *281*, 45. (h) Takeda, H.; Koike, K.; Morimoto, T.; Inumaru, H.; Ishitani, O. *Adv. Inorg. Chem.* **2011**, *63*, 137.

(2) (a) Hawecker, J.; Lehn, J. M.; Ziessel, R. *J. Chem. Soc., Chem. Commun.* **1983**, 536. (b) Fihri, A.; Artero, V.; Pereira, A.; Fontecave, M. *Dalton Trans.* **2008**, 5567. (c) Probst, B.; Kolano, C.; Hamm, P.; Alberto, R. *Inorg. Chem.* **2009**, *48*, 1836. (d) Probst, B.; Guttentag, M.; Rodenberg, A.; Hamm, P.; Alberto, R. *Inorg. Chem.* **2011**, *50*, 3404.

(3) (a) Kurz, P.; Probst, B.; Spingler, B.; Alberto, R. *Eur. J. Inorg. Chem.* **2006**, 2966. (b) Takeda, H.; Koike, K.; Inoue, H.; Ishitani, O. *J. Am. Chem. Soc.* **2008**, *130*, 2023. (c) Benson, E. E.; Kubiak, C. P.; Sathrum, A. J.; Smieja, J. M. *Chem. Soc. Rev.* **2009**, *38*, 89. (d) Yui, T.; Tamaki, Y.; Sekizawa, K.; Ishitani, O. *Top. Curr. Chem.* **2011**, *303*, 151. (e) Kumar, B.; Smieja, J. M.; Sasayama, A. F.; Kubiak, C. P. *Chem. Commun.* **2012**, *48*, 272.

(4) (a) Lewis, J. D.; Perutz, R. N.; Moore, J. N. *Chem. Commun.* **2000**, 1865. (b) Sun, S.-S.; Robson, E.; Dunwoody, N.; Silva, A. S.; Lees, A. J.; Brinn, I. M. *Chem. Commun.* **2000**, 201. (c) Yam, V. W.-W.; Zhang, Y. Y. J.; Chu, B. W.-K.; Zhu, N. *Organometallics* **2001**, *20*, 4911 . (d) Sun, S.-S.; Lees, A. J. *Organometallics* **2002**, *21*, 39. (e) Dattelbaum, D. M.; Itokazu, M. K.; Iha, N. Y. M.; Meyer, T. J. *J. Phys. Chem. A* **2003**, *107*, 4092 . (f) Wenger, O. S.; Henling, L. M.; Day, M. W.; Winkler, J. R.; Gray, H. B. *Inorg. Chem.* **2004**, *43*, 2043. (g) Patrocinio, A. O. T.; Brennaman, M. K.; Meyer, T. J.; Murakami Iha, N. Y. *J. Phys. Chem. A* **2010**, *114*, 12129 . (h) Frin, K. P. M.; Murakami Iha, N. Y. *Inorg. Chim. Acta* **2011**, *376*, 531. (i) Lin, J. L.; Chen, C. W.; Sun, S. S.; Lees, A. J. *Chem. Commun.* **2011**, *47*, 6030. (j) Kumar, A.; Sun, S.-S.; Lees, A. J. *Top. Organomet. Chem.* **2010**, *29*, 1. (k) Bossert, J.; Daniel, C. *Chem.Eur. J.* **2006**, *12*, 4835. (l) Gindensperger, E.; Koppel, H.; Daniel, C. *Chem. Commun.* **2010**, *46*, 8225. (m) Kayanuma, M.; Daniel, C.; Köppel, H.; Gindensperger, E. *Coord. Chem. Rev.* **2011**, *255*, 2693.

(5) (a) O'Donnell, J. L.; Zuo, X.; Goshe, A. J.; Sarkisov, L.; Snurr, R. Q.; Hupp, J. T.; Tiede, D. M. *J. Am. Chem. Soc.* **2007**, *129*, 1578. (b) Hanan, G. S.; Cooke, M. W.; Chartrand, D. *Coord. Chem. Rev.* **2008**, *252*, 903. (c) Casanova, M.; Zangrando, E.; Iengo, E.; Alessio, E.; Indelli, M. T.; Scandola, F.; Orlandi, M. *Inorg. Chem.* **2008**, *47*, 10407. (d) Hanan, G. S.; Chartrand, D. *Chem. Commun.* **2008**, 727. (e) Thanasekaran, P.; Lee, C.-C.; Lu, K.-L. *Acc. Chem. Res.* **2012**, *45*, 1403.

(6) (a) Waldeck, D. H. *Chem. Rev.* **1991**, *91*, 415. (b) Asmis, K. R.; Allan, M.; Schafer, O.; Fuelscher, M. *J. Phys. Chem. A* **1997**, *101*, 2089. (c) Barr, J. W.; Bell, T. W.;

Catalano, V. J.; Cline, J. I.; Phillips, D. J.; Procupez, R. *J. Phys. Chem. A* **2005**, *109*, 11650. (d) Alfalah, S.; Belz, S.; Deeb, O.; Leibscher, M.; Manz, J.; Zilberg, S. *J. Chem. Phys.* **2009**, *130*, 124318/1. (e) Ioffe, I.; Dobryakov, A. L.; Granovsky, A. A.; Ernsting, N. P.; Perez, L. J. L. *ChemPhysChem* **2011**, *12*, 1860. (f) Blancafort, L.; Gatti, F.; Meyer, H.-D. *J. Chem. Phys.* **2011**, *135*, 134303/1.(g) Belz, S.; Grohmann, T.; Leibscher, M. *J. Chem. Phys.* **2009**, *131*, 034305/1.

(7) (a) Passalacqua, R.; Loiseau, F.; Campagna, S.; Fang, Y.-Q.; Hanan, G. S. *Angew. Chem., Int. Ed.* **2003**, *42*, 1608. (b) Wang, J.; Hanan, G. S.; Loiseau, F.; Campagna, S. *Chem. Commun.* **2004**, 2068. (c) Wang, J.; Fang, Y.-Q.; Bourget-Merle, L.; Polson, M. I. J.; Hanan, G. S.; Juris, A.; Loiseau, F.; Campagna, S. *Chem.Eur. J.* **2006**, *12*, 8539. (d) Tyson, D. S.; Luman, C. R.; Zhou, X.; Castellano, F. N. *Inorg. Chem.* **2001**, *40*, 4063. (e) Wang, J.; Fang, Y.-Q.; Hanan, G. S.; Loiseau, F.; Campagna, S. *Inorg. Chem.* **2005**, *44*, 5. (f) Simon, J. A.; Curry, S. L.; Schmehl, R. H.; Schatz, T. R.; Piotrowiak, P.; Jin, X.; Thummel, R. P. *J. Am. Chem. Soc.* **1997**, *119*, 11012. (g) Ford, W. E.; Rodgers, M. A. J. *J. Phys. Chem.* **1992**, *96*, 2917.

(8) (a) Westmoreland, T. D.; Le Bozec, H.; Murray, R. W.; Meyer, T. J. *J. Am. Chem. Soc.* **1983**, *105*, 5952. (b) Westmoreland, T. D.; Schanze, K. S.; Neveux, P. E., Jr.; Danielson, E.; Sullivan, B. P.; Chen, P.; Meyer, T. J. *Inorg. Chem.* **1985**, *24*, 2596. (c) Chen, P.; Westmoreland, T. D.; Danielson, E.; Schanze, K. S.; Anthon, D.; Neveux, P. E., Jr.; Meyer, T. J. *Inorg. Chem.* **1987**, *26*, 1116.

(9) Connelly, N.; Geiger, W. *Chem. Rev.* **1996**, *96*, 877.

(10) Schmidt, S. P.; Trogler, W. C.; Basolo, F.; Urbancic, M. A.; Shapley, J. R. In *Inorganic Syntheses*; John Wiley & Sons, Inc.: New York, 2007; p 41.

(11) Hevia, E.; Perez, J.; Riera, V.; Miguel, D.; Kassel, S.; Rheingold, A. *Inorg. Chem.* **2002**, *41*, 4673.

(12) Caspar, J. V.; Meyer, T. J. *J. Phys. Chem.* **1983**, *87*, 952.

(13) Casey, C. P.; O'Connor, J. M. *Organometallics* **1985**, *4*, 384.

(14) Plater, M. J.; Kemp, S.; Lattmann, E. *J. Chem. Soc., Perkin Trans. 1* **2000**, 971.

(15) (a) Buu-Hoi, N. P.; Delbarre, F.; Jacqugnon, P.; Brouilhet, H.; Rose, A.; Sabathier, J. F.; Sinh, M. P. *Recl. Trav. Chim. Pays-Bas* **1963**, *82*, 1047. (b) Kolyadina, N. M.; Soldatenkov, A. T.; Gridunova, G. V.; Prostakov, N. S. *Chem. Heterocycl. Compd.* **1999**, *34*, 833.

(16) Ulmschneider, S.; Mueller-Vieira, U.; Klein, C. D.; Antes, I.; Lengauer, T.; Hartmann, R. W. *J. Med. Chem.* **2005**, *48*, 1563.

(17) Frisch, M. J.; Trucks, G. W.; Schlegel, H. B.; Scuseria, G. E.; Robb, M. A.; Cheeseman, J. R.; Montgomery, J., J. A.; Vreven, T.; Kudin, K. N.; Burant, J. C.; Millam, J. M.; Iyengar, S. S.; Tomasi, J.; Barone, V.; Mennucci, B.; Cossi, M.; Scalmani, G.; Rega, N.; Petersson, G. A.; Nakatsuji, H.; Hada, M.; Ehara, M.; Toyota, K.; Fukuda, R.; Hasegawa, J.; Ishida, M.; Nakajima, T.; Honda, Y.; Kitao, O.; Nakai, H.; Klene, M.; Li, X.; Knox, J. E.; Hratchian, H. P.; Cross, J. B.; Bakken, V.; Adamo, C.; Jaramillo, J.; Gomperts, R.; Stratmann, R. E.; Yazyev, O.; Austin, A. J.; Cammi, R.; Pomelli, C.; Ochterski, J. W.; Ayala, P. Y.; Morokuma, K.; Voth, G. A.; Salvador,

P.; Dannenberg, J. J.; Zakrzewski, V. G.; Dapprich, S.; Daniels, A. D.; Strain, M. C.; Farkas, O.; Malick, D. K.; Rabuck, A. D.; Raghavachari, K.; Foresman, J. B.; Ortiz, J. V.; Cui, Q.; Baboul, A. G.; Clifford, S.; Cioslowski, J.; Stefanov, B. B.; Liu, G.; Liashenko, A.; Piskorz, P.; Komaromi, I.; Martin, R. L.; Fox, D. J.; Keith, T.; Al-Laham, M. A.; Peng, C. Y.; Nanayakkara, A.; Challacombe, M.; Gill, P. M. W.; Johnson, B.; Chen, W.; Wong, M. W.; Gonzalez, C.; Pople, J. A.; *Gaussian 03*, Revision C.02; Gaussian, Inc.: Wallingford CT, 2004.

(18) (a) Lee, C.; Yang, W.; Parr, R. G. *Phys. Rev. B: Condens. Matter* **1988**, *37*, 785. (b) Becke, A. D. *J. Chem. Phys.* **1993**, *98*, 5648.

(19) (a) Hay, P. J.; Wadt, W. R. *J. Chem. Phys.* **1985**, *82*, 299. (b) Ehlers, A. W.; Boehme, M.; Dapprich, S.; Gobbi, A.; Hoellwarth, A.; Jonas, V.; Koehler, K. F.; Stegmann, R.; Veldkamp, A.; et, a. *Chem. Phys. Lett.* **1993**, *208*, 111.

(20) Cossi, M.; Rega, N.; Scalmani, G.; Barone, V. *J. Comput. Chem.* **2003**, *24*, 669.

(21) O'Boyle, N. M.; Tenderholt, A. L.; Langner, K. M. *J. Comput. Chem.* **2008**, *29*, 839.

(22) (a) Sheldrick, G. M.; *SADABS*, version 2008/1; Bruker AXS Inc.: Madison, WI, 2008. (b) *SAINT*, version 7.68A; Bruker AXS Inc.: Madison, 2009.

(23) Sheldrick, G. M. *Acta Crystallogr., Sect. A: Found. Crystallogr.* **2008**, *A64*, 112.

(24) (a) Farrugia, L. J. *J. Appl. Crystallogr.* **1997**, *30*, 565. (b) *POV-Ray*, version 3.6; Persistence of Vision Pty. Ltd.: Williamstown, Victoria, Australia, 2004.

(25) Casanova, M.; Zangrando, E.; Munini, F.; Iengo, E.; Alessio, E. *Dalton Trans.* **2006**, 5033.

(26) Kuehn, F. E.; Zuo, J.-L.; Fabrizi de Biani, F.; Santos, A. M.; Zhang, Y.; Zhao, J.; Sandulache, A.; Herdtweck, E. *New J. Chem.* **2004**, *28*, 43.

(27) Bergmann, E. D.; Hoarau, J.; Pacault, A.; Pullman, A.; Pullman, B. *J. Chim. Phys. Phys.-Chim. Biol.* **1952**, *49*, 474.

(28) Baková, R.; Chergui, M.; Daniel, C.; Vlček Jr, A.; Záliš, S. *Coord. Chem. Rev.* **2011**, *255*, 975.

(29) Neuenschwander, M.; Voegeli, R.; Fahrni, H. P.; Lehmann, H.; Ruder, J. P. *Helv. Chim. Acta* **1977**, *60*, 1073.

(30) Massi, M.; Werrett, M. V.; Chartrand, D.; Gale, J. D.; Hanan, G. S.; MacLellan, J. G.; Muzzioli, S.; Raiteri, P.; Skelton, B. W.; Silberstein, M.; Stagni, S. *Inorg. Chem.* **2011**, *50*, 1229.

(31) Oshin, K.; Landis, A. M.; Smucker, B. W.; Eichhorn, D. M.; Rillema, D. P. *Acta Crystallogr., Sect.E* **2004**, *E60*, m1126.

(32) Dufresne, S.; Skalski, T.; Skene, W. G. *Can. J. Chem.* **2011**, *89*, 173.

(33) Vlček, A.; Busby, M. *Coord. Chem. Rev.* **2006**, *250*, 1755.

Chapitre 3 : Optoelectronic Properties and Structural Effects of the Incremental Addition of Pyridyl Moieties on a Rhodium Dimer

3.1. Résumé

Dans ce chapitre, la fonctionnalisation d'un dimère de rhodium tétra(4-bromo-*N*,*N*-diphényl-benzamidinate) par couplage de type Suzuki est décrite. Le groupement 4-pyridyl est greffé à ce dimère, menant à cinq espèces différentes, selon le nombre de couplages effectué sur le dimère de départ (tétra, tris, *cis*-bis, *trans*-bis et mono).

Les propriétés structurales, électrochimiques et photophysiques de ces quatre complexes ont été évaluées, complétées par des calculs DFT et TD-DFT. Pour mieux évaluer le changement des propriétés selon le groupement aryle central de l'amidinate, cette série de dimères a été comparée avec d'autres dimères possédant des ligands *N*,*N*-diphényl-arylamidinate, où l'aryle est 4-pyridine, 4-aniline, 4-bromophényl ou phényle. Ceci a permis l'identification univoque de plusieurs transitions électroniques du dimère, dont la transition MLCT ou plutôt M_2LCT qui n'était pas identifiée dans la littérature.

Avec cette série étendue, une corrélation a pu être établie entre les propriétés électrochimiques, photophysiques et la nature du groupement aryle central. Une première corrélation a pu être effectuée avec le paramètre de Hammett, qui s'est montré insuffisant pour décrire le cas du groupement phénylpyridine, obtenu par couplage. Pour compenser cette lacune, les paramètres de Taft furent utilisés, car ceux-ci permettent d'établir un ratio entre les effets causés par le champ électrique et ceux causés par la délocalisation (résonnance) du groupement. Avec ces paramètres, une corrélation complète a pu être obtenue pour toutes les propriétés regardées.

De plus, le ratio entre les deux paramètres révèle la contribution du paramètre de résonnance qui peut-être minoritaire ou dominant : ceci est directement lié aux propriétés étudiées et reflète la localisation de celles-ci, soit centré sur le métal ou centré sur le ligand.

Contribution :

Daniel Chartrand : Tous les travaux présentés dans l'article ainsi que sa rédaction.

Garry S. Hanan : Supervision et révision de l'article.

Optoelectronic Properties and Structural Effects of the Incremental Addition of Pyridyl Moieties on a Rhodium Dimer

*Daniel Chartrand, Garry S. Hanan**

Department of Chemistry, Université de Montréal, Montréal, QC, H3T 1J4 Canada

* E-mail: Tel: 1-514-340-5156. Fax: 1-514-343-7586.

Received: March 4, 2014; Published(web): July 20, 2014

dx.doi.org/10.1021/jp502243c

Reproduced with permission from *J. Phys Chem. A*, **2014** (ASAP)
Special Issue: Current Topics of Photochemistry

KEYWORDS: Rhodium, Suzuki coupling, Photophysics, Electrochemistry, Density functional theory, Hammett parameter, Taft parameters

3.2. Table of Content Graphic

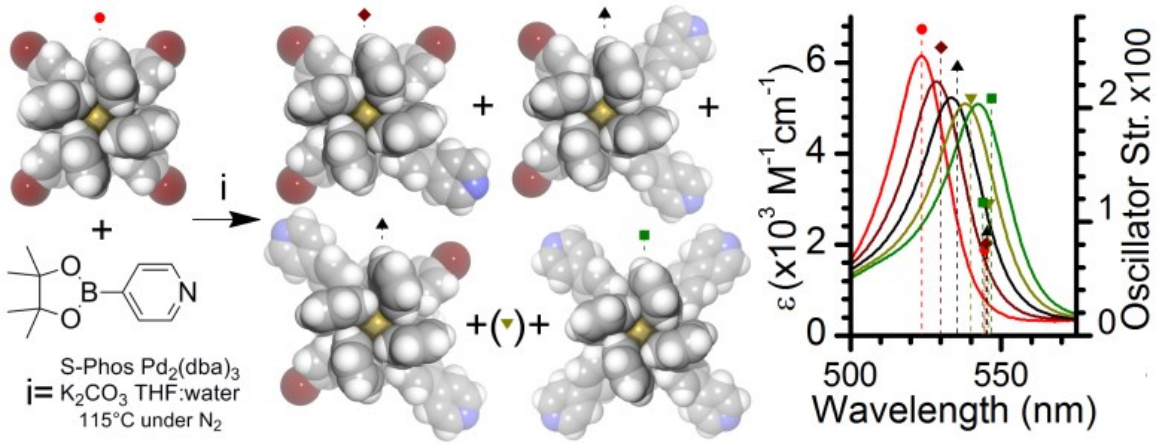

3.3. Abstract

The synthesis and characterization of five C–C coupling products obtained from the reaction of a paddlewheel tetrakis 4-bromo-*N*,*N*'-diphenylbenzamidinate dirhodium dimer with 4-pyridineboronic acid pinacol ester are reported. The coupling reactions occur on one to four amidinate ligands, leading to rhodium dimers containing [tetrakis, tris, *cis*-bis, *trans*-bis, or mono] -*N*,*N*'-diphenyl-4-(pyridin-4-yl)benzamidinate ligands, effectively creating new binding sites on the metal complexes. The new compounds were isolated by column chromatography, and the exact conformations were verified by X-ray crystallography. Redox processes showed only a small variation within the coupling products and included two oxidations (1.30 ± 0.02 V, 0.27 ± 0.01 V vs SCE) and one reduction (–1.55 ± 0.02 V vs SCE), all centered on the Rh–Rh core. Time-dependent density functional theory (TD-DFT) was used to analyze this series with four other fully characterized *N*,*N*'-diphenyl-aryl-amidinate rhodium dimers that were found in the literature. The two main absorption bands of these nine rhodium dimers were compared to TD-DFT calculations, both giving excellent correlation. The first, a metal-to-metal (MM) transition around 11800 cm^{-1} (845 nm) was blue-shifted in the calculation, with an average difference of 1378 cm^{-1} but had only a 15 cm^{-1} standard deviation, showing a strong correlation despite the energy difference. The second, a metal-to-ligand charge transfer (MLCT) transition around 18900 cm^{-1} (530 nm) was a near perfect match with only a 64 cm^{-1} average difference and a 35 cm^{-11} standard deviation. The electronic transition, redox potentials, HOMO, and LUMO energies of all dimers were plotted versus the Hammett parameter (σ) of the aryl group and Taft's model with 2 components: field effects (σ_F) and resonance (σ_R). The properties involving only the Rh–Rh core (MM band, all oxidation potentials, HOMO and LUMO) were fit with a single set of σ_F and σ_R contributions (73% and 27%), with a goodness-of-fit (R^2) value ranging from 90% to 99.7%. The metal-dimer to ligand charge-transfer band, involving the amidinate ligand, displayed different values of contribution with 45% and 55% for the σ_F and σ_R, respectively, with a fit of 94.8%. The accuracy of these fits enables the designed modification of amidinate-based dirhodium complexes to achieve desirable redox and spectroscopic properties.

3.4. Introduction

The paddle-wheel motif formed by many metal dimers offers a very modular and rigid scaffold to build up larger architectures. Many metals (*e.g.*, copper, molybdenum, and rhodium) form neutral, dimetallic assemblies with carboxylate ligands.[1-3] Among these complexes, rhodium tetracarboxylate dimers have been extensively developed for catalytic applications.[4-11] These rhodium dimers have also been used for supramolecular assemblies, using axial or equatorial linkers to form discrete or infinite structures.[12-24] Other families of ligands, such as amidines, can be used to form metal dimer assemblies. The amidine metal dimers show great stability and greater functionalization potential than the tetracarboxylate dimers, since moieties can be attached on both the central carbon and the nitrogen atoms.[25-33] The drawback to this is their limited catalytic activity,[34,35] although they have been shown to be photoactive to alkyl halide reduction[36] and mixed amidinate and diimine dimers have also gathered interest as an all-in-one chromophore–catalyst system for hydrogen production.[37] For their part, the tetraamidinate metal dimers have been used to form larger, often mixed-metal, assemblies.[38-44] In this study, we look at a postmodification of a dirhodium dimer formed with four 4-bromo-*N*,*N*'-diphenylbenzamidine ligands via a Suzuki coupling to attach a pyridyl motif,[45-50] thus creating new binding sites on the complex.[51-53]

Herein we present the synthesis and characterization of all five species formed by Suzuki coupling: mono- (**3-1**), *cis*-bis- (**3-2a**), *trans*-bis-(**3-2b**), tris- (**3-3**), and tetrakis- (**3-4**) *N*,*N*'-diphenyl-4-(pyridin-4-yl)bezamidinates; as illustrated in Chart 3.1. The properties of the synthesized complexes are compared to other Rh_2(*N*,*N'*-diphenylarylamidinate)$_4$ complexes (Chart 3.1, **3-5** to **3-9**), with an emphasis on the Hammett and Taft parameters, applied to an amidinate containing a central aryl group.[54,55] These parameters have successfully been correlated to electrochemical and/or catalytic properties upon functionalization of the ligand in both paddlewheel tetracarboxylate and tetraamidinate metal dimers in the past.[35,56,57] In these past studies, the amidinate dimers were always formamidinate -based, as such, no data exist for functionalization at the central position. The present study focuses on the electrochemical and photophysical properties of the benzamidinate-functionalized dirhodium tetraamidinate dimers.

Chart 3.1. Rh_2 Dimers **3-1** to **3-5** Prepared in This Study (Top); Other Dimers Used for Comparison (Bottom)

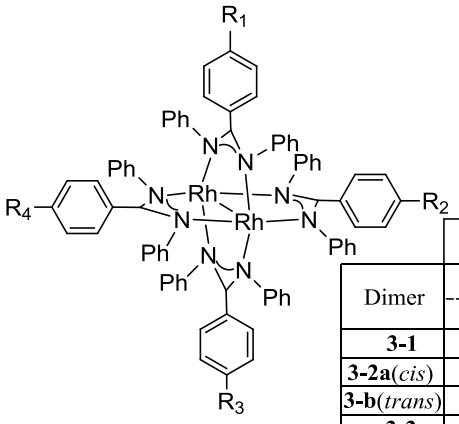

	R_n=	
Dimer	---Br	- - N
3-1	2,3,4	1
3-2a(*cis*)	3,4	1,2
3-b(*trans*)	2,4	1,3
3-3	4	1,2,3
3-4		1,2,3,4
3-5	1,2,3,4	

Dimer	R=
3-6	- - N
3-7	- -
3-8	- - NH_2
3-9	- - - H

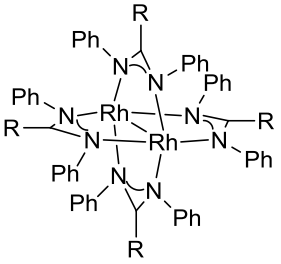

3.5. Experimental section

3.5.1. General considerations

All of the organic reagents were obtained from Sigma-Aldrich and rhodium(II) acetate from Pressure Chemical Co. Solvents from Fischer and Anachemia were used as received, except for acetone and dichloromethane (DCM) which were distilled. Nuclear magnetic resonance spectra were recorded using Bruker spectrometers at room temperature, with ^{1}H (400 MHz) and ^{13}C (100 MHz) chemical shifts referenced to residual solvent resonances (7.26 and 77.0 ppm, respectively, for $CHCl_3$). Elemental analyses were performed on the desolvated bulk samples by the university departmental service. Room temperature photophysical measurements were done in air-equilibrated and distilled DCM, using a 1 cm quartz cell. Absorption and emission spectra were recorded using a Cary 500i UV–vis–NIR spectrophotometer and a Cary Eclipse 300 fluorimeter, respectively. Electrochemical measurements were carried out in argon-purged DCM at room temperature with a BAS CV50W potentiostat. The working electrode was a Pt electrode, the counter electrode was a

Pt wire, and the pseudoreference electrode was a silver wire. The reference was set using an internal 1.0 mM ferrocene sample with its redox couple adjusted to 460 mV vs SCE in dichloromethane.[58] The concentration of the compounds was around 1 mM. Tetrabutylammonium hexafluorophosphate (TBAP) was used as the supporting electrolyte at a concentration of 0.10 M. Cyclic voltammograms (CVs) were obtained at scan rates of 50, 100, and 200 mV/s. For reversible processes, half-wave potentials (vs SCE) were measured with square-wave voltammetry (SWV) experiments performed with a step rate of 4 mV, a square-wave amplitude of 25 mV, and a frequency of 15 Hz. The criteria for reversibility were the separation of 60 mV between cathodic and anodic peaks, the close to unity ratio of the intensities of the cathodic and anodic currents, and the constancy of the peak potential on changing the scan rate. For irreversible processes, the peaks observed from square-wave voltammetry were used. Experimental uncertainties are as follows: absorption maxima, ± 0.5 nm; molar absorption coefficient, 10%; redox potentials, ± 30 mV.

3.5.2. Synthetic Methods

S-PHOS (2-dicyclohexylphosphino-2',6'-dimethoxybiphenyl),[59] 4-pyridineboronic acid pinacol ester (4,4,5,5-tetramethyl-2-(4-pyridyl)-1–3-dioxaborolane),[60] and $Pd_2(dba)_3$, (dba= dibenzylideneacetone)[61] were prepared from literature procedures. The synthesis of the tetrakis(4-bromo-*N*,*N*'-diphenylbenzamidinate) dirhodium(II) dimer (**3-5**) was previously reported,[43,62] and it is done by a neat melt reaction at 180 °C of rhodium acetate and 4-bromo-*N*,*N*'-diphenylbenzamidine (in 15-fold excess) under a flow of nitrogen for 10 min with a yield of up to 95% after removal of the excess ligand.[43,62]

Suzuki Coupling Reactions. The syntheses of species **3-1** to **3-4** were based on the same reaction conditions. However, synthesis of complex **3-4** could be optimized without any further attention to debromination, while the syntheses of **3-1** to **3-3** required optimization to lower debromination of the starting brominated benzamidinate rhodium dimer.

*Tetrakis(N,N'-diphenyl-(4-pyridin-4-yl)benzamidinate) dirhodium(II,II) (**3-4**).* Rhodium dimer **3-5** (121.3 mg, 75.2 μmol), $Pd_2(dba)_3$ (0.68 mg, 0.7 μmol), S-PHOS (0.57 mg, 1.3 μmol), potassium carbonate (69 mg, 522 μmol), and 4-pyridine boronic ester (122 mg, 594 μmol) were dispersed in THF:water (15 mL, 3:1, v:v) solution under nitrogen then were sealed in a 20 mL microwave pressure tube and heated by microwave at 115 °C for 1 h. The

red solution was reduced to 5 mL then 20 mL of water was added, leaving a red precipitate, which was collected by filtration and dissolved in DCM and MeOH (1:1, v:v) solution. This solution was evaporated to dryness to give **3-4**.

Purification: the bulk solid was dissolved in MeOH (5 mL) and concentrated HCl (3 drops) forming a brown solution. The solution was dried again to remove excess HCl, and the solid is dissolved in the eluent mixture [9 MeOH, 1 aqueous HCl (0.1M)) (v:v)] and applied to a Sephadex LH-20 column (1 cm diameter, 2 m length, flow rate of ~10 mL/hour). The second fraction was isolated; complex **3-4** was obtained as a precipitate after neutralization with aqueous KOH (1 M, 5 mL) and reduction with hydrazine (0.2 mL). The isolated red solid was dissolved in DCM (10 mL), and all salts were extracted into the water phase (10 mL × 3). The organic phase was dried under vacuum, to give 115 mg (yield 95%) of complex **3-4**.

^{1}H NMR (400 MHz, $CDCl_3$): δ 8.52 (d, J = 5 Hz, 8H: a), 7.27 (d, J = 6 Hz, 8H: b), 7.15 (d, J = 8 Hz, 8H: c), 7.04 (br, 16H: g), 6.98–6.93 (m, 8H: h), 6.93 (d, J = 6 Hz, 8H: d), 6.69 (br, 8H: e), 5.86 (br, 8H: f). $^{13}C\{^{1}H\}$ NMR (100 MHz**,** $CDCl_3$): δ 170.2; 151.3; 150.1; 147.3; 136.36; 136.22; 132.4; 128.5; 127.8; 125.6; 123.0; 121.1. HRMS (ESI, CH_2Cl_2) (m/z): $[M+4H]^{+4}$ $[C_{96}H_{72}N_{12}Rh_2]4H^{+4}$ calcd, 400.6106; found, 400.6124. Anal. Calcd for $C_{96}H_{72}N_{12}Rh_2+H_2O$: C, 71.28; H, 4.61; N, 10.39. Found: C, 71.03; H, 4.38; N, 10.40 (water confirmed by ^{1}H NMR and crystal structure).

*Suzuki Coupling Conditions for Species **3-1** to **3-3***. Rhodium dimer **3-5** (323.3 mg, 201 μmol), $Pd_2(dba)_3$ (1.74 mg, 1.9 μmol), S-PHOS (1.73 mg, 4.2 μmol), potassium carbonate (116 mg, 840 μmol), and 4-pyridine boronic ester (164.6 mg, 802 μmol) were dispersed in THF:water (45 mL, 3:1, v:v) solution under nitrogen then were sealed in a 100 mL pressure tube and heated at 115 °C for 15 min. The work up and purification is identical to **3-4**, although the purification by Sephadex column separated the mixture of products into four pure fractions where complex **3-4** elutes first, followed by complexes **3-3**, **3-2**, and **3-1**, respectively. Complex **3-2** was further purified into **3-2a** and **3-2b** by column chromatography (silica, hexane/AcOEt (v:v) (1:1): with a gradient to pure AcOEt). Rf of all species in AcOEt: **3-1,** 0.94; **3-2a**, 0.2; **3-2b,** 0.57; **3-3,** 0.05; **3-4,** 0; **3-5**, 1. Isolated yields are based on the removal of the starting material recovered mass (170 mg, 52%): **3-1**, 16.3 mg (10%); **3-2a** (*cis*), 26.5 mg (16%); **3-2b** (*trans*), 13.1 mg (8%); **3-3**, 17.1 mg (11%); **3-4**, 3.9 mg (2%).

*Tris(N,N'-diphenyl-4-bromo-benzamidinate)(N,N'-diphenyl-4-(pyridin-4-yl)benzamidinate) dirhodium(II,II) (**3-1**).* ^{1}H NMR (400 MHz, $CDCl_3$): δ 8.52 (d, J = 6 Hz, 2H: a), 7.27 (d, J = 6 Hz, 2H: b), 7.14 (d, J = 8 Hz, 2H: c), 7.10-6.98 (m, 16H: g,g'), 6.96 (d, J = 8 Hz, 6H: c'), 6.95–6.90 (m (br), 8H: h,h'), 6.89 (d, J = 8 Hz, 2H: d), 6.65 (dd, J = 9, 1 Hz, 6H: d'), 6.58 (br, 8H: e,e'), 5.78 (br, 8H: f,f'). ^{13}C{^{1}H} NMR (100 MHz**,** $CDCl_3$): δ 170.1; 169.7; 151.2; 151.09; 150.06; 147.3; 136.4; 136.1; 134.0; 133.1; 132.3; 130.4; 128.5 (br); 127.8 (br); 125.5; 123.04; 122.99; 121.7; 121.1. HRMS (ESI, CH_2Cl_2) (m/z): $[M]^+$ $[C_{81}H_{60}Br_3N_9Rh_2]^+$ calcd, 1601.0631; found, 1601.0613. Anal. Calcd for $C_{81}H_{60}Br_3N_9Rh_2$: C, 60.62; H, 3.77; N, 7.85. Found: C, 60.60; H, 3.74; N, 7.86.

*cis-Bis(N,N'-diphenyl-4-bromo-benzamidinate)bis(N,N'-diphenyl-4-(pyridin-4-yl)benzamidinate) dirhodium(II,II) (**3-2a**).* ^{1}H NMR (400 MHz, $CDCl_3$) δ 8.52 (d, J = 5 Hz, 4H: a), 7.28 (d, J = 6 Hz, 4H: b), 7.14 (dd, J = 7, 5 Hz, 4H: c), 7.10-6.99 (m (br), 16H: g,g'), 6.99–6.96 (m, 4H: c'), 6.95-6.92 (m, 8H: h,h'), 6.91 (d, J = 8 Hz, 4H: d), 6.66 (d, J = 8 Hz, 4H: d'), 6.61 (br, 8H: e,e'), 5.81 (br, 8H: f,f'). ^{13}C{^{1}H} NMR (100 MHz**,** $CDCl_3$): δ 170.1; 169.7; 151.26; 151.13; 150.1; 147.3; 136.37; 136.14; 134.1; 133.1; 132.3; 130.4; 128.5 (br); 127.8 (br); 125.6; 123.04; 122.98; 121.7; 121.1. HRMS (ESI, CH_2Cl_2) (m/z): $[M]^+$ $[C_{86}H_{64}Br_2N_{10}Rh_2]^+$ calcd, 1600.1792; found, 1600.1777. Anal. Calcd for $C_{86}H_{64}Br_2N_{10}Rh_2$: C, 64.43; H, 4.02; N, 8.74. Found: C, 64.40; H, 4.01; N, 8.74.

*trans-Bis(N,N'-diphenyl-4-bromo-benzamidinate)bis(N,N'-diphenyl-(4-pyridin-4-yl)benzamidinate) dirhodium(II,II) (**3-2b**).* ^{1}H NMR (400 MHz, $CDCl_3$): δ 8.52 (dd, J = 5, 1 Hz, 4H: a), 7.28 (dd, J = 5, 2 Hz, 4H: b), 7.14 (d, J = 8 Hz, 4H: c), 7.11–6.99 (m (br), 16H: g,g'), 6.95 (d, J = 8 Hz, 4H: c'), 6.95–6.91 (m, 8H: h,h'), 6.90 (d, J = 8 Hz, 4H: d), 6.66 (d, J = 8 Hz, 4H: d'), 6.62 (br, 8H: e,e'), 5.80 (br, 8H: f,f'). ^{13}C{^{1}H} NMR (100 MHz**,** $CDCl_3$): δ 170.1; 169.7; 151.26; 151.13; 150.0; 147.4; 136.35; 136.11; 134.1; 133.0; 132.3; 130.4; 128.5 (br); 127.7 (br); 125.6; 123.06; 123.01; 121.6; 121.1. HRMS (ESI, CH_2Cl_2) (m/z): $[M]^+$ $[C_{86}H_{64}Br_2N_{10}Rh_2]^+$ calcd, 1600.1792; found, 1600.1761. Anal. Calcd for $C_{86}H_{64}Br_2N_{10}Rh_2$: C, 64.43; H, 4.02; N, 8.74. Found: C, 64.40; H, 4.01; N, 8.74.

*(N,N'-Diphenyl-4-bromo-benzamidinate)tris(N,N'-diphenyl-(4-pyridin-4-yl)benzamidinate) dirhodium(II,II) (**3-3**).* ^{1}H NMR (400 MHz, $CDCl_3$): δ 8.55-8.49 (m, 6H: a), 7.30–7.25 (m, 6H: b), 7.17-7.11 (m, 6H: c), 7.04 (m (br), 16H: g,g'), 6.96 (d, J = 9 Hz, 2H: c'), 6.95–6.94 (m, 8H: h,h'), 6.92 (dd, J = 8, 1 Hz, 6H: d), 6.67 (d, J = 9 Hz, 2H: d'), 6.66 (br, 8H: e,e'), 5.83 (br, 8H: f,f'). ^{13}C{^{1}H} NMR (100 MHz**,** $CDCl_3$): δ 170.1; 169.7;

151.29; 151.17; 150.1; 147.3; 136.37; 136.17; 134.1; 133.1; 132.3; 130.4; 128.5 (br); 127.8 (br); 125.5; 123.04; 122.99; 121.7; 121.1. HRMS (ESI, CH_2Cl_2) (m/z): $[M]^+$ $[C_{91}H_{68}{}^{79}BrN_{11}Rh_2]^+$ calcd, 1599.29471; found, 1599.2953. Anal. Calcd for $C_{91}H_{68}{}^{79}BrN_{11}Rh_2+H_2O$: C, 67.50; H, 4.36; N, 9.51. Found: C, 67.18; H, 4.18; N, 9.53 (water confirmed by ^1H NMR).

3.5.3. Computational methods

All calculations were performed with Gaussian software (G03 and G09).[63,64] G09 was used mainly for gas phase optimization and vibrational frequency determinations of the bigger systems and gave identical result to G03. All TD-DFT was performed with G03, and although G09 gave similar results, G03 was kept for better uniformity in the comparison with older calculated data. All models used crystallographic structure data as the starting point for ground-state geometry optimizations. The geometry optimization and IR frequency determination was carried out with the DFT method using the B3LYP functional in the gas phase.[65,66] The 6-31G** basis set was used for C, H, N, and Br while relativistic LANL2DZ with effective core potentials and one additional f-type polarization functional was applied for the Rh atom ($\alpha_f = 1.350$).[67,68] No imaginary frequencies were observed for all optimized structures (Figure 3.S9 of the Supporting Information). The absorption spectral properties and molecular orbital (MO) energies were calculated by TD-DFT approach associated with the polarized continuum model (CPCM)[69] using DCM as solvent and with a smaller basis set: 3-21G was used for all atoms (N, C, H, and Br) except Rh atoms and the amidinate NCN core atoms, for which the previous basis set was left unchanged. Gaussview 3.09 was used to visualize MOs with an isodensity of 0.02; GaussSum 2.2 was employed to extract the absorption energies, oscillator strengths, and molecular orbital energies, and Chemissian program was used to sketch energies of MOs with their color-coded atomic orbital (AO) contributions, using 0.008 eV as the threshold for degeneracy for the MO.[70-72] Complex **3-6** was previously studied in our group using the same methods and was used for comparison; for completeness, its tabulated data are included in the Supporting Information.[44]

3.5.4. Crystal structure determination

X-ray quality crystals were obtained in various ways: for **3-1**, a slow diffusion of acetone into a DCM solution; for **3-2a**, slow diffusion of hexanes into a chloroform solution; for **3-2b**, slow diffusion of hexanes into an ethyl acetate solution; and for **3-4**, slow evaporation of

an ethyl acetate, methanol, and water (50/40/10% volume) solution. X-ray crystallographic data were collected from a single crystal sample, which was mounted on a loop fiber. For **3-1** and **2b**, data were collected with a Bruker Microstar diffractometer equipped with a Platinum 135 charged-coupled device (CCD) detector at 150 (2) K. For **3-2a**, data were collected with a Bruker Platform diffractometer, equipped with a Bruker SMART 4K CCD Area Detector and a Nonius FR591 rotating anode Cu Kα X-ray radiation source equipped with a Montel 200 optics at 200 (2) K. For **3-4**, data were collected with a Bruker Platform diffractometer, equipped with a Bruker APEX II CCD Area Detector and a Mo Kα X-ray radiation source at 200 (2) K. The data was integrated with APEX2 and corrected for absorption using the SADABS package, except for **3-2b**, where the crystal was nonmerohedrally twinned and was corrected for absorption using TWINABS, using HKLF 5 files for final refinement. This resulted in considerable removal of data, leading to 80% completeness.[73-75] Following analytical absorption corrections and solution by direct methods, the structures were refined against F^2 with full-matrix least-squares using the program SHELXL-97.[76] All nonwater H–atoms were added at calculated positions and refined by use of the riding model with isotropic displacement parameters based on those of the parent atom, water H atoms were refined with constraints. Anisotropic displacement parameters were employed throughout for the nonhydrogen atoms, except where disorder was too severe to be meaningful, where it was kept isotropic (i.e., the phenyl-pyridine moiety in **3-1**). For **3-2a**, a positional disorder was found between a bromine and a phenyl moiety, *trans* to each other, and it was refined to be in an 80% to 20% ratio. A second positional disorder implicating the other bromine was not modeled, as it only showed 5% contribution, it is the cause of the highest remaining electron density (1.67 e) in the model. Images were generated using Mercury, Ortep III and, Pov-Ray.[77-79] Specific parameters of each measurement are located in Table III-1.

Table III-1. Details of X-ray Diffraction Studies for the Different Dimers

	3-1a[a]	**3-2a**[b]	**3-2b**[a]	**3-4**[c]	**3-5**[d]
Formula	$[C_{81}H_{60}Br_3N_9Rh_2]$ $\cdot 1.5(CH_2Cl_2)$	$[C_{86}H_{64}Br_2N_{10}Rh_2]$ $\cdot 2.5(CH_2Cl_2)$	$[C_{86}H_{64}Br_2N_{10}Rh_2]$ $\cdot 2.5(C_4H_8O_2)$	$[C_{96}H_{72}N_{12}Rh_2]$ $\cdot 4(H_2O)$	$[C_{76}H_{56}Br_4N_8Rh_2]$ $\cdot 3(CH_2Cl_2)$
Color/form	red prism	red plate	red plate	red spearhead	brown prism
T (K); wavelength	150; 1.54178	200; 1.54178	150; 1.54178	200; 0.71073	150; 1.54178
Crystal System	tetragonal	triclinic	triclinic	orthorhombic	tetragonal
Space Group	*I*4	*P*-1	*P*-1	*Fddd*	*I*4
Unit Cell: *a* (Å)	14.7855(7)	13.6685(4)	13.0797(3)	15.689(4)	14.8465(1)
b (Å)	14.7855(7)	17.3026(5)	14.1503(4)	30.833(8)	14.8465(1)
c (Å)	17.6398(9)	19.4769(6)	25.3837(7)	33.866(8)	17.3717(2)
γ (deg)	90	73.857(2)	88.073(2)	90	90
β (deg)	90	74.732(1)	75.8300(12)	90	90
γ (deg)	90	79.393(1)	72.6550(12)	90	90
V (Å^3); Z	3856.3(3); 2	4237.9(2); 2	4344.0(2); 2	16382(7); 8	3829.04(6)
R1(F);wR(F^2)[I>σ(I)]	0.0578;0.1594	0.0683; 0.1689	0.0367; 0.1004	0.0375; 0.0659	0.0479;0.1231
R1(F); wR(F^2) (all)	0.0591;0.1614	0.1238; 0.1889	0.0440; 0.1048	0.0855; 0.0739	0.0513;0.1345
GoF(F^2)	1.076	0.980	1.039	0.962	1.077
Flack parameter	0.057(18)	n.a.	n.a.	n.a.	0.471(11)

[a]Bruker Microstar diffractometer (Platinum 135 CCD Detector, Helios optics and, Kappa goniometer). [b]Bruker/AXS Smart 6000 (4K) diffractometer (Mirror Montel 200-monochromated Cu Kα radiation, FR591 Rotating Anode). [c]Bruker Smart APEX 2, graphite monochromator. [a]From ref[62] (CCDC 942878).

3.6. Results and Discussion

The formation of complexes **3-1** to **3-4** by Suzuki coupling requires specific conditions (Scheme 3.1) due to the limited solubility of **3-5** (only chloroform, THF, and DMF). The synthesis of all of the species was quite effective using the optimized reaction and purification conditions outlined in the Supporting Information. Complexes **3-1**, **3-2**, and **3-3** were synthesized with four equivalents of boronic ester, and the reaction was stopped before completion to obtain a mixture of all three species, leading to 52% recovery of complex **3-5** that can be reused. In consideration of this recovery, the isolated yield was 47% for **3-1** to **3-4** (see Scheme 3.1 for distribution between species, for n = 4). The 53% loss of mass is due

to the chromatography which left mixed fractions. For complex **3-4**, efficient synthesis and purification was possible, leading to an isolated yield of 95% (98% from ^{1}H NMR analysis of the bulk material).

Scheme 3.1. Synthesis of the Rh Amidinate Dimer Assemblies; *n* is the Equivalents of Boronic Ester Added, *m* Is the Number of Coupled Pyridyls On the Product

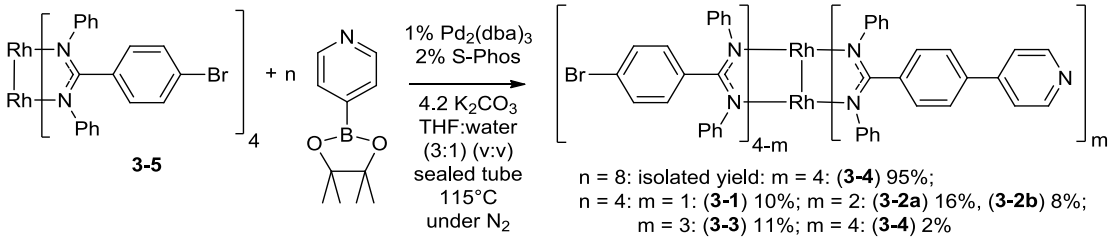

3-5

3.6.1. NMR spectroscopy

All of the proton NMR spectra of the dimers have two distinctive and broad signals (labeled *e* and *f* in Figure 3.1). These peaks are due to restricted rotation of the pendant phenyl rings and represent the splitting of the signal of the two protons *ortho* to the interannular bond. This rotation is known to be restricted and has a free-energy of activation of approximately 15 kcal/mol for various rhodium dimers with an aryl moiety in the amidinate backbone.[42-44] Proton *f* is shifted upfield due to the proximity of a phenyl ring core above it from neighboring ligands, while *e* is facing in the opposite direction, away from aryl rings. This broadening effect is also observed for the protons in the *meta* position, but these protons are in an almost chemically equivalent environment, being less affected by the nearby aromatic rings, and subsequently, their signals do not split.

By comparing ^{1}H NMR spectra of complexes **3-5** and **3-4**, a downfield shift of the protons *e* and *f* in complex **3-4** is observed as compared to *e'* and *f'* in **3-5**, suggesting that the phenyl-pyridine moiety is more electron withdrawing than the bromo-phenyl moiety on the center of the amidinate, which follows their Hammett parameter (0.44 and 0.23, respectively).[54,55] For **3-1** to **3-3**, a broader, averaged signal of the two positions is seen, confirmed by the very linear shift per number of pyridine coupled (Figure 3.S2 of the Supporting Information). This downfield shift is also observable in the ^{13}C NMR spectra where the amidinate carbon signal shifts from 169.7 ppm (in **3-1**) to 170.2 ppm (in **3-4**).

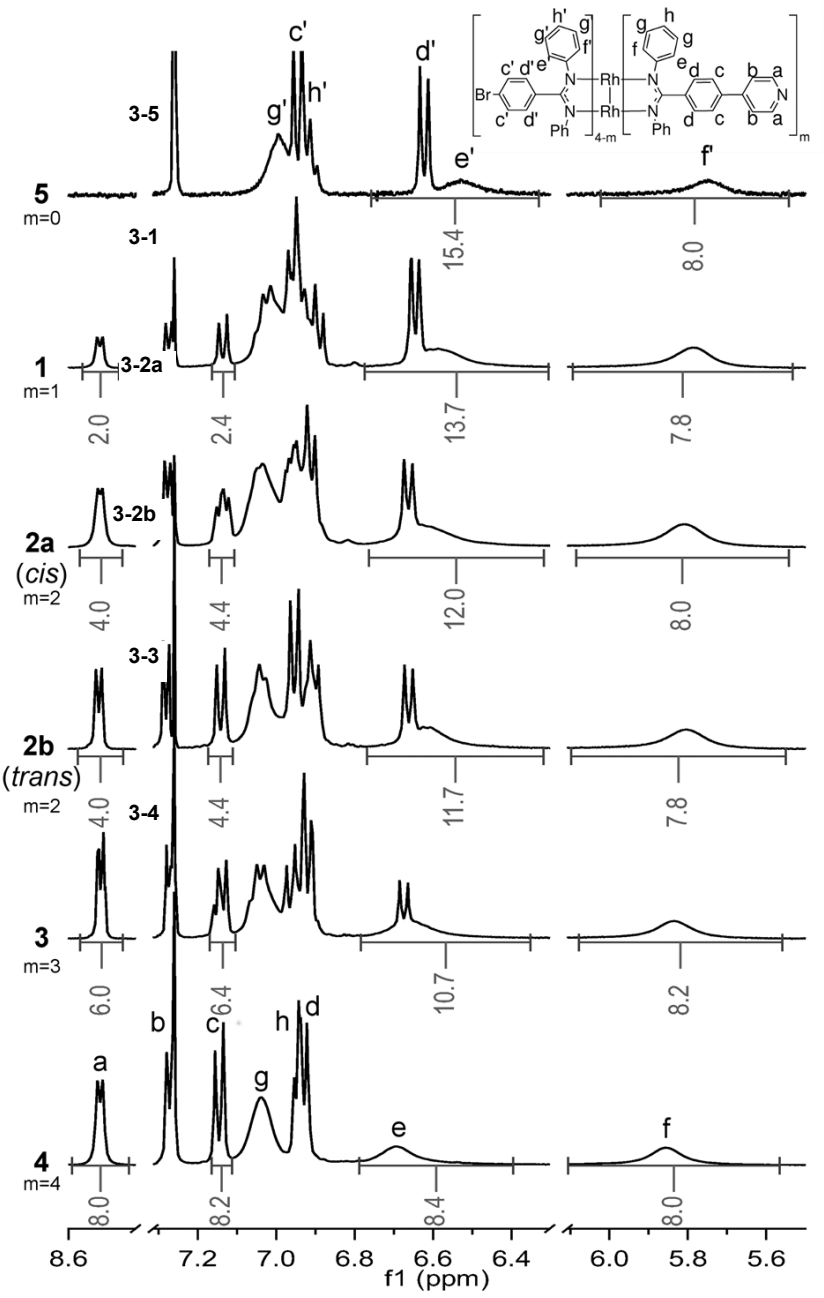

Figure 3.1. ^{1}H-NMR of **3-1** to **3-5** in $CDCl_3$ (room temperature, 400 MHz); labeling scheme of the protons (top right).

The proton NMR spectra can allow all of the species to be identified, including the **3-2a** and **3-2b** isomers, making it the only characterization method able to identify these isomers in solution. The identification is possible due to the protons on the central phenyl rings of the dimer (*c*, *d* and *c'*, *d'*). The central aromatic ring has restricted rotation, like the pendant rings

of the dimer, but due to the symmetrical chemical environment they do not split (extra information is available in the Supporting Information).[44]

Unlike the pendant ring, there is no broadening of the central aryl peak for **3-2a** (also observed for **3-1** and **3-3**). This well-resolved signal suggests a restricted rotation that is slower than the timescale of the NMR experiment leading to a higher free-energy activation barrier than that of the rotation of the pendant phenyl rings. The high restriction of the central phenyl ring is readily explained by looking at the crystal structure (Figure 3.2), in which the central ring is immobilized by the two pendant phenyl rings of the amidinate.

3.6.2. X-ray Structural Investigation

All of the dimers, except **3-3**, crystallize readily. Complexes **3-1** to **3-5** have a helical orientation of the 12 phenyl rings around the dimer, generating chirality in the solid state. As such, these molecules do not possess an inversion center; they can only contain C4, D4, and C2 rotation axes.

The geometry of the rhodium dimer core varies very little upon coupling of a pyridyl ring. This can be readily observed by looking at the two extremes, structures of **3-5** and **3-4**, where the Rh–Rh and Rh–N bond lengths and the N–Rh–Rh–N' torsion angle are not significantly different (< 3σ). The same can be concluded for structures of **3-1**, **3-2a**, and **3-2b**.

The Rh–Rh distance for the dimers is similar to other biphenyl-aryl-amidinate in the literature (complexes **3-6** to **3-8** in 0),suggesting that no observable structural changes are seen with the changes in polarity of the central aryl ring (here displayed as the average of the Hammett parameter of the 4 aryls groups in 0).[54,55]

The paddlewheel motif of the dimer induces a vectorial angular separation of 90° and/or 180° of the coordination vectors of the pyridines,[80,81] very similar to pyridyl -functionalized porphyrins.[82-84] Rhodium dimers **3-1** to **3-4** have a much longer span than both the porphyrins and **6**, with a radius (pyridine-to-center-of-mass) of 11.3(1) Å vs 7.7(1) Å for the porphyrins and 7.0(1) Å for **3-6**.[84] The angular separation between the coordination vectors of the two pyridine units in **3-2a** and **3-2b**, are 86° and 177°, respectively. The small deviations from 90° and 180° are due to the flexibility of the rhodium dimer core.

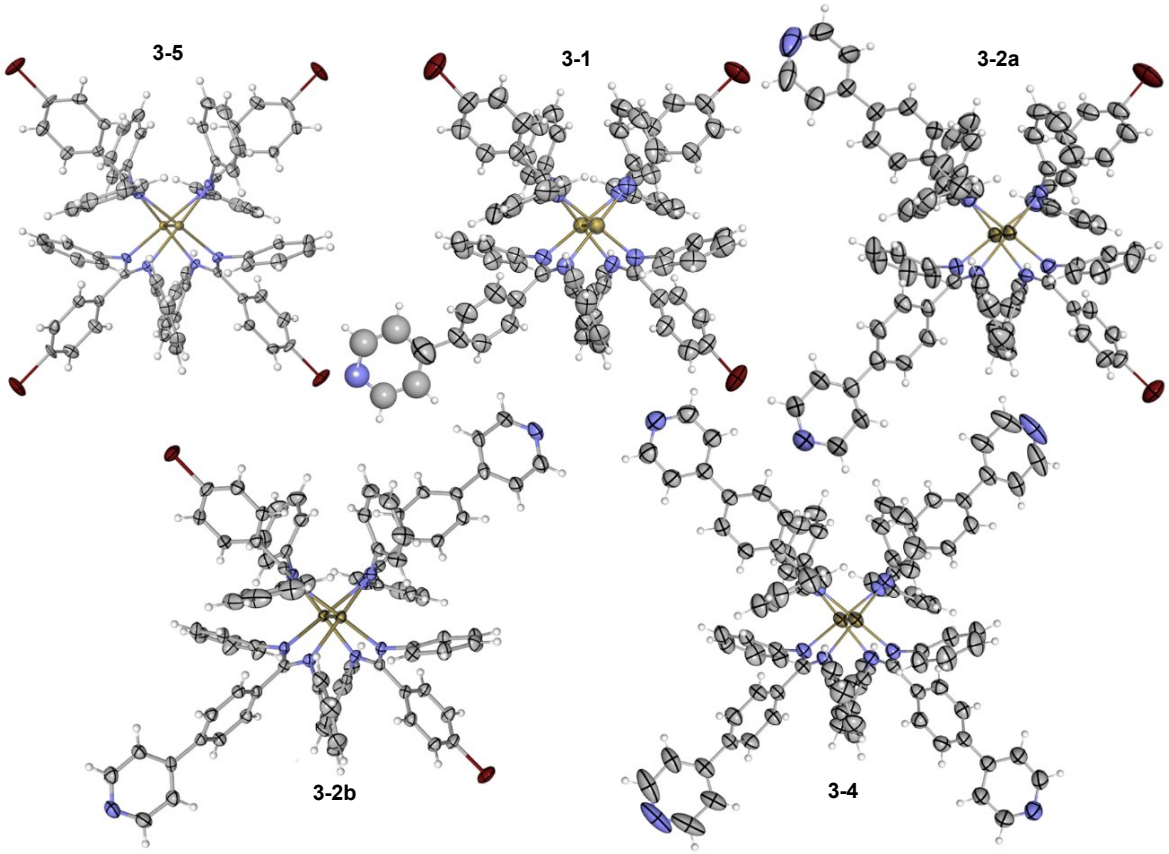

Figure 3.2. ORTEP view of the X-ray crystal structures of **3-5**[62] (top-left), **3-1** (top-center), **3-2a** (top-right), **3-2b** (bottom-right), and **3-4** (bottom-left) viewed at a 15° angle from the Rh–Rh axis (50% probability displacement ellipsoids; solvent and/or disordered elements have been removed for clarity; full labeling is available in Figure 3.S3 to Figure 3.S6 of the Supporting Information)

DFT calculations show the same trend in the optimized structures in the gas phase; the Rh–Rh distances (globally higher by about 0.02 Å vs experimental values) are not affected by the ligands although the Rh-N distances (higher by about 0.05 Å vs measured distances) do show a small correlation with the Hammett parameter (σ) ($d_{(Rh-N)}$ = (-0.0005 Σ(σ)+ 2.0989) Å), but it is far too small to be observed by crystallography. The calculated N-Rh-Rh-N torsion angle of the complexes is the same at 14° except for the formamidinate based dimer at 10°. The calculated difference re-emphasizes that the main cause of this distortion is the steric bulk of the central aryl ring.

Table III-2. Selected Crystallographic Parameters (Å,°) for **3-1**, **3-2a**, **3-2b**, **3-4**, **3-5** and Related Complexes with Computational Data of the Optimized Structure in Italics[a]

Complex	**3-1**	**3-2a** (*cis*)	**3-2b** (*trans*)	**3-4**	**3-5**	**3-6**[b]	**3-7**[c]	**3-8**[d]	**3-9**[e]
Central group	Ph-Br Ph-Py	Ph-Br Ph-Py	Ph-Br Ph-Py	Ph-Py	Ph-Br	Pyridine	Phenyl	Aniline	H
Σ(σ)[f]	1.13	1.34	1.34	1.76	0.92	3.8	0	-2.64	N/A
Rh1-Rh2	2.4012(9) *2.42257*	2.4022(7) *2.41939*	2.3983(3) *2.42270*	2.4034(9) *2.42276*	2.4017(6) *2.42257*	2.4055(8)[g] *2.42340*	2.389(1) *2.42316*	2.3950(9) *2.42110*	2.457(1) *2.48021*
Rh-N[g]	2.055(8) *2.0982*	2.057(7) *2.09890*	2.050(3) *2.0983*	2.047(8) *2.0984*	2.042(4) *2.0982*	2.054(9) *2.0975*	2.05(6) *2.0991*	2.050(4) *2.0995*	2.057(1) *2.0915*
$Rh_{2\ centroid}$-N_{py}	11.0	11.3	11.2	11.3		7			
N-Rh-Rh-N'[g]	12.4(2) *14.84*	13.0(4) *14.76*	15.1(4) *14.79*	11.7(3) *14.68*	12.0(2) *14.86*	12,6(4) *14.61*	17.3 *14.54*	17.6(1) *14.45*	3.5 *10.07*

[a]Gaussian03, gas phase B3LYP/6-31g**(CHNBr)LanL2DZ+f(Rh). [b]**3-6:** Rh_2(*N,N'*-diphenylisonicotinamidinate)$_4$.[42] [c]**3-7:** Rh_2(*N,N'*-diphenylbenzamidinate)$_4$.[30] [d]**3-8:** Rh_2(4-amino-*N,N'*-diphenylbenzamidinate)$_4$.[43] [e]**3-9:** Rh_2(*N,N'*-diphenylformadinate)$_4$.[29] [f]Sum of the Hammett parameter of the central aryl moiety.[54,55] [g]Averaged measurement, error represents the highest value between standard deviation and experimental error.

The monocoupled dimer, **3-1**, has very peculiar solid-state packing. It has a near-identical unit cell as the one obtained for **3-5** (Table III-1, Figure 3.3). Due to the *I*4 space group present for both dimers, a C_4 rotation axis is enforced through the Rh–Rh axis, leading to an asymmetric unit containing a single amidinate ligand. The phenyl-pyridine moiety is observable in 25% occupancy, the fragment shows heavy torsion due to the presence of the adjacent aryl rings on the neighboring molecule, as can be seen in Figure 3.2 and Figure 3.3 (top), where it occupies the cavity filled with DCM in the case of **3-5**. This positional disorder stems from entropy, since there is no preferential orientation for the moiety.

All the dimers exhibit similar packing arrangements, dominated by parallel-displaced π interactions between the pyridine fragments and bromine-to-π ring interactions. In the case of **3-4**, the packing creates cavities containing trapped water molecules interacting with the pyridines of the dimer. The packing of **3-1** to **3-5** is further described in the Figures 3.S7 and 3.S8 of the Supporting Information.

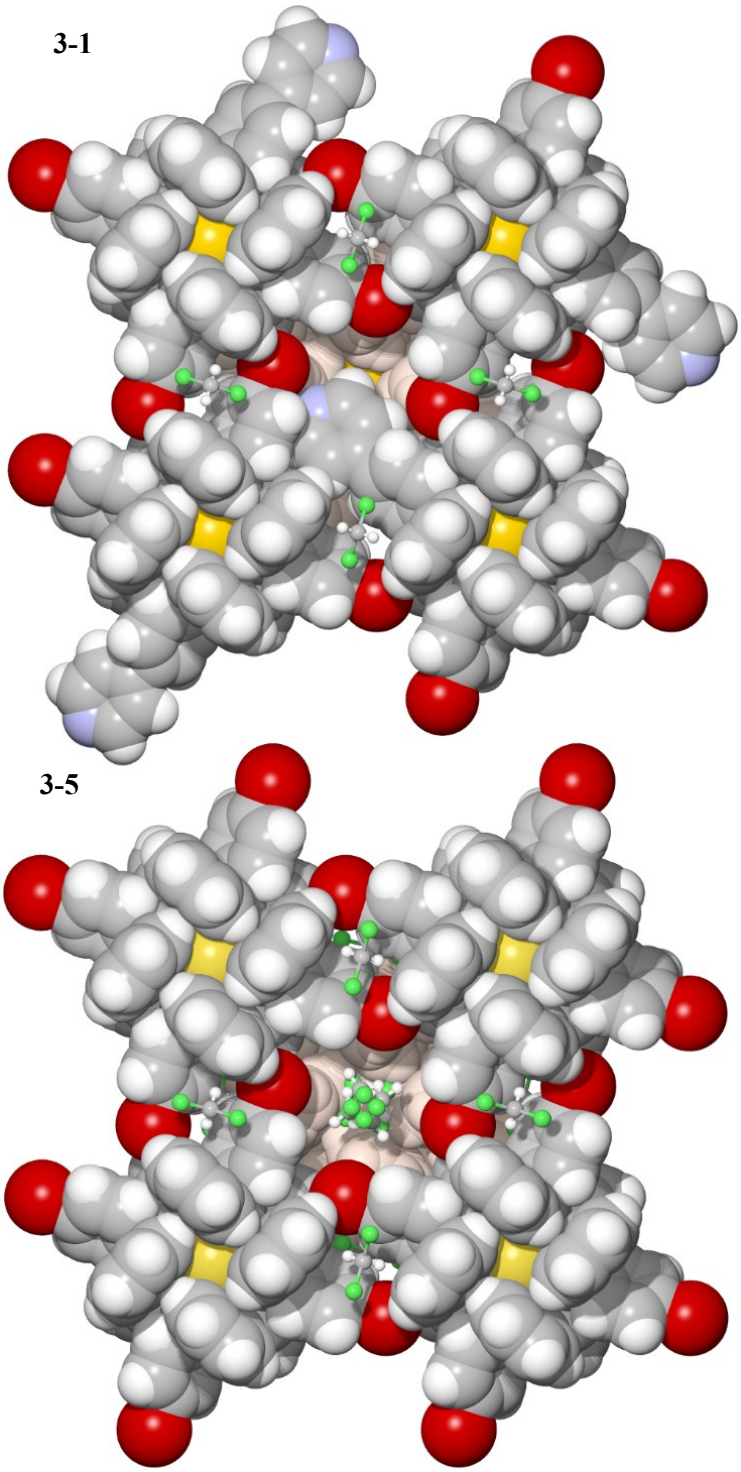

Figure 3.3. Spacefill views of the packing along the *c* axis; **3-1** (top) and **3-5** (bottom). View of **1** displays the four possible positions for the disordered phenyl-pyridine moiety. In the pink tint: the closest dimer along the *c* axis; the dichloromethane solvent is shown in the ball and stick model (showing disorder).

3.6.3. Electrochemistry

The rhodium amidinate dimers possess three reversible or quasi-reversible metal-based single-electron redox couples, corresponding to two oxidations and one reduction as seen on Figure 3.4 for complex **3-1**.[25-30,32,33,35,36,38] The redox processes should have a positive trend relative to the Hammett parameter (σ) since a higher positive σ correlates with a stronger electron withdrawing group on the ligand, making the coordinated metal harder to oxidize and easier to reduce. This trend has been observed in the literature for the pendant aryl groups of metal amidinates[35,56] and can be seen passing from **3-8** to **3-7** to **3-6** in in Figure 3.5 (top) (see also Table III-S29 of the Supporting Information for **3-1** to **3-4**). Correlation to σ is good except for the phenyl-pyridine from our present study, where a small negative trend is observed for the first oxidation and calculated MO values.

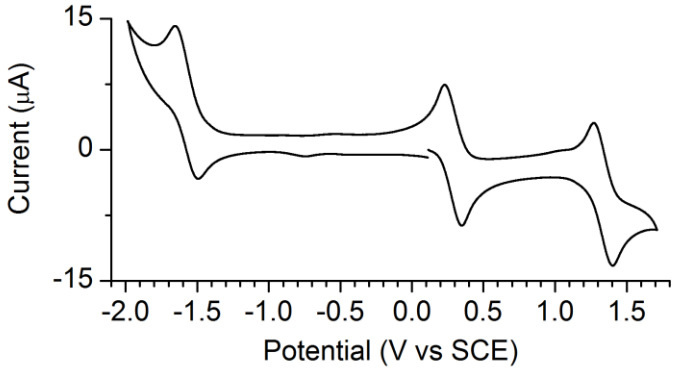

Figure 3.4. Cyclic voltammogram of **3-1** in DCM, 0.1 TBAP, scan rate = 200 mV/s.

To better model the data, the general Hammett parameter can be subdivided into its two main components using Taft parameters; σ_F or field effect, dipole–dipole or charge–charge interaction; and σ_R or resonance: delocalization and π electron bonding.[54,55,57] The σ_R parameter can have two additional forms, dependent on the studied property: σ_R^+ and σ_R^-, in this case σ_R^+ was used.[85] Figure 3.5 (bottom) shows the correlation of the fit (R^2), optimized for the HOMO and LUMO energies and the two oxidation processes, which goes from 99 % to 90 %, an increase of up to 10 % for the first oxidation. With the better fitting observed with the Taft parameters, it is clear that the main factor for these properties is the field effect (σ_F), with a contribution of (73 ± 7)%, while the resonance (σ_{R+}) plays only a smaller role at (27 ± 7) %. (The uncertainty calculated for contribution of the Taft parameters corresponds to a variation of ±10% of the slope of the fit being optimized.) This suggests that

the Hammett's original model could not fit the data because of the phenyl-pyridyl resonance effect being overestimated, while all other dimers only implied the core aryl ring delocalization, common for all species. A bigger pool of dimers containing aryl groups as R groups would be needed to confirm this hypothesis.

The observed deviation of the R^2 value for the oxidation processes comes mostly from **3-6**, where the aryl is 4-pyridyl. The 4-pyridyl is not a standard group for the Hammett parameter series, as the nitrogen atom is part of the aromatic ring, not a substituent. It has been studied in the past and also recently been subject of more analysis, but its parameter values are not precise, mainly due to the formation of a zwitterion during analysis.[86,87] In this case, the σ_p and σ_m parameters were obtained from alkaline hydrolysis[87] and passed through Taft's formula to make the corresponding σ_F (0.51) and σ_R (0.45) parameters.[54]

For the reduction process, the Taft parameter fit ($R^2 = 0.916$) is 3% worse than the Hammett parameter obtained ($R^2 = 0.942$). Applying the σ_R- value instead drops the fit to 78% (after optimization of the contributions), suggesting that no electron density is delocalized on the aryl motif, as will also be observed in the LUMO orbital atomic. The best fit with Taft parameters was obtained with the plain σ_R parameter, with a R^2 of 0.946, with (50 ± 10) % contribution on both factors, which is the default value of the Hammett parameter.

As previously mentioned the oxidation potential data follow the same trend observed for the calculated HOMO and LUMO energies. The HOMO orbital has, for all dimers (**3-1** to **3-8**), a 38% $Rh_2(\delta^*)$ contribution, a 46% amidinate core (N–C–N) contribution and the rest is on the pendant phenyls (15%) (Figure 3.6 and Table III-S20 to Table III-S28 of the Supporting Information). The central aryl contribution to the HOMO orbital is only 0.4%, suggesting that although it influences the polarity of the amidinate, it is not involved in delocalization. The contributions calculated fit well with the lower value of resonance seen on the Taft parameters, especially for **3-1** to **3-4** (e.g., the pendant pyridine group has less than 10^{-3} % contribution, truly negligible in this case). On the LUMO side, the contributions are the following: $Rh_2(\sigma^*)$: 83%, amidinate core: 9%, and pendant phenyls: 3%. Again, there is less than 1% contribution from the aryl, implying the same effects.

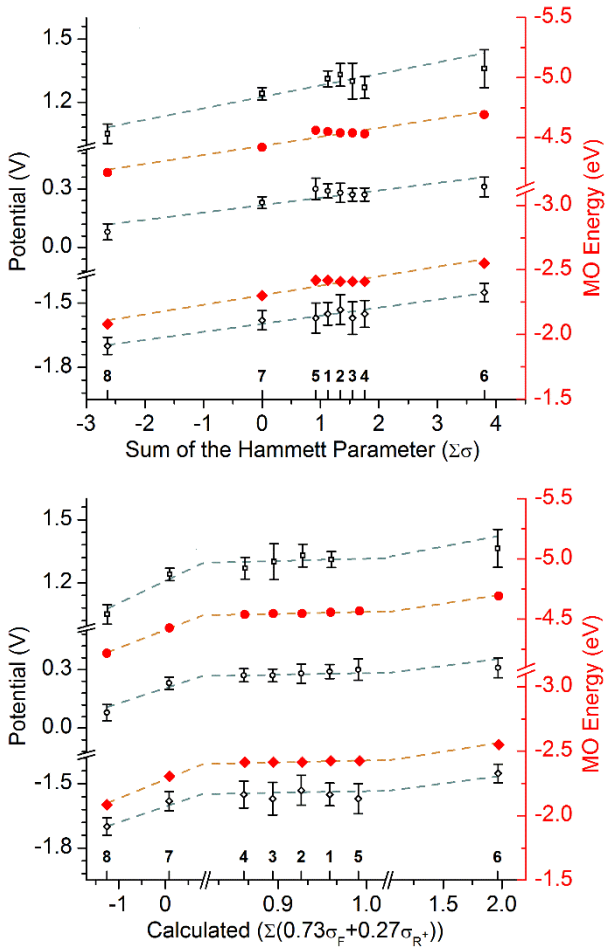

Figure 3.5. Redox potentials ($E_{1/2}$) of the Rh dimers referenced to SCE and calculated MO energies vs the sum of the empirical parameters of the four central aryl groups: Hammett (top) and fitted Taft parameters (bottom). Label of the complexes at the bottom; dashed lines represent linear fits of the series; 1st reduction (◇); 1st oxidation (○);2nd oxidation (□); error bars represent E_{pa} and E_{pc} positions; **3-1**, **3-2**, **3-3**, **3-4**, **3-6**[42],and **3-7**[25] in DCM; **3-5** in THF[62], **3-8** in MeCN(corrected for adduct formation);[62] HOMO (red ◆) and LUMO (red ●).

A reactivity parameter can be calculated to quantify the effect the aryl group has on a given property. It can be observed by looking at the slope obtained from the redox couples and the Taft parameters, represented by the following modified Hammett equation[56] applied to redox potentials, where $\Delta E_{1/2}$ is the change in volts observed for a given redox process:

(1) $\Delta E_{1/2} = \rho \sum \sigma \, V = \rho_T \sum 2(\rho_F \sigma_F + \rho_R \sigma_R) \, V$

The constants ρ_F and ρ_R are the same as described before (normalized to 1), the factor 2 appearing in the equation comes from the definition of the Taft parameters ($\sigma = \sigma_F + \sigma_R$). Hence, the reactivity parameter ρ_T will compare the global effect of the four central aryl groups to the shift in potential. All redox potentials have a similar reactivity parameter: 50 ± 6 mV for the second oxidation, 38 ± 5 mV for the first oxidation, and 37 ± 4 mV for the reduction (based on the Hammett parameter). The ρ_T can be compared with the previously reported ρ values obtained with the standard Hammett parameter for the 8 pendant aryls: in that case, the reactivity value was around 97 ± 2 mV for all three redox processes.[35,56] This suggests that the electronic properties of the Rh dimer core can be controlled in both positions, pendant, and central; however, the pendant position will have a bigger impact on the dimer's global redox properties.

The complexes all have a very similar HOMO to LUMO gap of around 1.82 ± 0.04 V (measured from redox potentials), consistent with the fact that the aryl groups affect both the oxidized and reduced states in a similar fashion and are comparable with the calculated values derived from the difference of the HOMO and LUMO energies, giving 2.13 ± 0.008 eV.

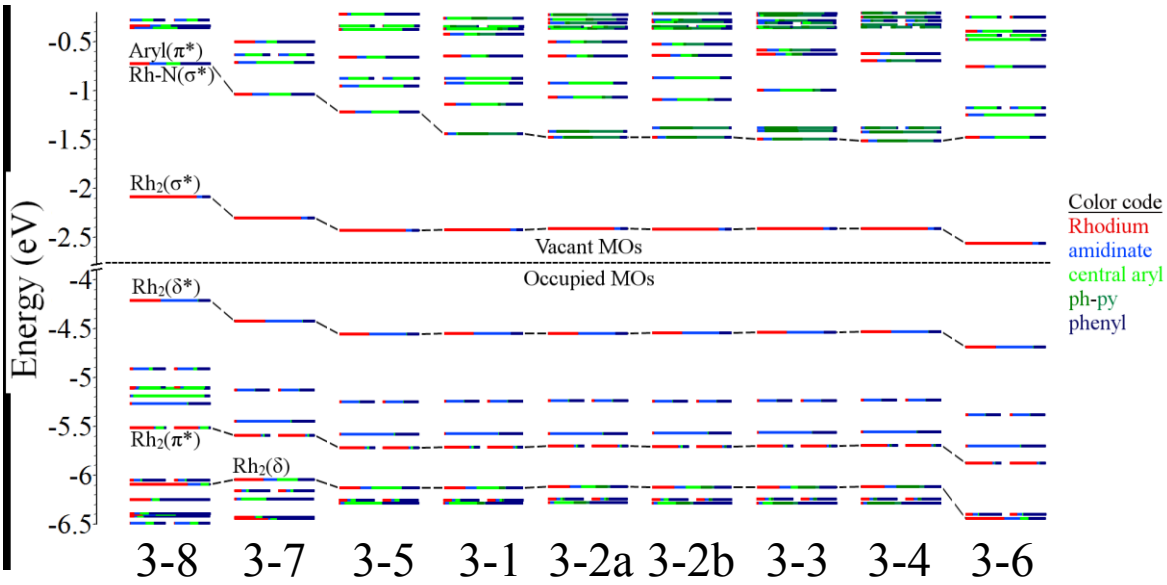

Figure 3.6. Calculated frontier MO energies of all the modeled Rh_2 complexes obtained from DFT(rb3lyp/LanL2DZ(f)[Rh]6-31G**[$NCN_{amidinate}$]3-21G[C,H,N,Br] with CPCM(CH_2Cl_2).

3.6.4. Photophysical Investigation

The absorption spectra of the tetraamidinate rhodium dimers are known, and no observable emission is seen for these systems, mostly due to the fact that they are absorbing well into the near IR.[29,30,44] In nonaxially coordinating solvents (all except nitrile or other linear coordinating solvents), they possess two strong characteristic bands, one in the near-IR, from 830 to 850 nm, the other in the visible range, between 500 to 600 nm, as can be seen in Figure 3.7Figure 3.7 (see Table III-S30 of the Supporting Information for tabulated values). TD-DFT was investigated for complexes **3-1** to **3-8** to assign and better understand the observed transition bands. In the phenyl–pyridine series, there are no differences in the absorption bands observed for **3-2a** and **3-2b**; the isomers showed the same intensities, moreover the TD-DFT models of both versions were calculated and gave very similar results. For example, the $^{1}M_2LCT$ band of both compounds varied by less than 0.01 %, while their oscillator strengths varied by less than 1%.

The TD-DFT results matched the band in the green region (550 nm) exceptionally well, as can be seen in the inset of Figure 3.7. In the case of the near-infrared (NIR) absorption near 830 nm, the band is significantly blue-shifted versus the experimental values with an averaged energy difference of 1378 cm^{-1}. However, this averaged difference displayed a very low (15 cm^{-1}) standard deviation for the nine complexes. This precision can be seen in Figure 3.8, where measured and calculated values of the green (uncorrected) and NIR (corrected by the averaged difference with experimental data) bands maxima are plotted against their Hammett parameters and optimized Taft parameters (σ_F and σ_R). The Hammett parameter was insufficient to describe the phenyl-pyridine species correctly, therefore, Taft parameters (σ_F and σ_R) were used to define them more accurately. In this case, the contribution of the field effect and resonance was dependent on the nature of the transition.

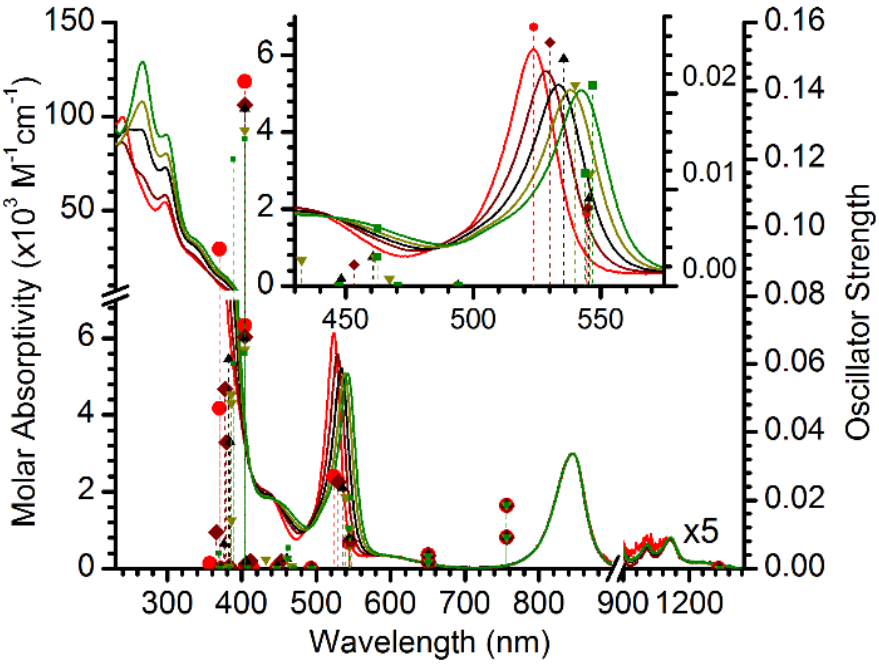

Figure 3.7. Absorption spectra in dichloromethane of **3-1** (dark red), **3-2** (black), **3-3** (dark yellow), **3-4** (green), **3-5** (red) with calculated oscillator strength positions from TD-DFT as symbols with vertical lines of matching color: **3-1** (◆),**3-2** (▲),**3-3** (▼),**3-4** (■),**3-5** (●) above 900 nm the spectra is amplified by a factor of 5; zoom of the spectra (inset).

The first intense band, near 845 nm, has previously been assigned in the literature.[26,28,44] It is due to a singlet MM [$Rh_2(\pi^* \rightarrow \sigma^*)$] transition (calculated to be the [HOMO–4, HOMO–5] to LUMO transition for all the dimers), and as such, this band is very sensitive to axial coordination, but not so sensitive to changes in the amidinate ligand. In this case only a very small bathochromic shift of about 2 nm is seen on passing from the starting dimer **3-5** to **3-4**. This shift goes in the opposite direction of the literature series when plotted against σ (Figure 3.8, top). The same reasons as explained in Electrochemistry can be applied here: the ^{1}MM transition implies that the orbitals are centered on the metals and the delocalization effect from the phenyl-pyridine is much less than expected. In fact, the ^{1}MM transition has the same optimized ratio of Taft's parameters as the oxidation and MO orbitals, and a R^2 value of 0.987 is obtained (Figure 3.8, bottom).

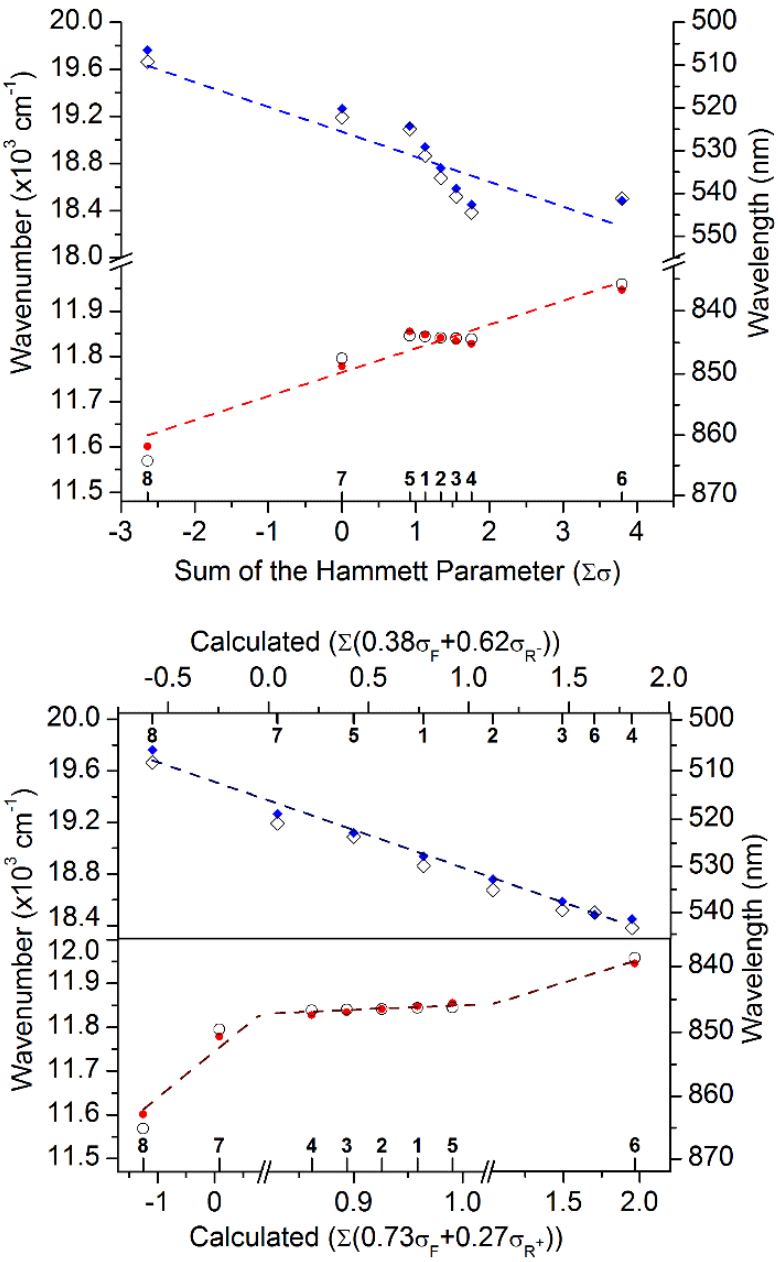

Figure 3.8. Absorption maximum (filled symbol, in DCM, except **3-8** in DMSO[62]) and calculated transition energy (hollow symbol) for the $^1Rh_2(\pi^*\rightarrow\sigma^*)$ transition (diamond, calculated energy adjusted by –1378 cm^{-1}) and the ^1M_2LCT transition (circle, unadjusted calculated values) vs the sum of the empirical parameters of the four central aryl groups: Hammett (top); fitted Taft parameters (bottom). Label of the complexes at the bottom; dashed lines represent linear fits of the series.

The second transition was previously assigned in our studies of **3-6**, with TD-DFT calculations as a singlet metal-dimer (M_2) to a ligand charge transfer (^1M_2LCT) transition {HOMO [$Rh_2(\delta^*)$] to LUMO+1}.[44] The ligand centered LUMO+1 is focused on the four amidinate cores, and their aryl ring π^* orbitals, as shown in Figure 3.9 for complexes **3-1** to **3-4**.[44] This assignment is supported by the TD-DFT data of the modeled dimers, having a near perfect fit in wavenumber and showing a strong correlation with peak intensity and oscillator strength (61 cm^{-1} averaged difference with a 35 cm^{-1} standard deviation). For the special cases of **3-1**, **3-2a**, **3-2b**, and **3-3**, where the four amidinate ligands are no longer equivalent, the LUMO+1 is focused on the phenyl-pyridine moiety; therefore, the ^1M_2LCT transition implies a mixture of HOMO to LUMO+1 and HOMO to LUMO+X (where X is the first empty MO located on the bromophenyl amidinate, as can be seen in Figure 3.9), leading to a single transition averaging the effects of the two different ligands. This single transition is in contrast to what was observed in **3-6** after binding a single rhenium chromophore: the signal was split in two and the transitions did not merge, due to a much larger shift in polarity of the ligands.[44]

The standard Hammett parameter still does not give a linear fit for the ^1M_2LCT transition. This time the phenyl-pyridine series transitions are more red-shifted than predicted, as opposed to the other trends observed so far (Figure 3.8, top). Once again, splitting the parameter into its field and resonance components enables a better understanding of the underlying process. Being a ^1M_2LCT transition, the excited state will place an electron directly on the aryl-amidinate system, thus it implies a strong contribution of the resonance parameter (chosen as σ_R- because of the implied negative charge on the ligand in the excited state). With these parameters, we obtained a linear fit that was a 10% R^2 factor increase and which has contributions of (45 ± 10)% and (55 ± 10) % for the field effect (σ_F) and resonance (σ_R-) parameters, respectively (Figure 3.8, bottom). The increase in the contribution of the resonance parameter, now in parity with the field effect parameter, emphasizes the nature of the excited state, centered on the ligand as can be observed in the LUMO +1 to +4 orbitals of the dimers (Figure 3.9). Thus, the energy of the transition will be lower as the electronic delocalization of the radical formed upon excitation is improved.[86]

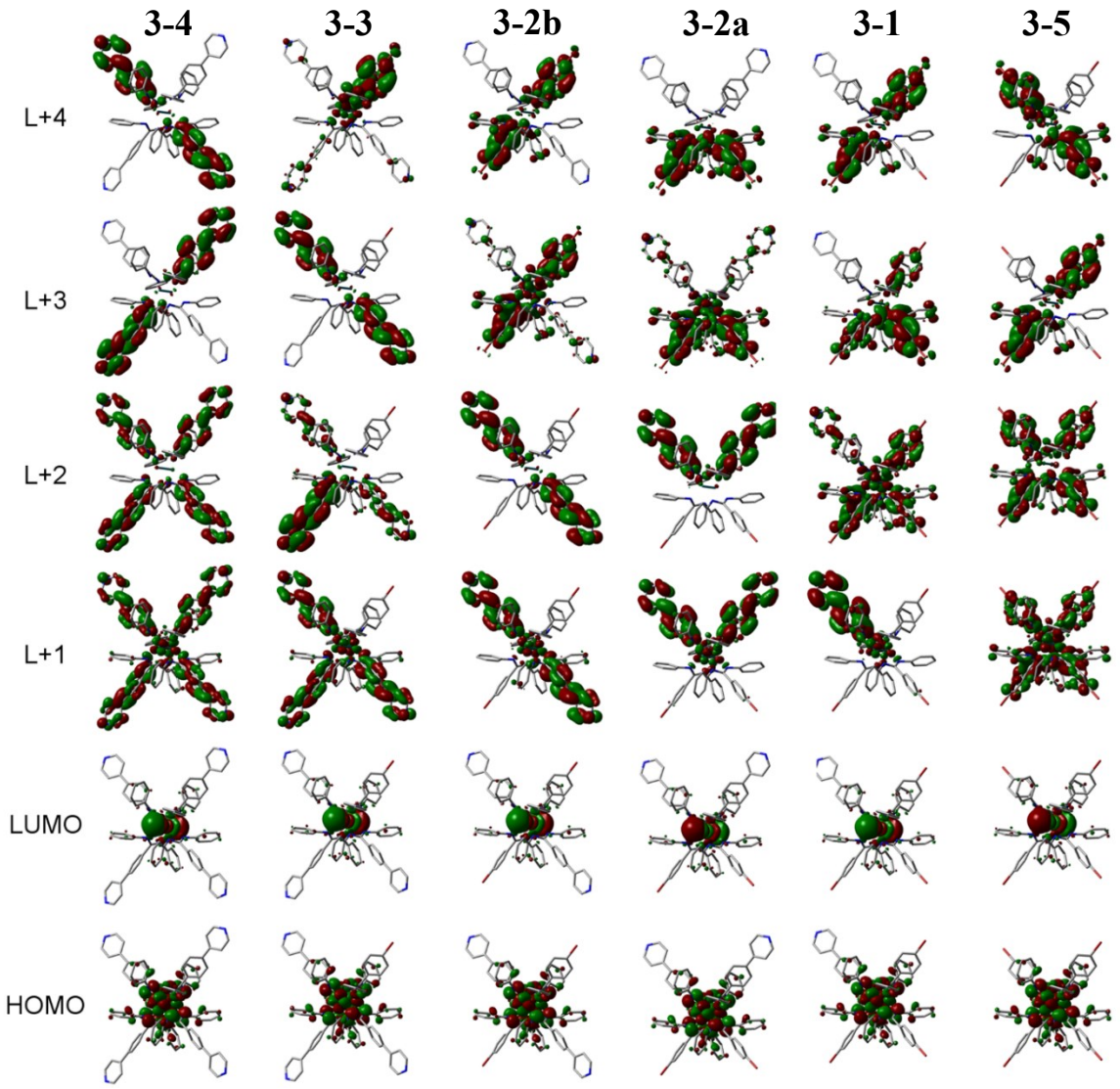

Figure 3.9. Calculated surfaces of the frontier MOs of the complexes obtained from DFT (rb3lyp/LanL2DZ(f)[Rh]6-31G**[$NCN_{amidinate}$]3-21G[C,H,N,Br] with CPCM(DCM)).

The shoulder at 600 nm, seen in all of the species, is assigned to a $^1LM_2CT$ (HOMO–1 to LUMO), evaluated at 650 ±2 nm across the whole series. The HOMO–1 is strictly aryl amidinate based. The absence of shifting can be explained since the HOMO–1 and LUMO have no contribution from the central aryl and both will shift by the same amount from the field effects induced by the aryl.

With the use of TD-DFT calculations, another $^1LM_2CT$ transition is calculated to be at 545 nm for the whole series. Its exact position in the experimental spectra is not clear, two plausible locations are the 430 nm peak or the 507 nm shoulder; both of these are present in all of the series. The strongest calculated oscillators in the visible come from a third $^1LM_2CT$

transition in the 400 nm region similar again to the modeled species and should correspond to the intense shoulder seen at 380 nm.

Complete assignment of the bands in the UV region was not attempted by TD-DFT, but from the spectra of complexes **3-1** to **3-5** (Figure 3.7), a clear additive effect in the UV region can be seen for the 265 and 290 nm bands going from **3-1** to **3-4**; these are brought by the additional pyridyl rings and should involve their π→π* transition. At the same time, the signal at 230 nm is less intense, suggesting that a bromo-phenyl based π→π* transition is located there, which is lost through the series.

The NIR region shows two other weak bands at 1000 nm (ε = 160 $cm^{-1}M^{-1}$) and 1100 nm (ε = 130 $cm^{-1}M^{-1}$) and an even weaker, broad shoulder extending from 1200 to 1300 nm (ε = 30 $cm^{-1}M^{-1}$). These transitions have been largely ignored in the literature, as they are easily missed due to their low intensity. They are not an artifact or due to partially oxidized product, since the Rh_2(II,III) species have a very strong and broad band near 1000 nm, quite different from these bands.[30,33,34,36,44] The two NIR bands are much too sharp to be from the trace oxidized dimer as we demonstrated recently.[44] These bands match well in energy of the lowest calculated HOMO→LUMO transition {singlet MM [Rh_2(δ*→σ*)] transition}. They are forbidden by symmetry and are calculated to be around 1335 ± 20 nm for the whole series (**3-1** to **3-8**). Since this ^{1}MM transition is forbidden by Laporte's rule, its calculated oscillator strength is zero, but relaxation of the selection rules by various vibration modes should make the ^{1}MM transition visible. It is suggested that these bands come from different components of the Rh_2(δ*→σ*) transition, but further studies would be required to confirm this assignment. Another origin could be from a triplet component of other permitted transitions, such as the Rh_2(π*→σ*), but no definitive answer is available at this point.

3.7. Conclusion

TThe rhodium dimer series was successfully synthesized by an efficient Suzuki coupling and was isolated by size-exclusion chromatography. The ability to prepare and isolate all isomers containing pyridyl moieties brings new synthons to supramolecular chemistry, similar in geometry to functionalized porphyrins, albeit more bulky and of longer reach. The most interesting complex for mixed-metal assemblies, **3-4**, can be synthesized in very high yield (95%). Complex **3-4** could be used as the phenyl spacer equivalent to the previously studied complex Rh_2(*N*,*N'*-diphenylisonicotinamidinate)$_4$ (**3-6**), where rhenium(I)-based

chromophores were grafted to furnish a light-harvesting assembly.[44] For discrete assemblies **3-2a** (*cis*) and **3-2b** (*trans*) are very promising as rigid bridging building blocks, as a corner of a square and a linear rod, respectively, but they are less trivial to obtain, due to the inherent statistical distribution during their synthesis.

The crystal structures showed the importance of the bromo-phenyl interactions on the solid-state packing, where **3-1** retained the same packing as **3-5**, despite strong deformation imposed on the phenyl-pyridyl group.

The phenyl-pyridine series showed similar electrochemical and distinctive spectroscopic properties, which were compared by both DFT and TD-DFT models with strong correlation to experimental data. In particular, the calculated ^1M_2LCT transitions matches the measured absorption bands in the green region both in wavelength and intensity for the nine rhodium dimers studied herein. The extension of the aryl ring with a pyridyl motif breaks the trend versus the electron withdrawing effect determined by the Hammett parameter when compared with other moieties found in the literature. An optimized Taft model, involving both resonance and field effects, showed the inherent differences between the $^1Rh_2(\pi^*\rightarrow\sigma^*)$ and the ^1M_2LCT transitions, coherent with the calculated models. The former is mostly affected by field effects, as for its redox properties, since the transition does not involve electron delocalization into the central ring. The ^1M_2LCT transition invokes a negative charge delocalization on the central aryl, which is modeled by the inclusion of the σ_R- Taft parameter. With both empirical and theoretical models, which fit very well with experimental results, the redox potentials as well as the absorption bands should be predicted reliably for a number of central aryl groups, although the current pool of synthesized complex is limited to a very small sampling. The central aryl variation can be combined with the already studied pendant aryl variations, allowing fine adjustment to be done on the electronic properties of the rhodium dimer, like the redox potentials which opens a –200 to +600 mV tuning window from the phenyl motif used in this study.[35]

3.8. Acknowledgment

We are grateful to the Natural Sciences and Engineering Research Council of Canada, the Ministère de l'Éducation du Québec and the Université de Montréal for financial support. The Université de Montréal's Altix and Briarée supercomputers are supported by le Réseau Québécois de Calculs de Haute Performances (RQCHP) and University of Manitoba's Grex supercomputer is supported by Westgrid, both networks being under the national supercomputing platform, Compute Canada Calcul Canada.

3.9. Supporting Information.

X-ray crystallographic data in CIF format, extended discussion on synthesis and NMR, extra figures and tabulated computational data. This material is available free of charge via the Internet at http://pubs.acs.org.

3.10. References

(1) Chifotides, H. T.; Dunbar, K. R. In *Multiple Bonds Between Metal Atoms*; Cotton, F. A., Murillo, C. A., Walton, R. A., Eds.; Springer: New York, 2005, pp 465-589.
(2) Cotton, F. In *Multiple Bonds Between Metal Atoms*; Cotton, F. A., Murillo, C. A., Walton, R. A., Eds.; Springer: New York, 2005, pp 707-796.
(3) Patmore, N. J. Recent Developments in the Chemistry of Metal-Metal Multiply Bonded Paddlewheel Compounds. *Organomet. Chem.* **2010**, *36*, 77-92.
(4) Timmons, D.; Doyle, M. In *Multiple Bonds Between Metal Atoms*; Cotton, F. A., Murillo, C. A., Walton, R. A., Eds.; Springer: New York, 2005, pp 591-632.
(5) Doyle, M. P. Perspective on Dirhodium Carboxamidates as Catalysts. *J. Org. Chem.* **2006**, *71*, 9253-9260.
(6) Tanaka, S.; Masaoka, S.; Yamauchi, K.; Annaka, M.; Sakai, K. Photochemical and Thermal Hydrogen Production from Water Catalyzed by Carboxylate-Bridged Dirhodium(II) Complexes. *Dalton Trans.* **2010**, *39*, 11218-11226.
(7) Doyle, M. P.; Duffy, R.; Ratnikov, M.; Zhou, L. Catalytic Carbene Insertion into C-H Bonds. *Chem. Rev.* **2010**, *110*, 704-724.
(8) Lebel, H. In *Catalyzed Carbon-Heteroatom Bond Formation*; Wiley-VCH: Weinheim, Germany, 2010, pp 137-155.
(9) Du, B. J. Rhodium-Catalyzed C-H Amination. An Enabling Method for Chemical Synthesis. *Org. Process Res. Dev.* **2011**, *15*, 758-762.
(10) Korotvicka, A.; Necas, D.; Kotora, M. Rhodium-catalyzed C-C bond cleavage reactions. *Curr. Org. Chem.* **2012**, *16*, 1170-1214.

(11) Lindsay, V. N. G.; Charette, A. B. Design and Synthesis of Chiral Heteroleptic Rhodium(II) Carboxylate Catalysts: Experimental Investigation of Halogen Bond Rigidification Effects in Asymmetric Cyclopropanation. *ACS Catal.* **2012**, *2*, 1221-1225.

(12) Cotton, F. A.; Daniels, L. M.; Lin, C.; Murillo, C. A. Square and Triangular Arrays Based on $Mo2^{4+}$ and $Rh2^{4+}$ Units. *J. Am. Chem. Soc.* **1999**, *121*, 4538-4539.

(13) Cotton, F. A.; Lin, C.; Murillo, C. A. Supramolecular Arrays Based on Dimetal Building Units. *Acc. Chem. Res.* **2001**, *34*, 759-771.

(14) Cooke, M. W.; Hanan, G. S.; Loiseau, F.; Campagna, S.; Watanabe, M.; Tanaka, Y. The Structural and Functional Roles of Rhodium(II)-Rhodium(II) Dimers in Multinuclear Ruthenium(II) Complexes. *Angew. Chem., Int. Ed.* **2005**, *44*, 4881-4884.

(15) Cotton, F. A.; Jin, J. Y.; Li, Z.; Liu, C. Y.; Murillo, C. A. A Deliberate Approach for the Syntheses of Heterometallic Supramolecules Containing Dimolybdenum $Mo(2)^{4+}$ Species Coordinated to Other Metal Units. *Dalton Trans.* **2007**, 2328-2335.

(16) Cooke, M. W.; Hanan, G. S.; Loiseau, F.; Campagna, S.; Watanabe, M.; Tanaka, Y. Self-assembled Light-harvesting Systems: Ru(II) Complexes Assembled about Rh-Rh Cores. *J. Am. Chem. Soc.* **2007**, *129*, 10479-10488.

(17) Cooke, M. W.; Chartrand, D.; Hanan, G. S. Self-assembly of Discrete Metallosupramolecular Luminophores. *Coord. Chem. Rev.* **2008**, *252*, 903-921.

(18) Cooke, M. W.; Santoni, M. P.; Hanan, G. S.; Loiseau, F.; Proust, A.; Hasenknopf, B. Spanning Pairs of $Rh_2(acetate)_4$ Units with Ru(II) Complexes. *Inorg. Chem.* **2008**, *47*, 6112-6114.

(19) Kataoka, Y.; Sato, K.; Miyazaki, Y.; Suzuki, Y.; Tanaka, H.; Kitagawa, Y.; Kawakami, T.; Okumura, M.; Mori, W. Photocatalytic Hydrogen Production from Water Using Heterogeneous Two-dimensional Rhodium Coordination Polymer $[Rh_2(p\text{-}BDC)_2]n$. *Chem. Lett.* **2010**, *39*, 358-359.

(20) Pogozhev, D.; Baudron, S. A.; Hosseini, M. W. From Insertion of Rhodium Acetate Paddlewheels into Functionalized 7-Azaindole Hydrogen-bonded Dimers to Infinite Architectures. *Dalton Trans.* **2011**, *40*, 7403-7411.

(21) Matsunaga, S.; Hasada, K.-i.; Sugiura, K.; Kitamura, N.; Kudo, Y.; Endo, N.; Mori, W. Hetero Bi-Paddlewheel Coordination Networks: a New Synthetic Route to Rh-Containing Metal-Organic Frameworks. *Bull. Chem. Soc. Jpn.* **2012**, *85*, 433-438.

(22) Amo-Ochoa, P.; Delgado, S.; Gallego, A.; Gomez-Garcia, C. J.; Jimenez-Aparicio, R.; Martinez, G.; Perles, J.; Torres, M. R. Structure and Properties of One-Dimensional Heterobimetallic Polymers Containing Dicyanoaurate and Dirhodium(II) Fragments. *Inorg. Chem.* **2012**, *51*, 5844-5849.

(23) Amo-Ochoa, P.; Jimenez-Aparicio, R.; Perles, J.; Torres, M. R.; Gennari, M.; Zamora, F. Structural Diversity in Paddlewheel Dirhodium(II) Compounds through Ionic Interactions: Electronic and Redox Properties. *Cryst. Growth Des.* **2013**, *13*, 4977-4985.

(24) Nickerl, G.; Stoeck, U.; Burkhardt, U.; Senkovska, I.; Kaskel, S. A Catalytically Active Porous Coordination Polymer Based on a Dinuclear Rhodium Paddle-Wheel Unit. *J. Mater. Chem. A* **2014**, *2*, 144-148.

(25) Le, J. C.; Chavan, M. Y.; Chau, L. K.; Bear, J. L.; Kadish, K. M. Synthesis and Characterization of Dirhodium Complexes with Four N,N'-Diphenylbenzamidine Bridging Ligands. Electrochemical Generation and ESR Properties of $[Rh_2(N_2R_2CR)_4]n$ where R = Phenyl and n = 1 and -1. *J. Am. Chem. Soc.* **1985**, *107*, 7195-7197.

(26) Rizzi, G. A.; Casarin, M.; Tondello, E.; Piraino, P.; Granozzi, G. UV Photoelectron Spectra and Calculations on Diatomic Rhodium Formamidinate Complexes. *Inorg. Chem.* **1987**, *26*, 3406-3409.

(27) Piraino, P.; Bruno, G.; Lo Schiavo, S.; Laschi, F.; Zanello, P. Synthesis, X-Ray Crystal Structure, and Electrochemical Properties of the Dirhodium(4+) Complex $Rh_2(form)_4$ (form = N,N'-Di-p-tolylformamidinate Anion). *Inorg. Chem.* **1987**, *26*, 2205-2211.

(28) Cotton, F. A.; Feng, X. Electronic Structures of the $Ru_2(RNNNR)_4$, $Rh_2(RNCHNR)_4$, and $Co_2(RNNNR)_4$ Molecules: Ordering and Separation of M-M δ* and π* Orbitals. *Inorg. Chem.* **1989**, *28*, 1180-1183.

(29) Bear, J. L.; Yao, C. L.; Lifsey, R. S.; Korp, J. D.; Kadish, K. M. Electrochemical, Spectroscopic, and Structural Characterization of Rh2(Dpf)4, Rh2(Dpf)4(Ch3cn), and $[Rh_2(dpf)_4(CH_3CN)]ClO_4$, Where dpf = N,N'-Diphenylformamidinate(1-). *Inorg. Chem.* **1991**, *30*, 336-340.

(30) He, L. P.; Yao, C. L.; Naris, M.; Lee, J. C.; Korp, J. D.; Bear, J. L. Molecular-Structure and Chemical and Electrochemical Reactivity of Co2(Dpb)4 and Rh2(Dpb)4 (Dpb = N,N'-Diphenylbenzamidinate). *Inorg. Chem.* **1992**, *31*, 620-625.

(31) Dequeant, M. Q.; Bradley, P. M.; Xu, G.-L.; Lutterman, D. A.; Turro, C.; Ren, T. Dirhenium Paddlewheel Compounds Supported by N,N'-Dialkylbenzamidinates: Synthesis, Structures, and Photophysical Properties. *Inorg. Chem.* **2004**, *43*, 7887-7892.

(32) Bear, J. L.; Han, B. C.; Li, Y. L.; Ngubane, S.; Van Caemelbecke, E.; Kadish, K. M. Synthesis, Spectroscopic Properties and Electrochemistry of Rh(2)(ap)(4)(R) where R = CH(3) or C(6)H(5) and ap=2-Anilinopyridinate Anion. *Polyhedron* **2009**, *28*, 1551-1555.

(33) Bear, J. L.; Van Caemelbecke, E.; Ngubane, S.; Da-Riz, V.; Kadish, K. M. Electrosynthesis of Rh(2)(dpf)(4)(R) where dpf = N,N '-Diphenylformamidinate Anion and R = CH(3), C(2)H(5), C(3)H(7), C(4)H(9) or C(5)H(11). *Dalton Trans.* **2011**, *40*, 2486-2490.

(34) Liu, L. M.; Bear, J. L. Photochemical Oxidation Studies of Dinuclear Rhodium (d(7)-d(7)) Complexes of Dinitrogen Bridging Ligands With Halohydrocarbons. *Acta Phys.-Chim. Sin.* **1989**, *5*, 644-651.

(35) Ren, T.; Lin, C.; Valente, E. J.; Zubkowski, J. D. The Influence of Remote Substituent in Tetrakis(μ-N,N′-diarylformamidinato)–dirhodium(II) Compounds.

Part 7. Linear Free Energy Relationships in Dinuclear Compounds. *Inorg. Chim. Acta* **2000**, *297*, 283-290.

(36) Lutterman, D. A.; Degtyareva, N. N.; Johnston, D. H.; Gallucci, J. C.; Eglin, J. L.; Turro, C. Photoinduced One-Electron Reduction of Alkyl Halides by Dirhodium(II,II) Tetraformamidinates and a Related Complex with Visible Light. *Inorg. Chem.* **2005**, *44*, 5388-5396.

(37) Li, Z.; Leed, N. A.; Dickson-Karn, N. M.; Dunbar, K. R.; Turro, C. Directional Charge Transfer and Highly Reducing and Oxidizing Excited States of New Dirhodium(ii,ii) Complexes: Potential Applications in Solar Energy Conversion. *Chem. Sci.* **2014**, *5*, 727-737.

(38) Bear, J. L.; Han, B.; Wu, Z.; Van Caemelbecke, E.; Kadish, K. M. Synthesis, Electrochemistry, and Spectroscopic Characterization of Bis-dirhodium Complexes Linked by Axial Ligands. *Inorg. Chem.* **2001**, *40*, 2275-2281.

(39) Cotton, F. A.; Lin, C.; Murillo, C. A. The Use of Dimetal Building Blocks in Convergent Syntheses of Large Arrays. *Proc. Natl. Acad. Sci. U.S.A.* **2002**, *99*, 4810-4813.

(40) Handa, M.; Yasuda, M.; Muraki, Y.; Yoshioka, D.; Mikuriya, M.; Kasuga, K. Polymer and "Trimer-of-Dimers" Complexes Derived from [Rh2(form)4] (form− = N,N′-Di-p-tolylformamidinate anion) and 1,4-Diisocyanobenzene. *Chem. Lett.* **2003**, *32*, 946-947.

(41) Zuo, J.-L.; Fabrizi de Biani, F.; Santos, A. M.; Kohler, K.; Kuehn, F. E. 4-Ethynylpyridine as a Bridging Moiety in Mixed Rh/Re Complexes. *Eur. J. Inorg. Chem.* **2003**, 449-452.

(42) Chartrand, D.; Hanan, G. S. Facile Synthesis of Multinuclear Complexes Based on a Tetra(4-pyridyl)amidinate Dirhodium(II) Dimer. *Chem. Commun.* **2008**, 727-729.

(43) Cooke, M. W.; Santoni, M. P.; Hanan, G. S.; Proust, A.; Hasenknopf, B. A Divergent Strategy for Covalently-tethered $(tpy)_2Ru(II)$ Systems Based on $Rh_2(N,N'$-diphenylbenzamidinates$)_4$. *Dalton Trans.* **2009**, 3671-3673.

(44) Chartrand, D.; Hanan, G. S. Rhodium Amidinate Dimers as Structural and Functional Hubs for Multimetallic Assemblies. *Inorg. Chem.* **2014**, *53*, 624-636.

(45) Suzuki, A. Synthetic Studies via the Cross-coupling Reaction of Organoboron Derivatives with Organic Halides. *Pure Appl. Chem.* **1991**, *63*, 419-422.

(46) Miyaura, N.; Suzuki, A. Palladium-Catalyzed Cross-Coupling Reactions of Organoboron Compounds. *Chem. Rev. (Washington, D. C.)* **1995**, *95*, 2457-2483.

(47) Cross-Coupling Reactions of Organoboron Compounds with Organic Halides. In Metal-Catalyzed Cross-Coupling Reactions, Diederich, F.; Stang, P. J., Eds.; Wiley-VCH: Weinheim, Germany,1998; pp 49-97.

(48) Suzuki, A. Recent Advances in the Cross-coupling Reactions of Organoboron Derivatives with Organic Electrophiles, 1995-1998. *J. Organomet. Chem.* **1999**, *576*, 147-168.

(49) Suzuki, A. Organoborane Coupling Reactions (Suzuki coupling). *Proc. Jpn. Acad., Ser. B* **2004**, *80*, 359-371.

(50) Suzuki, A.; Yamamoto, Y. Cross-Coupling Reactions of Organoboranes: an Easy Method for C-C Bonding. *Chem. Lett.* **2011**, *40*, 894-901.
(51) Fang, Y.-Q.; Polson, M. I. J.; Hanan, G. S. Creating New Binding Sites in Ligands and Metal Complexes Using the Negishi Cross-Coupling Reaction. *Inorg. Chem.* **2003**, *42*, 5-7.
(52) Polson, M. I. J.; Lotoski, J. A.; Johansson, K. O.; Taylor, N. J.; Hanan, G. S.; Hasenknopf, B.; Thouvenot, R.; Loiseau, F.; Passalaqua, R.; Campagna, S. Symmetric and Asymmetric Coupling of Pyridylpyrimidine for the Synthesis of Polynucleating Ligands. *Eur. J. Inorg. Chem.* **2002**, 2549-2552.
(53) Johansson, K. O.; Lotoski, J. A.; Tong, C. C.; Hanan, G. S. Toward High Nuclearity Ruthenium Complexes: Creating New Binding Sites in Metal Complexes. *Chem. Commun.* **2000**, 819-820.
(54) Hansch, C.; Leo, A.; Taft, R. W. A Survey of Hammett Substituent Constants and Resonance and Field Parameters. *Chem. Rev.* **1991**, *91*, 165-195.
(55) Johnson, C. D. *The Hammett Equation*; Cambridge University Press: Cambridge, 1973.
(56) Ren, T. Substituent Effects in Dinuclear Paddlewheel Compounds: Electrochemical and Spectroscopic Investigations. *Coord. Chem. Rev.* **1998**, *175*, 43-58.
(57) Pirrung, M. C.; Morehead, A. T., Jr. Electronic Effects in Dirhodium(II) Carboxylates. Linear Free Energy Relationships in Catalyzed Decompositions of Diazo Compounds and CO and Isonitrile Complexation. *J. Am. Chem. Soc.* **1994**, *116*, 8991-9000.
(58) Connelly, N.; Geiger, W. Chemical Redox Agents for Organometallic Chemistry. *Chem. Rev.* **1996**, *96*, 877-1787.
(59) Barder, T. E.; Walker, S. D.; Martinelli, J. R.; Buchwald, S. L. Catalysts for Suzuki-Miyaura Coupling Processes: Scope and Studies of the Effect of Ligand Structure. *J. Am. Chem. Soc.* **2005**, *127*, 4685-4696.
(60) Coudret, C.; Mazenc, V. Heteroarylation of Anthraquinone-triflate by Suzuki Cross-coupling. *Tetrahedron Lett.* **1997**, *38*, 5293-5296.
(61) Takahashi, Y.; Ito, T.; Sakai, S.; Ishii, Y. Novel Palladium(0) Complex; Bis(dibenzylideneacetone)palladium(0). *J. Chem. Soc. D* **1970**, 1065-1066.
(62) Cooke, M. W. The Synthesis and Characterization of Dirhodium(II,II) Templated Photoactive Assemblies. Ph.D. Dissertation, Université de Montréal, 2007.
(63) Frisch, M. J.; Trucks, G. W.; Schlegel, H. B.; Scuseria, G. E.; Robb, M. A.; Cheeseman, J. R.; Montgomery, J. A., Jr.; Vreven, T.; Kudin, K. N.; Burant, J. C. *et al.*; *Gaussian 03*, revision C.02, Gaussian, Inc.: Wallingford, CT, 2004.
(64) Frisch, M. J.; Trucks, G. W.; Schlegel, H. B.; Scuseria, G. E.; Robb, M. A.; Cheeseman, J. R.; Scalmani, G.; Barone, V.; Mennucci, B.; Petersson, G. A. *et al.*; *Gaussian 09*, revision D.01, Gaussian, Inc.: Wallingford, CT, 2009.
(65) Lee, C.; Yang, W.; Parr, R. G. Development of the Colle-Salvetti Correlation-Energy Formula into a Functional of the Electron Density. *Phys. Rev. B: Condens. Matter Mater. Phys.* **1988**, *37*, 785-789.

(66) Becke, A. D. Density-functional Thermochemistry. III. The Role of Exact Exchange. *J. Chem. Phys.* **1993**, *98*, 5648-5652.
(67) Hay, P. J.; Wadt, W. R. Ab Initio Effective Core Potentials for Molecular Calculations. Potentials for Potassium to Gold Including the Outermost Core Orbitals. *J. Chem. Phys.* **1985**, *82*, 299-310.
(68) Ehlers, A. W.; Boehme, M.; Dapprich, S.; Gobbi, A.; Hoellwarth, A.; Jonas, V.; Koehler, K. F.; Stegmann, R.; Veldkamp, A.; A Set of f-Polarization Functions for pseudopotential basis sets of the transition metals Sc-Cu, Y-Ag and La-Au. *Chem. Phys. Lett.* **1993**, *208*, 111-114.
(69) Cossi, M.; Rega, N.; Scalmani, G.; Barone, V. Energies, Structures, and Electronic Properties of Molecules in Solution with the C-PCM Solvation Model. *J. Comput. Chem.* **2003**, *24*, 669-681.
(70) Dennington II, R.; Keith, T.; Millam, J.; Eppinnett, K.; Hovell, W. L.; Gilliland, R. *Gaussview* 3.09, Semichem, Inc.: Shawnee Mission, KS, 2003.
(71) O'Boyle, N. M.; Tenderholt, A. L.; Langner, K. M. Software News and Updates cclib: A Library for Package-independent Computational Chemistry Algorithms. *J. Comput. Chem.* **2008**, *29*, 839-845.
(72) Skripnikov, L. V; *Chemissian*; Leonid V. Skripnikov: St. Petersubrg, Russia, 2005.
(73) Sheldrick, G. M. *SADABS*, version 2008/1; Bruker AXS Inc.: Madison, WI, 2008.
(74) *SAINT*, version 7.68A; Bruker AXS Inc.: Madison, WI, 2009.
(75) Sheldrick, G. M.; *TWINABS*; Bruker AXS Inc.: Madison, WI, 2001.
(76) Sheldrick, G. M. A Short History of SHELX. *Acta Crystallogr., Sect. A: Found. Crystallogr.* **2008**, *A64*, 112-122.
(77) Macrae, C. F.; Bruno, I. J.; Chisholm, J. A.; Edgington, P. R.; McCabe, P.; Pidcock, E.; Rodriguez-Monge, L.; Taylor, R.; van, d. S. J.; Wood, P. A. Mercury CSD 2.0 - New Features for the Visualization and Investigation of Crystal Structures. *J. Appl. Crystallogr.* **2008**, *41*, 466-470.
(78) Farrugia, L. J. ORTEP-3 for Windows - A Version of ORTEP-III with a Graphical User Interface (GUI). *J. Appl. Crystallogr.* **1997**, *30*, 565.
(79) *POV-Ray*, version 3.6; Persistence of Vision Pty. Ltd.: Williamstown, Victoria, Australia, 2004.
(80) Caulder, D. L.; Raymond, K. N. Supermolecules by Design. *Acc. Chem. Res.* **1999**, *32*, 975-982.
(81) Caulder, D. L.; Raymond, K. N. The Rational Design of High Symmetry Coordination Clusters. *J. Chem. Soc., Dalton Trans.* **1999**, 1185-1200.
(82) Fleischer, E. B.; Shachter, A. M. Coordination Oligomers and a Coordination Polymer of Zinc Tetraarylporphyrins. *Inorg. Chem.* **1991**, *30*, 3763-3769.
(83) Alessio, E.; Macchi, M.; Heath, S. L.; Marzilli, L. G. Ordered Supramolecular Porphyrin Arrays from a Building Block Approach Utilizing Pyridylporphyrins and Peripheral Ruthenium Complexes and Identification of a New Type of Mixed-Metal Building Block. *Inorg. Chem.* **1997**, *36*, 5614-5623.

(84) Casanova, M.; Zangrando, E.; Iengo, E.; Alessio, E.; Indelli, M. T.; Scandola, F.; Orlandi, M. Structural and Photophysical Characterization of Multichromophoric Pyridylporphyrin-Rhenium(I) Conjugates. *Inorg. Chem.* **2008**, *47*, 10407-10418.

(85) The choice of resonance parameter is determined by the propriety or reaction studied; for example, an oxidation should use a σR+ value, since it takes into account enhanced resonance for a para π-electron acceptor. Similarly, a reduction should favor the σR- parameter, since it is for enhanced resonance of the para π-electron donor.

(86) Schafman, B. S.; Wenthold, P. G. Regioselectivity of Pyridine Deprotonation in the Gas Phase. *J. Org. Chem.* **2007**, *72*, 1645-1651.

(87) Deady, L. W.; Shanks, R. A. Determination of the Sigma Zero Constant for the Pyridine Aza Group. *Aust. J. Chem.* **1972**, *25*, 431-432.

Chapitre 4 : Rhodium Amidinate Dimers as Structural and Functional Hubs for Multimetallic Assemblies

4.1. Résumé

Ce chapitre porte sur l'étude d'assemblages de dimères de rhodium tétra-*N*,*N*'-diphénylisonicotamidinate avec des chromophores de rhénium de type 2,2'-bipyridine tris carbonyle liés à travers le groupement pyridyle. Les propriétés photophysiques et électrochimiques des différents composés obtenus (mono-, bis-, tris- et tétrarhénium) ont été analysées.

La structure de deux de ces assemblages a été élucidée, établissant un point de départ pour la modélisation moléculaire de DFT. Celle-ci a été utilisée pour étudier les propriétés redox des assemblages. Cependant, des lacunes dans l'énergie des orbitales moléculaires calculées ont été décelées pour le système comprenant quatre chromophores de rhénium. Cela est possiblement causé par la présence d'une charge 4+ sur le système.

Les calculs TD-DFT ont permis d'établir une corrélation entre les transitions impliquées et les données spectrales de ces assemblages. La coordination axiale sur le dimère de rhodium d'une molécule d'acétonitrile a été modélisée, permettant de connaître la nature des nouvelles transitions électroniques observées. Cela a permis de conclure que la transition la plus basse en énergie devient le MLCT ou M_2LCT. Le dimère n'ayant qu'un seul chromophore de rhénium possède un spectre particulier avec de nouvelles bandes d'absorption près de la bande M_2LCT attendue. Celles-ci furent identifiées comme étant des bandes M_2LCT localisées soit sur l'amidinate contenant le chromophore de rhénium, soit sur les autres amidinates.

Les chromophores liés au dimère ne changent pas de propriétés spectrales. Ils sont très similaires au complexe de rhénium ne possédant qu'un groupement pyridine. Cependant, leur émission est désactivée par le dimère de rhodium.

Contribution :

Daniel Chartrand : Tous les travaux présentés dans l'article ainsi que sa rédaction.

Garry S. Hanan : Supervision et révision de l'article.

Rhodium Amidinate Dimers as Structural and Functional Hubs for Multimetallic Assemblies

*Daniel Chartrand, Garry S. Hanan**

Department of Chemistry, Université de Montréal, Montréal, QC, H3T 1J4 Canada

* Tel: 1-514-340-5156. Fax: 1-514-343-7586.

Received: 4 November 2013; Published: 17 December 2013

dx.doi.org/10.1021/ic4024585

Reproduced with permission from *Inorg. Chem*. **2014**, 53, 624−636.

KEYWORDS: rhodium, rhenium, chromophores, Photophysics, Electrochemistry, Density functional theory, Solvatochromism.

4.2. Table of Content Graphic

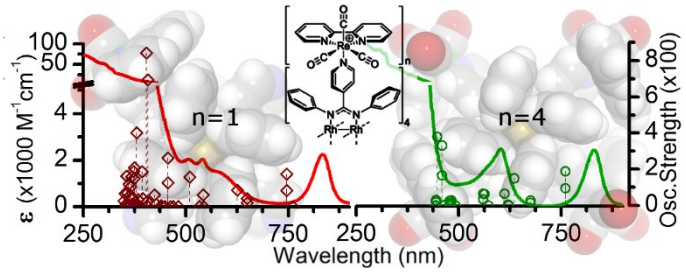

One to four *fac*-[Re(bpy)(CO)$_3$]$^+$ chromophores were grafted to a dirhodium tetra-*N*,*N*'-diphenylisonicotinamidinate dimer through its 4-pyridyl moieties. Spectral and electrochemical changes were observed to the dimer base properties. Extended calculations were performed to model these spectral changes, including a solvatochromism effect with acetonitrile. The chromophore emission was reductively quenched by electron transfer from the dirhodium core to the Re(bpy) MLCT state.

4.3. Abstract

The synthesis and characterization of multichromophore assemblies based on a dirhodium tetra-*N*,*N*'-diphenylisonicotinamidinate dimer are reported. The pyridyl moieties were used to coordinate up to four positively charged rhenium(I) chromophores of the form *fac*-[Re(bpy)(CO)$_3$**L**]PF$_6$ (bpy= 2,2'-bipyridine, **L** = a pyridyl group on the Rh_2 dimer). The mono-, bis-, tris- and tetrarhenium assemblies were isolated by size-exclusion chromatography and their spectroscopic and electrochemical properties were studied and compared with DFT and time-dependent (TD) DFT models of the original rhodium dimer and the mono- and tetrarhenium assembly. The rhenium chromophores modify the properties of the rhodium dimer: for example, the first oxidation of the Rh_2 dimer (Rh−Rh δ* orbital) increased from the original 210 mV versus SCE in acetonitrile, by 45 mV per rhenium complex added, finishing at 390 mV for the tetrarhenium complex. The rhodium dimer displays solvatochromism with acetonitrile (MeCN) due to the formation of an axial adduct and has an association constant that increased by a factor of 3.8 when the dimer has four rhenium chromophores. The absorption data clearly exhibited the cumulative effect of the addition of rhenium chromophores in the 230 to 400 nm range. The main visible band, a metal-dimer-to-ligand charge transfer (^1M_2LCT) transition determined by TD-DFT, red-shifts from 541 nm to 603 nm, while the main near-IR band, a $^1Rh_2(\pi^* \rightarrow \sigma^*)$ transition, has a small blue-shift (~26 cm^{-1}/Re), varying from 837 to 831 nm upon addition of the four Re(I) chromophores. This was observed in TD-DFT also with a total shift of 105 cm^{-1} for the tetrarhenium assembly. In terms of emission, the rhenium excited state was completely quenched upon coordination to the dimer, suggesting fast electron transfer of the rhodium dimer. All other aspects of the rhenium chromophore are similar to the parent complex where **L** = pyridine, showing similar redox couples and additive spectral characteristics.

4.4. Introduction

The rhodium dimer with its paddle-wheel motif is greatly affected by the nature of its four ligands.[1] Its tetra-acetate and tetracarboxamidinate forms are effective catalysts,[2] its bis-acetate form has anticancer properties,[3] and in general it serves as a building block for supramolecular assemblies.[4] Amidinate based rhodium dimers have a chemistry of their own and have been studied for the last 30 years.[5] They are in general more inert than their acetate analogues, but still possess rich electrochemistry and photochemistry, making them an interesting choice from which to build polynuclear complexes.[6]

Rhenium triscarbonyl diimine chromophores also possess a very rich history due to their high stability, high energy excited state, and capacity for reductive and oxidative quenching of their excited state.[7] They can also be functionalized to form supramolecular assemblies.[6a,6b] As such they are good candidates for functional assemblies, since they can act as photosensitizers that supply electrons for catalysts (e.g., hydrogen evolution),[8] as photocatalysts that reduce carbon dioxide to carbon monoxide,[9] or as photosensitizers for other processes, such as photoisomerisation.[10] The rhenium archetype used in this study is $[Re(bpy)(CO)_3L]^+$, where bpy = 2,2'-bipyridine and L is a neutral ligand.

In natural photosynthetic systems, light energy is gathered by light-harvesting antennae and is subsequently transferred to a reaction center.[11] Our approach to gather light energy involves attaching chromophores to the paddle-wheel motif of the rhodium dimer, thus grafting up to four chromophores in a very close space with a strict 90° angle between each metal center, similar to tetrapyridylporphyrin assemblies.[12] Both tetra -amidinate and tetra -acetate rhodium dimers have been designed to incorporate functional groups able to bond to metal ions.[6a,6b,13] The tetra -amidinate dimers were found to be more robust and allowed subsequent reactions to be performed on the metal dimer.[6a] We have already demonstrated the use of isonicotinic amidinate rhodium dimers to assemble four rhenium chromophores, but since the dimers themselves are not known as active catalysts, unsaturated assemblies (one to three chromophores) are more promising as they intrinsically possess further coordination sites to make larger assemblies of chromophores or even complete photocatalytic systems. The properties of these four units, **4-1** to **4-4** as seen in Chart 4.1 (full in Chart 4.S1), are presented herein, with a focus on the effect on the dimer core upon addition of each rhenium chromophore and the coordination of axial acetonitrile. To this end,

theoretical calculations were also performed to establish and correlate the structural and functional properties of the assemblies.

Chart 4.1. Rh_2 Complexes **4-1** to **4-5** Synthesized in This Study and Side-View with an MeCN Adduct.

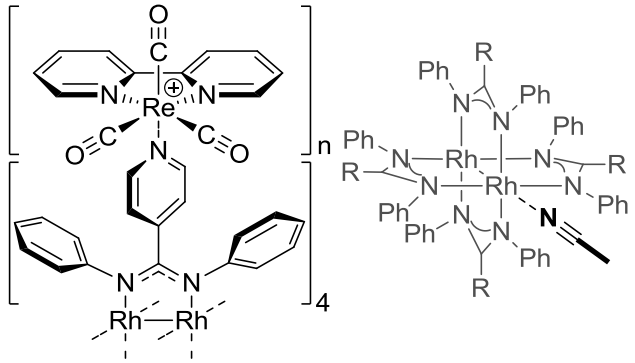

4-1, n = 1; **4-2**, n = 2; **4-3**, n = 3; **4-4**, n=4; **4-5**, n = 0.

4-n+MeCN

4.5. Experimental Section

4.5.1. General Considerations

The organic reagents were obtained from Sigma Aldrich, rhenium carbonyl and rhodium(II) acetate from Pressure Chemical Co., and solvents from Fischer and Anachemia. All were used as received. IR spectra were recorded on solid samples using a diamond ATR Perkin-Elmer Spectrum 100 FT-IR. Nuclear magnetic resonance spectra were recorded using Bruker spectrometers (300, 400 and 700 MHz) at room temperature, with ^{1}H and ^{13}C chemical shifts referenced to residual solvent resonances (1.94 and 1.24 ppm, respectively, for CD_3CN). Elemental analyses were performed on the desolvated bulk samples by the university departmental service. All photophysical measurements were done in air-equilibrated solvents, using a borosilicate cell. Absorption and emission spectra were recorded at room temperature using a Cary 500i UV−vis−NIR spectrophotometer and a Cary Eclipse 300 fluorimeter, respectively. Association constants were measured by titration of acetonitrile and were calculated using multiple wavelengths with the HypSpec software suite.[14] The emission spectra used the maximum of absorption of the lowest energy band of the sample as excitation wavelength. Electrochemical measurements were carried out in argon-purged solvent at room temperature with a BAS CV50W multipurpose apparatus. The

working electrode was a Pt electrode, the counter electrode was a Pt wire, and the pseudoreference electrode was a silver wire. The reference was set using an internal 1.0 mM ferrocene sample with its redox couple adjusted to 400 mV versus SCE in acetonitrile and 460 mV versus SCE in dichloromethane.[15] The concentration of the compounds was about 1.0 mM, tetrabutylammonium hexafluorophosphate (TBAP) was used as supporting electrolyte, and its concentration was 0.10 M. Cyclic voltammograms were obtained at scan rates of 10, 100, and 200 mV/s. For reversible processes, half-wave potentials (vs SCE) were measured as the average potential of the anodic and cathodic peak and compared with square wave voltammetry (SWV) experiments performed with a step rate of 4 mV, a square wave amplitude of 25 mV, and a frequency of 15 Hz. For irreversible oxidation processes, the cathodic peak was used as E, and the anodic peak was used for irreversible reduction processes. The criteria for reversibility were the separation of 60 mV between cathodic and anodic peaks, the close to unity ratio of the intensities of the cathodic and anodic currents, and the constancy of the peak potential on changing scan rate. Experimental uncertainties are as follows: absorption maxima, ±2 nm; molar absorption coefficient, 10%; emission maxima, ± 5 nm; redox potentials, ± 10 mV.

4.5.2. Synthetic Methods

The rhenium complexes $Re(CO)_5Br$,[16] *fac*-$[Re(bpy)(CO)_3Br]$,[17] *fac*-$[Re(bpy)(CO)_3(CH_3CN)][PF_6]$,[18] *fac*-$[Re(bpy)(CO)_3(pyridine)][PF_6]$[18] (**4-8**), and *fac*-$[Re(bpy)(CO)_3(THF)][PF_6]$[19] were prepared as described. The syntheses of the tetra(*N*,*N*'-diphenylisonicotinamidinate)dirhodium(II) dimer (**4-5**) and the tetra-$[Re(bpy)(CO)_3]-[Rh_2(dppy)_4]$ tetrahexafluorophosphate (**4-4**) were previously published by our group, with a more complete characterization given herein.[6b] See Figure 4.5 (top) for the labeling of the proton peaks in NMR.

General conditions for the synthesis of **4-1**, **4-2**, **4-3** and **4-4**: To a 50 mL round-bottomed flask were added **4-5** (0.312 g, 0.241 mmol) and $[Re(bpy)(CO)_3(NCCH_3)]PF_6$ (0.470 g (0.767 mmol) in acetone (20 mL). The solution was heated at reflux and was monitored by TLC. After 2 h, reaction equilibrium was reached (TLC R_f (7 CH_3CN:1 KNO_3(aq) (v/v)): 0.75 (**4-5**); 0.70 (**4-1**); 0.68 (**4-2**); 0.62 (**4-3**); 0.60 (**4-4**)). The solution was evaporated to dryness at room temperature and purified by multiple size-exclusion chromatography columns (Sephadex-LH20 gel; column: 3 cm diameter by 1.2 m length; solvent: 0.45

acetonitrile/0.45 methanol/0.1 water (v/v/v)), flow rate: 30 mL per hour, total elution time to first fraction: 16 h). The fractions were treated with dilute aqueous KPF_6 (5% of volume); then the solvent was reduced until precipitation of a green solid, which was filtered and washed with water and then dried under vacuum. Alternate synthesis: Using $[Re(bpy)(CO)_3(THF)]PF_6$ in dichloromethane yields comparable results, but in this case the reaction was left 18 h at room temperature.

(*N*''-(2,2'-Bipyridinetricarbonyl-rhenium(I))-*N*,*N*'-diphenylisonicotinamidinate)-tris(*N*,*N*'-diphenylisonicotinamidinate)dirhodium(II,II) Hexafluorophosphate, 4-1. Quantities of starting product: **4-5**, 0.354 g (0.273 mmol); $[Re(bpy)(CO)_3(NCCH_3)]PF_6$, 0.470 g (0.767 mmol). Yield: 23% (0.118 g, 0.0632 mmol). ^{1}H NMR (700 MHz, CD_3CN): δ 9.04 (ddd, *J* = 5.5, 1.4, 0.8 Hz, 1H, Hw), 8.99 (ddd, *J* = 5.3, 1.4, 0.8 Hz, 1H: Hw'), 8.32 (d, *J* = 8.0 Hz, 1H: Hv), 8.28 (ddd, *J* = 8.0, 7.5, 1.5 Hz, 1H: Hy), 8.25 (d, *J* = 7.5 Hz, 1H: Hv'), 8.23 (ddd, *J* = 8.2, 7.5, 1.5 Hz, 1H: Hy'), 8.04−8.00 (m, 6H: Ha'), 7.73 (ddd, *J* = 7.5, 5.5, 1.5 Hz, 1H: Hx), 7.67 (d, *J* = 6.8 Hz, 2H: Ha), 7.64 (ddd, *J* = 7.5, 5.5, 1.5 Hz, 1H: Hx'), 6.99 (br, 8H:He,He'), 6.96-6.82 (m, 22H: Hd',Hf), 6.81−6.79 (m, *J* = 5.3 Hz, 4H: Hd), 6.76 (dd, *J* = 10, 5.5 Hz, 4H: *cis*Hb'), 6.68 (d, *J* = 4.8 Hz, 2H: *trans*Hb'), 6.59 (d, *J* = 6.7 Hz, 2H: Hb), 6.52 (br, 2H: Hc), 5.91 (br, 6H: Hf'), 5.76 (br, 2H: Hf). ^{13}C{^{1}H} NMR (176 MHz, CD_3CN): δ 196.5; 192.5; 170.8; 170.6; 167.9; 156.1; 156.0; 154.7; 154.5; 152.4; 152.3; 151.7; 151.5; 149.68; 149.66; 149.63; 149.61; 149.5; 148.5; 144.5; 144.4; 142.2; 142.0; 129.9; 129.8; 129.7; 129.4; 128.9; 128.6; 126.57; 126.52; 125.34; 125.32; 124.7; 124.3; 124.1. HRMS (ESI, CH_3CN) (m/z): $[M-PF_6]^+$ ($C_{85}H_{64}N_{14}O_3ReRh_2$) calcd 1721.2948; found 1721.2961. IR (ATR, cm^{-1}): ν_{CO} 2032s, 1930sh, 1915s; ν_{PF} 838s. Anal. Calcd for $C_{85}H_{64}F_6N_{14}O_3PReRh_2$+DMSO: C, 5374; H, 3.63; N, 10.08; S, 1.65. Found: C, 53.56; H, 3.15; N, 9.94, S, 1.38.

Bis(*N*''-(2,2'-bipyridinetricarbonyl-rhenium(I))-*N*,*N*'-diphenylisonicotinamidinate)-bis(*N*,*N*'-diphenylisonicotinamidinate)dirhodium(II,II) Bis (hexafluorophosphate), 4-2. Quantities of starting product: **4-5**, 0.354 g (0.273 mmol); $[Re(bpy)(CO)_3(NCCH_3)]PF_6$, 0.470 g (0.767 mmol). Yield: 13 % (0.0859 g, 0.0352 mmol). ^{1}H NMR (700 MHz, CD_3CN): δ 9.27 (d, *J* = 4.5 Hz, 2H: Hw), 9.17 (d, *J* = 4.0 Hz, 2H: Hw'), 8.70-8.58 (m, 4H: Hz, Hv'), 8.50−8.35 (m, 4H: Hy, Hy'), 8.11−7.99 (m, 8H: Ha, Ha'), 7.98−7.86 (m, 2H: Hx), 7.79 (t, *J* = 6.0 Hz, 2H: Hx'), 7.08-6.81 (m, 24H: Hd, Hd', He, He'), 6.79−6.71 (m, 2H: Hb'), 6.71−6.65 (m, 2H: Hb), 6.62−6.13 (br, 8H: Hc), 6.13-5.44 (br, 8H: He). ^{13}C{^{1}H} NMR

(176 MHz, CD_3CN): δ 96.48; 196.46; 192.5; 156.11; 156.09; 156.03; 156.02; 154.7; 154.5; 151.76; 151.72; 151.70; 149.52; 149.47; 149.42; 149.41; 149.37; 149.28; 142.17; 142.14; 142.00; 141.98; 129.7; 129.40; 129.38; 128.7; 125.34; 125.32; 124.8; 124.5. HRMS (ESI, CH_3CN) (m/z): $[M-PF_6]^+$ ($C_{98}H_{72}F_6N_{16}O_6PRe_2Rh_2$) calcd 2293.2682; found 2293.2577. IR (ATR, cm^{-1}): ν_{CO} 2031s, 1930sh, 1910s; ν_{PF} 834s. Anal. Calcd for $C_{98}H_{72}F_{12}N_{16}O_6P_2Re_2Rh_2$: C, 48.28; H, 2.98; N, 9.19. Found: C, 48.10; H, 2.99; N, 9.16.

Tris(*N*''-(2,2'-bipyridinetricarbonyl-rhenium(I))-*N*,*N*'-diphenylisonicotinamidinate)-(*N*,*N*'-diphenylisonicotinamidinate)dirhodium(II,II) Tris (hexafluorophosphate), 4-3. Quantities of starting product: **4-5**, 0.100 g (0.072 mmol); $[Re(bpy)(CO)_3(THF)]PF_6$, 0.154 g (0.239 mmol). Yield: 27% (0.062 g, 0.021 mmol). ^1H NMR (700 MHz, CD_3CN): δ 9.04 (dd, *J* = 6.0, 1.5 Hz, 1H, *trans* Hw), 9.02 (dd, *J* = 5.5, 1.0 Hz, 2H: *cis* Hw), 9.00−8.98 (m, 1H: *trans* Hw'), 8.98 (dd, *J* = 5.5, 1.5 Hz, 2H: *cis* Hw'), 8.42 (d, *J* = 8.0 Hz, 1H: *trans* Hv), 8.37 (d, *J* = 8.0 Hz, 2H: *cis* Hv), 8.35 (d, *J* = 8.0 Hz, 1H: *trans* Hv'), 8.31−8.29 (m, 3H: *cis* Hv', *trans* Hy), 8.28 (td, *J* = 8.0, 1.5 Hz, 2H: *cis* Hy), 8.24 (td, *J* = 8.0, 1.5 Hz, 1H: *trans* Hy'), 8.22 (td, *J* = 8.0, 1.5 Hz, 2H: *cis* Hy'), 8.01 (br, 2H: Ha'), 7.74 (ddd, *J* = 7.5, 5.5, 1.0 Hz, 1H: *trans* Hx), 7.76 (ddd, *J* = 7.5, 5.5, 1.0 Hz, 1H: *cis* Hx), 7.66 (td, *J* = 5.5, 1.0 Hz, 1H: *trans* Hx'), 7.65−7.64 (m, 4H: *cis* Hx', *trans* Ha), 7.63 (d, *J* = 6.4 Hz, 4H: *cis* Ha), 6.93−6.91 (m, 6H: Hd', *trans* He), 6.89−6.85 (m, 6H:*cis* He, He'), 6.83 (t, *J* = 7.0 Hv 4H: *trans* Hd), 6.80−6.77 (m, 8H: *cis* Hd), 6.63−6.58 (br, 2H: Hb'), 6.52 (d, *J* = 6.0 Hz, 2H: *trans* Hb), 6.51−6.45 (br, 2H: Hc'), 6.44 (t, *J* = 6.2 Hz, 4H: *cis* Hb), 6.39−6.30 (br, 4H: *cis* Hc), 6.30−6.22 (br, 2H: *trans* Hc), 5.80−5.66 (br, 2H: Hf'), 5.65−6.55 (br, 6H, Hf). NOTE: *trans* refers to the rhenium complex *trans* to the free pyridyl, and *cis* refers to the rhenium complexes *cis* to the free pyridyl of the dimer. Peaks noted br are broad. $^{13}C\{^1H\}$ NMR (176 MHz, CD_3CN): δ 196.61; 196.59; 192.6; 170.7; 168.3; 168.2; 156.26; 156.22; 156.15; 156.13; 156.78; 154.75; 154.6; 151.97; 151.90; 151.8; 151.2; 151.1; 149.5; 148.3; 144.5; 142.3; 142.19; 142.12; 141.0; 133.9; 129.8; 129.64; 129.62; 129.56; 129.53; 129.4; 129.3; 128.9; 128.8; 128.6; 126.7; 125.62; 125.56; 125.52; 125.0; 124.9; 124.5. HRMS (ESI, CH_3CN) (m/z): $[M-PF_6]^{+2}$ ($C_{111}H_{80}F_6N_{18}O_9PRe_3Rh_2$) calcd 1360.1384; found 1360.1380. IR (ATR, cm^{-1}): ν_{CO} 2030s, 1930sh, 1905s; ν_{PF} 833s. Anal. Calcd for $C_{111}H_{80}F_{18}N_{18}O_9P_3Re_3Rh_2$: C, 44.30; H, 2.68; N, 8.38. Found: C, 44.35; H, 2.78; N, 8.38.

Tetrakis((*N*''-(2,2'-bipyridinetricarbonyl-rhenium(I))-*N*,*N*'-diphenyl-isonicotinamidinate)dirhodium(II,II) Tetrakis (hexafluorophosphate), 4-4. Quantities of starting product: **4-5**, 0.312 g (0.241 mmol); $[Re(bpy)(CO)_3(THF)]PF_6$, 1.376 g (2.247 mmol). Yield: 50% ^{1}H NMR (700 MHz, CD_3CN): δ 9.05 (ddd, *J* = 5.5, 1.5, 1.0 Hz, 4H: Hw), 9.01 (ddd, *J* = 5.0, 1.5, 1.0 Hz, 4H: Hw'), 8.34 (ddd, *J* = 8.0, 1.0, 0.5 Hz, 4H: Hv), 8.31 (ddd, *J* = 8.0, 7.0, 1.50 Hz, 4H: Hy), 8.27 (ddd, *J* = 8.0, 1.5, 0.5 Hz, 4H: Hv'), 8.25 (ddd, *J* = 8.0, 7.0, 1.50 Hz, 4H: Hy') 7.79 (ddd, *J* = 7.0, 5.5, 1.5 Hz, 4H: Hx), 7.68 (ddd, *J* = 7.0, 5.5, 1.5 Hz, 4H: Hx'), 7.65 (d, *J* = 7.0 Hz, 8H: Ha), 6.91 (t, *J* = 7.5 Hz, 8H: He), 6.78 (t, *J* = 7.5 Hz, 16H: Hd), 6.43 (d, *J* = 7.0 Hz, 8H: Hb), 5.65-5.47 (br, 8H: Hc), 6.31−6.14 (m, 8H:, Hf). $^{13}C\{^1H\}$ NMR (176 MHz, CD_3CN): δ 196.41; 196.37; 192.4; 168.2; 156.1; 155.9; 154.6; 154.5; 151.7; 150.8; 147.9; 141.9; 129.6; 129.4; 129.1; 128.90; 128.85; 128.68; 128.5; 125.3; 125.2; 124.9. HRMS (ESI, CH_3CN) (m/z): $[M-2(PF_6)]^{+2}$ ($C_{124}H_{88}F_{12}N_{20}O_{12}P_2Re_4Rh_2$) calcd 1646.1252; found 1646.1201. IR (ATR, cm^{-1}): ν_{CO} 2032s, 1930sh, 1908s; ν_{PF} 829s. Anal. Calcd for $C_{124}H_{88}F_{24}N_{20}O_{12}P_4Re_4Rh_2$: C, 41.59; H, 2.48; N, 7.82. Found: C, 41.23; H, 2.41; N, 7.60.

Tetrakis (*N*,*N*'-diphenyl-isonicotinamidinate)dirhodium(II,II) , 4-5. ^{1}H NMR (400 MHz, CD_3CN): δ 8.01 (d, J = 3 Hz, 8H: Ha'), 7.07 (s, 16H: Hd'), 6.87 (s, 8H: He'), 6.83 (d, J = 3 Hz, 8H: Hb'), 6.72 (s, 8H: Hc'), 5.89 (s, 8H: Hf') $^{13}C\{^1H\}$ NMR (176 MHz, DMSO-d_6): δ 168.0; 149.7; 149.1; 142.0; 128.8; 127.6(br); 126.6(br); 125.2; 123.8. HRMS (ESI, CH_3CN) (m/z): $[M+H]^+$ ($C_{72}H_{57}N_{12}Rh_2$) calcd 1295.2934; found 1295.2876.

4.5.3. Crystal Structure Determination

X-ray crystallographic data were collected from a single crystal sample, which was mounted on a loop fiber. Data were collected with a Bruker Microstar diffractometer equipped with a Platinum 135 CCD Detector at 150 (2) K. The data were integrated with APEX2 software and corrected for absorption using the SADABS package.[20] Following analytical absorption corrections and solution by direct methods, the structures were refined against F^2 with full-matrix least-squares using the program SHELXL-97.[21] All H atoms were added at calculated positions and refined by use of riding models with isotropic displacement parameters based on those of the parent atoms. Anisotropic displacement parameters were employed throughout for the non-hydrogen atoms. Images were generated using Ortep III.[22]

X-ray quality crystals of **4-1** were obtained by vapor diffusion of isopropyl ether into an acetonitrile solution containing the complex.

Crystal data for **4-1**, $[C_{87}H_{67}N_{15}O_3ReRh_2][F_6P]\cdot 2.5(C_2H_3N)$, were collected on a Bruker Microstar at 150(2) K using Cu-Kα radiation (λ = 1.54178 Å). Full-matrix, least-squares refinements on F_2 using all data; 15021 unique reflections, M =2010.18, triclinic, space group $P\bar{1}$, a = 12.692(2), b= 17.182(3), c = 21.751(3)Å, α = 75.315(8), β = 77.197(8), γ = 73.324(7)°, V = 4338.5(12) Å^3, Z = 2, $R1$ [$I > 2\sigma(I)$] =0.0605, wR^2 (all data) = 0.1422. Figure 4.S1 and Figure 4.S2 displays the asymmetric unit.

4.5.4. Computational Methods

All calculations were performed with Gaussian 03 and 09 software (G03 and G09).[23] G09 was used mainly for gas-phase optimization and vibrational frequency determinations of the bigger systems and gave identical result to G03. All TD-DFT was done on G03, G09 gave similar result, but G03 was kept for a better uniformity in the comparison with older calculated data. The initial model used before optimization comes from the solid-state structure, without any anion or solvent adducts. Optimization and IR frequency determination were carried out with the DFT method using the B3LYP functional[24] in the gas phase with the 6-31G** basis set for C, H, N, and O atoms and the relativistic LANL2DZ with effective core potentials and one additional f-type polarization function for Rh and Re atoms (α_f(Rh) = 1.350; α_f(Re) = 0.890).[25] All structures optimized successfully and had no imaginary frequencies, except **4-5+MeCN**. **4-5+MeCN** did not converge with tight conditions, and its lowest energy model still possessed a negative frequency centered on the axial rotation of the methyl group around the C−C axis of MeCN; this has minimal impact on the global properties of the dimer and was used as is. The absorption spectra and solution state molecular orbital (MO) energies were calculated by TD-DFT, using the same method associated with the polarized continuum model (CPCM)[26] and a smaller basis set: Rh, Re, N bond to metal, the amidinate C, and the carbonyls remained unchanged, while all other remaining atoms (C, H, N) used 3-21G. Gaussview 3.09 was used to visualize MOs with an isodensity of 0.02; GaussSum 2.2 was employed to extract the absorption energies, oscillator strengths, and molecular orbital energies: and Chemissian program was used to sketch energies of MOs with their color-coded atomic orbital (AO) contributions, using 0.01 eV as

the threshold for degeneracy for the MO.[27] A model of complex **4-8** has already been studied in our group using the same methods and was used for comparison.[10c]

4.6. Results and Discussion

The synthesis of the rhenium assemblies was straightforward, and specific assemblies were prepared by varying the ratio of rhenium complex to rhodium dimer. Separation of the rhenium species was not possible by traditional silica gel chromatography, which leads to dissociation of the assemblies, whereas size-exclusion chromatography permitted product separation with no observable Re(I) dissociation. The complexes proved stable in the solid state and in most solvents, but dimethylsulfoxide and acetone displayed slow dissociation of the rhenium chromophores after a few days. Note that in the case of **4-2** it was not possible to separate the two possible *cis* and *trans* isomers, and they were analyzed as a mixture (see Chart 4.S1 for a full scheme of these species).

4.6.1. X-ray Structural Investigation and Calculated Geometry

The structural characteristics of the assemblies have been reported for **4-4** and **4-5**.[6b] These dimers crystallize easily, presumably due to the high symmetry of the molecules. In the case of **4-4**, disorder from cocrystallized solvent and the hexafluorophosphate anions was observed. Both complexes **4-1** and **4-3** crystallized, but only **4-1** furnished X-ray quality crystals. In the case of **4-2**, no crystallization occurs in the same conditions used for the other complexes, possibly due to the presence of both *cis* and *trans* isomers in solution. Both complex **4-1** and **4-4** crystallized with an acetonitrile adduct in the axial position of the rhodium dimer (see Chart 4.1), while **4-5** is adduct free. Figure 4.1 illustrates the three dimers of the family, and a first general observation can be made: all these dimers are chiral in the solid state, due to the presence of a helicity in the amidinate phenyl rings and that the racemic mixture of the two forms is found for all of the structures.

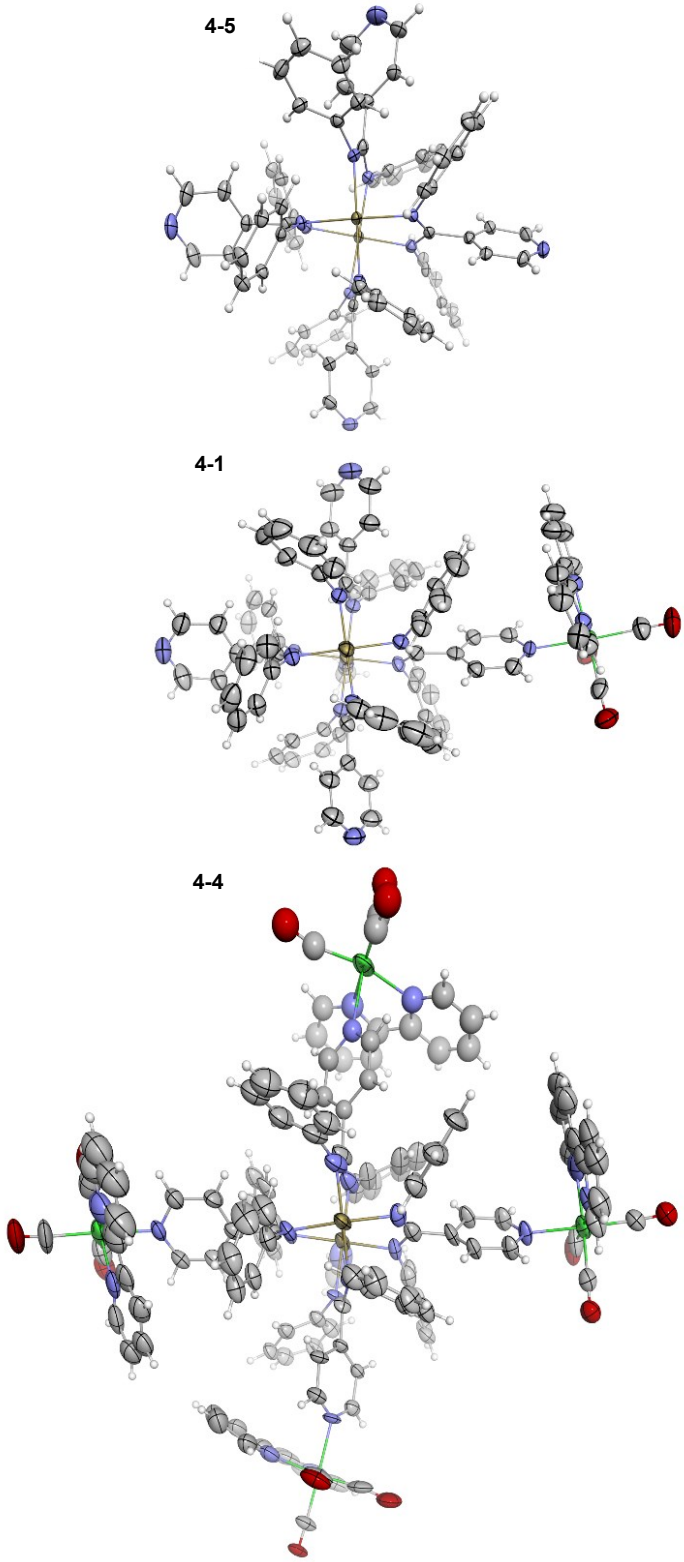

Figure 4.1. ORTEP view of the X-ray crystal structures of **4-5** (top), **4-1**+**MeCN** (center), and **4-4**+**MeCN** (bottom) (50% probability displacement ellipsoids; anion, solvent, and any other chemically equivalent molecule removed for the sake of clarity).

Complexes **4-5**, **4-5+MeCN**, **4-1**, and **4-4** had their geometry optimized from the crystallographic data (the latter two were modeled as charged species without anions). The computational modeling of these complexes, especially **4-4**, with its four attached rhenium and a total of 250 atoms, proved quite challenging, and they represent the first fully modeled structures of this class of rhodium amidinate dimers with the exception of the much smaller tetraethanimidamidate rhodium dimer.[28] Past calculations done for larger *N*,*N*'-arylamidinate dimers were all based on a minimalist formamidinate core model composed of 26 atoms, $[Rh_2(N_2H_2CH)_4]$; as such, they offered very little insight on functionalization effects of the amidinate.[5c,5h,5i,29] Due to the significant computational cost implied in modeling rhenium chromophores attached to the dimer, complexes **4-2** and **4-3** were not analyzed, as very limited knowledge would have been gained, since all their measured properties follow the trend between **4-1** and **4-4**. Complete modeling of the acetonitrile adducts of **4-1** and **4-4** was not attempted for the same reason and due to the optimization difficulty observed for **4-5+MeCN**. The optimized structure of **4-1** and **4-4** are good models, but the bipyridines of the Re are much farther away from the amidinate than they are in the solid state, as can be seen in Figure 4.2 for the case of **4-4**. This deviation can be explained by the absence of dispersion modeling in our chosen method, which neglects attractive π stacking observed between the bipyridine of the rhenium and the core phenyl rings and can be a small source of discrepancy in our modeling.

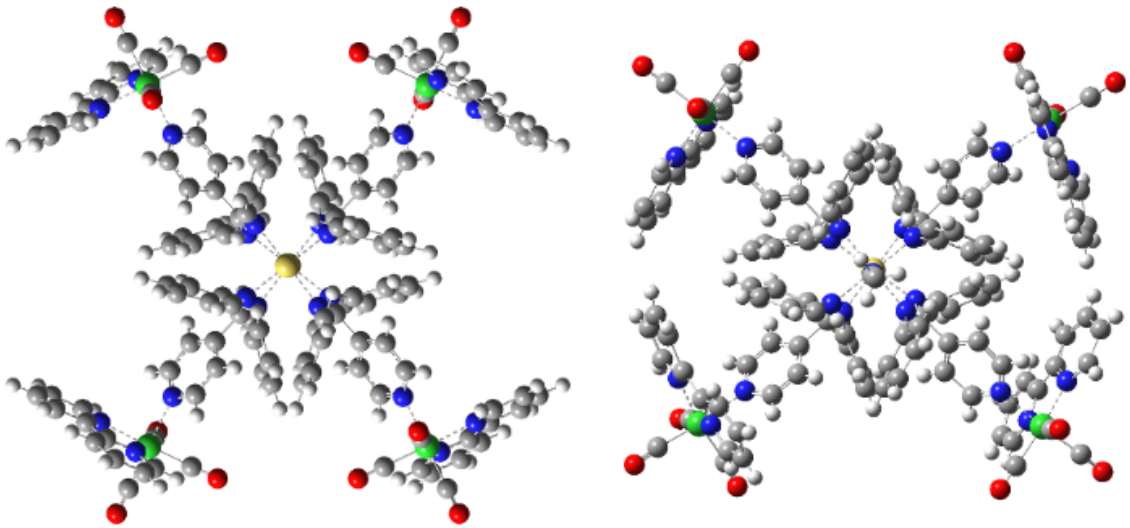

Figure 4.2. Optimized geometry (left) of **4-4** versus solid-state model **4-4+MeCN** (right).

The main crystallographic feature of the dimers is its Rh−Rh distances (Table IV-1). In our present study two elements modify it from the parent dimer **4-5**: the presence of an acetonitrile adduct and of the rhenium chromophores. Without the **4-1+MeCN** structure, our first analysis showed that **4-4+MeCN** and **5** have very similar Rh−Rh lengths, suggesting the acetonitrile adduct and the rhenium chromophores had little effect on the Rh−Rh bond distance. Literature examples were not conclusive in this regard: the tetradiphenylbenzamidinate (dpb) dimer (**4-6**), which is very similar to complex **4-5**, showed extensive increase in bond length when coordinated to CO, but due to the very different nature of CO and acetonitrile ligands no conclusion could be made.[5f] The tetradiphenylformamidinate (dpf) dirhodium dimer (**4-7**), without any central aryl ring and thus much less steric hindrance, showed no Rh−Rh bond length increase upon axial coordination either.[5g]

The dimer **4-1+MeCN** crystal structure has a significantly longer (> 3σ) Rh−Rh bond length when compared to both **4-5** and **4-4+MeCN**. This leads to the conclusion that an acetonitrile adduct increases the Rh−Rh bond length whereas the addition of a Re chromophore lowers it. The first statement can be confirmed by analyzing the optimized structure of **4-5**: it has a Rh−Rh bond 0.03 Å shorter than the **4-5+MeCN** model, despite slightly elongated Rh−Rh (+0.017 Å) and Rh−N bonds (+0.044 Å) versus the X-ray data. This compares very well with the difference of 0.031 Å seen experimentally between **4-5** and **4-1+MeCN**. The effect of the Re chromophores appears to be much more subtle on the calculated models; moving from **4-5** to **4-1** reduces the Rh−Rh bond length by 0.0023 Å, while it drops by a mere 0.0014 Å when passing from **4-1** to **4-4**. The measured effect seems much higher, suggesting the computed model of **4-4** is not quite adequate for evaluating these bond lengths.

The acetonitrile adduct has another measurable effect on the dimer geometry: the increased length of the Rh2−N bonds (where Rh2 is binding an axial adduct). From the DFT data of **4-5+MeCN** we have a 0.04 Å increase in these metal−ligand bonds upon coordination of the acetonitrile. This increase is similar to **4-1+MeCN** (+0.04 Å) and **4-4+MeCN** (+0.03 Å) although it is below the 3σ error of the individual bonds for **4-4+MeCN**. It is clearly visible for **4-1+MeCN**, which has more precise bond lengths (3σ = 0.018 Å). This increase is also observed in the case of $Rh_2(dpb)_4$ (**6**) upon coordination of CO with a 0.06 Å increase of the Rh2−N bonds, while again the formamidinate complex **7** has no significant changes. This

distortion on the Rh-N distances suggests very strong steric constraints imposed on any axial adduct, stronger than the diarylformamidinate family of dimers. The rhenium chromophores do not seem to increase this steric bulk around the axial site; they actually stabilize the adduct formation due to their electron withdrawing effect. This will be discussed later in more detail.

Table IV-1. Selected Parameters (Å,°) of the Solid-State Model and Computed DFT Models (in italics) of the Assemblies and Related Complexes.

	lengths (Å)								angles (deg)	
dimer	Rh1−Rh2	Rh1−N[e]	Rh2−N[f]	Rh2−L adduct	Re−N_{py}	Re−N_{bpy}[g]	Re−C[g]	C−O[g]	N_{bpy}−Re−N_{bpy}	N−Rh−Rh−N'[g]
4-1 +CH_3CN	2.4365(8)	2.04(1)[g]	2.08(1)[g]	2.114(7)	2.215(5)	2.18(2)	1.93(3)	1.14(3)	75.1(3)	14.4(4)
4-1 *(-PF_6)*	*2.4211*	*2.10(1)*[h]			*2.252*	*2.198(1)*[h]	*1.930(3)*[h]	*1.158(1)*[h]	*74.45*	*14.9*
4-4 +CH_3CN	2.414(3)	2.06(1)[g]	2.09(3)[g]	2.17(3)	2.22(3)[g]	2.15(6)	1.90(4)	1.15(5)	76.6(15)[g]	14.6(6)
4-4 *(-4PF_6)*	*2.4197*	*2.105*			*2.28*	*2.200(1)*[h]	*1.930(5)*[h]	*1.158(4)*[h]	*74.5*	*14.7*
4-5	2.4055(8)[g]	2.054(9)[g]								12,6(4)
4-5	*2.4234*	*2.0976*								*14.6*
4-5 *+CH_3CN*	*2.4551*	*2.093*	*2.135*	*2.178*						*14.5*
4-6[a]	2.389(1)	2.05(6)								17.3
4-6 +CO[a]	2.435(1)	2.056(6)	2.114(6)	1.97(2)						17
4-7[b]	2.457(1)	2.057(1)								3.5
4-7 +CH_3CN[b]	2.459(1)	2.062(2)	2.066(2)	2.106(4)						16.8
4-8[c]					2.194(6)	2.17(1)	1.92(1)	1.15(1)	74.5(2)	
4-8[d] *(-triflate)*					*2.266*	*2.198(1)*[h]	*1.930(2)*[h]	*1.158(2)*[h]	*74.5*	

[a] **4-6:** Rh_2(*N,N'*-diphenylbenzamidinate)$_4$.[5f] [b] **4-7:** Rh_2(*N,N'*-diphenylformadinate)$_4$.[5g] [c] **4-8**:[Re(bpy)$(CO)_3$(py)] triflate.[30] [d] From literature.[10c] [e] On the Rh without adduct. [f] On the Rh with adduct. [g] Averaged measurement; error represent the highest standard deviation between equivalent bonds and experimental error. [h] Averaged value of the calculated bonds.

The rhenium−ligand bonds show no deviation in bond lengths and angles as compared to the simplest model complex, Re(bpy)$(CO)_3Py^+$ (**4-8**) (Table IV-1),[30] thus confirming that the rhenium chromophore is not subject to steric hindrance from the amidinate ligand or the other rhenium chromophores. The theoretical models of **4-1**, **4-4** and **4-8** also show near identical parameters, except for the Re−N_{py} bond; in the case of **4-1** it is shorter by 0.014 Å versus **4-8** while for **4-4** it is the reverse it is 0.014 Å longer. These values make sense as the amidinate pyridyl can be more electron rich than a free pyridyl, but the effect of the +4 charge across

the dimer slightly lowers this effect. Although the crystal data reflect this trend, the bond resolution is too poor to confirm it. A survey of the Cambridge Structural Database (CSD) suggests very little changes to the Py−Re bond for functionalized pyridine derivatives, even with anionic or cationic charges attached to the pyridine, so no observable change is expected.[31]

The rhenium−rhodium assemblies can be compared to rhenium−porphyrin assemblies in the literature, both having mono- and tetrarhenium versions (although in the case of porphyrin the number of rhenium complexes was determined by the number of pyridyl units grafted to the porphyrin).[12a] The same square motif can be observed, although the porphyrin core is actually bigger, bringing the opposed rhenium chromophores 20 Å apart versus 18 Å in **4-4**. Like the porphyrin tetrarhenium assembly, the rhenium units are paired by two with the bipyridine ligand pointing toward each other always on the smallest side of the rectangle (14 Å by 12 Å). This arrangement seems to be due to the packing of the dimers (Figure 4.S3); the longer side shows two intercalating T-shaped π-stacks between a bpy ring and a phenyl ring of the dimer (3.1 Å and 3.4 Å apart). In the case of **4-1** no special interaction occurs in the packing of the crystal, and no H-bonding bridges are formed by any of the three remaining pyridyl moieties.

4.6.2. IR Spectroscopy

All of the complexes displayed IR spectra consistent with the facial configuration of the carbonyl ligands as indicated by the three intense CO absorptions. The peaks at 2032 cm^{-1} and the shoulder at 1930 cm^{-1} are identical for all of the species (**4-1** to **4-4**), but the last peak varies slightly, from 1915 to 1905 cm^{-1}. Although this vibration decreases with the increased number of coordinated rhenium complexes (up to three), the shift is at most marginal. The positions of these three bands are consistent with other pyridine bound complexes, such as **4-8**, which has bands at 2026, 1921 and 1907 cm^{-1} (in KBr, vs ATR bulk powder measurement herein).[32] The computed frequency between **4-1**, **4-4**, and **4-8** gave only small differences (8 cm^{-1} max), again showing very little measurable variation (Table IV-S1). No splitting of the IR bands of CO stretches for complexes **4-2** (*cis*/*trans* mix) and **4-3** was found, even if both these complexes have chemically different Re(I) centers. This fact, plus the similarity of all of the species, suggests that the rhenium complexes bonded to the dimer do not interact with one another: no effect is seen from steric tension or electron density brought

by the other rhenium complexes. This was also observed for tetrarhenium assemblies bonded to a tetrapyridylporphyrin.[12a]

4.6.3. NMR Spectroscopy

The proton NMR spectra of the assemblies display a split and a broadening of the signal of the protons *ortho* to the pendant phenyl groups (only a broadening is observed for the protons in *meta* position). This effect was reported before for this type of complex and has been studied in greater detail for **4-5** in this work.[6a,6b] The splitting of the signal is due to restricted rotation; at room temperature, the phenyl rings are sterically hindered and are in a slow-exchange regime on the NMR time scale. In the crystal structure model where the rotation is totally frozen, as shown in Figure 4.3, the proton labeled f (in red) is oriented toward the center of an adjacent phenyl ring, creating a strong shielding effect, while proton c (in magenta) is not facing the phenyl rings. At room temperature, the rotation is slow enough to distinguish the two positions, while their ^{1}H resonances coalesce to a single signal around 325 K and form a well-defined doublet at 383 K as they can freely rotate (in DMSO, Figure 4.3). From the variable temperature data we can calculate a free energy of activation of 14.9 kcal/mol based on the coalescence temperature (T_C) in Kelvin and the difference in the proton splitting at that temperature (Δν), in Hz using the following equation:[33] $\Delta G^* = 4.57\ T_C\{9.97 + \log(T_C\ /\Delta\nu)\}$(cal/mol). Note that these spectral features are seen in all solvents, even in acetonitrile, where one would expect a break in symmetry due to adduct formation, suggesting an exchange rate greater than the NMR time scale.

The proton chemical shifts clearly distinguish the species by the ratio of the peaks corresponding to the bipyridine ligand of the rhenium versus the peaks of the pyridyl moiety on the dimer. Upon coordination, the bpy loses its symmetry and all eight of its protons are seen as individual peaks in the rhenium assemblies due to the restricted rotation of the pyridyl ring in the presence of the phenyl rings of the amidinate. This lack of rotation of the pyridyl (either bonded or free) on the amidinate does not cause a split in its proton resonances like the phenyl rings due to a local pseudo-C_2 symmetry around the pyridine−amidinate axis (Figure 4.4). In the case of the rhenium-bonded pyridine, the rhenium chromophore breaks this symmetry but it possesses a mirror plane perpendicular to the pyridine plane, thus keeping the pyridine protons as pairs. The bipyridine itself sits on one side above a phenyl

ring from the dimer core where it π-stacks and thus breaks the symmetry of the bpy proton resonances (Figure 4.4).

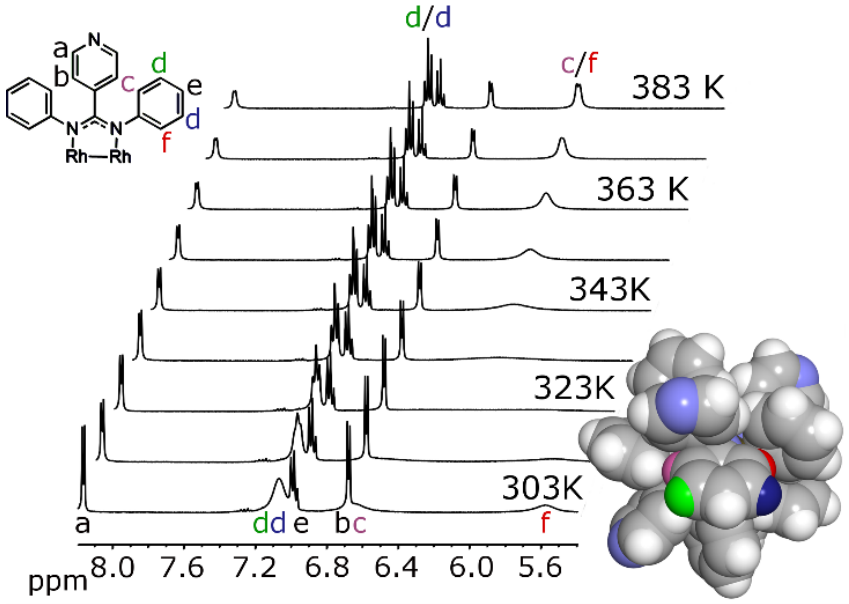

Figure 4.3. Variable-temperature H NMR of **4-5** in d_6-DMSO. Top left: Labeling scheme of the protons. Bottom right: Space-filling model of the crystal structure of **4-5**, with color-coded protons.

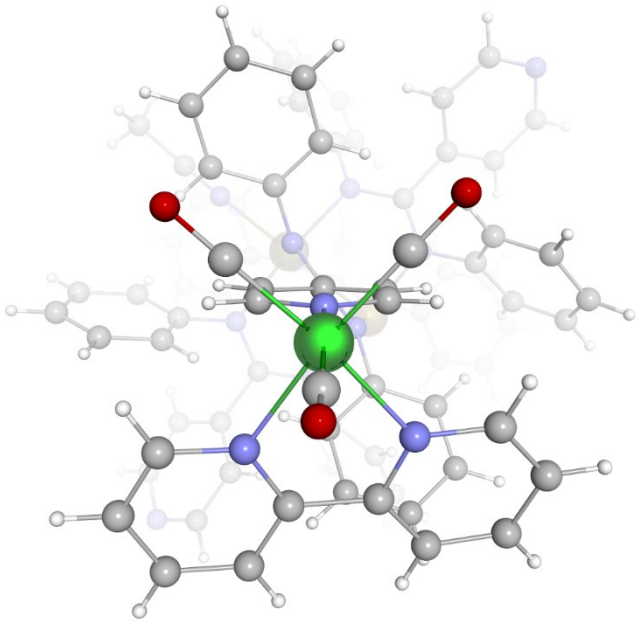

Figure 4.4. View of the crystal structure of **4-1** along the pyridine−amidinate axis.

Figure 4.5 shows the proton NMR spectra of all the rhenium assemblies, and further splitting between the rhenium chromophores can be seen on the bpy protons in the case of **4-2** and **4-3** (around 9.00, 8.35, and 7.75 ppm). In the case of **4-2**, a *cis/trans* two-to-one ratio can be measured and matches the expected statistical distribution (two possibilities for the *cis* isomer vs one for the *trans* isomer). In the case of **4-3** the splitting is more apparent with again a two-to-one ratio of the bipyridine resonances, this time due to the chemical differences between the rhenium opposed to the free pyridyl versus the two adjacent to it. The proton signals on the dimer amidinate ligand for complexes **4-1** to **4-3** also split; however, they are poorly resolved at room temperature.

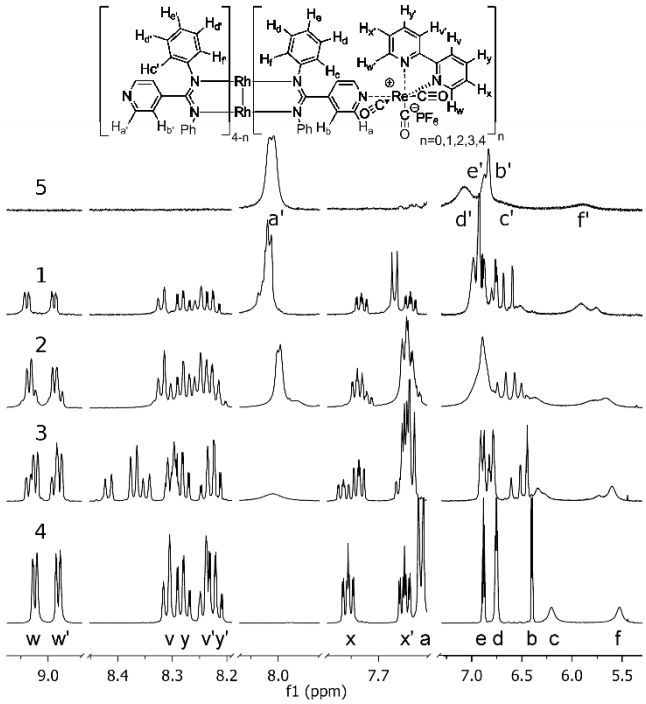

Figure 4.5. Proton NMR of the complexes **4-5**, **4-1**, **4-2**, **4-3,** and **4-4** (from top to bottom) in CD_3CN; labeling for **4-4** and **4-5** indicated as reference.

4.6.4. Electrochemistry

The rhodium amidinate dimers have a rich electrochemistry that is well documented. They possess three reversible or quasi-reversible metal-based single-electron redox couples, one reduction and two oxidations.[5f,5g,5k] The rhenium chromophores have four further redox couples (observable in MeCN), one irreversible rhenium-based oxidation, a first reversible bpy reduction, a second quasi-reversible bpy reduction, and a third irreversible reduction assumed to be centered on the rhenium. Note that in DCM only three are seen, the second

bpy reduction being pushed to −1.7 V.[34] All of the redox couples for our assemblies are tabulated in Table IV-2.

DCM was used as a solvent only for complexes **4-4** and **4-5** to observe the effect that polarity and the coordination of acetonitrile has on the redox potentials of the assemblies versus the very similar complex **4-6** ($Rh_2(dpb)_4$).[5k] For **6**, it had previously been shown that the rhodium dimer's first and second oxidation potential display a 170 mV cathodic shift in acetonitrile due to its coordination and not its polarity, as DMSO and DMF actually showed an anodic shift (~100 mV) for the first oxidation. At negative potentials, the acetonitrile adduct shows only a small anodic shift (60 mV) versus the other polar solvents (200 mV). In our assemblies, both **4-4** and **4-5** showed the expected cathodic shift for the oxidation. Complex **4-4** shows only a 40 mV cathodic shift, much less than the 100 mV seen in **4-5**, and is likely due to the presence of a +4 charge already present on the assembly, making the oxidation more difficult. The reduction of **4-5** in DCM is at more negative potential than in MeCN, which is probably due to the interaction of **4-5** with MeCN being weaker than with **4-4** or **4-6**. The adduct effect is only seen during oxidation, which is stabilized by the presence of MeCN.

Table IV-2. Redox Potentials[a] of the Assemblies in Acetonitrile and Dichloromethane

dimer	solvent	$E_{½}^{oxy}$ (V) (ΔE (mV))			$E_{½}^{red}$ (V) (ΔE (mV))			
		Re^{+}/Re^{2+}	Rh_2^{5+}/Rh_2^{6+}	Rh_2^{4+}/Rh_2^{5+}	$bpy^{-\cdot}/bpy$	$bpy^{2-}/bpy^{-\cdot}$	Rh_2^{3+}/Rh_2^{4+}	Re^{0}/Re^{+}
4-5	DCM		1.36 (180)	0.31 (100)			-1.45 (88)	
4-5	MeCN		1.24 (69)	0.21 (73)			-1.42 (88)	
4-1	MeCN	1.85	1.31 (60)	0.26 (70)	-1.18 (60)	-1.43 (120)	-1.43[b]	-1.72
4-2	MeCN	1.90	1.37 (130)	0.29 (87)	-1.18 (80)	-1.40 (90)	-1.51 (180)	-1.71
4-3	MeCN	1.86	1.38 (61)	0.36 (65)	-1.17 (63)	-1.42 (89)	-1.52 (80)	-1.73
4-4	MeCN	1.87	1.39 (97)	0.39 (83)	-1.17 (60)	-1.44 (89)	-1.61[c]	-1.74
4-4	DCM	1.86 (230)	1.43 (88)	0.43 (84)	-1.12 (90)	-1.75[d]	-1.41 (120)	
4-6[e]	MeCN		1.08	0.05			-1.52	
4-6[e]	DCM		1.24	0.23			-1.58	
4-8[f]	MeCN	1.74			-1.09	-1.39		
4-8[g]	DCM	1.85			-1.2	-1.7[d]		

[a]Potentials are vs SCE; potentials without ΔE values are irreversible. [b]Superimposed with previous reduction (total two electron transfer observed). [c]Seen as a weak shoulder in square-wave experiment. [d]Corresponds to the $bpy^{2-}/bpy^{-\cdot}$ redox couple in DCM. [e]**4-6:** $Rh_2(dpb)_4$ from ref 5k. [f]**4-8**: $Re(bpy)(CO)_3(pyridine)^{+}$, from ref 34a. [g]**4-8** in DCM from ref 34b.

Looking at assemblies **4-1** to **4-5** in acetonitrile, a few trends are observable. First, the rhenium chromophores attached to the dimer do not interact with each other, showing only one wave for all the expected redox couples. The overall charge of the assembly does not affect the potential of these couples, as all have very small variations, e.g., the reversible first reduction of bpy being essentially the same for all complexes with only 10 mV variation.

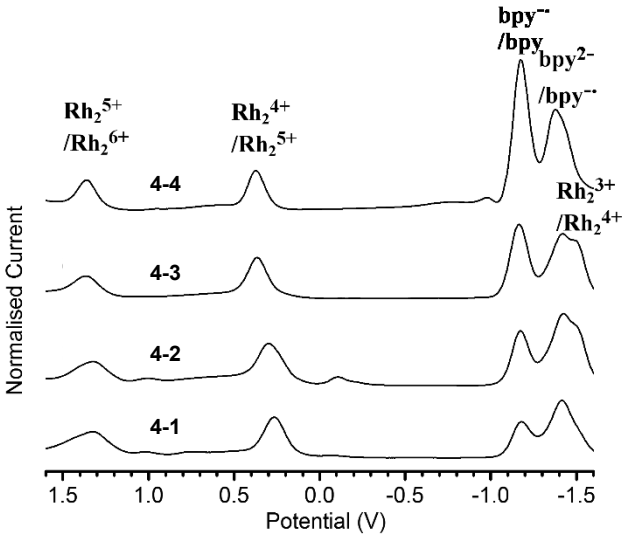

Figure 4.6. Square-wave voltammograms of complexes **4-1**, **4-2**, **4-3**, and **4-4** (from bottom to top) in CH_3CN. Scanning starts on the negative potential, reduction waves at −1.2 and −1.4 V are smaller due to their partial irreversibility at high negative current. Current normalized for the first oxidation maximum.

On the other hand, the dirhodium redox potentials are affected by each rhenium chromophore. Both oxidations exhibit an anodic shift, the first one with a linear slope of 45 mV per rhenium, while the second oxidation follows more of an exponential curve, showing less of an effect for each added rhenium (see Figure 4.S5). The reduction of the rhodium dimer coincides with the second bpy reduction: in **4-1** there is a complete superposition of the two coincidental one-electron reductions, as can be seen by square-wave (SW) voltammetry (Figure 4.6). The reduction of the rhodium follows a cathodic shift and is observed clearly in the SW curves of assemblies **4-2** and **4-3**. In the case of **4-4** the dimer reduction is almost completely masked by the four simultaneous one-electron reductions of the bipyridine on the rhenium chromophores. Only a plateau in CV suggests the presence of the dimer reduction, re-evaluated at −1.61 V herein. At first glance, this is unexpected, since each rhenium should make the dimer less electron rich, making it easier to reduce. But at

−1.4 V, the bpy in the rhenium chromophore itself undergoes its second reduction, making its total charge negative, thus the dimer actually has an increase in electron density for each rhenium chromophore present.

4.6.5. Calculated MO Energies

The main feature of the dimer, its metal−metal bond, is predominant in the frontier MO. The ordering of the bond interaction obtained for all of the calculated complexes is similar to previous calculations of the Rh_2 dimers.[5c,5h,5i] The Rh-Rh bond ordering remains the same with $\sigma^2\pi^4\delta^2\pi^{*4}\delta^{*2}$. The addition of many ligand-based or chromophore-based molecular orbitals in the upper valence region creates a further splitting of the Rh_2 δ and π bonds with strong contributions from the phenyl rings (Chart 4.S2 to Chart 4.S4 illustrate selected frontier MOs). The main metal bond orbitals are labeled in Figure 4.7. In this figure the MO lines contain different colors to illustrate the percentile of AO of each group, red being the rhodium atoms, for example. The numerical contribution of the AO to the frontier orbitals can be found in Table IV-S13 to Table IV-S18.

For all of the complexes the HOMO is the expected Rh−Rh δ* bond, which also has some Rh−N π* bond character. Below it, the HOMO −1 to −3 are centered on the phenyl amidinate ligand, with little metal contribution. This is followed by MOs focused on the Rh−Rh π* bonds, here split in two sets of two degenerate orbitals. (HOMO−4, −5 and −6, −7). The Rh−Rh δ bond is found mainly on HOMO−11, except for **4-4**. The Rh−Rh π and σ MOs are buried very deep beneath ligand−based MOs.

All of the orbitals are lowered in energy as the rhodium dimer loses core electron density by removal of the MeCN adduct or addition of the positive Re chromophore. The drop in energy among the dimers is constant for all of these orbitals, with 0.18 ± 0.03 eV from **4-5**+**MeCN** to **5**, then 0.25± 0.02 eV from **4-5** to **4-1**, and finally 0.70 ± 0.05 eV from **4-1** to **4-4**. This similar drop indicates that all of the occupied MOs are subject to an electrostatic effect, which is in contrast with the LUMO, the Rh−Rh σ* bond, which drops by 0.9 eV between **5**+**MeCN** and **5**. This change in value is expected due to the axial coordination of the acetonitrile which directly interacts with the orbital. The Rh−Rh σ* bond in **4-1** and **4-4** drops by the same energy as the other previously mentioned orbitals; however, the LUMO changes in **4-1** to the bpy π* orbital, as expected from the electrochemical data and the MO energies of complex **4-8**. The MO energies of **4-4** should show the same change; instead it

has an exaggerated lowering in energy of both its bpy π* (LUMO+1 to +5) and Rh−Rh σ* (LUMO) orbitals. The same effect is seen for the Re *d* orbitals: the first three occupied MOs in **4-8** show similar energy levels for **4-1** but are much lower in energy for **4-4**. The three reductions remain mostly constant for the series **4-1** to **4-4**, indicating that the model severely overestimates the effect of the +4 charge on both the rhenium- and rhodium-based MOs. A better model taking into account anions and/or adjacent solvent molecules is required.

Another issue observed in MOs of **4-4** is the extended delocalization of the orbitals centered on the Re chromophores, which form four closely spaced orbitals delocalized over the four rhenium sites (see Chart 4.S3 for an example). They would be better represented as four isolated and degenerate orbitals, each on an individual rhenium site, since the first reduction observed by electrochemistry clearly indicates no communication between rhenium centers.

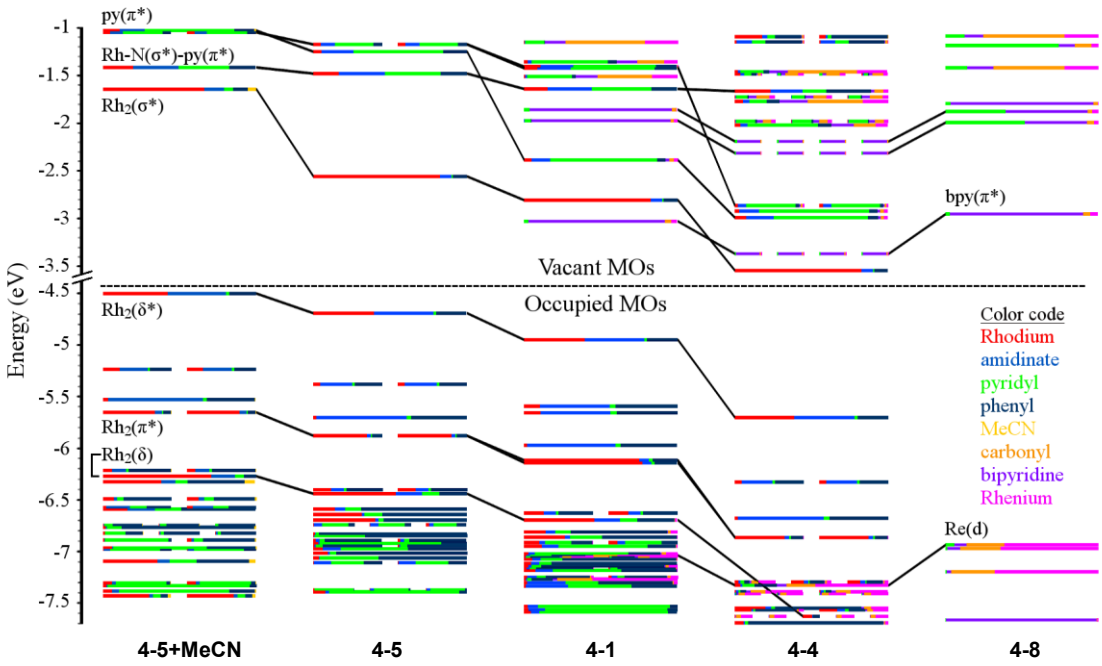

Figure 4.7. Frontier MO energies of modeled complexes **4-1**, **4-4**, **4-5**, **4-5+MeCN**, and **4-8** using a color code for the MO indicating the percentage of AO contribution of each group found in the legend. From rb3lyp/LanL2DZ(f)[Rh,Re] 6-31G**[$NCN_{amidinate}$, $N_{py\text{-}Re}$, CO], 3-21G[C_{aryl},H, N_{py}] with CPCM (DCM or MeCN).

4.6.6. Photophysical Investigation and Comparison with Theoretical Models

The tetra-amidinate rhodium dimers have well-documented electronic spectra.[5f,5g] In general, the amidinate dimers exhibit very small shifts in peak position in different solvents, the exception being cyano-group containing solvents, such as acetonitrile, where its axial coordination greatly perturbs the electronic spectra of the dimers, due to the destabilization of the LUMO.

Upon titration of acetonitrile into a dichloromethane solution of **4-4** and **4-5**, their spectra change radically with the collapse of the 830 nm band, known to be the $Rh_2(\pi^* \rightarrow \sigma^*)$ transition (Figure 4.8). The binding constants obtained for the association of acetonitrile are 5.540(4) and 1.451(8) for **4-4** and **4-5**, respectively, which are much lower than the binding constant of 58 reported for the dpf dimer (**4-7**).[5g] This is expected due to increased steric bulk around the axial coordination site of the dimers. As found for **4-7**, only one acetonitrile forms a bond, as shown by the experimental slope value of 0.98(2) (Figure 4.8, insets). Interestingly, the complexation of the rhenium chromophore enhances the association constant since a more electron-deficient rhodium dimer will be further stabilized with the electron density of the acetonitrile. All the dimers studied display this solvatochromism, passing from red to green upon contact with MeCN. This is observed as well in the solid state: powders of dimers **4-1** to **4-5** display this reversible color change in the presence of acetonitrile vapor.

The spectra of the assemblies in DCM are shown in Figure 4.9 and indicate that only certain bands are affected by the rhenium chromophore. Their transition energies were simulated by TD-DFT, albeit with a smaller basis set to save limited computational time. Comparison of basis sets and Gaussian versions of TD-DFT calculations on **4-5** led to the conclusion that a better fit was obtained with the smaller basis set and G03; G09 significantly overestimated the energy of the metal-centered transitions (Table IV-S10, Table IV-S19 to Table IV-S21).

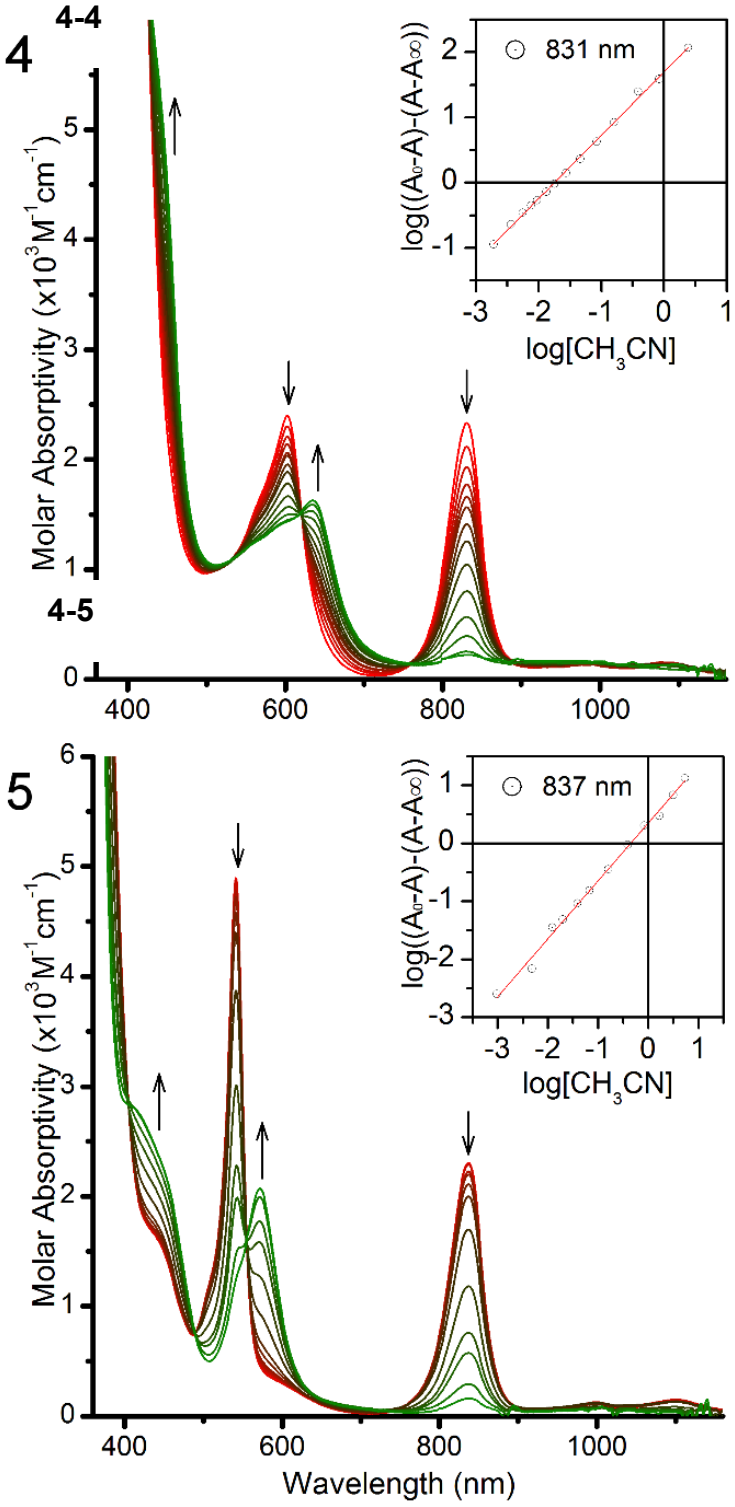

Figure 4.8. Changes in absorption spectra in dichloromethane of the complexes (top **4-4**; bottom: **4-5**) during titration with acetonitrile. Inset: Analysis of the spectroscopic data as a function of acetonitrile concentration.

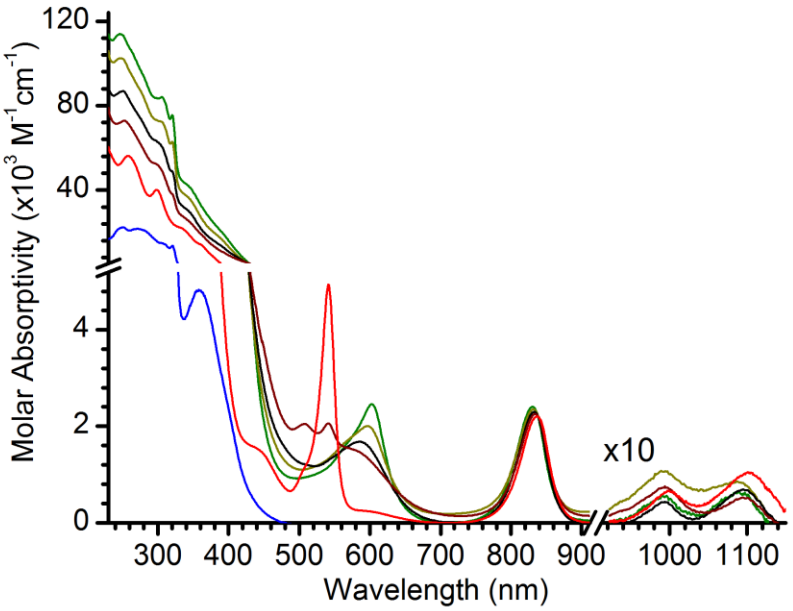

Figure 4.9. Absorption spectra in dichloromethane of **4-1** (dark red), **4-2** (black), **4-3** (dark orange), **4-4** (green), **4-5** (red), and **4-8** (blue); above 900 nm the signal is amplified by 10.

Complexes **4-5**, **4-1**, and **4-4** possess transitions of similar energies in DCM, **4-5**+**MeCN** having significantly shifted transitions (full data in Table IV-S8 to Table IV-S12). The first transition calculated for all of the complexes is the forbidden HOMO−LUMO transition $^1Rh_2(\delta^*\rightarrow\sigma^*)$ near 1300 nm (740 nm for **4-5**+**MeCN**) with zero oscillator strength, which may be the very weak peaks near 1000 and 1100 nm (50 to 100 $M^{-1}cm^{-1}$). These forbidden transitions may be observed due to a vibrational loss of symmetry, and/or they could be from the forbidden triplet transition of $^3Rh_2(\pi^*\rightarrow\sigma^*)$, calculated to be at 1075 cm^{-1}. To the best of our knowledge, these transitions have never been reported previously. These NIR bands are not a trace of partly oxidized product, since upon oxidation of the dimer they do not increase; they are replaced by very broad transitions centered at 1050 and 1200 nm (see Figure 4.S6).

The first well-known bands are the degenerate singlet $^1Rh_2(\pi^*\rightarrow\sigma^*)$ transitions calculated at 750 nm for **4-5**, corresponding to the peak at 838 nm. Upon coordination of the rhenium chromophores to the rhodium dimer, the peak at 838 nm is blue-shifted by about 26 cm^{-1} (approximately 2 nm) per rhenium added (Figure 4.9 and Table IV-S2), showing there is only a small net increase in the energy gap between $Rh_2(\pi^*)$ and $Rh_2(\sigma^*)$ MOs. This shift is also observed in the values of the averaged $^1Rh_2(\pi^*\rightarrow\sigma^*)$ transitions of **4-1** and **4-4** (no longer

degenerate due to a break in symmetry) with shifts of 48 cm^{-1} and 105 cm^{-1}, respectively. These calculated results are closer to a previously calculated $^1Rh_2(\pi^* \rightarrow \sigma^*)$ transition centered at 986 nm for the minimalist core, but it is still significantly different. If the full basis set was employed, the result was of higher energy, at 731 nm, with G09 giving less favorable results with 706 and 711 nm for the small and big basis set (Table IV-S19 to Table IV-S21). This result shows the limit of the method/basis set to correctly model the Rh−Rh bond, but at least the calculation gives trends of matching intensity and energy.[5c] In the case of **4-5+MeCN**, this transition should be blue-shifted due to the destabilization of the $^1Rh_2(\sigma^*)$ orbital. It is calculated to be at 555 nm and would fit well with the peak seen at 572 nm; however, another transition of higher intensity is also in this region.

The next two calculated transitions are more difficult to establish on the spectrum. Both are ligand-to-metal dimer charge-transfer ($^1LM_2CT$) based and are relatively weak: the first originates from a phenyl moiety and is located exactly at 650 nm for **4-1**, **4-4**, and **4-5**; the second is from the amidinate itself and is centered on 545 nm. The first band likely corresponds to the shoulder seen at 600 nm in the case of **4-5**, but in the case of **4-1** and **4-4**, this assignment is difficult due to overlapping bands.

This next transition corresponds to a Rh_2 δ^*-to-py π^* charge transfer (^1M_2LCT, HOMO to LUMO+1), with a relatively strong oscillator strength. In the case of **4-5**, the 541 nm band fits near perfectly with the calculated transition at 540 nm (0.023 o.s.). In the case of **4-5+MeCN**, the band calculated at 588 nm has about half the oscillator strength (0.012) and matches very well with the peak measured at 572 nm, which has half the molar absorptivity of the adduct free dimer (Figure 4.10a). This corresponds to a red-shift of the ^1M_2LCT by 1000 cm^{-1} upon coordination of MeCN, which is similar to that of **4-4** (860 cm^{-1}). This is in opposition with the $^1Rh_2(\pi^* \rightarrow \sigma^*)$ band blue-shift observed and is due to the pyridine π^* MO being away from the MeCN adduct. It is less destabilized and reduces the energy gap as can be observed in Figure 4.7. The addition of the Re chromophore will have the opposite effect; it will greatly reduce its energy in comparison to the Rh_2 core, thus generating another red-shift. This shift is measured at 1850 cm^{-1} (60 nm) for **4-4** and is calculated to be slightly higher (2330 cm^{-1}) with a transition at 619 nm (Figure 4.10b).

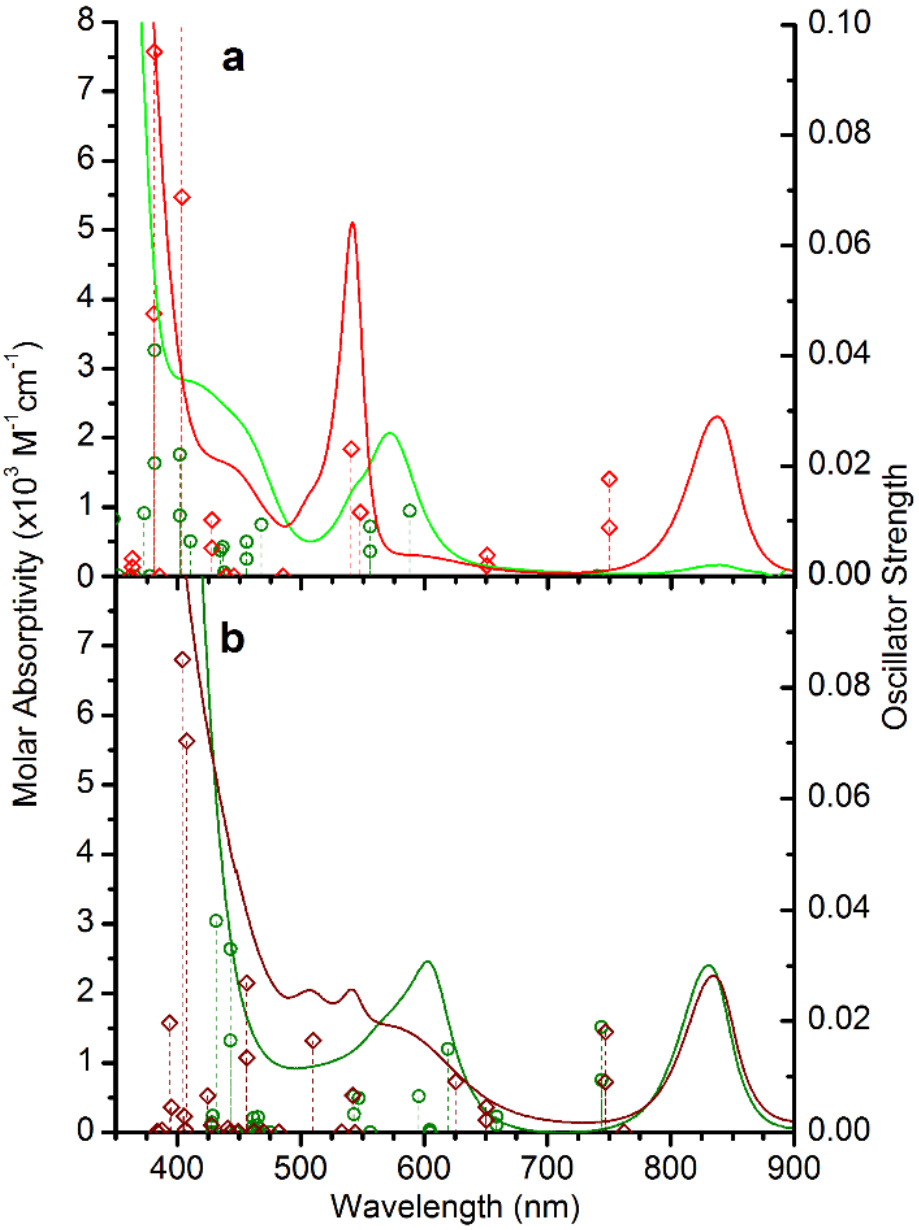

Figure 4.10. Absorption spectra (lines) compared to calculated TD-DFT oscillator strength (circles and diamonds); (a) **4-5** in DCM (red, diamonds) and acetonitrile (green, circles);(b) **4-1** (dark red, diamonds) and **4-4** (dark green, circles) both in DCM; rb3lyp/LanL2DZ(f)[Rh,Re] 6-31G**[$NCN_{amidinate}$, $N_{py\text{-}Re}$, CO], 3-21G[C_{aryl},H, N_{py}] with CPCM (DCM or MeCN).

For **4-2** and **4-3** the ^1M_2LCT shifts less, as expected, but for **4-1** there are two unexpected bands seen at 541 and 507 nm, although the expected band at 572 nm is still present. This suggests that in the case of **4-1** the $Rh_2(\delta^*)\rightarrow$pyridyl transitions are split. This is modeled in the TD-DFT results as two distinct ^1M_2LCT transitions, one at 510 nm and the other at 625 nm. The remaining transition should be the previously mentioned $^1LM_2CT$, calculated to be 542 nm. We do not observe a peak at 507 nm in the case of **4-2** or **4-3**, but a definite decrease in ε is observed in that area as rhenium chromophores are added, suggesting there is still a contribution from this secondary $^1LM_2CT$.

As can be seen in Figure 4.9, the model rhenium chromophore **4-8** starts absorbing around 480 nm, but is not responsible for the sharp increase in absorption observed near 442 nm for complexes **4-1** to **4-4**. This band due to the rhodium should correspond to a strong amidinate to pyridine transition (^{1}LL), calculated at 443 nm for **4-4**, 455 nm for **4-1**, and 427 nm for **4-5**. The calculation follows the measurements, as there is an initial red-shift when the first rhenium is bonded, followed by a small blue-shift as the other rhenium chromophores are bonded.

After this transition all others become less defined, due to heavy absorption observed in the UV region. A strong second degenerate $^1Rh_2(\pi^*\rightarrow\sigma^*)$ transition was calculated, centered on HOMO −6 and −7, with stronger phenyl−amidinate character in the MOs. It is located at 403 nm (0.13 o.s. total) for **4-5**; however, the position of the experimental band is less obvious, and it could be a shoulder around 380 nm. In the case of **4-1**, this is calculated as two transitions, one at 407 nm and the other at 403 nm, which may explain the red-shift observed in that region with the addition of chromophores.

The actual contribution of the rhenium chromophore is very noticeable in the UV region, where each rhenium adds its absorbance to the total. The chromophore behaves like $Re(bpy)(CO)_3(Py)^+$ (**4-8**), a complex well characterized with TD-DFT studies.[10c] Model **4-1** evaluates these MLCT transitions at 384, 365, and 361 nm (transition 30, 40, and 42). These values are in good agreement with **4-8**, with its first three calculated transition being 383, 375, and 361 nm. This is a nice display of reproducibility in the TD-DFT calculation, giving similar results even after 40 transitions were calculated. For the experimental spectra, the rhenium chromophore has two distinct elements: the rhenium ^{1}MLLCT, centered at 358 nm (4800 $M^{-1}cm^{-1}$) for **4-8**, seen as a shoulder for **4-1** to **4-4** and a sharp signature bpy ^{1}IL transition band, seen for **4-8** at 320 nm (13500 $M^{-1}cm^{-1}$), readily observable in **4-1** to **4-4** at

the same wavelength. It is a signature band and shows the presence of a coordinated pyridyl; for example it is fairly different from $Re(bpy)(CO)_3(MeCN)^+$, where this sharp ^{1}IL transition band is seen at 317 nm. If we plot the molar absorption versus number of chromophores at these two wavelengths we obtain a linear fit with a slope of 4800 ±300 and 12600 ±200 $M^{-1}cm^{-1}$ for 358 and 320 nm, respectively (see Figure 4.S4). These results match very well with the absorption coefficient of **4-8** measured at 4800 and 13500 $M^{-1}cm^{-1}$. At 320 nm, there is a 900 $M^{-1}cm^{-1}$ difference, due to the absorption contribution of the pyridyl motif already present on the dimer.

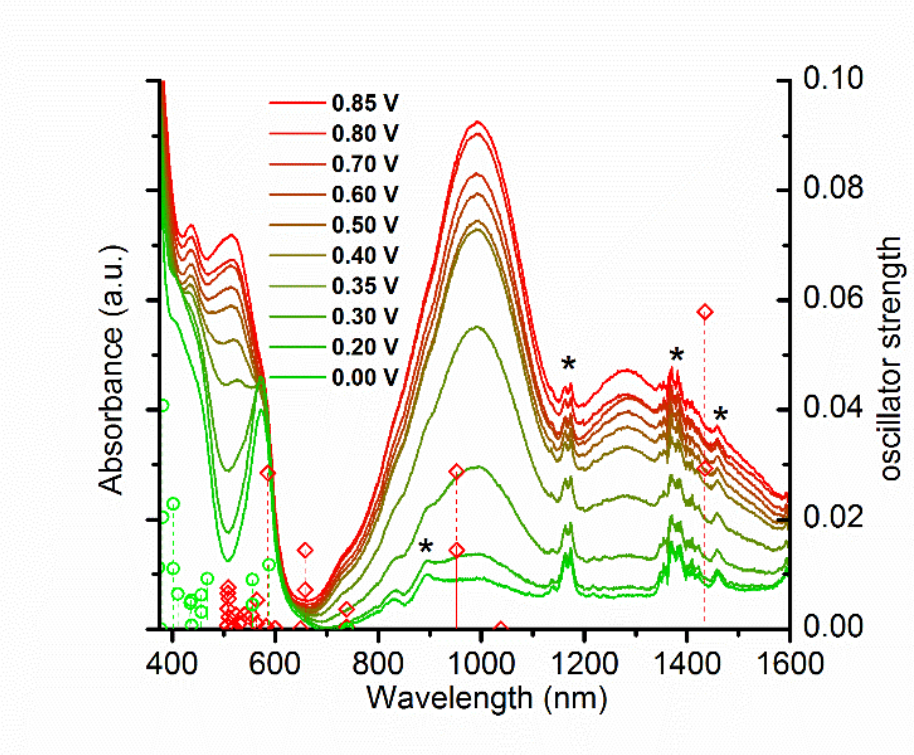

Figure 4.11. First oxidation of **4-5** in MeCN monitored by spectroscopy (applied voltage: 0.0 to 0.8 V green to red) vs silver wire (uncorrected); electrolyte 0.1 M Bu_4NPF_6) with calculated TD-DFT oscillator strength of **4-5+MeCN** (green, circles) and of **(4-5+MeCN)$^+$** (red, diamonds) from b3lyp/LanL2DZ(f)[Rh] 6-31G**[$NCN_{amidinate}$], 3-21G[C_{aryl},H,N] with CPCM (MeCN).*: artifacts.

The spectroelectrochemistry of **4-5** was also investigated in acetonitrile. At 0.35 V, two NIR bands appeared at 995 and 1280 nm (Figure 4.11). Similar bands have been observed for **7**$^+$ at 890 and 1150 nm when the potential was held at 0.65 V.[5g] These bands are expected to be due to new transitions toward the Rh_2 δ* MO, which is now missing an electron (see

Chart 4.S5 for calculated total electron spin density). Calculated transitions (Figure 4.11; vertical lines) show two main transitions in the NIR, an $^2LM_2CT$ at 1435 nm, centered on the amidinate and phenyl, and a $^2Rh_2(\pi^*\rightarrow\delta^*)$ at 952 nm. This is in agreement with the spectra, although the intensities do not match.

4.6.7. Emission

In terms of emission, the rhodium amidinate dimers are comparable to rhodium acetate dimers: both are known to be nonemissive and both possess a nonradiative excited state. [5c,35] The amidinate dimers also display photochemical activity toward reduction of halogenated compounds even with near-IR radiation (λ_{irr} > 715 nm).[5c] No emission was observed from the attached rhenium chromophores in assemblies **4-1** to **4-4** in DCM or acetonitrile, which suggests fast quenching of the excited state of the rhenium chromophores. The rhenium complex is known to rapidly form the ^{3}MLLCT excited state after initial irradiation (<200 fs), and it should be this triplet state that is quenched by the dimer.[36] As such two possible pathways are predicted. The first path is a triplet−triplet Dexter energy transfer from the ^{3}MLLCT state of the rhenium to a nonemissive, low−energy triplet state centered on the dimer. The second pathway is a true electron transfer, leading to a transient state in the form of Rh_2(II,III) Re(I)$bpy^{-\bullet}$, before charge recombination and return to the ground state. This last path would be more similar to the observed intermolecular electron transfer outer-sphere mechanism with halogenated molecules.[5c]

Chart 4.1. Scheme of the Described Amidinate (top) and Acetate (bottom) Based Rh_2 Ru_4 Assemblies[4b,6a]

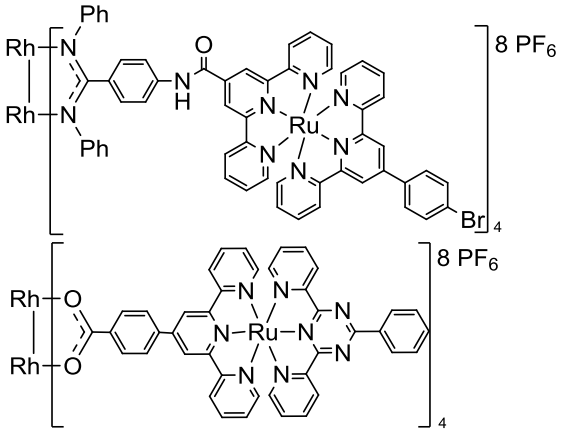

These rhenium-based assemblies can be compared to ruthenium-based assemblies previously synthesized (Chart 4.1).[6a,13] These complexes were based on a tridentate terpyridine or triazine ligand bonded to the ruthenium. It was shown, in the case of the rhodium acetate assemblies, where only a phenyl spacer separates the ruthenium from the rhodium core, that energy transfer was observed for a higher energy chromophore (above 1.7 eV). Below that point, the luminescence of the chromophore was retained.[13b,13c] It was shown that the nonradiative excited state of the rhodium acetate dimer was in the same range as the ^{3}MLCT of the ruthenium chromophore, thus containing insufficient driving force to quench the latter chromophores of lower energy.

An emission was still observed for amidinate-based rhodium dimers with bridged ruthenium complexes linked by an amide moiety to the dimer.[6a] The ruthenium is significantly farther away from the rhodium core than the rhenium in the present work and this distance is enough to prohibit fast quenching of the excited state of the ruthenium chromophores. As our assemblies are much more compact with the rhenium being only a pyridyl ring away from the core of the dimer, quenching still occurs.

4.7. Conclusion

In the different assemblies, the rhenium chromophore base properties are not altered significantly as demonstrated by the unchanged redox properties in electrochemistry and little change in the IR and UV−vis spectra. The rhodium dimer itself is affected, and with each rhenium chromophore added, the electron density around the dimer is lowered, making it harder to oxidize the rhodium core and giving rise to a bathochromic shift for the electronic transitions in the visible region. The presence of four chromophores also increased the binding strength of acetonitrile along the axial coordination site of the dimer, making its solvatochromism properties adjustable. Computed models were in good agreement and set a good basis for future computational modeling of rhodium dimers, thus allowing evaluation of their properties before synthesis. Although in the case of **4-4** the MO energies were flawed with lower energy values due to the high positive charge of the assembly, this limitation should be considered before evaluating systems using only *in silico* data.

Another interesting feature is the quenching of the rhenium emission observed in **4-1** to **4-4**. More research on the quenching of the rhenium chromophore is planned to uncover the

relaxation mechanism; of particular interest will be the transient absorption spectra of the assemblies, both in the visible and in the IR.

The ability to prepare and isolate these different species permits a stepwise pathway to make larger assemblies by using the free pyridyl sites for subsequent coordination. One such application is the studies of the assemblies as chromophores for the photocatalytic production of dihydrogen using different catalysts that have an affinity for pyridine, e.g., cobalt dimethylglyoxime. Preliminary results are promising, but without a deeper understanding of the active species via theoretical models, they cannot be fully discussed at this time.

4.8. Acknowledgements

We are grateful to the Natural Sciences and Engineering Research Council of Canada, the Ministère de l'Éducation du Québec and the Université de Montréal for financial support and for the Université de Montréal's Altix and Briarée supercomputers supported by le Réseau Québécois de Calculs de Haute Performances (RQCHP) and University of Manitoba's Grex supercomputer supported by Westgrid both networks under the national supercomputing platform, Compute Canada / Calcul Canada.

4.9. Supporting Information

Extra figures, tables, computational data, and data in CIF format. This material is available free of charge via the Internet at http://pubs.acs.org. X-ray crystallographic data in CIF format can be obtained from the Cambridge Structural Database (CCDC662536, 662537, 906876);

4.10. References

(1) (a) Chifotides, H. T.; Dunbar, K. R. In *Multiple Bonds between Metal Atoms*; 3rd ed.; Cotton, F. A., Murillo, C. A., Walton, R. A., Eds.; Springer: New York, 2005; p 465. (b) Cotton, F. In *Multiple Bonds between Metal Atoms*; 3rd ed.; Cotton, F. A., Murillo, C. A., Walton, R. A., Eds.; Springer: New York, 2005; p 707. (c) Patmore, N. J. *Organomet. Chem.* **2010**, *36*, 77.

(2) (a) Korotvicka, A.; Necas, D.; Kotora, M. *Curr. Org. Chem.* **2012**, *16*, 1170. (b) Du, B. J. *Org. Process Res. Dev.* **2011**, *15*, 758. (c) Tanaka, S.; Masaoka, S.; Yamauchi, K.; Annaka, M.; Sakai, K. *Dalton Trans.* **2010**, *39*, 11218. (d) Doyle, M. P.; Duffy, R.; Ratnikov, M.; Zhou, L. *Chem. Rev.* **2010**, *110*, 704. (e) Lebel, H. In *Catalyzed Carbon-Heteroatom Bond Formation*; Wiley-VCH Verlag GmbH & Co. KGaA: 2010; p 137. (f) Doyle, M. P. *J. Org. Chem.* **2006**, *71*, 9253. (g) Timmons, D.; Doyle, M. In *Multiple Bonds between Metal Atoms*; 3rd ed.; Cotton, F. A., Murillo,

C. A., Walton, R. A., Eds.; Springer: New York, 2005; p 591. (h) Lindsay, V. N. G.; Charette, A. B. *ACS Catal.* **2012**, *2*, 1221.

(3) (a) Aguirre, J. D.; Lutterman, D. A.; Angeles-Boza, A. M.; Dunbar, K. R.; Turro, C. *Inorg. Chem.* **2007**, *46*, 7494. (b) Angeles-Boza, A. M.; Bradley, P. M.; Fu, P. K. L.; Shatruk, M.; Hilfiger, M. G.; Dunbar, K. R.; Turro, C. *Inorg. Chem.* **2005**, *44*, 7262. (c) Burya, S. J.; Palmer, A. M.; Gallucci, J. C.; Turro, C. *Inorg. Chem.* **2012**, *51*, 11882. (d) Chifotides, H. T.; Lutterman, D. A.; Dunbar, K. R.; Turro, C. *Inorg. Chem.* **2011**, *50*, 12099. (e) Joyce, L. E.; Aguirre, J. D.; Angeles-Boza, A. M.; Chouai, A.; Fu, P. K. L.; Dunbar, K. R.; Turro, C. *Inorg. Chem.* **2010**, *49*, 5371. (f) Lutterman, D. A.; Fu, P. K. L.; Turro, C. *J. Am. Chem. Soc.* **2006**, *128*, 738.

(4) (a) Cooke, M. W.; Chartrand, D.; Hanan, G. S. *Coord. Chem. Rev.* **2008**, *252*, 903. (b) Cooke, M. W.; Hanan, G. S. *Chem. Soc. Rev.* **2007**, *36*, 1466. (c) Cotton, F. A.; Lin, C.; Murillo, C. A. *Acc. Chem. Res.* **2001**, *34*, 759.

(5) (a) Bear, J. L.; Van Caemelbecke, E.; Ngubane, S.; Da-Riz, V.; Kadish, K. M. *Dalton Trans.* **2011**, *40*, 2486. (b) Bear, J. L.; Han, B. C.; Li, Y. L.; Ngubane, S.; Van Caemelbecke, E.; Kadish, K. M. *Polyhedron* **2009**, *28*, 1551. (c) Lutterman, D. A.; Degtyareva, N. N.; Johnston, D. H.; Gallucci, J. C.; Eglin, J. L.; Turro, C. *Inorg. Chem.* **2005**, *44*, 5388. (d) Bear, J. L.; Han, B.; Wu, Z.; Van Caemelbecke, E.; Kadish, K. M. *Inorg. Chem.* **2001**, *40*, 2275. (e) Ren, T.; Lin, C.; Valente, E. J.; Zubkowski, J. D. *Inorg. Chim. Acta* **2000**, *297*, 283. (f) He, L. P.; Yao, C. L.; Naris, M.; Lee, J. C.; Korp, J. D.; Bear, J. L. *Inorg. Chem.* **1992**, *31*, 620. (g) Bear, J. L.; Yao, C. L.; Lifsey, R. S.; Korp, J. D.; Kadish, K. M. *Inorg. Chem.* **1991**, *30*, 336. (h) Cotton, F. A.; Feng, X. *Inorg. Chem.* **1989**, *28*, 1180. (i) Rizzi, G. A.; Casarin, M.; Tondello, E.; Piraino, P.; Granozzi, G. *Inorg. Chem.* **1987**, *26*, 3406. (j) Piraino, P.; Bruno, G.; Lo Schiavo, S.; Laschi, F.; Zanello, P. *Inorg. Chem.* **1987**, *26*, 2205. (k) Le, J. C.; Chavan, M. Y.; Chau, L. K.; Bear, J. L.; Kadish, K. M. *J. Am. Chem. Soc.* **1985**, *107*, 7195.

(6) (a) Cooke, M. W.; Santoni, M. P.; Hanan, G. S.; Proust, A.; Hasenknopf, B. *Dalton Trans.* **2009**, 3671. (b) Chartrand, D.; Hanan, G. S. *Chem. Commun.* **2008**, 727. (c) Zuo, J.-L.; Fabrizi de Biani, F.; Santos, A. M.; Kohler, K.; Kuehn, F. E. *Eur. J. Inorg. Chem.* **2003**, 449.

(7) Takeda, H.; Koike, K.; Morimoto, T.; Inumaru, H.; Ishitani, O. *Adv. Inorg. Chem.* **2011**, *63*, 137.

(8) Probst, B.; Guttentag, M.; Rodenberg, A.; Hamm, P.; Alberto, R. *Inorg. Chem.* **2011**, *50*, 3404.

(9) (a) Yui, T.; Tamaki, Y.; Sekizawa, K.; Ishitani, O. *Top. Curr. Chem.* **2011**, *303*, 151. (b) Kumar, B.; Smieja, J. M.; Sasayama, A. F.; Kubiak, C. P. *Chem. Commun.* **2012**, *48*, 272.

(10) (a) Kumar, A.; Sun, S.-S.; Lees, A. J. *Top. Organomet. Chem.* **2010**, *29*, 1. (b) Patrocinio, A. O. T.; Brennaman, M. K.; Meyer, T. J.; Murakami Iha, N. Y. *J. Phys. Chem. A* **2010**, *114*, 12129 . (c) Chartrand, D.; Castro, R. C. A.; Hanan, G. S. *Inorg. Chem.* **2012**, *51*, 12738.

(11) Barber, J. *Philos. Trans. R. Soc., A* **2007**, *365*, 1007.
(12) (a) Casanova, M.; Zangrando, E.; Iengo, E.; Alessio, E.; Indelli, M. T.; Scandola, F.; Orlandi, M. *Inorg. Chem.* **2008**, *47*, 10407. (b) Slone, R. V.; Hupp, J. T. *Inorg. Chem.* **1997**, *36*, 5422. (c) Kon, H.; Tsuge, K.; Imamura, T.; Sasaki, Y.; Ishizaka, S.; Kitamura, N. *Inorg. Chem.* **2006**, *45*, 6875. (d) Splan, K. E.; Keefe, M. H.; Massari, A. M.; Walters, K. A.; Hupp, J. T. *Inorg. Chem.* **2002**, *41*, 619.
(13) (a) Cooke, M. W.; Santoni, M. P.; Hanan, G. S.; Loiseau, F.; Proust, A.; Hasenknopf, B. *Inorg. Chem.* **2008**, *47*, 6112. (b) Cooke, M. W.; Hanan, G. S.; Loiseau, F.; Campagna, S.; Watanabe, M.; Tanaka, Y. *J. Am. Chem. Soc.* **2007**, *129*, 10479. (c) Cooke, M. W.; Hanan, G. S.; Loiseau, F.; Campagna, S.; Watanabe, M.; Tanaka, Y. *Angew. Chem. Int. Ed.* **2005**, *44*, 4881.
(14) (a) Gans, P.; Sabatini, A.; Vacca, A. *Anal. Chim.* **1999**, *89*, 45. (b) Gans, P.; Sabatini, A.; Vacca, A. *Talanta* **1996**, *43*, 1739.
(15) Connelly, N.; Geiger, W. *Chem. Rev.* **1996**, *96*, 877.
(16) Schmidt, S. P.; Trogler, W. C.; Basolo, F.; Urbancic, M. A.; Shapley, J. R. In *Inorganic. Syntheses*; John Wiley & Sons, Inc.: New York, 2007; p 41.
(17) Hevia, E.; Perez, J.; Riera, V.; Miguel, D.; Kassel, S.; Rheingold, A. *Inorg. Chem.* **2002**, *41*, 4673.
(18) Caspar, J. V.; Meyer, T. J. *J. Phys. Chem.* **1983**, *87*, 952.
(19) Casey, C. P.; O'Connor, J. M. *Organometallics* **1985**, *4*, 384.
(20) (a) *SAINT*, version 7.68A; Bruker AXS Inc.: Madison, WI, 2009. (b) Sheldrick, G. M.; *SADABS*, version 2008/1; Bruker AXS Inc.: Madison, WI, 2008.
(21) Sheldrick, G. M. *Acta Crystallogr., Sect. A: Found. Crystallogr.* **2008**, *A64*, 112.
(22) Farrugia, L. J. *J. Appl. Crystallogr.* **1997**, *30*, 565.
(23) (a) Frisch, M. J.; Trucks, G. W.; Schlegel, H. B.; Scuseria, G. E.; Robb, M. A.; Cheeseman, J. R.; Montgomery, J. A., Jr.; Vreven, T.; Kudin, K. N.; Burant, J. C.; Millam, J. M.; Iyengar, S. S.; Tomasi, J.; Barone, V.; Mennucci, B.; Cossi, M.; Scalmani, G.; Rega, N.; Petersson, G. A.; Nakatsuji, H.; Hada, M.; Ehara, M.; Toyota, K.; Fukuda, R.; Hasegawa, J.; Ishida, M.; Nakajima, T.; Honda, Y.; Kitao, O.; Nakai, H.; Klene, M.; Li, X.; Knox, J. E.; Hratchian, H. P.; Cross, J. B.; Bakken, V.; Adamo, C.; Jaramillo, J.; Gomperts, R.; Stratmann, R. E.; Yazyev, O.; Austin, A. J.; Cammi, R.; Pomelli, C.; Ochterski, J. W.; Ayala, P. Y.; Morokuma, K.; Voth, G. A.; Salvador, P.; Dannenberg, J. J.; Zakrzewski, V. G.; Dapprich, S.; Daniels, A. D.; Strain, M. C.; Farkas, O.; Malick, D. K.; Rabuck, A. D.; Raghavachari, K.; Foresman, J. B.; Ortiz, J. V.; Cui, Q.; Baboul, A. G.; Clifford, S.; Cioslowski, J.; Stefanov, B. B.; Liu, G.; Liashenko, A.; Piskorz, P.; Komaromi, I.; Martin, R. L.; Fox, D. J.; Keith, T.; Al-Laham, M. A.; Peng, C. Y.; Nanayakkara, A.; Challacombe, M.; Gill, P. M. W.; Johnson, B.; Chen, W.; Wong, M. W.; Gonzalez, C.; Pople, J. A.; *Gaussian 03*, Revision C.02; Gaussian, Inc.: Wallingford, CT, 2004. (b) Frisch, M. J.; Trucks, G. W.; Schlegel, H. B.; Scuseria, G. E.; Robb, M. A.; Cheeseman, J. R.; Scalmani, G.; Barone, V.; Mennucci, B.; Petersson, G. A.; Nakatsuji, H.; Caricato, M.; Li, X.; Hratchian, H. P.; Izmaylov, A. F.; Bloino, J.;

Zheng, G.; Sonnenberg, J. L.; Hada, M.; Ehara, M.; Toyota, K.; Fukuda, R.; Hasegawa, J.; Ishida, M.; Nakajima, T.; Honda, Y.; Kitao, O.; Nakai, H.; Vreven, T.; Montgomery, J. A., Jr.; Peralta, J. E.; Ogliaro, F.; Bearpark, M.; Heyd, J. J.; Brothers, E.; Kudin, K. N.; Staroverov, V. N.; Kobayashi, R.; Normand, J.; Raghavachari, K.; Rendell, A.; Burant, J. C.; Iyengar, S. S.; Tomasi, J.; Cossi, M.; Rega, N.; Millam, N. J.; Klene, M.; Knox, J. E.; Cross, J. B.; Bakken, V.; Adamo, C.; Jaramillo, J.; Gomperts, R.; Stratmann, R. E.; Yazyev, O.; Austin, A. J.; Cammi, R.; Pomelli, C.; Ochterski, J. W.; Martin, R. L.; Morokuma, K.; Zakrzewski, V. G.; Voth, G. A.; Salvador, P.; Dannenberg, J. J.; Dapprich, S.; Daniels, A. D.; Farkas, Ö.; Foresman, J. B.; Ortiz, J. V.; Cioslowski, J.; Fox, D. J.; *Gaussian 09*, Revision D.01, Gaussian, Inc.: Wallingford, CT, 2009.

(24) (a) Lee, C.; Yang, W.; Parr, R. G. *Phys. Rev. B: Condens. Matter* **1988**, *37*, 785. (b) Becke, A. D. *J. Chem. Phys.* **1993**, *98*, 5648.

(25) (a) Hay, P. J.; Wadt, W. R. *J. Chem. Phys.* **1985**, *82*, 299. (b) Ehlers, A. W.; Boehme, M.; Dapprich, S.; Gobbi, A.; Hoellwarth, A.; Jonas, V.; Koehler, K. F.; Stegmann, R.; Veldkamp, A.; et, a. *Chem. Phys. Lett.* **1993**, *208*, 111.

(26) (a) Barone, V.; Cossi, M. *J. Phys. Chem. A* **1998**, *102*, 1995. (b) Cossi, M.; Rega, N.; Scalmani, G.; Barone, V. *J. Comput. Chem.* **2003**, *24*, 669.

(27) (a) Dennington II, R.; Keith, T.; Millam, J.; Eppinnett, K.; Hovell, W. L.; Gilliland, R.; *Gaussview 3.09*, Semichem, Inc.: Shawnee Mission, KS, 2003. (b) O'Boyle, N. M.; Tenderholt, A. L.; Langner, K. M. *J. Comput. Chem.* **2008**, *29*, 839. (c) Skripnikov, L.; *Chemissian*, version 3.3; 2005.

(28) Pruchnik, F. P.; Pruchnik, H.; Kochel, A. *Polyhedron* **2009**, *28*, 769.

(29) Kawamura, T.; Maeda, M.; Miyamoto, M.; Usami, H.; Imaeda, K.; Ebihara, M. *J. Am. Chem. Soc.* **1998**, *120*, 8136.

(30) Oshin, K.; Landis, A. M.; Smucker, B. W.; Eichhorn, D. M.; Rillema, D. P. *Acta Crystallogr. Sect. E: Struct. Rep. Online* **2004**, *E60*, m1126.

(31) (a) Allen, F. H. *Acta Crystallogr. B* **2002**, *58*, 380. (b) Bruno, I. J.; Cole, J. C.; Edgington, P. R.; Kessler, M.; Macrae, C. F.; McCabe, P.; Pearson, J.; Taylor, R. *Acta Crystallogr. B* **2002**, *58*, 389.

(32) Casanova, M.; Zangrando, E.; Munini, F.; Iengo, E.; Alessio, E. *Dalton Trans.* **2006**, 5033.

(33) (a) Dickson, P. M.; McGowan, M. A. D.; Yearwood, B.; Heeg, M. J.; Oliver, J. P. *J. Organomet. Chem.* **1999**, *588*, 42. (b) Sanders, J. K. M.; Hunter, B. K. *Modern NMR Spectroscopy: A Guide for Chemists*; Oxford University Press: USA, 1993. (c) Michinori, O. *Methods in Stereochemical Analysis, Vol. 4: Applications of Dynamic NMR Spectroscopy to Organic Chemistry*; VCH: New York, 1985.

(34) (a) Sacksteder, L.; Zipp, A. P.; Brown, E. A.; Streich, J.; Demas, J. N.; DeGraff, B. A. *Inorg. Chem.* **1990**, *29*, 4335. (b) Kuehn, F. E.; Zuo, J.-L.; Fabrizi de Biani, F.; Santos, A. M.; Zhang, Y.; Zhao, J.; Sandulache, A.; Herdtweck, E. *New J. Chem.* **2004**, *28*, 43.

(35) (a) Bradley, P. M.; Bursten, B. E.; Turro, C. *Inorg. Chem.* **2001**, *40*, 1376. (b) Liu, L. M.; Bear, J. L. *Acta Phys.-Chim. Sin.* **1989**, *5*, 644.
(36) Vlček, A.; Busby, M. *Coord. Chem. Rev.* **2006**, *250*, 1755.

Chapitre 5: Design d'un photoréacteur et production d'hydrogène par photocatalyse utilisant des assemblages rhodium-rhénium

5.1. Introduction

Ce chapitre est divisé en deux grands volets : l'élaboration du photoréacteur et les études photocatalytiques effectuées avec celui-ci sur les assemblages du chapitre précédent.

À noter que les résultats de la production d'hydrogène sont présentés en TON (*Turnover Number*) et que celui-ci correspond au ratio entre le nombre de moles de H_2 générées et le nombre de moles du photosensibilisateur (PS) ou du catalyseur utilisés. Dans la littérature, le TON en fonction du PS est doublé, présenté en ½ mole de H_2 par mole de PS, faisant allusion au fait que le PS effectue deux cycles par mole d'hydrogène générée. À moins de notation contraire, les TON en fonction du PS présentés dans cette thèse ne sont pas doublés de cette façon.

5.1.1. La photocatalyse

Les principes de la photocatalyse des systèmes étudiés ont été abordés dans la section 1.4. Le Schéma 5.1 illustre les composés principaux qui seront discutés dans ce chapitre. Le complexe **5-0** correspond au complexe **3-6** et au complexe **4-5** des chapitres précédents. Les assemblages **5-1**, **5-2**, **5-3** et **5-4** correspondent respectivement aux assemblages **4-1**, **4-2**, **4-3** et **4-4** du chapitre précédent. Les chromophores de rhénium **5-5**, **5-6** et **5-8** correspondent respectivement aux chromophores **1-1**, **1-3** et **1-2** introduits dans le chapitre 1. Le complexe **5-6** est aussi les complexes **2-3** et **4-8** des chapitres 2 et 4. Les catalyseurs de cobalt **5-9** et **5-10** correspondent respectivement aux complexes **1-7** et **1-6**.

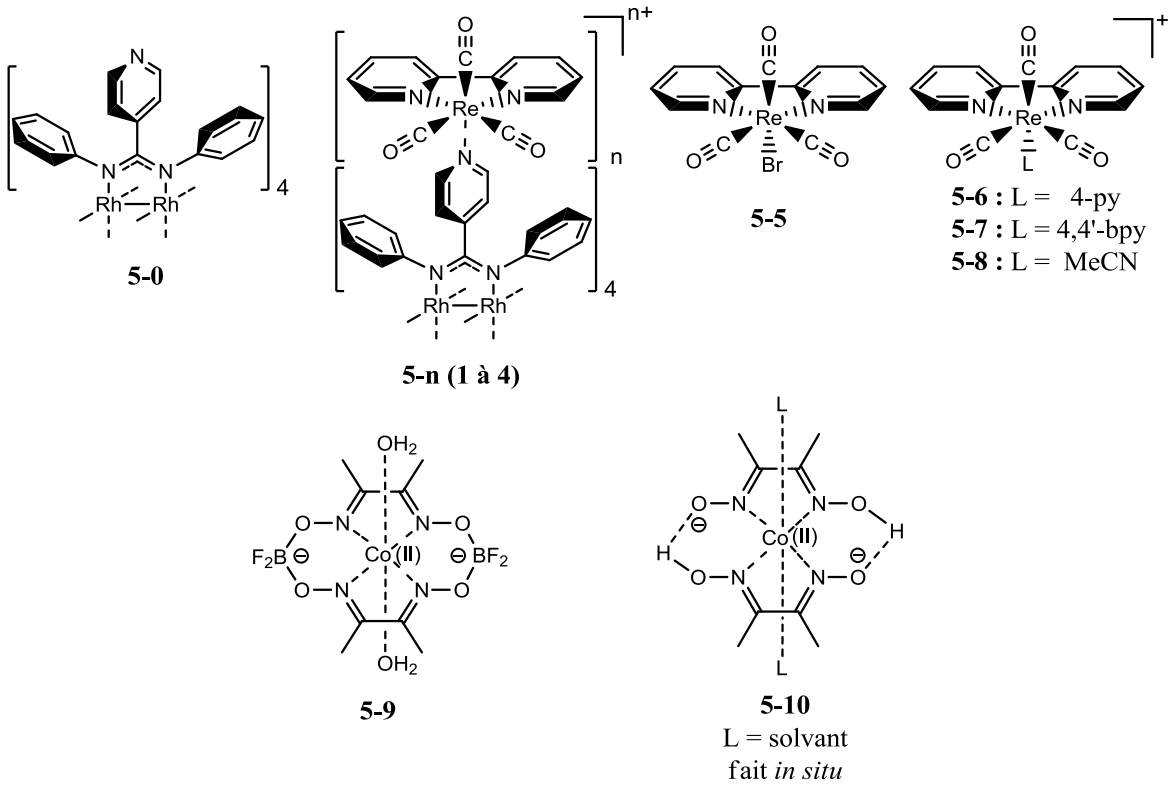

Schéma 5.1. Les molécules utilisées pour la photocatalyse.

5.1.2. Le Photoréacteur

Beaucoup de photoréacteurs commerciaux sont sur le marché, mais en général ils sont conçus pour des applications de très grand volume, avec irradiation UV, ou sont conçus pour imiter le flux lumineux solaire, sans grande sélection de longueur d'onde d'irradiation. Ces photoréacteurs ne viennent pas équipés d'équipements analytiques et ne sont souvent pas conçus pour accommoder un suivi de la réaction. Les photoréacteurs de recherche sont quant à eux de fabrication maison assemblés avec diverses technologies, ce qui a pour effet de rendre la comparaison littéraire très difficile, car les sources de lumière et les géométries vont être différentes entre chaque groupe de recherche. C'est pour ces raisons que nous avons fabriqué notre propre système.

Le premier point à considérer est la méthode d'analyse, qui dictera les contraintes expérimentales du photoréacteur. Plusieurs méthodes analytiques pour la quantification de l'hydrogène figurent sur le Tableau V-1. La première technique indiquée dans le tableau, par volumétrie, soit par burette inversée ou soit par déplacement d'eau dans un échantillon tenu sous vide statique, permet de déterminer le volume de gaz formé, mais pas sa composition.

Les expériences de Jean-Marie Lehn utilisaient ces deux techniques; la première, moins précise, pour obtenir une vitesse de réaction, la deuxième pour une mesure unique de gaz produit à la fin de la réaction.[1] Ces deux techniques étaient accompagnées par la chromatographie à phase gazeuse (GC) afin d'identifier le gaz. De nos jours, la technique de la burette s'appliquerait encore, mais elle est limitée à des systèmes qui génère de l'hydrogène à un débit assez rapide (1 mL/heure et plus). En dessous de ce volume, la détection va être trop facilement perturbée par la pression atmosphérique, la température ambiante et la diffusion de l'hydrogène dans l'eau. De plus, les méthodes volumétriques ne sont pas automatisables.

Tableau V-1. Les différentes méthodes d'analyse quantitative de dihydrogène.

Méthode	Système ouvert	Directe	Non-destructrice	Sensible < 25 ppm	Non spécifique	Isotopique (H_2,HD,D_2)	Applicable en série	Intervalle Analyse	Coût	Autre remarque
Volumétrique : Burette inversée			X		X			n.a.	100$	Affecté par P_{atm}, et diffusion H_2
Senseur de pression électronique			X	X	X			ms	100$	Dégradation à long terme?
Chromatographie à phase gazeuse	X	X	X	X	X	X	X	min	30k$	Séparation des gaz
Spectrométrie de masse	X	X	X	X	X	X	X	ms	80k$	Sans séparation
Détecteur H_2 électronique spécifique	X	X	X	X			X	ms	30k$	Dégradation à long terme?
Spectroscopie RMN		X	X	?		X		10 min	$$$	ardu

Le détecteur de pression électronique est la méthode moderne équivalant à la burette inversée. Elle requiert un système fermé hermétiquement à l'intérieur duquel le détecteur sera placé. Puisque ces détecteurs sont relativement peu dispendieux, il est peu onéreux de paralléliser ce type de montage, quoique l'acquisition de données requiert un traitement d'informations et un système de gestion électronique complexe. C'est la méthode de choix du groupe du Pr Bernhard qui ont développé un système à 16 canaux.[2] Ici encore, une injection par GC permet d'identifier les gaz formés en fin de réaction. Pour une réaction classique, ce système s'applique bien, mais il ne permet pas de suivre l'évolution de deux gaz et ne peut pas être appliqué si la réaction étudiée consomme un gaz, comme ce serait le cas pour les réactions impliquant le gaz carbonique.

Les GC utilisant un détecteur à conductivité thermique et la spectrométrie de masse (MS) sont excellents pour la mesure d'hydrogène et permettent des mesures à très basse concentration, de l'ordre du ppm. Les deux techniques permettent de regarder plusieurs espèces gazeuses. Elles peuvent aussi distinguer H_2 de D_2, ce qui les rend utiles pour une étude avec effet isotopique ou pour vérifier la source de proton. La grande différence entre les deux techniques est le temps d'analyse : le GC sépare les gaz et les analyse individuellement, tandis que le MS analyse tous les gaz en même temps. Pour l'hydrogène, le MS est idéal, mais pour d'autres gaz, tel le monoxyde de carbone, il y a un problème, car il a la même masse que le diazote. Il existe des détecteurs électroniques spécifiques à l'hydrogène qui offrent les mêmes avantages que le MS, mais ils sont généralement très coûteux compte tenu de leur fonctionnalité limitée.

La technique par RMN permet de détecter de l'hydrogène dans un échantillon, mais n'est pas pratique. Elle ne montre que ce qui est dissous dans l'échantillon, nécessite un tube scellé et requiert une calibration très spécifique pour chaque type de solvant ou de solution utilisé. Les avantages possibles d'une telle méthode sont le petit volume réactionnel utilisé, l'absence de prélèvement gazeux et la possibilité de suivre d'autres espèces en solution. Cependant, l'irradiation ne peut pas continuer pendant l'analyse, à moins d'avoir un RMN modifié dédié à cette seule fin, ce qui serait très dispendieux.

Le premier point du Tableau V-1, le système ouvert, est très important. Toutes les analyses présentées s'appliquent pour des systèmes fermés, mais quelques-unes seulement sont applicables pour des systèmes ouverts. Le Schéma 5.2 illustre la principale différence chimique des deux systèmes. Le premier accumule l'hydrogène, qui se trouve dans l'espace

libre au-dessus de la solution, mais une certaine partie reste dissoute dans le solvant. Ceci peut avoir des effets non souhaitables, comme un ralentissement de la réaction, dus à un empoisonnement du site actif, ou comme une réaction d'hydrogénation secondaire catalysée qui pourrait décomposer n'importe quel élément du système. L'augmentation de pression peut aussi entraîner des risques de fuite plus importante lors des analyses, ce qui peut être un problème pour des expériences effectuées sur de grands laps de temps ou avec des sceaux moins hermétiques. Également, le prélèvement gazeux peut être très peu reproductible s'il est fait manuellement sur de petits volumes.

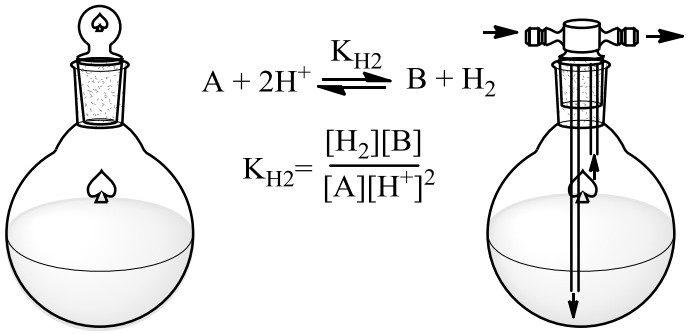

Schéma 5.2. Système fermé vs système ouvert.

Le système ouvert est quant à lui très simple à gérer. Le milieu réactionnel est purgé continuellement avec un débit constant de gaz inerte. Ce système ne possède aucun des problèmes du système fermé et la réaction de formation d'hydrogène est favorisée en tout temps par le principe de Le Chatelier puisqu'il est éliminé systématiquement. De plus, le système ouvert permet une quantification de la vitesse de réaction par une méthode directe (ce qui n'est pas le cas pour les méthodes de changement de volume ou de pression). Le seul inconvénient de ce système est que la concentration d'hydrogène à tout moment pendant la réaction est très faible comparée à la méthode fermée. Pour qu'elle soit utilisable, il faut une méthode très sensible sinon les réactions devraient être réalisées à très grande échelle.

D'autres analyses peuvent être intégrées au photoréacteur, soit au travers d'une sonde, soit avec une circulation en circuit fermé de la solution, soit par échantillonnage périodique du milieu réactionnel. Le dernier point, le plus difficile à automatiser, pourrait être utilisé pour faire un suivi de la réaction par chromatographie liquide ou par injection directe dans un MS. Il est à proscrire sans automatisation, car il peut facilement introduire de la

contamination ou des fuites. Une sonde optique est l'idéal pour suivre une réaction, cependant elle apporte des contraintes dimensionnelles importantes. La circulation fermée est facilement mise en œuvre, mais apporte un changement au niveau de la réaction. Il y a deux zones différentes : l'une irradiée et l'autre dans le noir. Cela a pour effet de créer un réservoir qui va ralentir les changements de vitesse réactionnelle et de vitesse de décomposition.

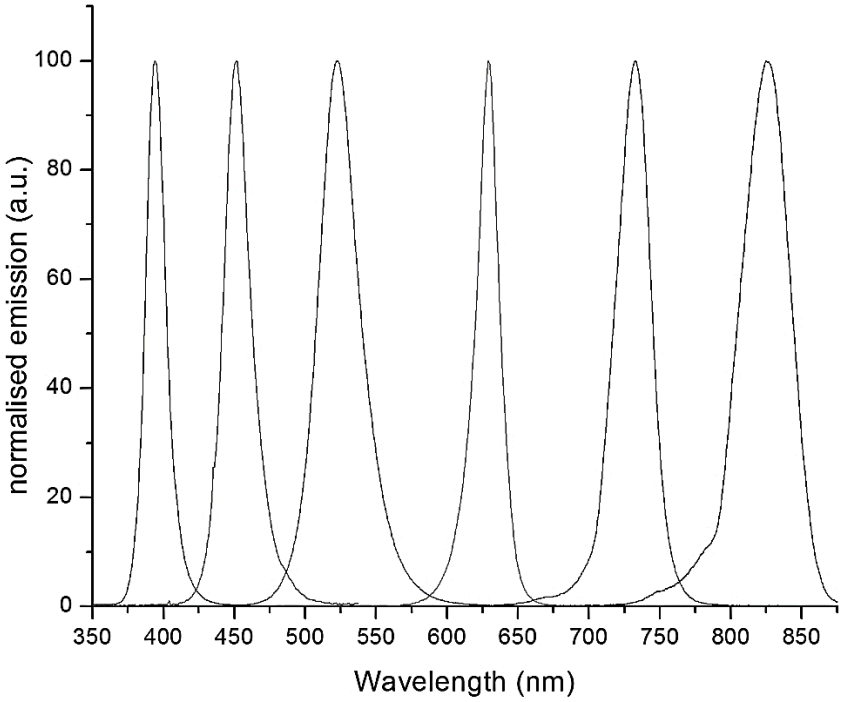

Figure 5.1. Spectres d'émission normalisés des différentes lampes DEL de notre photoréacteur.

L'élément le plus important du photoréacteur est sans doute la source de lumière. Le Tableau V-2 illustre les différents choix de sources lumineuses disponibles. Les diodes électroluminescentes (DEL) et les lumières à arc électrique sont les plus couramment utilisées. Ce sont les lampes à arc électrique les plus utilisées, car elles permettent une puissance lumineuse excellente qui peut être décomposée avec des filtres ou avec un réseau, ce qui les rend très polyvalentes. Cependant, les DEL ont plusieurs avantages sur celles-ci : elles sont beaucoup plus petites et d'une meilleure efficacité énergétique. De plus, elles ont une bande d'émission relativement fine (soit environ ±25 nm pour la zone à 10% d'intensité maximale), qui va du proche ultraviolet (UVC) (380 nm) jusqu'à le proche infrarouge (NIR) (850 nm) (voir Figure 5.1, exemple d'émission de DEL de notre système). Cette

caractéristique ne les rend pas intéressantes pour un simulateur solaire (qui devrait contenir plusieurs LED à différentes longueurs d'onde pour simuler le spectre d'un corps noir), mais les rend très utiles pour une étude où la longueur d'onde d'irradiation est importante, ce qui est notre cas. Une lampe à arc muni de filtre, ou encore mieux, munie d'un réseau optique, peut le faire aussi, mais requiert un système beaucoup plus lourd, énergétique, volumineux et complexe. L'avantage principal d'un système d'arc électrique avec réseau optique est la possibilité de faire un balayage spectral et de faire un simulateur solaire avec le même appareil.

Tableau V-2. Avantages et inconvénients des différentes lampes d'un photoréacteur*

Source de photon	Avantages	inconvénients
Lumière DEL • ***I*ndividuel ou en réseau :** • **Puissance variable, 10 mW à 10 W.**	• Coût • Longévité • Étroite fenêtre de λ • petite dimension : Intégration facile • Faible génération de chaleur	• Plage de λ fixe • *I* et λ variable d'un fournisseur à l'autre • *I* relativement faible • Simulateur solaire difficilement réalisable
Lumière incandescente • **Tungstène, halogène**	• *I* moyen • Grande fenêtre spectrale (corps noir) • Simulation solaire disponible • Coût	• Longévité • Grande dimension : intégration complexe • Filtres ou réseau requis pour plage de λ étroite • *I* variable selon λ
Lumière à arc électrique • **Xénon, Mercure**	• *I* fort • Grande fenêtre spectrale • (corps noir) • Simulation solaire disponible	• Coût • Longévité • Grande dimension : intégration complexe • Filtres ou réseau requis pour plage de λ étroite
Lumière fluorescente • **Néon** • **fluorocompacte**	• *I* moyen (pour UV) • Émission dans région UV • Coût	• Plage de λ fixe et large • Lumière commerciale blanche : loin du spectre solaire. (3 bandes d'émission) • *I* très faible (visible)
Lumière Laser	• Longévité • Étroite fenêtre de λ • *I* fort • Rendement quantique calculable directement	• Plage de λ fixe • Coût • *I* concentré en un point • Dangereux • Simulateur solaire impossible

* *I* = intensité lumineuse

La photoréaction consomme les photons, donc il serait nécessaire d'en déterminer le nombre consommé ou transmit, du moins si l'on désire suivre l'effet du flux lumineux sur la réaction. Mesurer le flux lumineux est très facile pour un laser, puisqu'il s'agit d'une source monochromatique ponctuelle. Un actinomètre optique peut mesurer directement la puissance reçue, mais pour toutes autres lumières polychromatiques, il est plus difficile d'avoir cette mesure puisqu'il faut la décomposer afin d'obtenir un flux par longueur d'onde. Plusieurs méthodes d'actinométrie chimique sont aussi disponibles pour déterminer le flux, mais sont spécifiques à une bande spectrale précise et sont applicables seulement dans une fenêtre spectrale donnée.[3]

Tableau V-3. Avantages et inconvénients des différentes géométries d'éclairage du réacteur.

Géométrie d'éclairage	Avantages	inconvénients
Éclairage rectiligne	• Flux constant • Idéal pour actinométrie chimique/optique	• Verrerie spécifique • Échantillon unique • Design complexe • Pénétration de la lumière • Coût
Éclairage diffus :	• Design simple	• Flux disperse • Actinométrie chimique seulement
Par le bas	• Design simple • Échantillons multiples • uniformisation du flux par rotation facile • Verrerie non-spécifique	• Bloqué par agitateur magnétique • Pénétration de la lumière (hauteur du solvant)
Enveloppant (ou latéral)	• Échantillons multiples • Absorption maximale	• Design complexe • Rotation plus difficile pour uniformisation • Verrerie spécifique
Enveloppé (à l'intérieur de l'échantillon)	• Absorption maximale • Efficace volume élevé	• Design complexe • Verrerie unique coûteuse • Échantillon unique

Le Tableau V-3 montre différentes géométries possibles. Une lumière focalisée adéquatement permet de former un faisceau rectiligne et rend facile la détermination du flux, idéal pour l'actinométrie optique et chimique, mais ne fonctionne que pour un échantillon à la fois. Il est possible de faire un montage multipuits avec ce type de système, mais il faut

une source lumineuse rectiligne par canal, calibré individuellement, ce qui peut devenir prohibitif. L'éclairage diffus (la lumière peut être focalisée, mais n'est pas rectiligne à travers l'échantillon) a le problème inhérent d'être moins intense plus l'échantillon est éloigné, ce qui impose des contraintes géométriques sur le système : la lumière doit être le plus près possible de l'échantillon. Pour les lampes DEL, ce n'est pas un problème, car elles ne génèrent que très peu de chaleur et sont très petites, donc il est facile de les positionner adéquatement. La géométrie enveloppée (lumière interne) semble excellente, mais n'est pas très utile, car elle ne devient qu'intéressante que pour des systèmes très volumineux où une lumière interne permet de maximiser l'absorption uniforme dans tout le photoréacteur. Elle n'est pas pratique pour un système à échantillon multiple.

Les deux autres géométries proposées dans le Tableau V-3, soit par le bas ou enveloppante, permettent de faire un design multiéchantillon. Un choix de design circulaire permet d'avoir un carrousel rotatif (ou mieux : une lampe rotative). Ceci permet d'uniformiser la lumière dans le photoréacteur, sans besoin de calibration pour chaque lumière individuelle ou pour chaque position possible dans le réacteur. Le design par le bas est le plus simple à mettre en œuvre, mais un système enveloppant est l'idéal.

Un autre détail à considérer pour le photoréacteur est le système de refroidissement. Il peut être à l'air, par immersion dans un liquide ou par contact thermique avec une plaque métallique. Pour un système DEL un refroidissement à l'air peut sembler suffisant. Cependant, pour toute expérience sérieuse de catalyse, la température ne devrait pas être une variable approximative, ce qui requiert un contrôle réel de la température, ajustable minimalement au degré près. Dans ce contexte, un refroidissement par immersion dans un bain d'eau est une méthode simple qui ne nuit pas à la transmission de lumière. Le modèle par contact thermique avec un bloc thermostaté a l'avantage d'éviter les dégâts d'eau, mais n'est pas très transparent. Un design judicieux (et complexe) d'un bloc de refroidissement incorporant les lumières dans les compartiments à échantillon pourrait maximiser l'intensité lumineuse sans compromettre le contrôle de température.

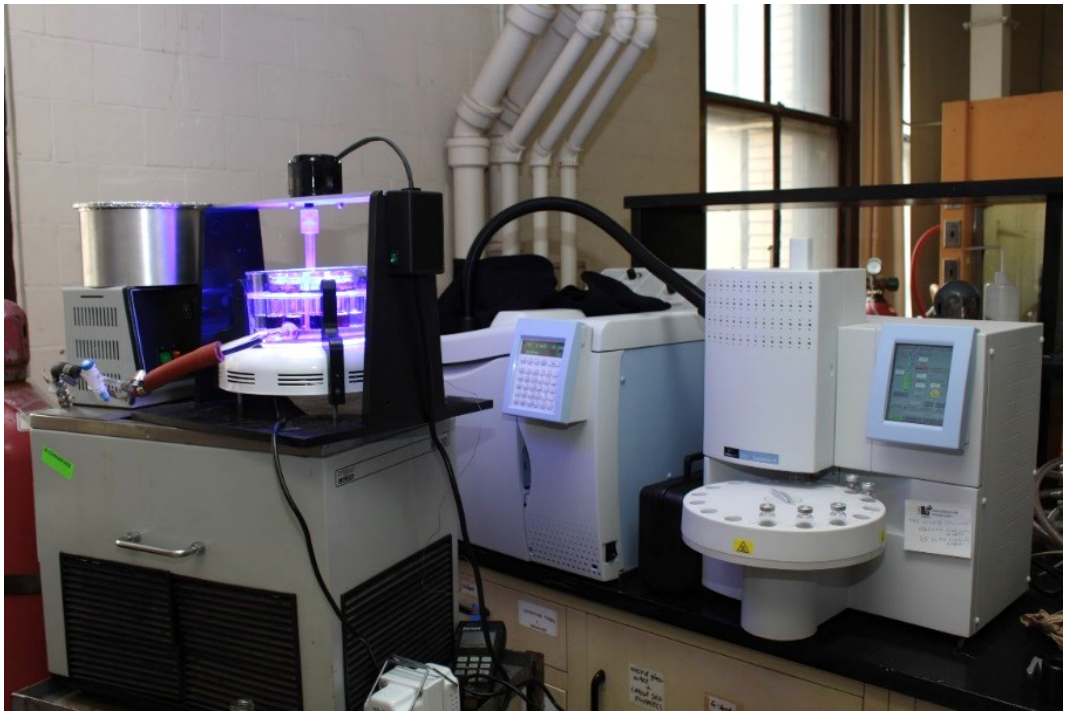

Figure 5.2. Le photoréacteur en mode système fermé, première version.

Finalement, le choix du photoréacteur s'est arrêté sur un modèle à base de DEL, utilisant une lampe commerciale circulaire composée de 90 DEL de 1 W chacune. Un bain thermostaté est monté au-dessus et les échantillons, scellés dans une fiole standard pour GC, sont placés dans un carrousel (Figure 5.2). Pour l'analyse d'hydrogène, un système GC-TCD avec un auto-injecteur de la phase gazeuse est utilisé. Celui-ci peut efficacement faire des mesures en circuit fermé de façon automatique. Il est aussi capable d'effectuer des mesures en circuit ouvert, avec un débit continu de gaz vecteur. De plus, le suivit par spectroscopie UV-vis a été intégré dans le design avec un système de circulation fermé.

5.2. Section expérimentale

La section expérimentale se retrouve en annexe. On y retrouve les détails concernant les études de photocatalyse. Elle est séparée en six parties :

- le système de mesure de dihydrogène généré pendant la réaction (section 5.S2);
- le photoréacteur et les conditions expérimentales utilisées avec celui-ci (section 5.S3);
- le suivi de la réaction par spectroscopie UV-vis (section 5.S4);
- les conditions expérimentales utilisées en Allemagne pour la photocatalyse (section 5.S5);
- les méthodes synthétiques des nouvelles espèces présentées dans cette section (section 5.S6);
- et une annexe informatique illustrant le fonctionnement du code développé pour le contrôle électronique du photoréacteur ainsi que le code source pour l'interface et le microcontrôleur (section 5.S7).

La synthèse des ligands isocyanures 1-bromo-4-isocyanobenzene (**CNPhBr)** et 4-isocyanopyridine (**CNPy)** suit une méthode de la littérature.[4,5] Cependant, une synthèse de **CNPy** n'a jamais été formellement reportée à cause de son instabilité malgré son utilisation dans plusieurs articles comme ligand.[6-8] La synthèse de celui-ci est présentée avec une caractérisation partielle à la section 5.S6.

Les conditions expérimentales des expériences photocatalytiques sont soit décrites dans un tableau soit incorporées à la légende des figures décrivant la production d'hydrogène.

Notez que les figures illustrant la compilation des spectres possèdent une échelle du temps changeant de sens selon les différentes expériences, afin d'obtenir la meilleure visualisation possible.

5.3. Résultats et discussion

5.3.1. Développement du photoréacteur

L'élaboration du photoréacteur pour la méthode système ouvert a été un défi important. La source d'inspiration majeure de celui-ci vient des travaux effectués par Benjamin Probst, du groupe du Pr R. Alberto, qui a développé un système similaire.[9,10] Plusieurs détails importants sont critiques pour le bon fonctionnement du système et le réacteur a évolué considérablement lors de son élaboration (Schéma 5.3), pour en arriver à la version actuelle (Schéma 5.4). Les points critiques sont les suivants :

1. Le flux de gaz vecteur doit être bullé dans la solution pour permettre un dégazage efficace de celle-ci. Une agitation magnétique est aussi conseillée pour le dégazage.
2. Les conduites en acier inoxydable sont idéales, mais ne devraient pas trempées directement dans la solution, une extension en PTFE est conseillée.
3. Le prébullage du gaz vecteur est essentiel pour tout solvant, afin d'éviter son évaporation à long terme.
4. Ce prébullage doit se faire à la même température, car s'il est plus chaud il y aura condensation et transfert de masse vers l'échantillon, suivi d'un possible débordement.
5. Une protection de débordement du liquide vers le GC est essentielle à cause du transfert potentiel de liquide vers les conduites par projection des bulles qui éclatent à la surface.
6. Limiter le volume réactionnel pour réduire la projection du point 5 (maximum 10 mL dans une fiole de 20 mL).
7. Le retour de pression après repositionnement de la valve d'injection doit être bloqué, un circuit en bobine utilisé au départ n'est qu'une solution temporaire.
8. Un débitmètre électronique ne peut pas être laissé en permanence sur le circuit, car il est endommagé par les vapeurs de solvants.

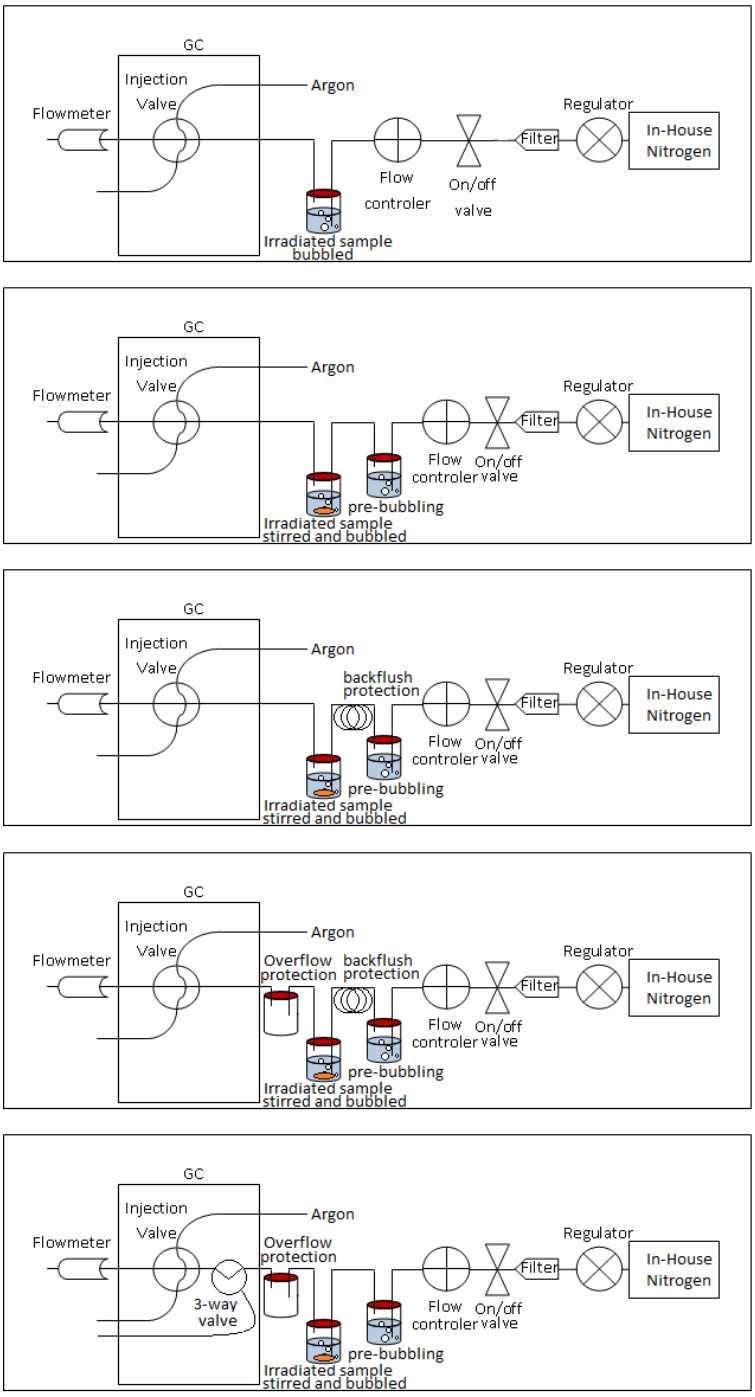

Schéma 5.3. Évolution du design du système à débit continu.

Dans le but d'augmenter le rendement des analyses à débit continu, le système final a été optimisé pour permettre l'analyse automatisée de deux échantillons. Plus de deux échantillons seraient possibles, mais deux problèmes surgissent : les coûts reliés à chaque

canal supplémentaire (notamment le contrôleur de débit) et le temps d'analyse du GC, qui se situe entre 2 et 3 minutes pour une analyse de la concentration en H_2 seulement. Puisque les analyses sont faites en série, le délai passerait au-delà de 5 minutes, ce qui est déjà long, surtout en début d'expérience ou les fluctuations sont rapides. Le Schéma 5.4 illustre le montage actuel, qui se retrouve aussi dans la Figure 5.3.

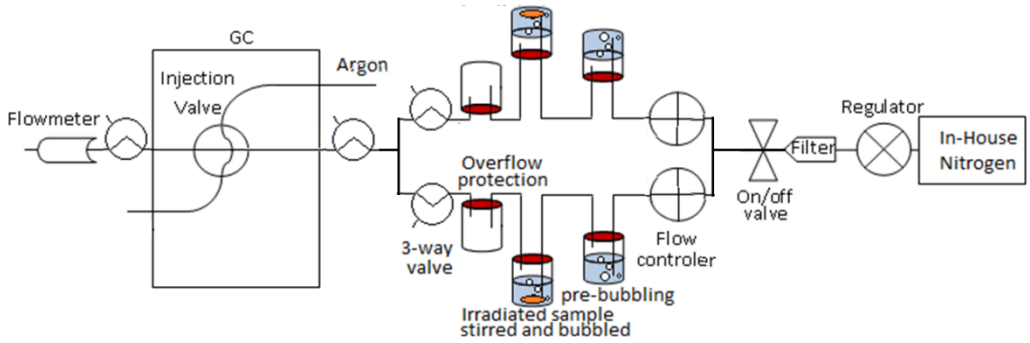

Schéma 5.4. Dessin schématique du système à débit continu pour l'analyse à deux canaux.

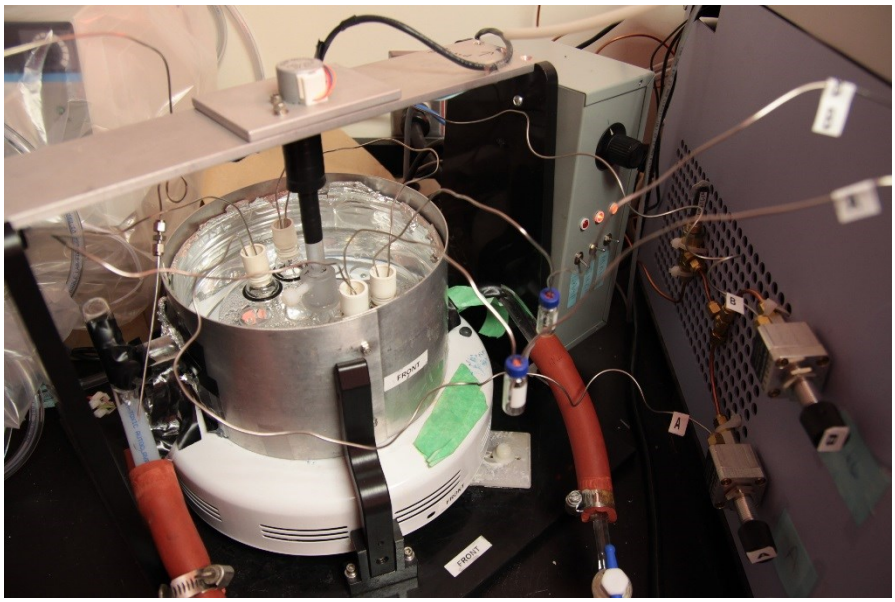

Figure 5.3. Le photoréacteur en mode système ouvert, deux canaux.

Le principal défi de ce design est le contrôle des valves externes. Comme décrit dans la section 5.S3, la synchronisation du GC et des valves est commandée par un microcontrôleur, qui reçoit lui-même ses ordres d'un logiciel sur un PC. L'équipement initial fourni par la compagnie du GC ne faisait qu'une chose : lorsqu'en marche, le microcontrôleur envoyait les signaux de départ à intervalle régulier, par une variable codée dans sa mémoire

interne. Pour changer cette variable, il était nécessaire de reprogrammer le microcontrôleur. Une interface a donc été créée pour permettre un plus grand contrôle, qui était nécessaire pour la gestion d'un système à deux canaux. Le circuit simplifié se retrouve dans le Schéma 5.5; des informations plus poussées se retrouvent en annexe dans la section 5.S7. Le microcontrôleur contrôle de façon autonome les cycles d'injection, mais l'usager peut facilement en modifier les paramètres : l'intervalle de temps entre les injections, le choix de canal et les temps où le flux est redirigé vers l'extérieur pour éviter le retour de pression du GC. En plus, un fichier de suivi est créé, notant les temps d'injection et l'état de la lampe, ce qui permet d'établir le début de l'irradiation à la seconde près.

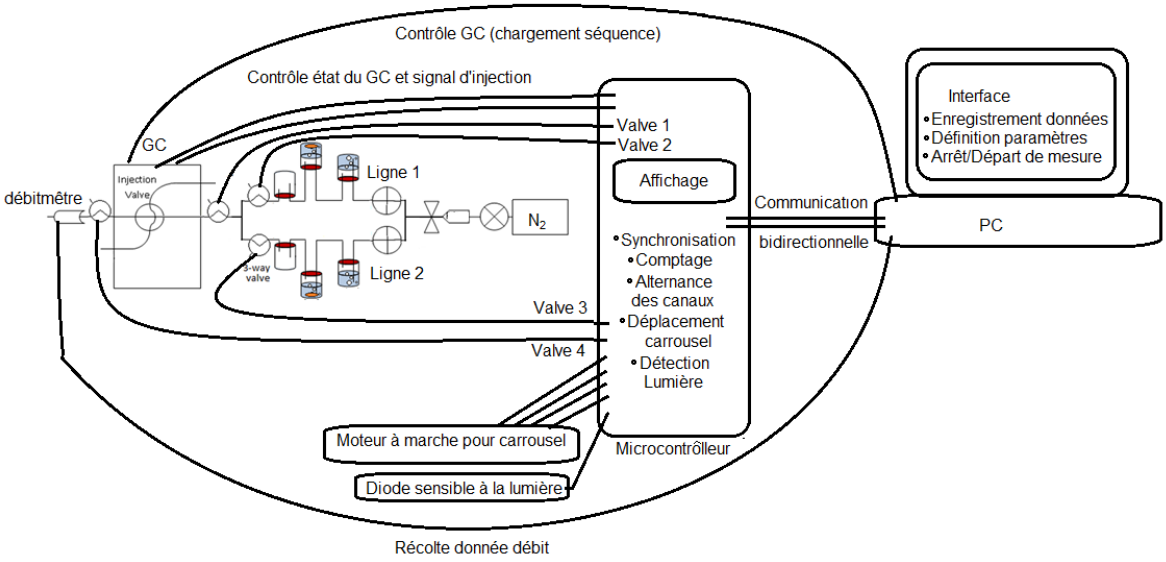

Schéma 5.5. Circuit électronique simplifié du contrôle automatisé.

Le GC est déclenché par le microcontrôleur à travers l'interface, mais l'acquisition des données et la configuration des paramètres utilisés pour obtenir les chromatogrammes sont prises en charge par le logiciel originel de gestion du GC. Celui-ci permet de traiter tous les chromatogrammes ainsi que de tabuler les temps d'injections et les aires d'intégration pour les différents gaz mesurés. Ensuite, le traitement de données se fait dans un chiffrier où une feuille de calcul établie permet de rapidement séparer les données par canal et de les convertir en concentration d'hydrogène, en mol_{H2}/min produit, en fréquence des cycles catalytiques (TOF :*turnover frequency*) et en nombre de cycle catalytique (TON : *turnover nomber*) après intégration de ces données dans le temps.

La seule partie tout à fait indépendante du système est le suivi par spectroscopie UV-vis, qui a été brièvement introduit plus tôt. Pour qu'elle soit efficace, elle doit se faire dans un circuit isolé de l'air, puisque les réactions étudiées sont très susceptibles à l'oxydation. Le problème est le type de conduit utilisable pour faire circuler la solution organique : seuls les tuyaux de PTFE (polytétrafluoroéthylène) sont utilisables avec un système de pompe péristaltique, toutefois ils sont très perméables à l'oxygène et ils doivent être isolés de l'air. Le problème fut réglé en passant les tuyaux de PTFE à travers des tuyaux de Nalgène et en plaçant la pompe dans un sac, le tout purgé avec une pression positive d'azote qui isole le système de l'atmosphère (voir Figure 5.4).

Le traitement de données spectroscopiques est relativement lourd, requérant un formatage initial des données spectrales pour inclure la date et l'heure d'analyse. Finalement, les données spectrales sont synchronisées avec les données des chromatogrammes. Un traitement cinétique est possible, en utilisant le logiciel SPECFIT32, mais la complexité du système photocatalytique rend l'analyse très difficile : il y a trop d'inconnues tant au niveau des espèces absorbantes qu'au niveau du modèle cinétique à définir. Par exemple, comment définir la quantité d'espèce excitée générée par les photons si la quantité de photons reçus change à cause des variations d'absorption causées par aux autres espèces pendant la réaction? Des artifices de calculs permettent une certaine modélisation, mais le modèle cinétique final perd beaucoup de son sens, même si le changement des espèces est bien modélisé par ce dernier.

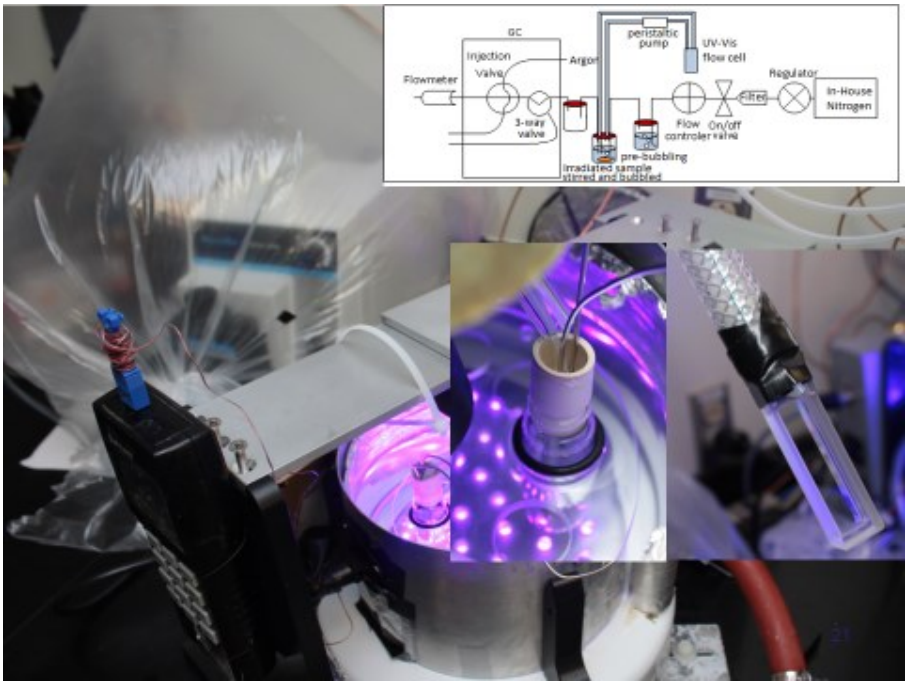

Figure 5.4. Le photoréacteur avec l'équipement de suivi par spectroscopie UV-vis. En haut à droite : circuit schématique.

L'étude par suivi UV-vis apporte un changement des conditions expérimentales. Il y aura toujours une quantité de solution non irradiée circulant dans les tuyaux et dans la cellule. Notre choix de cellule n'est pas optimal, car elle a un assez grand volume. Au total, il y a environ 7 mL de la solution qui circule en dehors du réacteur. Ce réservoir non irradié altère la quantité réelle soumise à l'irradiation (ce qui affecte la valeur du TOF) et crée un effet de réservoir qui va ralentir la cinétique.

5.3.2. Étude de la production d'hydrogène : système fermé du groupe du Pr Sven Rau

Les études de production d'hydrogène de nos assemblages de rhénium-rhodium ont commencé en système fermé, pendant un mois lors d'un stage chez le groupe du Pr Sven Rau. Leur photoréacteur, muni de DEL avec une longueur d'excitation à 470 nm, n'était pas optimal pour des chromophores à base de rhénium, car ils ont leurs maxima d'absorption entre 350 et 380 nm. Cependant, leurs bandes d'absorption sont très larges et absorbent jusqu'à environ 470 nm (voir Figure 2.2. et Figure 4.9). Les résultats des tests obtenus avec le système connu du Pr Fontecave étaient positifs avec un TON_{PS} mesuré de 42 (Tableau V-4 entrée 1) quoique inférieur à leur valeur publiée de 273 après 16 h.[11] Deux différences séparent les expériences :

- le chromophore utilisé par Fontecave était le $Re(phen)(CO)_3Br$;
- une lampe de mercure de 150W avec un filtre bloquant la lumière en bas de 380 nm.

Probablement qu'une plus longue irradiation aurait mené à un résultat plus similaire.

Pour les études avec nos assemblages, les conditions de Fontecave n'ont pas été utilisées. Ses conditions étaient les suivantes : l'acétone comme solvant avec une quantité modeste de triéthylamine (TEA) (750 fois la quantité de PS) et une source équivalente de proton initiale (sous forme de sel Et_3NHBF_4). Pour éviter la dissociation des assemblages de Rh-Re, nous avons testé les conditions du groupe Rau, i.e. sans acide (évitant la protonation des pyridyles), dans l'acétonitrile (qui ne montre pas de dissociation contrairement à l'acétone où le dimère perd lentement ses chromophores) et avec une quantité de TEA 10 fois supérieur (cela augmente la vitesse de réduction initiale et élimine la dépendance

cinétique à la concentration de TEA). Le chromophore **5-5**, dans ces nouvelles conditions, a donné un résultat plus faible (7 TON_{PS}) (Tableau V-4 entré 2 et 3) et la plupart des autres chromophores ont tous donné des résultats nuls, sauf **5-3** (Tableau V-4 entré 7 et 9). Le chromophore **5-3** a donné un résultat variant de 8 à 14 TON_{PS}. Après irradiation (donc une fois l'expérience de photocatalyse terminée), la solution ne contenait plus que l'espèce **5-0**. De plus, l'entrée 8 montre qu'il ne semblait pas actif en présence d'acide.

Tableau V-4. Résultats initiaux obtenus par le système du groupe du Pr Sven Rau avec le catalyseur $Co(dmgBF_2)_2$ (**5-9**)

Entrée	Cond.	Photosensibilisateur (PS)	Donneur electron/H^+	Solvant	Temps (h)	TON_{PS} (/mol de PS)
1	*a*	**5-5**	$Et_3N + Et_3NHBF_4$	Acétone	19	42*
2	*b*	**5-5**	Et_3N	Acétone	19	11*
3	*b*	**5-5**	Et_3N	CH_3CN	13	7*
4	*b*	**5-8**	Et_3N	CH_3CN	16	0*
5	*b*	**5-4**	Et_3N	CH_3CN	12	0
6	*b*	**5-4+CNPy**[f]	Et_3N	CH_3CN	12	0.5*
7	*b*	**5-3**	Et_3N	CH_3CN	12	14*
8	*b,c*	**5-3**	$Et_3N + Et_3NHBF_4$	CH_3CN	19	0*
9	*b*	**5-3+CNPhBr**[g]	Et_3N	CH_3CN	12	8*
10	*d*	**5-2**	Et_3N	CH_3CN	16	0*
11	*e*	**5-1**	Et_3N	CH_3CN	16	0*

*Coloration bleue détectable durant la réaction. *a*) 5.0 x 10^{-4} M du catalyseur et chromophore, 750 éq.de Et_3N et de sel acide. *b*) 5.0 x 10^{-5} M du catalyseur et chromophore, 7500 éq. de Et_3N. *c*) Avec 3250 eq. de sel acide. *d*) 5.0 x 10^{-5} M de chromophore et 1.0 x 10^{-5} M du catalyseur, 7500 éq. de Et_3N, sel. *e*) 5.0 x 10^{-5} M du Chromophore et 1.5 x 10^{-5} M du catalyseur, 7500 éq. de Et_3N. *f*) CNPy = 4-pyridylisocyanure. *g*) CNPhBr = 4-bromophényl isocyanure.

D'après ces résultats, il nous semblait que l'espèce **5-11** (voir Schéma 5.6) formée *in situ* serait l'espèce active, puisqu'aucune réaction n'a eu lieu avec **5-4** (pas de décomposition ou de formation d'espèce réduite de cobalt) et que les assemblages **5-1**et **5-2** ont montré la formation de l'intermédiaire de Co(I), sans produire d'hydrogène. Cette espèce de Co(I) forme un composé bleu très caractéristique. Si celui-ci est détecté, le chromophore est actif, l'absence d'hydrogène formé sera expliqué plus tard.[12] De plus, l'assemblage **5-4** avec un 4-isocyanopyridine semblait aussi être actif (quoique très faiblement), donnant donc à penser que l'espèce avec un complexe de cobalt lié (**5-12**) était aussi formé *in situ*. Ces deux espèces, **5-11** et **5-12** ont été synthétisées auparavant, cependant elles n'ont pas pu être isolées convenablement, le complexe de Co ayant tendance à se dissocier trop facilement du groupement pyridyl. Des preuves RMN de leurs existences sont illustrées dans les Figure 5.5

et Figure 5.6 pour les complexes **5-11** et **5-12** respectivement. Le complexe de Co(II) étant paramagnétique, il fait disparaître le signal des protons proche de lui (aucun signal en dehors de la fenêtre normale n'a été observé). Dans le cas de **5-11** seuls les protons des bipyridines sur les complexes de rhénium restent relativement non-affectés, les signaux de tous les autres deviennent plus affaissés et le signal à 7.95 ppm, correspondant au proton en alpha de l'azote du pyridyle libre, disparaît complètement.

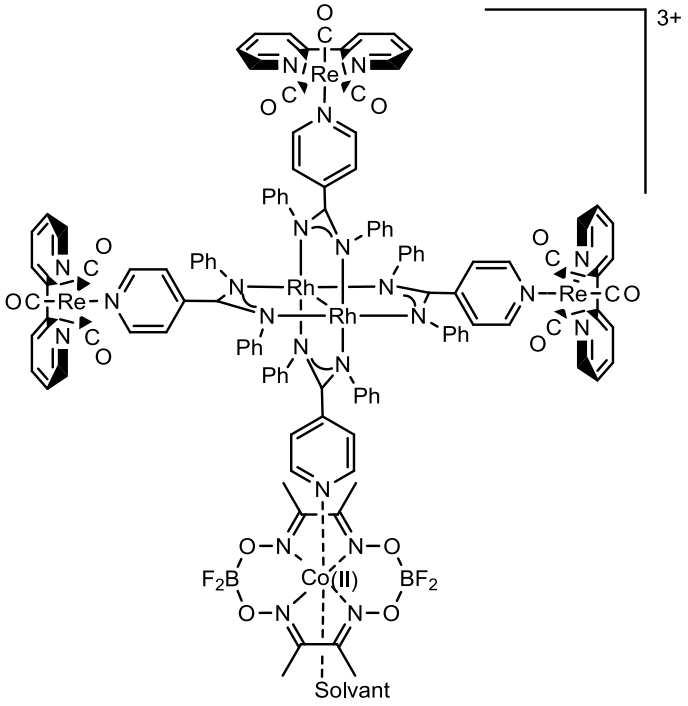

5-11

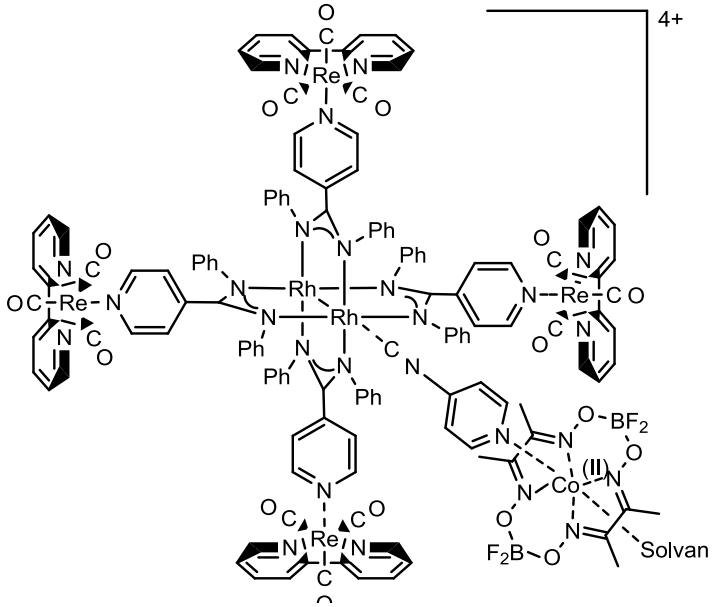

Schéma 5.6. L'espèce assemblée Rh_2Re_3Co (**5-11**) et Rh_2Re_4Co (**5-12**)

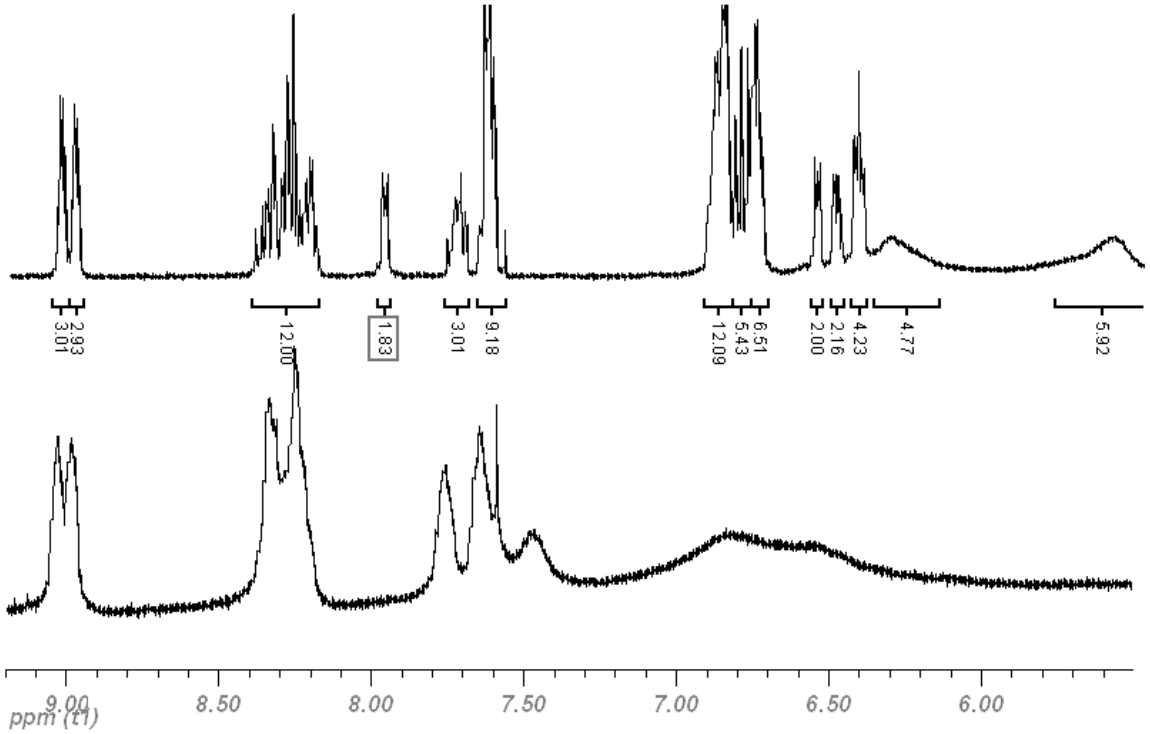

Figure 5.5. Spectres ^{1}H RMN de **5-3** (haut) et **5-11** (bas) dans l'acétonitrile.

Da façon similaire, le complexe **5-12** montre les mêmes tendances. Au milieu de la Figure 5.6 se retrouve l'espèce contenant seulement l'isocyanure. On peut y observer une perte de symétrie par le dédoublement des signaux des anneaux phényles du dimère (entre 5.5 et 7 ppm) et la présence du pyridyle libre de l'isocyanure qui se trouve à 8.65 ppm. À l'ajout du cobalt, ce dernier signal disparaît et le spectre conserve son asymétrie versus **5-4**, ce qui suggère que l'isocyanure est toujours lié au dimère et que le cobalt est coordonné à ce dernier à travers l'isocyanure. Puisque le centre métallique du cobalt est plus loin du dimère, il n'affecte pas autant les signaux de ces anneaux aromatiques.

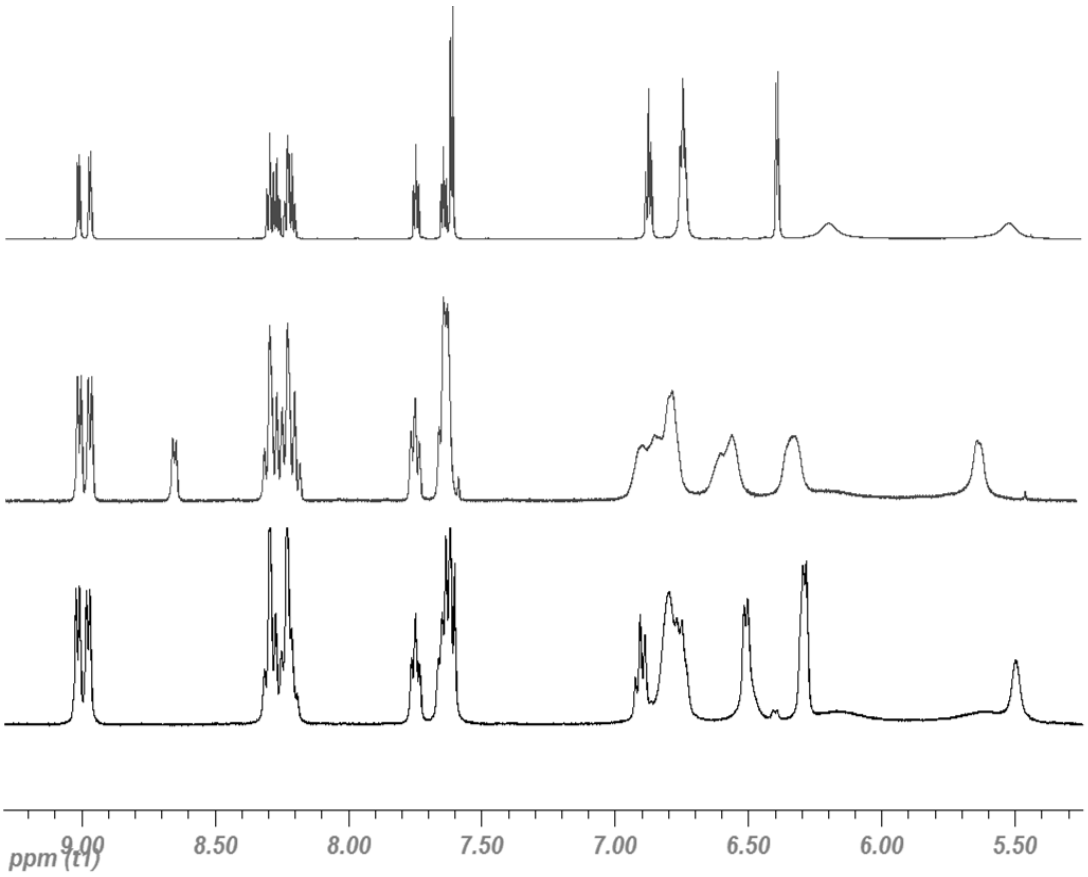

Figure 5.6. Spectres ^{1}H RMN de **5-4** (haut) et **5-4**+CNPy (milieu) et **5-12** (bas) dans l'acétonitrile.

Une preuve par spectrométrie de masse a aussi été obtenue, mais jamais en espèce majoritaire. Le catalyseur de cobalt n'est vu attaché sur le rhodium que par des signaux faibles et, de plus, il est altéré (perte d'un groupement BF2 avec ou sans ajout de OH pour **5-11** voir Figure 5.7). Dans le cas **5-12**, une preuve similaire a été trouvé (Figure 5.8). Ici l'espèce complète est visible, mais la masse exacte n'est pas parfaite. Dans ce cas-ci, il semble qu'il s'agit d'un problème de calibration, car toutes les masses sont décalées comme le montre la masse de [**5-4**+CNPy(-3PF_6)]$^{3+}$.

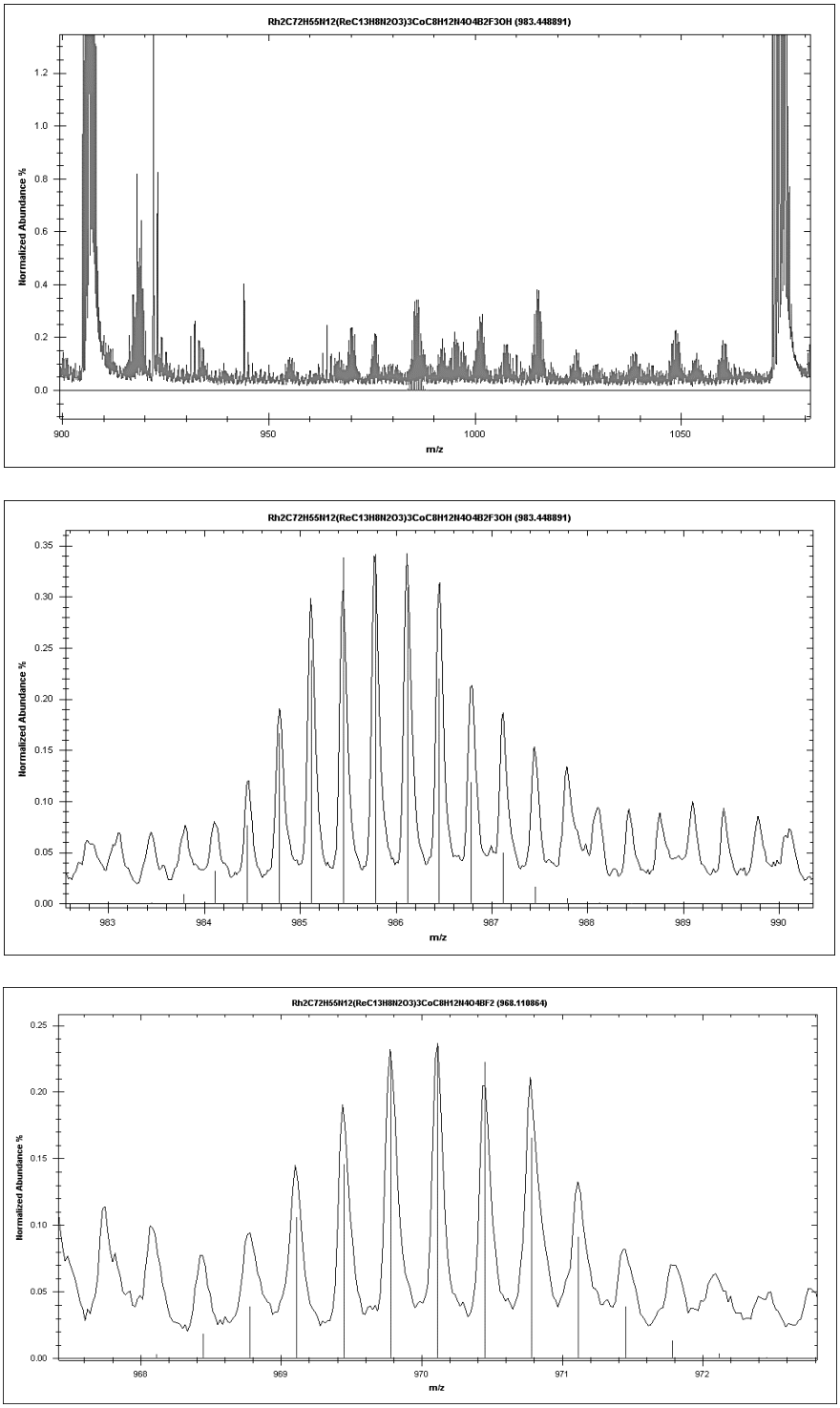

Figure 5.7. Spectres de masse du complexe **5-11**. En haut, zone 900 à 1100 M/z. Au milieu zoom sur l'espèce [**5-11**(-3PF_6 –BF_2 +OH)]$^{3+}$. En bas zoom sur l'espèce [**5-11**(-3PF_6 –BF_2)]^{3}.

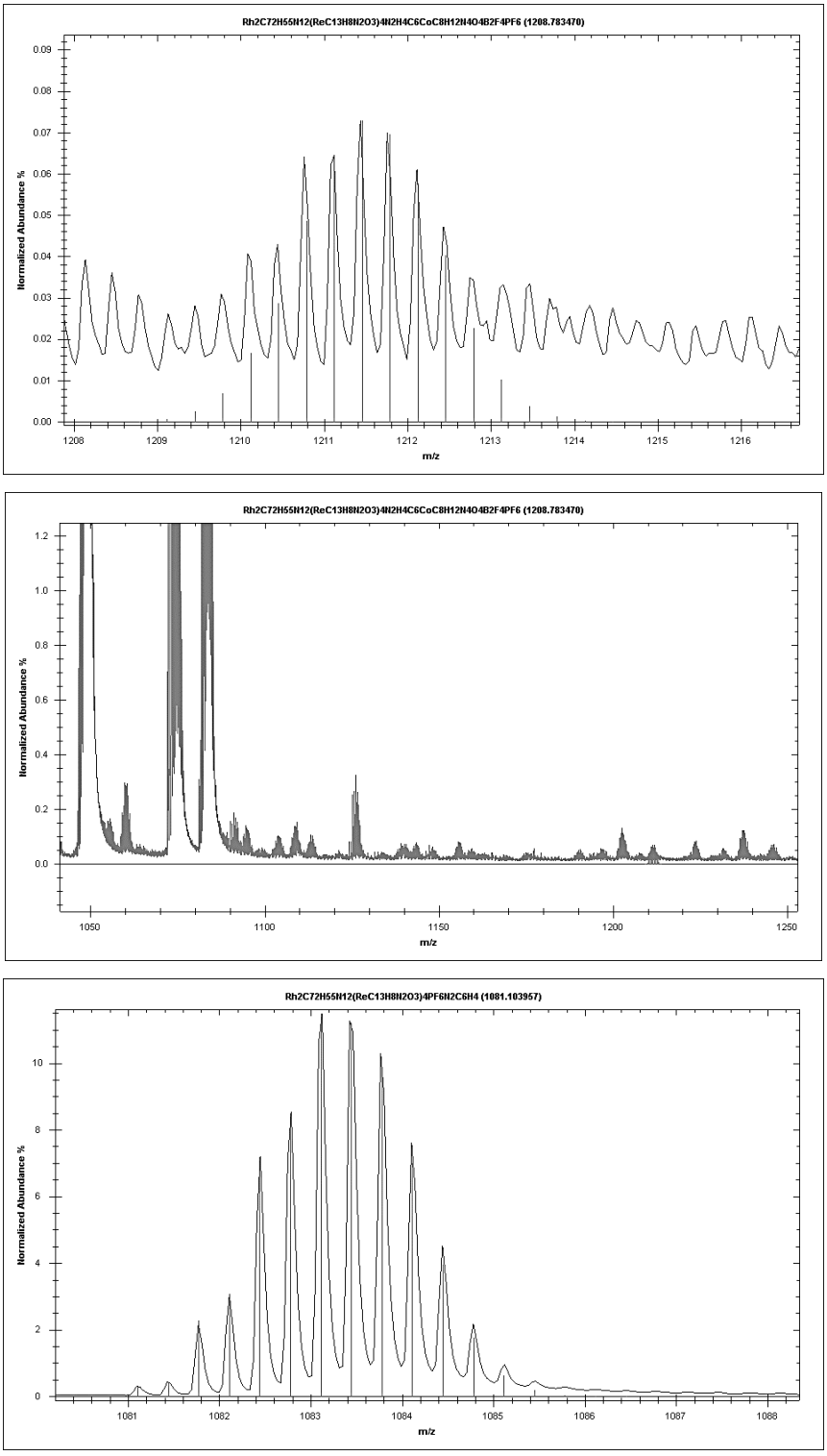

Figure 5.8. Spectres de masse du complexe **5-12**. En haut, zone 1000 à 1300 M/z. Au milieu zoom sur l'espèce [**5-12**(-3PF_6)]$^{3+}$. En bas, zoom sur un fragment, l'espèce [**5-4+CNPy**(-3PF_6)]$^{3+}$.

Ces résultats préliminaires ont été le point de départ pour la nouvelle étude avec notre propre photoréacteur. Beaucoup de ces résultats se sont avérés mauvais, surtout au niveau des chromophores supposément inactifs. Après répétition avec notre réacteur, certaines espèces inactives se sont avérées actives telles **5-8** et **5-4**. Avec ces nouveaux résultats, il n'était plus clair que le complexe **5-11** soit réellement l'espèce active, puisque **5-8** peut se former et devenir le chromophore actif. De plus, la liaison pyridyl-Cobalt n'est pas essentielle si le dimère **5-4** initie la catalyse aussi.

Afin de poursuivre l'étude des réactions de photocatalyse, il a été nécessaire d'améliorer quelques aspects du photoréacteur. En effet, un problème majeur des expériences avec le photoréacteur du groupe Rau sera corrigé lors de l'élaboration de notre photoréacteur. Il s'agit de la reproductibilité des expériences, reproductibilité difficilement réalisable découlant d'une préparation dans des fioles où l'herméticité n'était pas garantie ainsi que d'une injection manuelle pour l'analyse par GC.

5.3.3. Étude de production d'hydrogène : Photoréacteur du groupe du Pr Hanan

Les premières expériences effectuées en circuit fermé utilisent une lampe à 451 nm, notre première lampe reçue. Ces analyses, exécutées en duplicata, ont donné sensiblement les mêmes résultats qu'auparavant : (22 ± 2) TON_{PS} pour le complexe **5-3**. Ici la réaction contenait 1.6 mM de **5-3**, 3.2 mM **5-9**, 0.65 M de TEA et 0.063 M d'acide acétique, irradié pendant 17h. L'ajout d'acide rend ces conditions plus près de celles utilisées par le groupe du Pr Alberto.[10]. Tous les chromophores à base de rhénium testés étaient actifs dans ces conditions (**5-5**, **5-6**, **5-7**, **5-8** et même **2-1** et **2-2**). Le meilleur résultat, (66 ± 15) TON_{PS}, a été obtenu avec **5-8**. **2-1** arrive second avec 55 TON_{PS} et **2-2** a obtenu 12 TON_{PS} (ces deux dernières mesures n'ont pas été dupliquées dans ce cas-ci).

L'évolution de toutes les réactions était identique. Au départ, la solution était jaune (pour **5-5**, **5-6**, **5-7**, **5-8**, **2-1** et **2-2**) ou verte pour **5-3**. Il s'en suivait une coloration bleue très foncée, indicatif de la formation de cobalt(I), puis, après un certain temps, il y avait décoloration totale de la solution (qui avait une teinte rose pour **5-3**). Après la réaction, il ne restait pas d'espèces de rhénium identifiables. Seulement le complexe **5-0** (qui est rose) a pu être identifié dans le cas de la réaction avec **5-3**. Le suivi avec le système ouvert a pu démontrer rapidement qu'il y avait un long temps d'induction (pratiquement 1h) pour le complexe **5-3**, comme on peut le voir sur la Figure 5.9. On observe, à environ 2 heures, le

maximum de production d'hydrogène, où le TOF_{PS} atteint 0.50 min^{-1}, suivi d'un décroissement exponentiel très rapide. Un arrêt de la lampe montre l'interruption de la production d'hydrogène, qui redémarre aussitôt quand elle est rallumée, mais ne remonte pas au même niveau. En fin de réaction, après 24h, il y a toujours une faible production d'hydrogène, avec un TOF_{PS} résiduel de 0.02 min^{-1}.

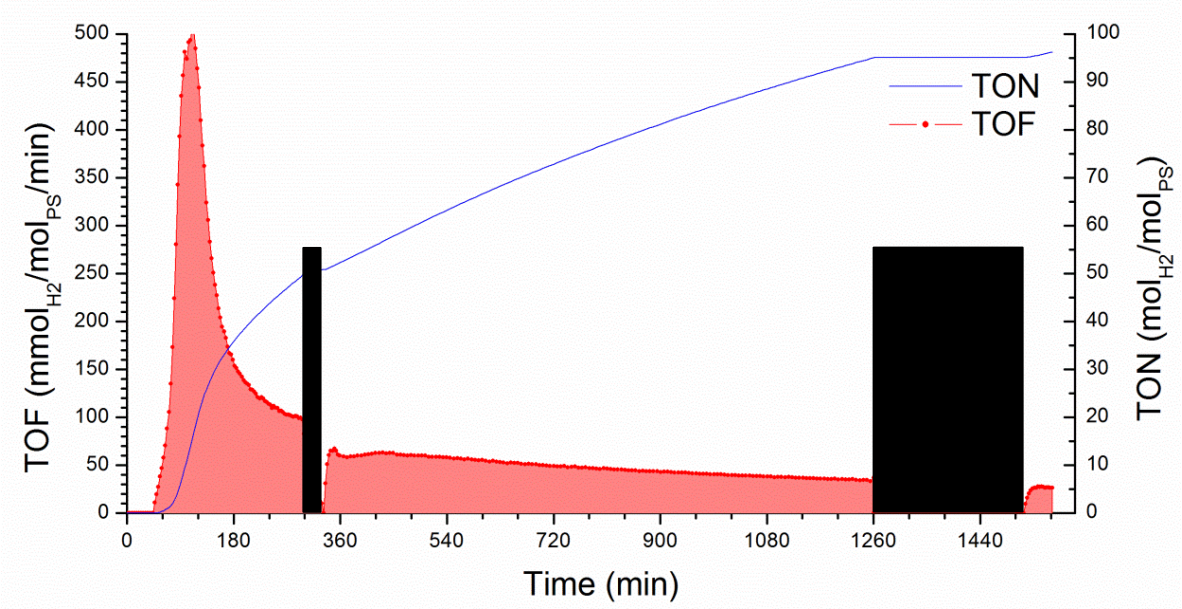

Figure 5.9. Photoproduction d'hydrogène avec 77 µM de **5-3**, 0.4 mM de **5-9** et 1 M TEA dans l'acétonitrile; 14 mL; irradiation à 450 nm; T = 20.0 °C. Dans les zones ombragées, la lampe a été éteinte.

5.3.4. Suivi spectral avec le catalyseur 5-9, $Co(II)(dmgBF_2)_2(H_2O)_2$

Le suivi spectral a permis de répondre à plusieurs questions sur notre système. Entre autres, l'utilisation du catalyseur **5-9** a été remise en question. En effet, tous les résultats obtenus avec celui-ci (avec ou sans source d'acide) dans l'acétonitrile comme dans le DMF, avec tous les chromophores à base de rhénium à notre disposition, mènent vers une seule et même conclusion : le chromophore réduit le catalyseur, mais celui-ci ne fait pas la réduction d'hydrogène. Il n'est activé que dans une deuxième étape par ce qui semble être un produit de décomposition du chromophore de Re de type $Re(bpy)(CO)_3X$ ou X serait un ligand anionique inconnu. Ceci est illustré sur le Schéma 5.7. Les analyses présentées dans cette section convergent toutes vers cette conclusion.

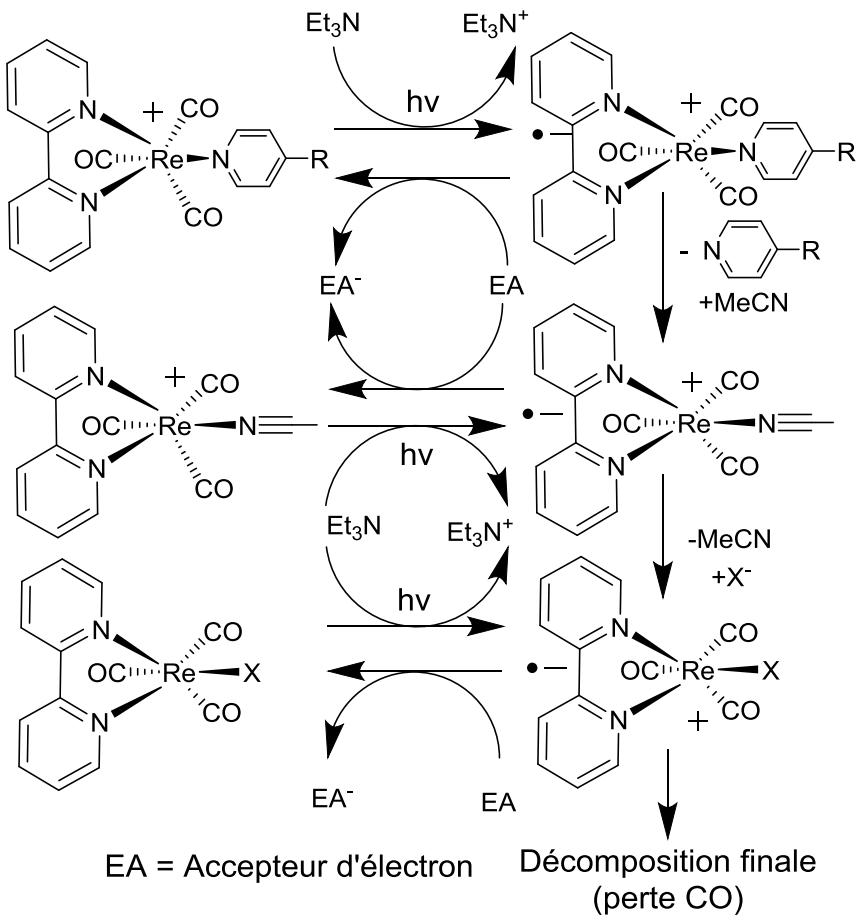

Schéma 5.7. Chemin de décomposition des chromophores de Re.

La Figure 5.10 (gauche) montre ce qu'il advient lorsque le chromophore **5-4** est soumis à une irradiation en présence d'un donneur d'électron (ici le TEA) dans le *N*,*N*-diméthylformamide. On y observe deux changements majeurs : la perte de la bande étroite à 320 nm et le déplacement hypsochromique de la bande associée au M_2LCT du dimère, située au départ vers 600 nm. Ceci correspond à la dissociation du rhénium : on peut voir l'apparition des espèces **5-1** et **5-0** en comparant avec les spectres des produits purs de la Figure 5.10 (droite). La réaction suit le même parcourt, illustré sur le Schéma 5.7, en ignorant le catalyseur qui n'est pas présent. Le même processus est observé dans l'acétonitrile, où la bande associée au M_2LCT passe de 630 à 570 nm.

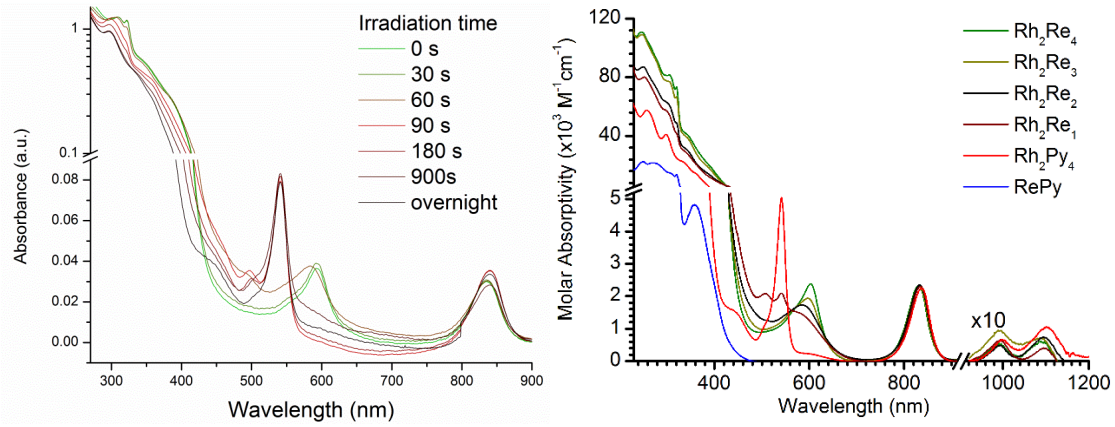

Figure 5.10. Gauche : Décomposition du complexe **5-4** dans le DMF en présence de TEA et sous irradiation à 390 nm. Droite : Spectre d'absorption des espèces **5-0** (Rh_2Py_4) à **5-4** (Rh_2Re_4) et **5-6** (RePy).

Lors de l'expérience effectué avec le chromophore **5-5** illustrée à la Figure 5.11, on constate qu'il n'y a pas de temps d'induction et que la production d'hydrogène, de très courte durée, chute très rapidement de façon exponentielle. Une espèce de cobalt réduit est visible immédiatement après l'allumage de la lampe et ne perdure que très peu de temps après le début de l'expérience (environ 10 minutes). Cette espèce de cobalt est identifié comment étant Co(II)H selon la littérature : le Co(I) réagit rapidement avec un proton pour former Co(III)H et se fait réduire de nouveau pour former Co(II)H.[13] Il est suivi par la bande à 550 nm, la bande à 365 nm correspondant à une autre espèce, possiblement à un nouveau chromophore de rhénium ou à une autre espèce de cobalt. La réaction est très peu productive, car le catalyseur se trouve en moins grande concentration que le chromophore. Ce dernier se décompose rapidement, car il se réduit plus vite que le catalyseur est capable de produire de l'hydrogène.

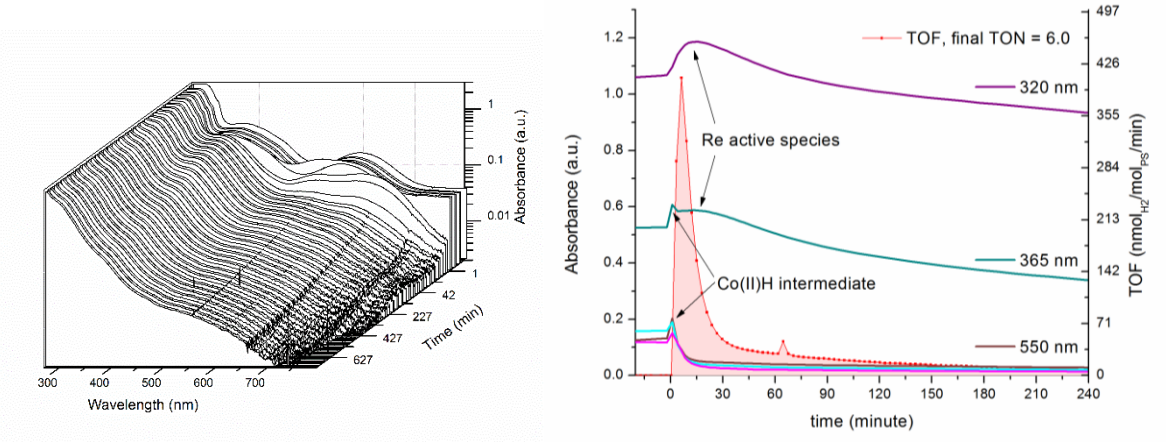

Figure 5.11. Photoproduction d'hydrogène avec 0.11 mM de **5-5**, 0.075 mM de **5-9** et 0.9 M TEA dans l'acétonitrile; 18.3 mL; irradiation à 390 nm, T= 20.0 °C. Gauche : compilation des spectres. Droite : suivi de la production d'hydrogène et d'une sélection d'absorption à différentes longueurs d'onde dans le temps mauve : 320 nm, ReX; turquoise : 370 nm, ReX inconnu; brun : 550 nm, Co(II)H.

Le chromophore **5-5** est neutre à cause de son ligand bromure ce qui le rend différent des chromophores de rhénium cationique sur le dimère. Le chromophore **5-8** avec un ligand acétonitrile est aussi cationique, ce qui le rend plus proche de celui sur nos assemblages. De plus, il représente le produit de dissociation le plus probable qui se formerait pendant la réaction dans l'acétonitrile. Ici le complexe **5-8** possède une bande signature se situant à 317 nm (bande très étroite). Lors de l'irradiation, dans l'acétonitrile, on voit immédiatement sa disparition, environ 10 minutes avant que la production d'hydrogène atteigne son maximum. Quant au cobalt, il se fait réduire en 5 minutes seulement, et après une analyse plus poussée, au moins deux autres espèces semblent présentes (Figure 5.13). Elles sont assignées comme étant les chromophores ReX et CoX. Le chromophore ReX se dégrade en suivant la dégradation de la production d'hydrogène et l'espèce CoX serait l'espèce catalytique active, qui se dégrade plus lentement. À noter que très peu d'hydrogène total est produit, encore une fois à cause du manque de catalyseur initial, celui-ci était ajouté en plus basse concentration afin d'être capable de suivre le chromophore de rhénium convenablement.

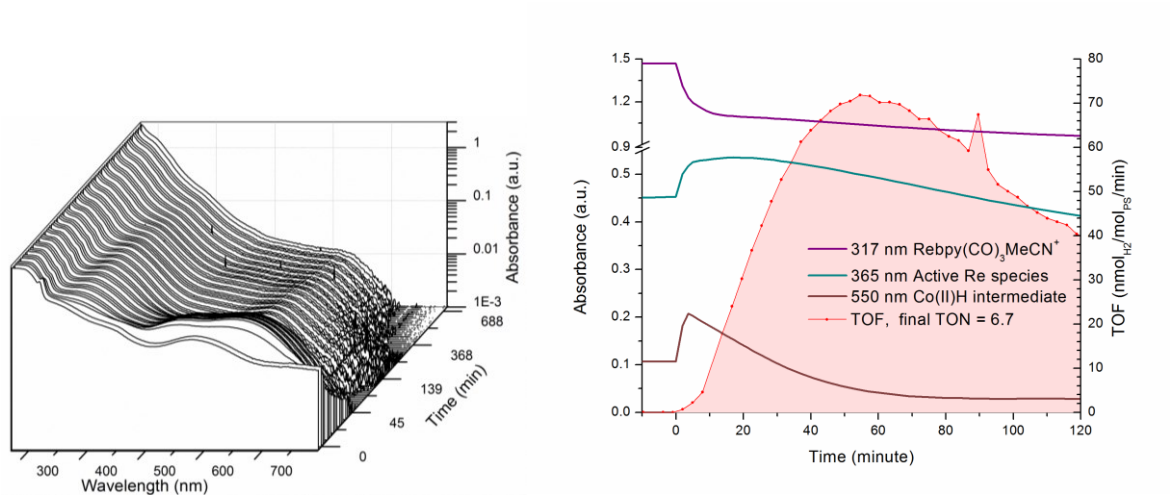

Figure 5.12. Photoproduction d'hydrogène avec 0.90 mM de **5-8**, 0.075 mM de **5-9** et 0.9 M TEA dans l'acétonitrile; 18.3 mL; irradiation à 390 nm, T= 20.0 °C. Gauche : compilation des spectres. Droite : suivi de la production d'hydrogène et d'une sélection d'absorption à différentes longueurs d'onde dans le temps. Mauve : 317 nm, Re-MeCN; turquoise : 365 nm, ReX inconnu; brun : 550 nm, Co(II)H

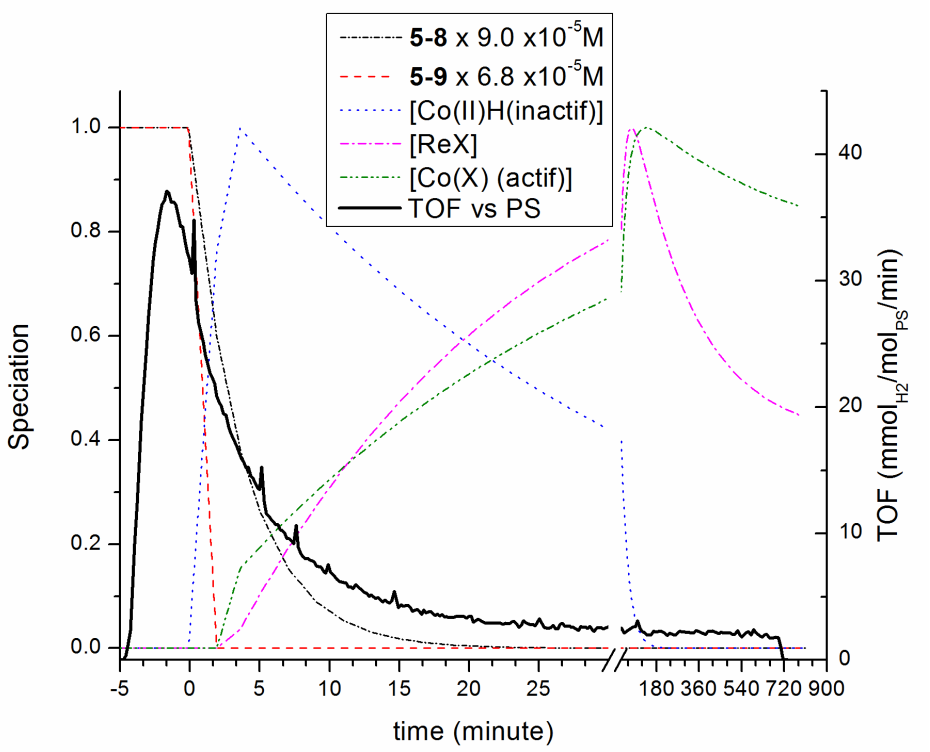

Figure 5.13. Spéciation à partir des espèces observées par spectroscopie pour la Photoproduction d'hydrogène avec 0.90 mM de **5-8**, 0.075 mM de **5-9** et 0.9 M TEA dans l'acétonitrile; 18.3 mL; irradiation à 390 nm, T= 20.0 °C; irradiation totale 18 h.

Ces résultats illustrent déjà un problème majeur : la vitesse de réaction du Co(II) étant trop lente, le chromophore se dégrade. Cependant, dans le cas du complexe **5-3**, le résultat était encore plus surprenant. Sur la Figure 5.14 on retrouve le premier suivi dans l'acétonitrile du complexe. Malheureusement, dû à un problème technique, le suivit par GC de l'hydrogène s'est interrompu après 50 min. Malgré tout, les données recueillies pendant ce court laps de temps sont suffisantes pour confirmer l'absence de réaction du catalyseur en début de réaction.

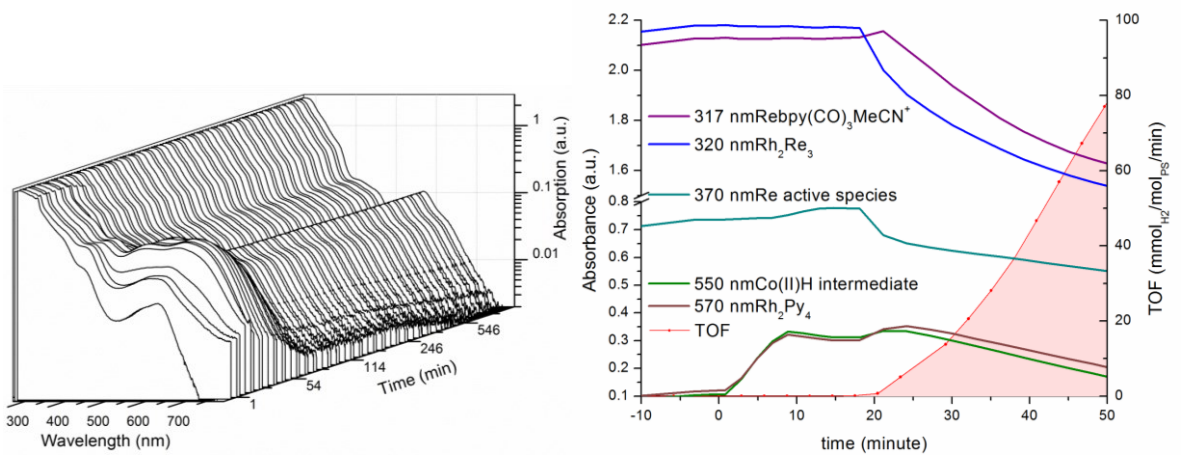

Figure 5.14. Photoproduction d'hydrogène avec 36 µM **5-3**, 64 µM de **5-9** et 0.9 M TEA dans l'acétonitrile; 18.3 mL; irradiation à 390 nm, T= 20.0 °C. Gauche : compilation des spectres. Droite : suivi de la production d'hydrogène et d'une sélection d'absorption à différentes longueurs d'onde dans le temps; mauve : 317 nm, Re-MeCN; bleu : 320 nm, Re-Pyridyl; turquoise : 370 nm, ReX inconnu; vert : 550 nm, Co(II)H; brun : 570 nm, M_2LCT de **5-0**.

La première chose à remarquer est le temps d'induction, pendant ce temps l'espèce Co(II)H se forme et le dimère reste stable, comme la bande à 320 nm le démontre, celle-ci étant une bande signature du complexe Re(bpy)(CO)$_3$Py$^+$. Cependant, vers la 19^e minute, cette bande diminue radicalement et à la 21^e minute, la bande se déplace vers l'espèce Re(bpy)(CO)$_3$MeCN$^+$, puis chute aussi rapidement (voir Figure 5.15).

Aussitôt que le signal de Co(II)H s'estompe, le signal du dimère **5-0** domine les spectres. Il est clair que l'assemblage **5-3** ne participe pas à la production d'hydrogène, cependant l'assemblage semble effectuer les premières réduction du Co(II) en Co(I) et du

Co(III)H en Co(II)H sans se dissocier, ce qui confirme au moins que l'assemblage peut faire la réduction.

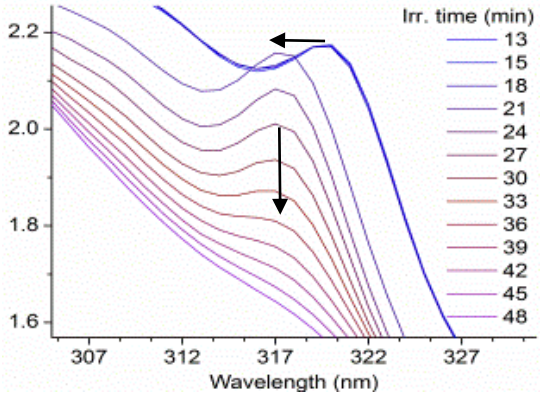

Figure 5.15. Zoom sur la région signature du chromophore de rhénium, de la minute 13 jusqu'à la minute 48. Photoproduction d'hydrogène avec 36 µM **5-3**, 64 µM de **5-9** et 0.9 M TEA dans l'acétonitrile; 18.3 mL; irradiation à 390 nm, T= 20.0 °C.

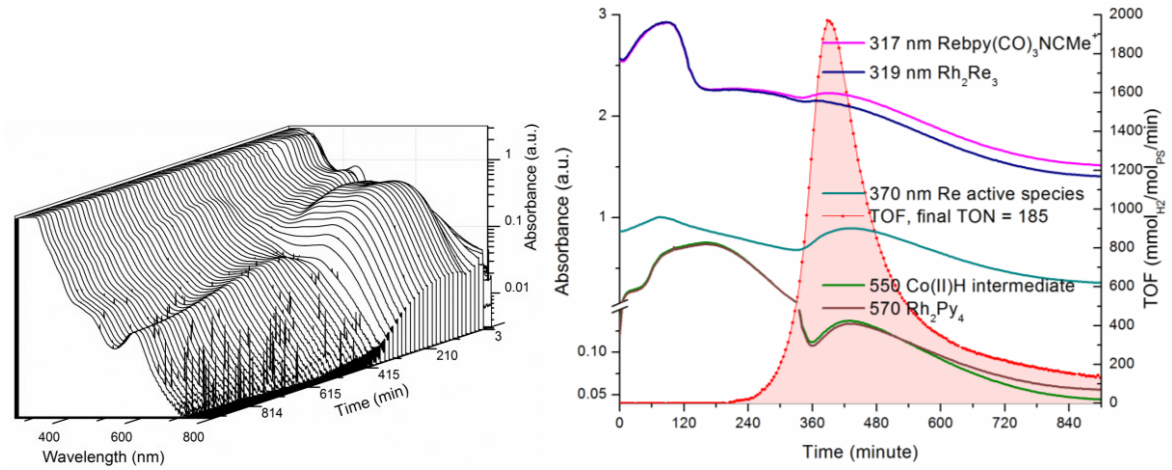

Figure 5.16. Photoproduction d'hydrogène avec 29 µM de **5-3**, 0.5 mM de **5-9**, 0.78 M TEA et 0.20 M de HPF_6 dans l'acétonitrile; 18.3 mL; irradiation à 390 nm, T= 20.0 °C. Gauche : compilation des spectres. Droite : suivi de la production d'hydrogène et d'une sélection d'absorption à différentes longueurs d'onde dans le temps; mauve : 317 nm, Re-MeCN; bleu : 319 nm, Re-Pyridyl; turquoise : 370 nm, ReX inconnu; vert : 550 nm, Co(II)H; brun : 570 nm, M_2LCT de **5-0**.

Le manque de proton initial (fournit par une source d'acide présente) pourrait expliquer l'absence de réaction. De plus, la trop faible concentration du catalyseur pourrait expliquer la décomposition hâtive du chromophore. L'expérience illustrée sur la Figure 5.16

démontre que ni l'ajout d'acide, ni l'ajout de catalyseur n'empêche la décomposition complète du chromophore avant la production maximale d'hydrogène.

La première observation est un temps d'induction plus long, tout à fait normal considérant que le nombre de molécules de catalyseur devant être réduites augmente. Ici le maximum de Co(II)H est atteint vers 180 min, une autre espèce semble s'être formée comme le témoignent les bandes à 317, 319 et 370 nm. Dès le début de la production d'hydrogène, vers 240 minutes, la bande à 319 nm diminue en intensité et la bande à 317 nm apparaît, pour ensuite s'estomper à nouveau comme dans le cas de l'expérience de la Figure 5.14. Une bande à 370 nm atteint son maximum en même temps que le maximum de la vitesse de production d'hydrogène, probablement due à une espèce de rhénium inconnu. Puis celle-ci s'estompe à son tour. La production d'hydrogène est plus intense, due à la concentration du catalyseur, mais le TOF_{PS} indiqué en fonction du photosensibilisateur initial n'est pas aussi significatif puisque l'assemblage libère trois équivalents de rhénium, diminuant donc ce résultat à 60 TOF_{PS} par chromophore.

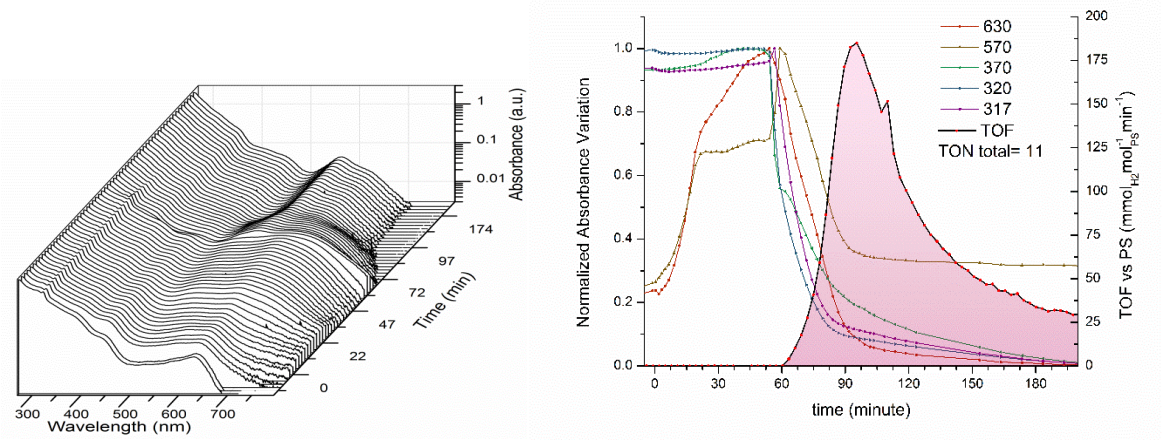

Figure 5.17. Photoproduction d'hydrogène avec 20 µM **5-4**, 69 µM de **5-9** et 0.9 M TEA dans l'acétonitrile; 18.3 mL; irradiation à 390 nm, T= 20.0 °C. Gauche : compilation des spectres. Droite : suivi de la production d'hydrogène et d'une sélection d'absorption à différentes longueurs d'onde dans le temps; mauve : 317 nm, Re-MeCN; bleu : 320 nm, Re-Pyridyl; turquoise : 370 nm, ReX inconnu; brun : 570 nm, M_2LCT de **5-0**; rouge : 630 nm, M_2LCT de **5-4**.

Le prochain point à observer est l'activé de l'assemblage **5-4** qui, selon les premiers résultats, était inactif. Les résultats affichés sur la Figure 5.17 démontrent le contraire : la production est similaire que celle du complexe **5-3**, incluant les mêmes décompositions. Les concentrations initiales sont légèrement différentes de celles vues dans la Figure 5.14. Le ratio de catalyseur sur PS est de 3.45 pour **5-4** versus 1.77 pour **5-3**, donnant une différence d'un facteur de 1.94 entre les deux expériences. En tenant compte de ce fait, le temps d'induction de 60 min est toujours plus long que celui observé avec le complexe **5-3**, (de 20 min), donnant un ratio de 3. Finalement, incluant les différences de concentration initiale des composantes, le temps d'induction normalisé serait 1.5 fois plus grand dans le cas de l'espèce **5-4**, mais ceci est une grosse approximation puisque les expériences n'ont pas été faites dans des conditions identiques. Pour conclure, on peut dire que l'espèce **5-4** est très similaire en activité à **5-3**.

Une dernière tentative avec le catalyseur **5-9** a été tentée avec le dimère **5-3**, cette fois-ci dans le dimethylformamide (DMF), en présence d'acide et avec 8 équivalents du catalyseur par rapport au chromophore. La Figure 5.18 montre encore une fois le même résultat, la décomposition du chromophore qui coïncide avec le début de la production d'hydrogène. Cependant dans le DMF, les bandes sont plus simples à suivre, car la dissociation du rhénium ne crée pas une espèce transitoire visible, comme c'était le cas dans l'acétonitrile. En effectuant la différence entre l'absorbance à 322 nm (bande étroite venant de l'espèce Re-Py) et celle à 318 nm, on voit sa dissociation rapide vers la minute 120. Les bandes entre 542 nm et 655 nm montrent l'augmentation en quantité de l'espèce Co(II)H, qui atteint également son maximum à la minute 120 avant de chuter avec l'apparition de l'hydrogène.

Dans le DMF, le signal du dimère **5-3** peut-être suivit à 588 nm, tandis que l'espèce libre **5-0** se situe à 542 nm. Toutefois, il est difficile de les suivre quand l'espèce Co(II)H est présente. Cependant, en suivant leur différence d'absorbance, on peut encore voir la dissociation rapide du rhénium à la minute 120 (le reste des variations provenant de l'espèce Co(II)H). Un dernier fait intéressant, le signal à 465 nm, correspondant à la bande d'absorption de l'espèce initiale de Co(II) (**5-9**), décroît et montre une discontinuité lui aussi à la minute 120. Comme expliqué plutôt, ceci correspond au point où tout le Co(II) initial est converti vers une espèce réduite inactive. Les chromophores de rhénium se dissocient, car ils sont réduits par le TEA, mais n'ont plus d'accepteur d'électron pour faire le transfert.

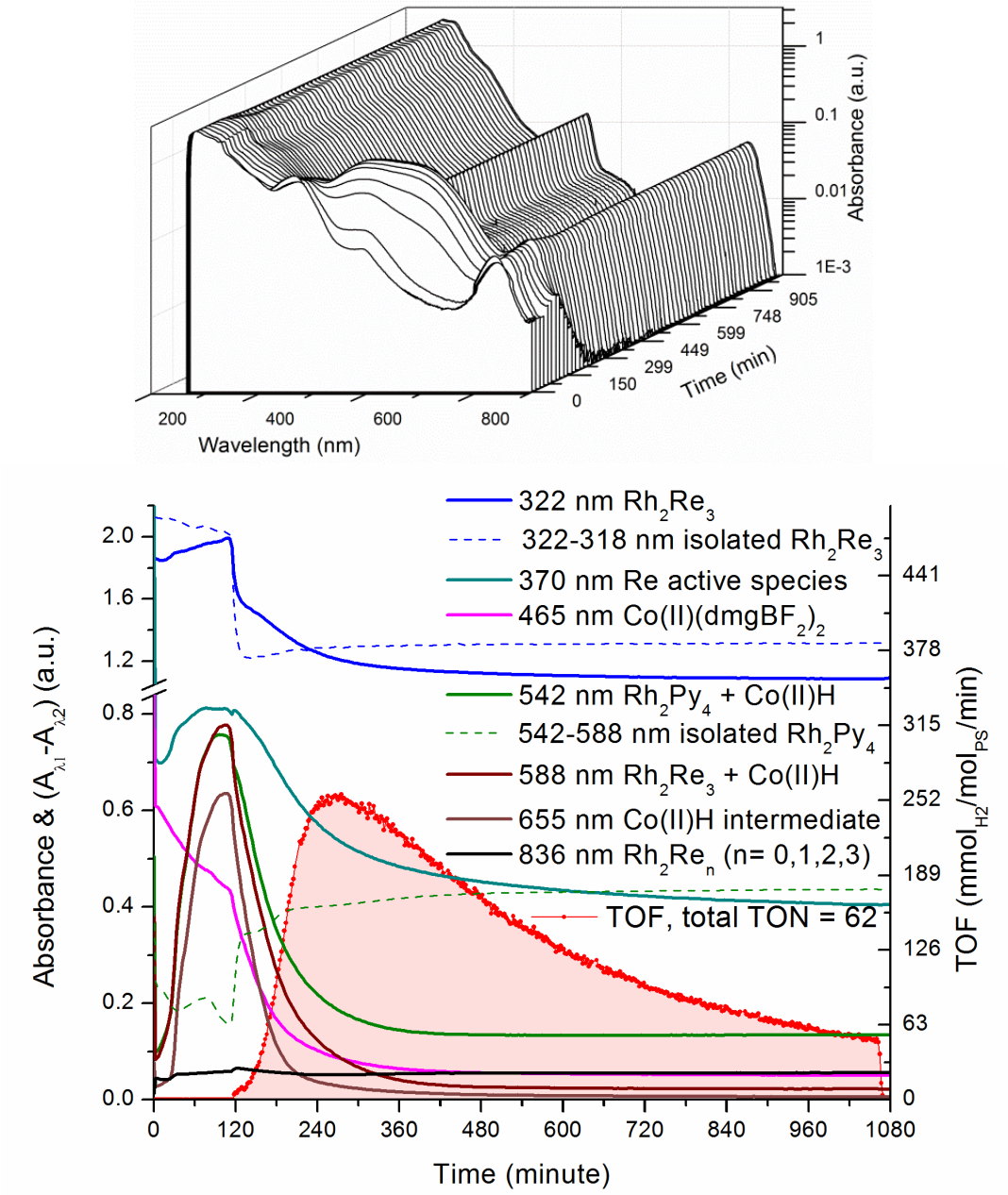

Figure 5.18. Photoproduction d'hydrogène avec 21 µM **5-3**, 0.18 mM de **5-9** et 0.8 M TEA 0.097 M HPF_6 dans le DMF; 15 mL; irradiation à 390 nm, T= 20.0 °C. Haut : compilation des spectres. Bas : suivi de la production d'hydrogène et d'une sélection d'absorption à différentes longueurs d'onde dans le temps (en pointillé des différences d'absorption normalisées).

En résumé, nos assemblages sont actifs, mais le catalyseur est le problème. Tous les chromophores testés réduisent le Co(II) en Co(I), mais celui-ci demeure inactif, sous la forme

Co(II)H. Il semble qu'après dissociation initiale du ligand du complexe de rhénium, il y a transformation du chromophore de rhénium vers une autre espèce, ce qui pousse le catalyseur à produire de l'hydrogène. L'hypothèse la plus probable est une attaque sur le ligand du cobalt, le $(dmgBF_2)_2$, qui pourrait expliquer une réactivation de celui-ci. Puisqu'à ce point nos chromophores ne sont plus impliqués, nous ne sommes plus intéressés par le suivi de la réaction du catalyseur **5-9**.

5.3.5. Suivi spectral avec le catalyseur 5-10, $Co(dmgOH)_2(H_2O)_2$ dans le DMF

Dans la littérature, les photoréactions avec le complexe **5-9** et des complexes de rhénium n'ont été que très sommairement étudiées, se limitant à deux communications.[11,14] En revanche, les systèmes photocatalytiques à base du complexe **5-10** et de rhénium ont été étudiés avec beaucoup plus de rigueur par le groupe du Pr R. Alberto.[9,10,15,16] Ils ont étudiés en détail les effets de la concentration pour toutes les espèces présentes et offrent donc des paramètres beaucoup plus optimisés pour analyser nos assemblages.

Les conditions expérimentales utilisées sont différentes de celles avec le catalyseur **5-9**, afin d'être plus près de celles du groupe d'Alberto. Les changements majeurs par rapport aux expériences impliquant **5-9** sont les suivants :

- Le donneur d'électron, qui passe au triéthanolamine (TEOA). Celui-ci a l'avantage d'être soluble dans l'eau, permettant un transfert éventuel vers un système aqueux;
- La source de proton devient l'acide tétrafluoroborique.
- Le catalyseur **5-10** est préparé *in situ*, à partir d'un sel inorganique de Co(II) (soit acétate ou tétrafluoroborate) et du diméthylglyoxime. Ce dernier est toujours en proportion de six équivalents par rapport au cobalt.

Pour la plupart des expériences, le complexe **5-10** est préparé en avance et est exposé à l'air. Il se retrouve donc sous sa forme oxydée (Co(III)). Il est par la suite réduit par le chromophore au début de l'expérience.

Le premier résultat avec le chromophore **5-3** et le catalyseur **5-10**, dans le DMF, est illustré dans la Figure 5.19. La courbe de production d'hydrogène montre une augmentation marquée du TON final par rapport à nos précédents résultats. Après un peu moins de 24h, le TON_{PS} observé est près de 700. Il y a toujours un temps d'induction, mais cela s'explique

par la présence du Co(III) qui doit être initialement réduit en Co(II). En effet, sur la Figure 5.19 (gauche), on remarque au départ le spectre du Co(III) qui domine de 300 à 800 nm, jusqu'à saturation dans la région de 300 à 350 nm. Les 26 équivalents de cobalt sont réduits en environ 75 min, puis l'hydrogène évolue, signe que le chromophore continue de réduire le Co(II) en Co(I), espèce active dans ce cas-ci.

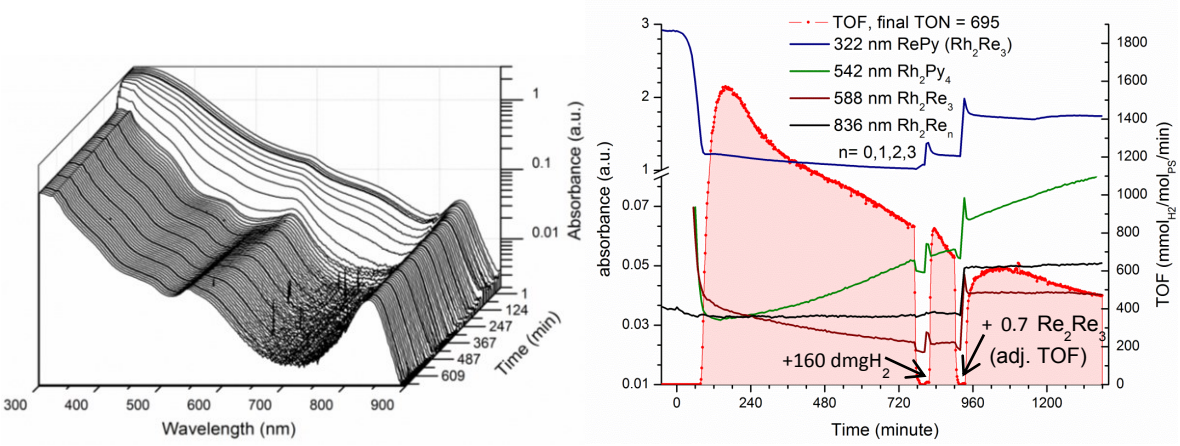

Figure 5.19. Photoproduction d'hydrogène avec 14.5 µM **5-3**, 379 µM de $Co(OAc)_2 \cdot 4(H_2O)$, 2.30 mM de $dmgH_2$, 0.75 M TEOA, 19 mM HBF_4 et 49 mM H_2O dans le DMF; 20 mL; irradiation à 390 nm, T= 20.0 °C; cobalt oxydé au départ. Gauche : compilation des spectres. Droite : suivi de la production d'hydrogène et d'une sélection d'absorption à différentes longueurs d'onde dans le temps; bleu : 322 nm, Re-Pyridyl; vert : 542 nm, M_2LCT de **5-0**; rouge vin : 588 nm, M_2LCT de **5-3**; noir : 836 nm MM du dimère (**5-0** à **5-4**).

Par spectroscopie, il est difficile de suivre le chromophore au départ, car les signaux sont enfuis sous le spectre du Co(III). Mais par la suite, on peut clairement voir l'apparition lente du dimère libre. Cette apparition coïncide avec la chute de la vitesse de production d'hydrogène.

Pour tester l'élément limitant dans la réaction, deux ajouts ont été faits durant cette expérience. Le premier est un ajout de diméthylglyoxime, qui est reconnu pour se décomposer pendant la réaction.[10,11] Lors de cet ajout, aucune accentuation de la vitesse n'est observée, signe qu'il n'y a pas eu décomposition importante du catalyseur. Le deuxième ajout, celui de chromophore (0.7 équivalent), cause une augmentation de la production d'hydrogène, qui sur la Figure 5.19 (droite) n'est pas visible, car les données sont reportées en TOF_{PS} vs la quantité de chromophores totale en solution. Mais les données brutes, sur la Figure 5.20, illustrent très bien cette augmentation. Une observation importante peut être

tirée de cet ajout de chromophore : malgré le nouvel apport de chromophore neuf, le TOF_{PS} n'augmente pas vers son maximum de 1.5 min^{-1}, il continue plutôt son lent déclin exponentiel. Ceci laisse suggérer que la catalyse est ralentie par les sous-produits durant la réaction. Par contre, l'augmentation immédiate de la catalyse au-dessus des niveaux précédents après l'ajout de **5-3** montre qu'il s'agit bel et bien de l'espèce active.

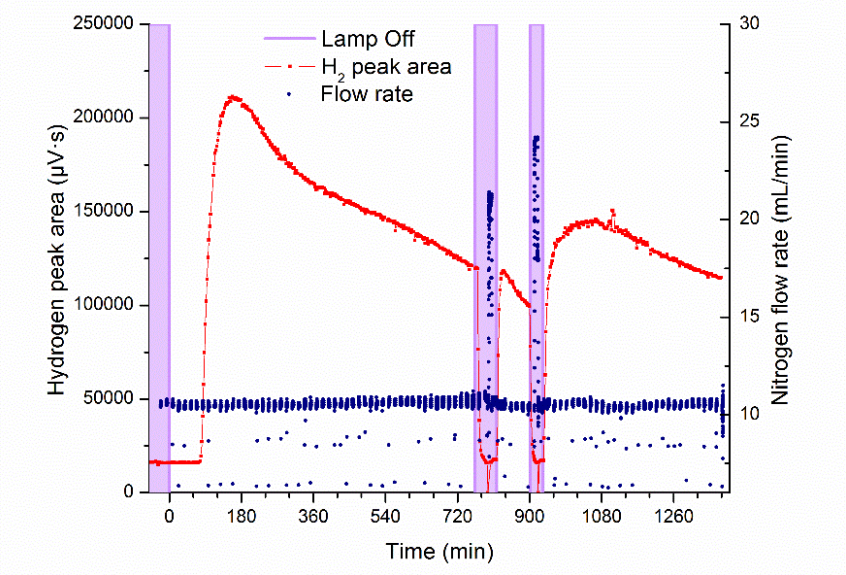

Figure 5.20. Données brutes pour l'expérience effectuée à la Figure 5.19

Le complexe **5-4**+CNPy, utilisé pour faire l'espèce **5-12** et mentionné dans la section 5.3.2, n'a pas été étudié avec le nouveau photoréacteur. Cependant, une expérience de stabilité dans les conditions de photocatalyse d'un ligand isocyanure a été effectuée pour en évaluer sa pertinence. Celle-ci est illustrée à la Figure 5.21. Pour se faire, du 4-bromophénylisocyanure a été ajouté au chromophore **5-3**. Le complexe formé perd sa bande d'absorption à 836 nm comme pour un adduit d'acétonitrile (voir section 4.6.10). Le suivi spectral de cette bande pendant la catalyse montre très bien une dissociation complète, qui commence dès le début de l'irradiation, pendant la phase de réduction du Co(III) et qui se complète rapidement au début de la phase de production d'hydrogène. Ce résultat illustre très bien que l'isocyanure sur le dimère se dissocie très rapidement, quoiqu''il n'y ait aucune interaction possible avec le catalyseur. Il est clair que l'isocyanure ayant un groupement pyridyle aura le même parcours et l'espèce équivalente à **5-12** n'existera pas pendant la catalyse. Plus positivement, on peut conclure que l'excitation lumineuse affecte l'isocyanure

lié au dimère, ce qui renforce l'idée que le dimère de rhodium est excité pendant l'irradiation et pas seulement les chromophores de rhénium liés. Le ligand d'isocyanure pourrait donc être une sonde de cet état excité.

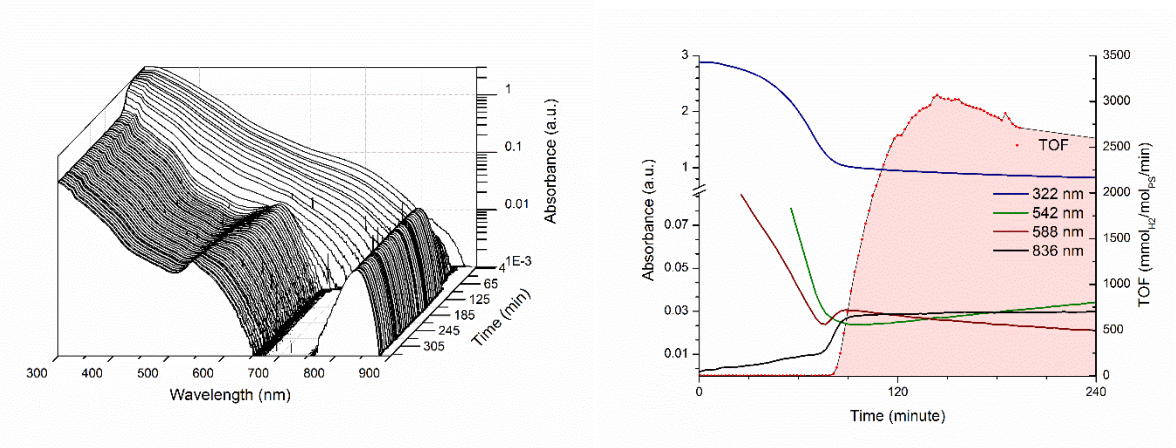

Figure 5.21. Photoproduction d'hydrogène avec 12.4 µM **5-3**, 13.1 µM de 4-bromophénylisocyanure, 369 µM de $Co(OAc)_2 \cdot 4(H_2O)$, 2.38 mM de $dmgH_2$, 0.75 M TEOA, 19 mM HBF_4 et 49 mM H_2O dans le DMF; 15 mL; irradiation à 390 nm, T= 20.0 °C; cobalt oxydé au départ. Gauche : compilation des spectres. Droite : suivi de la production d'hydrogène et d'une sélection d'absorption à différentes longueurs d'onde dans le temps; bleu : 322 nm, Re-Pyridyl; vert : 542 nm, M_2LCT de **5-0**; rouge vin : 588 nm, M_2LCT de **5-3**; noir : 836 nm MM du dimère (**5-0** à **5-4**) sans ligand isocyanure.

Il a déjà été démontré que le catalyseur **5-9** se fait autant réduire avec le **5-4** qu'avec le **5-3**. C'est aussi le cas avec l'utilisation du catalyseur **5-10**. Les expériences ont été répétées à plusieurs reprises sans suivi spectral, ce qui permet d'évaluer la décroissance de la production d'hydrogène sans avoir le problème du réservoir non irradié. Ce réservoir ralentit les processus de décomposition et modifie le TOF et le TON, puisque la quantité réelle du PS et du catalyseur irradiée est inférieure à la quantité totale présente dans le système. Le TOF est ajusté pour tenir compte de la quantité réelle irradiée. Cependant, le TON final correspond à la totalité du volume de la solution si l'on considère que l'étape limitante est la décomposition du système photocatalytique.

Les résultats sans suivis sont illustrés dans la Figure 5.22 et dans le Tableau V-5. Toutes les expériences utilisent les mêmes conditions avec le cobalt initial isolé de l'air pour éviter son oxydation, sauf l'entrée 4 qui sera analysée plus tard. Les entrées 1 et 2 comparent

5-3 et **5-4**, dans des conditions identiques. On observe que le TON augmente dans un ratio de quatre tiers, ce qui suggère que la quantité de rhénium sur le dimère est déterminante. Cela suppose deux possibilités :

- Soit le dimère **5-4**, en se dissociant, génère une plus grande quantité de rhénium finale que **5-3**. Ce rhénium dissocié va donc générer plus d'hydrogène.
- Soit les espèces Rh_2-Re_n, avec n=1 à 4, sont tous des espèces actives qui se décomposent pendant la réaction. Il est donc évident que le dimère **5-4** aura une plus longue durée de vie puisque n au départ est plus grand que **5-3**.

Il semble que le groupement pyridyle libre n'augmente pas la stabilité ni la vitesse de réaction, cependant il ne s'agit pas d'une preuve absolue, car le groupement pyridyle se libère avec la dissociation du rhénium.

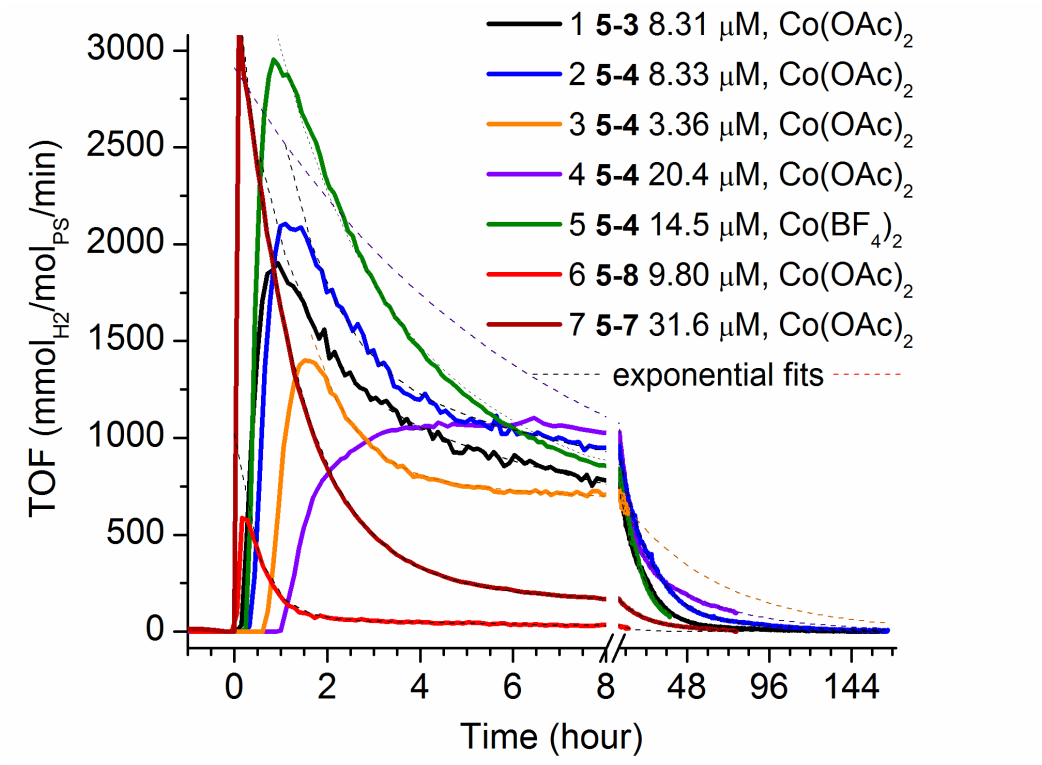

Figure 5.22. Production d'hydrogène obtenu pour différents systèmes catalytiques. Conditions communes : [Co] = 407(1) μM, [$dmgH_2$] = 2.45(1) mM, 1.0 M TEOA, 50 mM HBF_4 et 128 mM H_2O dans le DMF; 10 mL; irradiation à 390 nm, T= 20.0 °C. entré 4 Co départ oxydé.

Tableau V-5. Compilation des résultats de photoproduction* illustrés sur la Figure 5.22.

Entré	**1**	**2**	**3**	**4**[a]	**5**	**6**	**7**
PS	**5-3**	**5-4**	**5-4**	**5-4**	**5-4**	**5-8**	**5-7**
[PS] (μM)	8.31	8.33	3.35	20.4	14.5	9.8	31.6
source de cobalt	$Co(OAc)_2$ $4(H_2O)$	$Co(OAc)_2$ $4(H_2O)$	$Co(OAc)_2$ $4(H_2O)$	$Co(OAc)_2$ $4(H_2O)$ oxydé	$Co(BF_4)_2$ $n(H_2O)$	$Co(OAc)_2$ $4(H_2O)$	$Co(OAc)_2$ $4(H_2O)$
max. TOF_{PS} (mmol $_{H2}$/mol $_{PS}$/min)	1905	2106	1401	1105	2952	587	3186
max. $TOF_{Cat.}$ (mmol $_{H2}$/mol $_{cat}$/min)	39	43	12	55	105	14	247
TON_{PS} (mol $_{H2}$/mol $_{PS}$)	1250	1809	605 (2740)[b]	1547	1333	52	516
TON_{PS}[c] (mol $_{½H2}$/mol $_{PS}$)	2500	3618	1210 (5480)[b]	3094	2666	104	1032
temps d'induction (min)	3	12	37	60	9	0	0
courbes de tendance exponentielles							
début (min)	75	100	120	560	75	30	24
A1 (TOF mmol/mol/min)	1930(70)	3260(110)	4400(400)	2380(40)	2680(30)	950(12)	3200(5)
t1 (min)	66(2)	65(2)	56(3)	375(6)	122(2)	29.3(5)	74.0(2)
A2 (TOF mmol/mol/min)	1280(12)	1320(15)	800(12)	530(10)	1473(20)	70(3)	250(3)
t2 (min)	820(12)	1090(20)	3400(300)	2800(50)	810(10)	590(30)	1120(20)
A3 (TOF mmol/mol/min)	55(15)	90(20)					
t2 (min)	3000(450)	4000(500)					
$\%A1/A_{total}$	59	69	83	82	65	93	93
$\%A2/A_{total}$	40	29	17	18	35	7	7
$\%A3/A_{total}$	2	2					

*Conditions communes : [Co] = 407(1) μM, [$dmgH_2$] = 2.45(1) mM, 1.0 M TEOA, 50 mM HBF_4 et 128 mM H_2O dans le DMF; 10 mL; irradiation à 390 nm, T= 20.0 °C. incertitude sur les mesures 5%. [a]Co(III) au départ, irradié au paravent avec la lampe rouge (630 nm) et la lampe verte (520 nm) pendant une journée chacune. [b]Valeur finale projetée selon la courbe de tendance. [c]Valeur de TON doublé pour comparer avec valeur de la littérature utilisant mol(½H_2)/mol(PS).

L'entrée 4 correspond à une expérience avec le cobalt oxydé. La solution a d'abord été irradiée par une lumière rouge (630 nm), puis par une lumière verte (520 nm) pendant 16 h chacune, avant de commencer l'irradiation dans l'UV. Les irradiations avec les lumières rouge et verte n'ont donné aucune évolution d'hydrogène. L'évolution de cette réaction pendant l'irradiation dans l'UV est différente des autres expériences. Le temps d'induction est normal et ressemble aux expériences montrées précédemment (avec Co(III) au départ), il n'y a cependant pas un maximum qui décroît rapidement. On n'y observe qu'un long plateau, puis la production d'hydrogène devient très similaire aux autres expériences illustrées. Il se peut qu'il y ait eu altération des espèces initiales.

Le temps d'induction des expériences effectuées avec un cobalt non oxydé au départ chute considérablement, mais il n'est toujours pas nul, surtout en comparaison avec les chromophores des entrées 6 et 7 qui n'ont pas d'induction du tout. L'hypothèse la plus probable est la présence d'une faible fraction oxydée du Co(III) qui crée cette induction, et qui n'est pas observable avec les chromophores **5-7** et **5-8**, car leur rendement quantique et leur temps de vie de l'état excité sont beaucoup plus grand que les assemblages **5-1** à **5-4**. En effet les assemblages Rh_2-Re_n n'ont pas d'émission mesurable et ont probablement un temps de vie de l'état excité très court, ce qui limiterait leurs vitesses de réaction. Les complexes de $Re(bpy)(CO)_3L^+$ ont quant à eux des temps de vies variant entre 100 et 1200 ns et des rendements quantiques oscillant entre 2 et 41%, les valeurs maximums étant vu avec **5-8**. Pourtant **5-8** a un TOF maximal très faible, presque de 0.6 min^{-1} comparé à des TOF de 2 min^{-1} à 3 min^{-1} pour **5-4** et **5-7**. Ce faible TOF maximal s'expliquerait par la vitesse de dissociation initiale accrue. Cela diminue fortement le TOF avant même la première mesure d'hydrogène. **5-8** devrait se dissocier plus rapidement, car l'acétonitrile est plus labile que la pyridine. On peut l'observer dans les temps de vie très court de la bisexponentielle décrivant sa vitesse de réaction. En comparaison avec l'entrée 6 qui utilise **5-7**, où le ligand L sur le rhénium est le 4,4'-bipyridine, le premier temps de vie est 2.5 fois plus rapide.

Il se peut aussi que la différence des temps d'induction entre **5-4** et **5-3** est due à leur activité respective. **5-3** serait plus actif que **5-4**. Des expériences avec **5-2** et **5-1** pourraient élucider ce problème, si elles se montrent plus actives.

Pour mieux expliquer les observations, il faut définir la cinétique des réactions impliquées dans le cycle catalytique décrit dans la section 1.4. En effet, la localisation de l'étape limitante lors de la photocatalyse a de grandes répercussions sur la durée de vie du système catalytique. Voici les principales réactions impliquant le chromophore et le catalyseur :

(1) $$\mathrm{Re(bpy)(CO)_3L^+} \underset{K_{\mathrm{La}}}{\overset{K_{\mathrm{Ld}}}{\rightleftharpoons}} \mathrm{Re(bpy)(CO)_3^+ + L}$$

(2) $$\mathrm{Re(bpy)(CO)_3H_2O^+} \underset{K_{\mathrm{La}}}{\overset{K_{\mathrm{Ld}}}{\rightleftharpoons}} \mathrm{Re(bpy)(CO)_3^+ + H_2O}$$

(3) $$\mathrm{Re(bpy)(CO)_3H_2O^+} + h\nu \xrightarrow{K_{photo-acide}} \mathrm{Re(bpy)(CO)_3OH + H^+}$$

(4) $$\mathrm{Re(bpy)(CO)_3L^+} + h\nu \xrightarrow{K_{\mathrm{ex}}} \mathrm{Re(bpy)(CO)_3L^{+*}}$$

(5) $\mathrm{Re(bpy)(CO)_3L^{+*} + TEOA \xrightarrow{K_{red}} Re(bpy)(CO)_3L^{\cdot} + TEOA^{+\cdot}}$

(6) $\mathrm{Re(bpy)(CO)_3L^{\cdot} \xrightarrow{K_{Ld\ rad}} Re(bpy)(CO)_3^{\cdot} + L}$

(7) $\mathrm{Re(bpy)(CO)_3L^{\cdot} + Co(III) \xrightarrow{K_{ET1}} Re(bpy)(CO)_3L^{+} + Co(II)}$

(8) $\mathrm{Re(bpy)(CO)_3L^{\cdot} + Co(II) \xrightarrow{K_{ET2}} Re(bpy)(CO)_3L^{+} + Co(I)}$

(9) $\mathrm{Co(I) + HA^{+} \xrightarrow{K_{H1}} Co(III)H + A}$

(10) $\mathrm{2Co(III)H \xrightarrow{K_{H2(homoleptique)}} 2Co(II) + H_2}$

(11) $\mathrm{Co(III)H + e^{-} + \xrightarrow{K_{ET3}} Co(II)H}$

(12) $\mathrm{Co(II)H + HA^{+} \xrightarrow{K_{H2(heteroleptique)}} Co(II) + H_2 + A}$

(13) $\mathrm{Co(I) + Co(III) \xrightarrow{K_{recomb}} 2Co(II)}$

Dans cette liste, les réactions venant de la décomposition de la TEAO sont omises (illustrées au Chapitre 1, Schéma 1.10). Celles-ci engendrent la réduction directe du PS non excité et du catalyseur, semblables aux équations (5), (7) et (8). Ces réactions dépendent tous de la vitesse de la réaction indiquée dans l'équation (5).

L'équation (1) fait référence à une dissociation (ou association) du ligand L du PS au repos. En général, la constante de dissociation va dépendre du groupement L (selon la force du lien L–Re) et devrait être négligeable dans un solvant peu coordonnant. Cependant, la dissociation de l'espèce réduite, décrite dans l'équation (6), va être très importante, car l'espèce radicalaire sera beaucoup plus instable. Puisque dans nos réactions il y a présence d'eau, les équations (2) et (3) peuvent devenir la voie de décomposition principale du PS, puisque que $Re(bpy)(CO)_3OH$ est inactif tel que postulé dans la littérature.[16] Si le solvant est plus coordonnant, il peut remplacer le ligand L du départ (ceci sera vu dans la prochaine section).

La vitesse de la réaction de l'équation (4) sera limitée par le flux lumineux et par la concentration du PS, ou plutôt par l'absorption de celui-ci. Pour des systèmes de même absorption utilisant la même source lumineuse, le rendement quantique va définir la vitesse de réaction. Pour l'équation (5), la réduction du PS par le donneur d'électron, le K_{red} va dépendre du potentiel d'oxydation du donneur et du potentiel de réduction du PS excité.

Puisque tous nos PS ont une nature très semblable, ce facteur devrait être très similaire pour tous les systèmes étudiés. Par le même argument, les constantes de vitesse des réactions (7) et (8) ne devraient pas variées, de même que celles de (9). (10), (11) et (12) qui ne dépendent que du catalyseur et la concentration de proton. Cette concentration devrait être constante car le TEAO libère un proton pour chaque électron qu'il transfère (dans sa forme de départ ou en se décomposant). L'équation (13) décrit l'oxydation du Co(I) par le Co(III) et est extrêmement rapide, car il n'y a pas de production d'hydrogène observable en présence de Co(III).

L'étape limitante pour le cycle catalytique du cobalt est connue et se situe sur (10) lorsque le cycle est homoleptique. Cependant la concentration d'acide joue un rôle sur (9) et peut aussi influencer la vitesse de réaction si celle-ci est très faible.[17,18] Si la vitesse de formation du PS réduit (qui est directement proportionnelle au K_{ex} et la concentration du PS) est plus rapide que la vitesse de réaction de la formation de l'hydrogène, qui dépend de la concentration du catalyseur et du pH, il y aura accumulation du PS réduit, ce qui risque de grandement favoriser la décomposition de ce dernier.

La stabilité du PS pendant la catalyse va dépendre exclusivement de la vitesse des réactions de transfert d'électron vers le catalyseur par rapport à la vitesse de dissociation ou de décomposition de celui-ci à l'état réduit. Dans nos expériences, nous avons démontré qu'il s'agit du PS qui se décompose. Un test simple à effectuer est de rajouter un PS très actif à la fin de l'expérience. En général, la production d'hydrogène reprend et s'estompe de la même manière. Nous sommes donc dans des conditions où la vitesse de réaction n'est pas idéale. Il faut soit rendre le chromophore plus stable à l'état excité ou augmenter sa vitesse de réaction avec le catalyseur.

Dans le cas de l'expérience avec **5-7**, entrée 7, qui a été réalisée à plus haute concentration de PS, on atteint un TOF du catalyseur beaucoup plus haut, soit 0.247 min^{-1} vs un TOF inférieur à 0.05 min^{-1} pour tous les cas des entrées 1 à 4 et 6. Ceci laisse suggérer que le catalyseur n'est pas saturé (c'est-à-dire qu'il n'y a pas un manque de catalyseur à réduire, comme c'était le cas avec le $Co(dmgBF_2)_2$). Donc le problème est lié à la concentration de celui-ci, qui va dicter la vitesse de réaction.

Selon les travaux de Probst *et. al.*, la concentration minimale pour ces systèmes est de 0.4 mM. En deçà de cette valeur, le PS se décompose rapidement et il n'y a pas

d'hydrogène produit.[9] Si le cobalt était plus concentré, il y a très rapidement un effet de désactivation direct sur l'état excité décrit par l'équation (14), ou un transfert de charge, suivant l'équation (15). Ce transfert serait suivi d'une recombinaison de charge selon (7).

(14) $$\mathrm{Re(bpy)(CO)_3L^{+*} + Co(II) \xrightarrow{K_{Des}} Re(bpy)(CO)_3L^{+} + Co(II)^*}$$

(15) $$\mathrm{Re(bpy)(CO)_3L^{+*} + Co(II) \xrightarrow{K_{ET4}} Re(bpy)(CO)_3L^{\cdot} + Co(III)}$$

Nos tests ont montré les mêmes résultats. La source de Co(II) a été changée pour un sel de tétrafluoroborate, qui donne des résultats similaires, mais qui permet d'augmenter considérablement la concentration (voir entrée 5 Figure 5.22 et Tableau V-5). Une expérience avec une concentration de 10 mM de catalyseur n'a donné aucune production d'hydrogène en 24h avec **5-4**. Un suivit UV-vis a démontré que **5-4** ne se décompose pas pendant cette période et qu'il n'y avait que très peu de changement spectral. Avec cette concentration de Co(II), le spectre d'absorption est saturé jusqu'à 500 nm. Même si le cobalt ne désactive pas selon (14) ou (15), il absorbe la majorité des photons, anéantissant la photoréaction. Avec une concentration 10 fois plus diluée (1 mM), la catalyse reprend, comme indiqué sur la Figure 5.23 (gauche). On peut y voir l'influence d'une expérience avec suivi UV : le maximum de TOF passe d'environ 18 h pour l'expérience sans suivi, jusqu'à 36 h avec suivi. Le TON_{PS} total est de 2700 dans les deux cas, mais les données entre 0 et 80 h sont de mauvaise qualité à cause de l'utilisation de l'azote comme gaz vecteur à la place de l'argon dans le GC. Ceci fait chuter considérablement le signal sur bruit, à cause de cela, ce résultat n'est pas comparé avec les autres résultats répertoriés au Tableau V-5.

Le suivi spectral, illustré sur la Figure 5.23 (droite) et plus en détail sur la Figure 5.24, montre une certaine induction probablement due à une oxydation partielle du Co de départ. On l'observe par les bandes de 321 nm et 465 nm qui diminuent pendant la première heure. Pendant le premier 24 h, il semble que le dimère ne se décompose pas, par la suite une nouvelle bande plutôt large augmente l'absorption jusqu'à 750 nm. Ceci rend difficile le suivit des bandes associées au dimère **5-4**, mais on peut voir la bande à 318 nm rattraper celle de 321 nm, indiquant que la bande associée au $Re(bpy)(CO)_3Py^+$ est en train de s'estomper. Quant à la bande à 541 nm, correspondant au dimère **5-0**, elle commence à n'être observable que vers la 100^e heure.

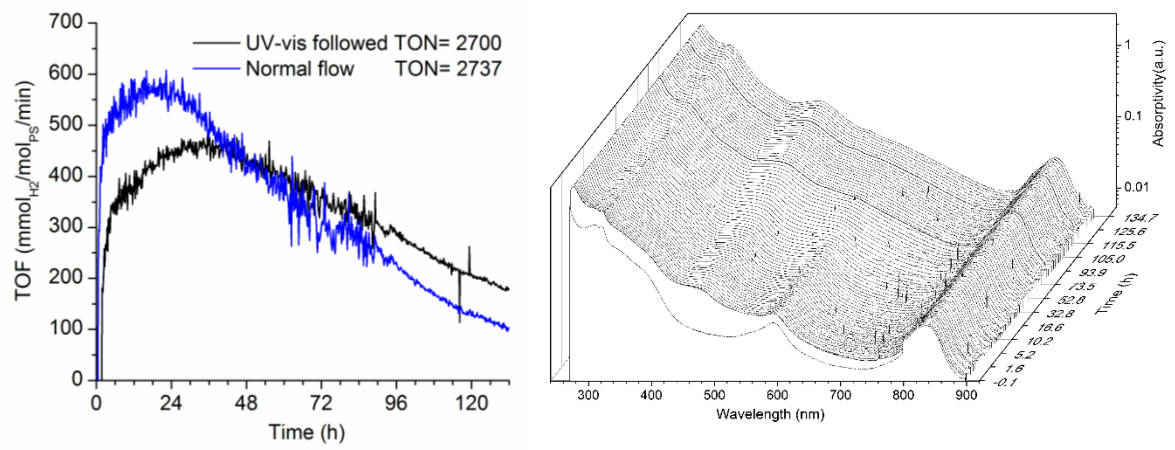

Figure 5.23. À Gauche : Photoproduction d'hydrogène avec 10.1 µM **5-4**, 1.01 mM de $Co(OAc)_2 \cdot 4(H_2O)$, 6.03 mM de $dmgH_2$, 1.00 M TEOA, 100 mM HBF_4 et 255 mM H_2O dans le DMF; irradiation à 390 nm, T= 20.0 °C. En noir, avec suivi spectral (16.9 mL) en gris, sans suivi (10 mL). À droite : Suivit spectral.

L'espèce qui se développe au cours de la réaction s'estompe au moment où l'irradiation est interrompue, laissant croire à une espèce de Co(I) qui se réoxyderait lentement en Co(II) (possiblement en formant de l'hydrogène). Cette oxydation ne semble pas être causée par l'air, car lorsque la purge d'azote est arrêtée, il y a une augmentation fulgurante de l'absorption due à la formation du Co(III), comme indiqué sur la Figure 5.24 (droite).

Quant à la décroissance de la réaction, toutes les réactions avec les assemblages Rh_2-Re_n montrent une décroissance soit bis- ou tris-exponentielle. En général, la dernière exponentielle possède un temps de vie très long (plus de 2000 min, voir Tableau V-5). Celle-ci représente l'hydrogène produit en fin de réaction où le système est plus ou moins à l'équilibre. Il s'agit soit de l'hydrogène produit par les chromophores de rhénium dissociés, soit par ceux qui restent associés si l'on considère qu'il y a équilibration entre la forme Rh2-Re_n et le rhénium dissocié en solution.

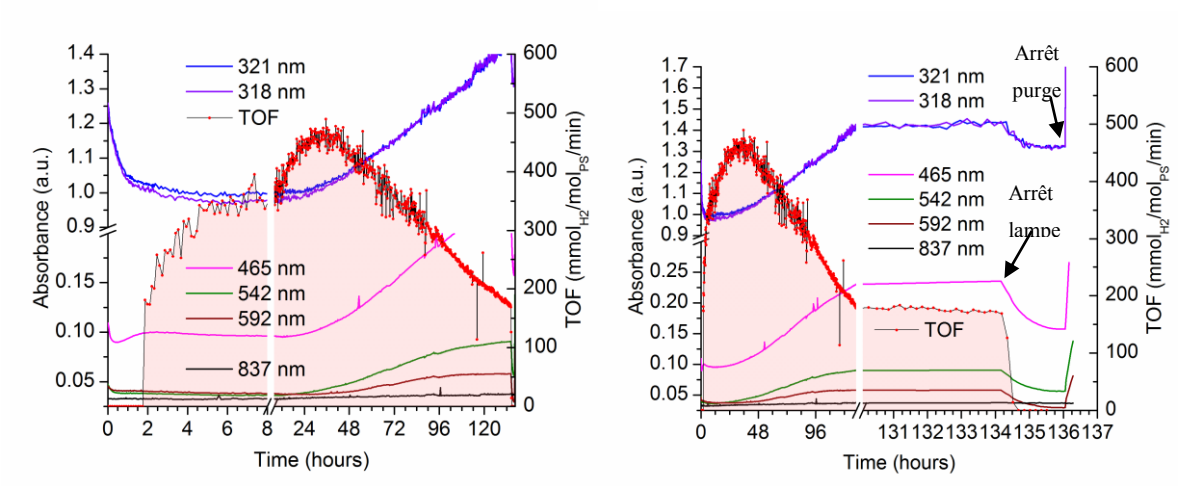

Figure 5.24. Photoproduction d'hydrogène avec 10.1 µM **5-4**, 1.01 mM de $Co(OAc)_2 \cdot 4(H_2O)$, 6.03 mM de $dmgH_2$, 1.00 M TEOA, 100 mM HBF_4 et 255 mM H_2O dans le DMF; 16.9 mL; irradiation à 390 nm, T= 20.0 °C. Gauche : Focus sur le début de la réaction Droite : Focus sur la fin de la réaction après l'arrêt de la lampe et ouverture à l'air. Couleur : mauve : 318 nm, Re (comparé avec l'absorption à 321 nm); bleu : 321 nm, Re-Pyridyl; rose : 465 nm Espèce Co inconnu; vert : 542 nm, M_2LCT de **5-0**; rouge vin : 592 nm, M_2LCT de **5-4**; noir : 837 nm MM du dimère (**5-0** à **5-4**).

Beaucoup d'hypothèses sont mises en jeu, mais il est très difficile d'établir des réponses claires. Il est cependant observable que dans le DMF et pour le catalyseur **5-10**, il y a toujours décomposition du chromophore à long terme, malgré une différence d'ordre 100 entre la concentration du chromophore et du catalyseur. Il est impossible d'augmenter la concentration du catalyseur davantage sans causer une désactivation du PS. Il est clair qu'un autre catalyseur ou d'autres conditions expérimentales doivent être trouvés pour minimiser la décomposition du PS.

5.3.6. Suivi spectral avec le catalyseur 5-10, $Co(dmgOH)_2(H_2O)_2$ dans l'acétonitrile

La dernière série de résultats dont nous allons discuter est celle obtenue dans l'acétonitrile. Le premier résultat, illustré à la Figure 5.25, montre ce qui semble être un résultat idéal : un temps d'induction seulement dû au Co(III) initial, puis une production d'hydrogène constante, sans décomposition du dimère, qui est suivit avec les bandes à 570 nm (le dimère libre) et à 620 nm (**5-3**). Cependant, le TOF_{PS} a chuté, il est d'environ 0.15 min^{-1}, soit au moins 10 fois moins que ceux observés dans le DMF. On peut observer,

grâce au spectre d'absorption, une espèce avec une bande à 432 nm qui s'estompe lentement et qui correspond fort probablement au Co(II).

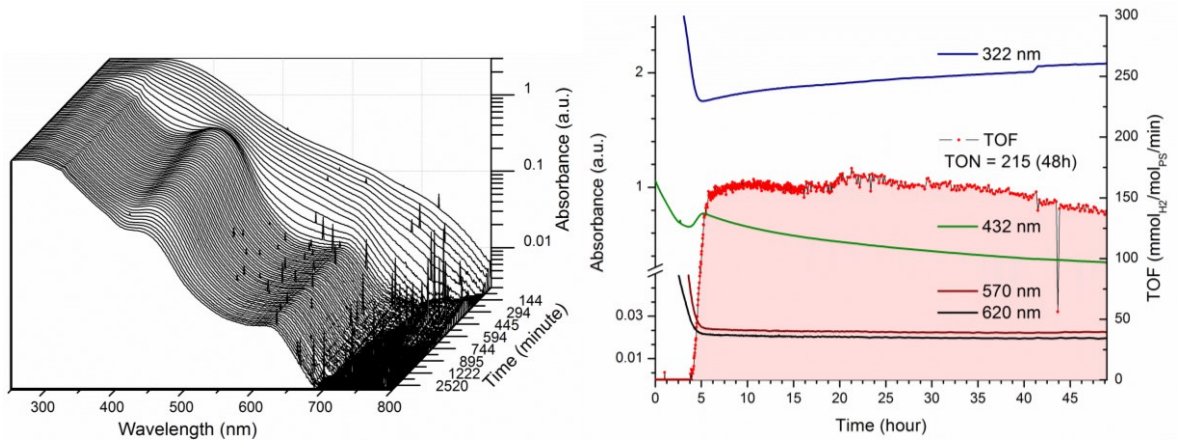

Figure 5.25. Photoproduction d'hydrogène avec 11.7 µM **5-3**, 372 µM de $Co(OAc)_2 \cdot 4(H_2O)$, 2.31 mM de $dmgH_2$, 1.00 M TEOA, 25.5 mM HBF_4 et 64.7 mM H_2O dans l'acétonitrile; 15 mL; irradiation à 390 nm, T= 20.0 °C; cobalt oxydé au départ. Gauche : compilation des spectres. Droite : suivi de la production d'hydrogène et d'une sélection d'absorption à différentes longueurs d'onde dans le temps; bleu : 322 nm, Re-Pyridyl; vert : 432 nm Espèce Co inconnu; rouge vin : 570 nm, M_2LCT de **5-0**; noir : 620 nm, M_2LCT de **5-4**.

Si le PS actif est **5-3** comme démontré dans le DMF, ce résultat demeure très intéressant. Par contre, ce n'est pas certain, car le dimère est électroniquement très différent dans l'acétonitrile, comme le montre son spectre d'absorption (voir chapitre 4, Figure 4.8). Les prochains tests ont mis un doute sur l'espèce active, qui semble être le complexe **5-8**. Celui-ci serait assurément formé si le rhénium se dissocie du dimère puisque le solvant est l'acétonitrile, comme ce qui a été observé, quoique brièvement, dans les expériences avec le catalyseur **5-9**.

Un suivit avec une basse concentration de catalyseur a démontré cela de façon spectaculaire et sans équivoque avec les PS **5-4** et **5-3**. La vitesse de production de l'hydrogène n'est pas conventionnelle, elle augmente de façon exponentielle pendant 25 à 31 h, jusqu'à un seuil critique où elle chute spontanément, pour ensuite produire un peu d'hydrogène à nouveau avant de s'éteindre complètement (Figure 5.26 et Figure 5.27 (droite)).

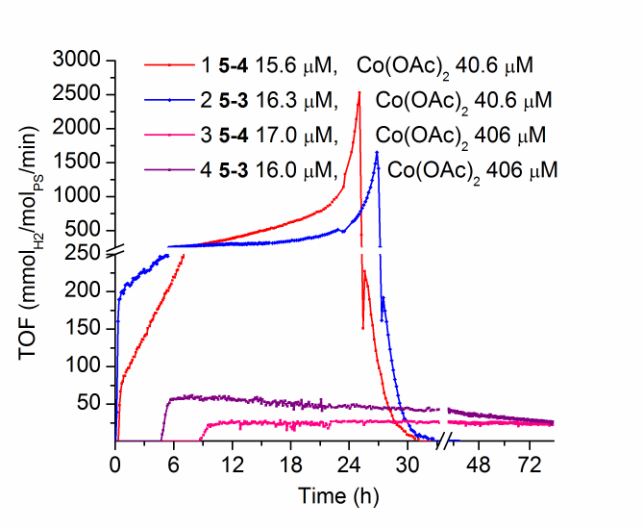

Figure 5.26. Photoproduction d'hydrogène avec différents équivalents de cobalt. Conditions communes : [dmgH_2] = 6 x [Co], 1.0 M TEOA, 50 mM HBF_4 et 128 mM H_2O dans l'acétonitrile; 10 mL; irradiation à 390 nm, T= 20.0 °C;cobalt oxydé au départ.

Le suivi spectral illustré à la Figure 5.27 montre que le dimère **5-4** se dissocie très lentement pendant les 24 premières heures (de façon presque imperceptible). Pal la suite, il se décomposer plus rapidement, atteignant environ 30% de décomposition à l'heure 31, puis est totalement décomposé après. Ceci se voit aussi avec la bande à 320 nm. La seule explication plausible à l'augmentation de la vitesse de production est la formation d'un PS plus actif pendant la réaction. **5-8** a toutes les qualités d'un chromophore très actif, car il a un long temps de vie (1,2 ms) et un rendement quantique de 41%.[19] Son seul défaut étant la rapide dissociation de l'acétonitrile, mais puisque l'expérience se fait dans ce solvant, il va se régénéré et rester actif beaucoup plus longtemps avant de se décomposer en espèce inactive par la voie des équations (2) et (3). L'hydrogène produit initialement peut-être due au chromophore **5-4**, mais peut aussi être due à des traces de **5-8**. Dans les premières 20 h, le dimère semble perdre environ 5% de son rhénium, mais la production d'hydrogène augmente d'un facteur de 10, donc en première approximation, si au départ l'hydrogène produit vient de **5-4** uniquement, **5-8** serait environ 200 fois plus actif.

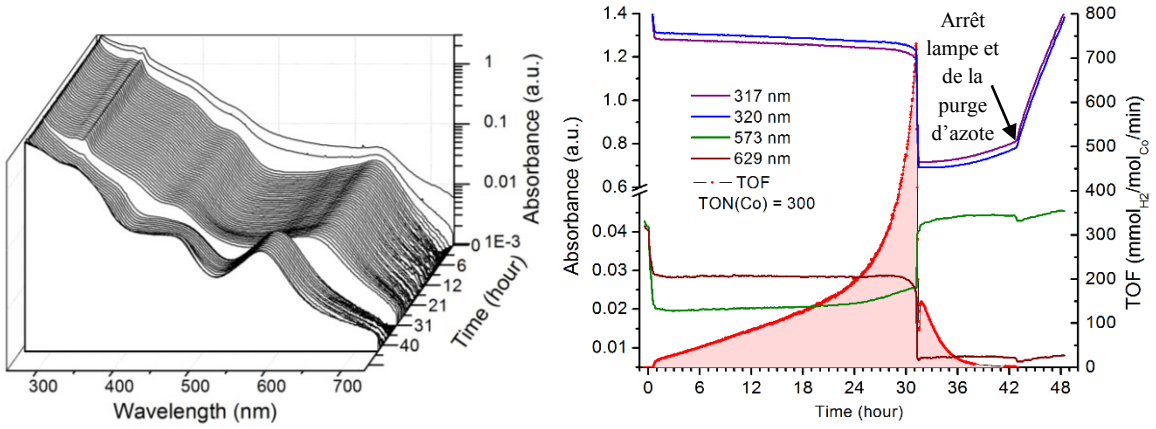

Figure 5.27. Photoproduction d'hydrogène avec 17.0 µM de **5-4**, 40.0 µM de $Co(OAc)_2 \cdot 4(H_2O)$, 245 µM de $dmgH_2$, 1.00 M TEOA, 50 mM HBF_4 et 128 mM H_2O dans l'acétonitrile; 15 mL; irradiation à 390 nm, T= 20.0 °C; cobalt oxydé au départ. Gauche : compilation des spectres. Droite : suivi de la production d'hydrogène et d'une sélection d'absorption à différentes longueurs d'onde dans le temps; mauve : 317 nm, Re (comparé avec l'absorption à 320 nm); bleu : 320 nm, Re-Pyridyl; vert : 573 nm, M_2LCT de **5-0**; rouge vin : 629 nm, M_2LCT de **5-4**.

Si l'on s'attarde seulement sur la première demi-heure de l'heure 31, comme illustré à la Figure 5.28, on peut observer le déplacement de la bande à 321 nm vers 319 nm, correspondant à la dissociation de **5-4** et à la formation de **5-8**. Mais celui disparaît aussi très rapidement, en environ 15 min. La situation est donc identique à celle étudiée avec le catalyseur **5-9** : le chromophore se décompose complètement en une autre espèce qui se forme due à un manque d'accepteur d'électron. Le catalyseur lui-même peut être dégradé, dans ce cas-ci il a atteint une fréquence maximale de 0.7 min^{-1}, fréquence largement supérieure au TOF du catalyseur observé dans les expériences dans le DMF (Tableau V-5).

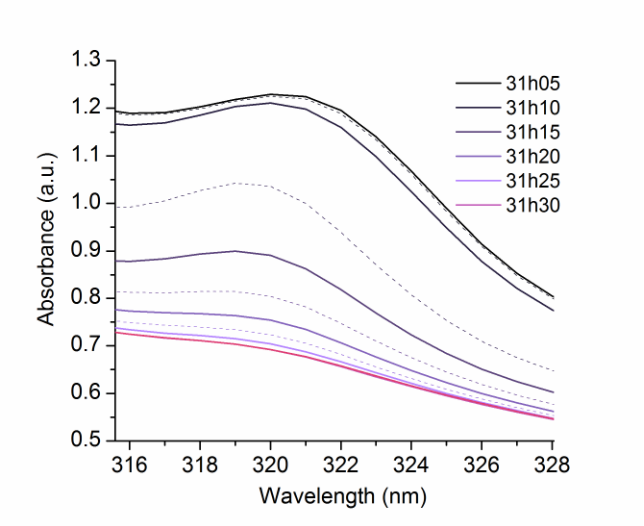

Figure 5.28. Zoom sur la région signature du chromophore de rhénium, de 31 h 05 min à 31 h 30 min. Photoproduction d'hydrogène avec 17.0 µM de **5-4**, 40.0 µM de $Co(OAc)_2 \cdot 4(H_2O)$, 245 µM de $dmgH_2$, 1.00 M TEOA, 50 mM HBF_4 et 128 mM H_2O dans l'acétonitrile; 15 mL; irradiation à 390 nm, T= 20.0 °C; cobalt oxydé au départ.

Par contre, pour que **5-4** se décompose de cette façon, il doit être actif au début de l'expérience ou être en mesure d'être réduit par un chromophore actif. Puisque **5-8** est au moins 200 fois plus actif que **5-4**, des traces de celui pourraient très bien initier cette réaction. En regardant l'émission attendue pour **5-8** (à 537 nm) dans une solution de **5-4** dans l'acétonitrile, on a pu voir grandir un signal émissif après quelques jours, et ce sans irradiation (Figure 5.29 gauche). Ceci nous ramène à l'équation (1), nous avons une dissociation très lente de **5-4** dans le noir à température ambiante. Après une semaine, la même solution commence à être visiblement différente par spectroscopie d'absorption (Figure 5.29 droite). Cette preuve est formelle : **5-4** décompose très lentement dans le noir et donc il y aura toujours une source de **5-8** disponible en début de réaction. Dans d'autres solvants, comme le DMF, des traces de **5-8** ne produiraient pas beaucoup d'hydrogène, car il dissocierait rapidement, mais dans l'acétonitrile il a une durée de vie beaucoup plus longue et est responsable de l'augmentation de la production d'hydrogène.

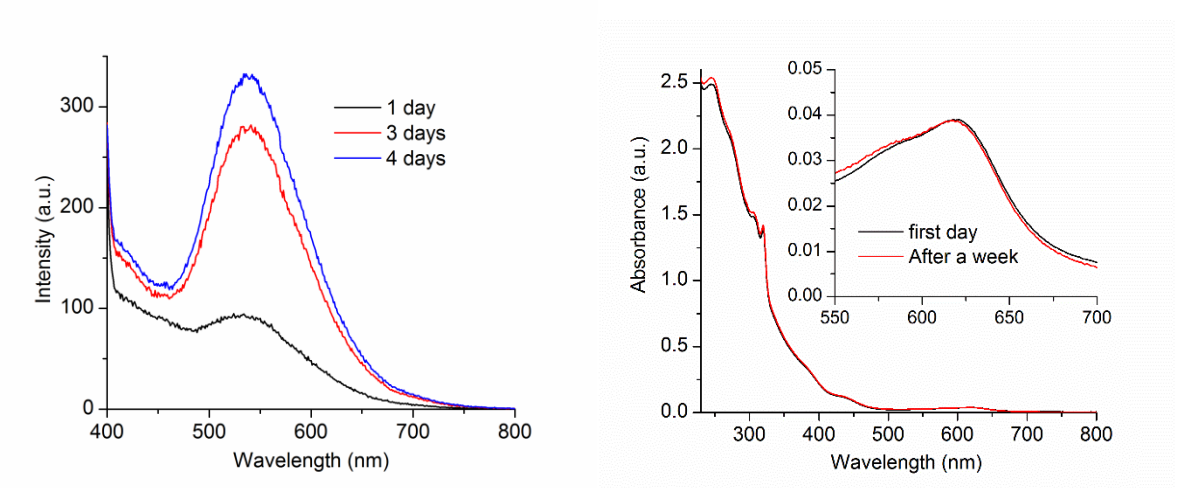

Figure 5.29. Gauche : Spectre d'émission d'une solution **5-4** dans l'acétonitrile après quelques jours laissé dans le noir. Droite : Spectre d'absorption de **5-4** dans l'acétonitrile, au départ (noir) et après une semaine laissé dans le noir.

Les résultats à plus haute concentration de catalyseur, comme ceux de la Figure 5.26, peuvent être expliqués par une faible concentration de **5-8** qui demeure plus ou moins constante à cause d'une vitesse de réaction assez grande avec le cobalt pour éviter la dissociation. Les dimères **5-3** et **5-4** sont soit inertes, soit très peu actifs dans l'acétonitrile, mais on ne peut pas le démontrer avec les expériences effectuées, car l'espèce **5-8** se forme intrinsèquement. Possiblement, une réaction à basse température pourrait résoudre ce problème.

5.3.7. Test d'implication du dimère de rhodium dans le cycle catalytique

Une expérience a pu démontrer l'implication possible du dimère de rhodium comme médiateur rédox lors de la catalyse. Une solution de PS et de catalyseur a donc été préparée sans donneur d'électron. Le catalyseur **5-9** a été choisi, car il est stable dans l'air sous sa forme Co(II), par contre sa forme Co(I) est très réactive et se fait rapidement oxyder. En irradiant la réaction, nous suivons un cycle similaire à la production d'hydrogène (illustré sur le Schéma 5.8). Le dimère de rhodium agit comme donneur d'électron sacrificiel. En effet, le dimère **5-3** a un potentiel d'oxydation de 0.36 V vs SCE dans l'acétonitrile, ce qui lui permet de réduire le chromophore de rhénium a l'état excité. Le potentiel de réduction du Re est de +1.13 V vs SCE à l'état excité (potentiel au GS : -1.17 V additionné de l'énergie de l'état excité de 2.30 eV). Le cobalt quant à lui à un potentiel de réduction de -0.60 V vs

SCE[20] et acceptera seulement l'électron du rhénium réduit, mais peut recombiner la charge avec le dimère de rhodium. Pour éviter cette recombinaison, le Co(I) réagit avec l'oxygène pour ainsi bloquer le dimère dans son état oxydé. La voie oxydative n'est pas possible avec le chromophore de Re, car son potentiel d'oxydation à l'état fondamental est trop haut à 1.86 V vs SCE. Additionné de l'énergie de l'état excité (2.30 eV) celui-ci atteint -0.44 V, ce qui est encore trop faible pour réduire directement le cobalt(II) à 0.60 V vs SCE. Pour la liste des potentiels de l'espèce **5-3,** voir Chapitre 4: Table IV-2.

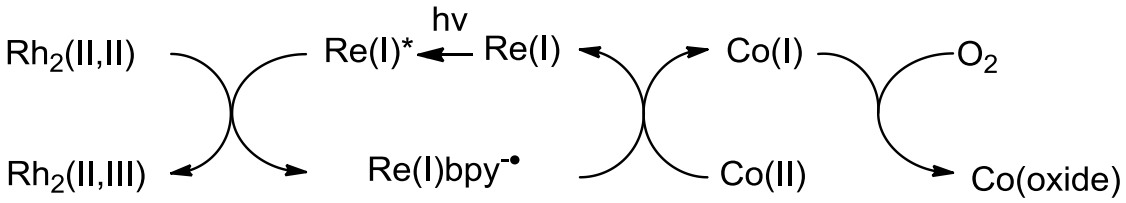

Schéma 5.8. L'oxydation du dimère de rhodium par photoréduction du cobalt

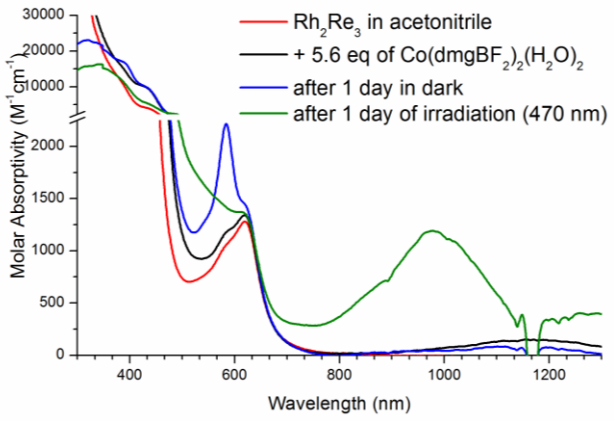

Figure 5.30. Changement d'absorption de **5-3** (rouge) après ajout de 5.6 équiv. de **5-9** (noir) et une journée avec irradiation (vert) ou sans irradiation (bleu) à 470 nm dans l'acétonitrile.

Ceci est démontré expérimentalement dans la Figure 5.30, par l'apparition d'une bande à 960 nm, typique de l'espèce Rh_2(II,III), tel que vu dans le précédent chapitre. Il est à noter que le test d'irradiation réalisé dans le même laps de temps avec seulement l'espèce **5-3** n'a donné aucune oxydation significative du dimère. Encore une fois, l'espèce excitée pourrait bien être le chromophore **5-8** probablement formé en très faible quantité (trace) pendant cette expérience. Cependant, il ne fait nul doute que le donneur d'électron soit le dimère et que le transfert d'électron du rhénium se fait par voie réductrice.

5.4. Conclusion

L'étude de la photocatalyse s'est heurtée à beaucoup de défis, tant du point de vue technique lors de l'utilisation du photoréacteur que du point de vue chimique lors de l'identification des espèces actives. Quant au photoréacteur lui-même, les objectifs ont été atteints. Le système permet en effet de suivre les réactions et d'en retirer une pléthore d'informations. Toutefois, les résultats des systèmes photocatalytiques qui y furent étudiés n'ont pas tout à fait donné les résultats escomptés.

Le catalyseur **5-9** s'est montré inactif dans nos conditions, sauf après décomposition totale de nos chromophores. Le meilleur rôle qui peut en être tiré maintenant est celui d'un indicateur, car il montrait clairement sa réduction initiale par son changement de couleur. Il pourrait être utilisé pour identifier visuellement si un chromophore est capable de le réduire, ce qui pourrait être utile si on n'a pas accès à un photoréacteur pour l'analyse ou comme test préliminaire.

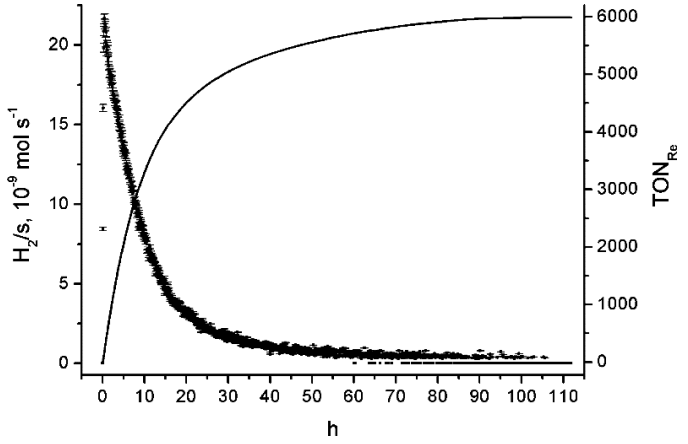

Figure 5.31. Meilleur résultat obtenu par le groupe d'Alberto. 30 μM de $Re(bpy)(CO)_3(NCS)$, 500.0 μM de $[Co(OH_2)_6](BF_4)_2$, 300 μM de $dmgH_2$, 1.00 M TEOA et 20 mM HBF_4, dans DMF, irradiation à 380 nm; TON_{Re}= mol(½H_2)/mol(PS). Reprinted with permission from reference 9. Copyright 2010 American Chemical Society.

Le catalyseur **5-10** a donné de meilleurs résultats : il a effectué la catalyse en milieu basique aussi bien dans le DMF que dans l'acétonitrile, et ce, en présence d'eau (de l'ordre d'environ 0.1 M). Utilisé en excès à une concentration de 0.4 à 1 mM, il donne des systèmes photocatalytiques avec les espèces **5-3** et **5-4** qui perdurent très longtemps et se comparent avec le meilleur résultat obtenu par le groupe d'Alberto illustré à la Figure 5.31.[9] Nos

meilleurs résultats ont un TON_{PS}, exprimé en (mol H/mol PS) entre 5400 et 5500, ce qui est très près de leur production finale optimisée.

Par contre, le suivi spectral laisse planer un doute sur l'espèce active, qui pourrait être un produit de dissociation, comme cela semble être réellement le cas dans l'acétonitrile. Cependant beaucoup de preuves dans le DMF laissent suggérer que le dimère est l'espèce active, tel le déclin de la production d'hydrogène qui suit le déclin du chromophore.

Il reste plusieurs mesures à effectuer pour confirmer le rôle du dimère avec ce catalyseur, cependant il serait peut-être plus judicieux de se tourner vers d'autres catalyseurs, plus performants, comme ceux développés récemment par les groupes d'Alberto et de Fontecave.[21] Si le point majeur de la décomposition provient réellement d'une vitesse de réaction trop lente du catalyseur, ceux-ci pourraient s'avérer un excellent choix. Il y a aussi la possibilité d'investiguer un dimère plus riche en électrons, qui pourrait stabiliser d'avantage les liens pyridyl-Re et, par ce fait même, les rendre plus durables pendant la photocatalyse.

Finalement, de nouvelles questions non-résolues ont été amenées par cette étude. La quête d'un TON toujours plus haut est importante, car pour une application commerciale, il se doit d'être très haut. Cependant, l'optimisation du TON dans les conditions actuelles ne devrait pas être le but ultime, car même avec un TON de l'ordre du milliard, un système photocatalytique nécessitant un donneur d'électron sacrificiel n'a aucune application commerciale. Il faut être capable de combiner ces systèmes avec un système photo- ou électrocatalytique d'oxydation de l'eau, l'autre réaction essentielle pour fermer la boucle catalytique sans requérir d'élément sacrificiel. Il faut donc comprendre le fonctionnement du catalyseur, du chromophore ainsi qu'identifier les espèces réellement actives en solution. L'optimisation du TON_{PS} doit se faire dans des conditions qui se dirigent vers des applications industrielles. Ces conditions impliquent généralement un milieu aqueux et une cellule photoélectrochimique, qui permet de séparer l'oxydation de la réduction de l'eau et d'éliminer le donneur d'électron sacrificiel.[24]

5.5. References

(1) Hawecker, J.; Lehn, J. M.; Ziessel, R. *Nouv. J. Chim.* **1983**, *7*, 271.

(2) Curtin, P. N.; Tinker, L. L.; Burgess, C. M.; Cline, E. D.; Bernhard, S. *Inorg. Chem.* **2009**, *48*, 10498.

(3) Hatchard, C. G.; Parker, C. A. *Proc. R. Soc. London, Ser. A* **1956**, *235*, 518.

(4) Samuel, D.; Weinraub, B.; Ginsburg, D. *J. Org. Chem.* **1956**, *21*, 376.

(5) Shingaki, T.; Takebayashi, M. *Bull. Chem. Soc. Jpn.* **1963**, *36*, 617.

(6) Bartolome, C.; Carrasco-Rando, M.; Coco, S.; Cordovilla, C.; Espinet, P.; Martin-Alvarez, J. M. *Dalton Trans.* **2007**, 5339.

(7) Ikezaki, A.; Nakamura, M.; Juillard, S.; Simonneaux, G. *Inorg. Chem.* **2006**, *45*, 6728.

(8) Guo, J.; Mayr, A. *Inorg. Chim. Acta* **1997**, *261*, 141.

(9) Probst, B.; Rodenberg, A.; Guttentag, M.; Hamm, P.; Alberto, R. *Inorg. Chem.* **2010**, *49*, 6453.

(10) Probst, B.; Kolano, C.; Hamm, P.; Alberto, R. *Inorg. Chem.* **2009**, *48*, 1836.

(11) Fihri, A.; Artero, V.; Pereira, A.; Fontecave, M. *Dalton Trans.* **2008**, 5567.

(12) Zhang, P.; Jacques, P.-A.; Chavarot-Kerlidou, M.; Wang, M.; Sun, L.; Fontecave, M.; Artero, V. *Inorg. Chem.* **2012**, *51*, 2115.

(13) (a) Zhang, P.; Jacques, P.-A.; Chavarot-Kerlidou, M.; Wang, M.; Sun, L.; Fontecave, M.; Artero, V. Inorg. Chem. 2012, 51, 2115. (b) Muckerman, J. T.; Fujita, E. Chem. Commun. 2011, 47, 12456.

(14) Fihri, A.; Artero, V.; Razavet, M.; Baffert, C.; Leibl, W.; Fontecave, M. *Angew. Chem. Int. Ed.* **2008**, *47*, 564.

(15) Guttentag, M.; Rodenberg, A.; Kopelent, R.; Probst, B.; Buchwalder, C.; Brandstaetter, M.; Hamm, P.; Alberto, R. *Eur. J. Inorg. Chem.* **2012**, *2012*, 59.

(16) Probst, B.; Guttentag, M.; Rodenberg, A.; Hamm, P.; Alberto, R. *Inorg. Chem.* **2011**, *50*, 3404.

(17) Dempsey, J. L.; Winkler, J. R.; Gray, H. B. *J. Am. Chem. Soc.* **2010**, *132*, 1060.

(18) Hu, X. L.; Brunschwig, B. S.; Peters, J. C. *J. Am. Chem. Soc.* **2007**, *129*, 8988.

(19) Caspar, J. V.; Meyer, T. J. *J. Phys. Chem.* **1983**, *87*, 952.

(20) Razavet, M.; Artero, V.; Fontecave, M. *Inorg. Chem.* **2005**, *44*, 4786.

(21) (a) Guttentag, M.; Rodenberg, A.; Bachmann, C.; Senn, A.; Hamm, P.; Alberto, R. *Dalton Trans.* **2013**, *42*, 334. (b) Smolentsev, G.; Guda, A.; Zhang, X.; Haldrup, K.; Andreiadis, E. S.; Chavarot-Kerlidou, M.; Canton, S. E.; Nachtegaal, M.; Artero, V.; Sundstrom, V. *J. Phys. Chem. C* **2013**, *117*, 17367. (c) Tran, P. D.; Chiam, S. Y.; Boix, P. P.; Ren, Y.; Pramana, S. S.; Fize, J.; Artero, V.; Barber, J. *Energy Environ. Sci.* **2013**, *6*, 2452. (d) Elgrishi, N.; Artero, V.; Fontecave, M. *Actual. Chim.* **2013**, *371-372*, 95. (e) Andreiadis, E. S.; Chavarot-Kerlidou, M.; Fontecave, M.; Artero, V. *Photochem. Photobiol.* **2011**, *87*, 946.

Chapitre 6: Conclusion générale et perspectives

L'objectif initial de la thèse était la synthèse de nouveaux assemblages de complexes métalliques oligonucléaires, servant d'antenne solaire au niveau moléculaire. La thèse va finalement beaucoup plus loin que cet objectif de synthèse. En effet, une part importante de la thèse se penche sur la modélisation des systèmes à l'étude et leurs applications dans la photocatalyse.

6.1. Conclusion et perspectives : Chapitre 2

Les chromophores du Chapitre 2 semblent éloignés avec ce sujet. Ceux-ci sont en effet le fruit d'un projet secondaire, mais l'étude du chromophore de rhénium avec le ligand fluorène/fulvène est un système intéressant de transfert d'énergie intramoléculaire entre deux chromophores. Cette étude cadre bien dans le concept d'antenne moléculaire, où l'électron de l'état excité d'un chromophore transfère vers d'autres chromophores avec des énergies excitées similaire ou plus basse ou encore vers un centre de réaction. Dans ce cas-ci, le chromophore de rhénium transfère son énergie vers le fulvène, ce dernier étant non émissif. Selon les calculs DFT et les précédents décrit dans la littérature énoncés dans le Chapitre 2, cette relaxation passe par une photoisomérisation du ligand. Cependant, à cause de la symétrie du fluorène, il n'est pas possible d'observer un tel changement, il faut donc fonctionnaliser le fluorène d'un côté avec un groupement R afin de les différencier (comme indiqué sur le Schéma 6.1).

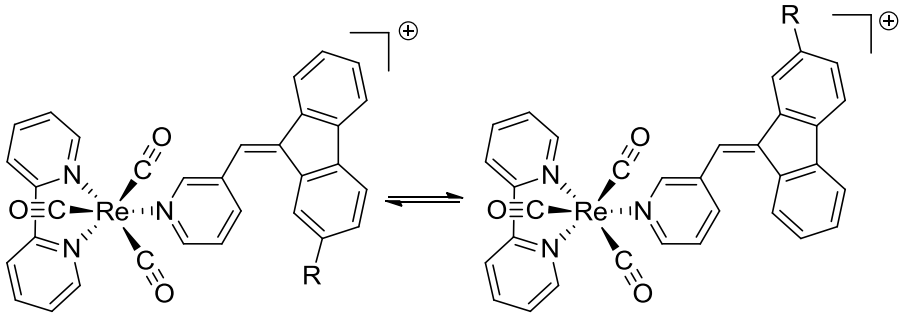

Schéma 6.1. Photoisomérisation avec un groupement R pour différencier les deux formes.

Puisque le groupement pyridyle du complexe de rhénium est légèrement labile, comme cela a été démontré à la fois avec les complexes **2-1** et **2-2** et avec le dimère de rhodium **4-4**, il serait préférable de déplacer le groupement fluorène sur la bipyridine, ce qui éliminerait les problèmes de dissociation. Sur le Schéma 6.2, on retrouve un tel exemple avec les trois formes d'isomères obtenus. S'ajoute à ces isomères une possible rotation libre du fulvène à travers le lien simple qui le relie à la pyridine. Un tel système serait intéressant, mais serait très difficilement caractérisable, le groupement R choisit doit permettre de distinguer tous ces différents isomères.

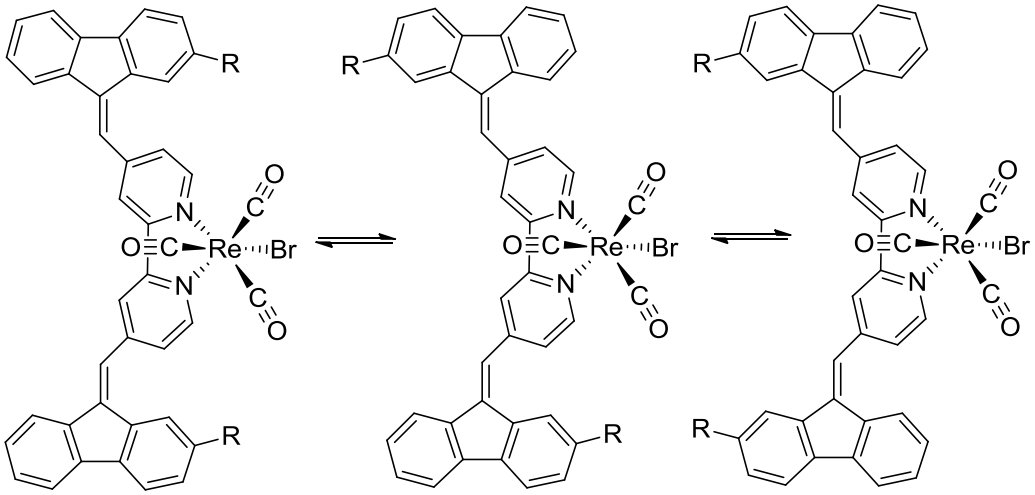

Schéma 6.2. Isomères possibles avec une fonctionnalisation de deux fulvènes sur le ligand bpy.

6.2. Conclusion et perspectives : Chapitre 3

Le chapitre 3 s'est concentré uniquement sur le centre de liaison, soit le dimère de rhodium. Les complexes obtenus, **3-1** à **3-4,** sont des molécules potentiellement très intéressantes pour les assemblages supramoléculaires. La formation de carrés est envisageable avec les complexes **3-2** *cis* et *trans*. Cependant, lors des premières synthèses de ces complexes, la pureté des produits obtenus n'était pas assez bonne à cause de la débromination partielle des autres groupements bromo-phényle. Quelques tests ont toutefois été effectués avec le couplage d'un dimère tétraacétate de rhodium.

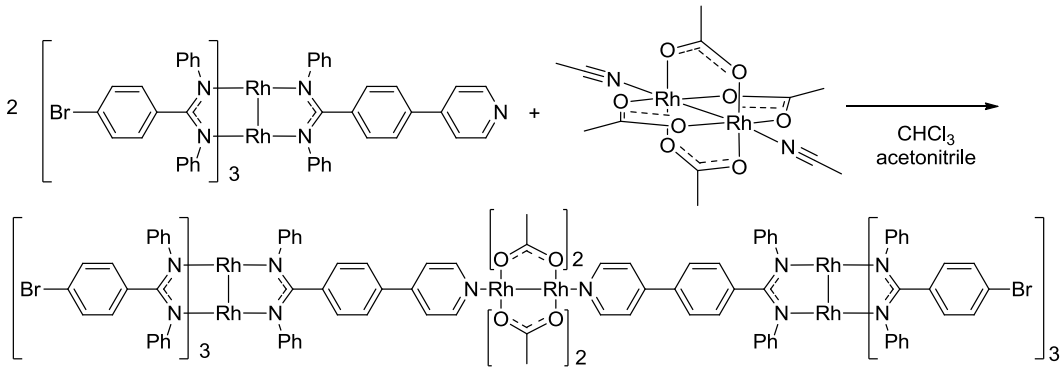

Schéma 6.3. Formation d'un dimère de (**3-1**)-($Rh_2(OAc)_4$)-(**3-1**).

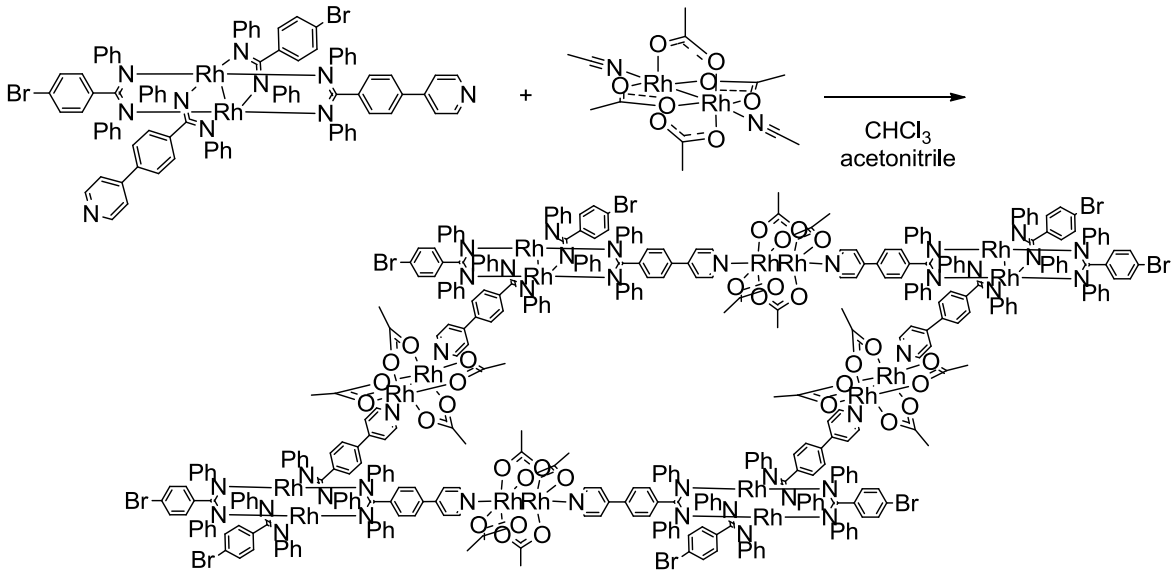

Schéma 6.4. Formation hypothétique d'un carré [(***cis* 3-2a**)-($Rh_2(OAc)_4$)]$_4$.

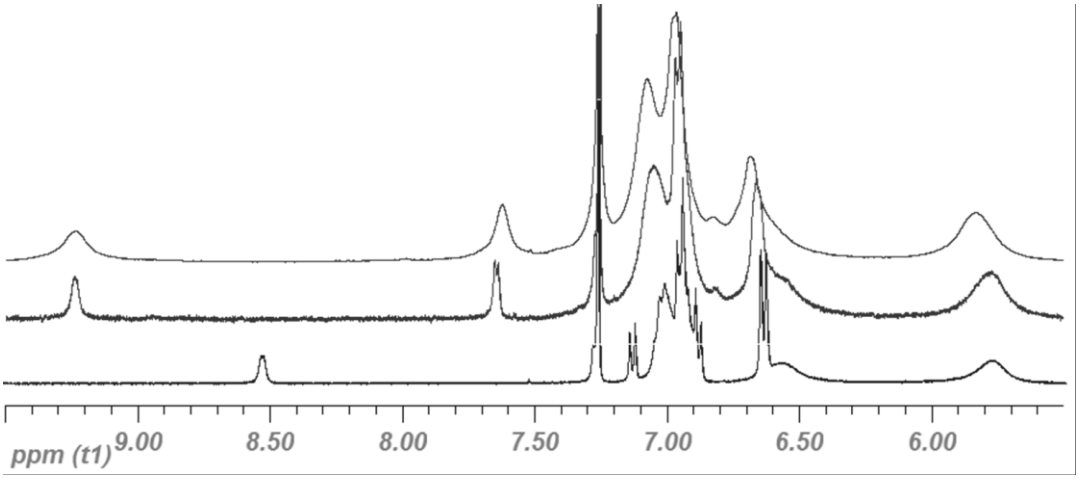

Figure 6.2. Comparaison ^{1}H-RMN dans le chloroforme deutéré : en bas **3-1**; au milieu (**3-1**)-($Rh_2(OAc)_4$)-(**3-1**); en haut la solution de la réaction [(***cis* 3-2a**)-($Rh_2(OAc)_4$)]$_4$.

Les réactions illustrées sur le Schéma 6.3 et Schéma 6.4 ont été faites à l'échelle RMN (soit environ 5 mg), l'espèce dimérique (**3-1**)-($Rh_2(OAc)_4$)-(**3-1**) a pu être confirmée par spectrométrie de masse, cependant l'espèce obtenue avec **3-2a** (*cis*) n'a que donnée des fragments avec le dimère d'acétate, jamais le carré complet. Le spectre RMN illustrée à la Figure 6.2 n'est pas suffisant pour affirmer qu'il s'agit d'un carré, mais il y a bel et bien coordination du dimère d'acétate, observable par le déplacement du signal du proton *ortho* à la pyridine de 8.50 ppm vers 9.25 ppm.

Malheureusement, ces expériences n'ont pas été effectuées à plus grande échelle, faute de temps et de matériel. En effet, les espèces **3-2a** et **3-2 b** donnaient les rendements les plus faibles. Ceci était causé par l'approche statistique de la réaction et par la purification par silice pour l'isolation finale des isomères *cis* et *trans*, qui réduisait considérablement le rendement.

Le dimère **3-4** est tout désigné pour fabriquer un complexe tétrarhénium, similaire à celui présenté dans le Chapitre 4. Encore une fois, une réaction à l'échelle RMN a été faite en utilisant les mêmes conditions que **4-4**. Elle montre la formation de l'espèce à la Figure 6.3. Dans cette synthèse, il n'y a pas tout à fait quatre chromophores de rhénium liés, car on peut voir des signaux faibles (comme celui à 8.60 ppm) du ligand amidinate avec la pyridine libre. On peut noter un fait intéressant : le bpy du chromophore de rhénium redevient symétrique dans le cas du complexe avec **3-4**, ce qui s'explique par la distance le séparant du dimère.

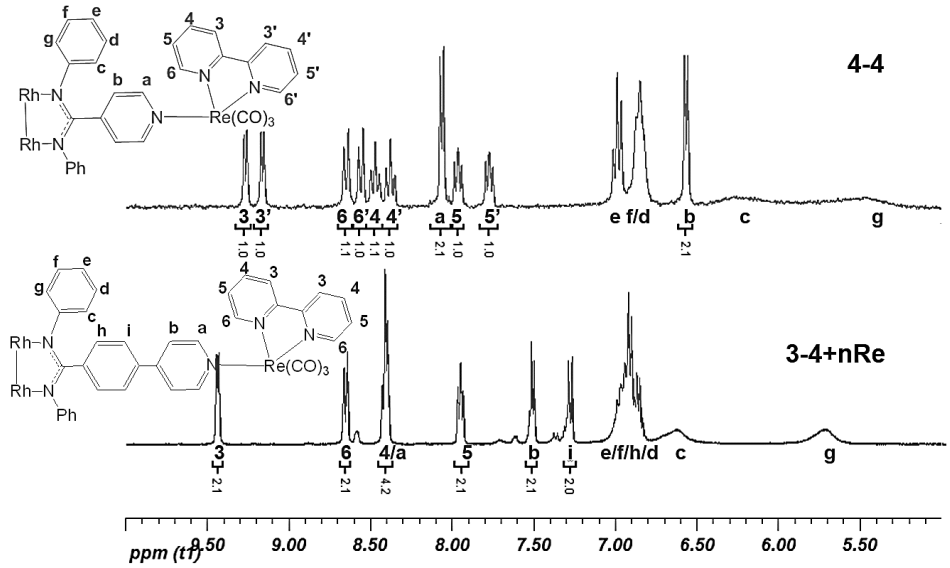

Figure 6.3. Comparaison ^{1}H-RMN dans l'acétone deutéré : en bas **3-4+nRe**, en haut **4-4**.

Ce composé purifié serait très intéressant pour les études de photocatalyse, ainsi que pour de simples comparaisons avec les propriétés spectrales du complexe **4-4**. Par exemple, est-ce que les chromophores de rhénium conservent leur émission ce cas?

Le chapitre 3 a aussi mis les balises nécessaires pour rapidement modéliser les dimères et d'en évaluer leurs propriétés optiques et électrochimiques. La corrélation avec les paramètres de Taft et de Hammett permettra de mieux cibler un dimère avec des propriétés électrochimiques et/ou optiques désirable. Par exemple, il serait intéressant d'optimiser le potentiel d'oxydation du dimère pour la réaction de photoréduction d'halogénure d'alkyle, une réaction qui a déjà été étudiée par le groupe du Pr C. Turro.[1]

6.3. Conclusion et perspectives : Chapitre 4

Le chapitre 4 a quantifié avec beaucoup de détails les propriétés de nos assemblages de chromophores de rhénium. Il s'agit d'une analyse poussée des propriétés spectrales et électrochimiques des complexes **4-1** à **4-4**, avec une modélisation TD-DFT qui a élucidé les changements observés. L'absence d'émission centrée sur le chromophore de rhénium suggère fortement une désactivation impliquant le dimère de rhodium. Il serait très intéressant de pousser l'étude de l'état excité par spectroscopie d'absorption transitoire résolue dans le temps. Ceci permettrait de voir si l'état excité passe par un transfert d'électron entre le dimère de rhodium et le rhénium. Cet état ressemblerait au spectre du dimère à l'état oxydé Rh_2(II,III) et serait très différentiable de l'état fondamental.

Une étude plus poussée du dimère à l'état oxydé pourrait aussi être effectuée. Celui-ci s'est montré très réactif à l'eau, où il se réduit à sa forme Rh_2(II,II). Un exemple de cette réduction est illustré à la Figure 6.4 où le dimère **4-4** a été oxydé avec du ferrocénium PF_6, puis isolé sous condition inerte. Le spectre du bas montre un signal très faible et large de l'espèce non oxydée résiduelle. Lorsqu'on y ajoute de l'eau, le spectre devient plus intense et beaucoup plus net, signe que l'espèce oxydée a disparu. Des preuves aussi convaincantes ont été obtenues par spectroscopie d'absorption.

Cette réduction s'est observée avec plusieurs dimères, dont ceux synthétisés au chapitre 3. L'application catalytique de cette réduction pourrait être très intéressante, car l'eau doit se faire oxyder au passage. Si le dimère de rhodium en soi peut servir de catalyseur à l'oxydation de l'eau, ce seul résultat pourrait permettre la réduction et l'oxydation de l'eau avec le même système photocatalytique.

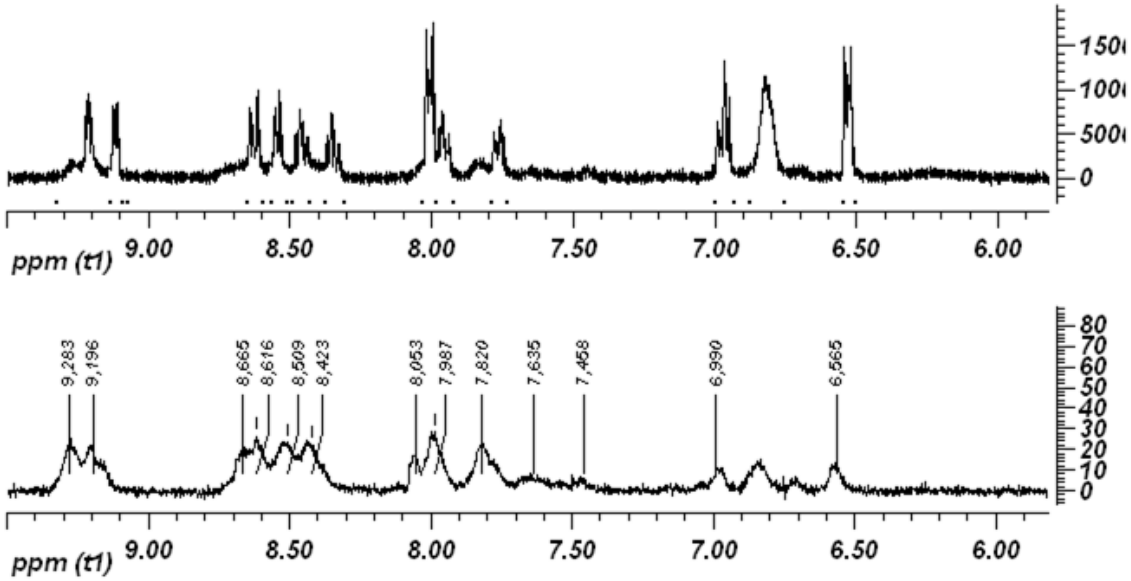

Figure 6.4. Comparaison ^{1}H-RMN dans l'acétone deutérée : en bas **4-4** oxydé avec ferrocénium hexafluorophosphate, en haut après ajout de 0.05 mL d'eau dans le noir.

Du point de vue de l'assemblage des chromophores, le groupement pyridyle n'est pas le meilleur choix pour lier les complexes de rhénium. La liaison pyridyl–rhénium est légèrement trop faible et a tendance à se dissocier à long terme. Idéalement, un ligand bidentate ou tridentate serait l'idéal dû à sa stabilité. Par couplage Suzuki, il serait possible de greffer un tel groupement directement sur le dimère, mais ce serait synthétiquement plus complexe et possiblement à trop faible rendement. Une autre possibilité est de fonctionnaliser le dimère avec un groupement tétrazole. Le tétrazole est facilement synthétisé à partir d'un groupement nitrile et d'un sel d'azoture de sodium. Il a déjà été utilisé avec succès pour la synthèse de chromophore de rhénium (voir Figure 6.5).[2] Le tétrazole est aussi un ligand monodentate, cependant il est chargé négativement, ce qui devrait le rendre plus stable.

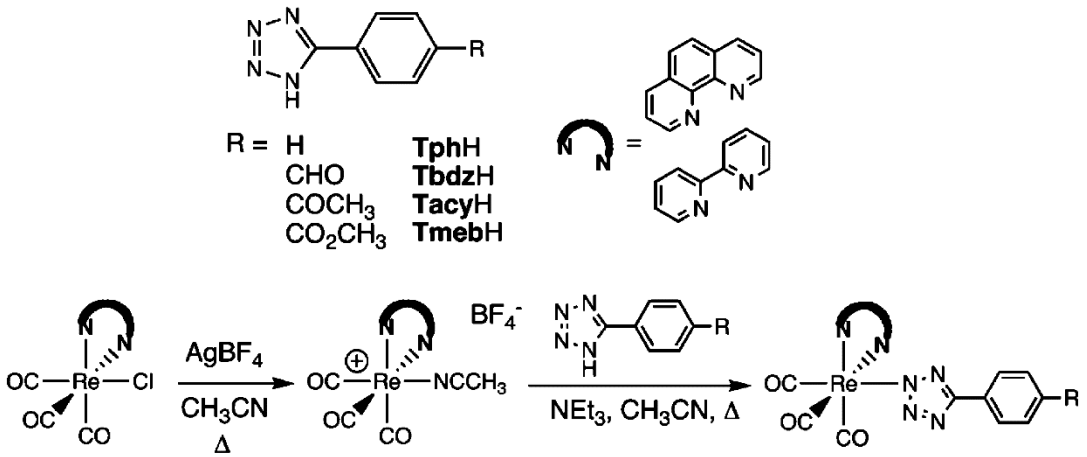

Figure 6.5. Chemin synthétique de la préparation de complexes tétrazolato de rhénium. Reprinted with permission from reference 2. Copyright 2010 American Chemical Society.

6.4. Conclusion et perspectives : Chapitre 5

Les conclusions ont déjà été bien établies dans le chapitre précédent au sujet des assemblages de rhodium–rhénium utilisés. Comme mentionnés plus tôt, les complexes du Chapitre 3 sont d'excellents candidats pour évaluer l'effet de la distance entre le chromophore de rhénium et le centre du dimère de rhodium sur maintes propriétés, y compris l'effet sur la photocatalyse. Cependant, il aurait été prématuré de faire cette comparaison dès le début des études décrites au Chapitre 5, car l'élaboration de conditions gagnantes où le chromophore ne se décompose pas rapidement est primordiale avant d'examiner des complexes avec un coût synthétique beaucoup plus haut.

Un point important qu'il reste à établir est le flux lumineux de la lampe. Une mesure avec un senseur électronique donne un flux lumineux d'environ 20 ± 5 mW/cm^2 à 3 cm de la lampe qui contient les DEL bleues (maximum à 451 nm). Par contre, il s'agit plutôt de caractériser le flux lumineux qui traverse les échantillons. Cette donnée est essentielle pour la comparaison des vitesses de réaction avec la littérature ou pour la mesure du rendement quantique de la réaction. À cause du choix d'un carrousel et de la forme de la lampe, seule l'actinométrie chimique peut répondre adéquatement à ce problème et nécessite un investissement considérable de temps, de plus les méthodes d'actinométrie applicables changent selon la longueur d'onde d'intérêt.

Le photoréacteur en soi est un succès majeur, sa mise en service permet beaucoup d'expérience connexe. Par exemple, un membre du groupe l'a utilisé pour tester un autoassemblage par irradiation lumineuse, ayant réussi à démontré la formation de

l'assemblage par voie thermique auparavant. Puisque son réactif absorbait la lumière jusqu'à 650 nm, il a pu évaluer l'effet de la longueur d'onde d'excitation, passant de l'UV jusqu'au rouge. Le photoréacteur offrant une température contrôlée et différents choix de longueur d'onde, cela a permis d'effectuer efficacement et rapidement ces réactions. Un autre exemple est son utilité en électrochimie. Dans ce cas, le GC est mis à contribution et le flux de gaz d'une expérience d'électrolyse à voltage constant est étudié, permettant de voir une production d'hydrogène ou d'oxygène. Bien entendu, il a été aussi utilisé pour son rôle principal dans l'analyse de l'hydrogène formé par photocatalyse sur plusieurs systèmes différents par différents membres du groupe.

6.5. Références

(1) Lutterman, D. A.; Degtyareva, N. N.; Johnston, D. H.; Gallucci, J. C.; Eglin, J. L.; Turro, C. *Inorg. Chem.* **2005**, *44*, 5388.

(2) Werrett, M. V.; Chartrand, D.; Gale, J. D.; Hanan, G. S.; MacLellan, J. G.; Massi, M.; Muzzioli, S.; Raiteri, P.; Skelton, B. W.; Silberstein, M.; Stagni, S. *Inorg. Chem.* **2011**, *50*, 1229.

Annexes

SI - Chapitre 2 : Informations supplémentaires

Supplementary Information

Diimine triscarbonyl Re(I) of isomeric pyridyl-fulvene ligands: an electrochemical, computational, and spectroscopic investigation

*Daniel Chartrand, Carlos A. Castro Ruiz, Garry S. Hanan**

Département de Chimie, Université de Montréal, Montréal, Québec, H3T-1J4, Canada

2.S1. Table of Contents

Chart 2.S1. Hydrogen labeling for proton NMR assignation of ligands and complexes.

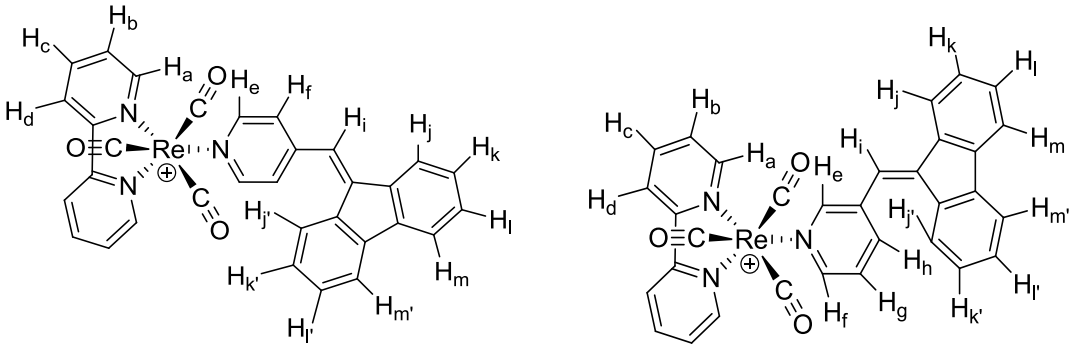

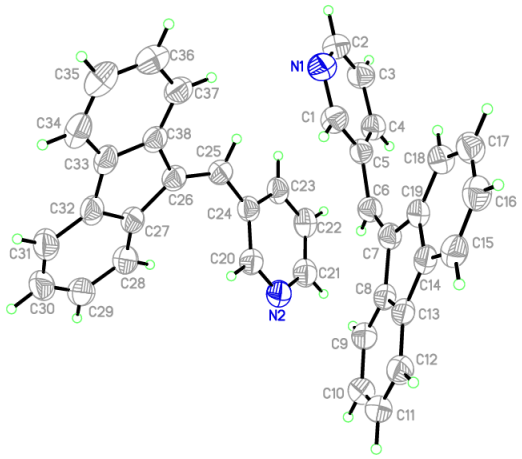

Figure 2.S1. ORTEP view of the X-ray crystal structure of ***m*Fpy** (50% probability displacement ellipsoids).

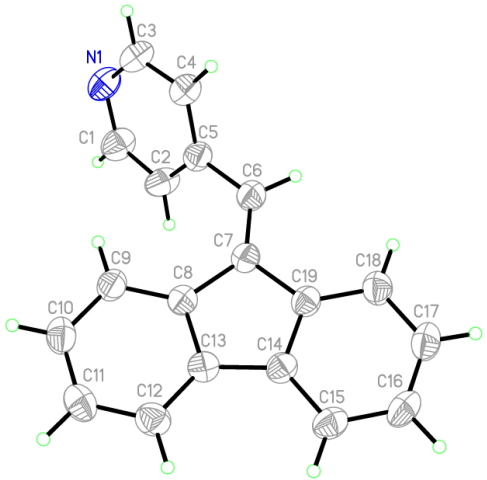

Figure 2.S2. ORTEP view of the X-ray crystal structure of ***p*Fpy** (50% probability displacement ellipsoids).

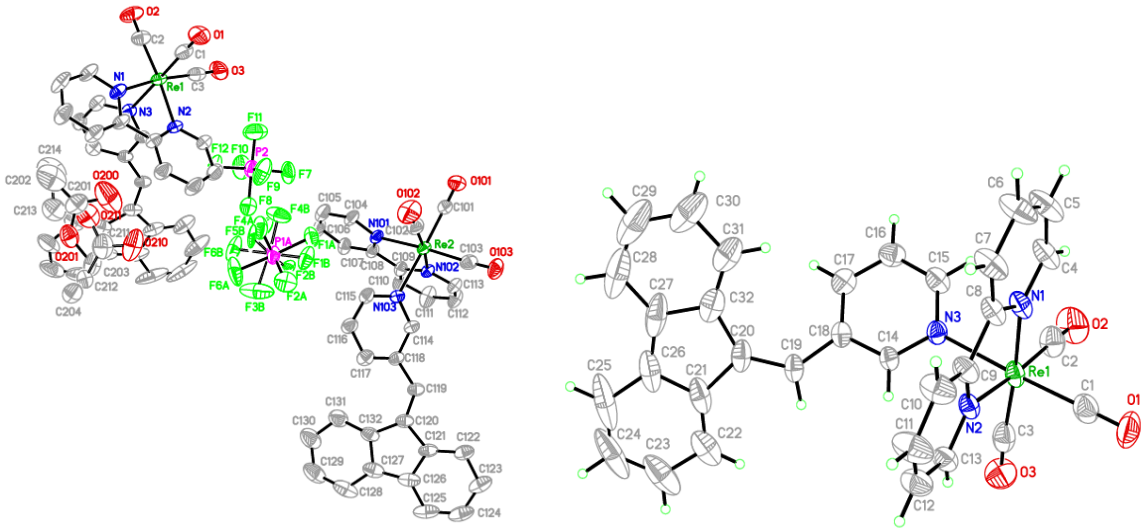

Figure 2.S3. ORTEP view of the X-ray crystal structure of **2-1** (50% probability displacement ellipsoids) (left: full asymmetric unit, right: full labelling of the first molecule).

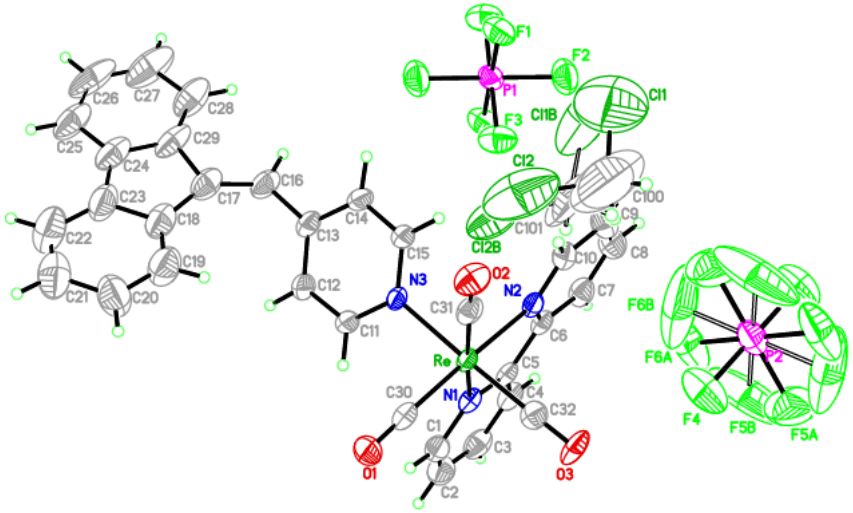

Figure 2.S4. ORTEP view of the X-ray crystal structure of **2-2** (50% probability displacement ellipsoids).

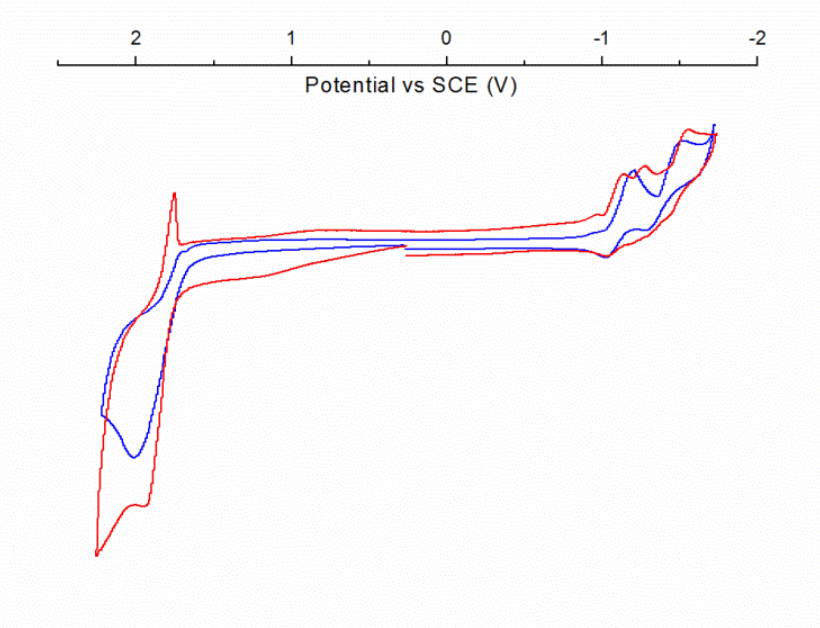

Figure 2.S5. Cyclic voltammetry of **2-1** (blue) and **2-2** (red) in a solution of 0.1 M $TBAPF_6$ in dichloromethane; platinum electrode.

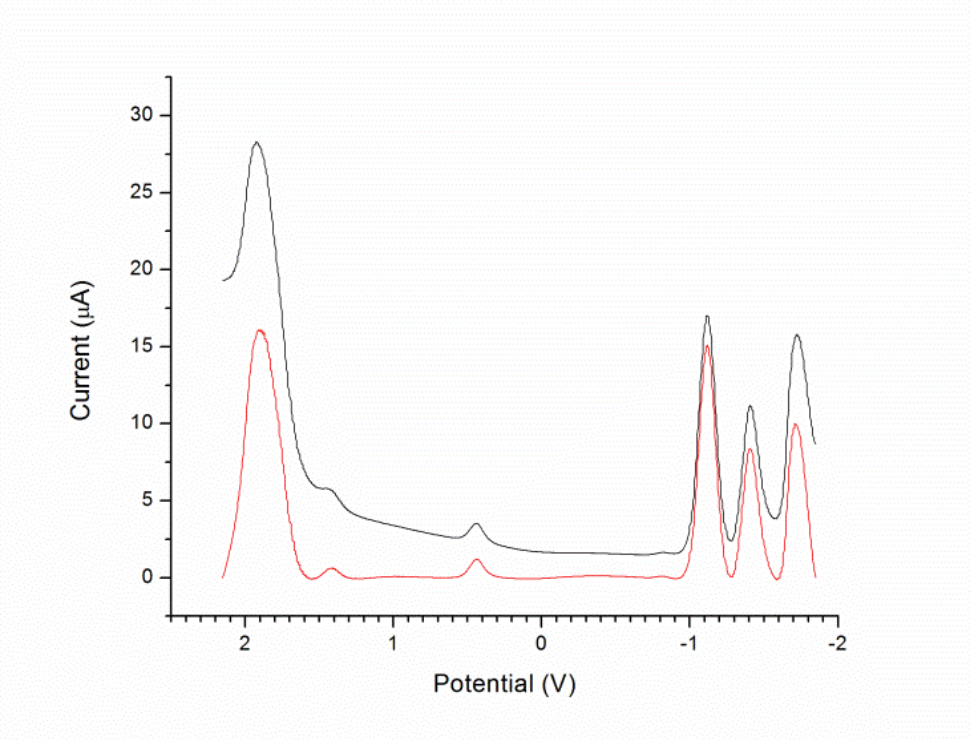

Figure 2.S6. Square-wave voltammetry of **2-1**: raw data (black), baseline corrected (red) in a solution of 0.1 M TBA PF_6 in dichloromethane; platinum electrode.

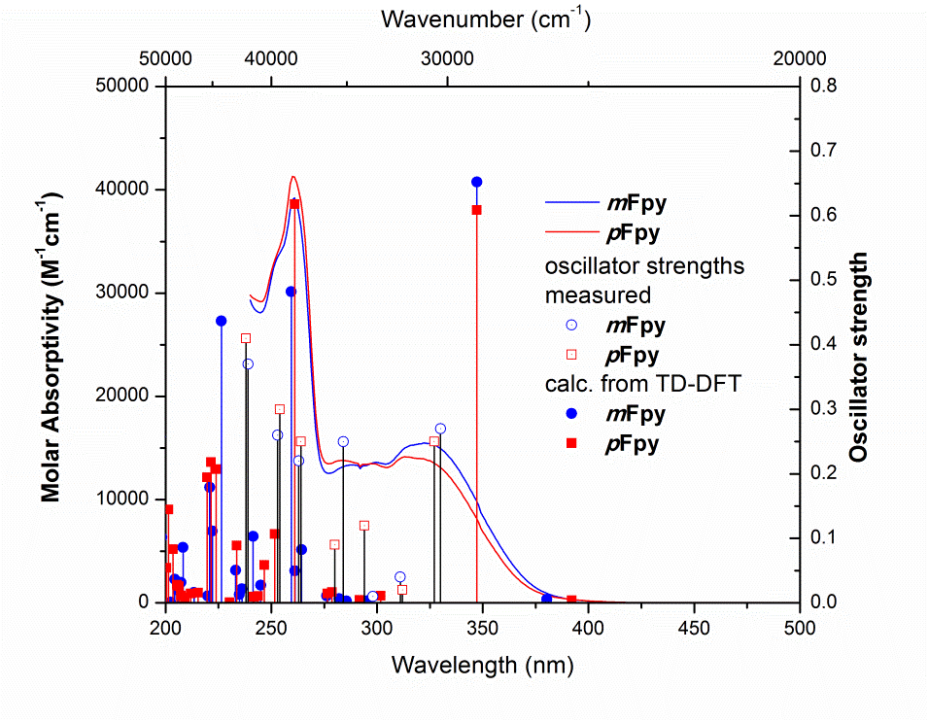

Figure 2.S7. Comparative absorption spectra of the ligands, the bars represent measured and calculated oscillator strengths (empty and full symbols).

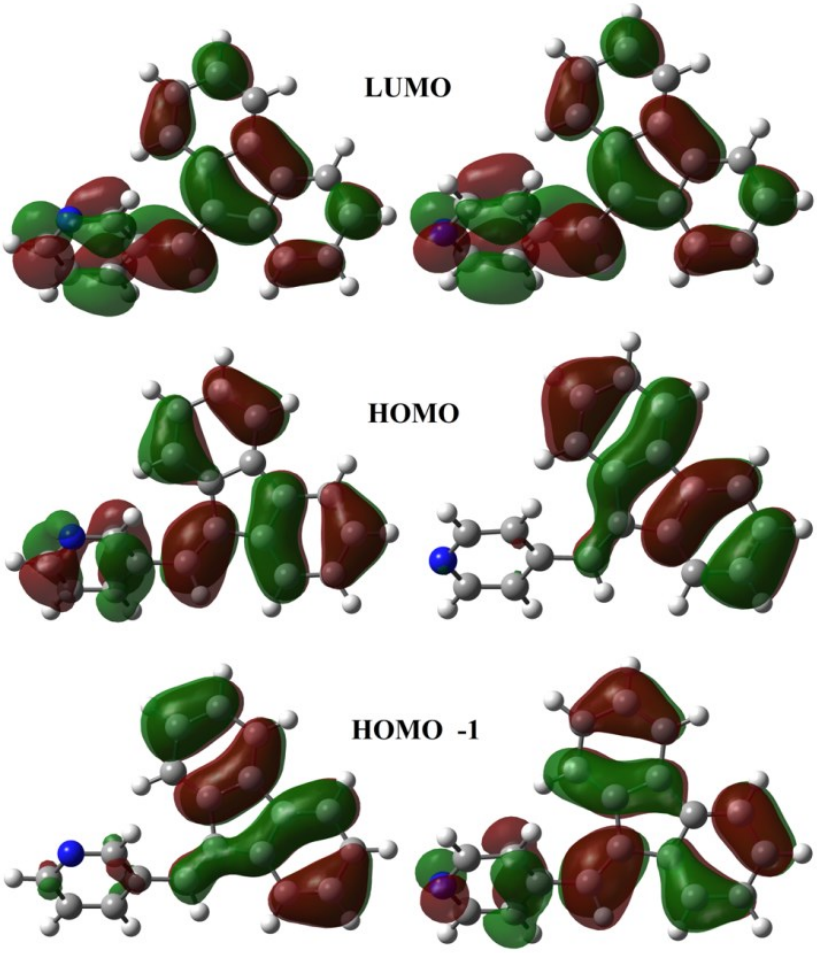

Figure 2.S8. Frontier molecular orbitals of the ligands ***m*Fpy** (left) and ***p*FPy** (right).

Table II-S1. Calculated triplet and singlet ground state energy levels and estimated triplet transition energy for **2-1**, **2-2** and **2-3**. (b3lyp/LanL2DZ(f)[Re]6-31G**[C,H,N,O], CPCM(CH_2Cl_2)).

	^{3}GS	^{1}GS	$\Delta(^3GS-^1GS)$	Estimated triplet transition energy		
	(Hartree)	(Hartree)	(Hartree)	(eV)	(cm^{-1})	(nm)
2-1	-1701.09612	-1701.15212	0.05600	1.52	12276	815
2-2	-1701.09971	-1701.15440	0.05469	1.49	11990	834
2-3	-1162.72758	-1162.82886	0.10128	2.76	22203	450

Table II-S2. Optimized atomic coordinates obtained from DFT for ***m*Fpy** singlet ground state (b3lyp/6-31G**[C,H,N,O]).

Atom	x /Å	y /Å	z /Å	Atom	x /Å	y /Å	z /Å
N1	-4.0791	0.4247	1.0447	H18	3.6657	-3.786	0.1472
C2	-2.7975	0.0726	0.9145	C19	4.2949	-1.725	0.1506
H3	-2.0986	0.5437	1.6016	H20	5.3505	-1.9737	0.2085
C4	-4.9697	-0.1694	0.2395	C21	3.8996	-0.3855	0.1137
H5	-6.0062	0.1401	0.358	H22	4.6428	0.4062	0.144
C6	-4.6235	-1.1441	-0.6974	C23	2.5402	-0.0874	0.0378
H7	-5.3865	-1.6101	-1.313	C24	1.8356	1.1981	-0.0284
C8	-3.2854	-1.5027	-0.8192	C25	2.3371	2.497	-0.074
H9	-2.979	-2.2608	-1.5352	H26	3.4069	2.6794	-0.0263
C10	-2.3209	-0.8676	-0.0192	C27	1.4441	3.5635	-0.1961
C11	-0.9098	-1.2663	-0.0959	H28	1.8202	4.5818	-0.2321
H12	-0.7649	-2.3417	-0.1967	C29	0.069	3.3268	-0.2855
C13	0.2194	-0.5188	-0.0511	H30	-0.6158	4.1622	-0.3963
C14	1.5761	-1.1194	0.002	C31	-0.4401	2.0262	-0.2337
C15	1.9786	-2.4532	0.0472	H32	-1.5087	1.8709	-0.315
H16	1.2518	-3.2606	0.0312	C33	0.4392	0.9508	-0.0859
C17	3.3425	-2.7498	0.1163				

Table II-S3. Optimized atomic coordinates obtained from DFT for ***p*Fpy** singlet ground state (b3lyp/6-31G**[C,H,N,O]).

Atom	x /Å	y /Å	z /Å	Atom	x /Å	y /Å	z /Å
N1	-5.0821	-0.21	0.1832	C17	0.1068	3.3352	-0.2968
C2	-4.1663	0.3904	0.9553	H18	-0.5692	4.1764	-0.4174
H3	-4.5454	1.1279	1.6607	C19	1.4831	3.5599	-0.1975
C4	-2.801	0.1166	0.9062	H20	1.8684	4.5747	-0.2336
H5	-2.1195	0.6218	1.5816	C21	2.3663	2.4858	-0.0682
C6	-4.6284	-1.1373	-0.6707	H22	3.4373	2.6591	-0.0154
H7	-5.3788	-1.6267	-1.2891	C23	1.8533	1.1915	-0.0241
C8	-3.2873	-1.4927	-0.7924	C24	2.5462	-0.1006	0.0429
H9	-2.9896	-2.2603	-1.5007	C25	3.9024	-0.4109	0.1235
C10	-2.324	-0.8418	-0.0032	H26	4.6525	0.374	0.1593
C11	-0.9139	-1.2485	-0.085	C27	4.2853	-1.7542	0.1573
H12	-0.7801	-2.325	-0.1849	H28	5.3384	-2.0126	0.2182
C13	0.2215	-0.5106	-0.0508	C29	3.324	-2.7702	0.1152
C14	0.4552	0.9569	-0.0882	H30	3.6379	-3.8094	0.1427
C15	-0.4138	2.0389	-0.246	C31	1.963	-2.4612	0.0418
H16	-1.4823	1.8896	-0.3388	H32	1.2292	-3.262	0.0183
				C33	1.5733	-1.1237	0.0003

Table II-S4. Optimized atomic coordinates obtained from DFT for **2-1** singlet ground state (b3lyp/LanL2DZ(f)[Re]6-31G**[C,H,N,O])

Atom	x /Å	y /Å	z /Å	Atom	x /Å	y /Å	z /Å
Re1	-2.6629	-0.8468	-0.2626	C31	-0.6584	0.8075	-2.0918
N2	-3.2591	1.267	-0.1449	H32	-1.6118	1.1666	-2.4586
N3	-1.9236	-0.1359	1.6821	C33	0.5366	1.2393	-2.656
N4	-0.696	-0.0915	-1.0845	H34	0.5136	1.9395	-3.484
O5	-5.3491	-1.7805	0.9417	C35	1.7417	0.7432	-2.1709
O6	-3.7121	-1.356	-3.1204	H36	2.6817	1.0379	-2.6237
O7	-1.5269	-3.7078	-0.0552	C37	1.7351	-0.1747	-1.1053
C8	-4.3433	-1.4372	0.4862	C38	2.9349	-0.8225	-0.5672
C9	-3.3158	-1.2021	-2.0428	H39	2.7939	-1.8778	-0.3397
C10	-1.9767	-2.6449	-0.1625	C40	4.1762	-0.3219	-0.3442
C11	-4.0013	1.8981	-1.078	C41	5.3258	-1.1827	0.0308
H12	-4.3173	1.2981	-1.9234	C42	5.403	-2.5622	0.2151
C13	-4.3584	3.2372	-0.977	H43	4.527	-3.1972	0.1143
H14	-4.9603	3.693	-1.7548	C44	6.6386	-3.1341	0.5333
C15	-3.9301	3.96	0.1351	H45	6.7114	-4.2067	0.6835
H16	-4.1868	5.0079	0.2502	C46	7.7824	-2.3375	0.6545
C17	-3.1739	3.3129	1.1076	H47	8.7345	-2.7993	0.8973
H18	-2.846	3.8588	1.9831	C48	7.7136	-0.9535	0.4626
C19	-2.8524	1.9606	0.953	H49	8.6074	-0.3435	0.5531
C20	-2.1016	1.184	1.9628	C50	6.4825	-0.3819	0.1532
C21	-1.6247	1.7355	3.1559	C51	6.0989	1.0161	-0.0877
H22	-1.7648	2.7875	3.3697	C52	6.8595	2.1803	-0.0272
C23	-0.97	0.9259	4.0793	H53	7.9229	2.1379	0.1888
H24	-0.5989	1.346	5.0082	C54	6.2309	3.4118	-0.2337
C25	-0.8102	-0.4284	3.7932	H55	6.8126	4.3277	-0.1908
H26	-0.3186	-1.1022	4.4856	C56	4.8561	3.4736	-0.478
C27	-1.299	-0.9162	2.587	H57	4.3762	4.4379	-0.6153
H28	-1.2008	-1.9636	2.3276	C58	4.09	2.3054	-0.5465
C29	0.4767	-0.5651	-0.62	H59	3.0224	2.3839	-0.7173
H30	0.4173	-1.2996	0.1752	C60	4.7102	1.0655	-0.376

Table II-S5. Optimized atomic coordinates obtained from DFT for **2-1** triplet ground state (b3lyp/LanL2DZ(f)[Re]6-31G**[C,H,N,O]).

Atom	x /Å	y /Å	z /Å	Atom	x /Å	y /Å	z /Å
Re1	-2.6604	-0.9017	0.082	H32	-1.1784	-0.4875	-2.6673
N2	-3.198	0.9225	-1.0217	C33	0.966	-0.2474	-2.5236
N3	-2.2877	0.7582	1.4737	H34	1.1018	-0.1715	-3.5971
N4	-0.5615	-0.5335	-0.6802	C35	2.0475	-0.1828	-1.6622
O5	-5.5419	-1.2817	1.1254	H36	3.0574	-0.0518	-2.0358
O6	-3.1985	-2.889	-2.2174	C37	1.8287	-0.2976	-0.2614
O7	-1.6388	-3.1504	1.9321	C38	2.8711	-0.2482	0.6977
C8	-4.4623	-1.1469	0.7343	H39	2.5899	-0.3539	1.7467
C9	-2.9939	-2.1719	-1.3306	C40	4.2867	-0.0729	0.3693
C10	-2.0405	-2.3333	1.2153	C41	5.2679	-1.1238	0.2524
C11	-3.7187	0.9302	-2.2656	C42	5.1468	-2.516	0.3778
H12	-3.8979	-0.0397	-2.7142	H43	4.186	-2.9721	0.6001
C13	-4.0239	2.1021	-2.9473	C44	6.2847	-3.3074	0.2127
H14	-4.4449	2.0493	-3.9449	H45	6.2087	-4.3861	0.3075
C15	-3.7792	3.3222	-2.32	C46	7.5261	-2.7238	-0.0731
H16	-4.001	4.2592	-2.8199	H47	8.3993	-3.3569	-0.1969
C17	-3.2536	3.3225	-1.0315	C48	7.659	-1.3315	-0.2009
H18	-3.0701	4.2628	-0.5274	H49	8.6298	-0.8961	-0.4205
C19	-2.9756	2.1094	-0.3939	C50	6.5371	-0.5312	-0.0394
C20	-2.473	2.0181	0.9937	C51	6.3435	0.9211	-0.1056
C21	-2.2357	3.1356	1.8003	C52	7.2174	1.9698	-0.3555
H22	-2.3812	4.135	1.4106	H53	8.2697	1.7854	-0.5517
C23	-1.8202	2.9628	3.1171	C54	6.7239	3.2845	-0.35
H24	-1.638	3.8249	3.7502	H55	7.4019	4.1101	-0.543
C25	-1.656	1.6686	3.6076	C56	5.3704	3.5462	-0.098
H26	-1.3489	1.4822	4.6304	H57	5.0148	4.5721	-0.0972
C27	-1.898	0.5983	2.7549	C58	4.4787	2.5023	0.1537
H28	-1.788	-0.4245	3.0952	H59	3.43	2.7077	0.3514
C29	0.4825	-0.4728	0.1565	C60	4.9601	1.1845	0.1497
H30	0.2657	-0.5742	1.2144				
C31	-0.3199	-0.4222	-2.0114				

Table II-S6. Optimized atomic coordinates obtained from DFT for **2-2** singlet ground state (b3lyp/LanL2DZ(f)[Re]6-31G**[C,H,N,O]).

Atom	x /Å	y /Å	z /Å	Atom	x /Å	y /Å	z /Å
Re1	-2.7294	-0.7349	-0.471	C31	1.2017	1.2371	-1.4502
N2	-2.7572	-0.1241	1.6415	H32	1.5005	1.9484	-2.2132
N3	-3.2567	1.3997	-0.4839	C33	-0.122	0.8404	-1.3817
N4	-0.5873	-0.0412	-0.4667	H34	-0.8472	1.2307	-2.086
O5	-1.8329	-3.647	0.0159	C35	3.538	1.1667	-0.6156
O6	-2.6409	-1.1089	-3.5333	H36	3.6296	2.2004	-0.9443
O7	-5.6983	-1.5878	-0.406	C37	4.7044	0.533	-0.3146
C8	-2.5556	-0.9648	2.6762	C38	5.0244	-0.8903	-0.0348
H9	-2.3988	-2.0061	2.421	C39	4.2586	-2.056	-0.1173
C10	-2.5542	-0.5431	4.0004	H40	3.2158	-2.027	-0.41
H11	-2.3903	-1.2634	4.7937	C41	4.8559	-3.2916	0.1525
C12	-2.7686	0.8072	4.271	H42	4.2624	-4.1982	0.0879
H13	-2.7721	1.1765	5.2911	C43	6.2091	-3.3705	0.4924
C14	-2.9902	1.6789	3.2092	H44	6.6565	-4.3372	0.7026
H15	-3.1701	2.7281	3.4054	C45	6.9981	-2.2163	0.5386
C16	-2.9871	1.1924	1.898	H46	8.0571	-2.2859	0.7684
C17	-3.2677	2.0379	0.718	C47	6.409	-0.9868	0.2627
C18	-3.5687	3.4009	0.8045	C48	7.0094	0.3505	0.1535
H19	-3.5737	3.9028	1.7636	C49	8.3164	0.7862	0.3478
C20	-3.8745	4.1167	-0.349	H50	9.0981	0.0956	0.6499
H21	-4.1126	5.1735	-0.2892	C51	8.6107	2.1393	0.1444
C22	-3.8801	3.4509	-1.5732	H52	9.6265	2.495	0.2873
H23	-4.1251	3.9612	-2.4977	C53	7.6115	3.039	-0.2415
C24	-3.5658	2.0974	-1.596	H54	7.8593	4.0842	-0.3974
H25	-3.5638	1.54	-2.5252	C55	6.2956	2.604	-0.4274
C26	0.3152	-0.5304	0.4161	H56	5.5306	3.3172	-0.722
H27	-0.066	-1.2205	1.1598	C57	5.9969	1.2562	-0.2338
C28	1.6568	-0.1918	0.4061	C58	-2.1803	-2.563	-0.2032
H29	2.3107	-0.609	1.1619	C59	-2.6759	-1.0053	-2.3797
C30	2.1581	0.7032	-0.5614	C60	-4.5853	-1.2747	-0.4341

Table II-S7. Optimized atomic coordinates obtained from DFT for **2-3** triplet ground state (b3lyp/LanL2DZ(f)[Re]6-31G**[C,H,N,O])

Atom	x /Å	y /Å	z /Å	Atom	x /Å	y /Å	z /Å
Re1	-2.7059	-0.8706	0.1126	C31	1.0069	-0.2296	-2.3431
N2	-2.346	0.7537	1.5499	H32	1.182	-0.1361	-3.41
N3	-3.1812	0.9853	-0.9671	C33	-0.2815	-0.3925	-1.8808
N4	-0.5943	-0.526	-0.5646	H34	-1.1115	-0.4299	-2.5761
O5	-1.7966	-3.1766	1.9519	C35	3.4323	-0.0355	-1.8753
O6	-3.1971	-2.7973	-2.2473	H36	3.5887	0.0612	-2.9509
O7	-5.6295	-1.2176	1.0544	C37	4.6007	0.0038	-0.9958
C8	-1.9919	0.5615	2.8368	C38	5.287	-1.1361	-0.4386
H9	-1.9107	-0.4695	3.1601	C39	5.0288	-2.5118	-0.5444
C10	-1.7486	1.6101	3.7158	H40	4.1905	-2.8765	-1.1315
H11	-1.4702	1.3977	4.7417	C41	5.873	-3.4066	0.115
C12	-1.8729	2.9165	3.2465	H42	5.6893	-4.4739	0.0413
H13	-1.6876	3.7624	3.9001	C43	6.9593	-2.9418	0.8684
C14	-2.2516	3.1228	1.9235	H44	7.605	-3.6544	1.3723
H15	-2.3648	4.1323	1.5493	C45	7.2282	-1.5677	0.9795
C16	-2.4922	2.026	1.0899	H46	8.0762	-1.2258	1.566
C17	-2.9562	2.1547	-0.3082	C47	6.3997	-0.6649	0.3287
C18	-3.1985	3.3855	-0.9262	C48	6.4094	0.799	0.2434
H19	-3.0138	4.3116	-0.397	C49	7.2537	1.7599	0.7815
C20	-3.6904	3.4214	-2.2274	H50	8.1009	1.4763	1.3995
H21	-3.8847	4.3723	-2.7122	C51	7.0031	3.1151	0.5118
C22	-3.9377	2.219	-2.8873	H52	7.661	3.8726	0.9264
H23	-4.3333	2.1944	-3.8963	C53	5.9198	3.5032	-0.2877
C24	-3.6689	1.028	-2.2235	H54	5.7504	4.5572	-0.4853
H25	-3.8511	0.071	-2.6977	C55	5.061	2.5488	-0.8358
C26	0.4404	-0.4983	0.3164	H56	4.2243	2.8537	-1.4587
H27	0.1817	-0.6191	1.3615	C57	5.3019	1.1921	-0.5727
C28	1.7579	-0.3383	-0.0566	C58	-2.1532	-2.3365	1.2381
H29	2.5348	-0.3341	0.6993	C59	-3.0129	-2.1039	-1.3371
C30	2.0989	-0.1944	-1.431	C60	-4.5351	-1.0947	0.7018

Table II-S8. Optimized atomic coordinates obtained from DFT for **2-3** singlet ground state (b3lyp/LanL2DZ(f)[Re]6-31G**[C,H,N,O]).

Atom	x /Å	y /Å	z /Å	Atom	x /Å	y /Å	z /Å
O1	2.4547	-2.6139	-0.9572	C20	1.6194	1.6781	1.4823
O2	2.462	1.6345	-2.2372	H21	1.3321	2.3983	0.726
N3	1.3683	0.3808	1.2028	C22	2.5888	1.1389	3.6099
O4	-0.7701	-1.0384	-3.4953	H23	3.0673	1.4318	4.5386
N5	-1.0737	1.2587	-0.4067	C24	-2.1207	-0.5446	0.7935
N6	-1.0596	-1.2866	0.3734	C25	-2.1272	0.8698	0.363
C7	-0.2974	-0.746	-2.4817	C26	-3.1537	1.7648	0.6797
C8	-1.0463	2.519	-0.8863	H27	-3.9861	1.4508	1.2963
H9	-0.1995	2.7726	-1.5128	C28	-2.0403	3.4512	-0.613
C10	1.7356	0.9018	-1.7103	H29	-1.9691	4.4499	-1.0281
C11	-3.1111	3.0677	0.1922	C30	-3.1444	-1.1203	1.5523
H12	-3.9056	3.7665	0.4312	H31	-3.9844	-0.5236	1.8839
C13	-1.0174	-2.5985	0.6839	C32	-2.0071	-3.2286	1.4287
H14	-0.163	-3.1502	0.3104	H33	-1.9248	-4.2876	1.6443
C15	1.7354	-1.7061	-0.9241	C34	-3.0889	-2.4726	1.8763
C16	2.2219	2.0947	2.6636	H35	-3.8815	-2.9273	2.461
H17	2.4038	3.1509	2.8266	C36	2.3313	-0.2028	3.332
C18	1.725	-0.5379	2.1271	H37	2.6007	-0.9869	4.0306
H19	1.5224	-1.5733	1.8814	Re38	0.4861	-0.2436	-0.789

Table II-S9. Optimized atomic coordinates obtained from DFT for **2-3** triplet ground state (b3lyp/LanL2DZ(f)[Re]6-31G**[C,H,N,O]).

Atom	x /Å	y /Å	z /Å	C20	1.4212	2.2425	-0.6499
O1	2.6908	-2.0375	1.6382	H21	1.1795	1.9476	-1.6636
O2	2.6417	-0.9749	-2.4869	C22	2.1808	3.8664	0.9449
N3	1.2385	1.3104	0.3104	H23	2.5503	4.8568	1.1907
O4	-0.7097	-3.5383	-0.9044	C24	-2.0931	0.2681	0.8293
N5	-1.0019	0.221	-1.2994	C25	-2.1188	0.619	-0.5341
N6	-0.9495	-0.4473	1.2684	C26	-3.1921	1.3121	-1.1748
C7	-0.2432	-2.5227	-0.6453	H27	-4.0462	1.6265	-0.5879
C8	-1.0064	0.4736	-2.6343	C28	-2.0301	1.1302	-3.2791
H9	-0.1412	0.1204	-3.1849	H29	-1.9715	1.3013	-4.3473
C10	1.8611	-0.9037	-1.6423	C30	-3.1335	0.5604	1.7641
C11	-3.1534	1.5668	-2.518	H31	-4.0004	1.1188	1.4334
H12	-3.972	2.0878	-3.0027	C32	-1.9033	-0.616	3.4749
C13	-0.9103	-0.8739	2.5616	H33	-1.81	-0.9832	4.4898
H14	-0.0328	-1.4457	2.8422	C34	-3.0476	0.1337	3.0592
C15	1.8901	-1.572	0.9513	H35	-3.8414	0.3528	3.765
C16	1.8882	3.522	-0.3739	C36	1.9901	2.9095	1.9411
H17	2.0186	4.2286	-1.1858	H37	2.2018	3.1262	2.9821
C18	1.5216	1.6504	1.5869	Re38	0.5198	-0.7601	-0.1996
H19	1.3607	0.8879	2.3391				

Table II-S10. Electronic transition obtained from TD-DFT for ***m*Fpy** from singlet ground state (b3lyp/6-31G**[C,H,N,O], CPCM(CH_2Cl_2)).

λ (nm)	Osc. Strength	Major contribs
380.317	0.0055	H-1→LUMO (81%), HOMO→LUMO (13%)
347.2145	0.652	H-1→LUMO (-12%), HOMO→LUMO (71%)
295.6489	0.0032	H-2→LUMO (76%), H-1→L+1 (-16%)
285.5377	0.0031	H-3→LUMO (93%)
282.1266	0.0065	H-1→L+1 (-10%), HOMO→L+1 (78%)
276.1998	0.0109	HOMO→L+2 (80%)
264.3173	0.0824	H-1→L+1 (26%), H-1→L+2 (57%)
261.1605	0.0499	H-4→LUMO (62%), H-1→L+2 (-10%)
259.4662	0.4821	H-4→LUMO (-16%), H-2→LUMO (10%), H-1→L+1 (27%), H-1→L+2 (-24%)
244.9876	0.0274	H-5→LUMO (-18%), H-3→L+2 (60%)
241.4006	0.1031	H-5→LUMO (62%), H-3→L+2 (13%)
236.1048	0.0216	H-2→L+1 (-12%), H-1→L+3 (41%), HOMO→L+3 (36%)
234.9371	0.0129	H-6→LUMO (-16%), H-1→L+3 (31%), HOMO→L+3 (-25%)
233.0864	0.0506	H-6→LUMO (48%), H-1→L+4 (28%)
226.3957	0.4369	HOMO→L+4 (68%)
222.1287	0.1111	H-4→L+1 (10%), H-2→L+1 (22%), H-1→L+4 (-20%)
220.831	0.179	H-2→L+1 (41%), H-1→L+4 (16%)
219.9144	0.011	H-2→L+2 (93%)
213.4552	0.0162	H-3→L+1 (65%), H-3→L+3 (15%)
208.2703	0.0859	H-4→L+2 (52%)
207.3404	0.0319	H-8→LUMO (59%), H-7→LUMO (16%), H-4→L+2 (-11%)
205.802	0.0196	H-3→L+1 (-19%), H-3→L+3 (56%)
204.3098	0.0366	H-4→L+1 (62%)
202.2996	0.0013	H-9→LUMO (54%), H-8→LUMO (10%), H-7→LUMO (-10%)
198.2972	0.1017	H-9→LUMO (-13%), H-5→L+1 (36%), H-2→L+3 (10%), H-1→L+5 (-16%)
197.5232	0.2572	H-2→L+3 (41%), HOMO→L+5 (-36%)
196.8896	0.0097	H-2→L+3 (36%), HOMO→L+5 (43%)
195.9994	0.0223	H-9→LUMO (15%), H-7→LUMO (30%), H-1→L+5 (-12%)
194.1912	0.0219	H-5→L+1 (-17%), H-2→L+4 (44%), H-1→L+5 (-17%)
192.452	0.0088	H-5→L+2 (78%), H-2→L+4 (11%)
188.8522	0.0804	H-6→L+1 (67%), H-5→L+1 (12%)
186.3682	0.0079	H-10→LUMO (51%), H-6→L+2 (-18%), H-4→L+3 (20%)
186.1975	0.0066	H-10→LUMO (41%), H-6→L+2 (20%), H-4→L+3 (-29%)
182.0126	0.0024	H-3→L+4 (95%)
180.5679	0.0014	H-12→LUMO (75%)
178.9365	0.0137	H-12→LUMO (10%), H-5→L+3 (18%), H-2→L+4 (-14%), H-1→L+5 (-10%), HOMO→L+6 (-12%)
178.0398	0.0412	H-11→LUMO (13%), H-4→L+4 (75%)
176.9118	0.0651	H-7→L+1 (-15%), H-5→L+3 (35%)
176.1677	0.0067	H-11→LUMO (43%), H-8→L+1 (25%)
175.8479	0.0058	H-11→LUMO (-23%), H-8→L+1 (43%)
174.45	0.0413	H-9→L+1 (51%)
173.3839	0.0157	H-5→L+4 (-34%), H-1→L+6 (42%)
173.2579	0.1082	H-9→L+1 (-11%), H-7→L+2 (19%), H-6→L+2 (-11%)
172.3978	0.0027	H-13→LUMO (77%)
170.7595	0.1072	H-9→L+1 (19%), H-7→L+1 (32%), H-6→L+3 (10%), HOMO→L+6 (13%)
168.5174	0.0468	H-5→L+4 (24%), H-1→L+6 (28%)
167.5813	0.2239	H-7→L+1 (-11%), H-6→L+3 (38%)
165.267	0.5625	H-7→L+2 (18%), H-6→L+4 (12%), H-2→L+5 (22%)
164.5585	0.1238	H-7→L+2 (-16%), H-5→L+3 (11%), H-2→L+5 (22%)
164.1381	0.0934	H-8→L+2 (-18%), H-6→L+4 (57%)

Table II-S11. Electronic transition obtained from TD-DFT for ***p*Fpy** from singlet ground state (b3lyp/6-31G**[C,H,N,O], CPCM(CH_2Cl_2)).

λ (nm)	Osc. Strength	Major contribs
392.1414	0.0042	HOMO→LUMO (91%)
347.1464	0.6086	H-1→LUMO (80%)
301.7434	0.011	H-2→LUMO (81%), HOMO→L+1 (-13%)
291.7804	0.0045	H-3→LUMO (84%)
278.7145	0.0169	H-4→LUMO (60%), H-1→L+1 (19%)
276.5572	0.0145	H-4→LUMO (-20%), H-1→L+1 (58%)
261.0505	0.6177	H-2→LUMO (12%), HOMO→L+1 (61%)
251.6611	0.1068	H-5→LUMO (62%), H-1→L+3 (14%)
246.6986	0.0588	H-1→L+2 (66%), HOMO→L+2 (-13%)
243.7881	0.0105	HOMO→L+2 (38%), HOMO→L+3 (42%)
241.796	0.0091	H-6→LUMO (-18%), H-1→L+2 (-14%), H-1→L+3 (26%), HOMO→L+2 (-24%)
241.4993	0.0099	H-6→LUMO (16%), H-5→LUMO (12%), HOMO→L+2 (-23%), HOMO→L+3 (35%)
233.6795	0.0888	H-6→LUMO (24%), H-1→L+3 (28%), HOMO→L+4 (30%)
230.2982	0.001	H-4→L+2 (12%), H-3→L+2 (75%)
223.8492	0.2074	H-2→L+1 (43%), H-1→L+4 (-32%)
221.4621	0.2181	H-2→L+1 (32%), H-1→L+4 (28%), HOMO→L+4 (-14%)
219.6611	0.1944	H-6→LUMO (-13%), H-1→L+4 (19%), HOMO→L+4 (23%)
215.3311	0.0158	H-3→L+1 (33%), H-3→L+3 (38%)
211.8794	0.0147	H-4→L+1 (79%), H-3→L+1 (-14%)
209.1487	0.0082	H-8→LUMO (81%), H-3→L+1 (10%)
207.2226	0.0114	H-3→L+1 (37%), H-3→L+3 (-32%)
206.3466	0.0258	H-9→LUMO (-33%), H-7→LUMO (52%)
205.4303	0.0279	H-2→L+2 (93%)
203.4515	0.083	H-4→L+3 (48%), H-2→L+3 (-19%)
201.3599	0.1447	H-4→L+3 (11%), H-3→L+3 (-13%), H-2→L+3 (61%)
200.4678	0.0542	H-9→LUMO (57%), H-7→LUMO (19%)
197.5263	0.0877	H-6→L+1 (11%), H-5→L+1 (29%), HOMO→L+5 (29%)
194.9485	0.0872	H-1→L+5 (68%), HOMO→L+5 (-12%)
193.9361	0.0161	H-2→L+4 (51%), H-1→L+5 (-13%)
193.0212	0.0374	H-6→L+1 (54%), H-5→L+1 (-25%)
189.6524	0.157	H-5→L+3 (-16%), H-4→L+2 (41%)
189.2875	0.0144	H-10→LUMO (87%)
183.5566	0.0133	H-12→LUMO (35%), H-11→LUMO (-22%), H-5→L+3 (-14%)
182.2239	0.0044	H-4→L+4 (39%), H-3→L+4 (-36%)
181.6446	0.0243	H-6→L+2 (10%), H-5→L+2 (59%)
180.7574	0.0089	H-4→L+4 (49%), H-3→L+4 (22%)
180.6626	0.012	H-13→LUMO (36%), H-5→L+3 (12%), H-3→L+4 (-14%)
180.5285	0.0108	H-13→LUMO (-16%), H-12→LUMO (28%), H-5→L+3 (14%), H-3→L+4 (-21%)
178.2369	0.0082	H-13→LUMO (29%), H-11→LUMO (47%), H-5→L+4 (-10%)
177.3547	0.0069	H-7→L+1 (17%), H-2→L+4 (10%), H-1→L+6 (-15%), HOMO→L+5 (12%)
175.7034	0.0016	H-8→L+1 (88%)
174.0874	0.0425	H-9→L+1 (16%), H-5→L+4 (29%), HOMO→L+6 (28%)
173.5198	0.0099	H-9→L+1 (32%), H-5→L+4 (-16%), H-1→L+6 (-16%)
172.7028	0.3061	H-6→L+2 (60%)
170.5762	0.1731	H-9→L+1 (-14%), H-6→L+3 (33%), H-1→L+6 (-10%)
169.0182	0.0558	H-9→L+1 (-12%), H-7→L+1 (-19%), H-6→L+4 (12%), H-5→L+4 (-16%), HOMO→L+6 (21%)
168.0788	0.1432	H-7→L+1 (22%), H-6→L+3 (15%)
166.2889	0.018	H-6→L+4 (58%)
165.1042	0.2733	H-14→LUMO (56%), H-2→L+5 (-20%)
164.8189	0.3357	H-14→LUMO (30%), H-2→L+5 (33%)

Table II-S12. Electronic transition obtained from TD-DFT for **2-1** from singlet ground state (b3lyp/LanL2DZ(f)[Re]6-31G**[C,H,N,O], CPCM(CH_2Cl_2)).

λ (nm)	Osc. Str.	bpy	Re	CO	pyridine	fulvene	Major contribs
425.69	0.0007	0→91 (91)	0→3 (3)	10→2 (-8)	1→3 (2)	88→1 (-87)	H-1→LUMO (12%), HOMO→LUMO (86%)
419.94	0.0026	0→89 (89)	1→3 (2)	11→2 (-9)	8→3 (-5)	80→3 (-77)	H-1→LUMO (84%), HOMO→LUMO (-11%)
416.89	0.0018	0→6 (6)	0→1 (1)	10→7 (-3)	1→19 (18)	89→67 (-22)	HOMO→L+1 (89%)
381.46	0.0027	17→92 (75)	64→3 (-61)	18→2 (-16)	1→3 (2)	1→0 (-1)	H-3→LUMO (93%)
373.03	0.1316	13→83 (70)	54→3 (-51)	16→2 (-14)	5→5 (0)	11→8 (-3)	H-2→LUMO (78%), H-1→L+1 (10%)
367.95	0.498	2→15 (13)	9→1 (-8)	12→7 (-5)	8→18 (10)	68→59 (-9)	H-1→L+1 (71%)
360.63	0.0217	11→91 (80)	67→3 (-64)	20→2 (-18)	1→3 (2)	1→1 (0)	H-5→LUMO (91%)
330.39	0.0323	0→41 (41)	1→1 (0)	10→2 (-8)	1→39 (38)	88→16 (-72)	HOMO→L+2 (72%), HOMO→L+3 (-17%)
327.27	0.1135	2→38 (36)	6→1 (-5)	11→3 (-8)	8→37 (29)	73→21 (-52)	H-1→L+2 (61%), H-1→L+3 (-16%)
321.90	0.0007	0→92 (92)	1→3 (2)	25→2 (-23)	0→3 (3)	74→0 (-74)	H-4→LUMO (99%)
317.22	0.0334	15→5 (-10)	59→1 (-58)	17→7 (-10)	3→22 (19)	6→66 (60)	H-3→L+1 (44%), H-2→L+1 (44%)
316.12	0.0432	14→5 (-9)	56→1 (-55)	17→7 (-10)	3→22 (19)	10→66 (56)	H-3→L+1 (49%), H-2→L+1 (-35%)
313.42	0.0136	0→25 (25)	1→1 (0)	16→4 (-12)	1→29 (28)	82→40 (-42)	H-4→L+1 (39%), HOMO→L+2 (11%), HOMO→L+3 (34%)
312.04	0.0303	1→22 (21)	3→1 (-2)	17→5 (-12)	1→28 (27)	79→44 (-35)	H-4→L+1 (41%), HOMO→L+3 (-38%)
309.46	0.0202	2→44 (42)	3→2 (-1)	11→2 (-9)	8→37 (29)	77→16 (-61)	H-1→L+2 (15%), H-1→L+3 (67%)
303.55	0.0018	0→81 (81)	0→1 (1)	10→1 (-9)	1→16 (15)	88→1 (-87)	HOMO→L+4 (88%)
300.50	0.0035	9→33 (24)	43→1 (-42)	16→5 (-11)	4→19 (15)	28→42 (14)	H-5→L+1 (58%), H-1→L+4 (30%)
300.36	0.0136	10→50 (40)	29→1 (-28)	14→4 (-10)	5→18 (13)	42→28 (-14)	H-5→L+1 (-37%), H-1→L+4 (43%)
298.81	0.1582	56→79 (23)	17→2 (-15)	6→2 (-4)	8→14 (6)	12→4 (-8)	H-6→LUMO (54%), H-3→L+2 (15%), H-1→L+4 (13%)
291.25	0.0192	19→46 (27)	61→5 (-56)	17→4 (-13)	2→32 (30)	1→13 (12)	H-3→L+2 (50%), H-3→L+3 (-12%), H-2→L+2 (-10%)
289.15	0.0279	16→44 (28)	60→6 (-54)	16→6 (-10)	4→31 (27)	4→13 (9)	H-3→L+2 (12%), H-2→L+2 (52%), H-2→L+5 (15%)
286.87	0.004	14→49 (35)	54→17 (-37)	16→13 (-3)	5→14 (9)	11→6 (-5)	H-2→L+2 (-19%), H-2→L+5 (48%)
283.46	0.0307	17→47 (30)	60→7 (-53)	17→5 (-12)	3→29 (26)	3→11 (8)	H-3→L+2 (-10%), H-3→L+3 (-18%), H-3→L+5 (15%), H-2→L+3 (38%)
282.42	0.0238	16→49 (33)	54→11 (-43)	16→8 (-8)	3→22 (19)	11→9 (-2)	H-3→L+3 (33%), H-2→L+3 (15%), H-1→L+5 (-10%)
278.25	0.0157	13→53 (40)	65→4 (-61)	19→4 (-15)	1→28 (27)	2→11 (9)	H-5→L+2 (45%), H-3→L+4 (-22%)
276.77	0.0154	3→46 (43)	10→22 (12)	11→17 (6)	2→5 (3)	74→9 (-65)	HOMO→L+5 (65%)
275.63	0.0277	5→35 (30)	21→14 (-7)	13→13 (0)	4→11 (7)	56→26 (-30)	H-1→L+5 (-10%), H-1→L+7 (-18%), HOMO→L+5 (27%)
275.09	0.0607	13→61 (48)	58→4 (-54)	18→4 (-14)	2→23 (21)	10→8 (-2)	H-5→L+2 (31%), H-3→L+4 (40%)
274.85	0.1228	17→62 (45)	50→6 (-44)	16→6 (-10)	5→14 (9)	13→12 (-1)	H-5→L+5 (10%), H-2→L+4 (44%)
274.28	0.0223	11→39 (28)	38→8 (-30)	15→9 (-6)	5→12 (7)	32→32 (0)	H-3→L+4 (-11%), H-3→L+5 (14%), H-2→L+3 (-10%), H-2→L+4 (10%), H-1→L+7 (26%)
273.26	0.001	0→91 (91)	1→3 (2)	12→2 (-10)	14→3 (-11)	73→1 (-72)	H-8→LUMO (13%), H-7→LUMO (83%)
272.47	0.0351	5→46 (41)	21→20 (-1)	13→17 (4)	7→5 (-2)	54→12 (-42)	H-3→L+5 (12%), H-1→L+5 (51%)
269.99	0.0336	12→46 (34)	66→6 (-60)	19→5 (-14)	1→31 (30)	2→13 (11)	H-5→L+3 (70%)
268.08	0.0276	13→69 (56)	65→8 (-57)	19→7 (-12)	1→14 (13)	2→2 (0)	H-5→L+4 (54%), H-3→L+6 (-17%)
267.63	0.1266	0→30 (30)	1→2 (1)	21→4 (-17)	0→30 (30)	78→34 (-44)	H-4→L+2 (49%), H-4→L+3 (-16%), HOMO→L+7 (-18%)
265.15	0.041	20→60 (40)	55→10 (-45)	17→9 (-8)	2→13 (11)	6→9 (3)	H-5→L+4 (39%), H-3→L+6 (21%)
264.66	0.0116	81→7 (-74)	6→1 (-5)	2→8 (6)	11→20 (9)	1→65 (64)	H-6→L+1 (90%)
261.60	0.0493	1→31 (30)	5→14 (9)	11→14 (3)	7→14 (7)	76→27 (-49)	H-7→L+1 (17%), H-1→L+6 (18%), HOMO→L+6 (29%), HOMO→L+8 (10%)

260.1413	0.1635	0→37 (37)	1→10 (9)	11→11 (0)	9→11 (2)	79→31 (-48)	H-8→LUMO (-12%), H-1→L+6 (11%), HOMO→L+6 (-22%), HOMO→L+7 (21%)
259.7326	0.0797	0→77 (77)	0→3 (3)	7→3 (-4)	31→6 (-25)	62→11 (-51)	H-8→LUMO (67%), H-7→LUMO (-11%)
259.2817	0.2152	0→26 (26)	0→9 (9)	13→11 (-2)	4→15 (11)	83→39 (-44)	H-7→L+1 (-14%), H-4→L+2 (16%), HOMO→L+6 (30%), HOMO→L+7 (21%)
258.1964	0.0788	1→34 (33)	6→13 (7)	12→14 (2)	8→15 (7)	73→25 (-48)	H-7→L+1 (-13%), H-1→L+6 (43%), HOMO→L+8 (-17%)
255.6779	0.02	1→19 (18)	3→7 (4)	12→12 (0)	2→25 (23)	82→37 (-45)	HOMO→L+6 (-15%), HOMO→L+8 (52%)
255.0258	0.0082	11→49 (38)	60→22 (-38)	18→18 (0)	2→8 (6)	8→4 (-4)	H-5→L+6 (49%), H-2→L+6 (-29%)
252.924	0.0139	0→44 (44)	1→2 (1)	24→2 (-22)	0→37 (37)	75→15 (-60)	H-4→L+2 (15%), H-4→L+3 (77%)
250.6841	0.0377	0→5 (5)	1→2 (1)	10→9 (-1)	17→24 (7)	72→60 (-12)	H-8→L+1 (25%), H-7→L+1 (-21%), H-1→L+8 (36%)
249.0475	0.0149	13→53 (40)	62→20 (-42)	18→18 (0)	3→6 (3)	4→3 (-1)	H-5→L+6 (34%), H-2→L+6 (37%)
247.818	0.0759	14→54 (40)	63→19 (-44)	18→17 (-1)	2→6 (4)	3→4 (1)	H-5→L+5 (34%), H-3→L+6 (26%)
246.8706	0.0079	0→81 (81)	1→1 (0)	25→1 (-24)	0→16 (16)	74→1 (-73)	H-4→L+4 (95%)
242.2922	0.0376	86→47 (-39)	1→2 (1)	0→2 (2)	11→36 (25)	1→14 (13)	H-6→L+2 (87%)
240.3057	0.0036	51→85 (34)	2→2 (0)	2→2 (0)	20→10 (-10)	24→2 (-22)	H-9→LUMO (32%), H-6→L+4 (46%)
238.8843	0.1218	3→8 (5)	1→4 (3)	7→10 (3)	22→21 (-1)	67→57 (-10)	H-8→L+1 (41%), H-1→L+8 (-27%), HOMO→L+11 (15%)
237.1389	0.0455	85→50 (-35)	1→2 (1)	0→2 (2)	11→33 (22)	2→13 (11)	H-6→L+3 (83%)
233.2838	0.0377	29→88 (59)	2→2 (0)	3→2 (-1)	29→6 (-23)	37→1 (-36)	H-9→LUMO (62%), H-6→L+4 (-23%)
232.2568	0.004	5→27 (22)	5→2 (-3)	9→5 (-4)	21→31 (10)	60→35 (-25)	H-9→L+1 (-25%), H-7→L+2 (33%), H-7→L+3 (-10%)
229.7605	0.0142	12→53 (41)	53→5 (-48)	17→12 (-5)	4→11 (7)	15→19 (4)	H-5→L+10 (11%), H-2→L+8 (-12%), H-2→L+9 (-12%), H-2→L+10 (13%), H-1→L+9 (10%)
228.967	0.0035	0→48 (48)	1→26 (25)	25→20 (-5)	0→2 (2)	74→4 (-70)	H-4→L+5 (95%)
227.6386	0.0036	2→71 (69)	6→2 (-4)	11→10 (-1)	1→9 (8)	79→8 (-71)	HOMO→L+9 (78%)
226.8555	0.01	14→25 (11)	51→7 (-44)	16→12 (-4)	2→15 (13)	16→41 (25)	H-3→L+7 (-18%), H-3→L+8 (27%)
225.9213	0.0036	9→35 (26)	37→2 (-35)	14→10 (-4)	7→15 (8)	33→38 (5)	H-2→L+7 (32%), H-2→L+8 (-15%), H-1→L+9 (-20%)
225.3833	0.0061	7→56 (49)	29→3 (-26)	14→11 (-3)	7→11 (4)	44→19 (-25)	H-1→L+9 (40%)
224.8968	0.0027	3→35 (32)	2→2 (0)	10→6 (-4)	19→27 (8)	67→30 (-37)	H-9→L+1 (19%), H-7→L+2 (38%), H-1→L+9 (-12%)
223.926	0.0387	2→10 (8)	8→4 (-4)	21→11 (-10)	2→7 (5)	68→68 (0)	H-4→L+7 (63%)
223.6795	0.0119	18→25 (7)	55→15 (-40)	17→14 (-3)	2→5 (3)	9→42 (33)	H-3→L+7 (-23%), H-3→L+12 (40%)
223.0077	0.0143	12→25 (13)	48→13 (-35)	16→14 (-2)	5→6 (1)	19→42 (23)	H-2→L+7 (-12%), H-2→L+12 (29%)
222.9074	0.0347	54→76 (22)	8→5 (-3)	4→6 (2)	11→5 (-6)	23→8 (-15)	H-12→LUMO (13%), H-11→LUMO (12%), H-10→LUMO (31%), H-6→L+5 (-10%)
222.2003	0.0061	4→74 (70)	4→2 (-2)	10→15 (5)	2→5 (3)	80→5 (-75)	HOMO→L+10 (78%)
221.4725	0.1235	2→29 (27)	3→9 (6)	12→10 (-2)	10→18 (8)	73→34 (-39)	H-7→L+3 (25%), H-1→L+11 (-18%), HOMO→L+11 (-12%)
221.4225	0.0662	1→35 (34)	1→7 (6)	12→7 (-5)	12→27 (15)	74→25 (-49)	H-7→L+3 (46%), H-1→L+11 (18%)
220.949	0.0172	51→48 (-3)	2→17 (15)	5→17 (12)	10→5 (-5)	32→12 (-20)	H-6→L+5 (54%), H-1→L+10 (-13%), H-1→L+11 (-10%)

Table II-S13. Electronic transition obtained from TD-DFT for **2-2** from singlet ground state (b3lyp/LanL2DZ (f)[Re]6-31G**[C,H,N,O], CPCM (CH_2Cl_2)).

λ (nm)	Osc. Str.	bpy	Re	CO	pyridine	fluorene	Major contribs
454.9847	0.0016	0→16 (16)	0→1 (1)	0→2 (2)	2→54 (52)	98→28 (-70)	HOMO→L+1 (89%)
417.7477	0.0771	4→78 (74)	5→3 (-2)	2→13 (11)	28→3 (-25)	61→3 (-58)	H-1→LUMO (68%), HOMO→LUMO (26%)
411.5356	0.0275	1→75 (74)	2→3 (1)	1→12 (11)	11→5 (-6)	85→4 (-81)	H-1→LUMO (-25%), HOMO→LUMO (69%)
397.8926	0.786	5→13 (8)	5→1 (-4)	2→1 (-1)	39→56 (17)	50→29 (-21)	H-1→L+1 (84%)
383.8256	0.0032	7→77 (70)	64→3 (-61)	18→13 (-5)	1→3 (2)	9→4 (-5)	H-2→LUMO (95%)
365.7433	0.0325	5→78 (73)	59→3 (-56)	18→13 (-5)	4→3 (-1)	14→4 (-10)	H-5→LUMO (-39%), H-3→LUMO (54%)
358.4784	0.0422	4→78 (74)	62→3 (-59)	19→13 (-6)	3→3 (0)	12→3 (-9)	H-5→LUMO (57%), H-3→LUMO (36%)
346.9036	0.0003	7→13 (6)	64→1 (-63)	18→1 (-17)	1→56 (55)	9→29 (20)	H-2→L+1 (96%)
336.4358	0.013	8→12 (4)	56→1 (-55)	16→1 (-15)	5→56 (51)	14→29 (15)	H-3→L+1 (90%)
332.4307	0.0563	0→16 (16)	1→2 (1)	0→2 (2)	1→51 (50)	98→29 (-69)	H-4→L+1 (83%)
325.2278	0.0076	2→13 (11)	67→1 (-66)	21→1 (-20)	1→56 (55)	10→29 (19)	H-5→L+1 (92%)
315.8007	0.0009	0→74 (74)	1→3 (2)	0→12 (12)	0→6 (6)	98→5 (-93)	H-4→LUMO (92%)
309.7957	0.0047	3→75 (72)	4→1 (-3)	1→21 (20)	21→1 (-20)	71→2 (-69)	H-1→L+2 (51%), HOMO→L+2 (45%)
307.0186	0.002	2→75 (73)	3→1 (-2)	1→21 (20)	18→1 (-17)	75→2 (-73)	H-1→L+2 (-44%), HOMO→L+2 (54%)
302.6198	0.0377	22→80 (58)	10→1 (-9)	9→15 (6)	22→2 (-20)	38→3 (-35)	H-6→LUMO (23%), H-1→L+3 (51%), HOMO→L+3 (10%)
298.2878	0.038	12→80 (68)	4→1 (-3)	5→16 (11)	1→1 (0)	78→2 (-76)	H-6→LUMO (-14%), HOMO→L+3 (77%)
296.469	0.0914	24→78 (54)	15→1 (-14)	11→16 (5)	16→2 (-14)	34→3 (-31)	H-6→LUMO (-25%), H-2→L+2 (-19%), H-1→L+3 (38%), HOMO→L+3 (-12%)
294.4133	0.0005	7→13 (6)	28→23 (-5)	8→18 (10)	23→9 (-14)	33→38 (5)	H-3→L+4 (-41%), H-1→L+4 (49%)
283.9226	0.1238	19→71 (52)	50→3 (-47)	19→18 (-1)	3→2 (-1)	10→5 (-5)	H-6→LUMO (-16%), H-2→L+2 (61%)
282.3064	0.0056	11→18 (7)	9→6 (-3)	3→6 (3)	28→33 (5)	49→38 (-11)	H-7→L+1 (-16%), H-1→L+5 (32%), H-1→L+6 (-17%)
281.9918	0.003	71→13 (-58)	2→1 (-1)	24→1 (-23)	1→56 (55)	2→29 (27)	H-6→L+1 (95%)
281.0521	0.0173	7→19 (12)	58→19 (-39)	17→16 (-1)	4→10 (6)	14→36 (22)	H-2→L+4 (64%)
280.3277	0.004	8→75 (67)	55→1 (-54)	16→19 (3)	5→2 (-3)	16→3 (-13)	H-3→L+2 (61%), H-2→L+3 (27%)
279.1914	0.0112	3→17 (14)	4→15 (11)	1→13 (12)	9→18 (9)	84→37 (-47)	H-7→L+1 (10%), HOMO→L+4 (51%), HOMO→L+6 (-13%)
278.0082	0.0207	7→19 (12)	6→11 (5)	2→10 (8)	21→25 (4)	65→36 (-29)	H-7→L+1 (-15%), H-1→L+6 (16%), HOMO→L+4 (26%)
276.7176	0.0675	8→73 (65)	60→2 (-58)	17→17 (0)	3→2 (-1)	12→6 (-6)	H-3→L+2 (-20%), H-2→L+3 (58%)
273.0069	0.0203	15→61 (46)	44→6 (-38)	14→15 (1)	13→5 (-8)	14→13 (-1)	H-8→LUMO (-19%), H-5→L+2 (-17%), H-5→L+4 (13%), H-3→L+3 (27%)
272.8026	0.015	5→68 (63)	62→3 (-59)	19→19 (0)	3→3 (0)	11→8 (-3)	H-5→L+2 (66%)
272.3951	0.012	32→69 (37)	16→5 (-11)	5→13 (8)	31→4 (-27)	15→9 (-6)	H-8→LUMO (62%), H-3→L+3 (11%)
271.4884	0.0406	0→15 (15)	0→6 (6)	0→5 (5)	2→29 (27)	97→45 (-52)	HOMO→L+5 (35%), HOMO→L+6 (27%), HOMO→L+8 (24%)
269.4177	0.0523	6→58 (52)	62→5 (-57)	19→15 (-4)	2→5 (3)	11→17 (6)	H-5→L+3 (42%), H-3→L+3 (-14%), H-2→L+7 (15%)
267.2861	0.0861	1→20 (19)	2→7 (5)	1→7 (6)	2→26 (24)	94→39 (-55)	HOMO→L+4 (-12%), HOMO→L+5 (42%), HOMO→L+6 (-37%)
266.3216	0.0527	6→64 (58)	58→4 (-54)	18→15 (-3)	4→5 (1)	14→12 (-2)	H-5→L+3 (52%), H-3→L+3 (16%)
264.4921	0.0997	4→27 (23)	3→3 (0)	1→6 (5)	21→29 (8)	72→36 (-36)	H-7→LUMO (20%), H-7→L+1 (27%), H-1→L+5 (27%)
263.8336	0.0211	14→14 (0)	26→17 (-9)	7→13 (6)	25→19 (-6)	28→38 (10)	H-8→L+1 (-17%), H-3→L+4 (28%), H-1→L+4 (30%)
262.6543	0.3441	1→17 (16)	1→8 (7)	0→8 (8)	5→20 (15)	92→47 (-45)	HOMO→L+7 (26%), HOMO→L+8 (27%)

262.2765	0.0756	6→56 (50)	1→3 (2)	0→10 (10)	12→15 (3)	82→16 (-66)	H-7→LUMO (56%), H-7→L+1 (-17%)
260.3325	0.0394	6→19 (13)	21→12 (-9)	6→12 (6)	27→16 (-11)	39→42 (3)	H-1→L+6 (25%), H-1→L+7 (32%)
258.2341	0.0201	16→16 (0)	11→7 (-4)	3→6 (3)	35→32 (-3)	34→39 (5)	H-8→L+1 (24%), H-1→L+6 (17%), H-1→L+7 (-11%), H-1→L+8 (14%)
254.9104	0.0008	1→10 (9)	5→12 (7)	2→10 (8)	2→15 (13)	90→53 (-37)	HOMO→L+7 (54%), HOMO→L+8 (-26%)
254.1111	0.0527	11→10 (-1)	21→7 (-14)	6→6 (0)	28→28 (0)	34→48 (14)	H-8→L+1 (-13%), H-5→L+7 (-12%), H-1→L+8 (32%)
253.6536	0.0048	4→13 (9)	42→10 (-32)	13→9 (-4)	14→20 (6)	27→48 (21)	H-5→L+7 (34%), H-1→L+8 (23%)
251.2989	0.1004	6→21 (15)	60→15 (-45)	18→16 (-2)	4→11 (7)	12→37 (25)	H-5→L+4 (37%), H-2→L+7 (-10%)
250.5422	0.0102	0→75 (75)	1→1 (0)	0→21 (21)	1→1 (0)	97→3 (-94)	H-4→L+2 (97%)
245.7257	0.0021	8→23 (15)	57→8 (-49)	17→9 (-8)	5→22 (17)	14→38 (24)	H-2→L+5 (-21%), H-2→L+6 (40%)
244.1578	0.0001	0→80 (80)	1→0 (-1)	0→16 (16)	1→1 (0)	97→2 (-95)	H-4→L+3 (97%)
242.8712	0.0031	12→39 (27)	35→8 (-27)	12→12 (0)	16→12 (-4)	25→29 (4)	H-9→LUMO (23%), H-3→L+6 (14%), H-3→L+7 (13%)
242.2354	0.0112	17→50 (33)	31→6 (-25)	12→10 (-2)	16→15 (-1)	24→19 (-5)	H-9→LUMO (30%), H-6→L+3 (10%), H-3→L+6 (-26%)
241.6452	0.0046	12→27 (15)	43→8 (-35)	14→10 (-4)	11→17 (6)	19→38 (19)	H-9→LUMO (-13%), H-3→L+5 (21%), H-3→L+6 (-10%), H-3→L+7 (17%)
240.7911	0.1658	10→12 (2)	3→2 (-1)	2→2 (0)	32→42 (10)	54→42 (-12)	H-9→L+1 (62%), HOMO→L+11 (13%)
239.6369	0.0819	75→75 (0)	2→2 (0)	22→19 (-3)	1→1 (0)	1→3 (2)	H-11→LUMO (-17%), H-6→L+2 (73%)
237.0573	0.0003	5→19 (14)	65→8 (-57)	19→8 (-11)	1→24 (23)	10→41 (31)	H-5→L+5 (-11%), H-5→L+6 (25%), H-2→L+5 (-18%), H-2→L+8 (-15%)
236.3794	0.0297	48→77 (29)	3→1 (-2)	15→14 (-1)	15→3 (-12)	20→4 (-16)	H-9→LUMO (-28%), H-6→L+3 (49%)
235.6023	0.0017	6→24 (18)	55→7 (-48)	16→12 (-4)	7→18 (11)	16→40 (24)	H-5→L+6 (16%), H-2→L+5 (12%), H-2→L+8 (11%)
234.0456	0.0044	7→11 (4)	52→9 (-43)	15→6 (-9)	6→24 (18)	19→49 (30)	H-3→L+5 (35%), H-3→L+6 (14%), H-3→L+8 (19%)
231.1957	0.0061	0→15 (15)	1→21 (20)	0→16 (16)	1→11 (10)	97→38 (-59)	H-4→L+4 (81%), H-4→L+6 (-13%)
229.4288	0.0329	4→30 (26)	44→7 (-37)	13→18 (5)	13→9 (-4)	25→36 (11)	H-5→L+6 (-14%), H-1→L+9 (20%)
228.2504	0.0399	1→11 (10)	2→4 (2)	0→4 (4)	4→27 (23)	93→54 (-39)	H-4→L+5 (62%), H-4→L+6 (11%)
226.6523	0.0113	3→12 (9)	60→10 (-50)	18→6 (-12)	3→25 (22)	16→48 (32)	H-5→L+5 (32%), H-5→L+6 (15%), H-5→L+8 (19%)
224.7256	0.0004	1→44 (43)	2→1 (-1)	1→25 (24)	3→2 (-1)	93→28 (-65)	HOMO→L+9 (91%)
224.4977	0.0419	25→13 (-12)	7→3 (-4)	7→2 (-5)	17→48 (31)	44→33 (-11)	H-13→L+1 (15%), H-12→L+1 (49%)
223.8007	0.0196	5→18 (13)	13→8 (-5)	4→7 (3)	8→20 (12)	71→47 (-24)	H-4→L+4 (10%), H-4→L+5 (-10%), H-4→L+6 (30%), H-1→L+11 (-14%)
223.486	0.0175	19→28 (9)	19→7 (-12)	9→10 (1)	11→18 (7)	42→37 (-5)	H-10→LUMO (12%)
223.2044	0.0055	9→34 (25)	19→6 (-13)	6→20 (14)	24→5 (-19)	42→35 (-7)	H-1→L+9 (41%), H-1→L+10 (-16%)
222.8633	0.0366	35→38 (3)	20→5 (-15)	13→10 (-3)	8→14 (6)	24→33 (9)	H-10→LUMO (30%), H-3→L+8 (-11%)
222.7352	0.0081	20→24 (4)	45→13 (-32)	16→12 (-4)	5→13 (8)	14→38 (24)	H-10→LUMO (13%), H-2→L+5 (15%), H-2→L+7 (-11%), H-2→L+8 (-15%), H-2→L+12 (17%)
222.4116	0.0806	12→11 (-1)	22→21 (-1)	9→9 (0)	13→11 (-2)	44→48 (4)	H-3→L+12 (-17%), H-1→L+12 (17%), HOMO→L+11 (13%)
222.0213	0.0096	68→15 (-53)	2→22 (20)	23→17 (-6)	1→8 (7)	5→38 (33)	H-6→L+4 (85%)
221.914	0.0703	4→11 (7)	7→11 (4)	3→7 (4)	13→15 (2)	73→57 (-16)	H-4→L+6 (17%), H-4→L+7 (-16%), H-4→L+8 (-15%), H-1→L+11 (22%)
221.3632	0.0005	41→75 (34)	0→1 (1)	0→21 (21)	41→1 (-40)	17→2 (-15)	H-8→L+2 (84%), H-7→L+2 (-14%)

Table II-S14. Electronic transition obtained from TD-DFT for **2-3** from singlet ground state (b3lyp/LanL2DZ (f)[Re]6-31G**[C,H,N,O], CPCM (CH_2Cl_2)).

λ (nm)	Osc. Strength	bpy	Re	carbonyls	pyridine	Major contribs
383.3153	0.0038	8→91 (83)	64→3 (-61)	26→5 (-21)	1→1 (0)	H-1→LUMO (91%)
375.1727	0.1002	9→92 (83)	61→3 (-58)	25→4 (-21)	6→1 (-5)	HOMO→LUMO (86%)
361.1516	0.0113	2→91 (89)	68→3 (-65)	29→4 (-25)	0→1 (1)	H-2→LUMO (95%)
299.8533	0.1449	65→77 (12)	24→2 (-22)	10→4 (-6)	1→17 (16)	H-3→LUMO (58%), H-1→L+1 (-24%)
294.5112	0.032	16→50 (34)	58→2 (-56)	24→5 (-19)	1→43 (42)	H-1→L+1 (59%), H-1→L+2 (22%)
291.28	0.0565	8→40 (32)	61→3 (-58)	25→9 (-16)	5→48 (43)	HOMO→L+1 (79%)
288.2663	0.0005	9→13 (4)	61→20 (-41)	25→47 (22)	6→20 (14)	HOMO→L+4 (75%)
285.6035	0.0202	9→45 (36)	61→6 (-55)	25→14 (-11)	5→35 (30)	H-1→L+4 (11%), HOMO→L+2 (68%)
283.8901	0.026	11→55 (44)	62→5 (-57)	25→12 (-13)	3→29 (26)	H-1→L+2 (46%), HOMO→L+3 (19%)
280.0364	0.0052	4→46 (42)	67→4 (-63)	28→11 (-17)	1→39 (38)	H-2→L+1 (60%), H-1→L+3 (-15%), H-1→L+4 (10%)
276.8536	0.1588	16→60 (44)	57→7 (-50)	24→17 (-7)	4→16 (12)	H-2→L+1 (-10%), H-2→L+4 (-12%), HOMO→L+3 (40%)
276.4092	0.0789	8→77 (69)	64→4 (-60)	26→10 (-16)	2→9 (7)	H-1→L+3 (72%), H-1→L+4 (11%)
275.8127	0.1125	9→41 (32)	62→9 (-53)	26→23 (-3)	2→27 (25)	H-2→L+1 (-22%), H-1→L+4 (22%), HOMO→L+3 (-13%)
272.7966	0.0014	0→92 (92)	1→3 (2)	0→4 (4)	99→1 (-98)	H-4→LUMO (99%)
271.0492	0.0211	3→49 (46)	68→5 (-63)	29→11 (-18)	1→36 (35)	H-2→L+2 (81%)
268.3157	0.0173	4→68 (64)	67→7 (-60)	29→19 (-10)	1→6 (5)	H-2→L+3 (65%), H-1→L+6 (-16%)
265.8761	0.0711	7→47 (40)	64→12 (-52)	27→32 (5)	1→8 (7)	H-2→L+3 (33%), H-2→L+4 (14%), H-1→L+6 (32%)
255.3304	0.008	5→11 (6)	65→23 (-42)	27→59 (32)	3→8 (5)	H-2→L+6 (43%), HOMO→L+6 (-39%)
251.8911	0.0338	7→11 (4)	59→11 (-48)	24→32 (8)	9→46 (37)	H-2→L+4 (-15%), H-1→L+6 (13%), HOMO→L+5 (48%)
249.8455	0.0109	5→12 (7)	65→19 (-46)	27→54 (27)	2→15 (13)	H-2→L+6 (42%), H-1→L+5 (13%), HOMO→L+6 (25%)
246.2625	0.043	6→13 (7)	60→13 (-47)	25→36 (11)	9→38 (29)	H-2→L+4 (23%), H-1→L+6 (-12%), HOMO→L+5 (34%)
244.4563	0.0214	9→6 (-3)	63→9 (-54)	26→24 (-2)	2→60 (58)	H-1→L+4 (10%), H-1→L+5 (72%)
242.8379	0.0307	98→44 (-54)	1→2 (1)	0→5 (5)	0→50 (50)	H-3→L+1 (89%)
240.0266	0.0018	69→89 (20)	3→1 (-2)	2→4 (2)	26→5 (-21)	H-5→LUMO (-29%), H-3→L+3 (53%)
237.8075	0.0516	97→61 (-36)	1→2 (1)	1→3 (2)	1→34 (33)	H-7→LUMO (-12%), H-3→L+2 (80%)
235.8398	0.0082	3→9 (6)	67→5 (-62)	29→20 (-9)	1→66 (65)	H-2→L+5 (79%)
229.6583	0.0661	43→91 (48)	2→3 (1)	2→5 (3)	54→2 (-52)	H-5→LUMO (64%), H-3→L+3 (20%)
227.8435	0.0005	6→33 (27)	51→11 (-40)	21→39 (18)	21→17 (-4)	H-4→L+1 (15%), H-1→L+9 (-14%), HOMO→L+7 (-16%), HOMO→L+8 (21%)
224.0109	0.0193	6→23 (17)	30→19 (-11)	12→24 (12)	52→35 (-17)	H-4→L+1 (45%), H-1→L+9 (28%)
223.2767	0.0266	9→24 (15)	50→23 (-27)	21→38 (17)	20→15 (-5)	H-4→L+1 (-15%), H-1→L+9 (19%), HOMO→L+9 (-19%)
222.9836	0.0069	20→27 (7)	54→29 (-25)	22→40 (18)	5→4 (-1)	H-6→LUMO (-13%), H-1→L+7 (-11%), H-1→L+9 (22%), HOMO→L+9 (28%)
222.4236	0.0197	74→67 (-7)	15→11 (-4)	6→18 (12)	5→4 (-1)	H-6→LUMO (59%), HOMO→L+9 (12%)
221.7988	0.0027	96→7 (-89)	2→23 (21)	1→55 (54)	0→15 (15)	H-3→L+4 (92%)
219.9183	0.0304	2→49 (47)	4→3 (-1)	2→6 (4)	92→42 (-50)	H-4→L+2 (83%)
218.7118	0.0039	86→90 (4)	3→3 (0)	10→5 (-5)	1→2 (1)	H-10→LUMO (78%), H-7→LUMO (12%)
217.8854	0.0386	9→17 (8)	61→24 (-37)	25→56 (31)	4→3 (-1)	H-2→L+11 (12%), H-1→L+7 (-12%), H-1→L+8 (16%), HOMO→L+11 (38%)

216.3003	0.0022	1→94 (93)	1→0 (-1)	1→3 (2)	98→2 (-96)	H-4→L+3 (98%)
215.7395	0.0289	56→61 (5)	28→9 (-19)	13→25 (12)	3→5 (2)	H-10→LUMO (-11%), H-7→LUMO (32%), H-2→L+7 (-10%)
214.5337	0.0038	28→42 (14)	48→19 (-29)	21→35 (14)	2→3 (1)	H-7→LUMO (14%), H-2→L+7 (17%), H-2→L+10 (14%), HOMO→L+10 (13%)
212.9895	0.0148	12→18 (6)	60→30 (-30)	25→50 (25)	4→2 (-2)	H-2→L+10 (-12%), H-1→L+11 (37%), HOMO→L+7 (16%), HOMO→L+10 (13%)
212.7629	0.0452	44→73 (29)	21→5 (-16)	11→17 (6)	24→5 (-19)	H-8→LUMO (58%)
211.0139	0.0076	22→38 (16)	51→11 (-40)	21→48 (27)	6→3 (-3)	H-1→L+11 (-11%), HOMO→L+7 (28%), HOMO→L+8 (33%)
210.5266	0.0006	13→21 (8)	55→35 (-20)	24→41 (17)	8→3 (-5)	H-2→L+9 (29%), H-1→L+10 (29%)
209.807	0.0098	94→11 (-83)	1→4 (3)	1→13 (12)	4→72 (68)	H-3→L+5 (90%)
209.0394	0.0233	24→57 (33)	41→10 (-31)	18→29 (11)	16→4 (-12)	H-11→LUMO (-11%), H-9→LUMO (-22%), H-2→L+9 (-11%), H-1→L+7 (26%), H-1→L+8 (14%)
207.9036	0.0007	89→18 (-71)	7→21 (14)	3→56 (53)	1→4 (3)	H-3→L+6 (77%)
206.5838	0.0563	62→79 (17)	18→4 (-14)	11→14 (3)	10→4 (-6)	H-11→LUMO (56%), H-1→L+7 (11%)
205.5631	0.0056	1→6 (5)	1→22 (21)	1→54 (53)	97→19 (-78)	H-4→L+4 (90%)
205.25	0.0001	9→9 (0)	62→39 (-23)	26→50 (24)	3→1 (-2)	H-2→L+10 (-21%), H-1→L+11 (-29%), HOMO→L+10 (29%)
203.5784	0.0015	8→11 (3)	61→36 (-25)	26→52 (26)	5→2 (-3)	H-2→L+11 (30%), H-1→L+10 (-20%), HOMO→L+11 (-19%)
202.3194	0.0009	3→47 (44)	67→6 (-61)	29→45 (16)	1→2 (1)	H-2→L+7 (49%), H-2→L+8 (38%)
202.0885	0.0574	45→78 (33)	12→4 (-8)	8→10 (2)	35→7 (-28)	H-11→LUMO (-20%), H-9→LUMO (43%)
199.3846	0.0134	31→40 (9)	4→3 (-1)	4→6 (2)	61→51 (-10)	H-9→L+1 (21%), H-8→L+1 (15%), H-5→L+1 (28%)
196.2041	0.0041	1→7 (6)	11→28 (17)	5→60 (55)	83→4 (-79)	H-4→L+6 (81%)
195.7518	0.0285	9→9 (0)	60→47 (-13)	25→40 (15)	6→4 (-2)	H-2→L+11 (-11%), H-1→L+12 (33%), HOMO→L+13 (-14%)
195.3663	0.0076	25→33 (8)	6→5 (-1)	4→9 (5)	65→54 (-11)	H-8→L+1 (-11%), H-5→L+1 (28%), H-4→L+5 (23%)
194.9209	0.0176	7→8 (1)	52→45 (-7)	21→42 (21)	20→4 (-16)	H-4→L+6 (-14%), HOMO→L+10 (13%), HOMO→L+12 (32%)
193.3916	0.0087	33→40 (7)	11→12 (1)	5→11 (6)	51→36 (-15)	H-5→L+2 (46%), H-4→L+5 (10%)
193.3644	0.0103	13→13 (0)	52→52 (0)	22→24 (2)	13→11 (-2)	H-1→L+13 (40%), HOMO→L+12 (-11%)
191.7911	0.008	55→74 (19)	3→2 (-1)	2→4 (2)	40→20 (-20)	H-7→L+1 (25%), H-5→L+3 (50%)
190.5267	0.0449	15→10 (-5)	56→53 (-3)	23→30 (7)	6→6 (0)	H-1→L+10 (10%), HOMO→L+13 (39%)
189.5799	0.0253	73→49 (-24)	7→7 (0)	3→16 (13)	16→29 (13)	H-6→L+1 (29%), H-3→L+7 (23%)
188.7918	0.1904	69→70 (1)	3→1 (-2)	2→5 (3)	26→24 (-2)	H-7→L+1 (33%), H-6→L+3 (-17%), H-5→L+3 (-30%)
188.436	0.0083	86→52 (-34)	2→2 (0)	1→9 (8)	11→37 (26)	H-6→L+1 (28%), H-6→L+2 (32%), H-3→L+7 (-15%)
186.75	0.0306	92→56 (-36)	4→2 (-2)	1→4 (3)	3→37 (34)	H-7→L+1 (25%), H-7→L+2 (56%), H-6→L+3 (12%)
186.0271	0.0115	68→52 (-16)	11→8 (-3)	12→8 (-4)	10→32 (22)	H-10→L+1 (34%), H-10→L+2 (-28%), H-5→L+3 (-11%)
185.1797	0.0029	12→11 (-1)	60→49 (-11)	26→33 (7)	2→7 (5)	H-2→L+12 (62%)
184.5375	0.0055	92→45 (-47)	3→2 (-1)	1→46 (45)	4→7 (3)	H-3→L+7 (-23%), H-3→L+8 (57%)
183.6627	0.0055	79→74 (-5)	4→2 (-2)	9→6 (-3)	8→18 (10)	H-11→L+1 (11%), H-11→L+2 (-11%), H-10→L+3 (49%)
183.3205	0.004	82→69 (-13)	5→3 (-2)	4→13 (9)	9→15 (6)	H-8→L+1 (12%), H-7→L+3 (42%), H-3→L+8 (-15%)

Table II-S15. Energy and contribution of MO obtained from DFT for ***m*Fpy** from singlet ground state (b3lyp/6-31G**[C,H,N,O], CPCM(CH_2Cl_2)).

MO		eV	Symmetry	67	HOMO	-5.86	A
88	L+20	5.33	A	66	H-1	-5.91	A
87	L+19	5.28	A	65	H-2	-6.84	A
86	L+18	5.2	A	64	H-3	-7.13	A
85	L+17	4.83	A	63	H-4	-7.32	A
84	L+16	4.67	A	62	H-5	-7.64	A
83	L+15	4.6	A	61	H-6	-7.91	A
82	L+14	4.54	A	60	H-7	-8.72	A
81	L+13	4.35	A	59	H-8	-8.91	A
80	L+12	4.19	A	58	H-9	-9.01	A
79	L+11	3.74	A	57	H-10	-9.52	A
78	L+10	3.42	A	56	H-11	-9.66	A
77	L+9	3.05	A	55	H-12	-9.67	A
76	L+8	2.99	A	54	H-13	-10.02	A
75	L+7	2.87	A	53	H-14	-10.64	A
74	L+6	1.96	A	52	H-15	-10.86	A
73	L+5	1.08	A	51	H-16	-10.93	A
72	L+4	0.17	A	50	H-17	-11.05	A
71	L+3	-0.06	A	49	H-18	-11.16	A
70	L+2	-0.7	A	48	H-19	-11.39	A
69	L+1	-0.79	A	47	H-20	-11.51	A
68	LUMO	-1.93	A				

Table II-S16. Energy and contribution of MO obtained from DFT for ***p*Fpy** from singlet ground state (b3lyp/6-31G**[C,H,N,O], CPCM(CH_2Cl_2)).

MO		eV	Symmetry	67	HOMO	-5.94	A
88	L+20	5.34	A	66	H-1	-6	A
87	L+19	5.27	A	65	H-2	-6.87	A
86	L+18	5.15	A	64	H-3	-7.14	A
85	L+17	4.98	A	63	H-4	-7.18	A
84	L+16	4.65	A	62	H-5	-7.62	A
83	L+15	4.62	A	61	H-6	-7.88	A
82	L+14	4.55	A	60	H-7	-8.77	A
81	L+13	4.31	A	59	H-8	-8.95	A
80	L+12	4.01	A	58	H-9	-9.06	A
79	L+11	3.77	A	57	H-10	-9.54	A
78	L+10	3.38	A	56	H-11	-9.68	A
77	L+9	3.14	A	55	H-12	-9.71	A
76	L+8	3	A	54	H-13	-9.85	A
75	L+7	2.86	A	53	H-14	-10.51	A
74	L+6	1.94	A	52	H-15	-10.82	A
73	L+5	1.05	A	51	H-16	-11.09	A
72	L+4	0.14	A	50	H-17	-11.12	A
71	L+3	-0.24	A	49	H-18	-11.36	A
70	L+2	-0.34	A	48	H-19	-11.46	A
69	L+1	-0.82	A	47	H-20	-11.56	A
68	LUMO	-2.06	A				

Table II-S17. Energy and contribution of MO obtained from DFT for **2-1** from singlet ground state (b3lyp/LanL2DZ(f)[Re]6-31G**[C,H,N,O], CPCM(CH_2Cl_2)).

MO		eV	Symmetry	bpy	Re	carbonyls	pyridine	fulvene
157	L+20	1.63	A	23	59	1	5	13
156	L+19	1.51	A	5	11	4	10	69
155	L+18	0.85	A	11	84	3	0	3
154	L+17	0.78	A	0	1	9	0	89
153	L+16	0.66	A	23	70	3	2	1
152	L+15	0.63	A	34	53	8	5	1
151	L+14	0.24	A	50	33	15	1	1
150	L+13	0.18	A	41	47	11	1	1
149	L+12	-0.12	A	23	27	18	2	30
148	L+11	-0.13	A	15	18	17	1	49
147	L+10	-0.32	A	80	1	15	4	0
146	L+9	-0.44	A	79	1	10	8	2
145	L+8	-0.83	A	7	1	10	36	46
144	L+7	-1.08	A	1	0	10	5	84
143	L+6	-1.12	A	51	24	19	5	1
142	L+5	-1.41	A	49	27	21	2	2
141	L+4	-1.8	A	83	0	1	15	1
140	L+3	-1.88	A	44	2	2	38	15
139	L+2	-2	A	42	1	2	40	15
138	L+1	-2.54	A	1	0	8	20	71
137	LUMO	-2.97	A	93	3	2	2	0
136	HOMO	-6.2	A	0	0	10	0	90
135	H-1	-6.33	A	0	1	11	9	79
134	H-2	-6.98	A	15	60	16	5	3
133	H-3	-7	A	17	64	18	1	0
132	H-4	-7.14	A	0	0	25	0	74
131	H-5	-7.22	A	10	68	21	0	0
130	H-6	-7.68	A	88	1	0	11	0
129	H-7	-7.9	A	0	0	13	10	77
128	H-8	-8.19	A	0	0	4	41	54
127	H-9	-8.73	A	7	1	4	39	49
126	H-10	-9.1	A	46	1	2	16	35
125	H-11	-9.17	A	89	4	1	2	4
124	H-12	-9.17	A	62	1	2	15	20
123	H-13	-9.24	A	1	0	14	2	84
122	H-14	-9.31	A	33	1	8	3	56
121	H-15	-9.54	A	31	4	4	10	52
120	H-16	-9.72	A	72	3	2	18	6
119	H-17	-9.73	A	27	3	3	40	27
118	H-18	-9.85	A	1	0	17	5	77
117	H-19	-9.96	A	1	0	17	2	80
116	H-20	-10	A	31	2	6	4	58

Table II-S18. Energy and contribution of MO obtained from DFT for **2-2** from singlet ground state (b3lyp/LanL2DZ(f)[Re]6-31G**[C,H,N,O], CPCM(CH_2Cl_2)).

MO		eV	Symmetry	bpy	Re	carbonyls	pyridine	fulvene
157	L+20	1.67	A	8	70	1	2	19
156	L+19	1.53	A	5	4	0	37	53
155	L+18	0.9	A	1	83	2	2	13
154	L+17	0.77	A	0	2	0	2	96
153	L+16	0.68	A	4	70	3	2	22
152	L+15	0.66	A	4	52	9	1	33
151	L+14	0.27	A	2	33	15	1	48
150	L+13	0.2	A	5	47	11	0	37
149	L+12	-0.09	A	3	45	13	3	36
148	L+11	-0.15	A	0	0	0	0	99
147	L+10	-0.3	A	30	1	25	1	43
146	L+9	-0.42	A	45	1	25	2	27
145	L+8	-0.96	A	5	4	3	32	56
144	L+7	-1.08	A	8	16	14	6	56
143	L+6	-1.16	A	36	7	7	27	23
142	L+5	-1.18	A	8	3	3	32	54
141	L+4	-1.42	A	12	24	18	7	39
140	L+3	-1.78	A	81	0	16	1	2
139	L+2	-1.92	A	75	1	21	1	2
138	L+1	-2.82	A	12	1	1	57	29
137	LUMO	-2.94	A	79	3	13	2	3
136	HOMO	-6.22	A	0	0	0	1	99
135	H-1	-6.34	A	5	5	1	40	49
134	H-2	-6.96	A	7	64	18	1	9
133	H-3	-6.99	A	8	56	16	5	14
132	H-4	-7.14	A	0	1	0	0	99
131	H-5	-7.19	A	1	68	21	0	9
130	H-6	-7.66	A	74	1	25	0	0
129	H-7	-7.94	A	1	0	0	7	91
128	H-8	-8.09	A	48	0	0	46	5
127	H-9	-8.5	A	9	1	1	41	48
126	H-10	-9.1	A	75	1	16	5	3
125	H-11	-9.14	A	84	4	11	1	1
124	H-12	-9.19	A	33	1	8	21	37
123	H-13	-9.27	A	6	0	1	22	71
122	H-14	-9.3	A	30	1	7	4	58
121	H-15	-9.57	A	17	2	3	44	33
120	H-16	-9.7	A	73	3	13	1	10
119	H-17	-9.71	A	23	4	3	39	32
118	H-18	-9.91	A	8	1	1	18	72
117	H-19	-9.96	A	1	0	0	2	97
116	H-20	-9.99	A	32	2	5	10	52

Table II-S19. Energy and contribution of MO obtained from DFT for **2-3** from singlet ground state (b3lyp/LanL2DZ(f)[Re]6-31G**[C,H,N,O], CPCM(CH_2Cl_2)).

MO		eV	Symmetry	bpy	Re	carbonyls	pyridine
111	L+20	2.82	A	92	4	1	2
110	L+19	2.47	A	40	17	2	41
109	L+18	2.24	A	83	3	2	12
108	L+17	1.91	A	73	16	3	8
107	L+16	1.72	A	4	62	16	17
106	L+15	1.67	A	8	70	19	2
105	L+14	0.89	A	2	87	10	1
104	L+13	0.68	A	3	70	24	3
103	L+12	0.66	A	5	54	39	2
102	L+11	0.27	A	2	32	64	1
101	L+10	0.19	A	5	47	48	0
100	L+9	-0.11	A	3	46	48	3
99	L+8	-0.3	A	35	1	64	1
98	L+7	-0.42	A	64	1	33	3
97	L+6	-1.08	A	7	25	65	4
96	L+5	-1.18	A	3	4	13	80
95	L+4	-1.42	A	4	24	57	15
94	L+3	-1.79	A	95	0	3	2
93	L+2	-1.87	A	55	2	3	40
92	L+1	-1.99	A	41	1	4	54
91	LUMO	-2.95	A	92	3	4	1
90	HOMO	-6.93	A	8	61	25	6
89	H-1	-6.97	A	8	65	27	1
88	H-2	-7.19	A	2	69	29	0
87	H-3	-7.66	A	99	1	0	0
86	H-4	-8.09	A	0	0	0	99
85	H-5	-8.87	A	23	1	1	76
84	H-6	-9.14	A	93	1	0	5
83	H-7	-9.15	A	94	4	1	1
82	H-8	-9.33	A	56	5	5	34
81	H-9	-9.63	A	25	5	6	63
80	H-10	-9.71	A	85	3	12	0
79	H-11	-10.05	A	83	5	7	5
78	H-12	-10.75	A	1	0	0	99
77	H-13	-11.03	A	100	0	0	0
76	H-14	-11.2	A	96	0	3	0
75	H-15	-11.85	A	3	1	33	63
74	H-16	-11.9	A	29	1	13	57
73	H-17	-11.91	A	76	1	19	4
72	H-18	-11.95	A	68	1	27	4
71	H-19	-12.12	A	33	1	44	22
70	H-20	-12.26	A	4	0	95	1

Table II-S20. Energy and contribution of alpha MO obtained from DFT for **2-1** from triplet ground state (b3lyp/LanL2DZ(f)[Re]6-31G**[C,H,N,O], CPCM(CH_2Cl_2)).

MO		eV	Symmetry	bpy	Re	carbonyls	pyridine	fulvene
158	L+20	1.72	A	21	64	1	11	3
157	L+19	1.64	A	27	68	1	2	3
156	L+18	0.87	A	11	84	2	0	3
155	L+17	0.73	A	3	10	9	1	77
154	L+16	0.73	A	9	31	9	1	49
153	L+15	0.66	A	30	57	6	2	5
152	L+14	0.59	A	17	28	11	3	42
151	L+13	0.26	A	49	33	15	1	1
150	L+12	0.19	A	40	47	11	1	1
149	L+11	-0.1	A	36	45	13	3	3
148	L+10	-0.27	A	1	0	24	1	74
147	L+9	-0.31	A	77	1	17	4	2
146	L+8	-0.42	A	78	1	8	10	3
145	L+7	-0.79	A	10	1	3	50	35
144	L+6	-1.09	A	1	0	11	0	88
143	L+5	-1.1	A	51	24	20	4	2
142	L+4	-1.4	A	50	27	20	2	1
141	L+3	-1.79	A	87	1	1	11	1
140	L+2	-1.91	A	64	2	1	29	4
139	L+1	-2.06	A	19	2	2	57	21
138	LUMO	-2.96	A	93	3	2	3	0
137	HOMO	-5.29	A	0	0	11	1	88
136	H-1	-5.96	A	0	0	3	30	66
135	H-2	-6.17	A	0	0	11	0	88
134	H-3	-6.97	A	16	62	17	3	1
133	H-4	-6.99	A	16	64	18	2	1
132	H-5	-7.2	A	10	68	20	1	1
131	H-6	-7.23	A	0	0	23	0	76
130	H-7	-7.67	A	88	1	0	11	0
129	H-8	-8.03	A	0	0	16	0	84
128	H-9	-8.58	A	0	0	6	11	82
127	H-10	-8.64	A	2	1	2	60	36
126	H-11	-9.08	A	62	1	1	16	20
125	H-12	-9.16	A	77	2	2	11	8
124	H-13	-9.18	A	58	2	3	8	30
123	H-14	-9.23	A	17	0	17	6	59
122	H-15	-9.35	A	30	2	5	10	53
121	H-16	-9.58	A	3	2	12	27	56
120	H-17	-9.64	A	33	4	2	29	32
119	H-18	-9.72	A	87	3	2	8	0
118	H-19	-9.98	A	0	0	17	0	82
117	H-20	-10.02	A	41	2	3	4	50

Table II-S21. Energy and contribution of alpha MO obtained from DFT for **2-2** from triplet ground state (b3lyp/LanL2DZ(f)[Re]6-31G**[C,H,N,O], CPCM(CH_2Cl_2)).

MO		eV	Symmetry	bpy	Re	carbonyls	pyridine	fulvene
158	L+20	1.78	A	7	64	1	10	19
157	L+19	1.68	A	9	71	0	1	18
156	L+18	0.91	A	1	85	2	2	10
155	L+17	0.74	A	1	21	1	1	76
154	L+16	0.71	A	2	38	1	5	54
153	L+15	0.67	A	4	50	8	2	36
152	L+14	0.63	A	2	16	1	16	65
151	L+13	0.28	A	2	33	15	2	48
150	L+12	0.21	A	5	47	11	0	37
149	L+11	-0.07	A	2	46	13	4	34
148	L+10	-0.28	A	2	0	2	0	96
147	L+9	-0.29	A	28	1	24	0	47
146	L+8	-0.42	A	46	1	25	2	27
145	L+7	-1.05	A	8	21	17	14	40
144	L+6	-1.09	A	4	1	1	4	90
143	L+5	-1.17	A	31	4	4	42	18
142	L+4	-1.23	A	22	5	5	55	13
141	L+3	-1.41	A	11	24	19	7	39
140	L+2	-1.78	A	83	0	14	1	2
139	L+1	-1.92	A	74	1	22	1	2
138	LUMO	-2.93	A	81	3	13	1	3
137	HOMO	-5.29	A	1	0	0	39	61
136	H-1	-6.16	A	6	4	1	28	61
135	H-2	-6.2	A	7	5	2	38	48
134	H-3	-6.95	A	7	65	18	0	9
133	H-4	-7.06	A	9	55	16	11	9
132	H-5	-7.19	A	2	67	20	2	9
131	H-6	-7.24	A	0	0	0	1	99
130	H-7	-7.65	A	74	1	25	0	0
129	H-8	-8.04	A	0	0	0	4	96
128	H-9	-8.25	A	50	0	0	49	0
127	H-10	-8.6	A	1	0	0	25	74
126	H-11	-9.09	A	76	1	15	6	3
125	H-12	-9.14	A	87	4	8	0	0
124	H-13	-9.2	A	40	0	13	15	32
123	H-14	-9.24	A	12	0	4	7	77
122	H-15	-9.35	A	21	2	4	10	64
121	H-16	-9.69	A	41	2	5	23	29
120	H-17	-9.7	A	48	2	11	16	23
119	H-18	-9.78	A	27	5	4	52	13
118	H-19	-9.99	A	0	0	0	0	100
117	H-20	-9.99	A	17	1	2	11	68

Table II-S22. Energy and contribution of alpha MO obtained from DFT for **2-3** from triplet ground state (b3lyp/LanL2DZ(f)[Re]6-31G**[C,H,N,O], CPCM(CH_2Cl_2)).

MO		eV	Symmetry	bpy	Re	carbonyls	pyridine
112	L+20	3	A	92	3	1	4
111	L+19	2.85	A	1	2	1	97
110	L+18	2.42	A	47	7	1	44
109	L+17	2.21	A	94	4	0	2
108	L+16	1.96	A	53	15	1	31
107	L+15	1.5	A	8	77	13	1
106	L+14	1.25	A	2	89	6	4
105	L+13	0.76	A	1	94	5	0
104	L+12	0.34	A	8	74	18	1
103	L+11	0.16	A	4	61	30	5
102	L+10	-0.27	A	89	1	8	2
101	L+9	-0.46	A	12	22	62	4
100	L+8	-0.5	A	7	26	64	3
99	L+7	-0.79	A	4	31	61	5
98	L+6	-0.94	A	3	2	91	4
97	L+5	-1.28	A	10	3	8	80
96	L+4	-1.44	A	62	7	24	7
95	L+3	-1.69	A	83	1	10	7
94	L+2	-1.74	A	4	21	69	6
93	L+1	-1.78	A	35	14	49	2
92	LUMO	-2.11	A	1	3	8	87
91	HOMO	-4.39	A	93	3	4	1
90	H-1	-7.37	A	88	9	3	1
89	H-2	-7.55	A	16	56	20	8
88	H-3	-7.78	A	2	72	25	0
87	H-4	-7.81	A	35	47	14	4
86	H-5	-8.22	A	0	3	1	96
85	H-6	-8.92	A	33	0	1	66
84	H-7	-9.16	A	99	0	0	1
83	H-8	-9.22	A	80	15	4	1
82	H-9	-9.44	A	49	13	5	33
81	H-10	-9.61	A	88	3	8	0
80	H-11	-9.88	A	14	6	7	74
79	H-12	-10.02	A	83	4	5	9
78	H-13	-10.77	A	99	1	0	0
77	H-14	-10.84	A	68	0	3	29
76	H-15	-10.87	A	29	0	1	70
75	H-16	-11.73	A	90	2	2	5
74	H-17	-11.84	A	65	0	12	23
73	H-18	-11.9	A	80	1	17	2
72	H-19	-12.08	A	28	1	11	60
71	H-20	-12.21	A	15	1	12	72

SI - Chapitre 3 : Informations supplémentaires

Supplementary Information

Creating new binding sites on rhodium dimers via Suzuki coupling reactions

*Daniel Chartrand, Garry S. Hanan**

Département de Chimie, Université de Montréal, Montréal, Québec, H3T-1J4, Canada

3.S1. Table of Contents

3.S2. Extra discussion

3.S2.1. Optimization of the synthetic conditions

Our first Suzuki coupling trial, based on previously successful Buchwald coupling on **3-5**,[1] using a simple phenyl-boronic acid and $Pd_2(dba)_3$, S-PHOS and K_2CO_3, in dry THF at 140 °C under nitrogen in a pressure vessel, showed positive result (observed by HRMS), and we moved on to the target coupling with 4-pyridyl boronic ester. Electron withdrawing groups like 4-pyridine are known to be harder to couple and usually requires high temperature and anhydrous solvent, to avoid hydrolytic deboronation.[2] Although these conditions proved to work with the with 4-pyridine motif, the reaction was very slow (over 16 h) and showed a critical issue: the formation of debrominated product. In our first attempt to form **3-4** we obtained a 50% yield with excess boronic ester, all other species formed showed partial pyridine coupling while the unreacted sites were converted to phenyl instead of 4-bromo-phenyl. This debromination is generally seen in literature when alcohol or DMF is present and is due to ß-hydride elimination from the coordinated solvent on the palladium, generating Ar-H.[3] THF being a cyclic ether, can potentially undergo ß-hydride elimination to some extent. To verify if this ß-hydride elimination from the solvent was the real cause, the reaction was tried in DMF and led to the expected total debromination of the dimer, making (*N*,*N*'-diphenylbenzamidinate)$_4Rh_2$ (**3-7**) the major isolated product with some minor coupling products.

Being one of the few useable solvents due to limited solubility of complex **3-5**, THF was kept unchanged and other conditions like temperature, and water content of the solvent were varied.

It was observed that temperature was an important factor in this debromination side-reaction and was lowered to 130 °C, but this led to longer reaction time (2 to 3 days). Partial debromination was still observable and was very variable between experiments, going from 0% up to 40% debromination, perhaps due to variations in temperature over the time of the experiment.

Water content was next studied. On a 1% water in THF (by volume) reaction no significant increase in debromination side-reaction was observed as expected from the literature.[3] More water was added to the reaction mixture in hope to better dissolve the carbonate base as it was shown in the literature to greatly affect the reactivity of the coupling reaction.[4] When the

water content was raised to 25%, despite the lower solubility of the starting dimer, we observed much faster reaction time (less than 5 minutes with microwave heating at 130 °C). The temperature was further reduced to 115 °C, the minimum temperature required to completely dissolve all the starting materials, and complete coupling was achieved in less than one hour. It is to note that microwave heating did not show any differences in reactivity, but was more efficient due to better temperature control. The debromination side-reaction is greatly reduced to below 2%. By ^{1}H NMR the debrominated product can be differentiated with one signal coming at around 6.8 ppm. It is barely observable as a trace peak in Figure 3.1.

The scope of the Suzuki coupling reaction was not explored beyond this successful test with phenylboronic acid, but high yields were obtained for **3-4**, giving a yield of 99% per bromine site by ^{1}H NMR. Since the 4-pyridylboronic ester is a very electron-poor boronic ester, and is known to be less reactive, the reaction should proceed with a wide range of arylboronic acid. The only limiting factor would be the steric hindrance near the boron, due to the rhodium dimer's own bulkiness. Achieving high yields is very important when multiple coupling sites are present in the substrate, as the final yield will be exponentially dependent to the number of coupling. Other examples, where both 4-pyridylboronic acid and 3-pyridylboronic acid (or ester) have been used for multiple coupling, show that the 4-pyridyl moiety is usually harder to couple; for a sextuple coupling (the formation of 1,3,5-tris[3,5-bis(pyridyl)phenyl]benzene), the 4-pyridyl yield is at 40% (or 85% yield per bromine site) and is significantly lower than the 3-pyridyl yield of 66% (93% yield per site).[5] The same trend is also seen for a triple coupling in the formation 1,3,5-tri(*m*-pyridylphenyl)benzene where the yield pass from 72% (89% per site) for the 4-pyridyl to 84% (94% per site) for the 3-pyridyl.[6] For the geometrically closer porphyrin analogues, no Suzuki coupling of a pyridyl moiety was attempted in literature as other pathways were available.[7] Other quadruple Suzuki coupling on tetra *meso*-(tetrabromophenyl)porphine or *meso*-tetrabromoporphine are reported. Their yield ranges from good (80%), for electron rich boronic acid (2,5-dimethoxyboronic acid)[8] to average (42%), for electron poor boronic acid (3-nitroboronic acid)[9], this contrasts **3-5**'s excellent coupling of electron poor boronic acids.

Due to their high disparity in polarity, the differently coupled dimers have very different Rf and can be separated by chromatography on silica and good separation conditions were obtainable for all species, including **3-2a** and **3-2b**. But due to the poor solubility of the

reaction mixture these conditions precluded scaling up (> 20 mg) of the reaction. Another problem during column purification was the tendency of the complexes to slowly oxidize and being retained on silica, reducing the effective yield of the reaction.

To increase the solubility of the bulk product, the best approach was protonation of the pyridyl moieties with HCl, making the dimer very soluble in methanol solutions (100 mg/mL). It is to note that under these acidic conditions, the Rh_2(II,II) core slowly oxidizes to Rh_2(II,III), but it has no effect on the afore mentioned separation as long as the bulk is left to oxidize completely. This oxidized state does not lead to decomposition of the assembly and is totally reversible; the dimer can be reduced back by addition of reductant like triethylamine or hydrazine. Due to the necessity of keeping the eluent under a constant acidic pH, a size-exclusion chromatography technique compatible with acid solution was used (LH-20 Sephadex) for separation. Normally the effective size of the unprotonated forms of the dimers **3-1** to **3-4** would not be enough to differentiate them using this technique, their effective solvation sphere vary greatly as they will have one to four positive charges due to protonation. The dimers were easily separated by their charge, leaving only **3-2a** and **3-2b** as a mixture. These were further separated by silica, the solubility being less of a problem with only these two species to separate, but the recovery of these two was not 100% due to the previously mentioned issues.

3.S2.2. NMR spectroscopy additional information

This extend the discussion of the central ring proton NMR signal for the complex **3-2a**, **3-2b** and **3-3**. For the *cis* complex, **3-2a,** a frozen rotation of the central ring would make the protons on either side chemically different, since their neighboring amidinate would be different all the time. This is observable for both the proton *c* or *c'* in *meta* position relative to the amidinate as they are the closest to the neighboring bromine or pyridine moiety, it can clearly be seen that a triplet arises from the splitting of the expected doublet for these protons. In contrast, the *trans* complex **3-2b** shows the expected perfect symmetry with doublet signals for all the protons concerned, since their neighbors are identical. However this splitting is only seen for the *meta* protons, in all cases the signals of the protons in *ortho* position on the central phenyl ring (*d*, *d'*) are not split, as being closer to the core it has a more similar chemical environment.

In the case of **3-3,** the proton signals for the phenyl-pyridine moiety are split into two due to the two geometrically different positions, leading to the observed two-to-one ratio. On top of that, the two central phenyls adjacent to the bromo-phenyl amidinate are split further due to the aforementioned splitting induced by the restricted rotation.

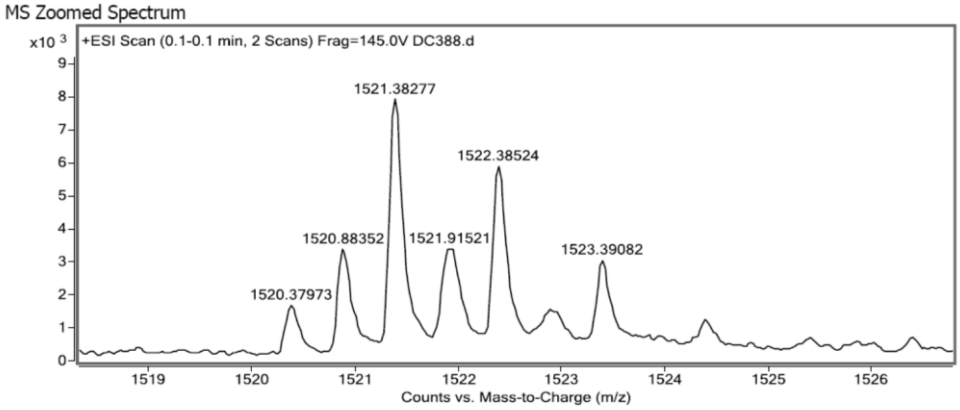

MS Spectrum Peak List

Ion	Ion Formula	Abund	*Expe. m/z*	*Calc. m/z*	Diff(ppm)
M2+	Rh4 C182 H136 N22		1520.37973	1520.37638	-2.21

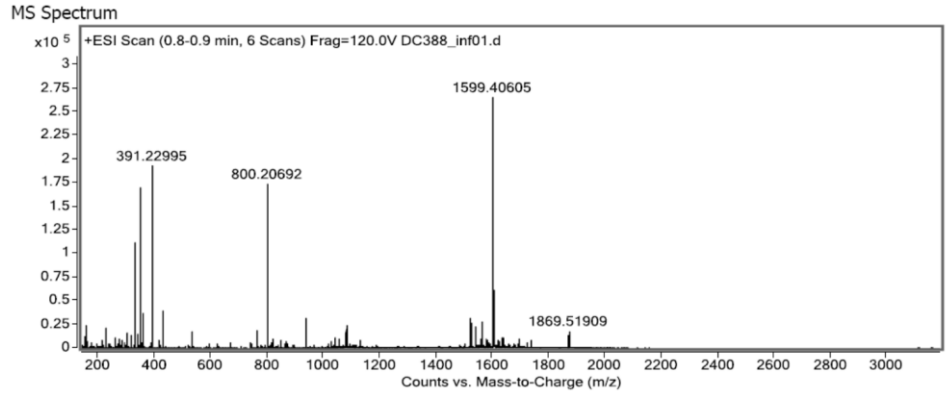

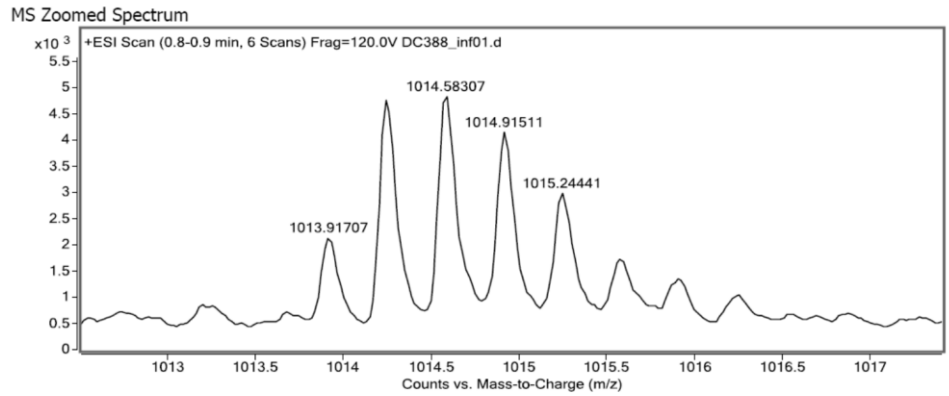

MS Spectrum Peak List

Ion	Ion Formula	Abund	*Expe. m/z*	*Calc. m/z*	Diff(ppm)
(M+H)3+	Rh4 C182 H137 N22		1013.91707	1013.92001	2.9

Figure 3.S1. ESI-MS spectrograms showing the presence of **3-3-3**.

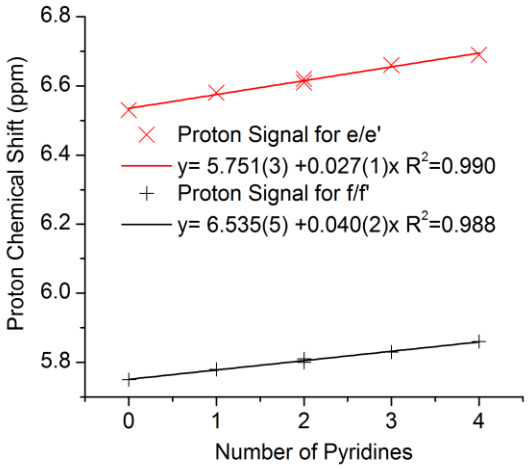

Figure 3.S2. Proton NMR shift observed for unresolved *e/e'* and *f/f'* in function of the number of pyridine present.

3.S3. Crystallography additional information

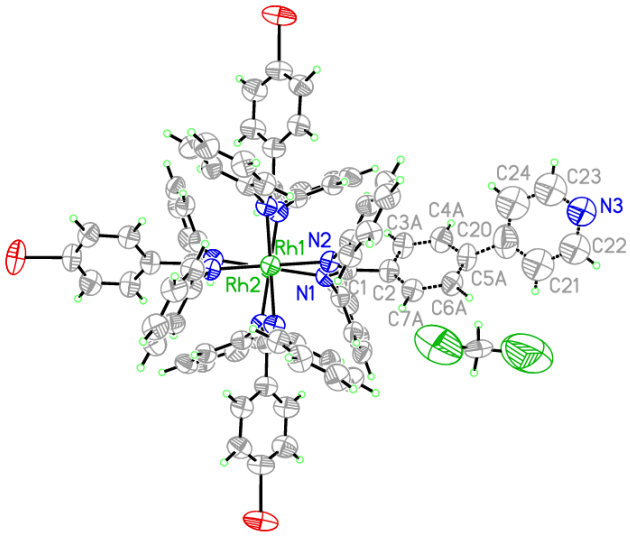

Figure 3.S3. ORTEP view of the X-ray crystal structure of **3-1** with the labeling scheme (50% probability displacement ellipsoids).

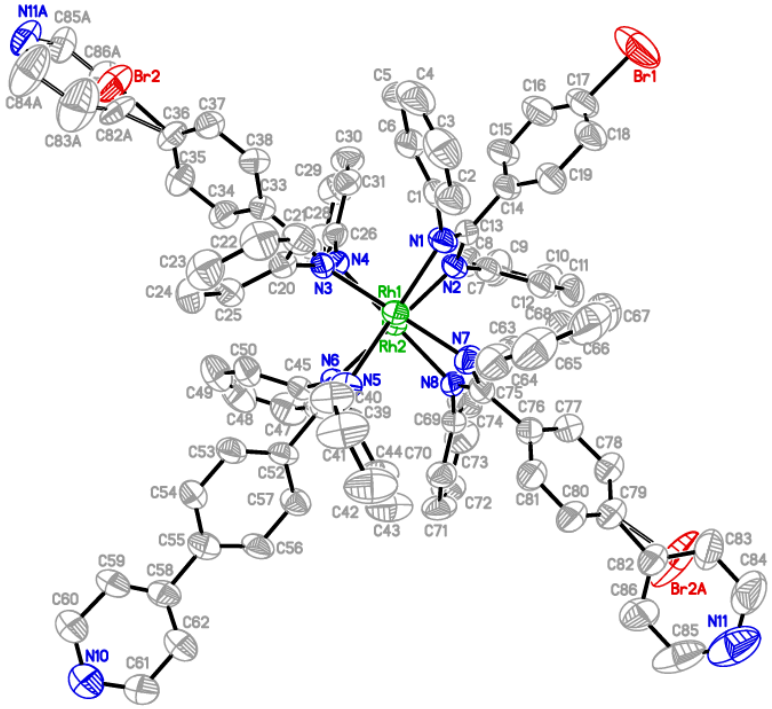

Figure 3.S4. ORTEP views of the X-ray crystal structure of **3-2a** with the labeling scheme (50% probability displacement ellipsoids; hydrogen atoms and solvent molecules removed for the sake of clarity).

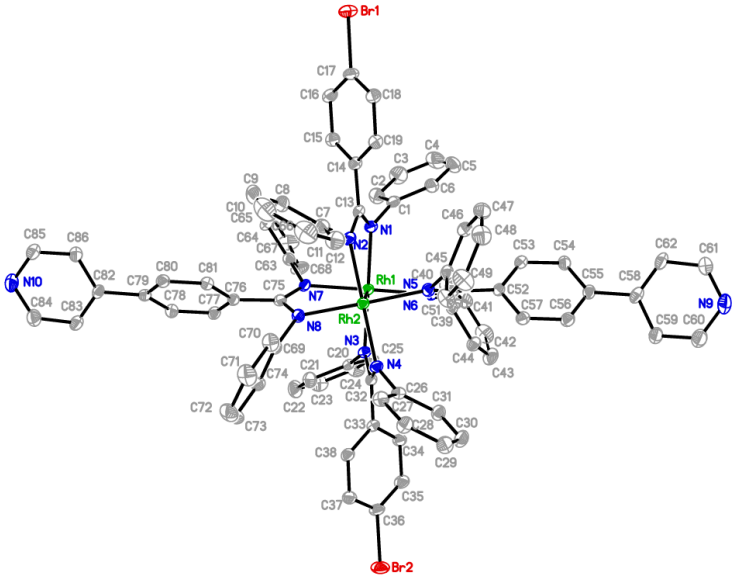

Figure 3.S5. ORTEP view of the X-ray crystal structure of **3-2b** with the labeling scheme (50% probability displacement ellipsoids; hydrogen atoms and solvent molecules removed for the sake of clarity).

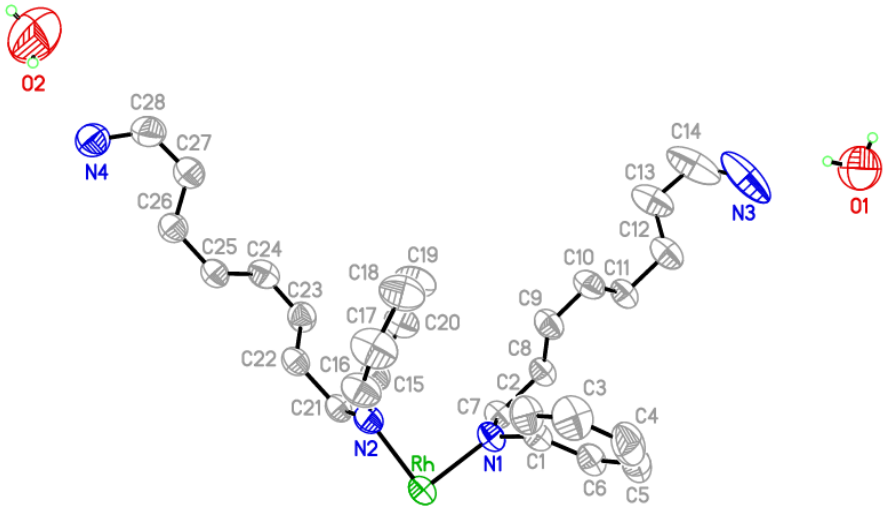

Figure 3.S6. ORTEP view of the X-ray crystal structure asymmetric unit of **3-4** with the labeling scheme (50% probability displacement ellipsoids; hydrogen atoms of non-water removed for the sake of clarity).

3.S3.1. Extended crystallography discussion

The overall packing of **3-1** remains identical to **3-5** and consists of a square motif of dimers, all on the same plane (*a*-*b*), with their Rh_2 axis perpendicular to it, with co-crystallized solvent in the cavity formed at the center. The strongest intermolecular interaction seen is the bromine-to-π ring interaction between the dimers. The pyridine does T-shaped π-π interaction to the adjacent bromophenyl as can be seen in Figure 3.3 (top, main article). Note that different crystals of **1** showed varied values of the Flack parameter, from near zero to 0.25, suggesting that the chirality is preserved in large domains but that the bulk remains racemic.

The *cis* and *trans* dimers **3-2a** and **3-2b**, respectively, offered better data, with the introduction of a second pyridine, the packing is distorted and favors a staggered arrangement of dimers. In the case of the *cis* **3-2a**, two different types of interactions are observed: a parallel-displaced π interaction to an adjacent pyridine on a neighboring dimer and a bromine-to-π ring interaction to a second dimer (Figure 3.S7, top). There is a positional disorder for the bromine atom labeled Br2 and the pyridyl ring *trans* to it and despite being in a ratio of 80% to 20%, this disorder was totally resolved. In Figure 3.S7 top image, the non-tinted molecule has the minor occupancy configuration (Br2a label) and all other display the major configuration. Co-crystallized chloroform is trapped in small cavities, one of them forms a H-bridge interaction between its proton and one of the pyridine nitrogen atom.

Packing of **2b** is similar to **3-2a** (Figure 3.S7, bottom), with the dimer staggered to accommodate the same type of Br-π and π-π interactions. The nitrogen atom of pyridine ring, in this case, is involved in non-classical H– bond interaction with a proton of an adjacent phenyl ring. Crystal packing of complex **3-2b** shows solvent canals along the *b* axis (left to right in Figure 3.S7, bottom) with other smaller cavities perpendicular to them.

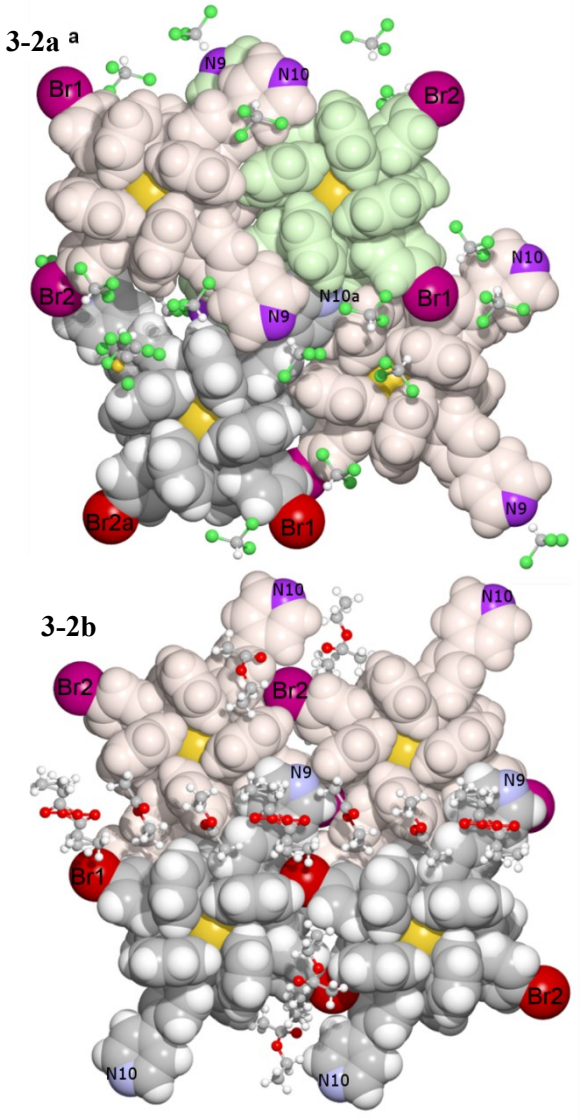

Figure 3.S7. Spacefill view of the packing: **3-2a** (Top), **3-2b** (Bottom); **3-2a**: in non-tinted colors: showing the 20% occupancy positional disorder model and in green and pink the showing the 80% occupancy model; the different tints highlight the two enantiomers; **3-2b**: pink tint distinguish the second enantiomer. Solvent showed in ball and stick model (showing disorder).

In the case of **3-4**, the crystallization conditions were different and required the presence of water. It afforded an orthorhombic (*Fddd*) packing arrangement, where the pyridines form dominating H-bond interactions to water, sequestered in a rectangular cavity sandwiched between two rhodium centers. This cavity contains 4 water molecules, in 8 possible positions (Figure 3.S8). This packing, illustrated in Figure S8, forms a very large grid with intercalating layers of opposed chirality.

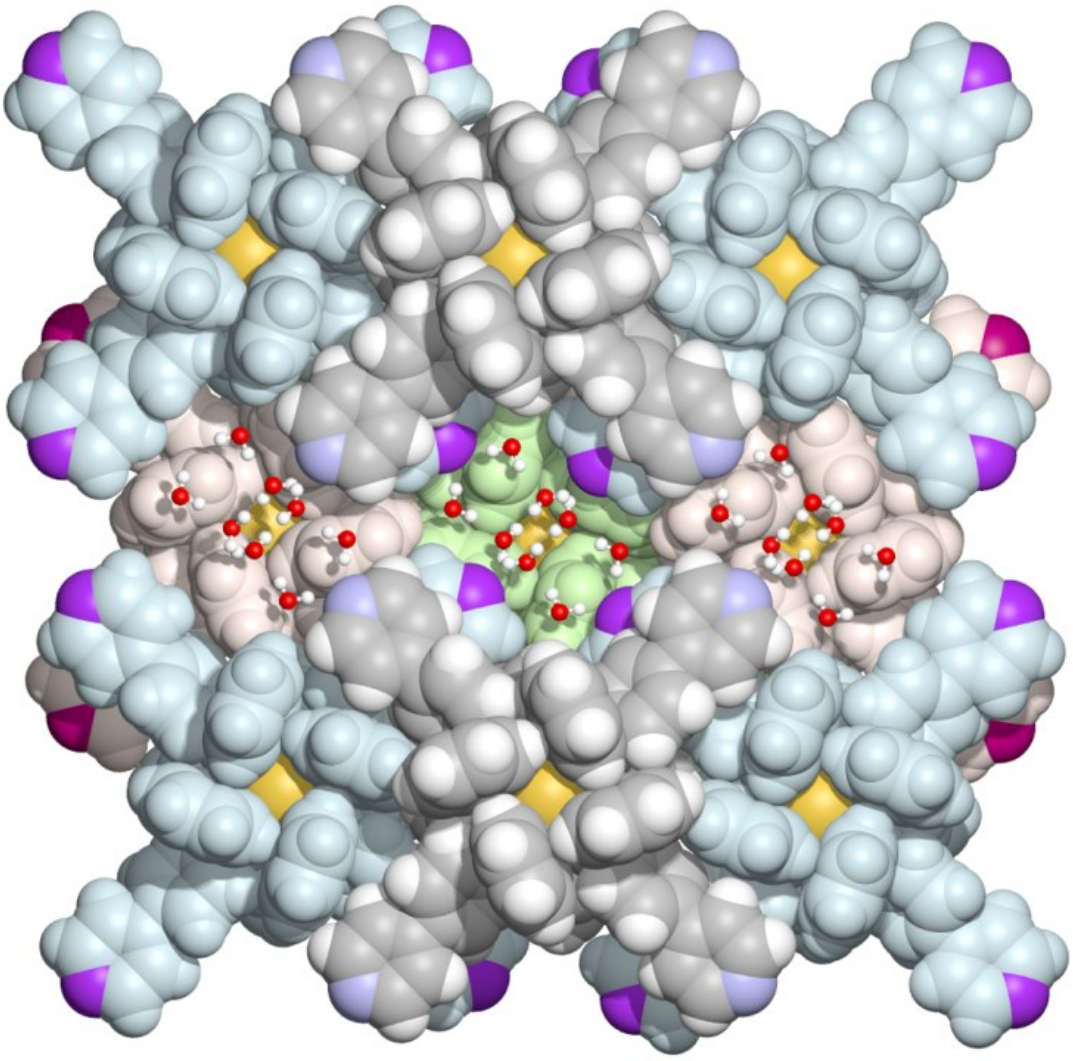

Figure 3.S8. Spacefill view of the packing along the *a* axis of **3-4** (in non-tinted colors the first layer; in cyan tint the second; in pink tint the third and in green tint the fourth. Solvent showed in ball and stick model (showing disorder).

3.S4. References

(1) M. W. Cooke, M. P. Santoni, G. S. Hanan, A. Proust, B. Hasenknopf, *Dalton Trans.* **2009**, 3671-3673.

(2) C. Klein, E. Graf, M. W. Hosseini, C. A. De, N. Kyritsakas-Gruber, *Eur. J. Org. Chem.* **2002**, 802-809.

(3) a) S. Kappaun, M. Zelzer, K. Bartl, R. Saf, F. Stelzer, C. Slugovc, *J. Polym. Sci., Part A: Polym. Chem.* **2006**, *44*, 2130-2138; b) L. Ghosez, C. Franc, F. Denonne, C. Cuisinier, R. Touillaux, *Can. J. Chem.* **2001**, *79*, 1827-1839.

(4) a) C. Amatore, A. Jutand, D. G. Le, *Chem. Eur. J.* **2012**, *18*, 6616-6625; b) C. Amatore, A. Jutand, D. G. Le, *Chem. Eur. J.* **2011**, *17*, 2492-2503.

(5) Y.-J. Li, H. Sasabe, S.-J. Su, D. Tanaka, T. Takeda, Y.-J. Pu, J. Kido, *Chem. Lett.* **2010**, *39*, 140-141.

(6) S.-J. Su, Y. Takahashi, T. Chiba, T. Takeda, J. Kido, *Adv. Funct. Mater.* **2009**, *19*, 1260-1267.

(7) E. B. Fleischer, A. M. Shachter, *Inorg. Chem.* **1991**, *30*, 3763-3769.

(8) G. J. Capitosti, C. D. Guerrero, D. E. Binkley, Jr., C. S. Rajesh, D. A. Modarelli, *J. Org. Chem.* **2003**, *68*, 247-261.

(9) D.-F. Shi, R. T. Wheelhouse, *Tetrahedron Lett.* **2002**, *43*, 9341-9342.

3.S5. Calculation data

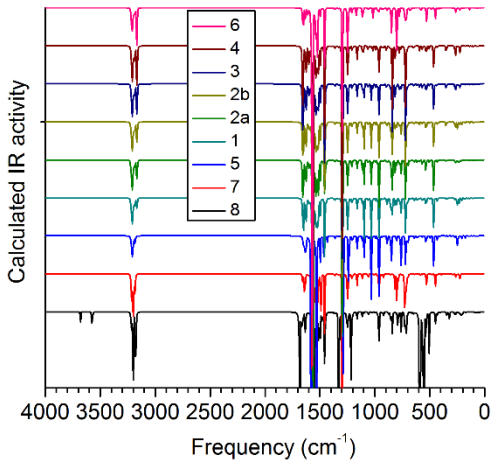

Figure 3.S9. Calculated IR vibration frequencies for complex **3-1** to **3-8** (b3lyp/LanL2DZ(f)[Rh] 6-31G**[C,H,N,Br])

Table III-S1. Optimized atomic coordinates obtained from DFT for **3-1** singlet ground state (b3lyp/LanL2DZ(f)[Rh] 6-31G**[C,H,N,Br]); E = -11549.93401090 Hartree.

Atom	x /Å	y /Å	z /Å
Rh	-0.122519	-0.00202	-1.211296
Rh	-0.122481	0.002132	1.211275
N	1.956449	0.269092	-1.127728
N	1.956593	-0.268103	1.127673
C	4.841427	-0.774261	-0.923414
H	4.302013	-1.371795	-1.650932
C	4.127067	0.000895	-0.000089
C	4.84123	0.776215	0.92325
H	4.301666	1.373622	1.650761
C	6.232357	0.781792	0.916868
H	6.764999	1.376255	1.652791
C	6.232553	-0.779636	-0.916907
H	6.765348	-1.374019	-1.652785
C	2.621876	0.000604	-0.000043
C	2.573522	-0.933747	2.21686
C	2.48111	-0.386167	3.507438
H	1.995399	0.573919	3.639501
C	3.027218	-1.055942	4.603291
H	2.95314	-0.608648	5.590647
C	3.675671	-2.280766	4.43646
H	4.102911	-2.797946	5.290134
C	3.77187	-2.831968	3.156654
H	4.274795	-3.784013	3.010613
C	3.221236	-2.171988	2.059399
H	3.294074	-2.607811	1.069123
C	2.573138	0.934989	-2.216893
C	2.480925	0.387453	-3.507502
H	1.995547	-0.572792	-3.639628
C	3.026801	1.05749	-4.603312
H	2.952886	0.610231	-5.590696
C	3.674839	2.282524	-4.436402
H	4.101902	2.799903	-5.290043
C	3.770873	2.833663	-3.156557
H	4.273486	3.785863	-3.010451
C	3.220457	2.173425	-2.059348
H	3.293177	2.609185	-1.069036
N	-0.39379	2.077086	-1.130794
N	0.147808	2.081	1.123797
C	0.651469	4.958032	-0.936754
H	1.251998	4.41605	-1.659898
C	-0.121777	4.24924	-0.007675
C	-0.893766	4.963547	0.918206
H	-1.495601	4.425958	1.643526
C	-0.901786	6.356891	0.916082
H	-1.505488	6.906945	1.62874
C	0.662194	6.351348	-0.940647
H	1.266754	6.897169	-1.655838
C	-0.122795	2.743825	-0.004629
C	0.814626	2.700345	2.211237
C	0.266444	2.61368	3.501907
H	-0.694279	2.129744	3.63565
C	0.936671	3.163132	4.595836
H	0.488952	3.093566	5.583319
C	2.162323	3.809371	4.426731
H	2.679638	4.239633	5.278801
C	2.714075	3.89973	3.146761
H	3.666595	4.401144	2.998908
C	2.053793	3.345519	2.051547
H	2.490444	3.413307	1.061297
C	-1.06258	2.692111	-2.219327
C	-0.518132	2.59811	-3.511072
H	0.441493	2.112005	-3.644989
C	-1.190681	3.142831	-4.605954
H	-0.745823	3.067523	-5.594315
C	-2.41501	3.791577	-4.436856
H	-2.934152	4.218079	-5.289692
C	-2.963103	3.88941	-3.155837
H	-3.914428	4.393039	-3.007876
C	-2.300446	3.33996	-2.059616
H	-2.734069	3.414132	-1.068468
N	-2.201634	-0.273338	-1.12677
N	-2.20172	0.27254	1.126815
C	-5.083573	0.770116	-0.928621
H	-4.543934	1.370388	-1.653723
C	-4.371843	-0.000911	0.00005
C	-5.083173	-0.772296	0.92873
H	-4.543223	-1.372302	1.653821
C	-6.4765	-0.782049	0.929607
H	-7.024285	-1.385316	1.644378
C	-6.476905	0.779165	-0.929481
H	-7.025004	1.382147	-1.644253
C	-2.866449	-0.00053	0.000029
C	-2.819002	0.943187	2.212992
C	-2.729776	0.399825	3.505511
H	-2.245663	-0.560464	3.641822
C	-3.276724	1.074324	4.59809
H	-3.205173	0.630292	5.587098
C	-3.922884	2.299585	4.42584
H	-4.351114	2.820248	5.276881
C	-4.015976	2.846588	3.144003
H	-4.517667	3.798556	2.993601
C	-3.464388	2.181906	2.050087
H	-3.5349	2.614602	1.058264
C	-2.818659	-0.944313	-2.212887
C	-2.729723	-0.400999	-3.505445
H	-2.24604	0.559495	-3.641839
C	-3.276409	-1.075817	-4.597959
H	-3.205091	-0.63182	-5.587
C	-3.92202	-2.301353	-4.425603
H	-4.350045	-2.822265	-5.276595
C	-4.014838	-2.848302	-3.143724
H	-4.516108	-3.800479	-2.993237
C	-3.463504	-2.1833	-2.049874
H	-3.533801	-2.615949	-1.058016
N	0.148675	-2.080773	-1.123815
N	-0.392834	-2.077094	1.130802
C	-0.891891	-4.963701	-0.918119
H	-1.494088	-4.426318	-1.643292
C	-0.120001	-4.249127	0.007639
C	0.65374	-4.957652	0.93651
H	1.254216	-4.415463	1.659542
C	0.665059	-6.350964	0.940308
H	1.270016	-6.896574	1.655323
C	-0.899323	-6.357049	-0.916082
H	-1.502932	-6.907313	-1.628656
C	-0.121606	-2.743714	0.004624
C	-1.061373	-2.692384	2.219341
C	-0.516944	-2.598143	3.511078
H	0.44248	-2.111633	3.644978
C	-1.189248	-3.143132	4.605976

Atom	x /Å	y /Å	z /Å
H	-0.744408	-3.067626	5.594329
C	-2.413304	-3.792399	4.436901
H	-2.932254	-4.219113	5.289747
C	-2.961374	-3.890477	3.15589
H	-3.912489	-4.39451	3.007949
C	-2.298967	-3.340757	2.059653
H	-2.732572	-3.415128	1.068512
C	0.815752	-2.699838	-2.21125
C	0.267569	-2.613349	-3.50193
H	-0.693349	-2.129799	-3.635678
C	0.938036	-3.162508	-4.59586
H	0.490306	-3.0931	-5.58335
C	2.163957	-3.808235	-4.426753
H	2.681462	-4.238264	-5.278824
C	2.715737	-3.898373	-3.14678
H	3.668466	-4.399389	-2.998923
C	2.055198	-3.344478	-2.051562
H	2.491887	-3.412059	-1.061315
C	6.955439	0.001124	0.000018
C	-0.119074	7.038206	-0.013715
C	-7.160785	-0.001615	0.000067
C	-0.116118	-7.038092	0.0135
Br	-0.11704	8.950016	-0.017781
Br	-9.07257	-0.002082	0.000091
Br	-0.113301	-8.949901	0.017463
C	8.438299	0.001189	0.000104
C	9.176376	-1.158009	-0.283933
C	9.176259	1.160461	0.284142
C	10.568525	-1.104165	-0.27141
H	8.674054	-2.098206	-0.487311
C	10.568414	1.10673	0.27171
H	8.673849	2.100637	0.487394
N	11.274102	0.00131	0.000182
H	11.147702	-2.00082	-0.485421
H	11.147503	2.003436	0.485748

Table III-S2. Optimized atomic coordinates obtained from DFT for **3-2a** singlet ground state (b3lyp/LanL2DZ(f)[Rh] 6-31G**[C,H,N,Br]) ; E = -9225.92972186 Hartree.

Atom	x /Å	y /Å	z /Å
Rh	-1.20968	-0.00038	-0.170828
Rh	1.20968	0.00038	-0.170828
N	-1.126955	-1.280691	-1.83232
N	-1.126888	-1.661495	1.109529
N	-0.005345	-8.061844	7.888663
C	-2.212715	-1.237781	-2.742849
C	-3.506875	-1.552432	-2.295359
H	-3.644965	-1.890211	-1.274469
C	-4.599569	-1.453751	-3.157979
H	-5.58992	-1.711631	-2.793128
C	-4.425927	-1.042427	-4.480509
H	-5.277107	-0.969976	-5.150564
C	-3.142379	-0.729024	-4.933616
H	-2.990839	-0.40924	-5.960912
C	-2.04821	-0.817359	-4.074753
H	-1.055201	-0.566818	-4.431367
C	0.000546	-1.941651	-2.112305
C	0.000601	-3.006665	-3.176691
C	-0.941105	-4.044004	-3.145571
H	-1.67592	-4.077544	-2.348203
C	-0.942847	-5.035877	-4.124118
H	-1.668399	-5.84057	-4.093779
C	0.000206	-4.979731	-5.148215
C	-2.21252	-2.571788	1.065499
C	-3.507263	-2.123654	1.377025
H	-3.645573	-1.102557	1.714135
C	-4.600101	-2.985833	1.276549
H	-5.590874	-2.620387	1.531976
C	-4.426164	-4.308704	0.866364
H	-5.277546	-4.978318	0.792067
C	-3.14206	-4.762485	0.556208
H	-2.990444	-5.789916	0.236745
C	-2.047642	-3.904139	0.646536
H	-1.05412	-4.261192	0.39871
C	0.000378	-1.941778	1.771145
C	0.000205	-3.00619	2.835851
C	0.942074	-4.043657	2.809701
H	1.683888	-4.072249	2.018687
C	0.935455	-5.030959	3.789664
H	1.685791	-5.814918	3.759992
C	-0.001598	-5.006791	4.83573
C	-0.002814	-6.055743	5.883951
C	0.323121	-7.38955	5.594002
H	0.561532	-7.693684	4.579944
C	0.307638	-8.336577	6.615763
H	0.554386	-9.374103	6.397017
N	1.127658	-1.661043	-1.451116
C	2.214595	-2.570239	-1.408788
C	3.50796	-2.121094	-1.724462
H	3.644516	-1.100063	-2.062411
C	4.601815	-2.982333	-1.626864
H	5.591462	-2.61625	-1.885677
C	4.430151	-4.305062	-1.21537
H	5.282217	-4.974105	-1.14385
C	3.147494	-4.759547	-0.900434
H	2.997582	-5.78693	-0.580139
C	2.052143	-3.902149	-0.987778
H	1.059964	-4.259605	-0.735258
C	0.942281	-2.976707	-4.214083
H	1.677278	-2.179546	-4.248443
C	0.94345	-3.955869	-5.205362
H	1.668705	-3.926143	-6.010338
N	1.12735	-1.279982	1.490492
C	2.213896	-1.237095	2.399715
C	3.508004	-1.54938	1.950174
H	3.645174	-1.885951	0.928753
C	4.601682	-1.450572	2.811441
H	5.591883	-1.706694	2.444945
C	4.429241	-1.04121	4.134765
H	5.281275	-0.968321	4.803717
C	3.145858	-0.72991	4.589705
H	2.99548	-0.410696	5.617403
C	2.050578	-0.818576	3.73234
H	1.057733	-0.569093	4.09007

Atom	x /Å	y /Å	z /Å
C	-0.942243	-2.979289	3.872779
H	-1.683425	-2.18766	3.900884
C	-0.937504	-3.9597	4.85963
H	-1.688542	-3.929681	5.642911
C	-0.33015	-5.766348	7.21754
H	-0.567851	-4.752224	7.52203
C	-0.317137	-6.788768	8.163876
H	-0.564948	-6.570452	9.20125
N	-1.12735	1.279982	1.490492
N	-1.127658	1.661043	-1.451116
N	0.005345	8.061844	7.888663
C	-2.213896	1.237095	2.399715
C	-3.508004	1.54938	1.950174
H	-3.645174	1.885951	0.928753
C	-4.601682	1.450572	2.811441
H	-5.591883	1.706694	2.444945
C	-4.429241	1.04121	4.134765
H	-5.281275	0.968321	4.803717
C	-3.145858	0.72991	4.589705
H	-2.99548	0.410696	5.617403
C	-2.050578	0.818576	3.73234
H	-1.057733	0.569093	4.09007
C	-0.000378	1.941778	1.771145
C	-0.000205	3.00619	2.835851
C	-0.942074	4.043657	2.809701
H	-1.683888	4.072249	2.018687
C	-0.935455	5.030959	3.789664
H	-1.685791	5.814918	3.759992
C	0.001598	5.006791	4.83573
C	0.002814	6.055743	5.883951
C	-0.323121	7.38955	5.594002
H	-0.561532	7.693684	4.579944
C	-0.307638	8.336577	6.615763
H	-0.554386	9.374103	6.397017
C	-2.214595	2.570239	-1.408788
C	-3.50796	2.121094	-1.724462
H	-3.644516	1.100063	-2.062411
C	-4.601815	2.982333	-1.626864
H	-5.591462	2.61625	-1.885677
C	-4.430151	4.305062	-1.21537
H	-5.282217	4.974105	-1.14385
C	-3.147494	4.759547	-0.900434
H	-2.997582	5.78693	-0.580139
C	-2.052143	3.902149	-0.987778
H	-1.059964	4.259605	-0.735258

Atom	x /Å	y /Å	z /Å
C	-0.000546	1.941651	-2.112305
C	-0.000601	3.006665	-3.176691
C	0.941105	4.044004	-3.145571
H	1.67592	4.077544	-2.348203
C	0.942847	5.035877	-4.124118
H	1.668399	5.84057	-4.093779
C	-0.000206	4.979731	-5.148215
N	1.126888	1.661495	1.109529
C	2.21252	2.571788	1.065499
C	3.507263	2.123654	1.377025
H	3.645573	1.102557	1.714135
C	4.600101	2.985833	1.276549
H	5.590874	2.620387	1.531976
C	4.426164	4.308704	0.866364
H	5.277546	4.978318	0.792067
C	3.14206	4.762485	0.556208
H	2.990444	5.789916	0.236745
C	2.047642	3.904139	0.646536
H	1.05412	4.261192	0.39871
C	0.942243	2.979289	3.872779
H	1.683425	2.18766	3.900884
C	0.937504	3.9597	4.85963
H	1.688542	3.929681	5.642911
C	0.33015	5.766348	7.21754
H	0.567851	4.752224	7.52203
C	0.317137	6.788768	8.163876
H	0.564948	6.570452	9.20125
N	1.126955	1.280691	-1.83232
C	2.212715	1.237781	-2.742849
C	3.506875	1.552432	-2.295359
H	3.644965	1.890211	-1.274469
C	4.599569	1.453751	-3.157979
H	5.58992	1.711631	-2.793128
C	4.425927	1.042427	-4.480509
H	5.277107	0.969976	-5.150564
C	3.142379	0.729024	-4.933616
H	2.990839	0.40924	-5.960912
C	2.04821	0.817359	-4.074753
H	1.055201	0.566818	-4.431367
C	-0.942281	2.976707	-4.214083
H	-1.677278	2.179546	-4.248443
C	-0.94345	3.955869	-5.205362
H	-1.668705	3.926143	-6.010338
Br	-0.000205	-6.332369	-6.499921
Br	0.000205	6.332369	-6.499921

Table III-S3. Optimized atomic coordinates obtained from DFT for **3-2b** singlet ground state (b3lyp/LanL2DZ(f)[Rh] 6-31G**[C,H,N,Br]) ; E = -9225.92937943 Hartree.

Atom	x /Å	y /Å	z /Å
Rh	0	0	0
Rh	0	0	2.4226996
N	2.0967706	0	0.0839003
N	0.0000683	-2.0965196	0.083823
N	11.3019653	-1.4670831	1.2113498
C	2.7947877	0.5826406	-1.0039379
C	2.6354035	0.0524766	-2.2952314
H	2.0317426	-0.8379065	-2.4290497
C	3.2637628	0.6485185	-3.3896014

Atom	x /Å	y /Å	z /Å
H	3.1348722	0.215233	-4.3775704
C	4.0623137	1.7808909	-3.2205303
H	4.5530164	2.2404209	-4.0730645
C	4.225973	2.3141464	-1.9399694
H	4.8456181	3.194406	-1.7921865
C	3.5944098	1.7283508	-0.8442035
H	3.7205797	2.1503713	0.1466997
C	2.7217321	-0.353302	1.2113498
C	4.2144189	-0.5470644	1.2113498

Atom	x /Å	y /Å	z /Å
C	4.8230114	-1.4073121	0.2875776
H	4.211148	-1.9299734	-0.4402651
C	6.2018644	-1.5918053	0.2940136
H	6.6537092	-2.2494541	-0.4422009
C	7.0192494	-0.9111532	1.2113498
C	8.4897659	-1.1020377	1.2113498
C	9.0724388	-2.3464462	0.9265361
H	8.4532419	-3.213986	0.7225173
C	10.4599333	-2.4723037	0.939007
H	10.9188365	-3.4359412	0.7244496
C	0.5815267	-2.7944584	-1.0049098
C	0.0501372	-2.6339021	-2.2955484
H	-0.839398	-2.0287777	-2.4282917
C	0.6439814	-3.2629132	-3.3907426
H	0.2097552	-3.1331217	-4.3781736
C	1.7751256	-4.0634376	-3.2230188
H	2.2326798	-4.555061	-4.0760797
C	2.3096696	-4.2280136	-1.9431344
H	3.1889113	-4.8492695	-1.7963457
C	1.7263256	-3.5955425	-0.8466344
H	2.150004	-3.7219458	0.1435071
C	-0.3532037	-2.7209747	1.2113498
C	-0.5469976	-4.2139045	1.2113498
C	0.128256	-5.0190652	2.1382677
H	0.7943274	-4.561174	2.8621389
C	-0.0417848	-6.4020204	2.1391749
H	0.4872243	-7.0232052	2.8527498
C	-0.9060192	-6.9796982	1.2113498
N	2.0272801	-0.5353339	2.3387994
C	2.5534077	-1.276878	3.4266375
C	2.5346638	-0.7235916	4.7179311
H	2.1783361	0.2914055	4.8517493
C	2.9900207	-1.4603083	5.8123011
H	2.9760254	-1.0084751	6.80027
C	3.4729962	-2.7590328	5.6432299
H	3.830112	-3.3286163	6.4957641
C	3.4950843	-3.3163998	4.362669
H	3.8694511	-4.3256899	4.2148861
C	3.0340137	-2.5887718	3.2669031
H	3.0482546	-3.0290187	2.276
C	5.0224745	0.1292914	2.135122
H	4.5643318	0.7908478	2.8629647
C	6.4027336	-0.0443696	2.128686
H	7.0075102	0.4761215	2.8649005
C	9.3708424	-0.0476353	1.4961635
H	8.9936613	0.9492421	1.7001823
C	10.7444861	-0.280195	1.4836927
H	11.4342102	0.5343417	1.69825
N	-0.5353358	-2.02702	2.3388766
C	-1.2757169	-2.5533737	3.4276095
C	-0.7209464	-2.5338094	4.718248
H	0.2936045	-2.1758502	4.8509913
C	-1.4557046	-2.9903576	5.8134422
H	-1.0027319	-2.9757314	6.8008732
C	-2.7537456	-3.4755548	5.6457184
H	-3.3216537	-3.8340652	6.4987793
C	-3.3125923	-3.4982002	4.365834
H	-4.3213095	-3.8743844	4.2190453
C	-2.5871029	-3.0356259	3.269334
H	-3.0290123	-3.0496691	2.2791926
C	-1.4054406	-4.8199794	0.2844319
H	-1.9325314	-4.2072065	-0.4394393
C	-1.5941225	-6.2005149	0.2835247
H	-2.2641962	-6.6660494	-0.4300501

Atom	x /Å	y /Å	z /Å
N	-2.0967706	0	0.0839003
N	-0.0000683	2.0965196	0.083823
N	-11.3019653	1.4670831	1.2113498
C	-2.7947877	-0.5826406	-1.0039379
C	-2.6354035	-0.0524766	-2.2952314
H	-2.0317426	0.8379065	-2.4290497
C	-3.2637628	-0.6485185	-3.3896014
H	-3.1348722	-0.215233	-4.3775704
C	-4.0623137	-1.7808909	-3.2205303
H	-4.5530164	-2.2404209	-4.0730645
C	-4.225973	-2.3141464	-1.9399694
H	-4.8456181	-3.194406	-1.7921865
C	-3.5944098	-1.7283508	-0.8442035
H	-3.7205797	-2.1503713	0.1466997
C	-2.7217321	0.353302	1.2113498
C	-4.2144189	0.5470644	1.2113498
C	-4.8230114	1.4073121	0.2875776
H	-4.211148	1.9299734	-0.4402651
C	-6.2018644	1.5918053	0.2940136
H	-6.6537092	2.2494541	-0.4422009
C	-7.0192494	0.9111532	1.2113498
C	-8.4897659	1.1020377	1.2113498
C	-9.0724388	2.3464462	0.9265361
H	-8.4532419	3.213986	0.7225173
C	-10.4599333	2.4723037	0.939007
H	-10.9188365	3.4359412	0.7244496
C	-0.5815267	2.7944584	-1.0049098
C	-0.0501372	2.6339021	-2.2955484
H	0.839398	2.0287777	-2.4282917
C	-0.6439814	3.2629132	-3.3907426
H	-0.2097552	3.1331217	-4.3781736
C	-1.7751256	4.0634376	-3.2230188
H	-2.2326798	4.555061	-4.0760797
C	-2.3096696	4.2280136	-1.9431344
H	-3.1889113	4.8492695	-1.7963457
C	-1.7263256	3.5955425	-0.8466344
H	-2.150004	3.7219458	0.1435071
C	0.3532037	2.7209747	1.2113498
C	0.5469976	4.2139045	1.2113498
C	-0.128256	5.0190652	2.1382677
H	-0.7943274	4.561174	2.8621389
C	0.0417848	6.4020204	2.1391749
H	-0.4872243	7.0232052	2.8527498
C	0.9060192	6.9796982	1.2113498
N	-2.0272801	0.5353339	2.3387994
C	-2.5534077	1.276878	3.4266375
C	-2.5346638	0.7235916	4.7179311
H	-2.1783361	-0.2914055	4.8517493
C	-2.9900207	1.4603083	5.8123011
H	-2.9760254	1.0084751	6.80027
C	-3.4729962	2.7590328	5.6432299
H	-3.830112	3.3286163	6.4957641
C	-3.4950843	3.3163998	4.362669
H	-3.8694511	4.3256899	4.2148861
C	-3.0340137	2.5887718	3.2669031
H	-3.0482546	3.0290187	2.276
C	-5.0224745	-0.1292914	2.135122
H	-4.5643318	-0.7908478	2.8629647
C	-6.4027336	0.0443696	2.128686
H	-7.0075102	-0.4761215	2.8649005
C	-9.3708424	0.0476353	1.4961635
H	-8.9936613	-0.9492421	1.7001823
C	-10.7444861	0.280195	1.4836927
H	-11.4342102	-0.5343417	1.69825

Atom	x /Å	y /Å	z /Å
N	0.5353358	2.02702	2.3388766
C	1.2757169	2.5533737	3.4276095
C	0.7209464	2.5338094	4.718248
H	-0.2936045	2.1758502	4.8509913
C	1.4557046	2.9903576	5.8134422
H	1.0027319	2.9757314	6.8008732
C	2.7537456	3.4755548	5.6457184
H	3.3216537	3.8340652	6.4987793
C	3.3125923	3.4982002	4.365834
H	4.3213095	3.8743844	4.2190453
C	2.5871029	3.0356259	3.269334
H	3.0290123	3.0496691	2.2791926
C	1.4054406	4.8199794	0.2844319
H	1.9325314	4.2072065	-0.4394393
C	1.5941225	6.2005149	0.2835247
H	2.2641962	6.6660494	-0.4300501
Br	1.1521272	8.8756398	1.2113498
Br	-1.1521272	-8.8756398	1.2113498

Table III-S4. Optimized atomic coordinates obtained from DFT for **3-3** singlet ground state (b3lyp/LanL2DZ(f)[Rh] 6-31G**[C,H,N,Br]); E = -6901.92471098 Hartree.

Atom	x /Å	y /Å	z /Å
Rh	0	0	0
Rh	0	0	2.4227403
N	2.0967919	0	0.0836546
N	-0.0001549	-2.0967685	0.0837415
N	-1.4642434	-11.3025359	1.207783
C	2.7948091	0.5812152	-1.0051777
C	2.6359939	0.0484505	-2.2954529
H	2.0320658	-0.8419259	-2.4279144
C	3.2651465	0.6421293	-3.3906628
H	3.1367185	0.2068526	-4.3778092
C	4.0640456	1.7744825	-3.223317
H	4.5557702	2.2318992	-4.0763949
C	4.2268984	2.3103941	-1.9437825
H	4.8469209	3.1905562	-1.7972842
C	3.5943179	1.7271726	-0.8472837
H	3.7193268	2.1518863	0.1425981
C	2.7213962	-0.3522671	1.2113701
C	4.2144151	-0.5455287	1.2113701
C	4.8207349	-1.404719	0.2853138
H	4.2080961	-1.9328052	-0.437946
C	6.2013487	-1.5928393	0.2844252
H	6.66707	-2.2634627	-0.4285122
C	6.9803421	-0.9035599	1.2113701
C	0.5821193	-2.7943879	-1.0045096
C	0.0515917	-2.6344166	-2.2955899
H	-0.8387258	-2.0305554	-2.4288946
C	0.6472756	-3.2623346	-3.3904062
H	0.2137356	-3.1329347	-4.3781984
C	1.7796293	-4.0610623	-3.222029
H	2.2388865	-4.5514063	-4.0749171
C	2.3132696	-4.2252917	-1.9416955
H	3.1935729	-4.8450039	-1.7944541
C	1.7278571	-3.5941397	-0.8454896
H	2.150247	-3.7206743	0.1452124
C	-0.3522658	-2.7219492	1.211458
C	-0.5458064	-4.214696	1.2111392
C	0.1314008	-5.0231459	2.1338993
H	0.7934543	-4.5653035	2.86147
C	-0.0420003	-6.403435	2.1268694
H	0.4792068	-7.0084814	2.8623567
C	-0.9093273	-7.0196556	1.2098523
C	-1.0998512	-8.4902177	1.2091326
C	-0.0451587	-9.371214	1.4930982
H	0.9517268	-8.9939171	1.6968435
C	-0.2773795	-10.7449094	1.4799562
H	0.5373793	-11.4345499	1.6939199
N	2.0276838	-0.5338866	2.3390857
C	2.5547056	-1.2736752	3.427918
C	2.5367777	-0.7180322	4.7181932
H	2.1794627	0.2967709	4.8506547
C	2.9940312	-1.4523392	5.8134031
H	2.9806665	-0.9987084	6.8005495
C	3.4782788	-2.7507874	5.6460573
H	3.8373289	-3.3183314	6.4991352
C	3.49931	-3.3105016	4.3665228
H	3.8747897	-4.319525	4.2200245
C	3.0360789	-2.5854344	3.270024
H	3.0488267	-3.0279798	2.2801422
C	5.0195189	0.130962	2.1374265
H	4.5615337	0.7976336	2.8606863
C	6.4025283	-0.0386507	2.1383151
H	7.0236544	0.4912873	2.8512525
N	-0.5335456	-2.0277708	2.3391077
C	-1.2725955	-2.5549603	3.42816
C	-0.7165045	-2.5370384	4.7182737
H	0.2985462	-2.180233	4.8502279
C	-1.4504859	-2.9939455	5.8138108
H	-0.9964931	-2.9805918	6.8007943
C	-2.7492203	-3.4777095	5.6470686
H	-3.3166607	-3.8361129	6.5005034
C	-3.3093633	-3.4987153	4.3677238
H	-4.3188469	-3.8733335	4.2218535
C	-2.5845508	-3.0360249	3.2708171
H	-3.0271868	-3.0487113	2.2809779
C	-1.4066315	-4.822967	0.2877283
H	-1.9298033	-4.2107746	-0.4394767
C	-1.5908181	-6.201866	0.2935011
H	-2.2487581	-6.653449	-0.4426229
C	-2.3442014	-9.0730768	0.9244402
H	-3.2119673	-8.4539719	0.7210907
C	-2.4697516	-10.4605949	0.9362522
H	-3.433331	-10.9196349	0.7216961
N	-2.0964834	0.0004248	0.0836534
N	0.0003519	2.0967893	0.0836326
N	-11.3025326	1.4630394	1.2113701
N	1.4618759	11.3028423	1.2149573
C	-2.794044	-0.5798549	-1.0057186
C	-2.6329901	-0.0475054	-2.2959359
H	-2.0282137	0.8424183	-2.4276293
C	-3.2611994	-0.6407147	-3.3918983

Atom	x /Å	y /Å	z /Å
H	-3.130986	-0.2057504	-4.3789538
C	-4.0613196	-1.772377	-3.2255157
H	-4.5519789	-2.22968	-4.079283
C	-4.2263096	-2.3079192	-1.9460985
H	-4.8467875	-3.1879663	-1.8005118
C	-3.5948153	-1.7250898	-0.848753
H	-3.7213117	-2.1494112	0.1411011
C	-2.7216927	0.3523054	1.2113701
C	-4.2144923	0.5455386	1.2113701
C	-4.8233281	1.4061197	0.2881056
H	-4.2115747	1.9292896	-0.4394618
C	-6.202254	1.5900969	0.2944636
H	-6.6542364	2.2478623	-0.4415726
C	-7.0195461	0.9086346	1.2113702
C	-8.4901293	1.0989921	1.2113702
C	-9.073291	2.3431751	0.9261897
H	-8.4543994	3.2108962	0.7220225
C	-10.4608183	2.4685867	0.9386801
H	-10.9200814	3.4319748	0.7237676
C	-0.5801063	2.7947805	-1.0054197
C	-0.0469068	2.6358571	-2.2955334
H	0.8438388	2.0323587	-2.4274876
C	-0.6403589	3.2645918	-3.3910705
H	-0.2047294	3.1360823	-4.378054
C	-1.773112	4.0630961	-3.2243283
H	-2.2305932	4.5541689	-4.0777632
C	-2.3094448	4.2260335	-1.9449835
H	-3.1902712	4.8453401	-1.7991132
C	-1.7263318	3.5940407	-0.8480768
H	-2.1511489	3.7190132	0.1417624
C	0.3524091	2.7219307	1.2112823
C	0.5453316	4.2147575	1.2116011
C	-0.1322432	5.0221644	2.135012
H	-0.7940487	4.5633596	2.862217
C	0.040737	6.4025139	2.1292392
H	-0.4805356	7.0067384	2.8653632
C	0.9079927	7.0198283	1.212888
C	1.0981838	8.4904336	1.2136077
C	0.0432541	9.3709195	1.4983001
H	-0.953548	8.9931708	1.7016496
C	0.2751327	10.744674	1.4864881
H	-0.539807	11.4339318	1.7010442

Atom	x /Å	y /Å	z /Å
N	-2.0274935	0.5333972	2.3390869
C	-2.5543121	1.2721648	3.4284588
C	-2.5341135	0.7163534	4.7186762
H	-2.1758629	-0.2982279	4.8503696
C	-2.9905744	1.4499662	5.8146386
H	-2.9754036	0.9961828	6.8016941
C	-3.4761788	2.7480572	5.648256
H	-3.8342276	3.31522	6.5020233
C	-3.4993708	3.3079583	4.3688388
H	-3.8753201	4.3169865	4.2232521
C	-3.0370903	2.5835469	3.2714933
H	-3.0513765	3.0260917	2.2816392
C	-5.0223832	-0.1316563	2.1346347
H	-4.5640025	-0.7933481	2.8622021
C	-6.4027055	0.0415333	2.1282767
H	-7.0072717	-0.4794688	2.8643129
C	-9.3708653	0.0443012	1.4965506
H	-8.9933115	-0.9524033	1.7007178
C	-10.7445935	0.2763161	1.4840602
H	-11.4340182	-0.5383818	1.6989726
N	0.5337308	2.0277006	2.3389988
C	1.2744421	2.5540681	3.4272499
C	0.7206682	2.5344526	4.7183302
H	-0.2940608	2.1771873	4.8516349
C	1.4566	2.9900016	5.8131465
H	1.004401	2.9752548	6.8009387
C	2.755005	3.4740833	5.6447693
H	3.3239773	3.8313297	6.4976574
C	3.3128732	3.4970241	4.3644358
H	4.3219542	3.8721678	4.2171944
C	2.586051	3.0357324	3.2682299
H	3.0267376	3.0505473	2.2775279
C	1.4060668	4.8241307	0.288841
H	1.9297236	4.2128059	-0.4387297
C	1.589831	6.2030784	0.2958709
H	2.2479169	6.655473	-0.4396164
C	2.3424346	9.0738466	0.9296421
H	3.2103962	8.4551573	0.7258968
C	2.4676387	10.4613946	0.9427841
H	3.4311407	10.9208508	0.7288204
Br	8.8763755	-1.1489891	1.2113701

Table III-S5. Optimized atomic coordinates obtained from DFT for **3-4** singlet ground state (b3lyp/LanL2DZ(f)[Rh] 6-31G**[C,H,N]); E = -4577.92004131 Hartree.

Atom	x /Å	y /Å	z /Å
Rh	0	0	0
Rh	0	0	2.4227565
N	2.0967505	0	0.0834776
N	0	-2.0967505	0.0834776
N	11.3037506	-1.4562609	1.2113782
N	-1.4562609	-11.3037506	1.2113782
C	2.7942147	0.5801447	-1.0060459
C	2.6349252	0.0463579	-2.2958793
H	2.0314912	-0.8445128	-2.4272334
C	3.2630704	0.6395096	-3.3919156
H	3.1342219	0.2034609	-4.3786713
C	4.0613888	1.772515	-3.225983
H	4.5519972	2.2297611	-4.0798116

Atom	x /Å	y /Å	z /Å
C	4.2246924	2.3094424	-1.946928
H	4.8437943	3.1905172	-1.801689
C	3.5932514	1.726658	-0.8495316
H	3.718415	2.1520094	0.1400577
C	2.7222008	-0.3507008	1.2113782
C	4.2151386	-0.5430358	1.2113782
C	4.8244196	-1.4040479	0.2888948
H	4.2129084	-1.9282889	-0.4381056
C	6.2034603	-1.5871617	0.2952451
H	6.6557506	-2.2453609	-0.4402143
C	7.020434	-0.9044417	1.2113782
C	8.4911303	-1.0939113	1.2113782
C	9.0750302	-2.3379164	0.9274292

Atom	x /Å	y /Å	z /Å
H	8.4566522	-3.2062332	0.7242383
C	10.4626377	-2.4624732	0.9398677
H	10.9224502	-3.425807	0.7258826
C	0.5801447	-2.7942147	-1.0060459
C	0.0463579	-2.6349252	-2.2958793
H	-0.8445128	-2.0314912	-2.4272334
C	0.6395096	-3.2630704	-3.3919156
H	0.2034609	-3.1342219	-4.3786713
C	1.772515	-4.0613888	-3.225983
H	2.2297611	-4.5519972	-4.0798116
C	2.3094424	-4.2246924	-1.946928
H	3.1905172	-4.8437943	-1.801689
C	1.726658	-3.5932514	-0.8495316
H	2.1520094	-3.718415	0.1400577
C	-0.3507008	-2.7222008	1.2113782
C	-0.5430358	-4.2151386	1.2113782
C	0.135438	-5.0227514	2.1338617
H	0.7975507	-4.564078	2.8608621
C	-0.0369495	-6.4031739	2.1275113
H	0.4851234	-7.0075186	2.8629707
C	-0.9044417	-7.020434	1.2113782
C	-1.0939114	-8.4911303	1.2113782
C	-0.0385173	-9.3712616	1.4953273
H	0.9581768	-8.9931526	1.6985181
C	-0.2697211	-10.7451297	1.4828888
H	0.5456167	-11.4340882	1.6968738
N	2.0282867	-0.5314281	2.3392788
C	2.5559375	-1.2694042	3.4288024
C	2.5371392	-0.7126744	4.7186358
H	2.1792027	0.3020496	4.8499898
C	2.9944378	-1.4456636	5.814672
H	2.9803144	-0.9911959	6.8014277
C	3.4795253	-2.7440101	5.6487394
H	3.8382238	-3.3106723	6.502568
C	3.5014108	-3.3047954	4.3696845
H	3.8769863	-4.3140144	4.2244455
C	3.0382963	-2.5809996	3.272288
H	3.0515664	-3.0241853	2.2826988
C	5.0227514	0.135438	2.1338617
H	4.564078	0.7975507	2.8608621
C	6.4031739	-0.0369495	2.1275113
H	7.0075186	0.4851234	2.8629707
C	9.3712616	-0.0385173	1.4953273
H	8.9931526	0.9581768	1.6985181
C	10.7451297	-0.2697211	1.4828888
H	11.4340882	0.5456167	1.6968738
N	-0.5314281	-2.0282867	2.3392788
C	-1.2694042	-2.5559375	3.4288024
C	-0.7126744	-2.5371392	4.7186358
H	0.3020496	-2.1792027	4.8499898
C	-1.4456636	-2.9944378	5.814672
H	-0.9911959	-2.9803144	6.8014277
C	-2.7440101	-3.4795253	5.6487394
H	-3.3106723	-3.8382238	6.502568
C	-3.3047954	-3.5014108	4.3696845
H	-4.3140144	-3.8769863	4.2244455
C	-2.5809996	-3.0382963	3.272288
H	-3.0241853	-3.0515664	2.2826988
C	-1.4040479	-4.8244196	0.2888948
H	-1.9282889	-4.2129084	-0.4381056
C	-1.5871617	-6.2034603	0.2952451
H	-2.2453609	-6.6557506	-0.4402143
C	-2.3379164	-9.0750302	0.9274292
H	-3.2062332	-8.4566522	0.7242383

Atom	x /Å	y /Å	z /Å
C	-2.4624732	-10.4626377	0.9398677
H	-3.425807	-10.9224502	0.7258826
N	-2.0967505	0	0.0834776
N	0	2.0967505	0.0834776
N	-11.3037506	1.4562609	1.2113782
N	1.4562609	11.3037506	1.2113782
C	-2.7942147	-0.5801447	-1.0060459
C	-2.6349252	-0.0463579	-2.2958793
H	-2.0314912	0.8445128	-2.4272334
C	-3.2630704	-0.6395096	-3.3919156
H	-3.1342219	-0.2034609	-4.3786713
C	-4.0613888	-1.772515	-3.225983
H	-4.5519972	-2.2297611	-4.0798116
C	-4.2246924	-2.3094424	-1.946928
H	-4.8437943	-3.1905172	-1.801689
C	-3.5932514	-1.726658	-0.8495316
H	-3.718415	-2.1520094	0.1400577
C	-2.7222008	0.3507008	1.2113782
C	-4.2151386	0.5430358	1.2113782
C	-4.8244196	1.4040479	0.2888948
H	-4.2129084	1.9282889	-0.4381056
C	-6.2034603	1.5871617	0.2952451
H	-6.6557506	2.2453609	-0.4402143
C	-7.020434	0.9044417	1.2113782
C	-8.4911303	1.0939113	1.2113782
C	-9.0750302	2.3379164	0.9274292
H	-8.4566522	3.2062332	0.7242383
C	-10.4626377	2.4624732	0.9398677
H	-10.9224502	3.425807	0.7258826
C	-0.5801447	2.7942147	-1.0060459
C	-0.0463579	2.6349252	-2.2958793
H	0.8445128	2.0314912	-2.4272334
C	-0.6395096	3.2630704	-3.3919156
H	-0.2034609	3.1342219	-4.3786713
C	-1.772515	4.0613888	-3.225983
H	-2.2297611	4.5519972	-4.0798116
C	-2.3094424	4.2246924	-1.946928
H	-3.1905172	4.8437943	-1.801689
C	-1.726658	3.5932514	-0.8495316
H	-2.1520094	3.718415	0.1400577
C	0.3507008	2.7222008	1.2113782
C	0.5430358	4.2151386	1.2113782
C	-0.135438	5.0227514	2.1338617
H	-0.7975507	4.564078	2.8608621
C	0.0369495	6.4031739	2.1275113
H	-0.4851234	7.0075186	2.8629707
C	0.9044417	7.020434	1.2113782
C	1.0939114	8.4911303	1.2113782
C	0.0385173	9.3712616	1.4953273
H	-0.9581768	8.9931526	1.6985181
C	0.2697211	10.7451297	1.4828888
H	-0.5456167	11.4340882	1.6968739
N	-2.0282867	0.5314281	2.3392788
C	-2.5559375	1.2694042	3.4288024
C	-2.5371392	0.7126744	4.7186358
H	-2.1792027	-0.3020496	4.8499898
C	-2.9944378	1.4456636	5.814672
H	-2.9803144	0.9911959	6.8014277
C	-3.4795253	2.7440101	5.6487394
H	-3.8382238	3.3106723	6.502568
C	-3.5014108	3.3047954	4.3696845
H	-3.8769863	4.3140144	4.2244455
C	-3.0382963	2.5809996	3.272288
H	-3.0515664	3.0241853	2.2826988

Atom	x /Å	y /Å	z /Å
C	-5.0227514	-0.135438	2.1338617
H	-4.564078	-0.7975507	2.8608621
C	-6.4031739	0.0369495	2.1275113
H	-7.0075186	-0.4851234	2.8629707
C	-9.3712616	0.0385173	1.4953273
H	-8.9931526	-0.9581768	1.6985181
C	-10.7451297	0.2697211	1.4828887
H	-11.4340882	-0.5456166	1.6968738
N	0.5314281	2.0282867	2.3392788
C	1.2694042	2.5559375	3.4288024
C	0.7126744	2.5371392	4.7186358
H	-0.3020496	2.1792027	4.8499898
C	1.4456636	2.9944378	5.814672
H	0.9911959	2.9803144	6.8014277
C	2.7440101	3.4795253	5.6487394
H	3.3106723	3.8382238	6.502568
C	3.3047954	3.5014108	4.3696845
H	4.3140144	3.8769863	4.2244455
C	2.5809996	3.0382963	3.272288
H	3.0241853	3.0515664	2.2826988
C	1.4040479	4.8244196	0.2888948
H	1.9282889	4.2129084	-0.4381056
C	1.5871617	6.2034603	0.2952451
H	2.2453609	6.6557506	-0.4402143
C	2.3379164	9.0750302	0.9274292
H	3.2062332	8.4566522	0.7242383
C	2.4624732	10.4626377	0.9398677
H	3.425807	10.9224502	0.7258826

Table III-S6. Optimized atomic coordinates obtained from DFT for **3-5** singlet ground state (b3lyp/LanL2DZ(f)[Rh] 6-31G**[C,H,N,Br]); E = -13873.93792480 Hartree.

Atom	x /Å	y /Å	z /Å
Rh	0	0	1.211702
Rh	0	0	-1.211702
N	0.266446	2.078908	1.128826
N	-0.266446	2.078908	-1.128826
C	-0.788251	4.971969	0.901036
H	-1.415107	4.460227	1.623349
C	0	4.248163	0
C	0.788251	4.971969	-0.901036
H	1.415107	4.460227	-1.623349
C	0.755482	6.365035	-0.853827
H	1.367828	6.946213	-1.540969
C	-0.755482	6.365035	0.853827
H	-1.367828	6.946213	1.540969
N	0	7.06734	0
C	0	2.740564	0
C	-0.923522	2.700898	-2.221369
C	-0.364231	2.616008	-3.507214
H	0.597092	2.131456	-3.634136
C	-1.025206	3.168745	-4.604974
H	-0.569812	3.101203	-5.589011
C	-2.251567	3.815998	-4.443951
H	-2.761357	4.248855	-5.299175
C	-2.814051	3.904336	-3.168659
H	-3.766964	4.406718	-3.027526
C	-2.163206	3.346436	-2.069511
H	-2.608447	3.411253	-1.082767
C	0.923522	2.700898	2.221369
C	0.364231	2.616008	3.507214
H	-0.597092	2.131456	3.634136
C	1.025206	3.168745	4.604974
H	0.569812	3.101203	5.589011
C	2.251567	3.815998	4.443951
H	2.761357	4.248855	5.299175
C	2.814051	3.904336	3.168659
H	3.766964	4.406718	3.027526
C	2.163206	3.346436	2.069511
H	2.608447	3.411253	1.082767
N	2.078908	-0.266446	1.128826
N	2.078908	0.266446	-1.128826
C	4.971969	0.788251	0.901036
H	4.460227	1.415107	1.623349
C	4.248163	0	0
C	4.971969	-0.788251	-0.901036
H	4.460227	-1.415107	-1.623349
C	6.365035	-0.755482	-0.853827
H	6.946213	-1.367828	-1.540969
C	6.365035	0.755482	0.853827
H	6.946213	1.367828	1.540969
N	7.06734	0	0
C	2.740564	0	0
C	2.700898	0.923522	-2.221369
C	2.616008	0.364231	-3.507214
H	2.131456	-0.597092	-3.634136
C	3.168745	1.025206	-4.604974
H	3.101203	0.569812	-5.589011
C	3.815998	2.251567	-4.443951
H	4.248855	2.761357	-5.299175
C	3.904336	2.814051	-3.168659
H	4.406718	3.766964	-3.027526
C	3.346436	2.163206	-2.069511
H	3.411253	2.608447	-1.082767
C	2.700898	-0.923522	2.221369
C	2.616008	-0.364231	3.507214
H	2.131456	0.597092	3.634136
C	3.168745	-1.025206	4.604974
H	3.101203	-0.569812	5.589011
C	3.815998	-2.251567	4.443951
H	4.248855	-2.761357	5.299175
C	3.904336	-2.814051	3.168659
H	4.406718	-3.766964	3.027526
C	3.346436	-2.163206	2.069511
H	3.411253	-2.608447	1.082767
N	-0.266446	-2.078908	1.128826
N	0.266446	-2.078908	-1.128826
C	0.788251	-4.971969	0.901036
H	1.415107	-4.460227	1.623349
C	0	-4.248163	0
C	-0.788251	-4.971969	-0.901036
H	-1.415107	-4.460227	-1.623349
C	-0.755482	-6.365035	-0.853827

Atom	x /Å	y /Å	z /Å
H	-1.367828	-6.946213	-1.540969
C	0.755482	-6.365035	0.853827
H	1.367828	-6.946213	1.540969
N	0	-7.06734	0
C	0	-2.740564	0
C	0.923522	-2.700898	-2.221369
C	0.364231	-2.616008	-3.507214
H	-0.597092	-2.131456	-3.634136
C	1.025206	-3.168745	-4.604974
H	0.569812	-3.101203	-5.589011
C	2.251567	-3.815998	-4.443951
H	2.761357	-4.248855	-5.299175
C	2.814051	-3.904336	-3.168659
H	3.766964	-4.406718	-3.027526
C	2.163206	-3.346436	-2.069511
H	2.608447	-3.411253	-1.082767
C	-0.923522	-2.700898	2.221369
C	-0.364231	-2.616008	3.507214
H	0.597092	-2.131456	3.634136
C	-1.025206	-3.168745	4.604974
H	-0.569812	-3.101203	5.589011
C	-2.251567	-3.815998	4.443951
H	-2.761357	-4.248855	5.299175
C	-2.814051	-3.904336	3.168659
H	-3.766964	-4.406718	3.027526
C	-2.163206	-3.346436	2.069511
H	-2.608447	-3.411253	1.082767
N	-2.078908	0.266446	1.128826
N	-2.078908	-0.266446	-1.128826
C	-4.971969	-0.788251	0.901036
H	-4.460227	-1.415107	1.623349
C	-4.248163	0	0
C	-4.971969	0.788251	-0.901036
H	-4.460227	1.415107	-1.623349
C	-6.365035	0.755482	-0.853827
H	-6.946213	1.367828	-1.540969
C	-6.365035	-0.755482	0.853827
H	-6.946213	-1.367828	1.540969
N	-7.06734	0	0
C	-2.740564	0	0
C	-2.700898	-0.923522	-2.221369
C	-2.616008	-0.364231	-3.507214
H	-2.131456	0.597092	-3.634136
C	-3.168745	-1.025206	-4.604974
H	-3.101203	-0.569812	-5.589011
C	-3.815998	-2.251567	-4.443951
H	-4.248855	-2.761357	-5.299175
C	-3.904336	-2.814051	-3.168659
H	-4.406718	-3.766964	-3.027526
C	-3.346436	-2.163206	-2.069511
H	-3.411253	-2.608447	-1.082767
C	-2.700898	0.923522	2.221369
C	-2.616008	0.364231	3.507214
H	-2.131456	-0.597092	3.634136
C	-3.168745	1.025206	4.604974
H	-3.101203	0.569812	5.589011
C	-3.815998	2.251567	4.443951
H	-4.248855	2.761357	5.299175
C	-3.904336	2.814051	3.168659
H	-4.406718	3.766964	3.027526
C	-3.346436	2.163206	2.069511
H	-3.411253	2.608447	1.082767

Table III-S7. Optimized atomic coordinates obtained from DFT for **3-6** singlet ground state (b3lyp/LanL2DZ(f)[Rh] 6-31G**[C,H,N]); E = -3653.66095020 Hartree.

Atom	x /Å	y /Å	z /Å
Rh	0	0	0
Rh	0	0	2.4085721
N	2.09587	0	0.080846
N	2.0279335	-0.5292986	2.3277261
C	4.824602	-1.385543	0.270745
H	4.213589	-1.904428	-0.460252
C	4.2162866	-0.541169	1.204286
C	5.018125	0.1222089	2.1378271
H	4.5579588	0.7785819	2.8688241
C	6.403974	-0.044007	2.143488
H	7.023983	0.476491	2.864243
C	6.2075062	-1.5747022	0.2650841
H	6.6759694	-2.2349079	-0.4556709
C	2.7231773	-0.3495254	1.204286
C	2.552147	-1.270133	3.423299
C	2.540579	-0.724017	4.717657
H	2.196686	0.294351	4.859045
C	2.986773	-1.473226	5.807493
H	2.977768	-1.02718	6.798154
C	3.453762	-2.776799	5.631095
H	3.803373	-3.355742	6.480383
C	3.470367	-3.326304	4.346986
H	3.833423	-4.338699	4.192625
C	3.018253	-2.586307	3.255913
H	3.027047	-3.020602	2.262171
C	2.7901844	0.5844339	-1.0147269
C	2.6410733	0.0589414	-2.3090849
H	2.0511451	-0.8395688	-2.4504729
C	3.2620121	0.6711817	-3.3989209
H	3.1406529	0.2418682	-4.3895819
C	4.0430729	1.8145649	-3.2225229
H	4.5275598	2.2864498	-4.0718109
C	4.1979137	2.3420645	-1.9384139
H	4.8048753	3.2299558	-1.7840529
C	3.5735732	1.7402327	-0.8473409
H	3.6917606	2.1582293	0.1464011
N	0	2.09587	0.080846
N	0.5292986	2.0279335	2.3277261
C	1.385543	4.824602	0.270745
H	1.904428	4.213589	-0.460252
C	0.541169	4.2162866	1.204286
C	-0.1222089	5.018125	2.1378271
H	-0.7785819	4.5579588	2.8688241
C	0.044007	6.403974	2.143488
H	-0.476491	7.023983	2.864243
C	1.5747022	6.2075062	0.2650841

Atom	x /Å	y /Å	z /Å
H	2.2349079	6.6759694	-0.4556709
C	0.3495254	2.7231773	1.204286
C	1.270133	2.552147	3.423299
C	0.724017	2.540579	4.717657
H	-0.294351	2.196686	4.859045
C	1.473226	2.986773	5.807493
H	1.02718	2.977768	6.798154
C	2.776799	3.453762	5.631095
H	3.355742	3.803373	6.480383
C	3.326304	3.470367	4.346986
H	4.338699	3.833423	4.192625
C	2.586307	3.018253	3.255913
H	3.020602	3.027047	2.262171
C	-0.5844339	2.7901844	-1.0147269
C	-0.0589414	2.6410733	-2.3090849
H	0.8395688	2.0511451	-2.4504729
C	-0.6711817	3.2620121	-3.3989209
H	-0.2418682	3.1406529	-4.3895819
C	-1.8145649	4.0430729	-3.2225229
H	-2.2864498	4.5275598	-4.0718109
C	-2.3420645	4.1979137	-1.9384139
H	-3.2299558	4.8048753	-1.7840529
C	-1.7402327	3.5735732	-0.8473409
H	-2.1582293	3.6917606	0.1464011
N	-2.09587	0	0.080846
N	-2.0279335	0.5292986	2.3277261
C	-4.824602	1.385543	0.270745
H	-4.213589	1.904428	-0.460252
C	-4.2162866	0.541169	1.204286
C	-5.018125	-0.1222089	2.1378271
H	-4.5579588	-0.7785819	2.8688241
C	-6.403974	0.044007	2.143488
H	-7.023983	-0.476491	2.864243
C	-6.2075062	1.5747022	0.2650841
H	-6.6759694	2.2349079	-0.4556709
C	-2.7231773	0.3495254	1.204286
C	-2.552147	1.270133	3.423299
C	-2.540579	0.724017	4.717657
H	-2.196686	-0.294351	4.859045
C	-2.986773	1.473226	5.807493
H	-2.977768	1.02718	6.798154
C	-3.453762	2.776799	5.631095
H	-3.803373	3.355742	6.480383
C	-3.470367	3.326304	4.346986
H	-3.833423	4.338699	4.192625
C	-3.018253	2.586307	3.255913
H	-3.027047	3.020602	2.262171
C	-2.7901844	-0.5844339	-1.0147269
C	-2.6410733	-0.0589414	-2.3090849
H	-2.0511451	0.8395688	-2.4504729

Atom	x /Å	y /Å	z /Å
C	-3.2620121	-0.6711817	-3.3989209
H	-3.1406529	-0.2418682	-4.3895819
C	-4.0430729	-1.8145649	-3.2225229
H	-4.5275598	-2.2864498	-4.0718109
C	-4.1979137	-2.3420645	-1.9384139
H	-4.8048753	-3.2299558	-1.7840529
C	-3.5735732	-1.7402327	-0.8473409
H	-3.6917606	-2.1582293	0.1464011
N	0	-2.09587	0.080846
N	-0.5292986	-2.0279335	2.3277261
C	-1.385543	-4.824602	0.270745
H	-1.904428	-4.213589	-0.460252
C	-0.541169	-4.2162866	1.204286
C	0.1222089	-5.018125	2.1378271
H	0.7785819	-4.5579588	2.8688241
C	-0.044007	-6.403974	2.143488
H	0.476491	-7.023983	2.864243
C	-1.5747022	-6.2075062	0.2650841
H	-2.2349079	-6.6759694	-0.4556709
C	-0.3495254	-2.7231773	1.204286
C	-1.270133	-2.552147	3.423299
C	-0.724017	-2.540579	4.717657
H	0.294351	-2.196686	4.859045
C	-1.473226	-2.986773	5.807493
H	-1.02718	-2.977768	6.798154
C	-2.776799	-3.453762	5.631095
H	-3.355742	-3.803373	6.480383
C	-3.326304	-3.470367	4.346986
H	-4.338699	-3.833423	4.192625
C	-2.586307	-3.018253	3.255913
H	-3.020602	-3.027047	2.262171
C	0.5844339	-2.7901844	-1.0147269
C	0.0589414	-2.6410733	-2.3090849
H	-0.8395688	-2.0511451	-2.4504729
C	0.6711817	-3.2620121	-3.3989209
H	0.2418682	-3.1406529	-4.3895819
C	1.8145649	-4.0430729	-3.2225229
H	2.2864498	-4.5275598	-4.0718109
C	2.3420645	-4.1979137	-1.9384139
H	3.2299558	-4.8048753	-1.7840529
C	1.7402327	-3.5735732	-0.8473409
H	2.1582293	-3.6917606	0.1464011
C	6.9830941	-0.8962944	1.204286
C	0.8962944	6.9830941	1.204286
C	-6.9830941	0.8962944	1.204286
C	-0.8962944	-6.9830941	1.204286
Br	8.8793449	-1.139682	1.204286
Br	1.139682	8.8793449	1.204286
Br	-8.8793449	1.139682	1.204286
Br	-1.139682	-8.8793449	1.204286

Table III-S8. Optimized atomic coordinates obtained from DFT for **3-7** singlet ground state (b3lyp/LanL2DZ(f)[Rh] 6-31G**[C,H,N]); E = -3589.52443365 Hartree.

Atom	x /Å	y /Å	z /Å
Rh	0	0	1.2115789
Rh	0	0	-1.2115789
N	0.2653935	2.0805471	1.1281224
N	-0.2653935	2.0805471	-1.1281224
C	-0.7863867	4.961969	0.9180613

Atom	x /Å	y /Å	z /Å
H	-1.3949187	4.4173336	1.6326917
C	0	4.2524185	0
C	0.7863867	4.961969	-0.9180613
H	1.3949187	4.4173336	-1.6326917
C	0.7908293	6.3560052	-0.9121325

Atom	x /Å	y /Å	z /Å
H	1.4101729	6.8949335	-1.623309
C	-0.7908293	6.3560052	0.9121325
H	-1.4101729	6.8949335	1.623309
C	0	2.7466148	0
C	-0.9259096	2.6977693	-2.2198748
C	-0.3730908	2.6055216	-3.5082694
H	0.5876184	2.1201972	-3.636304
C	-1.038711	3.1506174	-4.6071445
H	-0.5871727	3.0758892	-5.5926156
C	-2.2646602	3.7982412	-4.4457607
H	-2.7790165	4.2242604	-5.3019109
C	-2.8208666	3.8946538	-3.1680672
H	-3.7741514	4.3964042	-3.0257797
C	-2.1650698	3.3451642	-2.0679687
H	-2.604953	3.4179855	-1.079609
C	0.9259096	2.6977693	2.2198748
C	0.3730908	2.6055216	3.5082694
H	-0.5876184	2.1201972	3.636304
C	1.038711	3.1506174	4.6071445
H	0.5871727	3.0758892	5.5926156
C	2.2646602	3.7982412	4.4457607
H	2.7790165	4.2242604	5.3019109
C	2.8208666	3.8946538	3.1680672
H	3.7741514	4.3964042	3.0257797
C	2.1650698	3.3451642	2.0679687
H	2.604953	3.4179855	1.079609
N	2.0805471	-0.2653935	1.1281224
N	2.0805471	0.2653935	-1.1281224
C	4.961969	0.7863867	0.9180613
H	4.4173336	1.3949187	1.6326917
C	4.2524185	0	0
C	4.961969	-0.7863867	-0.9180613
H	4.4173336	-1.3949187	-1.6326917
C	6.3560052	-0.7908293	-0.9121325
H	6.8949335	-1.4101729	-1.623309
C	6.3560052	0.7908293	0.9121325
H	6.8949335	1.4101729	1.623309
C	2.7466148	0	0
C	2.6977693	0.9259096	-2.2198748
C	2.6055216	0.3730908	-3.5082694
H	2.1201972	-0.5876184	-3.636304
C	3.1506174	1.038711	-4.6071445
H	3.0758892	0.5871727	-5.5926156
C	3.7982412	2.2646602	-4.4457607
H	4.2242604	2.7790165	-5.3019109
C	3.8946538	2.8208666	-3.1680672
H	4.3964042	3.7741514	-3.0257797
C	3.3451642	2.1650698	-2.0679687
H	3.4179855	2.604953	-1.079609
C	2.6977693	-0.9259096	2.2198748
C	2.6055216	-0.3730908	3.5082694
H	2.1201972	0.5876184	3.636304
C	3.1506174	-1.038711	4.6071445
H	3.0758892	-0.5871727	5.5926156
C	3.7982412	-2.2646602	4.4457607
H	4.2242604	-2.7790165	5.3019109
C	3.8946538	-2.8208666	3.1680672
H	4.3964042	-3.7741514	3.0257797
C	3.3451642	-2.1650698	2.0679687
H	3.4179855	-2.604953	1.079609
N	-0.2653935	-2.0805471	1.1281224
N	0.2653935	-2.0805471	-1.1281224
C	0.7863867	-4.961969	0.9180613
H	1.3949187	-4.4173336	1.6326917

Atom	x /Å	y /Å	z /Å
C	0	-4.2524185	0
C	-0.7863867	-4.961969	-0.9180613
H	-1.3949187	-4.4173336	-1.6326917
C	-0.7908293	-6.3560052	-0.9121325
H	-1.4101729	-6.8949335	-1.623309
C	0.7908293	-6.3560052	0.9121325
H	1.4101729	-6.8949335	1.623309
C	0	-2.7466148	0
C	0.9259096	-2.6977693	-2.2198748
C	0.3730908	-2.6055216	-3.5082694
H	-0.5876184	-2.1201972	-3.636304
C	1.038711	-3.1506174	-4.6071445
H	0.5871727	-3.0758892	-5.5926156
C	2.2646602	-3.7982412	-4.4457607
H	2.7790165	-4.2242604	-5.3019109
C	2.8208666	-3.8946538	-3.1680672
H	3.7741514	-4.3964042	-3.0257797
C	2.1650698	-3.3451642	-2.0679687
H	2.604953	-3.4179855	-1.079609
C	-0.9259096	-2.6977693	2.2198748
C	-0.3730908	-2.6055216	3.5082694
H	0.5876184	-2.1201972	3.636304
C	-1.038711	-3.1506174	4.6071445
H	-0.5871727	-3.0758892	5.5926156
C	-2.2646602	-3.7982412	4.4457607
H	-2.7790165	-4.2242604	5.3019109
C	-2.8208666	-3.8946538	3.1680672
H	-3.7741514	-4.3964042	3.0257797
C	-2.1650698	-3.3451642	2.0679687
H	-2.604953	-3.4179855	1.079609
N	-2.0805471	0.2653935	1.1281224
N	-2.0805471	-0.2653935	-1.1281224
C	-4.961969	-0.7863867	0.9180613
H	-4.4173336	-1.3949187	1.6326917
C	-4.2524185	0	0
C	-4.961969	0.7863867	-0.9180613
H	-4.4173336	1.3949187	-1.6326917
C	-6.3560052	0.7908293	-0.9121325
H	-6.8949335	1.4101729	-1.623309
C	-6.3560052	-0.7908293	0.9121325
H	-6.8949335	-1.4101729	1.623309
C	-2.7466148	0	0
C	-2.6977693	-0.9259096	-2.2198748
C	-2.6055216	-0.3730908	-3.5082694
H	-2.1201972	0.5876184	-3.636304
C	-3.1506174	-1.038711	-4.6071445
H	-3.0758892	-0.5871727	-5.5926156
C	-3.7982412	-2.2646602	-4.4457607
H	-4.2242604	-2.7790165	-5.3019109
C	-3.8946538	-2.8208666	-3.1680672
H	-4.3964042	-3.7741514	-3.0257797
C	-3.3451642	-2.1650698	-2.0679687
H	-3.4179855	-2.604953	-1.079609
C	-2.6977693	0.9259096	2.2198748
C	-2.6055216	0.3730908	3.5082694
H	-2.1201972	-0.5876184	3.636304
C	-3.1506174	1.038711	4.6071445
H	-3.0758892	0.5871727	5.5926156
C	-3.7982412	2.2646602	4.4457607
H	-4.2242604	2.7790165	5.3019109
C	-3.8946538	2.8208666	3.1680672
H	-4.3964042	3.7741514	3.0257797
C	-3.3451642	2.1650698	2.0679687
H	-3.4179855	2.604953	1.079609

Atom	x /Å	y /Å	z /Å
C	0	7.0569462	0
H	0	8.1431431	0
C	7.0569462	0	0
H	8.1431431	0	0

Atom	x /Å	y /Å	z /Å
C	0	-7.0569462	0
H	0	-8.1431431	0
C	-7.0569462	0	0
H	-8.1431431	0	0

Table III-S9. Optimized atomic coordinates obtained from DFT for **3-8** singlet ground state (b3lyp/LanL2DZ(f)[Rh] 6-31G**[C,H,N]); E = -3810.96292630 Hartree.

Atom	x /Å	y /Å	z /Å
Rh	0	0	0
Rh	0	0	2.421103
N	2.0981677	0	0.0810259
N	2.0313935	-0.5231863	2.3365384
C	4.8457992	-1.3479497	0.2590795
H	4.2453529	-1.8476944	-0.4938665
C	4.2183763	-0.5314601	1.2113724
C	5.0224288	0.0992267	2.1722001
H	4.5611222	0.7388354	2.9175762
C	6.4005632	-0.0753228	2.1826213
H	7.004777	0.433136	2.9299397
C	6.2217539	-1.5401154	0.2719881
H	6.6850042	-2.1837736	-0.4718657
C	2.730363	-0.3443081	1.2085226
C	2.5455911	-1.2795977	3.4177238
C	2.5248361	-0.7408701	4.7156041
H	2.1790012	0.2767785	4.857365
C	2.9620422	-1.4941318	5.8063592
H	2.9438294	-1.0519081	6.7988667
C	3.43074	-2.796816	5.6284447
H	3.77225	-3.3805225	6.4781453
C	3.456741	-3.3395828	4.3413411
H	3.8180743	-4.352603	4.1849304
C	3.0138937	-2.595538	3.2495229
H	3.0311894	-3.0269444	2.2547362
C	2.785182	0.5884438	-1.0089014
C	2.6310806	0.0535008	-2.2991538
H	2.0433877	-0.8479884	-2.4299944
C	3.244018	0.6588675	-3.3972754
H	3.1179411	0.2212213	-4.3838996
C	4.0228565	1.8054963	-3.233922
H	4.5011583	2.2728887	-4.0894915
C	4.1833531	2.3422207	-1.9540087
H	4.7885355	3.2331523	-1.8093374
C	3.5675	1.7471528	-0.8548409
H	3.6927682	2.1695946	0.1358782
N	0.0004018	2.0980211	0.081436
N	0.5234954	2.0309784	2.3368153
C	1.3475007	4.8451959	0.2579348
H	1.8462562	4.2445521	-0.4955013
C	0.5324615	4.2180833	1.2116083
C	-0.0959362	5.0228338	2.1735828
H	-0.7346993	4.5620379	2.9199947
C	0.0783861	6.4008066	2.183218
H	-0.429129	7.0053605	2.930909
C	1.5411417	6.2209227	0.2707096
H	2.1846279	6.6833202	-0.4738963
C	0.3448697	2.7303151	1.2089432
C	1.2787558	2.5439772	3.4191822
C	0.7400099	2.5173694	4.7169905
H	-0.2767756	2.1684188	4.8574018
C	1.4920129	2.9527778	5.8093052
H	1.0497974	2.9299063	6.8017181
C	2.7933882	3.4257289	5.6330558
H	3.3761168	3.7659785	6.4839325
C	3.3361731	3.4575389	4.3460603
H	4.3482261	3.822128	4.1909698
C	2.5934927	3.0162885	3.2526689
H	3.024904	3.0379157	2.2579968
C	-0.5882274	2.7844954	-1.0086481
C	-0.0542311	2.6285372	-2.2990778
H	0.8468833	2.0401754	-2.4296598
C	-0.6600147	3.240423	-3.3975605
H	-0.2231308	3.1128729	-4.3843356
C	-1.8061407	4.0200525	-3.234377
H	-2.273901	4.4975083	-4.0902196
C	-2.3419522	4.182359	-1.9542858
H	-3.2325439	4.788085	-1.8097885
C	-1.7464847	3.567537	-0.8547673
H	-2.1682586	3.6940494	0.1360777
N	-2.0983191	-0.000056	0.0811012
N	-2.0312585	0.5232849	2.3365786
C	-4.8468929	1.3458476	0.2598909
H	-4.2471	1.8460829	-0.4932491
C	-4.2185495	0.5299515	1.2120408
C	-5.0216564	-0.1013464	2.1732941
H	-4.5595281	-0.740649	2.9184369
C	-6.3999767	0.0718283	2.1839161
H	-7.0036835	-0.4373475	2.9311187
C	-6.2230499	1.5370299	0.2735454
H	-6.6871112	2.1807486	-0.4697446
C	-2.7303676	0.343935	1.2087295
C	-2.5452435	1.2798764	3.4176643
C	-2.5219911	0.7421671	4.7159295
H	-2.1741857	-0.2747806	4.8579252
C	-2.9590139	1.4955138	5.8066764
H	-2.9388523	1.0540718	6.7994945
C	-3.4299827	2.7973259	5.6283683
H	-3.7713828	3.3811215	6.4780517
C	-3.4583222	3.3391516	4.3409064
H	-3.8213231	4.35153	4.1842244
C	-3.015671	2.5950179	3.2490635
H	-3.0347713	3.0257114	2.2540016
C	-2.7854569	-0.5892968	-1.0083585
C	-2.6334397	-0.0538328	-2.2986199
H	-2.0474647	0.8487297	-2.4297412
C	-3.2462788	-0.6601149	-3.3962963
H	-3.1218585	-0.2220886	-4.3829639
C	-4.0228694	-1.8082053	-3.2324638
H	-4.5009927	-2.2763555	-4.0877163

Atom	x /Å	y /Å	z /Å
C	-4.1814097	-2.3453608	-1.9524863
H	-4.7849206	-3.2373615	-1.8074297
C	-3.565719	-1.7493078	-0.8537591
H	-3.6895461	-2.1719777	0.1370536
N	-0.0003162	-2.0983294	0.081211
N	-0.5232607	-2.0311464	2.3366388
C	-1.3441838	-4.8480868	0.260059
H	-1.8438389	-4.2489388	-0.4939785
C	-0.5292383	-4.2188197	1.2125374
C	0.1021628	-5.0212857	2.1740982
H	0.7405083	-4.558617	2.9197052
C	-0.0710083	-6.3996777	2.1856499
H	0.4368952	-7.0023347	2.9345866
C	-1.5335104	-6.2244191	0.2731558
H	-2.1743603	-6.6891807	-0.4721656
C	-0.3439265	-2.7305179	1.2089088
C	-1.2778853	-2.5446876	3.4191399
C	-0.7396924	-2.5156842	4.7171564
H	0.2761881	-2.164118	4.8576859
C	-1.4910854	-2.9518449	5.8095737
H	-1.0492824	-2.9270913	6.8021237
C	-2.791328	-3.4279051	5.6332903
H	-3.3735736	-3.7687545	6.4842557
C	-3.3336423	-3.4618772	4.346165
H	-4.3448995	-3.8286709	4.1910646
C	-2.5915949	-3.019866	3.2526363
H	-3.0227883	-3.0430718	2.2578956

Atom	x /Å	y /Å	z /Å
C	0.5878265	-2.7846569	-1.0092338
C	0.0527526	-2.6288745	-2.299238
H	-0.8484982	-2.0405794	-2.429106
C	0.6578328	-3.2406388	-3.3981582
H	0.2201426	-3.113268	-4.3845951
C	1.8043126	-4.0199257	-3.2358238
H	2.2715078	-4.4973283	-4.0920002
C	2.3412509	-4.1819391	-1.9561852
H	3.2321772	-4.7873322	-1.8123976
C	1.7464741	-3.5672351	-0.8562118
H	2.1692409	-3.6933193	0.1342621
C	7.025079	-0.9047653	1.2347674
C	0.9073375	7.0247325	1.2341319
C	-7.0254753	0.9007853	1.2363452
C	-0.8982485	-7.02625	1.237356
N	-8.4129835	1.0428766	1.2180532
H	-8.8736077	0.8793254	2.1026766
H	-8.7538039	1.879346	0.7644092
N	1.0499502	8.4110731	1.2146758
H	0.8880927	8.8754641	2.0973875
H	1.8805478	8.7532746	0.7520353
N	8.4118228	-1.0475464	1.2152436
H	8.8744675	-0.8779175	2.0975502
H	8.7528709	-1.8855396	0.7647698
N	-1.0388689	-8.4132772	1.2184859
H	-0.8738966	-8.8740244	2.1027254
H	-1.8744563	-8.755792	0.7646712

Table III-S10. Optimized atomic coordinates obtained from DFT for **3-9** singlet ground state (b3lyp/LanL2DZ(f)[Rh] 6-31G**[C,H,N]); E = -2665.32197248 Hartree.

Atom	x /Å	y /Å	z /Å
Rh	0	0	0
N	0	0	2.0915155
N	2.0915129	0	0.0033253
C	-0.4140486	1.1155877	2.852157
C	0.0907428	2.3942715	2.5560213
H	0.8279196	2.5047865	1.7681406
C	-0.3199819	3.5034931	3.2936506
H	0.0899731	4.4811064	3.05575
C	-1.2323292	3.3635101	4.3422124
H	-1.546792	4.2299207	4.9159757
C	-1.7384781	2.0978495	4.6411817
H	-2.4583258	1.9751613	5.445648
C	-1.3448542	0.9849964	3.8990179
H	-1.7748156	0.0104287	4.1086696
C	0.2817835	-1.1215941	2.7355583
C	2.8516384	1.1450127	0.328445
C	2.5564649	2.3794454	-0.2770229
H	1.7697676	2.4309154	-1.0219103
C	3.2935828	3.5178475	0.0452537
H	3.056456	4.4597165	-0.4416151
C	4.3406797	3.4509502	0.967516
H	4.9140536	4.3396478	1.2129086
C	4.6386862	2.2296074	1.5733048
H	5.4419951	2.1646231	2.3019137
C	3.8970062	1.0889469	1.2683564
H	4.1058529	0.1517067	1.7748808
C	2.7358595	-1.140469	-0.1872379
N	0.4573132	-2.296468	2.1515832
C	1.0039247	-3.3455835	2.9230236
C	0.4653622	-4.6412013	2.8288545
H	-0.3951338	-4.8135535	2.1914847
C	1.0047065	-5.6859281	3.5777325
H	0.5673183	-6.6772975	3.498576
C	2.0822474	-5.4631105	4.4383792
H	2.4968579	-6.2793032	5.0220625
C	2.6227299	-4.1802338	4.5362159
H	3.4689069	-3.9941991	5.191788
C	2.0994283	-3.1324061	3.7796437
H	2.5517058	-2.1466482	3.8279076
N	2.1520145	-2.3255887	-0.269595
C	2.9241874	-3.4148948	-0.7297133
C	2.8290009	-4.663519	-0.0898539
H	2.1902463	-4.7668112	0.7806186
C	3.5786006	-5.7478717	-0.5431133
H	3.4986254	-6.7012689	-0.0283072
C	4.440982	-5.6115556	-1.6336044
H	5.0252184	-6.4581684	-1.9809848
C	4.5398376	-4.3757849	-2.2743575
H	5.1967734	-4.2577136	-3.1316169
C	3.7825696	-3.2896184	-1.8373489
H	3.8316751	-2.3430005	-2.3665994
N	0.00664	-0.1665266	-2.084865
N	-2.0848729	-0.1665266	0.0033253
C	0.3331089	0.9143296	-2.9332255
C	-0.2726698	2.1683451	-2.7382377
H	-1.0187965	2.2822887	-1.9593212
C	0.0509188	3.2444436	-3.5631418
H	-0.436206	4.2022025	-3.4025338
C	0.9748309	3.0943887	-4.6001204
H	1.2212444	3.9346127	-5.2420413
C	1.5809366	1.853196	-4.7989739
H	2.3108095	1.7244584	-5.593399
C	1.2746688	0.7752094	-3.9693149
H	1.7814049	-0.1756836	-4.1020698
C	-0.1830462	-1.3546779	-2.6366639
C	-2.9325781	0.8849047	-0.4095135
C	-2.7383919	2.1831712	0.0948065
H	-1.9606445	2.3561598	0.8307297
C	-3.5626459	3.2300893	-0.3147449
H	-3.4026889	4.2235925	0.0948312
C	-4.598178	3.0069486	-1.225424
H	-5.2396011	3.8248857	-1.5389742
C	-4.7962277	1.7214381	-1.731097
H	-5.5895114	1.5349966	-2.4496648
C	-3.9671916	0.671259	-1.3386535
H	-4.0992637	-0.3169617	-1.768281
C	-2.6371221	-1.335803	0.2861324
N	-0.2664785	-2.4895493	-1.9604448
C	-0.7255103	-3.6368778	-2.6441662
C	-0.0859606	-4.8739592	-2.4488492
H	0.7834854	-4.9260657	-1.8025152
C	-0.5381687	-6.0145526	-3.1104525
H	-0.0236107	-6.9585554	-2.9540033
C	-1.6272745	-5.9473322	-3.9826823
H	-1.9738356	-6.8377742	-4.4982081
C	-2.2677136	-4.7233557	-4.1806348
H	-3.1239159	-4.6579645	-4.846248
C	-1.8317682	-3.5803437	-3.5115577
H	-2.3608204	-2.6406408	-3.6367185
N	-1.9611798	-2.4604286	0.4607334
C	-2.6457731	-3.5675664	1.0085707
C	-2.4495993	-4.8516415	0.4698592
H	-1.8018948	-4.972808	-0.3916491
C	-3.1120628	-5.952609	1.0103934
H	-2.9549178	-6.934584	0.5728799
C	-3.9860091	-5.7988872	2.0893013
H	-4.5021962	-6.658909	2.5048393
C	-4.1848214	-4.5278045	2.6299386
H	-4.8517824	-4.39445	3.4771569
C	-3.5149096	-3.4231314	2.1054348
H	-3.6407897	-2.4442885	2.5577885
Rh	0.0987373	-2.476272	0.0988944
H	-0.2773399	-1.4019605	-3.7264536
H	0.3760772	-1.0743115	3.825348
H	-3.7270659	-1.3754278	0.3821586
H	3.8258032	-1.1008442	-0.2832642

Table III-S11. Singlet electronic transition obtained from TD-DFT for **3-1** from singlet ground state (b3lyp/LanL2DZ(f)[Rh] 6-31G**[N, C, N amidinate core], 3-21G[C, H, N, Br]).

Wavelength (nm)	Osc. Str.	Rh_2 (%)	Amidine (%)	Ph(2) (%)	Ph-Br (%)	**Ph-**Py (%)	Ph-**Py** (%)	Major contributions
1335.0	0	38→83	46→7	16→9	0→0	0→0	0→0	HOMO→LUMO (82%)
756.4	0.0093	62→82	9→8	23→10	3→0	3→0	0→0	H-7→LUMO (10%), H-4→LUMO (72%)
756.3	0.0091	62→82	9→8	23→10	7→0	0→0	0→0	H-8→LUMO (10%), H-5→LUMO (72%)
651.4	0.0019	13→83	45→7	40→9	1→0	1→0	0→0	H-1→LUMO (89%)
650.3	0.002	14→83	45→7	40→9	2→0	0→0	0→0	H-2→LUMO (89%)
545.1	0.0081	3→83	65→7	30→9	1→0	0→0	0→0	H-3→LUMO (97%)
530.1	0.0253	37→11	45→14	17→19	1→16	0→20	0→20	HOMO→L+1 (45%), HOMO→L+2 (37%)
493.6	0	36→83	10→7	27→9	21→0	5→0	1→0	H-10→LUMO (34%), H-6→LUMO (56%)
453.0	0.0022	38→10	46→15	16→16	0→18	0→20	0→21	HOMO→L+1 (47%), HOMO→L+2 (48%)
446.8	0	38→20	42→12	18→39	2→20	1→7	0→2	HOMO→L+5 (70%)
411.6	0.0021	38→4	46→22	16→18	0→54	0→0	0→1	HOMO→L+3 (96%)
405.6	0.0014	37→5	45→25	17→16	1→54	0→0	0→0	HOMO→L+4 (93%)
404.4	0.0727	30→80	11→8	46→10	6→2	5→0	1→0	H-7→LUMO (76%), H-4→LUMO (10%)
404.1	0.0632	30→82	10→8	47→9	13→0	0→0	0→0	H-8→LUMO (78%), H-5→LUMO (11%)
383.0	0.0007	26→81	5→8	64→9	3→1	2→1	0→1	H-11→LUMO (87%)
379.4	0.0369	11→10	45→12	41→11	1→6	1→31	0→30	H-1→L+1 (76%), H-1→L+2 (10%)
377.7	0.0526	11→9	46→12	41→12	2→8	0→30	0→29	H-2→L+1 (74%), H-2→L+2 (15%)
371.8	0	26→83	7→7	37→9	24→0	5→0	1→0	H-10→LUMO (35%), H-9→LUMO (38%), H-6→LUMO (23%)
371.6	0	18→83	6→7	40→9	27→0	6→0	2→0	H-10→LUMO (24%), H-9→LUMO (58%), H-6→LUMO (15%)
365.5	0.0106	36→13	42→16	20→34	2→17	0→5	0→14	HOMO→L+6 (58%)

Table III-S12. Singlet electronic transition obtained from TD-DFT for **3-2a** from singlet ground state (b3lyp/LanL2DZ(f)[Rh] 6-31G**[N, C, N amidinate core], 3-21G[C, H, N, Br]).

Wavelength (nm)	Osc. Str.	Rh_2 (%)	Amidine (%)	Ph(2) (%)	Ph-Br (%)	**Ph-**Py (%)	Ph-**Py** (%)	Major contributions
1320.7	0	38→83	46→7	16→9	0→0	0→0	0→0	HOMO→LUMO (83%)
756.1	0.0094	62→82	9→8	23→10	3→0	3→0	0→0	H-8→LUMO (10%), H-4→LUMO (73%)
756.1	0.0094	62→82	9→8	23→10	3→0	3→0	1→0	H-7→LUMO (10%), H-5→LUMO (73%)
649.6	0.002	13→83	45→7	40→9	1→0	1→0	0→0	H-1→LUMO (89%)
649.6	0.002	13→83	45→7	40→9	1→0	1→0	0→0	H-2→LUMO (89%)
542.6	0.0101	4→82	65→8	30→9	1→0	1→1	0→1	H-3→LUMO (96%)
534.7	0.0232	37→11	45→14	17→16	1→10	0→25	0→24	HOMO→L+1 (60%), HOMO→L+3 (20%)
492.7	0	35→83	11→7	28→9	14→0	10→0	2→0	H-11→LUMO (32%), H-6→LUMO (57%)
466.8	0.0013	38→1	46→9	16→5	0→0	0→41	0→42	HOMO→L+2 (96%)
447.4	0	37→20	41→12	18→39	1→15	1→11	0→3	HOMO→L+5 (70%)
442.9	0.0037	37→10	46→17	16→18	0→24	0→14	0→16	HOMO→L+1 (30%), HOMO→L+3 (63%)
412.1	0.0031	37→4	46→23	16→18	0→55	0→0	0→0	HOMO→L+4 (96%)
404.4	0.0657	30→82	11→8	47→9	5→0	6→1	1→0	H-7→LUMO (79%), H-5→LUMO (11%)
404.4	0.0656	30→82	11→8	47→9	7→0	5→1	1→0	H-8→LUMO (79%), H-4→LUMO (11%)
384.1	0.0307	16→36	31→10	49→10	1→2	2→22	0→20	H-10→LUMO (32%), H-1→L+1 (54%)
383.6	0.0503	11→10	46→12	41→11	1→4	1→33	0→31	H-2→L+1 (82%)
383.0	0.0172	21→56	19→9	56→10	2→2	2→12	0→11	H-10→LUMO (57%), H-1→L+1 (30%)
375.6	0.013	36→12	44→17	19→30	1→16	1→7	0→17	HOMO→L+6 (64%)
371.2	0.0002	3→82	6→8	48→9	24→0	16→1	4→1	H-9→LUMO (95%)
371.0	0	41→83	8→7	32→9	11→0	7→0	2→0	H-11→LUMO (61%), H-6→LUMO (37%)

Table III-S13. Singlet electronic transition obtained from TD-DFT for **3-2b** from singlet ground state (b3lyp/LanL2DZ(f)[Rh] 6-31G**[N, C, N amidinate core], 3-21G[C, H, N, Br]).

Wavelength (nm)	Osc. Str.	Rh_2 (%)	Amidine (%)	Ph(2) (%)	Ph-Br (%)	**Ph**-Py (%)	Ph-**Py** (%)	Major contributions
1336.9	0	38→83	46→7	16→9	0→0	0→0	0→0	HOMO→LUMO (82%)
756.7	0.0095	62→82	9→8	23→10	0→0	5→0	1→0	H-7→LUMO (10%), H-4→LUMO (73%)
756.3	0.0091	62→82	9→8	23→10	7→0	0→0	0→0	H-8→LUMO (10%), H-5→LUMO (73%)
652.1	0.0019	13→83	45→7	40→9	1→0	1→0	0→0	H-1→LUMO (89%)
649.6	0.002	13→83	45→7	40→9	1→0	1→0	0→0	H-2→LUMO (89%)
545.6	0.0091	3→82	65→8	30→9	1→0	1→0	0→0	H-3→LUMO (97%)
535.5	0.0236	37→11	45→13	17→16	1→11	1→25	0→24	HOMO→L+1 (59%), HOMO→L+3 (21%)
493.9	0	35→83	10→7	28→9	13→0	10→0	2→0	H-10→LUMO (32%), H-6→LUMO (57%)
460.3	0.003	38→1	46→9	16→5	0→0	0→41	0→44	HOMO→L+2 (96%)
447.8	0.0007	38→11	46→16	16→18	0→25	0→15	0→15	HOMO→L+1 (31%), HOMO→L+3 (63%)
446.9	0	38→20	41→12	18→39	1→14	1→11	0→3	HOMO→L+5 (70%)
406.1	0.0022	37→4	46→25	16→16	0→55	0→0	0→0	HOMO→L+4 (94%)
404.6	0.074	30→80	11→8	47→9	0→1	9→0	2→0	H-7→LUMO (78%), H-4→LUMO (11%)
403.8	0.0608	29→82	10→8	47→9	13→0	0→1	0→0	H-8→LUMO (78%), H-5→LUMO (11%)
384.0	0.0369	10→10	46→11	41→11	1→3	1→34	0→31	H-1→L+1 (84%)
383.2	0	28→80	5→8	61→10	2→1	3→1	0→1	H-11→LUMO (83%)
382.1	0.0613	11→9	46→11	41→12	1→4	1→33	0→31	H-2→L+1 (84%)
376.4	0.0071	35→15	43→14	20→29	1→13	1→8	0→20	HOMO→L+6 (62%)
371.4	0	18→83	6→7	41→9	18→0	13→0	3→0	H-10→LUMO (23%), H-9→LUMO (58%), H-6→LUMO (16%)
371.3	0	26→83	7→7	38→9	15→0	11→0	3→0	H-10→LUMO (36%), H-9→LUMO (38%), H-6→LUMO (22%)

Table III-S14. Singlet electronic transition obtained from TD-DFT for **3-3** from singlet ground state (b3lyp/LanL2DZ(f)[Rh] 6-31G**[N, C, N amidinate core], 3-21G[C, H, N, Br]).

Wavelength (nm)	Osc. Str.	Rh_2 (%)	Amidine (%)	Ph(2) (%)	Ph-Br (%)	**Ph-**Py (%)	Ph-**Py** (%)	Major contributions
1338.2	0	38→83	46→7	16→9	0→0	0→0	0→0	HOMO→LUMO (82%)
756.7	0.0094	62→82	9→8	23→10	0→0	5→0	1→0	H-7→LUMO (10%), H-4→LUMO (74%)
756.5	0.0092	62→82	9→8	23→10	3→0	3→0	1→0	H-8→LUMO (10%), H-5→LUMO (74%)
651.2	0.0019	13→83	45→7	40→9	0→0	2→0	0→0	H-1→LUMO (89%)
650.1	0.0019	13→83	45→7	40→9	1→0	1→0	0→0	H-2→LUMO (89%)
546.1	0.0117	4→80	65→8	30→9	0→0	1→1	0→1	H-3→LUMO (94%)
540.0	0.0209	36→13	46→13	17→15	0→6	1→27	0→26	HOMO→L+1 (66%), HOMO→L+4 (11%)
494.0	0	33→83	10→7	31→9	7→0	15→0	3→0	H-10→LUMO (25%), H-6→LUMO (57%)
467.0	0.0007	38→2	46→9	15→6	0→0	0→41	0→42	HOMO→L+2 (95%)
461.2	0.003	38→1	46→9	15→5	0→0	0→41	0→44	HOMO→L+3 (96%)
447.0	0	37→21	41→13	18→39	1→8	2→16	0→4	HOMO→L+5 (71%)
432.3	0.0027	38→10	46→18	16→18	0→30	0→11	0→13	HOMO→L+1 (19%), HOMO→L+4 (72%)
404.3	0.0665	30→82	11→8	48→9	0→0	9→1	2→0	H-7→LUMO (79%), H-4→LUMO (11%)
404.0	0.0619	29→81	11→8	48→9	6→0	5→1	1→1	H-8→LUMO (78%), H-5→LUMO (11%)
386.3	0.0142	28→16	43→14	27→21	1→9	1→16	0→23	H-2→L+1 (30%), HOMO→L+6 (41%)
386.3	0.0484	10→11	46→11	41→11	0→2	2→34	0→31	H-1→L+1 (86%)
385.2	0.051	20→12	45→13	33→17	1→6	1→25	0→27	H-2→L+1 (55%), HOMO→L+6 (23%)
382.7	0.0005	33→78	8→8	52→10	2→1	5→1	1→2	H-11→LUMO (64%), H-10→LUMO (19%)
371.1	0	9→82	6→7	46→9	11→0	22→1	6→0	H-9→LUMO (78%)
371.0	0	30→83	7→7	40→9	6→0	14→0	3→0	H-11→LUMO (11%), H-10→LUMO (39%), H-9→LUMO (18%), H-6→LUMO (30%)

Table III-S15. Singlet electronic transition obtained from TD-DFT for **3-4** from singlet ground state (b3lyp/LanL2DZ(f)[Rh] 6-31G**[N, C, N amidinate core], 3-21G[C, H, N]).

Wavelength (nm)	Osc. Str.	Rh_2 (%)	Amidine (%)	Ph(2) (%)	**Ph-**Py (%)	Ph-**Py** (%)	Major contributions
1339.8	0	38→83	46→7	16→9	1→0	0→0	HOMO→LUMO (82%)
756.6	0.0093	62→82	9→8	23→10	5→0	1→0	H-7→LUMO (10%), H-4→LUMO (74%)
756.6	0.0093	62→82	9→8	23→10	5→0	1→0	H-8→LUMO (10%), H-5→LUMO (74%)
650.4	0.0019	13→83	45→7	40→9	2→0	0→0	H-2→LUMO (89%)
650.4	0.0019	13→83	45→7	40→9	2→0	0→0	H-1→LUMO (89%)
546.9	0.0208	10→68	61→9	27→10	1→7	0→7	H-3→LUMO (76%), HOMO→L+1 (16%)
544.0	0.0117	30→28	50→11	19→14	1→24	0→23	H-3→LUMO (22%), HOMO→L+1 (58%), HOMO→L+5 (12%)
494.1	0	36→83	11→7	28→9	21→0	5→0	H-11→LUMO (32%), H-6→LUMO (58%)
470.2	0	38→2	46→9	15→6	0→42	0→42	HOMO→L+2 (97%)
462.2	0.003	38→1	46→9	15→5	0→41	0→44	HOMO→L+3 (96%)
462.2	0.003	38→1	46→9	15→5	0→41	0→44	HOMO→L+4 (96%)
447.2	0	38→22	41→13	18→39	2→21	0→5	HOMO→L+6 (71%)
408.2	0.0002	37→18	44→14	17→26	1→15	0→28	HOMO→L+1 (22%), HOMO→L+5 (61%)
404.0	0.0629	29→81	11→8	48→9	9→1	2→1	H-7→LUMO (78%), H-4→LUMO (10%)
404.0	0.063	29→81	11→8	48→9	9→1	2→1	H-8→LUMO (78%), H-5→LUMO (10%)
388.6	0.06	10→12	46→11	41→12	2→35	0→31	H-2→L+1 (87%)
388.6	0.0599	10→12	46→11	41→12	2→35	0→31	H-1→L+1 (87%)
382.9	0	25→81	4→8	63→9	6→1	1→1	H-10→LUMO (88%)
370.6	0	41→83	8→7	32→9	15→0	3→0	H-11→LUMO (62%), H-6→LUMO (36%)
369.1	0.0044	9→3	48→9	41→6	2→41	0→41	H-2→L+2 (92%)

Table III-S16. Singlet electronic transition obtained from TD-DFT for **3-5** from singlet ground state (b3lyp/LanL2DZ(f)[Rh] 6-31G**[N, C, N amidinate core], 3-21G[C, H, N, Br]).

Wavelength (nm)	Osc. Str.	Rh_2 (%)	Amidine (%)	Ph(2) (%)	Ph-Br (%)	Major contributions
1333.4	0	38→83	46→7	16→9	1→0	HOMO→LUMO (82%)
756.3	0.0092	61→82	9→8	23→10	7→1	H-7→LUMO (11%), H-4→LUMO (73%)
756.3	0.0092	61→82	9→8	23→10	7→1	H-8→LUMO (10%), H-5→LUMO (73%)
650.9	0.002	14→83	45→7	40→9	2→0	H-1→LUMO (89%)
650.9	0.002	14→83	45→7	40→9	2→0	H-2→LUMO (89%)
544.6	0.0075	3→83	65→7	30→9	1→0	H-3→LUMO (98%)
523.8	0.0269	37→20	44→19	17→28	1→32	HOMO→L+1 (82%)
493.4	0	36→83	10→7	27→9	27→0	H-10→LUMO (35%), H-6→LUMO (55%)
446.7	0	38→21	41→12	18→39	3→28	HOMO→L+5 (70%), HOMO→L+11 (10%)
414.6	0	38→5	46→21	16→20	0→54	HOMO→L+2 (96%)
405.1	0.0003	37→7	44→24	18→16	1→52	HOMO→L+3 (90%)
405.1	0.0002	37→8	44→24	18→16	1→52	HOMO→L+4 (90%)
404.3	0.0713	30→77	12→9	45→10	13→4	H-7→LUMO (74%), H-4→LUMO (10%)
404.2	0.0714	30→77	12→9	45→10	13→4	H-8→LUMO (74%), H-5→LUMO (10%)
382.9	0	27→82	4→8	65→9	5→1	H-11→LUMO (89%)
372.1	0	40→83	8→7	30→9	22→0	H-10→LUMO (57%), H-6→LUMO (38%)
372.0	0	4→83	5→8	46→9	45→1	H-9→LUMO (94%)
370.0	0.0469	16→23	42→19	39→26	3→32	H-1→L+1 (80%)
370.0	0.0468	16→23	42→19	39→26	3→32	H-2→L+1 (80%)
357.3	0.0015	55→27	12→18	26→26	7→29	H-4→L+1 (61%)
357.3	0.0015	55→27	12→18	25→26	7→29	H-5→L+1 (61%)
355.2	0.0089	33→24	39→11	24→37	4→27	H-14→LUMO (15%), HOMO→L+9 (43%), HOMO→L+22 (11%)
351.4	0.0508	11→75	18→9	50→12	22→5	H-20→LUMO (14%), H-17→LUMO (33%), H-13→LUMO (29%)
351.4	0.0509	11→75	18→9	50→12	22→5	H-21→LUMO (14%), H-18→LUMO (33%), H-12→LUMO (29%)
340.9	0	37→3	46→1	16→21	0→74	HOMO→L+6 (97%)
339.7	0.0088	24→77	13→8	34→12	29→3	H-32→LUMO (22%), H-18→LUMO (13%), H-12→LUMO (45%)
339.7	0.0087	24→77	13→8	34→12	29→3	H-31→LUMO (22%), H-17→LUMO (13%), H-13→LUMO (45%)
338.9	0.0186	22→57	29→10	43→17	7→16	H-14→LUMO (61%), HOMO→L+9 (15%)
337.9	0	4→18	62→21	33→24	1→37	H-3→L+1 (80%)
336.8	0.0149	37→3	46→2	16→16	1→80	HOMO→L+7 (94%)

Table III-S17. Singlet electronic transition obtained from TD-DFT for **3-6** from singlet ground state (b3lyp/LanL2DZ(f)[Rh] 6-31G**[N, C, N amidinate core], 3-21G[C, H, N]).

Wavelength (nm)	Osc. Str.	Rh_2 (%)	Amidine (%)	Ph(2) (%)	Py (%)	Major contributions
1335.5	0	38→83	46→7	16→9	1→0	HOMO→LUMO (82%)
749.6	0.0088	65→82	9→8	24→10	2→1	H-4→LUMO (75%)
749.6	0.0088	65→82	9→8	24→10	2→1	H-5→LUMO (75%)
650.6	0.0019	12→83	45→8	41→9	2→0	H-1→LUMO (90%)
650.6	0.0019	12→83	45→8	41→9	2→0	H-2→LUMO (90%)
547.7	0.0117	4→81	64→8	31→9	1→1	H-3→LUMO (95%)
540.4	0.0231	37→20	45→18	17→23	1→39	HOMO→L+1 (81%)
485.0	0	44→83	15→7	32→9	9→0	H-11→LUMO (21%), H-8→LUMO (69%)
445.3	0	38→21	42→13	19→38	2→28	HOMO→L+5 (70%), HOMO→L+10 (10%)
438.7	0	38→4	46→19	16→14	0→63	HOMO→L+2 (97%)
427.7	0.0051	37→2	46→22	16→12	1→63	HOMO→L+3 (96%)
427.7	0.0051	37→2	46→22	16→12	1→63	HOMO→L+4 (96%)
403.3	0.0688	26→82	14→8	57→9	3→1	H-6→LUMO (81%), H-4→LUMO (10%)
403.3	0.0688	26→82	14→8	57→9	3→1	H-7→LUMO (81%), H-5→LUMO (10%)
385.3	0	24→83	3→8	61→9	12→1	H-10→LUMO (88%)
380.7	0.0476	11→20	45→18	42→21	3→41	H-1→L+1 (85%)
380.7	0.0476	11→20	45→18	42→21	3→41	H-2→L+1 (85%)
366.8	0.0129	33→21	40→12	21→36	5→31	HOMO→L+1 (10%), HOMO→L+9 (51%)
362.9	0.0016	63→23	10→17	22→22	6→38	H-4→L+1 (69%)
362.9	0.0016	63→23	10→17	22→22	6→38	H-5→L+1 (69%)
361.5	0	36→83	6→7	54→9	5→0	H-11→LUMO (75%), H-8→LUMO (24%)
356.9	0.0167	6→74	22→9	24→10	48→6	H-25→LUMO (15%), H-13→LUMO (62%)
356.9	0.0167	6→74	22→9	24→10	48→7	H-26→LUMO (15%), H-14→LUMO (62%)
356.7	0	6→81	6→8	78→9	10→2	H-9→LUMO (95%)
351.4	0	5→13	59→20	35→18	1→50	H-3→L+1 (63%), H-2→L+4 (16%), H-1→L+3 (16%)
348.4	0.0001	13→46	29→13	33→15	25→26	H-12→LUMO (43%), H-2→L+4 (13%), H-1→L+3 (13%), HOMO→L+9 (10%)
347.8	0.002	8→8	46→19	41→14	4→59	H-1→L+2 (89%)
347.8	0.002	8→8	46→19	41→14	4→59	H-2→L+2 (89%)
339.4	0.0035	40→70	12→9	27→15	22→7	H-34→LUMO (12%), H-32→LUMO (41%), H-20→LUMO (10%), H-4→L+5 (10%)
339.4	0.0034	39→70	12→9	27→15	22→7	H-33→LUMO (12%), H-31→LUMO (41%), H-21→LUMO (10%), H-5→L+5 (10%)
339.1	0	6→7	53→21	39→15	2→56	H-3→L+1 (32%), H-2→L+4 (32%), H-1→L+3 (32%)
338.2	0	17→2	47→16	35→15	1→67	H-2→L+3 (38%), H-1→L+4 (31%), HOMO→L+6 (30%)
338.1	0	8→2	47→22	43→12	2→64	H-2→L+3 (45%), H-1→L+4 (53%)
337.8	0	28→3	47→8	24→18	1→72	H-2→L+3 (15%), H-1→L+4 (15%), HOMO→L+6 (67%)
337.8	0.2295	11→32	35→17	37→14	17→38	H-12→LUMO (30%), H-2→L+4 (27%), H-1→L+3 (27%)
334.4	0	2→82	1→7	96→10	1→0	H-15→LUMO (98%)
333.6	0.0115	37→2	46→2	16→15	1→82	HOMO→L+7 (95%)
333.5	0.0115	37→2	46→2	16→15	1→82	HOMO→L+8 (95%)
332.0	0	1→83	1→8	70→9	28→1	H-19→LUMO (13%), H-16→LUMO (85%)
329.5	0.0127	2→83	5→8	84→9	9→1	H-17→LUMO (89%)
329.5	0.0127	2→83	5→8	84→9	9→1	H-18→LUMO (89%)
328.6	0	37→15	43→9	18→21	1→55	HOMO→L+5 (22%), HOMO→L+10 (62%)
324.3	0.0002	5→80	4→8	81→10	10→2	H-20→LUMO (79%)
324.3	0.0002	5→80	4→8	81→10	10→2	H-21→LUMO (79%)
322.8	0	37→9	46→0	16→89	0→1	HOMO→L+11 (97%)
320.9	0.0002	6→83	9→8	51→9	35→0	H-24→LUMO (20%), H-22→LUMO (70%)
318.3	0	4→80	2→8	92→9	2→3	H-23→LUMO (95%)
316.7	0	8→5	61→19	30→18	1→58	H-3→L+2 (78%)
316.2	0.0534	22→15	45→13	30→46	3→26	H-3→L+3 (10%), H-2→L+5 (41%), HOMO→L+12 (31%)

316.2	0.0535	22→15	45→13	30→46	3→26	H-3→L+4 (10%), H-1→L+5 (41%), HOMO→L+13 (31%)
316.1	0	4→83	1→7	34→9	61→0	H-19→LUMO (82%), H-16→LUMO (14%)
314.8	0.0367	21→12	47→14	31→44	2→30	H-3→L+3 (15%), H-2→L+5 (41%), HOMO→L+12 (28%)
314.8	0.0366	21→12	47→14	31→44	2→30	H-3→L+4 (15%), H-1→L+5 (41%), HOMO→L+13 (28%)
311.8	0.0278	27→4	47→17	24→34	2→44	H-4→L+2 (15%), H-3→L+3 (44%), HOMO→L+12 (32%)
311.8	0.0278	27→4	47→17	24→34	2→44	H-5→L+2 (15%), H-3→L+4 (44%), HOMO→L+13 (32%)
310.6	0.0001	41→41	16→12	24→22	19→25	H-25→LUMO (28%), H-5→L+2 (23%), H-4→L+5 (21%)
310.6	0.0001	41→41	16→12	24→22	19→25	H-26→LUMO (28%), H-5→L+5 (21%), H-4→L+2 (24%)
310.5	0.0267	14→61	16→11	50→21	20→8	H-24→LUMO (53%), HOMO→L+21 (13%)
310.1	0.0119	48→15	21→18	23→15	7→52	H-5→L+2 (55%), H-3→L+4 (20%)
310.1	0.0119	48→16	21→18	23→15	8→51	H-26→LUMO (10%), H-4→L+2 (54%), H-3→L+3 (20%)
306.7	0	37→6	46→6	16→78	1→10	HOMO→L+14 (31%), HOMO→L+15 (65%)
306.4	0.2702	23→41	29→14	36→30	12→15	H-24→LUMO (25%), H-22→LUMO (10%), HOMO→L+9 (15%), HOMO→L+21 (25%)
306.1	0.001	29→62	18→9	28→18	26→10	H-32→LUMO (13%), H-25→LUMO (35%), H-4→L+5 (20%)
306.1	0.001	29→62	18→9	28→18	26→10	H-31→LUMO (13%), H-26→LUMO (36%), H-5→L+5 (20%)
305.7	0	73→2	6→22	18→13	2→63	H-5→L+3 (48%), H-4→L+4 (48%)
305.1	0	51→12	19→17	25→19	6→52	H-8→L+1 (37%), H-5→L+3 (13%), H-4→L+4 (14%), HOMO→L+10 (16%)
304.5	0.0002	72→2	7→22	18→13	2→63	H-5→L+4 (34%), H-4→L+3 (61%)
304.5	0	65→3	16→18	18→27	2→52	H-5→L+4 (51%), H-4→L+3 (24%), HOMO→L+14 (16%)
303.9	0	46→5	36→9	16→59	1→28	H-5→L+4 (12%), H-4→L+3 (12%), HOMO→L+14 (50%), HOMO→L+15 (24%)
302.5	0	63→8	11→20	21→15	4→56	H-8→L+1 (17%), H-5→L+3 (33%), H-4→L+4 (33%)
300.4	0	37→5	46→2	16→70	1→23	HOMO→L+16 (95%)
297.9	0.0015	37→1	46→2	16→94	1→3	HOMO→L+17 (96%)
297.9	0.0015	37→1	46→2	16→94	1→3	HOMO→L+18 (96%)
294.9	0	3→22	64→12	32→39	1→26	H-3→L+5 (89%)
291.1	0.0007	37→2	46→2	17→78	1→17	HOMO→L+19 (93%)
291.1	0.0007	37→2	46→2	17→78	1→17	HOMO→L+20 (93%)
288.6	0.0296	29→17	14→18	55→23	3→42	H-6→L+1 (73%)
288.6	0.0296	29→17	14→18	55→23	3→42	H-7→L+1 (73%)
288.2	0	37→0	46→0	17→92	1→7	HOMO→L+22 (96%)
287.1	0	2→83	1→7	3→9	94→0	H-29→LUMO (98%)

Table III-S18. Singlet electronic transition obtained from TD-DFT for **3-7** from singlet ground state (b3lyp/LanL2DZ(f)[Rh] 6-31G**[N, C, N amidinate core], 3-21G[C, H]).

Wavelength (nm)	Osc. Str.	Rh_2 (%)	Amidine (%)	Ph(2) (%)	Ph (%)	Major contributions
1347.9	0	38→83	46→7	16→9	1→0	HOMO→LUMO (82%)
759.1	0.0087	65→82	8→8	22→10	5→1	H-5→LUMO (76%)
759.1	0.0087	65→82	8→8	22→10	5→1	H-4→LUMO (76%)
649.4	0.002	13→83	46→7	39→9	2→0	H-1→LUMO (90%)
649.3	0.002	13→83	46→7	39→9	2→0	H-2→LUMO (90%)
547.9	0.0071	3→83	66→7	29→9	1→0	H-3→LUMO (98%)
521.1	0.0278	38→22	44→20	17→32	1→26	HOMO→L+1 (83%)
495.7	0	38→83	13→7	29→9	21→0	H-11→LUMO (25%), H-6→LUMO (65%)
448.2	0	38→24	42→14	18→45	3→17	HOMO→L+5 (75%)
402.8	0	38→6	46→22	16→26	1→46	HOMO→L+2 (96%)
401.6	0.0629	28→82	12→8	53→10	8→1	H-7→LUMO (82%)
401.5	0.0626	28→82	12→8	53→10	8→1	H-8→LUMO (82%)
393.4	0.0084	38→3	46→28	16→22	1→47	HOMO→L+3 (96%)
393.4	0.0085	38→3	46→28	16→22	1→47	HOMO→L+4 (96%)
381.1	0	25→82	4→8	61→10	10→1	H-10→LUMO (87%)
366.8	0	40→83	7→7	39→9	13→0	H-11→LUMO (69%), H-6→LUMO (29%)
365.7	0.042	19→26	41→20	38→30	2→25	H-1→L+1 (75%)
365.7	0.0435	18→26	41→20	38→30	2→25	H-2→L+1 (77%)
365.5	0	4→82	6→8	59→9	31→1	H-9→LUMO (97%)
355.9	0.0015	49→37	14→17	28→26	10→19	H-13→LUMO (11%), H-5→L+1 (51%)

Table III-S19. Singlet electronic transition obtained from TD-DFT for **3-8** from singlet ground state (b3lyp/LanL2DZ(f)[Rh] 6-31G**[N, C, N amidinate core], 3-21G[C, H, N]).

Wavelength (nm)	Osc. Str.	Rh_2 (%)	Amidine (%)	Ph(2) (%)	Ph-NH_2 (%)	Major contributions
1340.7	0	38→83	46→7	15→10	1→0	HOMO→LUMO (82%)
772.4	0.0087	44→82	11→8	14→10	31→0	H-9→LUMO (50%), H-4→LUMO (24%), H-1→LUMO (11%)
772.4	0.0088	44→82	11→7	14→10	31→0	H-8→LUMO (50%), H-3→LUMO (23%), H-2→LUMO (11%)
645.5	0.0021	13→83	37→7	31→10	19→0	H-4→LUMO (15%), H-1→LUMO (77%)
645.3	0.0021	13→83	37→7	31→10	19→0	H-3→LUMO (15%), H-2→LUMO (77%)
540.4	0.0062	3→83	68→7	28→10	1→0	H-7→LUMO (98%)
534.9	0	26→83	8→7	6→10	59→0	H-12→LUMO (29%), H-5→LUMO (64%)
508.5	0.0281	39→24	44→21	15→38	2→17	HOMO→L+1 (82%)
471.2	0	1→83	4→7	7→10	88→0	H-6→LUMO (96%)
469.1	0.0008	33→83	10→7	14→10	44→0	H-8→LUMO (32%), H-3→LUMO (54%)
468.8	0.0008	33→83	10→7	14→10	43→0	H-9→LUMO (32%), H-4→LUMO (56%)
452.0	0	40→24	42→14	15→48	3→14	HOMO→L+3 (75%)
435.8	0	48→83	12→7	5→10	35→0	H-12→LUMO (61%), H-5→LUMO (33%)
386.4	0	37→13	42→21	19→37	2→28	HOMO→L+2 (87%)
385.2	0.0793	18→81	18→8	58→11	6→1	H-11→LUMO (75%)
385.2	0.0797	18→81	18→8	58→10	6→1	H-10→LUMO (75%)
378.7	0.0134	38→4	46→32	15→33	1→31	HOMO→L+4 (95%)
378.5	0.0135	38→4	46→32	15→33	1→31	HOMO→L+5 (95%)
377.3	0	27→75	8→9	55→13	10→3	H-13→LUMO (80%), HOMO→L+2 (10%)
360.4	0.0625	25→28	31→20	28→36	16→16	H-8→L+1 (12%), H-2→L+1 (58%)

Table III-S20. Energy and contribution of frontier MO obtained from DFT for **3-1** from singlet ground state (b3lyp/LanL2DZ(f)[Rh] 6-31G**[N, C, N amidinate core], 3-21G[C, H, N, Br]).

MO	eV	Symmetry	Rh_2	Amidine	Ph(2)	Ph-Br	**Ph**-Py	Ph-**Py**
L+20	0.18	A	0.03565073	0.01231346	0.71883423	0.18178881	0.02348854	0.02792274
L+19	0.14	A	0.04365899	0.01858808	0.68280954	0.17049595	0.08192422	0.00252791
L+18	0.13	A	0.00593861	0.01887315	0.92448775	0.04952116	0.0010944	9.56E-05
L+17	0.13	A	0.01145366	0.02111728	0.88286456	0.08256984	0.0017403	0.00025085
L+16	0.08	A	0.057995	0.06760777	0.85294381	0.01639725	0.00502628	3.26E-05
L+15	0	A	0.03611416	0.02260318	0.73722303	0.14953023	0.02111957	0.03341415
L+14	-0.03	A	0.0215409	0.06411796	0.74312726	0.12014052	0.04898321	0.00209195
L+13	-0.11	A	0.09267736	0.05476383	0.16277048	0.37070638	0.28094151	0.03813375
L+12	-0.12	A	0.04586889	0.09136331	0.54158803	0.23952834	0.02449002	0.0571581
L+11	-0.17	A	0.07986395	0.00018083	0.88271621	0.03459666	0.00259909	4.97E-05
L+10	-0.26	A	0.02755984	0.01799996	0.13832846	0.30252944	0.19910118	0.31448436
L+9	-0.34	A	0.01220579	0.01160917	0.1483041	0.82514721	0.0009905	0.00174599
L+8	-0.35	A	0.00512762	0.00563361	0.06488576	0.18857818	0.16840936	0.56736352
L+7	-0.37	A	0.02981401	0.01186617	0.19408964	0.62956073	0.06307138	0.07160379
L+6	-0.43	A	0.08289194	0.17349346	0.35328427	0.16206535	0.03517846	0.19308196
L+5	-0.65	A	0.22719054	0.12113566	0.4241684	0.18967783	0.03692862	0.00090496
L+4	-0.87	A	0.01927713	0.25572437	0.1616676	0.56313614	0.00018751	2.66E-06
L+3	-0.92	A	0.03550634	0.2247623	0.18422749	0.54919325	0.00168627	0.00462843
L+2	-1.14	A	0.15086359	0.19128917	0.21816762	0.33747512	0.03776479	0.06443271
L+1	-1.44	A	0.0569667	0.10473601	0.08317351	0.01932362	0.37567068	0.36012231
LUMO	-2.42	A	0.83347252	0.07442023	0.0900244	0.00152886	0.00053277	1.85E-05
HOMO	-4.55	A	0.37845015	0.46355323	0.15333168	0.00348917	0.0011826	2.04E-06
H-1	-5.24	A	0.08404854	0.48150757	0.41644804	0.01108066	0.00691014	1.14E-05
H-2	-5.25	A	0.08436261	0.48096691	0.41660481	0.01580844	0.0019602	0.00029201
H-3	-5.58	A	0.02581487	0.66000981	0.3031832	0.00836024	0.00262208	7.77E-06
H-4	-5.71	A	0.71255538	0.05858312	0.17002542	0.02954775	0.0251546	0.00413473
H-5	-5.71	A	0.71344485	0.05806798	0.16914437	0.05916034	0.00018405	2.37E-06
H-6	-6.12	A	0.27349978	0.13899312	0.22039837	0.28108718	0.07050108	0.01551697
H-7	-6.25	A	0.23339382	0.1011207	0.537173	0.06631563	0.05114554	0.01085657
H-8	-6.25	A	0.23248059	0.098963	0.53144191	0.13648955	0.00062483	6.50E-06
H-9	-6.28	A	0.02382006	0.04845078	0.47156325	0.35264665	0.08299576	0.02051176
H-10	-6.54	A	0.50711435	0.0466781	0.35029193	0.08280352	0.01100277	0.00212327
H-11	-6.54	A	0.26447866	0.01537775	0.67376667	0.02946433	0.01573912	0.00115685
H-12	-6.59	A	0.00711359	0.12210021	0.32761678	0.54066884	0.00234137	0.00014281
H-13	-6.6	A	0.00828747	0.12092447	0.34992738	0.2684023	0.18484811	0.06762103
H-14	-6.73	A	0.17304779	0.18771397	0.50057632	0.06863913	0.05047782	0.01954822
H-15	-6.74	A	0.01054707	0.01219724	0.94274973	0.02652605	0.00576922	0.00223113
H-16	-6.79	A	0.01348452	0.00316433	0.97786089	0.00342863	0.00185111	0.00020955
H-17	-6.8	A	0.01364614	0.23769535	0.59671706	0.04288468	0.03360632	0.07544114
H-18	-6.81	A	0.01036018	0.23780197	0.69793755	0.04959406	0.00322844	0.0010756
H-19	-6.85	A	0.00709517	0.00458421	0.19998818	0.00255364	0.02615676	0.7596202
H-20	-6.86	A	0.04316989	0.03665694	0.67107384	0.20314516	0.0299694	0.01598271

Table III-S21. Energy and contribution of frontier MO obtained from DFT for **3-2a** from singlet ground state (b3lyp/LanL2DZ(f)[Rh] 6-31G**[N, C, N amidinate core], 3-21G[C, H, N, Br]).

MO	eV	Symmetry	Rh_2	Amidine	Ph(2)	Ph-Br	**Ph**-Py	Ph-**Py**
L+20	0.15	A	0.007601784	0.011454613	0.920000263	0.037649076	0.01086605	0.01242505
L+19	0.13	B	0.007042436	0.019257474	0.916663151	0.050181744	0.00646304	0.000389407
L+18	0.09	B	0.057374847	0.066825591	0.854210708	0.011334503	0.010166982	9.49742E-05
L+17	0.07	A	0.023743458	0.008260056	0.773167543	0.048463305	0.069108655	0.077251167
L+16	0	B	0.028939952	0.038484532	0.737811949	0.109533374	0.071855746	0.013384196
L+15	-0.07	A	0.027313254	0.096979958	0.599694125	0.178076648	0.05145857	0.046488164
L+14	-0.07	B	0.085490021	0.050609174	0.161994452	0.20079785	0.447407414	0.053700199
L+13	-0.16	A	0.075658498	0.000958349	0.863477972	0.030888136	0.024190363	0.004834717
L+12	-0.22	A	0.022950805	0.012037917	0.204744577	0.025857203	0.426136842	0.308273012
L+11	-0.27	B	0.029764068	0.027897964	0.138280257	0.415298021	0.097969241	0.290801368
L+10	-0.31	B	0.030455315	0.185944455	0.372705954	0.010457043	0.058234073	0.342198712
L+9	-0.35	A	0.007822015	0.00634928	0.080895361	0.306386962	0.129424464	0.469126835
L+8	-0.35	B	0.005917082	0.01674364	0.077915096	0.139322067	0.183000171	0.577124551
L+7	-0.36	A	0.025026601	0.0098707	0.167851716	0.460213748	0.128334041	0.20870275
L+6	-0.5	A	0.10587957	0.176431845	0.31990362	0.171810455	0.033439629	0.192524404
L+5	-0.64	B	0.23276473	0.123669057	0.427117176	0.136285561	0.077895991	0.002260751
L+4	-0.92	B	0.030608959	0.234642073	0.175344829	0.554603091	0.001421351	0.003380233
L+3	-1.07	A	0.119513606	0.200297208	0.19992535	0.356760371	0.040947194	0.082563151
L+2	-1.41	B	0.012386925	0.092826722	0.048860772	0.001581594	0.418620609	0.425712095
L+1	-1.47	A	0.07184569	0.110134126	0.092907866	0.016374356	0.369289681	0.339447103
LUMO	-2.41	B	0.83274939	0.074568087	0.09065706	0.000980406	0.00100989	2.55485E-05
HOMO	-4.55	B	0.377289705	0.463313447	0.154704605	0.002306392	0.002376306	3.86801E-06
H-1	-5.24	A	0.083876904	0.479631547	0.418177098	0.008881592	0.009127912	0.000303365
H-2	-5.24	B	0.083883424	0.479544996	0.418237833	0.009130941	0.008894056	0.000307153
H-3	-5.57	A	0.025981327	0.656825929	0.305907976	0.005849045	0.005422231	1.49782E-05
H-4	-5.7	A	0.712801977	0.058902626	0.1690116	0.029017494	0.026006796	0.004278359
H-5	-5.7	B	0.712898947	0.058923279	0.168897034	0.029289121	0.025762818	0.004238708
H-6	-6.11	A	0.277053127	0.141432058	0.219640738	0.183239409	0.146303768	0.032344974
H-7	-6.24	B	0.232696957	0.10319049	0.53762174	0.052652903	0.060898324	0.012935539
H-8	-6.24	A	0.233084364	0.103167371	0.536755422	0.069079225	0.047932486	0.009972102
H-9	-6.28	B	0.025051668	0.050495442	0.478515187	0.248156918	0.158355219	0.039443092
H-10	-6.53	B	0.266343601	0.015172843	0.66626872	0.01918475	0.030879314	0.002137338
H-11	-6.54	A	0.498209765	0.043621288	0.370148671	0.063264227	0.020773827	0.003981334
H-12	-6.6	B	0.006785086	0.119462937	0.354840591	0.272077546	0.180475755	0.06635107
H-13	-6.6	A	0.009187914	0.119073096	0.357036872	0.255676487	0.189982727	0.069045825
H-14	-6.72	A	0.163101489	0.186747023	0.48024924	0.03925828	0.097850553	0.032778939
H-15	-6.74	A	0.011566615	0.012027147	0.943098269	0.017869684	0.01112308	0.00430946
H-16	-6.78	B	0.012565405	0.003706122	0.978949656	0.001825236	0.002727775	0.000231459
H-17	-6.8	B	0.009607301	0.229213777	0.603135179	0.028487206	0.043462722	0.086103797
H-18	-6.8	A	0.014589396	0.232778935	0.637948197	0.036488236	0.025517043	0.052678536
H-19	-6.85	B	0.003887773	0.000834493	0.227307911	0.001449944	0.040774659	0.725740038
H-20	-6.85	A	0.011429634	0.008845864	0.226036243	0.004865521	0.029295675	0.719531374

Table III-S22. Energy and contribution of frontier MO obtained from DFT for **3-2b** from singlet ground state (b3lyp/LanL2DZ(f)[Rh] 6-31G**[N, C, N amidinate core], 3-21G[C, H, N, Br]).

MO	eV	Symmetry	Rh_2	Amidine	Ph(2)	Ph-Br	**Ph-**Py	Ph-**Py**
L+20	0.15	?C	0.0049743	0.010157926	0.945270131	0.022081736	0.009288307	0.008227829
L+19	0.14	?C	0.003870375	0.016524848	0.946348149	0.014734215	0.017528587	0.001000905
L+18	0.09	B3	0.057849478	0.067468567	0.853164088	0.011025914	0.010431017	6.74439E-05
L+17	0.03	?C	0.032637781	0.005180768	0.784546381	0.103967585	0.029599823	0.044066475
L+16	-0.01	?C	0.017903339	0.067485503	0.760418151	0.089395527	0.062691134	0.002110727
L+15	-0.05	?L	0.051304958	0.044516785	0.57100647	0.215636821	0.040698932	0.076835306
L+14	-0.08	?L	0.090680942	0.05209377	0.162862763	0.240417524	0.40922505	0.044716601
L+13	-0.17	?L	0.080302886	0.000204313	0.88734824	0.026585186	0.005507803	5.69007E-05
L+12	-0.21	B1	0.010349112	0.013401503	0.161683101	0.004316378	0.541113573	0.269134716
L+11	-0.28	B2	0.01272621	0.232435508	0.375791786	0.08731632	0.059763601	0.231972657
L+10	-0.3	A	0.030014444	0.01323189	0.102374568	0.233553055	0.041481378	0.579348502
L+9	-0.34	?L	0.010170648	0.040920106	0.171219136	0.753524818	0.0063462	0.017808879
L+8	-0.35	?L	0.00329088	0.003737074	0.042186305	0.000882675	0.225126321	0.724781336
L+7	-0.36	?L	0.021065215	0.008560278	0.139114697	0.235622314	0.228882672	0.366759211
L+6	-0.52	B3	0.121060592	0.132844221	0.348444027	0.137010724	0.036588671	0.224049616
L+5	-0.64	A	0.230798194	0.122940804	0.428951251	0.137516092	0.077772134	0.002026547
L+4	-0.87	B1	0.019182105	0.255274804	0.161431273	0.563719526	0.000390975	5.3029E-06
L+3	-1.09	B3	0.128986819	0.19024597	0.215654087	0.374918281	0.031272676	0.058935428
L+2	-1.38	B2	0.007826119	0.090672445	0.041372752	9.22019E-05	0.415804303	0.444237219
L+1	-1.48	B3	0.071321246	0.10600715	0.093694272	0.009949729	0.377907469	0.341111706
LUMO	-2.41	B3	0.833233068	0.074395063	0.090250229	0.001020749	0.001065371	3.74299E-05
HOMO	-4.54	A	0.378746098	0.463550148	0.153057163	0.00231009	0.002341284	4.04502E-06
H-1	-5.24	?C	0.083653921	0.482222312	0.41613841	0.004281409	0.013680385	2.27256E-05
H-2	-5.24	?C	0.084335997	0.481229033	0.416345098	0.013607118	0.003901834	0.000581804
H-3	-5.57	A	0.025762355	0.660886604	0.302397372	0.005499402	0.005443115	1.5775E-05
H-4	-5.7	?C	0.712784413	0.058782539	0.170341653	0.000373126	0.049592769	0.008129626
H-5	-5.71	?C	0.71584518	0.057678445	0.167722315	0.058392049	0.000361078	4.73561E-06
H-6	-6.12	B3	0.279499446	0.141013077	0.219438568	0.187041151	0.14180232	0.031200156
H-7	-6.24	?C	0.233298185	0.103471524	0.543451232	0.001066778	0.098059525	0.020641205
H-8	-6.25	?C	0.230323865	0.099458375	0.533071692	0.13591247	0.00122734	1.06217E-05
H-9	-6.28	B3	0.024388371	0.049186911	0.479394866	0.22947324	0.174411758	0.043143348
H-10	-6.53	?C	0.494483603	0.04362254	0.371956598	0.04761201	0.034688387	0.007641332
H-11	-6.54	?C	0.26971924	0.016175013	0.661211954	0.019162729	0.031314859	0.0024243
H-12	-6.59	?C	0.006978363	0.123972754	0.328348346	0.534686867	0.005649932	0.000368379
H-13	-6.61	?C	0.006590703	0.121603787	0.371034512	0.005004736	0.361304182	0.13447231
H-14	-6.72	?L	0.170092474	0.182859486	0.49174654	0.049336771	0.0793727	0.026594782
H-15	-6.74	?L	0.010377739	0.01177871	0.944881455	0.018595589	0.0103921	0.003974909
H-16	-6.78	?L	0.013435329	0.001579014	0.980442836	0.002243772	0.002146952	0.000154411
H-17	-6.79	?L	0.010098666	0.23948194	0.509242885	0.018701901	0.092947607	0.129533002
H-18	-6.81	?L	0.01014502	0.239217737	0.698524939	0.039788615	0.008844141	0.003483447
H-19	-6.85	?L	0.00248277	0.000801244	0.342786329	0.001989293	0.032955014	0.618992705
H-20	-6.85	?L	0.012164379	0.008422349	0.024921594	0.001803776	0.022256019	0.930435805

Table III-S23. Energy and contribution of frontier MO obtained from DFT for **3-3** from singlet ground state (b3lyp/LanL2DZ(f)[Rh] 6-31G**[N, C, N amidinate core], 3-21G[C, H, N, Br]).

MO	eV	Symmetry	Rh_2	Amidine	Ph(2)	Ph-Br	**Ph-**Py	Ph-**Py**
L+20	0.09	A	0.057620782	0.06778451	0.851145132	0.005386387	0.016715324	0.001351162
L+19	0.08	A	0.017830094	0.008796247	0.779782878	0.022295813	0.080123204	0.091172706
L+18	0.04	A	0.029899454	0.00591965	0.813886066	0.04982274	0.057151073	0.043320695
L+17	-0.02	A	0.025059794	0.067403322	0.688439519	0.131688949	0.058221639	0.029183726
L+16	-0.06	A	0.083826731	0.04929109	0.155252558	0.093166196	0.565126935	0.053346205
L+15	-0.16	A	0.079356396	0.000146897	0.886069462	0.01304303	0.01894158	0.002453248
L+14	-0.21	A	0.010970109	0.011321354	0.157897113	0.003488711	0.549512543	0.266805843
L+13	-0.23	A	0.021932587	0.019834967	0.190473659	0.046189406	0.421337495	0.300238108
L+12	-0.28	A	0.015048709	0.218214657	0.358677639	0.047097307	0.072069892	0.288890248
L+11	-0.31	A	0.020816045	0.036277343	0.097957905	0.231819794	0.016611266	0.596517145
L+10	-0.31	A	0.039341917	0.184310299	0.419155088	0.002776721	0.063261633	0.291155265
L+9	-0.35	A	0.003755825	0.00846862	0.050907906	0.004483512	0.226107088	0.706275041
L+8	-0.35	A	0.004731237	0.014889548	0.072660653	0.172794359	0.166515529	0.568413561
L+7	-0.36	A	0.017907976	0.007933252	0.123160993	0.177376595	0.244101042	0.429524482
L+6	-0.59	A	0.135127171	0.148519866	0.317742325	0.135376995	0.03845791	0.224779809
L+5	-0.63	A	0.235280975	0.125260111	0.434831458	0.074863258	0.126260974	0.003503073
L+4	-1	A	0.094087902	0.202540589	0.196938654	0.403205502	0.030536259	0.07269272
L+3	-1.38	A	0.007811646	0.090388966	0.041232666	4.67975E-05	0.41594242	0.444564079
L+2	-1.41	A	0.014217803	0.089125505	0.050705442	0.001789922	0.417604012	0.426545242
L+1	-1.49	A	0.082686049	0.108496234	0.100373184	0.007539204	0.372751349	0.328164303
LUMO	-2.41	A	0.833081849	0.074345711	0.090392519	0.00051046	0.001603461	5.72704E-05
HOMO	-4.54	A	0.379066221	0.463531854	0.152760441	0.001138177	0.003487247	6.07295E-06
H-1	-5.24	A	0.083582712	0.482468065	0.415935567	0.002125924	0.015582537	0.000307253
H-2	-5.24	A	0.083896405	0.481923286	0.41610705	0.006719925	0.010759946	0.000584127
H-3	-5.56	A	0.025696091	0.661728978	0.301649558	0.002852221	0.00804867	2.39799E-05
H-4	-5.7	A	0.715158338	0.05834221	0.168917181	0.000183142	0.04933552	0.008052292
H-5	-5.7	A	0.716311438	0.057846842	0.16795335	0.028539062	0.025264017	0.004087811
H-6	-6.12	A	0.285269997	0.142934599	0.218710768	0.092702376	0.21348497	0.046906835
H-7	-6.24	A	0.23111915	0.103887136	0.544990002	0.000513198	0.098838237	0.020652071
H-8	-6.24	A	0.229935555	0.101956964	0.540349217	0.062472114	0.054080271	0.011200847
H-9	-6.28	A	0.024825749	0.049761418	0.48655401	0.123281345	0.253028869	0.06254564
H-10	-6.53	A	0.442740242	0.037081149	0.436670184	0.02887941	0.046022301	0.008607921
H-11	-6.53	A	0.311745719	0.021441779	0.602330403	0.015258665	0.044574951	0.004655249
H-12	-6.6	A	0.008296401	0.124053765	0.351447471	0.258850732	0.190094797	0.067264213
H-13	-6.61	A	0.006878491	0.123650118	0.371859661	0.002716961	0.361600529	0.133292805
H-14	-6.72	A	0.162680969	0.179198716	0.477670601	0.019344886	0.124025087	0.037088686
H-15	-6.74	A	0.010039076	0.011267074	0.947904441	0.008651116	0.016041625	0.006098709
H-16	-6.78	A	0.014061185	0.003395743	0.975833772	0.000911319	0.005212017	0.000575329
H-17	-6.79	A	0.010029246	0.240440062	0.515609354	0.012472533	0.095281472	0.126168965
H-18	-6.8	A	0.012183793	0.238984999	0.608910097	0.026386004	0.044208594	0.06931754
H-19	-6.85	A	0.002688645	0.000769584	0.349433445	0.001277139	0.035433788	0.610395086
H-20	-6.85	A	0.0036885	0.000684758	0.139095252	8.69261E-05	0.037660298	0.818784754

Table III-S24. Energy and contribution of frontier MO obtained from DFT for **3-4** from singlet ground state (b3lyp/LanL2DZ(f)[Rh] 6-31G**[N, C, N amidinate core], 3-21G[C, H, N]).

MO	eV	Symmetry	Rh_2	Amidine	Ph(2)	**Ph-**Py	Ph-**Py**
L+20	0.06	E	0.026581204	0.006423575	0.854727654	0.069168268	0.043103382
L+19	0.06	E	0.026581286	0.006423575	0.854722488	0.069168269	0.043103382
L+18	-0.04	B1	0.082250832	0.048939064	0.149148041	0.665239074	0.05443228
L+17	-0.16	A1	0.079900578	2.39744E-05	0.892540284	0.025313801	0.002218937
L+16	-0.2	E	0.010325593	0.016271756	0.156045702	0.564417976	0.252935512
L+15	-0.2	E	0.010325593	0.016271756	0.156045702	0.564417976	0.25293664
L+14	-0.25	A1	0.030645048	0.010177182	0.201214286	0.373357633	0.384626993
L+13	-0.28	E	0.012183396	0.250528451	0.384118978	0.073102151	0.280072003
L+12	-0.28	E	0.012183395	0.250528452	0.384118978	0.073102215	0.280071931
L+11	-0.33	A2	0.054901627	0.148157513	0.448328627	0.064177141	0.284445382
L+10	-0.33	B1	0.011063508	0.005772902	0.00711917	0.039865137	0.936169254
L+9	-0.35	E	0.003104556	0.00896319	0.047481404	0.224461948	0.715996426
L+8	-0.35	E	0.003104556	0.00896319	0.047481404	0.224461948	0.715996426
L+7	-0.36	A1	0.012369926	0.005333041	0.086657376	0.290895773	0.604732228
L+6	-0.62	B1	0.240743752	0.128051094	0.442014444	0.183705911	0.005494054
L+5	-0.69	B2	0.200959287	0.114658667	0.323886913	0.059763852	0.300748598
L+4	-1.38	E	0.007765429	0.089843722	0.040913814	0.415665864	0.445818635
L+3	-1.38	E	0.007765429	0.089843722	0.040913814	0.415665864	0.445818635
L+2	-1.42	A2	0.015871087	0.087790234	0.05359622	0.421210687	0.421545251
L+1	-1.51	B2	0.089307199	0.108579248	0.103965371	0.376133293	0.322029031
LUMO	-2.41	A2	0.832925222	0.07431433	0.090547475	0.002143301	7.77567E-05
HOMO	-4.53	B1	0.37942728	0.463526618	0.152447377	0.004600552	8.07665E-06
H-1	-5.23	E	0.083476832	0.482666779	0.415831868	0.017448604	0.000585633
H-2	-5.23	E	0.083476832	0.482666779	0.415831868	0.017448604	0.000585633
H-3	-5.56	A1	0.025600338	0.66268688	0.300831675	0.010848308	3.13333E-05
H-4	-5.7	E	0.717297214	0.057940367	0.167840373	0.048999591	0.007946206
H-5	-5.7	E	0.717297214	0.057940367	0.167840373	0.048999591	0.007946206
H-6	-6.12	B2	0.291568819	0.145001971	0.217726363	0.283571822	0.06213921
H-7	-6.24	E	0.229227334	0.104465708	0.546990483	0.098869993	0.020426801
H-8	-6.24	E	0.229227334	0.104465708	0.546990483	0.098869993	0.020426801
H-9	-6.28	A2	0.025196102	0.050474542	0.495411163	0.344096624	0.084812165
H-10	-6.53	B1	0.258747059	0.01492186	0.666731107	0.055864902	0.003729752
H-11	-6.53	B2	0.488481915	0.041215441	0.383176604	0.071152663	0.016007799
H-12	-6.61	E	0.006774105	0.12566124	0.373540267	0.362399777	0.131625696
H-13	-6.61	E	0.006774105	0.12566124	0.373540267	0.362399777	0.131625696
H-14	-6.71	A1	0.160453882	0.176452362	0.471860574	0.151299004	0.039921143
H-15	-6.73	B2	0.00984428	0.010708675	0.950388768	0.021140883	0.007923901
H-16	-6.78	B1	0.014123352	0.001341388	0.979615906	0.004861994	3.79723E-05
H-17	-6.79	E	0.009909615	0.242547922	0.532446915	0.099913863	0.115146201
H-18	-6.79	E	0.009909615	0.242547922	0.532446915	0.099913863	0.115146201
H-19	-6.85	E	0.002797481	0.001734557	0.372495946	0.041018109	0.5819571
H-20	-6.85	E	0.002797479	0.001734593	0.372507416	0.041020829	0.581957252

Table III-S25. Energy and contribution of frontier MO obtained from DFT for **3-5** from singlet ground state (b3lyp/LanL2DZ(f)[Rh] 6-31G**[N, C, N amidinate core], 3-21G[C, H, Br]).

MO	eV	Symmetry	Rh_2	Amidine	Ph(2)	Ph-Br
L+20	0.27	E	0.012769972	0.014004012	0.26228853	0.7109129
L+19	0.26	B1	0.003370115	0.002682341	0.094373886	0.899585159
L+18	0.13	A1	0.04727443	0.01936863	0.252182202	0.681170049
L+17	0.13	E	0.003669779	0.020226454	0.043843535	0.932260569
L+16	0.13	E	0.003676994	0.020210785	0.043893551	0.932237093
L+15	0.12	A2	0.057736115	0.022085343	0.291918068	0.628249495
L+14	0.08	A2	0.057797093	0.067843751	0.021396068	0.85298687
L+13	-0.04	E	0.02348525	0.062155309	0.169366246	0.744983265
L+12	-0.04	E	0.023446422	0.062245149	0.169482315	0.74480548
L+11	-0.14	B1	0.111227488	0.063148514	0.688923747	0.136697825
L+10	-0.18	A1	0.079223747	2.31495E-05	0.040223417	0.880526484
L+9	-0.22	B2	0.101951165	0.048741029	0.409938124	0.439372679
L+8	-0.34	E	0.010780407	0.012649386	0.828017096	0.148555922
L+7	-0.34	E	0.010762211	0.012622356	0.828368547	0.14823279
L+6	-0.37	A1	0.033026976	0.012643349	0.743890694	0.210434866
L+5	-0.65	B1	0.224165704	0.119576558	0.236131433	0.420130575
L+4	-0.87	E	0.019225628	0.256396023	0.562180604	0.162203627
L+3	-0.87	E	0.019217806	0.256329922	0.562385668	0.162066183
L+2	-0.95	A2	0.042763287	0.2121567	0.549358759	0.195717406
L+1	-1.22	B2	0.204766935	0.20210426	0.340113092	0.253029675
LUMO	-2.42	A2	0.833427397	0.074500807	0.002035227	0.090033704
HOMO	-4.56	B1	0.378346844	0.463511105	0.004689232	0.153442591
H-1	-5.25	E	0.084393688	0.480813671	0.018034768	0.416755569
H-2	-5.25	E	0.084411835	0.480811409	0.018039383	0.416730523
H-3	-5.58	A1	0.025857845	0.65940466	0.011022612	0.303693118
H-4	-5.72	E	0.71156093	0.058419622	0.059842207	0.170189628
H-5	-5.72	E	0.7117652	0.058398067	0.059760969	0.170084596
H-6	-6.13	B2	0.267585542	0.136942778	0.374652513	0.220814862
H-7	-6.25	E	0.234153625	0.098447293	0.13790836	0.529499795
H-8	-6.25	E	0.233972055	0.098523512	0.137761882	0.529754553
H-9	-6.28	A2	0.023285312	0.047697871	0.465310532	0.463713257
H-10	-6.54	B2	0.515268146	0.047930448	0.094854845	0.341945509
H-11	-6.55	B1	0.266759107	0.015319253	0.040512097	0.677401692
H-12	-6.59	E	0.006876422	0.121279798	0.545957653	0.325907999
H-13	-6.59	E	0.006877906	0.121245157	0.545662367	0.326209229
H-14	-6.74	A1	0.183220394	0.194505074	0.101542126	0.520719796
H-15	-6.75	B2	0.01074866	0.012583187	0.036577224	0.940083646
H-16	-6.79	B1	0.012953255	0.001219533	0.003929431	0.981912443
H-17	-6.81	E	0.010446464	0.238043998	0.053866537	0.697648436
H-18	-6.81	E	0.010431467	0.237602497	0.05365963	0.698281245
H-19	-6.86	A2	0.04449032	0.038112725	0.271154216	0.646221986
H-20	-6.89	E	0.011583601	0.214989859	0.041082389	0.732346679

Table III-S26. Energy and contribution of frontier MO obtained from DFT for **3-6** from singlet ground state (b3lyp/LanL2DZ(f)[Rh] 6-31G**[N, C, N amidinate core], 3-21G[C, H, N]).

MO	eV	Symmetry	Rh_2	Amidine	Ph(2)	Py
L+20	0.15	E	0.015713441	0.012772817	0.80584137	0.16568267
L+19	0.15	E	0.015713441	0.012772817	0.80584137	0.16568267
L+18	0.06	E	0.004646881	0.017466638	0.951484069	0.026402086
L+17	0.06	E	0.004646861	0.017466616	0.951476048	0.026402083
L+16	0.05	A1	0.051228509	0.019805942	0.72235907	0.206602544
L+15	-0.01	A2	0.059954048	0.077202161	0.83759612	0.025244866
L+14	-0.02	A2	0.058551307	0.024464481	0.688083684	0.228900428
L+13	-0.13	E	0.018877574	0.102768624	0.749213764	0.129141652
L+12	-0.13	E	0.018877574	0.102768624	0.749213764	0.129141652
L+11	-0.24	A1	0.085269855	0.000179186	0.903743553	0.010789811
L+10	-0.25	B1	0.10800799	0.061761386	0.121257959	0.708960353
L+9	-0.39	B2	0.146958324	0.064960909	0.413276404	0.374794169
L+8	-0.44	E	0.008676587	0.011968574	0.137043713	0.842317499
L+7	-0.44	E	0.008676587	0.011968574	0.137043713	0.842317499
L+6	-0.47	A1	0.030855476	0.012026022	0.197753039	0.759354052
L+5	-0.75	B1	0.237125599	0.126500818	0.414745213	0.221636276
L+4	-1.17	E	0.017836727	0.224898633	0.118247387	0.639019462
L+3	-1.17	E	0.017836727	0.224898633	0.118247387	0.639019462
L+2	-1.25	A2	0.037873434	0.193645343	0.139614983	0.628859262
L+1	-1.48	B2	0.177630959	0.18817182	0.201840961	0.432349508
LUMO	-2.55	A2	0.833011703	0.075015421	0.089482333	0.002489532
HOMO	-4.69	B1	0.377764044	0.463880048	0.15387836	0.004477915
H-1	-5.38	E	0.080746172	0.475035928	0.427464978	0.016750818
H-2	-5.38	E	0.080746172	0.475035928	0.427464978	0.016750818
H-3	-5.7	A1	0.025604292	0.652872673	0.310966384	0.010553731
H-4	-5.87	E	0.742820961	0.060024915	0.175953333	0.021206581
H-5	-5.87	E	0.742820961	0.060024915	0.175953333	0.021206581
H-6	-6.4	E	0.205735878	0.134481799	0.634412298	0.025365266
H-7	-6.4	E	0.205735878	0.134481799	0.634412298	0.025365266
H-8	-6.44	B2	0.479172115	0.197964629	0.215479927	0.107344085
H-9	-6.58	A2	0.046683423	0.058473136	0.795053821	0.099778045
H-10	-6.64	B1	0.243827207	0.012937611	0.645204689	0.098011267
H-11	-6.69	B2	0.318164175	0.014253246	0.636423614	0.031173105
H-12	-6.74	A1	0.096536038	0.114339548	0.302165309	0.48696894
H-13	-6.74	E	0.007754875	0.21883729	0.174144349	0.599247017
H-14	-6.74	E	0.007754707	0.218838707	0.174144265	0.599247031
H-15	-6.83	B2	0.008352089	0.002944627	0.976425291	0.012257658
H-16	-6.84	B1	0.001967835	0.001326899	0.775503541	0.221180139
H-17	-6.89	E	0.016481413	0.035339913	0.887734236	0.060445718
H-18	-6.89	E	0.016481415	0.035339911	0.887734236	0.060446674
H-19	-6.92	B1	0.031344572	0.009093424	0.25279544	0.706763597
H-20	-6.94	E	0.006351297	0.008955412	0.924627604	0.060066319

Table III-S27. Energy and contribution of frontier MO obtained from DFT for **3-7** from singlet ground state (b3lyp/LanL2DZ(f)[Rh] 6-31G**[N, C, N amidinate core], 3-21G[C, H]).

MO	eV	Symmetry	Rh_2	Amidine	Ph(2)	Ph
L+20	0.42	B2	0.193968529	0.27268653	0.435060772	0.098288887
L+19	0.39	B1	0.010232682	0.005156666	0.761832237	0.222766434
L+18	0.31	A1	0.0311524	0.012720173	0.527736669	0.428385697
L+17	0.29	A2	0.056020924	0.019247163	0.586105609	0.338622169
L+16	0.23	E	0.003302436	0.01791464	0.922198854	0.056575158
L+15	0.23	E	0.003287031	0.018007909	0.921936637	0.056768471
L+14	0.17	A2	0.060094859	0.069543116	0.849493595	0.020883998
L+13	0.13	B1	0.064688611	0.041188176	0.261078324	0.633052926
L+12	0.1	E	0.01828936	0.037564217	0.780733087	0.16341859
L+11	0.1	E	0.018266652	0.03758256	0.780168658	0.164000662
L+10	-0.01	B2	0.065804193	0.037963539	0.514671159	0.381561069
L+9	-0.05	E	0.017518161	0.022224877	0.307614587	0.652664808
L+8	-0.05	E	0.017525867	0.022219767	0.307642707	0.652622495
L+7	-0.08	A1	0.074666852	0.000623175	0.862984983	0.061728275
L+6	-0.12	A1	0.060379727	0.019557896	0.439432269	0.480611246
L+5	-0.5	B1	0.259662804	0.137252003	0.472356504	0.130721552
L+4	-0.63	E	0.020635788	0.284217127	0.218126155	0.477021614
L+3	-0.63	E	0.020637265	0.284198883	0.217986304	0.477182597
L+2	-0.71	A2	0.049688326	0.222439353	0.261511137	0.466357287
L+1	-1.03	B2	0.226499067	0.207192855	0.295314124	0.271003209
LUMO	-2.3	A2	0.832776027	0.073803691	0.091469887	0.001945876
HOMO	-4.42	B1	0.381198631	0.463331078	0.150885906	0.004572739
H-1	-5.13	E	0.083225908	0.487618803	0.411409542	0.017739353
H-2	-5.13	E	0.083238854	0.487707433	0.411326607	0.017737079
H-3	-5.44	A1	0.025279526	0.669496373	0.294402462	0.010835196
H-4	-5.59	E	0.739225422	0.05661608	0.158561604	0.045600554
H-5	-5.59	E	0.739362188	0.056596564	0.158425715	0.045604797
H-6	-6.04	B2	0.363990898	0.167638263	0.212052533	0.256303287
H-7	-6.16	E	0.209855458	0.119342973	0.590160246	0.08062946
H-8	-6.16	E	0.209710856	0.119378379	0.590143798	0.080769172
H-9	-6.24	A2	0.031338426	0.057541853	0.595875503	0.315240322
H-10	-6.43	B1	0.251940769	0.015338767	0.646933892	0.085794343
H-11	-6.44	B2	0.420773786	0.027777481	0.468150639	0.08331189
H-12	-6.59	A1	0.149698574	0.165447698	0.438577137	0.246258694
H-13	-6.6	E	0.0106124	0.203966931	0.48344231	0.301973014
H-14	-6.6	E	0.010607613	0.203689154	0.483728797	0.301970364
H-15	-6.66	B2	0.006972507	0.007301016	0.966825305	0.0189113
H-16	-6.7	E	0.00962769	0.217055173	0.593233547	0.180088489
H-17	-6.7	E	0.009624352	0.216836418	0.593543425	0.180014969
H-18	-6.7	B1	0.016221384	0.001638646	0.970240305	0.011919877
H-19	-6.78	E	0.008252194	0.056938015	0.853346994	0.081443605
H-20	-6.78	E	0.008239732	0.056665653	0.85341602	0.081679232

Table III-S28. Energy and contribution of frontier MO obtained from DFT for **3-8** from singlet ground state (b3lyp/LanL2DZ(f)[Rh] 6-31G**[N, C, N amidinate core], 3-21G[C, H, N]).

MO	eV	Symmetry	Rh_2	Amidine	Ph(2)	Ph-NH_2
L+20	0.63	A	0.249255452	0.367509364	0.232087425	0.151147177
L+19	0.6	A	0.059399281	0.059307143	0.480519585	0.400770448
L+18	0.52	A	0.022815223	0.011998327	0.586708205	0.37847768
L+17	0.49	A	0.022226068	0.010428829	0.43555007	0.531795393
L+16	0.36	A	0.003559734	0.018213922	0.883363723	0.09486917
L+15	0.36	A	0.003566941	0.018592373	0.882683219	0.095153263
L+14	0.34	A	0.049389795	0.033728796	0.434911144	0.481962222
L+13	0.32	A	0.062692717	0.071287113	0.843866649	0.022163983
L+12	0.28	A	0.013480706	0.010157651	0.813296428	0.163073997
L+11	0.28	A	0.013641441	0.010301366	0.814111844	0.161950552
L+10	0.27	A	0.023147256	0.025064637	0.712452423	0.239338786
L+9	0.13	A	0.027261255	0.020462758	0.421232865	0.531051033
L+8	0.13	A	0.027251166	0.020489615	0.421780026	0.530472206
L+7	0.09	A	0.060867241	0.01200551	0.668387378	0.258738554
L+6	0.02	A	0.081742935	0.010372672	0.727696061	0.180186548
L+5	-0.28	A	0.021376555	0.323921888	0.335489342	0.319215325
L+4	-0.28	A	0.021333802	0.32473061	0.335453852	0.31848521
L+3	-0.34	A	0.248794445	0.129975743	0.498538248	0.122677855
L+2	-0.36	A	0.05939345	0.229117366	0.403231334	0.308263848
L+1	-0.72	A	0.245014905	0.207671262	0.375133464	0.172176898
LUMO	-2.08	A	0.8302708	0.072898937	0.095145501	0.001682374
HOMO	-4.21	A	0.386093531	0.46268274	0.146573939	0.004647636
H-1	-4.91	A	0.094979136	0.440338977	0.355666976	0.109009381
H-2	-4.91	A	0.095111206	0.439566716	0.353984782	0.111333977
H-3	-5.1	A	0.171657144	0.094192781	0.139355491	0.594785879
H-4	-5.1	A	0.174480387	0.093357197	0.13958679	0.592572589
H-5	-5.11	A	0.058095191	0.048329507	0.077194633	0.81638174
H-6	-5.19	A	0.005230074	0.034621965	0.069521384	0.890628331
H-7	-5.26	A	0.025517275	0.683542022	0.279553783	0.011378978
H-8	-5.51	A	0.667133562	0.043013664	0.055499477	0.234351901
H-9	-5.51	A	0.667126501	0.04295715	0.055046167	0.23486593
H-10	-6.05	A	0.108564727	0.191108273	0.656452934	0.043874199
H-11	-6.05	A	0.109366617	0.191068756	0.655786736	0.043782395
H-12	-6.09	A	0.718758005	0.163781498	0.011398308	0.106071687
H-13	-6.25	A	0.260201505	0.019197327	0.627425812	0.093167912
H-14	-6.39	A	0.057391589	0.067891334	0.766243252	0.108479695
H-15	-6.41	A	0.158870887	0.160688464	0.428640949	0.251793563
H-16	-6.42	A	0.052743819	0.035200587	0.826690101	0.085371956
H-17	-6.49	A	0.019060779	0.417028243	0.334954272	0.228955001
H-18	-6.49	A	0.019113198	0.417328866	0.333485644	0.230077652
H-19	-6.57	A	0.005506801	0.001878043	0.965234225	0.027375193
H-20	-6.58	A	0.009133882	0.001499191	0.970450862	0.018918235

3.S6. Tabulated electrochemical and photophysical data

Table III-S29. Redox potentials vs. SCE of **3-1** to **3-4** in dichloromethane.

	$E_{½}^{red}$ (V) (ΔE (mV))		$E_{½}^{red}$ (V) (ΔE (mV))
	Rh_2^{+5}/ Rh_2^{+6}	Rh_2^{+4}/ Rh_2^{+5}	Rh_2^{+3}/ Rh_2^{+4}
3-1	1.31 (76)	0.29 (72)	-1.55 (106)
3-2a/3-2b	1.33 (109)	0.28 (97)	-1.53 (138)
3-3	1.30 (171)	0.27 (64)	-1.57 (152)
3-4	1.27 (103)	0.26 (67)	-1.55 (126)

Table III-S30. UV-vis absorption peak data of **3-1** to **3-5** in dichloromethane

λ (nm) (ε ($M^{-1}cm^{-1}$))				
3-1	**3-2a/3-2b**	**3-3**	**3-4**	**3-5**
265 (69k)	265 (92k)	266 (108k)	266 (129k)	240 (100k)
296 (57k)	297(72k)	298 (80k)	299 (90k)	296 (54k)
334s (26k)	336s (31k)	339s (32k)	341s (33k)	334s (25k)
372s (10k)	372s (13k)	377s (14k)	381s (14k)	357s (16k)
434s (2k)	438s (1.9k)	441s (1.8k)	450s (1.7k)	433s (2k)
528 (5.7k)	533 (5.2k)	538 (5.0k)	542 (5.0k)	523 (6.2k)
590 (0.3k)	590 (0.3k)	590 (0.3k)	590 (0.3k)	589
844.0 (3.0k)	844.5 (3.0k)	845.0 (3.0k)	845.5 (3.0k)	843.5 (3.0k)
1009(130)	1009(130)	1009(130)	1009(130)	1009
1116 (160)	1116 (160)	1116 (160)	1116 (160)	1116

SI - Chapitre 4 : Informations supplémentaires

Supplementary Information

Rhodium Amidinate Dimers as Structural and Functional Hubs for Multimetallic Assemblies.

Daniel Chartrand, Garry S. Hanan*

Department of Chemistry, Université de Montréal, Montréal, QC, H3T 1J4 Canada

4.S1. Table of Contents

Chart 4.S1. Rh2 complexes **4-1** to **4-4** synthesized in this study (anions omitted).

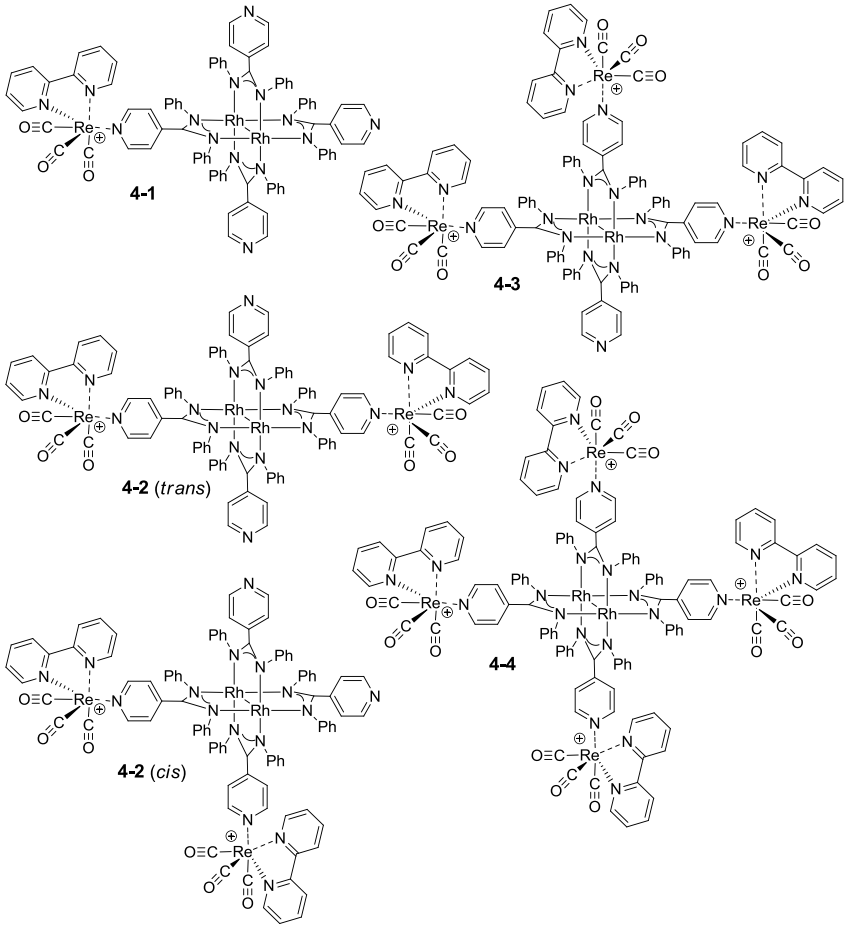

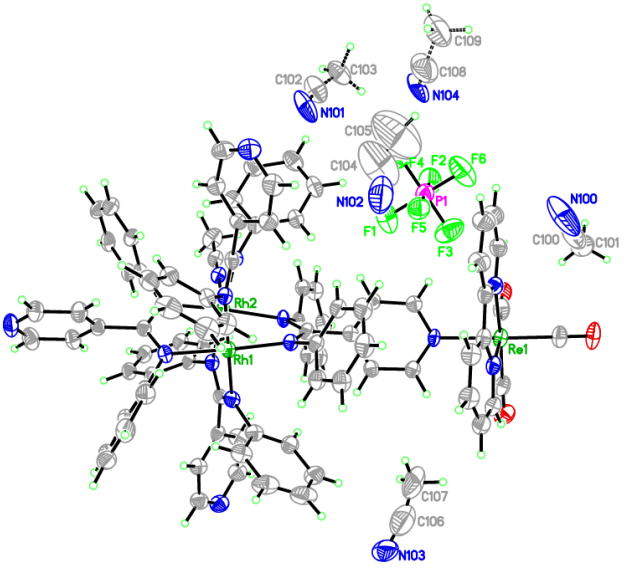

Figure 4.S1. ORTEP view of the asymmetric unit of the X-ray crystal structure of **4-1** (50% probability displacement ellipsoids); Showing labeling for anion and solvent molecules.

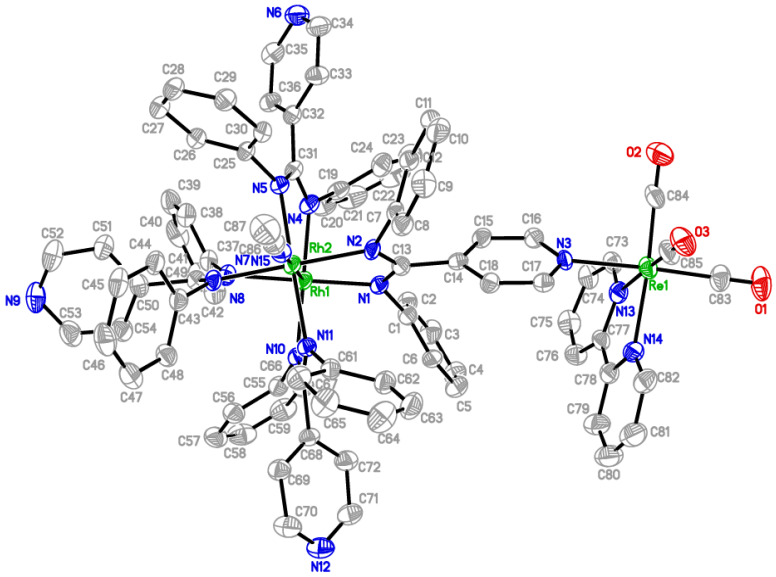

Figure 4.S2. ORTEP view and labeling of the X-ray crystal structure of **4-1** (50% probability displacement ellipsoids; hydrogen atoms, anion and solvent molecules removed for the sake of clarity).

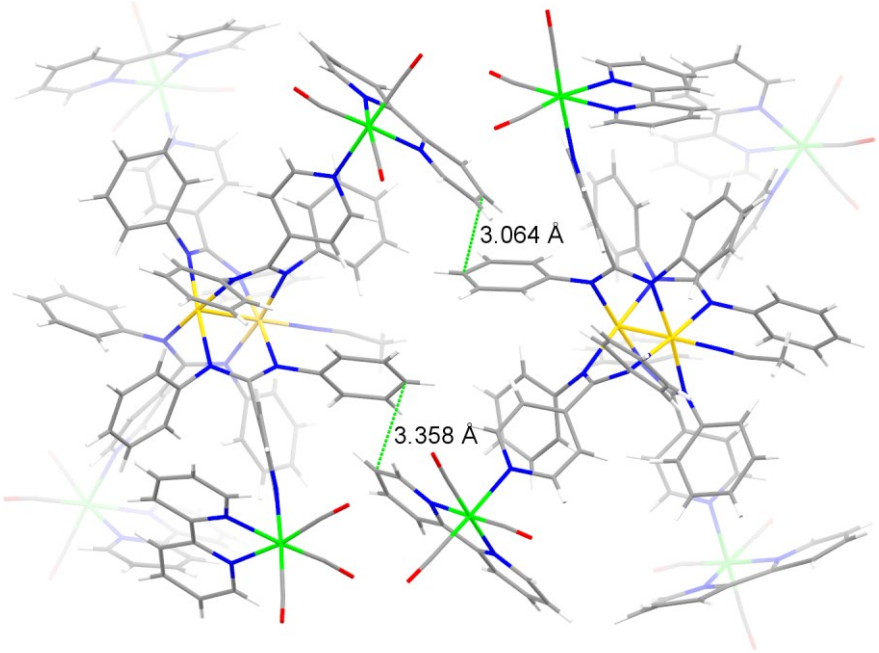

Figure 4.S3. Wireframe view of **4-4** showing the π stacking interactions between adjacent molecules; cocrystallised solvent and anions are omitted for the sake of clarity.

Table IV-S1. Unadjusted computed IR CO bands for **4-1**, **4-4** and **4-8**.

complex	CO stretches (cm^{-1})		
4-1	2037.49	2047.73	2118.25
4-4	2029.82	2033.79	2124.73
	2029.9	2055.88	2125.11
4-8	2041.15	2053.05	2122.7

Table IV-S2. UV-vis absorption bands data of **4-1** to **4-5** and **4-8** in dichloromethane

Band	Complex λ_{exp} (nm); (ε ($M^{-1}cm^{-1}$))					
assignment	**4-1**	**4-2**	**4-3**	**4-4**	**4-5**	**4-8**
^{1}Ph($\pi\rightarrow\pi^*$) Re ^{1}MLCT	305 (50k)	307 (60k)	308 (71k)	310 (82k)	298 (40k)	306 (15k)
^{1}Bpy ($\pi\rightarrow\pi^*$)	320 (38k)	320 (49k)	320 (63k)	320 (75k)	—	321 (14k)
Re ^{1}MLCT	344s (25k)	344s (30k)	344s (36k)	344s (42k)	—	358 (4.8k)
Rh_2 ^1M_2LCT	507; 541*; 571 (2k; 2k; 1.5k)	586 (1.7k)	595 (2.0k)	603 (2.5k)	541 (4.9k)	—
$^1Rh_2$ ($\pi^*\rightarrow\sigma^*$)	835 (2.2k)	833 (2.3k)	832 (2.3k)	831 (2.4k)	837 (2.2k)	—
$^1Rh_2$ ($\delta^*\rightarrow\sigma^*$)	992 (60)	994 (50)	989 (100)	991 (50)	993 (60)	—
$^1Rh_2$ ($\delta^*\rightarrow\sigma^*$)	1095 (40)	1095 (70)	1089 (70)	1084 (60)	1101 (100)	—

*: calculated as being a $^1LM_2CT$

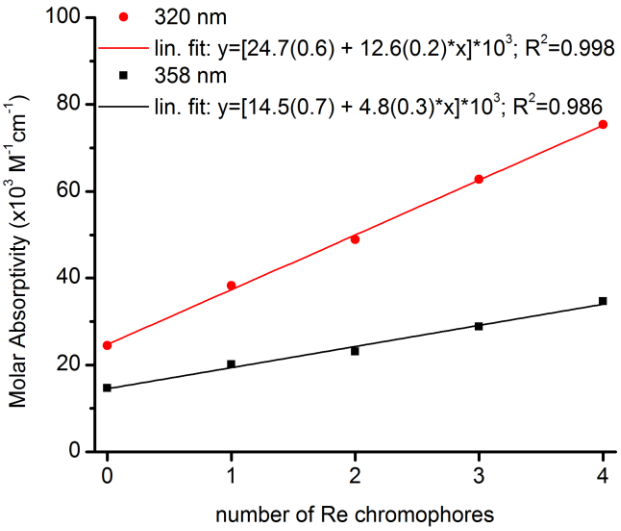

Figure 4.S4. Molar absorptivity at specific wavelengths for complexes **4-1** to **4-4** in function of the number of rhenium chromophores (in dichloromethane).

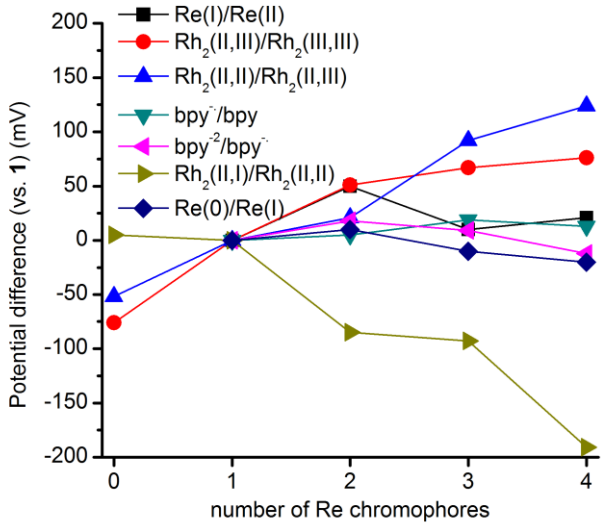

Figure 4.S5. Variation in potential in function of the number of Re chromophores, all redox couples are referenced vs. **4-1** redox couple (in acetonitrile).

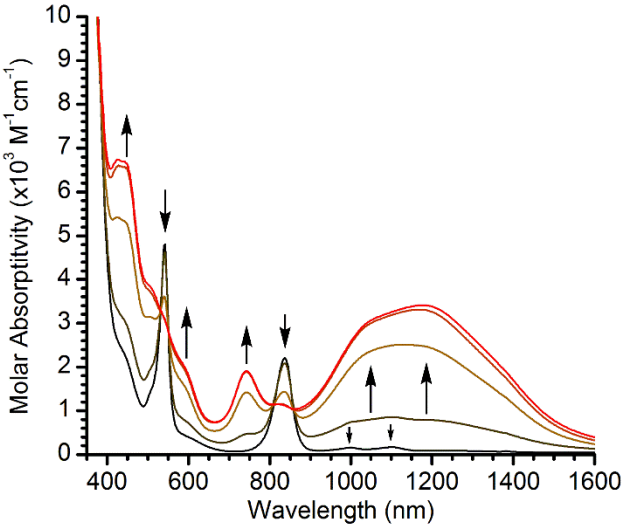

Figure 4.S6. Spectral changes of **4-5** during chemical oxidation in DCM (using *meta*-chloroperoxybenzoic acid). Black line: starting material, grey line: final oxidized product.

Chart 4.S2. Frontier MO orbital diagrams of **4-1**; rb3lyp/LanL2DZ(f)[Rh,Re] 6-31G**[$NCN_{amidinate}$, $N_{py\text{-}Re}$, CO], 3-21G[C_{aryl},H, N_{py}] with CPCM (DCM).

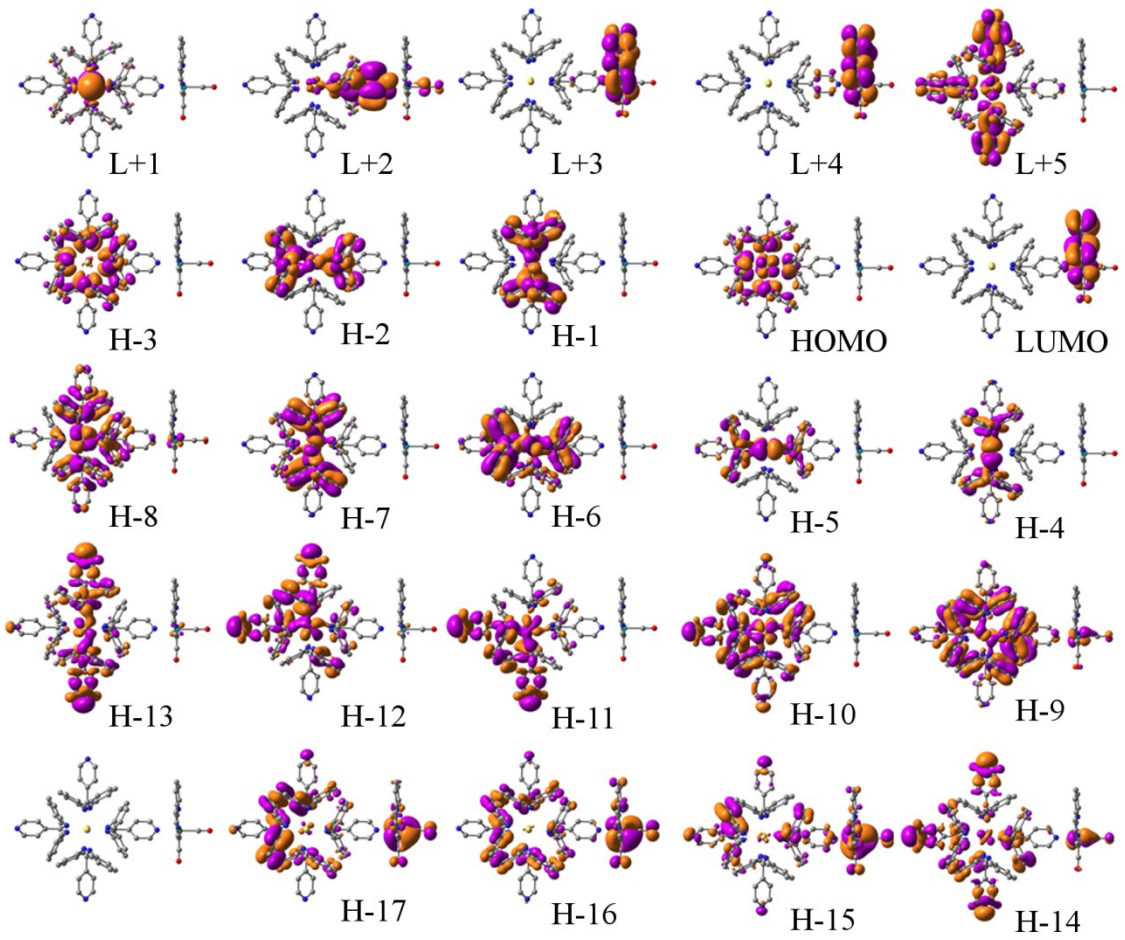

Chart 4.S3. Selected MO orbital diagrams of **4-4**; rb3lyp/LanL2DZ(f)[Rh,Re] 6-31G**[$NCN_{amidinate}$, $N_{py\text{-}Re}$, CO], 3-21G[C_{aryl},H, N_{py}] with CPCM (DCM).

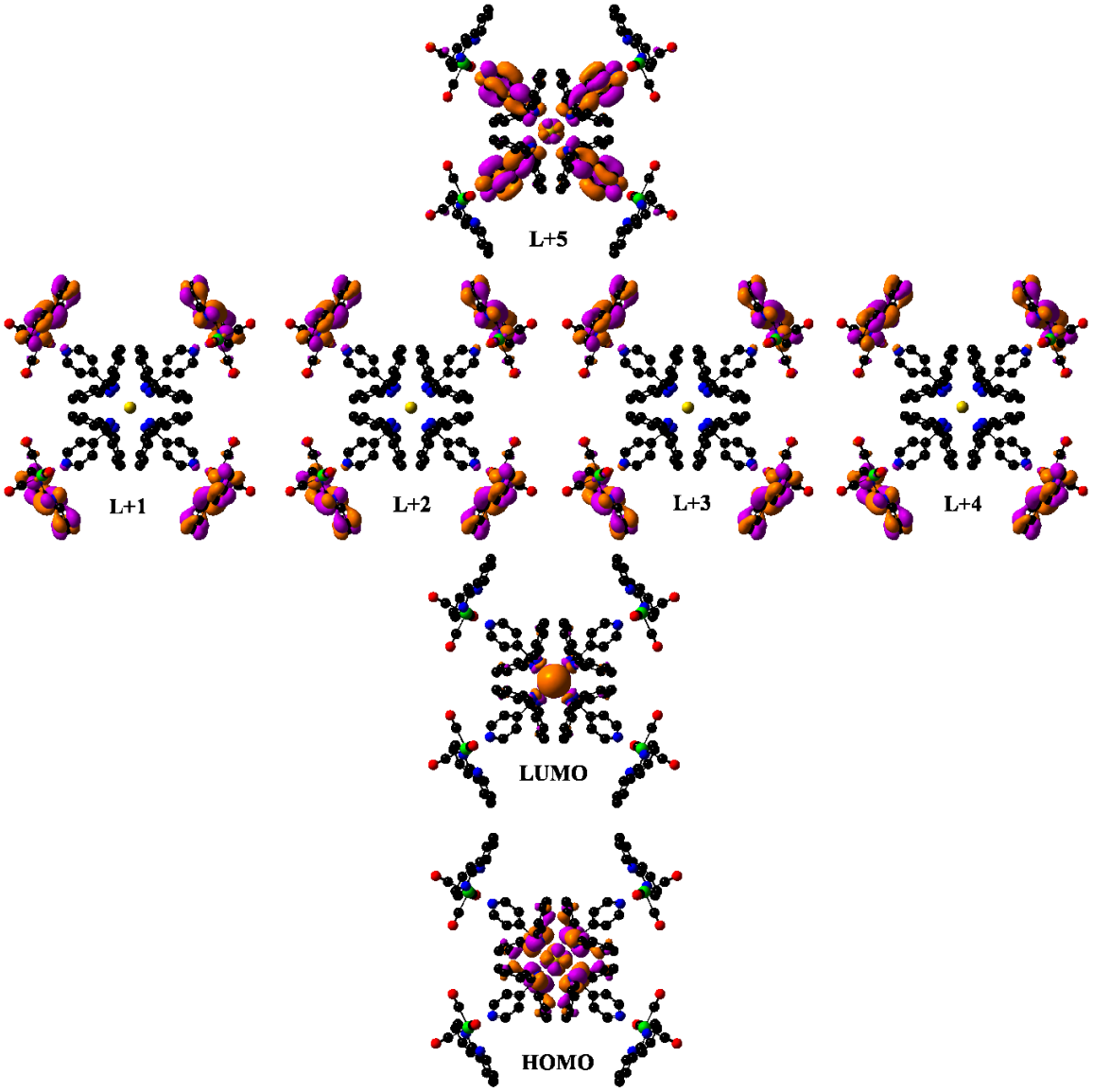

Chart 4.S4. Selected MO orbital diagrams of **4-5+MeCN**; rb3lyp/LanL2DZ(f)[Rh] 6-31G**[$NCN_{amidinate}$,, CO], 3-21G[C_{aryl},H, N_{py}] with CPCM (DCM).

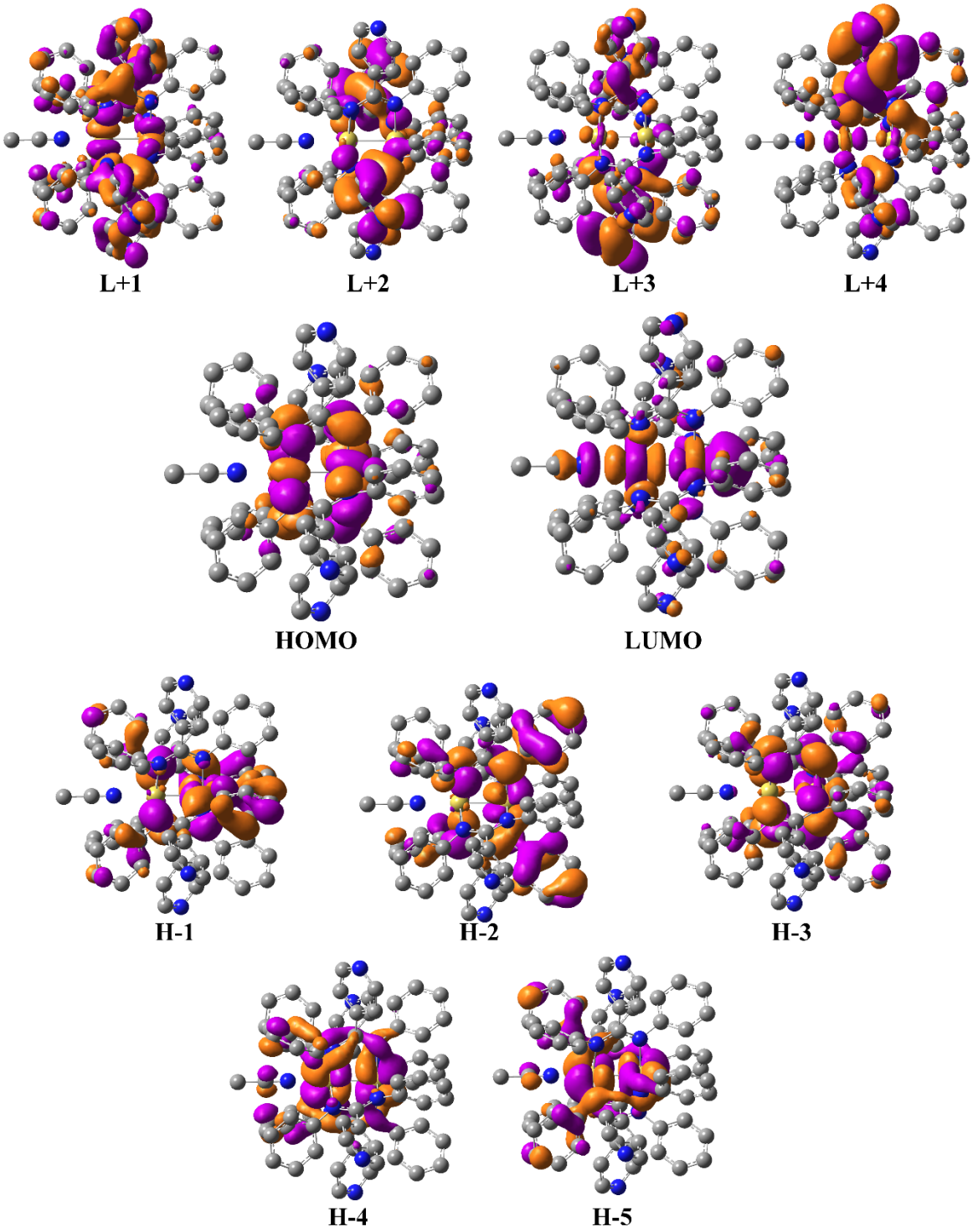

Chart 4.S5. Total electron spin density of (**4-5+MeCN**)$^{+}$; ub3lyp/LanL2DZ(f)[Rh] 6-31G**[$NCN_{amidinate}$,, CO], 3-21G[C_{aryl},H, N_{py}] with CPCM (DCM).(isovalue = 0.0004)

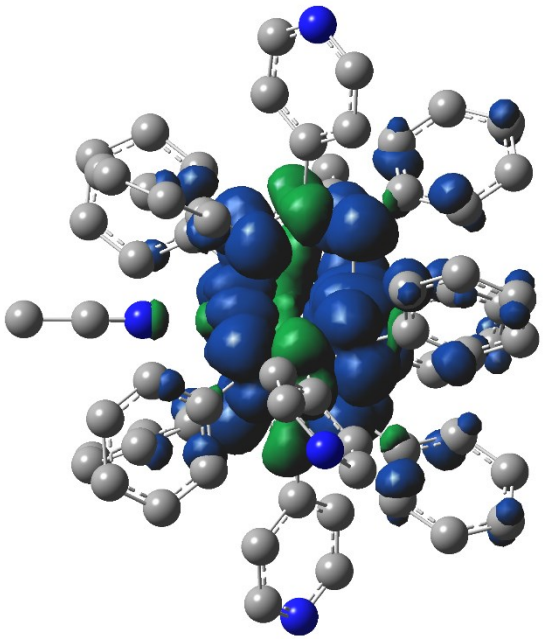

Table IV-S3. Optimized atomic coordinates obtained from DFT for **4-1** singlet ground state (b3lyp/LanL2DZ(f)[Rh,Re] 6-31G**[C,H,N]) E= -4568.16047523 Hartree.

Atom	x /Å	y /Å	z /Å
Re	7.078802	-0.737771	-0.520865
Rh	-2.128412	0.089657	1.196838
Rh	-2.26695	-0.095151	-1.213186
N	-0.026209	0.199741	0.986602
N	-0.197107	-0.50194	-1.227753
N	4.840888	-0.527855	-0.378956
N	-1.998888	-2.005471	1.259991
N	-2.664081	-2.133652	-0.956861
N	-2.73604	-7.024916	0.581298
N	-4.206622	-0.034485	1.242314
N	-4.298425	0.323679	-1.045233
N	-9.220253	0.501257	0.348602
N	-2.253694	2.169909	0.967069
N	-1.851684	1.963471	-1.306971
N	-1.714751	7.028831	-0.579177
N	7.101634	-0.133936	1.592768
N	7.114132	1.460802	-0.536085
O	10.16261	-0.922482	-0.624425
O	6.867258	-3.777567	-0.028324
O	6.914804	-1.111247	-3.580848
C	0.722662	0.903156	1.963132
C	0.732199	0.45229	3.294359
H	0.204324	-0.460381	3.547171
C	1.418787	1.164247	4.278
H	1.413813	0.796838	5.300278
C	2.107213	2.337227	3.958936
H	2.628415	2.895128	4.731055
C	2.100737	2.793325	2.639282

Atom	x /Å	y /Å	z /Å
H	2.615458	3.714224	2.377807
C	1.41271	2.088413	1.651556
H	1.388471	2.46182	0.633222
C	0.336453	-1.293207	-2.280186
C	0.281716	-0.824228	-3.602735
H	-0.127755	0.160122	-3.799471
C	0.761805	-1.611245	-4.650216
H	0.718019	-1.228963	-5.665915
C	1.30125	-2.8753	-4.401443
H	1.672542	-3.484369	-5.219505
C	1.352204	-3.350596	-3.089554
H	1.759309	-4.336311	-2.882923
C	0.868436	-2.57141	-2.038554
H	0.886996	-2.953942	-1.023424
C	0.532528	-0.197787	-0.157685
C	2.035479	-0.313031	-0.236717
C	2.753284	-1.084673	0.684171
H	2.239106	-1.623518	1.472207
C	4.132506	-1.170511	0.576056
H	4.700572	-1.777763	1.270532
C	4.145145	0.216061	-1.267495
H	4.724105	0.716359	-2.034495
C	2.765415	0.344157	-1.233866
H	2.26184	0.949485	-1.979235
C	-1.30012	-2.577513	2.350166
C	-1.717953	-2.299436	3.663113
H	-2.616713	-1.712859	3.818252
C	-1.006585	-2.797073	4.755909

Atom	x /Å	y /Å	z /Å
H	-1.357917	-2.581801	5.761006
C	0.131965	-3.582471	4.565867
H	0.675778	-3.978219	5.417974
C	0.552504	-3.867492	3.26464
H	1.427256	-4.491073	3.100071
C	-0.147527	-3.364801	2.168524
H	0.181401	-3.597614	1.16127
C	-3.422277	-2.776336	-1.971661
C	-4.701009	-3.300924	-1.718566
H	-5.101916	-3.258838	-0.711761
C	-5.447803	-3.876066	-2.745409
H	-6.430665	-4.284054	-2.528003
C	-4.942039	-3.925427	-4.046463
H	-5.526774	-4.37161	-4.844633
C	-3.675532	-3.400033	-4.307293
H	-3.264924	-3.442016	-5.312039
C	-2.919193	-2.830634	-3.28168
H	-1.927358	-2.442919	-3.485501
C	-2.382759	-2.730783	0.202386
C	-2.506137	-4.227373	0.328747
C	-1.871592	-5.090317	-0.571761
H	-1.281098	-4.700232	-1.393568
C	-2.013782	-6.466434	-0.397826
H	-1.522944	-7.154796	-1.083255
C	-3.345912	-6.191616	1.433175
H	-3.933959	-6.657976	2.221206
C	-3.260417	-4.801685	1.357673
H	-3.772338	-4.179429	2.083663
C	-4.802192	-0.573777	2.413753
C	-5.521895	-1.780693	2.385152
H	-5.666082	-2.289318	1.438166
C	-6.057555	-2.316204	3.55518
H	-6.621506	-3.243433	3.509808
C	-5.871181	-1.6695	4.779146
H	-6.288501	-2.088784	5.689216
C	-5.151049	-0.474533	4.817085
H	-5.011619	0.04747	5.759461
C	-4.620826	0.072578	3.647331
H	-4.085649	1.014683	3.679422
C	-4.926417	0.949093	-2.155459
C	-4.96797	0.28911	-3.394494
H	-4.581127	-0.720594	-3.472141
C	-5.527357	0.915015	-4.509993
H	-5.562314	0.383328	-5.456541
C	-6.054968	2.203483	-4.411166
H	-6.495394	2.684712	-5.278714
C	-6.018748	2.864459	-3.18119
H	-6.432048	3.864726	-3.088545
C	-5.45276	2.249191	-2.065969
H	-5.423605	2.767938	-1.113966
C	-4.914312	0.192399	0.132257
C	-6.414483	0.30038	0.208698
C	-7.236817	-0.482053	-0.609093
H	-6.808797	-1.182369	-1.317872
C	-8.619986	-0.347079	-0.495138
H	-9.278452	-0.951392	-1.116101
C	-8.4248	1.249551	1.122931

Atom	x /Å	y /Å	z /Å
H	-8.925937	1.936693	1.801957
C	-7.031952	1.185885	1.09848
H	-6.440816	1.812555	1.757479
C	-2.801943	2.90967	2.047509
C	-3.996723	3.638259	1.917777
H	-4.492508	3.677327	0.954073
C	-4.54099	4.309456	3.01153
H	-5.461024	4.873551	2.888852
C	-3.915366	4.254745	4.25914
H	-4.343697	4.775296	5.10982
C	-2.732918	3.526273	4.398431
H	-2.230797	3.482515	5.36075
C	-2.178152	2.859755	3.304977
H	-1.249863	2.30993	3.412629
C	-1.205752	2.43839	-2.474658
C	0.06864	3.03351	-2.433125
H	0.544852	3.196103	-1.471844
C	0.705964	3.435475	-3.606406
H	1.68216	3.910044	-3.549985
C	0.097149	3.237496	-4.847756
H	0.594271	3.551437	-5.760193
C	-1.164469	2.64169	-4.898729
H	-1.658493	2.494563	-5.854784
C	-1.812442	2.24671	-3.727743
H	-2.801609	1.805269	-3.77375
C	-2.010641	2.727608	-0.221182
C	-1.91276	4.226913	-0.341748
C	-2.671376	4.928793	-1.284538
H	-3.352348	4.406876	-1.948112
C	-2.539325	6.315474	-1.356253
H	-3.125727	6.880524	-2.078067
C	-0.992353	6.348187	0.319073
H	-0.328184	6.940089	0.946485
C	-1.055756	4.965256	0.482063
H	-0.452884	4.472813	1.237277
C	7.159922	-0.998278	2.625814
H	7.226548	-2.04791	2.365992
C	7.145968	-0.587964	3.952896
H	7.198659	-1.326861	4.74404
C	7.06551	0.775212	4.229023
H	7.04867	1.135457	5.252049
C	7.01732	1.674277	3.168677
H	6.965755	2.736829	3.367903
C	7.043105	1.200022	1.853852
C	7.05209	2.086396	0.670661
C	7.038979	3.481831	0.755823
H	6.985975	3.972276	1.719238
C	7.102965	4.246584	-0.404422
H	7.096914	5.329781	-0.345912
C	7.185408	3.597924	-1.634785
H	7.250507	4.149191	-2.565693
C	7.186752	2.208857	-1.655556
H	7.254316	1.664113	-2.589557
C	9.008245	-0.858722	-0.590943
C	6.957336	-2.643398	-0.249791
C	6.98299	-1.00891	-2.428492

Table IV-S4. Optimized atomic coordinates obtained from DFT for **4-4** singlet ground state (b3lyp/LanL2DZ(f)[Rh,Re] 6-31G**[C,H,N]) E= -7311.41466425 Hartree.

Atom	x /Å	y /Å	z /Å
Rh	0	0	1.209872
Rh	0	0	-1.209872
Re	7.298783	-5.651819	-0.639793
Re	7.298783	5.651819	0.639793
Re	-7.298783	-5.651819	0.639793
Re	-7.298783	5.651819	-0.639793
N	1.286141	-1.661263	1.126552
N	1.663169	1.278094	1.133364
N	-1.663169	-1.278094	1.133364
N	-1.286141	1.661263	1.126552
N	1.663169	-1.278094	-1.133364
N	1.286141	1.661263	-1.126552
N	-1.286141	-1.661263	-1.126552
N	-1.663169	1.278094	-1.133364
C	1.946649	-1.927169	-0.002284
C	1.260821	-2.586382	2.20303
C	1.946649	1.927169	0.002284
C	2.571642	1.234023	2.226674
C	-1.946649	-1.927169	0.002284
C	-2.571642	-1.234023	2.226674
C	-1.946649	1.927169	-0.002284
C	-1.260821	2.586382	2.20303
C	2.571642	-1.234023	-2.226674
C	1.260821	2.586382	-2.20303
C	-1.260821	-2.586382	-2.20303
C	-2.571642	1.234023	-2.226674
C	3.062691	-2.948968	-0.001639
C	1.560217	-2.149035	3.504262
C	0.878956	-3.926098	2.012687
C	3.062691	2.948968	0.001639
C	3.899377	0.799582	2.069187
C	2.122488	1.57459	3.512998
C	-3.062691	-2.948968	0.001639
C	-3.899377	-0.799582	2.069187
C	-2.122488	-1.57459	3.512998
C	-3.062691	2.948968	-0.001639
C	-1.560217	2.149035	3.504262
C	-0.878956	3.926098	2.012687
C	3.899377	-0.799582	-2.069187
C	2.122488	-1.57459	-3.512998
C	1.560217	2.149035	-3.504262
C	0.878956	3.926098	-2.012687
C	-1.560217	-2.149035	-3.504262
C	-0.878956	-3.926098	-2.012687
C	-2.122488	1.57459	-3.512998
C	-3.899377	0.799582	-2.069187
C	3.125506	-3.973462	-0.953257
C	4.118228	-2.864136	0.914236
H	1.866531	-1.120481	3.661365
C	1.48483	-3.032815	4.581704
C	0.814514	-4.806331	3.093057
H	0.632535	-4.270017	1.013095
C	3.125506	3.973462	0.953257
C	4.118228	2.864136	-0.914236
H	4.254475	0.52209	1.082147
C	4.760267	0.734356	3.165056
C	2.985663	1.496373	4.607428
H	1.102806	1.919143	3.645006
C	-3.125506	-3.973462	0.953257
C	-4.118228	-2.864136	-0.914236

Atom	x /Å	y /Å	z /Å
H	-4.254475	-0.52209	1.082147
C	-4.760267	-0.734356	3.165056
C	-2.985663	-1.496373	4.607428
H	-1.102806	-1.919143	3.645006
C	-3.125506	3.973462	-0.953257
C	-4.118228	2.864136	0.914236
H	-1.866531	1.120481	3.661365
C	-1.48483	3.032815	4.581704
C	-0.814514	4.806331	3.093057
H	-0.632535	4.270017	1.013095
H	4.254475	-0.52209	-1.082147
C	4.760267	-0.734356	-3.165056
C	2.985663	-1.496373	-4.607428
H	1.102806	-1.919143	-3.645006
H	1.866531	1.120481	-3.661365
C	1.48483	3.032815	-4.581704
C	0.814514	4.806331	-3.093057
H	0.632535	4.270017	-1.013095
H	-1.866531	-1.120481	-3.661365
C	-1.48483	-3.032815	-4.581704
C	-0.814514	-4.806331	-3.093057
H	-0.632535	-4.270017	-1.013095
H	-1.102806	1.919143	-3.645006
C	-2.985663	1.496373	-4.607428
C	-4.760267	0.734356	-3.165056
H	-4.254475	0.52209	-1.082147
H	2.332047	-4.107529	-1.679377
C	4.240748	-4.799159	-1.001118
C	5.20208	-3.723336	0.79322
H	4.119174	-2.109714	1.692192
H	1.727401	-2.679465	5.579451
C	1.112598	-4.364446	4.383806
H	0.522966	-5.839633	2.926636
H	2.332047	4.107529	1.679377
C	4.240748	4.799159	1.001118
C	5.20208	3.723336	-0.79322
H	4.119174	2.109714	-1.692192
H	5.787852	0.412289	3.021673
C	4.308055	1.08018	4.440766
H	2.624828	1.776167	5.592606
H	-2.332047	-4.107529	1.679377
C	-4.240748	-4.799159	1.001118
C	-5.20208	-3.723336	-0.79322
H	-4.119174	-2.109714	-1.692192
H	-5.787852	-0.412289	3.021673
C	-4.308055	-1.08018	4.440766
H	-2.624828	-1.776167	5.592606
H	-2.332047	4.107529	-1.679377
C	-4.240748	4.799159	-1.001118
C	-5.20208	3.723336	0.79322
H	-4.119174	2.109714	1.692192
H	-1.727401	2.679465	5.579451
C	-1.112598	4.364446	4.383806
H	-0.522966	5.839633	2.926636
H	5.787852	-0.412289	-3.021673
C	4.308055	-1.08018	-4.440766
H	2.624828	-1.776167	-5.592606
H	1.727401	2.679465	-5.579451
C	1.112598	4.364446	-4.383806
H	0.522966	5.839633	-2.926636

Atom	x /Å	y /Å	z /Å
H	-1.727401	-2.679465	-5.579451
C	-1.112598	-4.364446	-4.383806
H	-0.522966	-5.839633	-2.926636
H	-2.624828	1.776167	-5.592606
C	-4.308055	1.08018	-4.440766
H	-5.787852	0.412289	-3.021673
N	5.29769	-4.664189	-0.170615
H	4.316408	-5.572793	-1.755907
H	6.045096	-3.641392	1.468883
H	1.055448	-5.048045	5.224729
N	5.29769	4.664189	0.170615
H	4.316408	5.572793	1.755907
H	6.045096	3.641392	-1.468883
H	4.978777	1.030675	5.292291
N	-5.29769	-4.664189	0.170615
H	-4.316408	-5.572793	1.755907
H	-6.045096	-3.641392	-1.468883
H	-4.978777	-1.030675	5.292291
N	-5.29769	4.664189	-0.170615
H	-4.316408	5.572793	-1.755907
H	-6.045096	3.641392	1.468883
H	-1.055448	5.048045	5.224729
H	4.978777	-1.030675	-5.292291
H	1.055448	5.048045	-5.224729
H	-1.055448	-5.048045	-5.224729
H	-4.978777	1.030675	-5.292291
C	9.005758	-6.474363	-1.037747
C	6.956252	-5.457977	-2.526581
C	8.12858	-3.912808	-0.615902
N	7.515542	-6.119564	1.499933
N	6.335572	-7.610606	-0.365518
C	9.005758	6.474363	1.037747
C	6.956252	5.457977	2.526581
C	8.12858	3.912808	0.615902
N	7.515542	6.119564	-1.499933
N	6.335572	7.610606	0.365518
C	-9.005758	-6.474363	1.037747
C	-6.956252	-5.457977	2.526581
C	-8.12858	-3.912808	0.615902
N	-7.515542	-6.119564	-1.499933
N	-6.335572	-7.610606	0.365518
C	-9.005758	6.474363	-1.037747
C	-6.956252	5.457977	-2.526581
C	-8.12858	3.912808	-0.615902
N	-7.515542	6.119564	1.499933
N	-6.335572	7.610606	-0.365518
O	10.022195	-6.968383	-1.269509
O	6.705745	-5.383404	-3.656287
O	8.606247	-2.858236	-0.54341
C	8.191377	-5.349419	2.377946
C	6.992199	-7.300754	1.929266
C	6.335653	-8.127555	0.893919
C	5.810717	-8.341634	-1.370125
O	10.022195	6.968383	1.269509
O	6.705745	5.383404	3.656287
O	8.606247	2.858236	0.54341
C	8.191377	5.349419	-2.377946
C	6.992199	7.300754	-1.929266
C	6.335653	8.127555	-0.893919
C	5.810717	8.341634	1.370125
O	-10.022195	-6.968383	1.269509
O	-6.705745	-5.383404	3.656287
O	-8.606247	-2.858236	0.54341
C	-8.191377	-5.349419	-2.377946

Atom	x /Å	y /Å	z /Å
C	-6.992199	-7.300754	-1.929266
C	-6.335653	-8.127555	-0.893919
C	-5.810717	-8.341634	1.370125
O	-10.022195	6.968383	-1.269509
O	-6.705745	5.383404	-3.656287
O	-8.606247	2.858236	-0.54341
C	-6.992199	7.300754	1.929266
C	-8.191377	5.349419	2.377946
C	-5.810717	8.341634	-1.370125
C	-6.335653	8.127555	0.893919
H	8.614773	-4.433906	1.982025
C	8.365826	-5.700466	3.710714
C	7.127052	-7.703995	3.261214
C	5.786197	-9.386694	1.15288
C	5.259199	-9.602035	-1.17676
H	5.857618	-7.899371	-2.357994
H	8.614773	4.433906	-1.982025
C	8.365826	5.700466	-3.710714
C	7.127052	7.703995	-3.261214
C	5.786197	9.386694	-1.15288
C	5.259199	9.602035	1.17676
H	5.857618	7.899371	2.357994
H	-8.614773	-4.433906	-1.982025
C	-8.365826	-5.700466	-3.710714
C	-7.127052	-7.703995	-3.261214
C	-5.786197	-9.386694	-1.15288
C	-5.259199	-9.602035	1.17676
H	-5.857618	-7.899371	2.357994
C	-7.127052	7.703995	3.261214
C	-8.365826	5.700466	3.710714
H	-8.614773	4.433906	1.982025
H	-5.857618	7.899371	-2.357994
C	-5.259199	9.602035	-1.17676
C	-5.786197	9.386694	1.15288
H	8.928954	-5.049288	4.369282
C	7.818033	-6.899535	4.162183
H	6.712032	-8.646286	3.594803
H	5.794368	-9.794501	2.155462
C	5.24389	-10.133	0.111241
H	4.866264	-10.152425	-2.023822
H	8.928954	5.049288	-4.369282
C	7.818033	6.899535	-4.162183
H	6.712032	8.646286	-3.594803
H	5.794368	9.794501	-2.155462
C	5.24389	10.133	-0.111241
H	4.866264	10.152425	2.023822
H	-8.928954	-5.049288	-4.369282
C	-7.818033	-6.899535	-4.162183
H	-6.712032	-8.646286	-3.594803
H	-5.794368	-9.794501	-2.155462
C	-5.24389	-10.133	-0.111241
H	-4.866264	-10.152425	2.023822
H	-6.712032	8.646286	3.594803
C	-7.818033	6.899535	4.162183
H	-8.928954	5.049288	4.369282
H	-4.866264	10.152425	-2.023822
C	-5.24389	10.133	0.111241
H	-5.794368	9.794501	2.155462
H	7.937236	-7.212229	5.194078
H	4.830619	-11.117595	0.302652
H	7.937236	7.212229	-5.194078
H	4.830619	11.117595	-0.302652
H	-7.937236	-7.212229	-5.194078
H	-4.830619	-11.117595	-0.302652

Atom	x /Å	y /Å	z /Å
H	-7.937236	7.212229	5.194078

Atom	x /Å	y /Å	z /Å
H	-4.830619	11.117595	0.302652

Table IV-S5. Optimized atomic coordinates obtained from DFT for **4-5** singlet ground state (b3lyp/LanL2DZ(f)[Rh] 6-31G**[C,H,N]) E= -3653.66095020 Hartree

Atom	x /Å	y /Å	z /Å
Rh	0	0	1.211702
Rh	0	0	-1.211702
N	0.266446	2.078908	1.128826
N	-0.266446	2.078908	-1.128826
C	-0.788251	4.971969	0.901036
H	-1.415107	4.460227	1.623349
C	0	4.248163	0
C	0.788251	4.971969	-0.901036
H	1.415107	4.460227	-1.623349
C	0.755482	6.365035	-0.853827
H	1.367828	6.946213	-1.540969
C	-0.755482	6.365035	0.853827
H	-1.367828	6.946213	1.540969
N	0	7.06734	0
C	0	2.740564	0
C	-0.923522	2.700898	-2.221369
C	-0.364231	2.616008	-3.507214
H	0.597092	2.131456	-3.634136
C	-1.025206	3.168745	-4.604974
H	-0.569812	3.101203	-5.589011
C	-2.251567	3.815998	-4.443951
H	-2.761357	4.248855	-5.299175
C	-2.814051	3.904336	-3.168659
H	-3.766964	4.406718	-3.027526
C	-2.163206	3.346436	-2.069511
H	-2.608447	3.411253	-1.082767
C	0.923522	2.700898	2.221369
C	0.364231	2.616008	3.507214
H	-0.597092	2.131456	3.634136
C	1.025206	3.168745	4.604974
H	0.569812	3.101203	5.589011
C	2.251567	3.815998	4.443951
H	2.761357	4.248855	5.299175
C	2.814051	3.904336	3.168659
H	3.766964	4.406718	3.027526
C	2.163206	3.346436	2.069511
H	2.608447	3.411253	1.082767
N	2.078908	-0.266446	1.128826
N	2.078908	0.266446	-1.128826
C	4.971969	0.788251	0.901036
H	4.460227	1.415107	1.623349
C	4.248163	0	0
C	4.971969	-0.788251	-0.901036
H	4.460227	-1.415107	-1.623349
C	6.365035	-0.755482	-0.853827
H	6.946213	-1.367828	-1.540969
C	6.365035	0.755482	0.853827
H	6.946213	1.367828	1.540969
N	7.06734	0	0
C	2.740564	0	0
C	2.700898	0.923522	-2.221369
C	2.616008	0.364231	-3.507214
H	2.131456	-0.597092	-3.634136

Atom	x /Å	y /Å	z /Å
C	3.168745	1.025206	-4.604974
H	3.101203	0.569812	-5.589011
C	3.815998	2.251567	-4.443951
H	4.248855	2.761357	-5.299175
C	3.904336	2.814051	-3.168659
H	4.406718	3.766964	-3.027526
C	*3.346436*	2.163206	-2.069511
H	3.411253	2.608447	-1.082767
C	2.700898	-0.923522	2.221369
C	2.616008	-0.364231	3.507214
H	2.131456	0.597092	3.634136
C	3.168745	-1.025206	4.604974
H	3.101203	-0.569812	5.589011
C	3.815998	-2.251567	4.443951
H	4.248855	-2.761357	5.299175
C	3.904336	-2.814051	3.168659
H	4.406718	-3.766964	3.027526
C	3.346436	-2.163206	2.069511
H	3.411253	-2.608447	1.082767
N	-0.266446	-2.078908	1.128826
N	0.266446	-2.078908	-1.128826
C	0.788251	-4.971969	0.901036
H	1.415107	-4.460227	1.623349
C	0	-4.248163	0
C	-0.788251	-4.971969	-0.901036
H	-1.415107	-4.460227	-1.623349
C	-0.755482	-6.365035	-0.853827
H	-1.367828	-6.946213	-1.540969
C	0.755482	-6.365035	0.853827
H	1.367828	-6.946213	1.540969
N	0	-7.06734	0
C	0	-2.740564	0
C	0.923522	-2.700898	-2.221369
C	0.364231	-2.616008	-3.507214
H	-0.597092	-2.131456	-3.634136
C	1.025206	-3.168745	-4.604974
H	0.569812	-3.101203	-5.589011
C	2.251567	-3.815998	-4.443951
H	2.761357	-4.248855	-5.299175
C	2.814051	-3.904336	-3.168659
H	3.766964	-4.406718	-3.027526
C	2.163206	-3.346436	-2.069511
H	2.608447	-3.411253	-1.082767
C	-0.923522	-2.700898	2.221369
C	-0.364231	-2.616008	3.507214
H	0.597092	-2.131456	3.634136
C	-1.025206	-3.168745	4.604974
H	-0.569812	-3.101203	5.589011
C	-2.251567	-3.815998	4.443951
H	-2.761357	-4.248855	5.299175
C	-2.814051	-3.904336	3.168659
H	-3.766964	-4.406718	3.027526
C	-2.163206	-3.346436	2.069511

Atom	x /Å	y /Å	z /Å
H	-2.608447	-3.411253	1.082767
N	-2.078908	0.266446	1.128826
N	-2.078908	-0.266446	-1.128826
C	-4.971969	-0.788251	0.901036
H	-4.460227	-1.415107	1.623349
C	-4.248163	0	0
C	-4.971969	0.788251	-0.901036
H	-4.460227	1.415107	-1.623349
C	-6.365035	0.755482	-0.853827
H	-6.946213	1.367828	-1.540969
C	-6.365035	-0.755482	0.853827
H	-6.946213	-1.367828	1.540969
N	-7.06734	0	0
C	-2.740564	0	0
C	-2.700898	-0.923522	-2.221369
C	-2.616008	-0.364231	-3.507214
H	-2.131456	0.597092	-3.634136
C	-3.168745	-1.025206	-4.604974
H	-3.101203	-0.569812	-5.589011
C	-3.815998	-2.251567	-4.443951
H	-4.248855	-2.761357	-5.299175
C	-3.904336	-2.814051	-3.168659
H	-4.406718	-3.766964	-3.027526
C	-3.346436	-2.163206	-2.069511
H	-3.411253	-2.608447	-1.082767
C	-2.700898	0.923522	2.221369
C	-2.616008	0.364231	3.507214
H	-2.131456	-0.597092	3.634136
C	-3.168745	1.025206	4.604974
H	-3.101203	0.569812	5.589011
C	-3.815998	2.251567	4.443951
H	-4.248855	2.761357	5.299175
C	-3.904336	2.814051	3.168659
H	-4.406718	3.766964	3.027526
C	-3.346436	2.163206	2.069511
H	-3.411253	2.608447	1.082767

Table IV-S6. Optimized atomic coordinates obtained from DFT for **4-5+MeCN** singlet ground state (b3lyp/LanL2DZ(f)[Rh] 6-31G**[C,H,N]) E= -3786.42119891 Hartree.

Atom	x /Å	y /Å	z /Å
Rh	0.013651	-0.018687	1.157388
Rh	-0.019378	0.023767	-1.296967
N	1.860457	-1.072118	0.98443
N	1.999092	-0.529353	-1.272581
N	6.452314	-2.888348	-0.412961
N	-1.047989	-1.865072	1.008779
N	-0.571307	-1.995235	-1.263671
N	-2.925044	-6.441968	-0.358561
N	-1.8313	1.044541	1.071851
N	-2.03668	0.57546	-1.196543
N	-6.450631	2.927925	-0.134513
N	1.070298	1.827023	1.046813
N	0.534101	2.040489	-1.205806
N	2.893961	6.461714	-0.190667
C	2.278625	-1.948269	2.027079
C	2.806719	-1.437597	3.223165
H	2.924646	-0.364945	3.32689
C	3.200191	-2.297366	4.24878
H	3.631837	-1.883604	5.156872
C	3.072743	-3.681614	4.105018
H	3.387585	-4.348435	4.902126
C	2.553977	-4.198164	2.917129
H	2.461689	-5.272556	2.784322
C	2.157483	-3.339851	1.890251
H	1.757716	-3.741782	0.965698
C	2.806221	-0.173907	-2.384228
C	3.901786	0.69766	-2.254377
H	4.164192	1.076464	-1.272572
C	4.649443	1.07564	-3.368918
H	5.496085	1.744818	-3.242723
C	4.312672	0.60464	-4.639336
H	4.894042	0.901723	-5.506799
C	3.22164	-0.25522	-4.779009
H	2.952132	-0.638705	-5.759172
C	2.474149	-0.642389	-3.666281
H	1.63789	-1.322098	-3.779916
C	2.529648	-1.062724	-0.173137
C	3.901245	-1.692149	-0.247726
C	4.954205	-1.273504	0.572579
H	4.811263	-0.479916	1.297059
C	6.196159	-1.893894	0.446256
H	7.028526	-1.574494	1.071028
C	5.437412	-3.285816	-1.190762
H	5.654933	-4.095411	-1.88518
C	4.161056	-2.725889	-1.153889
H	3.384351	-3.084483	-1.820403
C	-1.901896	-2.281019	2.070936
C	-1.368179	-2.828547	3.247889
H	-0.295108	-2.965173	3.320682
C	-2.206002	-3.21761	4.293255
H	-1.774967	-3.662838	5.186565
C	-3.591289	-3.067302	4.187884
H	-4.241378	-3.378515	5.000083
C	-4.131192	-2.530261	3.018616
H	-5.207166	-2.420269	2.915491
C	-3.2946	-2.137876	1.972607
H	-3.714645	-1.723269	1.062921
C	-0.249981	-2.799633	-2.387518
C	0.622775	-3.89722	-2.285776
H	1.030077	-4.162252	-1.316085
C	0.96615	-4.643155	-3.412624
H	1.636974	-5.491457	-3.308164
C	0.45854	-4.302535	-4.66782
H	0.728642	-4.882554	-5.544952
C	-0.402754	-3.209403	-4.779684
H	-0.814369	-2.936939	-5.747545
C	-0.755361	-2.463628	-3.654402
H	-1.436448	-1.625731	-3.745962
C	-1.074716	-2.528756	-0.151704
C	-1.712501	-3.897141	-0.214731
C	-1.274853	-4.956768	0.586822
H	-0.459608	-4.82178	1.288385
C	-1.904387	-6.195231	0.472146
H	-1.570402	-7.03259	1.082467

Atom	x /Å	y /Å	z /Å
C	-3.340748	-5.420763	-1.11839
H	-4.17167	-5.630606	-1.789575
C	-2.774002	-4.147173	-1.091071
H	-3.148779	-3.365023	-1.742106
C	-2.202354	1.902704	2.146835
C	-2.676529	1.371619	3.356032
H	-2.791743	0.297409	3.445172
C	-3.021442	2.213086	4.41343
H	-3.4056	1.783658	5.335171
C	-2.90074	3.599297	4.287738
H	-3.177182	4.251888	5.110441
C	-2.436911	4.136815	3.08634
H	-2.349975	5.213356	2.968111
C	-2.087286	3.296736	2.028413
H	-1.728838	3.714878	1.094328
C	-2.87682	0.257594	-2.294827
C	-3.975112	-0.609757	-2.15974
H	-4.212797	-1.015937	-1.182557
C	-4.757001	-0.948914	-3.263267
H	-5.605043	-1.615511	-3.132861
C	-4.452732	-0.442451	-4.528209
H	-5.060843	-0.709226	-5.387139
C	-3.359291	0.41348	-4.673335
H	-3.11471	0.824302	-5.64895
C	-2.577474	0.761766	-3.571439
H	-1.739659	1.439059	-3.688555
C	-2.532697	1.077157	-0.066402
C	-3.901924	1.716004	-0.081238
C	-4.927902	1.287813	0.767879
H	-4.763819	0.481354	1.473338
C	-6.170017	1.916586	0.696849
H	-6.981609	1.58996	1.344792
C	-5.461158	3.335	-0.939701
H	-5.698115	4.158775	-1.610673
C	-4.187505	2.768175	-0.958049
H	-3.432374	3.136275	-1.643839
C	1.953643	2.199367	2.100371

Atom	x /Å	y /Å	z /Å
C	1.450111	2.653219	3.329115
H	0.377319	2.74981	3.45084
C	2.316552	3.001076	4.365079
H	1.908079	3.370481	5.302279
C	3.700334	2.902777	4.198749
H	4.372027	3.181663	5.005099
C	4.21013	2.458281	2.978106
H	5.284023	2.388652	2.828455
C	3.345313	2.105923	1.9411
H	3.741871	1.762914	0.991795
C	0.182145	2.882869	-2.292003
C	-0.683211	3.978931	-2.128985
H	-1.060225	4.214266	-1.139689
C	-1.056944	4.762028	-3.2204
H	-1.721251	5.608273	-3.068456
C	-0.587882	4.461264	-4.500519
H	-0.881629	5.070332	-5.34992
C	0.265816	3.370116	-4.673247
H	0.647877	3.128245	-5.661146
C	0.648654	2.587111	-3.583714
H	1.323935	1.751048	-3.722667
C	1.066554	2.5338	-0.088602
C	1.69764	3.906377	-0.115363
C	1.289081	4.925449	0.751577
H	0.504431	4.753117	1.479349
C	1.909042	6.171262	0.668629
H	1.597472	6.977677	1.330295
C	3.282234	5.478772	-1.012946
H	4.084532	5.723745	-1.706689
C	2.721844	4.202177	-1.021411
H	3.073358	3.452714	-1.721993
C	0.058275	-0.18206	4.485456
N	0.042905	-0.082288	3.334583
C	0.078142	-0.333566	5.931711
H	0.04251	0.646288	6.415077
H	-0.785497	-0.924881	6.248899
H	0.994152	-0.850851	6.231005

Table IV-S7. Optimized atomic coordinates obtained from DFT for (**4-5+MeCN**)$^+$ doublet ground state (b3lyp/LanL2DZ(f)[Rh] 6-31G**[C,H,N]) E= -3786.22305851 Hartree.

Atom	x /Å	y /Å	z /Å
Rh	0.014461	-0.005428	1.1604031
Rh	-0.016304	0.0061251	-1.2903551
N	2.0506412	-0.522931	1.0018701
N	2.0402422	0.0261211	-1.2553991
N	6.9670375	-1.0198287	-0.382362
N	-0.509023	-2.0435651	1.0257211
N	0.004614	-2.0504321	-1.2400201
N	-1.0393228	-6.9681544	-0.316654
N	-2.0231401	0.5186021	1.0577851
N	-2.0713452	-0.0157899	-1.2024671
N	-6.9717504	1.0395709	-0.198923
N	0.5337371	2.0303462	1.0337831
N	-0.0371289	2.0613943	-1.2177931
N	1.0222488	6.9707506	-0.26636
C	2.7094979	-1.2108804	2.0713842
C	3.0763092	-0.535877	3.2434933
H	2.8858783	0.5281054	3.3228233

Atom	x /Å	y /Å	z /Å
C	3.7106469	-1.2217933	4.2795184
H	4.016292	-0.6801169	5.1704924
C	3.9829883	-2.587563	4.1659683
H	4.4849043	-3.115193	4.9707694
C	3.6229539	-3.2628533	2.9993633
H	3.8441788	-4.3204278	2.8909772
C	2.9885962	-2.580352	1.9600592
H	2.7193731	-3.1029645	1.0486031
C	2.7335763	0.5490237	-2.3864332
C	3.5473686	1.6882792	-2.2710552
H	3.6878825	2.14845	-1.2991701
C	4.1768517	2.224219	-3.3931982
H	4.8092105	3.1002588	-3.2847262
C	3.9972636	1.6408683	-4.6493453
H	4.4895294	2.0585884	-5.5216134
C	3.1853583	0.5120578	-4.7704353
H	3.0475123	0.0413941	-5.7392014

Atom	x /Å	y /Å	z /Å
C	2.5553172	-0.032753	-3.6505023
H	1.9416434	-0.9199108	-3.7480913
C	2.7033186	-0.3367283	-0.148105
C	4.1921202	-0.5684812	-0.22167
C	5.0870407	0.1317081	0.5939051
H	4.7345141	0.8615088	1.3134281
C	6.4520843	-0.1258136	0.4694811
H	7.1659904	0.414058	1.0881491
C	6.1038142	-1.6879281	-1.1561171
H	6.5365318	-2.411991	-1.8433171
C	4.7221785	-1.4984813	-1.1221181
H	4.0764373	-2.0612551	-1.7869051
C	-1.1938774	-2.6896818	2.1051012
C	-0.511997	-3.0643552	3.2705883
H	0.5560714	-2.8919753	3.3369133
C	-1.1966043	-3.6836149	4.3166694
H	-0.6503639	-3.9944	5.2029964
C	-2.5678019	-3.9338322	4.2191343
H	-3.0945959	-4.4241152	5.0316204
C	-3.2499272	-3.5672688	3.0585273
H	-4.3120427	-3.7717937	2.9624893
C	-2.568668	-2.9476221	2.0097392
H	-3.0965445	-2.6721001	1.1033481
C	0.5106927	-2.7538552	-2.3725732
C	1.6515831	-3.5665015	-2.2663722
H	2.1260319	-3.6975504	-1.2999961
C	2.1708309	-4.2067275	-3.3903112
H	3.0483328	-4.8382393	-3.2888952
C	1.5689472	-4.0388883	-4.6392973
H	1.9737773	-4.5393612	-5.5129724
C	0.4384767	-3.2279581	-4.7513693
H	-0.0462761	-3.0990381	-5.7143994
C	-0.0896911	-2.587291	-3.6294973
H	-0.9783029	-1.9745712	-3.7197393
C	-0.3428213	-2.7044865	-0.122684
C	-0.5789133	-4.1932421	-0.182356
C	0.137167	-5.0849646	0.6228271
H	0.8840748	-4.73004	1.3233651
C	-0.1254237	-6.4502072	0.5119301
H	0.426708	-7.1616433	1.1225771
C	-1.7232261	-6.107936	-1.0798871
H	-2.463431	-6.5430466	-1.7481091
C	-1.5302564	-4.7265343	-1.0582321
H	-2.1075732	-4.0833221	-1.7129101
C	-2.6458008	1.2172094	2.1417312
C	-2.9794551	0.552965	3.3293833
H	-2.7937462	-0.5118605	3.4094873
C	-3.5763288	1.2500312	4.3798494
H	-3.8516669	0.7182467	5.2862424
C	-3.8457731	2.6159118	4.2641963
H	-4.3180361	3.1523188	5.0810424
C	-3.5209258	3.2805382	3.0810793
H	-3.7405197	4.3383378	2.9715453
C	-2.9229471	2.587159	2.0280012
H	-2.6807031	3.1011596	1.1042921
C	-2.7949102	-0.5323295	-2.3174052
C	-3.6065515	-1.671354	-2.1859781
H	-3.7203585	-2.1370008	-1.2131931
C	-4.2674016	-2.2003087	-3.2933102
H	-4.8974674	-3.0763755	-3.1723752
C	-4.1224815	-1.609653	-4.5504903
H	-4.6393193	-2.021858	-5.4110914
C	-3.3133162	-0.4806895	-4.6875563
H	-3.2021042	-0.0044636	-5.6570234

Atom	x /Å	y /Å	z /Å
C	-2.6513921	0.0567153	-3.5825413
H	-2.0405893	0.9444981	-3.6920013
C	-2.7052415	0.3428184	-0.07686
C	-4.1945852	0.5803264	-0.110905
C	-5.0705166	-0.120865	0.7242171
H	-4.702018	-0.8542288	1.4319841
C	-6.4375732	0.1408707	0.6359681
H	-7.1368113	-0.3995329	1.2707071
C	-6.1266331	1.7085822	-0.9916901
H	-6.5746787	2.4366752	-1.6646571
C	-4.7451404	1.5154255	-0.9936651
H	-4.1153282	2.0794573	-1.6724491
C	1.2392654	2.6653448	2.1058962
C	0.586208	2.9941871	3.3011453
H	-0.4744755	2.7932102	3.3968733
C	1.2889282	3.6051078	4.3396414
H	0.7653197	3.8773159	5.2517564
C	2.6494079	3.8924882	4.2049763
H	3.1900519	4.3754411	5.0127244
C	3.3029333	3.5710768	3.0147573
H	4.3562548	3.8040258	2.8905902
C	2.6040121	2.9594412	1.9731582
H	3.1095306	2.7204152	1.0438201
C	-0.5732945	2.7758534	-2.3293832
C	-1.712345	3.5853187	-2.1854131
H	-2.1620288	3.7058236	-1.2060031
C	-2.2615438	4.2360188	-3.2888752
H	-3.1372606	4.8646256	-3.1581972
C	-1.6916181	4.0826847	-4.5546013
H	-2.1195671	4.5915956	-5.4122354
C	-0.5628476	3.2754834	-4.7041003
H	-0.1024038	3.1579555	-5.6804194
C	-0.0050168	2.6240153	-3.6029713
H	0.8822021	2.0143365	-3.7225263
C	0.3373934	2.7041356	-0.102351
C	0.5706883	4.1936663	-0.15085
C	-0.131382	5.0753917	0.6773481
H	-0.8619898	4.7112821	1.3902651
C	0.1265247	6.4422283	0.5753481
H	-0.4143859	7.1461194	1.2044821
C	1.6919842	6.1199832	-1.0524451
H	2.4174131	6.5636258	-1.7311881
C	1.5023965	4.7380405	-1.0409761
H	2.0660693	4.1029983	-1.7152471
C	0.0727279	-0.0925381	4.4782084
N	0.046297	-0.032956	3.3255353
C	0.1143147	-0.1858452	5.9284075
H	-0.1974825	0.7617435	6.3752725
H	-0.5570689	-0.9820059	6.2620505
H	1.1333793	-0.4191782	6.2493425

Table IV-S8. Singlet electronic transitions obtained from TD-DFT for **4-1** from singlet ground state; G03 rb3lyp/LanL2DZ(f)[Rh,Re] 6-31G**[$C_{amidinate}$,N,CO], 3-21G[C_{aryl},H] with CPCM (DCM).

Wavelength (nm)	Osc. Strength	Symm.	Major contributions
1316.5	0	A	HOMO→L+1 (83%)
761.9	0.0001	A	HOMO→LUMO (100%)
748.4	0.009	A	H-4→L+1 (72%)
745.8	0.0091	A	H-5→L+1 (72%)
659.4	0.0017	A	H-1→L+1 (88%)
641.8	0.0028	A	H-2→L+1 (87%)
625.5	0.0092	A	HOMO→L+2 (89%)
543.8	0	A	H-1→LUMO (100%)
542.0	0.0067	A	H-3→L+1 (98%)
533.3	0.0001	A	H-2→LUMO (97%)
509.8	0.0165	A	HOMO→L+5 (76%)
482.1	0.0001	A	H-12→L+1 (12%), H-8→L+1 (56%)
469.7	0.0001	A	H-3→LUMO (97%)
462.2	0.0002	A	HOMO→L+3 (97%)
456.8	0.0097	A	H-1→L+2 (98%)
455.4	0.0172	A	H-2→L+2 (86%)
449.3	0.0002	A	HOMO→L+4 (32%), HOMO→L+11 (34%)
442.9	0	A	H-4→LUMO (99%)
442.2	0	A	HOMO→L+4 (67%), HOMO→L+11 (20%)
440.6	0.0008	A	H-5→LUMO (99%)
427.8	0.0013	A	HOMO→L+7 (93%)
424.4	0.0066	A	HOMO→L+8 (91%)
407.4	0.0701	A	H-7→L+1 (67%), H-6→L+1 (12%), H-4→L+1 (12%)
406.6	0.0005	A	HOMO→L+6 (66%), HOMO→L+9 (15%), HOMO→L+11 (12%)
405.8	0.0029	A	H-3→L+2 (81%)
404.1	0.0849	A	H-7→L+1 (13%), H-6→L+1 (63%), H-5→L+1 (10%)
395.2	0.0045	A	H-4→L+2 (80%)
393.8	0.0195	A	H-5→L+2 (87%)
387.5	0.0004	A	H-10→L+1 (77%)
383.8	0.0041	A	H-17→LUMO (41%), H-16→LUMO (45%)
383.5	0.0002	A	HOMO→L+6 (24%), HOMO→L+9 (71%)
380.8	0.0409	A	H-15→LUMO (14%), H-9→LUMO (18%), H-8→LUMO (24%), H-6→LUMO (21%)
374.3	0.0217	A	H-1→L+3 (27%), H-1→L+5 (61%)
373.9	0.0158	A	HOMO→L+12 (46%)
373.6	0.0011	A	H-7→LUMO (92%)
372.9	0.0197	A	H-15→LUMO (17%), H-6→LUMO (68%)
371.1	0.005	A	H-1→L+3 (72%), H-1→L+5 (23%)
368.2	0.0168	A	H-2→L+3 (42%), H-2→L+5 (41%)
365.8	0.011	A	H-2→L+3 (52%), H-2→L+5 (34%)
365.4	0.0048	A	H-26→LUMO (20%), H-15→LUMO (11%), H-8→LUMO (49%)
364.9	0.0065	A	H-12→L+1 (32%), H-11→L+1 (25%), H-8→L+1 (27%)
361.8	0.0125	A	H-26→LUMO (52%), H-8→LUMO (17%)
360.2	0.0002	A	H-1→L+4 (98%)
358.5	0.0008	A	H-9→L+1 (73%)
356.9	0.0077	A	H-28→L+1 (15%), H-13→L+1 (56%)
356.4	0.0171	A	H-12→L+1 (25%), H-11→L+1 (24%)
355.9	0.0017	A	H-2→L+4 (91%)
353.6	0.001	A	HOMO→L+10 (95%)
351.6	0.0074	A	H-15→LUMO (16%), H-9→LUMO (67%)
349.6	0.0033	A	H-4→L+5 (55%)

Table IV-S9. Singlet electronic transitions obtained from TD-DFT for **4-4** from singlet ground state; G03 rb3lyp/LanL2DZ(f)[Rh,Re] 6-31G**[$C_{amidinate}$,N,CO], 3-21G[C_{aryl},H] with CPCM (DCM).

Wavelength (nm)	Osc. Strength	Symm.	Major contributions
1288.1	0	A	HOMO→LUMO (83%)
744.2	0.0092	B2	H-6→LUMO (13%), H-5→LUMO (68%)
743.7	0.0097	B3	H-7→LUMO (14%), H-4→LUMO (69%)
659.4	0.0013	B3	H-2→LUMO (89%)
658.6	0.0015	B2	H-1→LUMO (87%)
619.3	0.015	B1	HOMO→L+1 (38%), HOMO→L+5 (54%)
605.2	0	A	HOMO→L+2 (97%)
604.5	0.0004	B3	HOMO→L+4 (99%)
604.4	0	B2	HOMO→L+3 (99%)
595.7	0.0065	B1	HOMO→L+1 (62%), HOMO→L+5 (34%)
556.1	0	A	HOMO→L+6 (95%)
547.0	0.0062	B1	H-3→LUMO (98%)
543.4	0.0035	B2	HOMO→L+7 (95%)
542.6	0.003	B3	HOMO→L+8 (95%)
475.1	0	B1	H-21→LUMO (40%), H-17→LUMO (26%), H-8→LUMO (17%)
465.7	0.0027	B3	H-2→L+2 (30%), H-1→L+1 (65%)
465.5	0.0002	B2	H-2→L+1 (47%), H-1→L+2 (47%)
464.8	0.0013	B1	H-2→L+3 (39%), H-1→L+4 (58%)
464.8	0	A	H-2→L+4 (39%), H-1→L+3 (58%)
461.5	0.0026	B2	H-2→L+1 (47%), H-1→L+2 (50%)
461.3	0.001	B3	H-2→L+2 (68%), H-1→L+1 (29%)
460.7	0	A	H-2→L+4 (59%), H-1→L+3 (40%)
460.7	0.0002	B1	H-2→L+3 (59%), H-1→L+4 (40%)
447.3	0	A	HOMO→L+17 (25%), HOMO→L+21 (16%), HOMO→L+26 (29%)
443.3	0.0194	B3	H-1→L+5 (86%)
442.8	0.0136	B2	H-2→L+5 (85%)
431.3	0.038	B1	H-2→L+7 (31%), H-1→L+8 (32%), HOMO→L+25 (19%)
428.8	0.003	B2	H-1→L+6 (89%)
428.5	0	A	H-3→L+5 (11%), H-2→L+8 (38%), H-1→L+7 (45%)
428.2	0.0018	B3	H-2→L+6 (90%)

Table IV-S10. Singlet and triplet electronic transitions obtained from TD-DFT for **4-5** from singlet ground state; G03 b3lyp/LanL2DZ(f)[Rh] 6-31G**[$NCN_{amidinate}$], 3-21G[C_{aryl},H, N_{py}] with CPCM (DCM).

Wavelength (nm)	Osc. Strength	Symm.	Major contributions
2210.8	0	^{3}B2	HOMO(A)→LUMO(A) (64%), HOMO(B)→LUMO(B) (64%)
1335.5	0	^{1}B2	HOMO→LUMO (82%)
1075.8	0	^{3}E	H-4(A)→LUMO(A) (55%), H-4(B)→LUMO(B) (55%)
1075.8	0	^{3}E	H-4(A)→LUMO(A) (55%), H-4(B)→LUMO(B) (55%)
749.6	0.0088	^{1}E	H-4→LUMO (75%)
749.6	0.0088	^{1}E	H-5→LUMO (75%)
702.5	0	^{3}E	H-1(A)→LUMO(A) (47%), H-1(B)→LUMO(B) (47%)
702.5	0	^{3}E	H-1(A)→LUMO(A) (47%), H-1(B)→LUMO(B) (47%)
650.6	0.0019	^{1}E	H-1→LUMO (90%)
650.6	0.0019	^{1}E	H-2→LUMO (90%)
547.7	0.0117	^{1}A2	H-3→LUMO (95%)
540.4	0.0231	^{1}A2	HOMO→L+1 (81%)
485.0	0	^{1}B1	H-11→LUMO (21%), H-8→LUMO (69%)
445.3	0	^{1}A1	HOMO→L+5 (70%), HOMO→L+10 (10%)
438.7	0	^{1}B2	HOMO→L+2 (97%)
427.7	0.0051	^{1}E	HOMO→L+3 (96%)
427.7	0.0051	^{1}E	HOMO→L+4 (96%)
403.3	0.0688	^{1}E	H-6→LUMO (81%), H-4→LUMO (10%)
403.3	0.0688	^{1}E	H-7→LUMO (81%), H-5→LUMO (10%)
385.3	0	^{1}B2	H-10→LUMO (88%)
380.7	0.0476	^{1}E	H-1→L+1 (85%)
380.7	0.0476	^{1}E	H-2→L+1 (85%)
366.8	0.0129	^{1}A2	HOMO→L+1 (10%), HOMO→L+9 (51%)
362.9	0.0016	^{1}E	H-4→L+1 (69%)
362.9	0.0016	^{1}E	H-5→L+1 (69%)
361.5	0	^{1}B1	H-11→LUMO (75%), H-8→LUMO (24%)
356.9	0.0167	^{1}E	H-25→LUMO (15%), H-13→LUMO (62%)
356.9	0.0167	^{1}E	H-26→LUMO (15%), H-14→LUMO (62%)
356.7	0	^{1}A1	H-9→LUMO (95%)
351.4	0	^{1}B2	H-3→L+1 (63%), H-2→L+4 (16%), H-1→L+3 (16%)
348.4	0.0001	^{1}A2	H-12→LUMO (43%), H-2→L+4 (13%), H-1→L+3 (13%), HOMO→L+9 (10%)
347.8	0.002	^{1}E	H-1→L+2 (89%)
347.8	0.002	^{1}E	H-2→L+2 (89%)
339.4	0.0035	^{1}E	H-34→LUMO (12%), H-32→LUMO (41%), H-20→LUMO (10%), H-4→L+5 (10%)
339.4	0.0034	^{1}E	H-33→LUMO (12%), H-31→LUMO (41%), H-21→LUMO (10%), H-5→L+5 (10%)
339.1	0	^{1}B2	H-3→L+1 (32%), H-2→L+4 (32%), H-1→L+3 (32%)
338.2	0	^{1}E	H-2→L+3 (38%), H-1→L+4 (31%), HOMO→L+6 (30%)
338.1	0	^{1}E	H-2→L+3 (45%), H-1→L+4 (53%)
337.8	0	^{1}B1	H-2→L+3 (15%), H-1→L+4 (15%), HOMO→L+6 (67%)
337.8	0.2295	^{1}A2	H-12→LUMO (30%), H-2→L+4 (27%), H-1→L+3 (27%)
334.4	0	^{1}B1	H-15→LUMO (98%)
333.6	0.0115	^{1}E	HOMO→L+7 (95%)
333.5	0.0115	^{1}E	HOMO→L+8 (95%)
332.0	0	^{1}B2	H-19→LUMO (13%), H-16→LUMO (85%)
329.5	0.0127	^{1}E	H-17→LUMO (89%)
329.5	0.0127	^{1}E	H-18→LUMO (89%)
328.6	0	^{1}A1	HOMO→L+5 (22%), HOMO→L+10 (62%)
324.3	0.0002	^{1}E	H-20→LUMO (79%)
324.3	0.0002	^{1}E	H-21→LUMO (79%)
322.8	0	^{1}B1	HOMO→L+11 (97%)
320.9	0.0002	^{1}A2	H-24→LUMO (20%), H-22→LUMO (70%)
318.3	0	^{1}A1	H-23→LUMO (95%)
316.7	0	^{1}A2	H-3→L+2 (78%)
316.2	0.0534	^{1}E	H-3→L+3 (10%), H-2→L+5 (41%), HOMO→L+12 (31%)
316.2	0.0535	^{1}E	H-3→L+4 (10%), H-1→L+5 (41%), HOMO→L+13 (31%)
316.1	0	^{1}B2	H-19→LUMO (82%), H-16→LUMO (14%)

Wavelength (nm)	Osc. Strength	Symm.	Major contributions
314.8	0.0367	^{1}E	H-3→L+3 (15%), H-2→L+5 (41%), HOMO→L+12 (28%)
314.8	0.0366	^{1}E	H-3→L+4 (15%), H-1→L+5 (41%), HOMO→L+13 (28%)
311.8	0.0278	^{1}E	H-4→L+2 (15%), H-3→L+3 (44%), HOMO→L+12 (32%)
311.8	0.0278	^{1}E	H-5→L+2 (15%), H-3→L+4 (44%), HOMO→L+13 (32%)
310.6	0.0001	^{1}E	H-25→LUMO (28%), H-5→L+2 (23%), H-4→L+5 (21%)
310.6	0.0001	^{1}E	H-26→LUMO (28%), H-5→L+5 (21%), H-4→L+2 (24%)
310.5	0.0267	^{1}A2	H-24→LUMO (53%), HOMO→L+21 (13%)
310.1	0.0119	^{1}E	H-5→L+2 (55%), H-3→L+4 (20%)
310.1	0.0119	^{1}E	H-26→LUMO (10%), H-4→L+2 (54%), H-3→L+3 (20%)
306.7	0	^{1}B2	HOMO→L+14 (31%), HOMO→L+15 (65%)
306.4	0.2702	^{1}A2	H-24→LUMO (25%), H-22→LUMO (10%), HOMO→L+9 (15%), HOMO→L+21 (25%)
306.1	0.001	^{1}E	H-32→LUMO (13%), H-25→LUMO (35%), H-4→L+5 (20%)
306.1	0.001	^{1}E	H-31→LUMO (13%), H-26→LUMO (36%), H-5→L+5 (20%)
305.7	0	^{1}E	H-5→L+3 (48%), H-4→L+4 (48%)
305.1	0	^{1}A1	H-8→L+1 (37%), H-5→L+3 (13%), H-4→L+4 (14%), HOMO→L+10 (16%)
304.5	0.0002	^{1}E	H-5→L+4 (34%), H-4→L+3 (61%)
304.5	0	^{1}E	H-5→L+4 (51%), H-4→L+3 (24%), HOMO→L+14 (16%)
303.9	0	^{1}B2	H-5→L+4 (12%), H-4→L+3 (12%), HOMO→L+14 (50%), HOMO→L+15 (24%)
302.5	0	^{1}E	H-8→L+1 (17%), H-5→L+3 (33%), H-4→L+4 (33%)
300.4	0	^{1}B1	HOMO→L+16 (95%)
297.9	0.0015	^{1}E	HOMO→L+17 (96%)
297.9	0.0015	^{1}E	HOMO→L+18 (96%)
294.9	0	^{1}B1	H-3→L+5 (89%)
291.1	0.0007	^{1}E	HOMO→L+19 (93%)
291.1	0.0007	^{1}E	HOMO→L+20 (93%)
288.6	0.0296	^{1}E	H-6→L+1 (73%)
288.6	0.0296	^{1}E	H-7→L+1 (73%)
288.2	0	^{1}A1	HOMO→L+22 (96%)
287.1	0	?Sym	H-29→LUMO (98%)

Table IV-S11. Singlet electronic transitions obtained from TD-DFT for **4-5+MeCN** from singlet ground state; G03 rb3lyp/LanL2DZ(f)[Rh] 6-31G**[$NCN_{amidinate}$], 3-21G[C_{aryl},H, N_{py}] with CPCM (MeCN).

Wavelength (nm)	Osc. Strength	Symm.	Major contributions
740.2	0	A	HOMO→LUMO (86%)
587.9	0.0117	A	HOMO→L+1 (82%)
555.9	0.0045	A	H-4→LUMO (56%), H-2→LUMO (27%)
555.6	0.0045	A	H-5→LUMO (56%), H-1→LUMO (27%)
467.9	0.0092	A	HOMO→L+5 (69%)
456.0	0.0031	A	H-5→LUMO (26%), H-1→LUMO (61%)
455.0	0.0031	A	H-4→LUMO (26%), H-2→LUMO (61%)
437.6	0.0007	A	HOMO→L+3 (53%), HOMO→L+4 (34%)
436.7	0.0052	A	HOMO→L+2 (88%)
434.6	0.0047	A	HOMO→L+3 (37%), HOMO→L+4 (59%)
410.4	0.0064	A	H-3→LUMO (96%)
401.8	0.011	A	H-4→L+1 (15%), H-2→L+1 (36%), H-1→L+1 (34%)
401.6	0.0118	A	H-5→L+1 (14%), H-2→L+1 (34%), H-1→L+1 (36%)
381.3	0.0204	A	H-5→L+1 (25%), H-4→L+1 (30%), H-1→L+1 (17%)
381.2	0.0204	A	H-5→L+1 (31%), H-4→L+1 (25%), H-2→L+1 (18%)
377.6	0	A	H-8→LUMO (80%)
372.8	0.0112	A	HOMO→L+1 (10%), HOMO→L+9 (35%), HOMO→L+10 (26%)
364.9	0	A	H-3→L+1 (88%)
352.2	0.0001	A	HOMO→L+6 (97%)
348.1	0.0112	A	HOMO→L+7 (72%)
347.9	0.0111	A	HOMO→L+8 (73%)
346.4	0.0031	A	H-1→L+3 (23%), H-1→L+4 (39%), HOMO→L+7 (14%)
346.2	0.0125	A	H-2→L+3 (38%), H-2→L+4 (21%), HOMO→L+8 (11%)
345.7	0.0346	A	H-1→L+2 (62%)
344.4	0.0067	A	H-2→L+3 (27%), H-2→L+4 (26%), H-1→L+2 (13%)
343.3	0.0124	A	H-2→L+3 (16%), HOMO→L+5 (12%), HOMO→L+9 (16%), HOMO→L+10 (21%)
342.7	0.0021	A	H-5→L+5 (13%), H-1→L+5 (43%)
342.4	0.0037	A	H-4→L+5 (10%), H-2→L+4 (20%), H-2→L+5 (36%)
341.4	0.0001	A	H-2→L+2 (93%)
340.5	0	A	H-1→L+3 (62%), H-1→L+4 (34%)

Table IV-S12. Doublet electronic transitions obtained from TD-DFT for (**4-5**+**MeCN**)$^+$ from doublet ground state; G03 ub3lyp/LanL2DZ(f)[Rh] 6-31G**[$NCN_{amidinate}$], 3-21G[C_{aryl},H, N_{py}] with CPCM (MeCN).

Wavelength (nm)	Osc. Strength	Symm.	Major contributions
1436.7	0.0293	A	HOMO(B)→LUMO(B) (83%)
1432.2	0.0286	A	H-1(B)→LUMO(B) (83%)
1037.8	0	A	H-2(B)→LUMO(B) (94%)
952.7	0.0144	A	H-11(B)→LUMO(B) (38%), H-3(B)→LUMO(B) (36%), H-1(B)→LUMO(B) (13%)
951.7	0.0143	A	H-12(B)→LUMO(B) (37%), H-4(B)→LUMO(B) (36%), HOMO(B)→LUMO(B) (13%)
738.4	0.0004	A	HOMO(A)→LUMO(A) (85%)
738.2	0.0036	A	H-19(B)→LUMO(B) (13%), H-16(B)→LUMO(B) (23%), H-6(B)→LUMO(B) (37%)
660.4	0.0072	A	H-11(B)→LUMO(B) (31%), H-3(B)→LUMO(B) (59%)
657.1	0.0072	A	H-12(B)→LUMO(B) (31%), H-4(B)→LUMO(B) (58%)
649.1	0.0001	A	H-30(B)→LUMO(B) (15%), H-18(B)→LUMO(B) (19%), H-7(B)→LUMO(B) (23%), H-5(B)→LUMO(B) (33%)
599.9	0.0001	A	H-19(A)→LUMO(A) (14%), H-4(A)→LUMO(A) (11%), H-11(B)→L+1(B) (27%), H-3(B)→L+1(B) (13%)
599.0	0.0001	A	H-20(A)→LUMO(A) (14%), H-5(A)→LUMO(A) (11%), H-12(B)→L+1(B) (27%), H-4(B)→L+1(B) (14%)
585.2	0.0285	A	H-10(B)→LUMO(B) (44%), H-9(B)→LUMO(B) (14%), H-6(B)→LUMO(B) (25%)
581.8	0.0005	A	H-7(B)→LUMO(B) (19%), H-5(B)→LUMO(B) (61%)
564.4	0.0053	A	H-24(B)→LUMO(B) (18%), H-8(B)→LUMO(B) (60%)
562.9	0.0052	A	H-25(B)→LUMO(B) (18%), H-10(B)→LUMO(B) (17%), H-9(B)→LUMO(B) (41%)
554.1	0.0025	A	H-19(B)→LUMO(B) (31%), H-16(B)→LUMO(B) (20%), H-6(B)→LUMO(B) (31%)
541.0	0.0027	A	HOMO(B)→L+1(B) (74%)
539.7	0.0027	A	H-1(B)→L+1(B) (74%)
529.4	0.001	A	H-16(B)→LUMO(B) (32%), H-13(B)→LUMO(B) (49%)
524.0	0.0026	A	HOMO(A)→L+1(A) (67%)
520.2	0.0003	A	H-14(B)→LUMO(B) (67%)
519.7	0.0003	A	H-20(B)→LUMO(B) (10%), H-15(B)→LUMO(B) (66%)
515.1	0.0001	A	H-17(B)→LUMO(B) (71%), H-14(B)→LUMO(B) (10%)
509.5	0.0022	A	H-33(A)→LUMO(A) (17%), HOMO(A)→L+1(A) (12%), H-30(B)→L+1(B) (19%), H-2(B)→L+1(B) (24%)
508.8	0.0056	A	H-1(A)→LUMO(A) (24%), H-20(B)→LUMO(B) (29%)
508.5	0.0076	A	H-2(A)→LUMO(A) (30%), H-1(A)→LUMO(A) (11%), H-21(B)→LUMO(B) (18%)
507.3	0.0066	A	H-2(A)→LUMO(A) (16%), H-1(A)→LUMO(A) (24%), H-20(B)→LUMO(B) (19%)
507.1	0.0037	A	H-2(A)→LUMO(A) (12%), H-1(A)→LUMO(A) (11%), H-21(B)→LUMO(B) (23%), H-20(B)→LUMO(B) (14%)
506.5	0.0007	A	H-21(B)→LUMO(B) (17%), H-18(B)→LUMO(B) (34%), H-7(B)→LUMO(B) (27%)

Table IV-S13. Energy and contribution of MO obtained from DFT for **4-1** from singlet ground state; G03 rb3lyp/LanL2DZ(f)[Rh,Re] 6-31G**[$C_{amidinate}$,N,CO], 3-21G[C_{aryl},H] with CPCM (DCM).

MO	eV	Symm.	Rh2	Amidinate	Pyridine	Phenyl	Carbonyl	Bipyridine	Re
L+20	-0.35	A	0.0194344	0.0820708	0.128642	0.628221497	0.08569367	0.0543856	0.0015399
L+19	-0.36	A	0.0057015	0.0162625	0.0354408	0.121163705	0.48536743	0.3282585	0.0078047
L+18	-0.43	A	0.0517297	0.1473281	0.1970809	0.521290594	0.05707049	0.0062981	0.0192005
L+17	-0.46	A	0.0750002	0.0192995	0.305868	0.495266091	0.02890778	0.0738336	0.0018172
L+16	-0.48	A	0.044834	0.0098528	0.1009752	0.383565946	0.17297216	0.2827723	0.0050366
L+15	-0.5	A	0.0424728	0.025355	0.3407043	0.182469983	0.16843925	0.2363143	0.0042403
L+14	-0.63	A	0.0187055	0.0136314	0.8004695	0.166241544	0.00036243	0.0004223	0.000163
L+13	-0.64	A	0.0293005	0.0144472	0.7584878	0.196819853	0.00061288	0.0002447	7.69E-05
L+12	-0.73	A	0.1422747	0.134705	0.282412	0.417116167	0.01410345	0.0021277	0.007256
L+11	-0.95	A	0.2526385	0.1344561	0.2138726	0.393201373	0.00338339	0.001609	0.0008428
L+10	-1.15	A	0.0010007	0.0025232	0.029349	0.003255846	0.6520407	0.0658941	0.2459228
L+9	-1.36	A	0.01186	0.0106307	0.5471662	0.052313035	0.238374	0.0454764	0.0941757
L+8	-1.41	A	0.019475	0.2375883	0.6130528	0.11908028	0.00714775	0.0007835	0.0028783
L+7	-1.42	A	0.0340343	0.2187435	0.6138984	0.132399529	0.0005673	0.0001624	0.000191
L+6	-1.51	A	0.0041875	0.003848	0.3118003	0.021512294	0.43584956	0.0404758	0.1823276
L+5	-1.64	A	0.150884	0.2001756	0.4551971	0.190767	0.00157481	0.0007684	0.0006367
L+4	-1.86	A	0.0001953	0.0001601	0.028202	0.001085725	0.03135213	0.9363769	0.0026412
L+3	-1.97	A	0.0013992	0.0032257	0.0191353	0.002054683	0.02689811	0.934079	0.0132142
L+2	-2.38	A	0.030743	0.1002773	0.753674	0.05095446	0.03202995	0.017457	0.0148702
L+1	-2.8	A	0.83099	0.0756485	0.0037943	0.089480783	4.96E-05	6.64E-06	3.06E-05
LUMO	-3.02	A	4.49E-05	0.0001178	0.0079127	6.91E-05	0.04258955	0.9224173	0.0268459
HOMO	-4.95	A	0.3741408	0.4636251	0.0045965	0.157614593	-4.87E-07	1.79E-06	1.56E-05
H-1	-5.59	A	0.0793107	0.4656124	0.0169273	0.438055405	3.18E-05	5.58E-06	5.32E-05
H-2	-5.66	A	0.0832046	0.4687463	0.0169483	0.431058315	4.30E-06	7.37E-06	3.36E-05
H-3	-5.97	A	0.0287479	0.6360135	0.0111532	0.324060637	2.77E-06	5.55E-06	2.19E-05
H-4	-6.11	A	0.7124772	0.0664973	0.0234683	0.197562028	1.29E-07	1.64E-07	1.10E-06
H-5	-6.14	A	0.7376467	0.0601164	0.0206295	0.179959269	0.00050469	9.68E-05	0.0010485
H-6	-6.62	A	0.2288387	0.1315617	0.0328369	0.606343408	0.00011062	3.23E-05	0.0002818
H-7	-6.63	A	0.2300476	0.1303078	0.0253857	0.614154993	2.98E-05	4.88E-06	6.70E-05
H-8	-6.69	A	0.3949537	0.1820253	0.1051149	0.297117883	0.00575583	0.001441	0.013582
H-9	-6.81	A	0.0565166	0.054783	0.0908673	0.73935074	0.01582069	0.0043289	0.0383331
H-10	-6.86	A	0.2105435	0.0299184	0.1714591	0.585022277	0.00080896	0.0002261	0.0020235
H-11	-6.91	A	0.124843	0.1078281	0.462423	0.299182638	0.00152247	0.0004407	0.0037556
H-12	-6.92	A	0.1979769	0.08135	0.3246339	0.386186472	0.00261804	0.0007563	0.0064844
H-13	-6.95	A	0.1096867	0.1141189	0.5217674	0.241307663	0.00346275	0.0010391	0.0086246
H-14	-7.02	A	0.0285271	0.0403911	0.5213811	0.292389745	0.03057455	0.0096214	0.0771057
H-15	-7.03	A	0.0083804	0.0206687	0.11523	0.282337811	0.14869826	0.0492896	0.3753929
H-16	-7.04	A	0.0036224	0.0050514	0.0215359	0.405309837	0.15092454	0.0411395	0.3724087
H-17	-7.05	A	0.0097802	0.0082246	0.039245	0.508620266	0.1163553	0.0310999	0.2866764
H-18	-7.07	A	0.0401511	0.0378646	0.088729	0.825565331	0.00213994	0.0004784	0.0050782
H-19	-7.11	A	0.020626	0.0329592	0.061915	0.882194892	0.00062654	0.0001321	0.001543
H-20	-7.14	A	0.016244	0.0129619	0.0392117	0.861887281	0.01791889	0.0060611	0.0457195

Table IV-S14. Energy and contribution of MO obtained from DFT for **4-4** from singlet ground state; G03 rb3lyp/LanL2DZ(f)[Rh,Re] 6-31G**[$C_{amidinate}$,N,CO], 3-21G[C_{aryl},H] with CPCM (DCM).

MO	eV	Symm.	Rh2	Amidinate	Pyridine	Phenyl	Carbonyl	Bipyridine	Re
L+20	-1.98	B2	0.00235636	0.00295604	0.521938024	0.0235484	0.24354125	0.09207424	0.11359866
L+19	-1.98	B3	0.0029142	0.0047791	0.51659074	0.02626197	0.23958508	0.09711126	0.11274482
L+18	-1.98	A	0.00598489	0.00398147	0.519510684	0.03010031	0.23275614	0.09813247	0.10952644
L+17	-2.02	B1	0.03689657	0.02209411	0.501675017	0.08878983	0.15141982	0.12434079	0.07478378
L+16	-2.19	B2	0.00014659	0.00027042	0.066212746	0.00220242	0.03996026	0.88919819	0.00201134
L+15	-2.19	B3	0.00039432	0.00038614	0.069574822	0.00287091	0.04038592	0.88421903	0.002173
L+14	-2.19	A	0.00087882	0.0004527	0.070418569	0.00333107	0.04043342	0.88235942	0.00212305
L+13	-2.19	B1	0.00262377	0.00169409	0.086721096	0.00827159	0.0418657	0.85625483	0.00255811
L+12	-2.31	B2	5.89E-05	0.00033477	0.012262795	0.00022214	0.03329585	0.93899812	0.01482143
L+11	-2.31	A	0.00022651	0.00028282	0.011955492	0.00036533	0.03326794	0.93925815	0.01465718
L+10	-2.31	B3	0.00013787	0.00040469	0.012767508	0.00030824	0.03334421	0.93820632	0.01483435
L+9	-2.31	B1	0.00037876	0.00048447	0.014178209	0.00077078	0.03336825	0.93623043	0.01459798
L+8	-2.86	B2	0.01123472	0.1231015	0.771162435	0.04240836	0.02911413	0.00771294	0.01527324
L+7	-2.86	B3	0.01103936	0.12409097	0.769229448	0.04379492	0.02888642	0.0073474	0.01560044
L+6	-2.92	B1	0.02052902	0.11893454	0.759372746	0.04861777	0.02831028	0.00902652	0.01522139
L+5	-2.99	A	0.07719252	0.11572028	0.678164299	0.07942933	0.02483964	0.01070081	0.01392506
L+4	-3.36	B2	0.0001572	0.00070967	0.014025619	0.00029649	0.04340949	0.9122479	0.02913378
L+3	-3.36	B3	0.00013944	0.00074324	0.013823365	0.00023818	0.04344043	0.91239949	0.02920563
L+2	-3.36	B1	0.00032945	0.00097571	0.015586796	0.00036185	0.04309059	0.91062509	0.02903559
L+1	-3.37	A	0.00069786	0.00115424	0.017142873	0.00075467	0.04274	0.90848879	0.02901044
LUMO	-3.54	B1	0.83355163	0.07678144	0.003898906	0.08558248	5.33E-05	0.00010281	2.46E-05
HOMO	-5.7	B1	0.36487615	0.46237885	0.004692492	0.16797367	-8.45E-07	3.79E-06	8.06E-05
H-1	-6.32	B3	0.07584434	0.45158245	0.015978666	0.45600403	0.00015019	5.39E-05	0.00039341
H-2	-6.33	B2	0.07717421	0.44987674	0.015555666	0.45704221	8.43E-05	2.26E-05	0.00025407
H-3	-6.67	A	0.02681963	0.60570368	0.011381472	0.35593263	2.93E-05	2.71E-05	0.00014948
H-4	-6.86	B2	0.66252452	0.06705666	0.02082436	0.23644694	0.00360846	0.00100472	0.00854208
H-5	-6.87	B3	0.6749495	0.06737592	0.020369073	0.22449007	0.00356904	0.00091699	0.00834131
H-6	-7.29	B3	0.24916797	0.08938659	0.028609918	0.49308701	0.03618452	0.01188013	0.09167253
H-7	-7.29	B2	0.25423788	0.08573923	0.030537531	0.46386741	0.0425571	0.01451945	0.10855039
H-8	-7.3	A	0.07265082	0.04988509	0.086769894	0.1631425	0.16180761	0.05431771	0.41142986
H-9	-7.33	B1	0.00987432	0.01413722	0.074925688	0.18978696	0.18250364	0.0624928	0.46628995
H-10	-7.39	B3	0.0152273	0.03318998	0.029200596	0.10951208	0.21022365	0.0686195	0.53400241
H-11	-7.39	B2	0.01655563	0.03305181	0.026873123	0.11177247	0.21049753	0.06775642	0.53347977
H-12	-7.4	A	0.00725549	0.00293276	0.009523763	0.0010843	0.25984947	0.07367411	0.64569309
H-13	-7.4	B1	0.00221661	0.00064703	0.009896219	0.0107573	0.25888499	0.07376314	0.64384911
H-14	-7.41	B3	0.00176665	0.0074176	0.016847001	0.0269055	0.24764849	0.07646241	0.62294159
H-15	-7.41	B2	0.00636152	0.01172503	0.016702069	0.04495574	0.24036714	0.07452956	0.6053427
H-16	-7.55	B1	0.13508633	0.02906013	0.018561804	0.65784384	0.04035789	0.0147806	0.10433543
H-17	-7.56	A	0.21379329	0.11657828	0.038543032	0.29562011	0.0850689	0.02937819	0.22101446
H-18	-7.56	B1	0.16372265	0.02152963	0.019935459	0.68959469	0.02706831	0.00814107	0.06998586
H-19	-7.63	B2	8.99E-05	0.00081185	0.002072728	0.00256671	0.29255166	0.01717302	0.6847192
H-20	-7.63	B3	5.50E-05	0.00045267	0.002103017	0.00245271	0.29273859	0.01720555	0.68500326

Table IV-S15. Energy and contribution of MO obtained from DFT for **4-5** from singlet ground state; G03 rb3lyp/LanL2DZ(f)[Rh] 6-31G**[$NCN_{amidinate}$], 3-21G[C_{aryl},H, N_{py}] with CPCM (MeCN).

MO	eV	Symmetry	Rh_2	Amidinate	Pyridine	Phenyl
L+20	0.15	E	0.015713441	0.012772817	0.16568267	0.80584137
L+19	0.15	E	0.015713441	0.012772817	0.16568267	0.80584137
L+18	0.06	E	0.004646881	0.017466638	0.026402086	0.951484069
L+17	0.06	E	0.004646861	0.017466616	0.026402083	0.951476048
L+16	0.05	A1	0.051228509	0.019805942	0.206602544	0.72235907
L+15	-0.01	A2	0.059954048	0.077202161	0.025244866	0.83759612
L+14	-0.02	A2	0.058551307	0.024464481	0.228900428	0.688083684
L+13	-0.13	E	0.018877574	0.102768624	0.129141652	0.749213764
L+12	-0.13	E	0.018877574	0.102768624	0.129141652	0.749213764
L+11	-0.24	A1	0.085269855	0.000179186	0.010789811	0.903743553
L+10	-0.25	B1	0.10800799	0.061761386	0.708960353	0.121257959
L+9	-0.39	B2	0.146958324	0.064960909	0.374794169	0.413276404
L+8	-0.44	E	0.008676587	0.011968574	0.842317499	0.137043713
L+7	-0.44	E	0.008676587	0.011968574	0.842317499	0.137043713
L+6	-0.47	A1	0.030855476	0.012026022	0.759354052	0.197753039
L+5	-0.75	B1	0.237125599	0.126500818	0.221636276	0.414745213
L+4	-1.17	E	0.017836727	0.224898633	0.639019462	0.118247387
L+3	-1.17	E	0.017836727	0.224898633	0.639019462	0.118247387
L+2	-1.25	A2	0.037873434	0.193645343	0.628859262	0.139614983
L+1	-1.48	B2	0.177630959	0.18817182	0.432349508	0.201840961
LUMO	-2.55	A2	0.833011703	0.075015421	0.002489532	0.089482333
HOMO	-4.69	B1	0.377764044	0.463880048	0.004477915	0.15387836
H-1	-5.38	E	0.080746172	0.475035928	0.016750818	0.427464978
H-2	-5.38	E	0.080746172	0.475035928	0.016750818	0.427464978
H-3	-5.7	A1	0.025604292	0.652872673	0.010553731	0.310966384
H-4	-5.87	E	0.742820961	0.060024915	0.021206581	0.175953333
H-5	-5.87	E	0.742820961	0.060024915	0.021206581	0.175953333
H-6	-6.4	E	0.205735878	0.134481799	0.025365266	0.634412298
H-7	-6.4	E	0.205735878	0.134481799	0.025365266	0.634412298
H-8	-6.44	B2	0.479172115	0.197964629	0.107344085	0.215479927
H-9	-6.58	A2	0.046683423	0.058473136	0.099778045	0.795053821
H-10	-6.64	B1	0.243827207	0.012937611	0.098011267	0.645204689
H-11	-6.69	B2	0.318164175	0.014253246	0.031173105	0.636423614
H-12	-6.74	A1	0.096536038	0.114339548	0.48696894	0.302165309
H-13	-6.74	E	0.007754875	0.21883729	0.599247017	0.174144349
H-14	-6.74	E	0.007754707	0.218838707	0.599247031	0.174144265
H-15	-6.83	B2	0.008352089	0.002944627	0.012257658	0.976425291
H-16	-6.84	B1	0.001967835	0.001326899	0.221180139	0.775503541
H-17	-6.89	E	0.016481413	0.035339913	0.060445718	0.887734236
H-18	-6.89	E	0.016481415	0.035339911	0.060446674	0.887734236
H-19	-6.92	B1	0.031344572	0.009093424	0.706763597	0.25279544
H-20	-6.94	E	0.006351297	0.008955412	0.060066319	0.924627604

Table IV-S16. Energy and contribution of MO obtained from DFT for **4-5+MeCN** from singlet ground state; G03 rb3lyp/LanL2DZ(f)[Rh] 6-31G**[$NCN_{amidinate}$], 3-21G[C_{aryl},H, N_{py}] with CPCM (MeCN).

MO	eV	Symmetry	Rh_2	Amidinate	Pyridine	Phenyl	MeCN
L+20	0.26	A	0.033909726	0.057268115	0.140641519	0.76236896	0.005814501
L+19	0.24	A	0.018301083	0.045885893	0.186114311	0.72018471	0.029514927
L+18	0.23	A	0.018229018	0.040171797	0.167304608	0.74436691	0.029922697
L+17	0.2	A	0.004821305	0.014224817	0.061355198	0.90500508	0.014583255
L+16	0.2	A	0.004874958	0.014799751	0.060400625	0.90505497	0.014871295
L+15	0.15	A	0.042545454	0.015087419	0.215156965	0.71996925	0.007240666
L+14	0.08	A	0.046537206	0.035414481	0.03442041	0.87669714	0.00692257
L+13	0.03	A	0.019819754	0.075193633	0.057042347	0.80496562	0.042981996
L+12	0.02	A	0.019438637	0.07897997	0.062852664	0.79521123	0.043512064
L+11	-0.02	A	0.054442941	0.009088332	0.067454941	0.86705657	0.001967891
L+10	-0.16	A	0.120789993	0.057069857	0.379824748	0.44060857	0.001709649
L+9	-0.34	A	0.087867461	0.048841331	0.667047485	0.19616358	8.29E-05
L+8	-0.4	A	0.005494026	0.009342837	0.815164013	0.16870522	0.001293002
L+7	-0.4	A	0.005883149	0.008843146	0.815524764	0.16844558	0.001306789
L+6	-0.44	A	0.024298941	0.00969661	0.745542063	0.21921629	0.001247274
L+5	-0.76	A	0.24298153	0.150246654	0.218575259	0.38756664	0.000625
L+4	-1.03	A	0.072667158	0.16845616	0.641909872	0.11214878	0.0048234
L+3	-1.04	A	0.040073147	0.183552935	0.663786469	0.11001472	0.002568493
L+2	-1.05	A	0.016308849	0.192853254	0.680053411	0.10997917	0.000798132
L+1	-1.41	A	0.21721745	0.167455539	0.408034975	0.20717393	0.000121458
LUMO	-1.64	A	0.699998469	0.081627228	0.069447823	0.10997211	0.038956117
HOMO	-4.5	A	0.4173868	0.460796519	0.005224656	0.11658509	7.78E-06
H-1	-5.23	A	0.212272802	0.442206847	0.015240178	0.32921312	0.001083721
H-2	-5.23	A	0.217354519	0.43703488	0.014599602	0.32987506	0.001121191
H-3	-5.53	A	0.034776687	0.725977977	0.007722226	0.22968641	0.001838226
H-4	-5.65	A	0.732677511	0.115453063	0.015190538	0.12341732	0.013256033
H-5	-5.65	A	0.737297453	0.113406789	0.01537188	0.12056443	0.013367153
H-6	-6.21	A	0.086078351	0.152565765	0.030424221	0.7226721	0.008250038
H-7	-6.22	A	0.095111798	0.150754078	0.03150472	0.71452921	0.008097775
H-8	-6.27	A	0.675347412	0.187268443	0.049687259	0.08742666	0.000264732
H-9	-6.32	A	0.35251183	0.085982256	0.099778045	0.45243421	0.040979752
H-10	-6.48	A	0.130161837	0.062603706	0.098011267	0.69099446	0.003033741
H-11	-6.49	A	0.119267476	0.032023708	0.031173105	0.76423026	7.16E-05
H-12	-6.57	A	0.072382681	0.275318107	0.48696894	0.45307508	0.002297685
H-13	-6.57	A	0.041219527	0.332890545	0.599247017	0.39926491	0.002655078
H-14	-6.59	A	0.128325358	0.157066697	0.599247031	0.56650522	0.001047154
H-15	-6.74	A	0.003114459	0.004404087	0.012257658	0.93870615	0.002465831
H-16	-6.75	A	0.008871692	0.011302279	0.221180139	0.87078968	0.007639807
H-17	-6.75	A	0.009156069	0.016407003	0.060445718	0.81821813	0.014199655
H-18	-6.76	A	0.010118388	0.005361708	0.060446674	0.90926668	0.005337267
H-19	-6.82	A	0.007016483	0.025453538	0.706763597	0.9057315	0.001204305
H-20	-6.82	A	0.006639686	0.026511042	0.060066319	0.91803117	0.001420748

Table IV-S17. Energy and contribution of the α MO obtained from DFT (**4-5+MeCN**)$^+$ from doublet ground state; G03 ub3lyp/LanL2DZ(f)[Rh] 6-31G**[$NCN_{amidinate}$], 3-21G[C_{aryl},H, N_{py}] with CPCM (MeCN).

MO	eV	Symm	Rh_2	Amidinate	Pyridine	Phenyl	MeCN
L+20	-0.21	A	0.013421664	0.016900313	0.005063642	0.718910007	0.075519216
L+19	-0.21	A	0.014003453	0.014472337	0.005248493	0.712435948	0.07688535
L+18	-0.24	A	0.009693354	0.043649748	0.00582362	0.825001351	0.021111115
L+17	-0.24	A	0.010568529	0.049547508	0.005384554	0.801278147	0.024128774
L+16	-0.28	A	0.037503402	0.008963413	0.001021876	0.634062023	0.005667031
L+15	-0.31	A	0.066051525	0.266163005	0.038610532	0.548313712	0.003228111
L+14	-0.39	A	0.038576197	0.057893348	0.044623864	0.863014732	0.005285268
L+13	-0.45	A	0.02062526	0.091310691	0.010640365	0.712993096	0.067519879
L+12	-0.45	A	0.019617439	0.098396307	0.010272755	0.696292852	0.062428352
L+11	-0.48	A	0.056840522	0.008377562	0.049802479	0.862380897	0.001460039
L+10	-0.64	A	0.044031891	0.034715318	0.038474335	0.172049906	0.001306354
L+9	-0.74	A	0.006518612	0.011921398	0.003781962	0.240155978	0.004023366
L+8	-0.74	A	0.006359348	0.011044465	0.003660627	0.241164327	0.003688839
L+7	-0.8	A	0.033982611	0.012802931	0.012625149	0.328194658	0.001613552
L+6	-0.9	A	0.194211054	0.191648684	0.145671765	0.183331532	0.000127227
L+5	-1.53	A	0.044088209	0.254266492	0.033150646	0.122722644	0.002058669
L+4	-1.54	A	0.11876725	0.270307245	0.057258238	0.180609051	0.000716405
L+3	-1.54	A	0.178035388	0.258523348	0.08635714	0.214152504	0.001053456
L+2	-1.56	A	0.06983801	0.271594995	0.036517855	0.145451286	0.00185667
L+1	-2.19	A	0.332493137	0.237040754	0.075320176	0.199251283	0.000105271
LUMO	-2.82	A	0.747531014	0.101486695	0.309755416	0.078374448	0.053076492
HOMO	-5.79	A	0.277611227	0.517307375	0.150502423	0.200446356	1.02E-05
H-1	-6.18	A	0.067493778	0.391956286	0.057014151	0.51448014	0.000617317
H-2	-6.18	A	0.067483553	0.393805793	0.057102253	0.512209242	0.000609857
H-3	-6.5	A	0.029430814	0.581356854	0.01996802	0.37545926	0.000650176
H-4	-6.66	A	0.104708278	0.100636322	0.048333533	0.731808169	0.001216244
H-5	-6.67	A	0.107222846	0.099049737	0.049416738	0.73077124	0.00121918
H-6	-6.93	A	0.034383546	0.039443248	0.001329095	0.811836317	0.011408049
H-7	-7	A	0.027625843	0.038071389	0.005794051	0.786498916	0.000256912
H-8	-7.03	A	0.033267985	0.061573542	0.022680888	0.113436206	0.00292966
H-9	-7.05	A	0.011446236	0.063508369	0.002282802	0.119905443	0.001136314
H-10	-7.05	A	0.01311985	0.059752643	0.003194034	0.125964457	0.001234598
H-11	-7.08	A	0.020083021	0.009966253	0.008915931	0.123305206	6.77E-05
H-12	-7.13	A	0.010292563	0.004102617	0.006044935	0.891790373	0.000990242
H-13	-7.15	A	0.064158863	0.014236724	0.033317984	0.829898837	0.013772136
H-14	-7.15	A	0.122760249	0.018339747	0.06391525	0.741872451	0.02155956
H-15	-7.16	A	0.134195225	0.017108703	0.076392546	0.76144392	0.005915171
H-16	-7.17	A	0.31383792	0.037082842	0.176402135	0.56887917	0.016055705
H-17	-7.18	A	0.234437539	0.03368439	0.133433622	0.661550815	0.011255746
H-18	-7.25	A	0.058464375	0.062391704	0.047932211	0.819382287	0.007709307
H-19	-7.3	A	0.34378232	0.023139549	0.17939991	0.568256792	0.011557418
H-20	-7.3	A	0.347081983	0.023017715	0.181311921	0.563543171	0.011865451

Table IV-S18. Energy and contribution of the β MO obtained from DFT (**4-5+MeCN**)$^+$ from doublet ground state; G03 ub3lyp/LanL2DZ(f)[Rh] 6-31G**[$NCN_{amidinate}$], 3-21G[C_{aryl},H, N_{py}] with CPCM (MeCN).

MO	eV	Symm	Rh_2	Amidinate	Pyridine	Phenyl	MeCN
L+21	-0.2	A	0.008471009	0.014028834	0.017844996	0.173868857	0.722085287
L+20	-0.2	A	0.0086192	0.013935549	0.013769429	0.175913565	0.72257501
L+19	-0.23	A	0.005553889	0.013705554	0.05352167	0.104072169	0.805103221
L+18	-0.23	A	0.005894659	0.012910323	0.056311454	0.110890194	0.801754069
L+17	-0.25	A	0.038583978	0.080428934	0.221246491	0.086074009	0.601519567
L+16	-0.28	A	0.035547557	0.038751048	0.009925086	0.30621377	0.639294049
L+15	-0.39	A	-0.006074629	0.041044148	0.056238246	0.032889513	0.864513575
L+14	-0.44	A	0.010128857	0.02058044	0.089346867	0.105516493	0.715545742
L+13	-0.45	A	0.009485652	0.019645532	0.095940546	0.120102359	0.700183967
L+12	-0.47	A	0.007077827	0.05589005	0.008943566	0.072950627	0.860273603
L+11	-0.63	A	0.004347496	0.052537198	0.037655777	0.726757702	0.18158954
L+10	-0.74	A	0.002822637	0.006669692	0.012011258	0.742087289	0.235296476
L+9	-0.74	A	0.002787356	0.006505339	0.011127185	0.742671182	0.236086657
L+8	-0.8	A	0.020935427	0.033303701	0.013281166	0.630631098	0.321165901
L+7	-0.84	A	0.045927272	0.166829241	0.137733788	0.481739011	0.213579858
L+6	-1.48	A	0.159713786	0.304133447	0.237019145	0.1464047	0.312254294
L+5	-1.51	A	0.008048308	0.041585712	0.239410402	0.594465223	0.122312854
L+4	-1.52	A	0.011064201	0.024665349	0.267979203	0.58335507	0.122649184
L+3	-1.53	A	0.010359847	0.031407046	0.26078974	0.581576816	0.124253459
L+2	-2.14	A	0.2626029	0.33378282	0.228976762	0.232918246	0.204211144
L+1	-2.71	A	0.417764397	0.749996761	0.098165744	0.02023628	0.08149661
LUMO	-4.21	A	0.132557993	0.440150763	0.450272969	0.005812042	0.103751289
HOMO	-5.98	A	0.009451582	0.068941585	0.481122767	0.018672006	0.430765485
H-1	-5.98	A	0.009545382	0.06965676	0.476520606	0.018202583	0.435121456
H-2	-6.24	A	0.006940685	0.031883202	0.687248168	0.008185359	0.271833294
H-3	-6.64	A	0.077319568	0.149354864	0.101683712	0.061209697	0.686511595
H-4	-6.65	A	0.079255703	0.153482234	0.099736704	0.061184734	0.684312306
H-5	-6.92	A	0.037794137	0.04116332	0.043927096	0.103317842	0.799972059
H-6	-6.95	A	0.095052215	0.179606967	0.117770353	0.156410007	0.545785151
H-7	-7.02	A	0.016196467	0.048627372	0.05722232	0.706480123	0.184236513
H-8	-7.02	A	0.028280902	0.04965522	0.111067615	0.679563098	0.155851662
H-9	-7.03	A	0.024605635	0.075777022	0.08924209	0.589557356	0.242130767
H-10	-7.03	A	0.010936372	0.109091637	0.035013948	0.408093319	0.44654828
H-11	-7.07	A	0.220077604	0.546919467	0.042244824	0.10629509	0.284620772
H-12	-7.08	A	0.213009487	0.532608659	0.042303755	0.116918508	0.288772859
H-13	-7.1	A	0.012344423	0.050565344	0.010927549	0.516969714	0.421425021
H-14	-7.14	A	0.007447275	0.015096124	0.013297319	0.079995567	0.881421305
H-15	-7.15	A	0.014101463	0.022801225	0.020629891	0.103443826	0.836378062
H-16	-7.16	A	0.10011709	0.221845837	0.055108516	0.125815371	0.59684359
H-17	-7.16	A	0.015578335	0.038569245	0.015265575	0.073734164	0.865491855
H-18	-7.23	A	0.018984924	0.072138613	0.071604222	0.168172522	0.681625765
H-19	-7.26	A	0.25030067	0.270680065	0.050901074	0.117093535	0.561017569

Table IV-S19. Singlet electronic transition obtained from TD-DFT for **4-5** from singlet ground state; G09 rb3lyp/LanL2DZ(f)[Rh] 6-31G**[$NCN_{amidinate}$], 3-21G[C_{aryl},H, N_{py}] with CPCM (DCM).

Wavelength (nm)	Osc. Strength	Symm.	Major contributions
1056.4	0	B	HOMO→LUMO (99%)
706.1	0.0075	E	H-5→LUMO (38%), H-4→LUMO (50%)
706.1	0.0075	E	H-5→LUMO (50%), H-4→LUMO (38%)
573.3	0.0025	E	H-2→LUMO (91%)
573.3	0.0025	E	H-1→LUMO (91%)
543.8	0.0311	A	HOMO→L+1 (85%)
486.5	0.005	A	H-3→LUMO (99%)
446.6	0	B	H-11→LUMO (11%), H-6→LUMO (87%)
445.0	0	B	HOMO→L+2 (99%)
436.8	0.0054	E	HOMO→L+3 (98%)

Table IV-S20. Singlet electronic transition obtained from TD-DFT for **4-5** from singlet ground state; G09 rb3lyp/LanL2DZ(f)[Rh] 6-31G**[C,H,N]) with CPCM (DCM).

Wavelength (nm)	Osc. Strength	Symm.	Major contributions
1056.3	0	B	HOMO→LUMO (98%)
711.3	0.0082	E	H-4→LUMO (85%)
711.3	0.0082	E	H-5→LUMO (85%)
578.1	0.0027	E	H-2→LUMO (91%)
578.1	0.0027	E	H-1→LUMO (91%)
550.3	0.0313	A	HOMO→L+1 (85%)
487.3	0.0064	A	H-3→LUMO (99%)
456.7	0	B	HOMO→L+2 (99%)
447.7	0	B	H-11→LUMO (25%), H-8→LUMO (73%)
447.4	0.0053	E	HOMO→L+3 (98%)

Table IV-S21. Singlet electronic transition obtained from TD-DFT for **4-5** from singlet ground state; G03, optimized and TD with rb3lyp/LanL2DZ(f)[Rh] 6-31G**[C,H,N]) with CPCM (DCM).

Wavelength (nm)	Osc. Strength	Symm.	Major contributions
1273.6	0	B	HOMO→LUMO (83%)
731.2	0.011	E	H-6→LUMO (10%), H-4→LUMO (70%), H-2→LUMO (10%)
731.2	0.011	E	H-7→LUMO (10%), H-5→LUMO (70%), H-1→LUMO (10%)
645.1	0.0016	E	H-5→LUMO (10%), H-1→LUMO (85%)
644.9	0.0017	E	H-4→LUMO (10%), H-2→LUMO (85%)
537.0	0.0364	A	HOMO→L+1 (85%)
522.2	0.0045	A	H-3→LUMO (98%)
475.5	0	B	H-11→LUMO (21%), H-8→LUMO (69%)
460.1	0	B	HOMO→L+2 (97%)
446.6	0.0067	E	HOMO→L+3 (96%)

SI - Chapitre 5 : Information supplémentaire

5.S1. Table of Contents

5.S2. Gas (Hydrogen) Measurement Description

For open experiment (rate studies) Gas chromatograms were recorded using a gas chromatograph (GC) [Perkin Elmer Clarus-480] with a TCD detector, argon as the carrier gas and a 7' HayeSep N 60/80 pre-column and 9' molecular sieve 13X45/60 column and a 2 mL injection loop. The gas flow was set to 34.5 mL min^{-1} when both columns are in-line. Samples solutions were prepared in standard 20 mL headspace vials. These were sealed with a rubber septum and were connected to a nitrogen flow of 10.5(4) mL/min (adjusted with a manual flow controller [Porter, 1000] and referenced with a digital flowmeter [Perkin Elmer FlowMark]) and were pre-bubbled in pure solvent. This flow passed through a 2 mL overflow protection vial, then through a 3-way selection valve [Clippard] before being sent to the GC sample loop. A microprocessor [Arduino Uno] coupled with custom PC interface allowed for timed injections of both channels in alternation. For calibration of H_2 production rate at a specific nitrogen flow, a syringe pump [New Era Pump] equipped with a gas-tight syringe [SGE] and a 26s gauge needle [Hamilton] was used to bubble different rates of pure hydrogen gas into the sample, to a minimum of 0,5 µL/minute. This gave a linear fit for peak area for H_2 versus the flow rates of H_2 used in the experiements. For general calibration, stock cylinders of known concentration of H_2 in nitrogen replaced the nitrogen flow (inserted at the pre-bubbler, to keep the vapor matrix consistent). The measured results, independent of flow rate (under same pressure) can be easily converted into a rate of hydrogen following equation 1.

(1) H_2 rate (uL/min) = [H_2 standard] (ppm) × N_2 flow rate (L/min)

For closed system studies, an auto-sampler [PerkinElmer TurboMatrix HS-16] was used to directly measure hydrogen concentration in the sealed vial. Calibration was done by injecting by gas-tight syringe different quantities of pure hydrogen in blank samples containing the same solvent matrix as the analyzed samples.

5.S3. Photochemical Reactor Description and Application Exemple

The prepared solutions each containing up to 10 mL solution (or 10 mL plus the volume of the flowcell circuit when combined with a UV-vis flow-cell) were kept in the dark and thoroughly degassed by the nitrogen carrier gas bubbling into the solution until no oxygen was seen by gas chromatography. The vials contained a Teflon stirrer and were agitated during the whole experiment. The samples are fitted in a carousel submerged inside a thermostated borosilicate waterbath at 20.0 ± 0.3 ºC and irradiated from below with interchangeable light sources consisting of a 90 x 1 watt LED UFO lamp [Nanning LvXing Lighting Electronics Co.Ltd] centered at 394 nm or 451 nm (see emission band in Figure 5.1). The flow was monitored at defined time intervals (up to a minimum of 2 minutes) and the resulting H_2 rates of production were integrated over time to yield the total quantity of H_2 evolved.

For closed systems. 2 to 10 mL samples were prepared, sealed under nitrogen, and inserted in the carousel. Mixing of the samples was afforded by roto-shaking the carousel. After a set time, the headspace was directly analyzed by the GC autosampler.

5.S4. Spectral Monitoring of Hydrogen Production

Using the flow monitoring experiment setup seen on Figure 5.4, two PTFE tube (1/16') were inserted through the seal of the headspace vial into the solution and were connected to a peristaltic pump and a UV-vis flow cell (total volume of flow path: 8.3 mL to 6.9 mL (volume was minimised over the course of development). The pump and PTFE tubing were kept under nitrogen atmosphere to avoid O_2 diffusion in the system. The solvent was circulated with an approximate rate of 5 mL/min during the whole experiment. Spectra were taken at regular intervals and plotted versus time. Between experiments the line was washed with the solvent used than methanol and finally dried with N_2 gas. The turn-over frequency (TOF) was adjusted to take into account only the irradiated volume, since only that fraction produces hydrogen. The turn-over number (TON) was left unadjusted, since the observed H_2 rate decays to nothing, consuming all PS and/or WRC and that the totality of both PS and WRC are irradiated over the total time of the experiment.

5.S5. Germany Internship Experimental conditions

All samples were prepared under nitrogen as 2 mL solutions, in small 4 mL MS vials which were capped with a standard septum (Figure 5.S1). The samples were irradiated in sets of four in an air cooled reactor by a high-intensity blue LED diodes array stick (470 nm max emission, see Figure 5.S2). After a set of time, a headspace aliquot was taken manually with an airtight 500 µL syringe and injected in a GC, where the concentration of H_2 was measured by peak integration.

Figure 5.S1. Experimental setup for preparation of samples, done under flux of nitrogen gas.

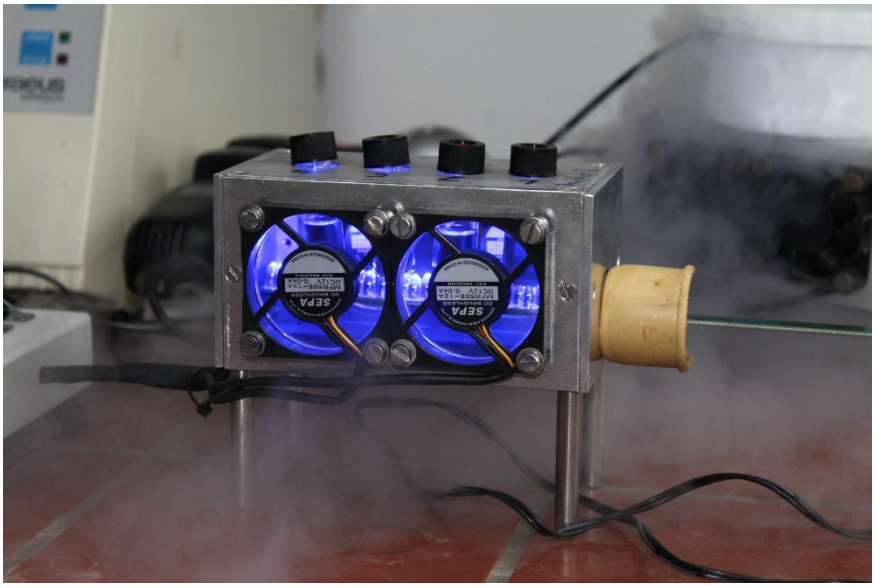

Figure 5.S2. LED photoreactor with air-cooling, showing the vials inside under irradiation.

5.S6. Synthetic Methods

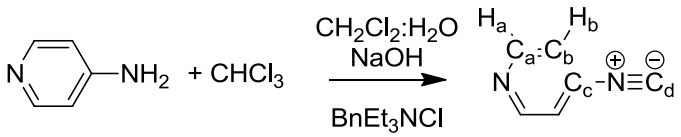

Scheme 5.S1. Reaction scheme for the synthesis of **CNPy** and proton and carbon labeling.

4-isocyanopyridine, **CNPy**

4-pyridylamine (9.45 g, 0.100 mol), benzyltriethylammonium chloride, (0.15 g , 0.0011 mol) and chloroform (8.1 mL, 0.100 mol) are mixed in a solution of dichloromethane (25 mL) and (30 ml) 50% NaOH aq solution (30 mL) in a round bottom flask. After stirring for 30 minutes at room temperature and exothermic reaction occurs and a brown precipitate forms. After 2 hours, the solution was filtered, the organic layer isolated, washed with water and dried under Na_2SO_4. The organic solution was reduced to 5 mL and the product was purified by flash chromatography (Silica gel; column 3 cm diameter by 10 cm length; solvent: AcOEt; Product Rf at 0.6 on TLC using same conditions). For storage, the product was kept as a 0.010 M solution in ethyl acetate at -10 °C. The fraction that was dried for nNMR characterization, leading to partial decomposition. Yield: 10% determined by UV-Vis titration using **5-4**. ^{1}H NMR ($CDCl_3$ 300 MHz) δ ppm 8.72 (dd, J = 5, 2 Hz, 2H, H2), , 7.29 (dd, J = 5, 2 Hz, 2H, H3). Peaks due to decomposion: (15%): 8.27 (dd, J = 5, 2 Hz, 2H), 7.68 (dd, J = 5, 2 Hz, 2H). 13C{1H} NMR (75 MHz, CDCl3) δ ppm 151.43 (2C), 150.17 (1C), 133.04 (1C), 120.35 (2C).

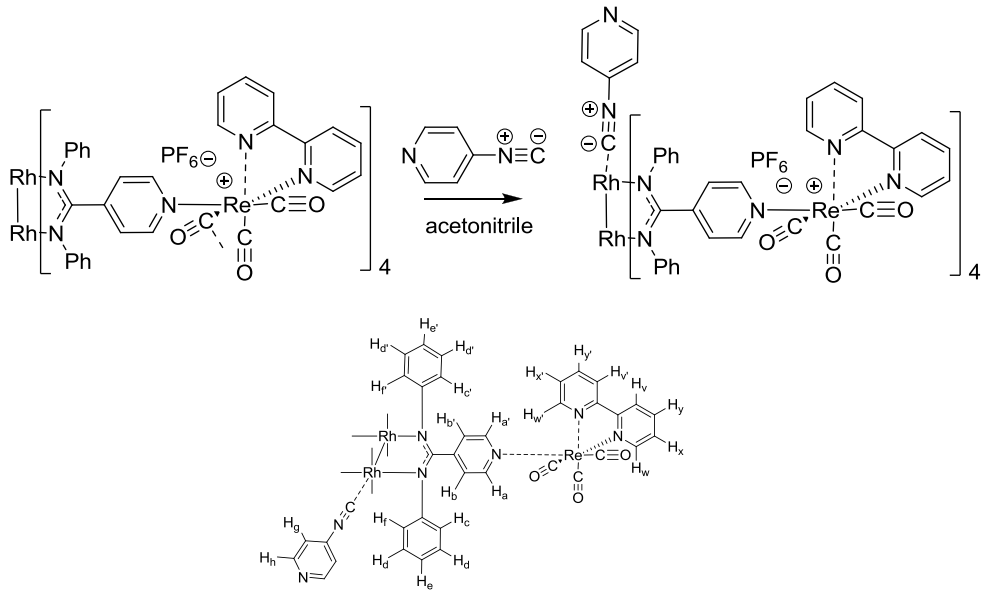

Scheme 5.S2. Top: Reaction scheme for the synthesis of **5-4+CNPy**. Bottom: Proton labeling for the complex **5-4+CNPy**.

tetrakis hexafluoropotassium tetrakis(*N*''-(2,2'-bipyridinetricarbonyl-rhenium(I))-*N*,*N*'-diphenyl-isonicotinamidate)-(4-isocyanopyridine)dirhodium(II,II), **5-4+CNPy**

In a 50 mL beaker, **2-4** (88 mg, 24 μmol) was dissolved in acetonitrile (10 mL), then a solution of 4-isocyanopyridine (2.4 mL, 0.010 M in ethyl acetate) was added. The olution changed from green to brown. The solvent was evaporated andreplaced by acetone and and the product was crystallized by diisopropyl ether diffusion. Quantitative yield by NMR and UV-Vis, isolated mass 0.090 g (99%). ^{1}H NMR (400 MHz, CD_3CN) δ ppm 9.02 (d, *J* = 5.5 Hz, 4H: Hw), 8.98 (d, *J* = 5.5 Hz, 4H: Hw'), 8.66 (d, *J* = 5.5 Hz, 2H, Hh), 8.33-8.25 (m, 8H, Hv, Hy), 8.26-8.17 (m, 8H, Hv', Hy'), 7.75 (t, *J* = 6.0 Hz, 4H: Hx), 7.68-7.60 (m, 12H, Ha',Ha, Hx), 6.96-6.87 (m, 4H: He), 6.87-6.81 (m, 8H, Hd), 6.81-6.70 (m, 8H, Hd'), 6.68-6.58 (m, 4H: He'), 6.58-6.51 (m, 6H, Hg, Hc), 6.38-6.27 (m, 8H, Hb, Hb'), 6.26-6.06 (br, 4H: Hc'), 5.68-5.57 (br, 4H: Hf'), 5.91-5.69 (m, 4H: Hf). HRMS (ESI, MeCN) (m/z): $[M-2PF_6]^{+2}$ ($C_{130}H_{92}F_{12}N_{22}O_{12}P_2Re_4Rh_2$) calcd 1698.1439; found 1698.1421.IR (ATR, cm^{-1})

$\nu_{N\equiv C}$: 2133s; $\nu_{C=O}$: 2031s, 1908s; ν_{PF} 832s. Anal. Calcd for $C_{130}H_{92}F_{24}N_{22}O_{12}P_4Re_4Rh_{22}$: C42.37; H, 2.52; N, 8.36. Found: C, 42.20; H, 2.51; N, 8.28.

5.S7. Microcontroller and software information

The control scheme illustrated in the section 5.3.1 (Schéma 5.5) displays the main properties of the control software and microcontroller and gives a simplified wiring to each component of the reactor. Herein we will elaborate in more details the workings of the flow interface software and the microcontroller.

5.S7.1. Arduino Flow Interface

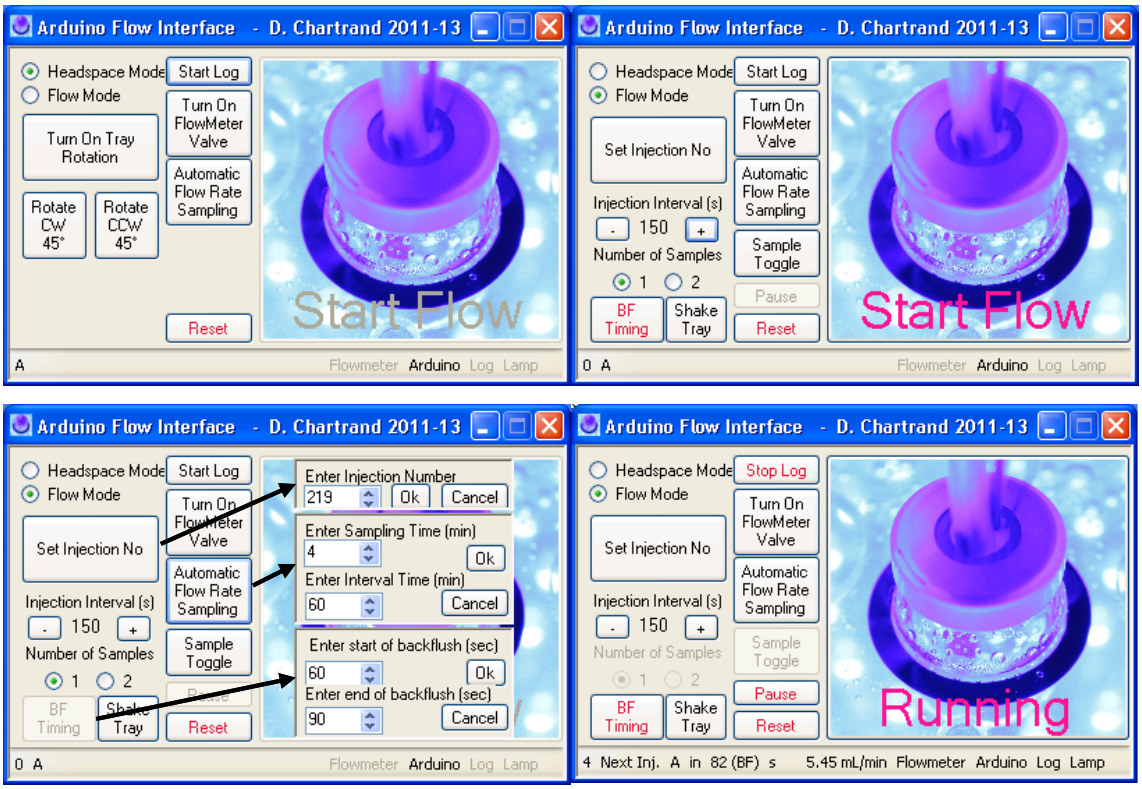

Figure 5.S3. Screenshots of the interface. Top Left: Default Headspace mode; Top Right: Selected flow system mode; Bottom Left: Selection windows opens for injection time, automatic flow rate sampling, and backflush timing; Bottom Right: During an on-going flow experiment.

The flow interface software has two main modes, Headspace and Flow. In the Figure 5.S3 (Top Left) the Headspace mode interface is shown, it is the default mode when the software is started. In this mode the interface sets valve 1 to the eluent gas of the GC. This valve is the first valve connected to the GC and it selects the flow going through the sample loop. In Headspace mode, the injection of the sample is done with the headspace autosampler directly into the carrier gas and does not use the sample loop. Because of the GC internal valve system, the sample loop is still part of the circuit and must be kept under the eluent gas to avoid injection of air in the GC with each sample. It is very important to select this mode before loading the headspace method in the GC software, failure to do so will inject air into the column and the trace CO_2 which will deactivate the primary column slightly, changing the elution time.

There are four selections that are identical in both Headspace and Flow mode. The *Start Log* button enables time-stamped data logging to a file selected by the user and will log the following information: Lamp turn-on, lamp turn-off, start of injection, injection number and channel, and flow rate (if a flowmeter is connected to the computer). The *Turn On Flowmeter Valve* directs the exhaust gas to the flowmeter (valve 4 in Schéma 5.5). This was made to preserve the flowmeter lifespan, which is shortened by organic vapors. The next button, *Automatic Flow Rate Sampling*, opens a selection windows (Figure 5.S3 (Bottom Left)) where sampling time and interval can be set for the flowmeter. These last two buttons are not in use in the current version, as the automatic flow monitoring was disabled after the early demise of our first flowmeter and we no longer log the flow rate during the whole experiment. The last common button, *Reset*, is self-explanatory and resets all parameters in the Arduino controller, by doing a soft reset (akin to restarting a computer via its shutdown menu).

The Headspace mode only has 3 other buttons, controlling the step-motor of the carousel, and they are self-explanatory. The rotation of the microcontroller is programmed to also shake the sample. This is done by moving forward by X steps, then backward by Y steps and repeating, with $X > Y$ there is a net rotation over time and the rapid inversion of direction shakes the samples well. This rotation should not be turned on with flow monitored samples inside the reactor, since the tubing cannot rotate around. Due to the motor low power, no damage should occur, although the tubes could get disconnected.

The Flow mode main interface is shown in Figure 5.S3 (Top Right) and it introduce a few more buttons. The *Set Injection No* is used to synchronize the injection number to the

experiment number in the sequence set in the GC software. By default it is set to 0, but should match the number of sequences due to a timing issue that arises every 98th injection. At this injection the GC needs extra time to upload the sequence information from the computer and will not inject when the microcontroller orders it, creating a disparity in the injection number of the microcontroller and the GC. This disparity creates confusion when the experiment is done with the two channels, as their numbering scheme no longer matches. The microcontroller has been programmed to add an extra five minutes for this particular injection, thus removing the problem, as long as the sequence number matches and was started at 0. The current injection number is displayed at the bottom left of the interface window, the maximum injection is 999 in the GC software.

The interval time can be increased or decreased in steps of 5 seconds via the + and – buttons; there is a strict minimum of 130 seconds, but no maximum. The *Sample Toggle* button toggles between channel A and B (switching on and off the appropriate valves), the current channel is displayed beside the injection number at the bottom left of the window. The *Number of Samples* checkboxes will tell the microcontroller to alternate between channel A and B during injections. The *Shake Tray* button is similar to the rotation in Headspace mode, but here X = Y so there is no net motion and the speed is much slower, to avoid detaching the stainless steel lines.

The last parameter button, *BF Timing*, controls the backflush parameters. These are very important to set properly, since backflushing pressure in the sample will result in solution transfer to the pre-bubbling vial. There are two parameters to set: the start and the end of the backflushing window. This window time depends on the method, but the default value, 60 to 90 seconds, covers all of the default methods. The timing can be optimized to minimize the windows size, since the sample should pass for about a full minute in the sample loop before injection. With less time there can be cross-contamination between channels.

The last button is the big *Start Flow* icon, which when pushed displays the current BF timing values and warns the user to verify them, after which the log starts automatically if it was not previously started. The first injection starts with a three-second delay, then the other injections use the timing value. During the experiment, most parameters can be changed. By changing the interval time, the acquisitions can be slowed which allows the experiments to be monitored over a very long period. The experiment can be halted, via the *Pause* button,

which waits until “backflush window” of the current run is passed, which avoids backflushing into to the sample vial.

The interface software polls the microcontroller every 0.6 second to follow the experient. An auto-detection routine is in place to detect the flowmeter activity as well. Note that in case of a cut in communication from the computer to the microcontroller, the experiment continues normally since all the parameters are stored within the microcontroller.

5.S7.2. Arduino Microcontroller

The microcontroller has a display that gives information similar to what is available with the software interface. Schéma 5.5 shows all of the microcontroller’s wiring. It communicates to the computer via a virtual serial port on a USB cable. The Microcontroller surveys the port for character strings that correspond to different commands. It only sends information (again via character strings) when a command is received that requests information. It communicates to the GC via two 5 V wires, which controls the state of readiness of the GC and sends the start signal to begin an injection. The microcontroller controls the 24 V electronic valves by turning them on and off, via an opto-isolated 4 channel relay board that separates the 24 V valve circuit from the Arduino’s relay board. This circuit is optically isolated from the valves, but the valve circuit requires a capacitor at each valve to absorb the electro-magnetic pulse generated by the switching of the valve states, which in turn affects both the microcontroller and the flowmeter near the valves. The 5 V step-motor is controlled through a ULN2803AG 8x Transistor Darlington Array integrated circuit, which isolates the current of the motor from the microcontroller Input/Output (I/O) pin current. Lastly there is an I/O pin dedicated to a photo-diode, which is used to determine when the photoreactor light is turned on. This diode cannot detect IR light and has difficulty detecting UV light. It should always be tested before an experiment to see if it is functioning properly (a moon/sun symbol display the current status on the microcontroller display). The detection of light is only used to log the time the lamp has been switched on and is not a critical component.

By design, the Arduino microcontroller resets its internal time every 50 days. If this occurs during an experiment, it would create problems with the injection timing and backflush timing. To alleviate this, a message will appear if the reset time is near (less than

a week), so the user can reset the microcontroller. It is suggested to reset via the interface of the controller every week to avoid this message altogether.

5.S7.3. Interface Windows – Code (compiled with Microsoft Visual Studio Express)

```
#pragma once
#define StepInjP L"+25 injections"
#define StepInjM L"-25 injections"
#define StepTimerP L"+5 seconds"
#define StepTimerM L"-5 seconds"
#define TimeOutPerkin 50
#define TimeOutArduino 50
#define TimeOutFLowValve 10 // in minutes set maximum time for the flow valve be on.
#define DefaultPathNameLog L"c:\\daniel"
#define FILEFORMAT "Time,Date,FlowMeter_data, Sample, Current_no_of_Inj,Ing_timer, Lamp_status"
namespace Interface_Arduino {

	using namespace System;
	using namespace System::ComponentModel;
	using namespace System::Collections;
	using namespace System::Windows::Forms;
	using namespace System::Data;
	using namespace System::Drawing;
	using namespace System::IO::Ports;
	using namespace System::IO;
	using namespace System::Text;



	/// <summary>

	/// Summary for Form1
	/// </summary>


	public ref class Form1 : public System::Windows::Forms::Form
	{
	public:

		Form1(void)
		{

			InitializeComponent();
			//
			//TODO: Add the constructor code here
			//
		}

	protected:
		/// <summary>
		/// Clean up any resources being used.
		/// </summary>
		~Form1()
		{

			if (components)
			{
				delete components;
			}
		}

	protected:

	private: System::IO::Ports::SerialPort^  serialPort1;

	private: System::Windows::Forms::Label^  textBox2;


	private: System::Windows::Forms::Button^  button3;
	private: System::Windows::Forms::Button^  button4;
	private: System::Windows::Forms::Button^  button5;
	private: System::Windows::Forms::Button^  button6;
	private: System::Windows::Forms::ToolTip^  toolTip1;
```

```
            private: System::Windows::Forms::Label^  textBox3;
            private: System::Windows::Forms::Panel^  panel2;
            private: System::Windows::Forms::RadioButton^  radioButton3;
            private: System::Windows::Forms::RadioButton^  radioButton4;
            private: System::Windows::Forms::RadioButton^  radioButton1;
            private: System::Windows::Forms::RadioButton^  radioButton2;
            private: System::Windows::Forms::Panel^  panel1;
            private: System::Windows::Forms::Button^  button7;
            private: System::Windows::Forms::Button^  button8;

            private: System::Windows::Forms::Label^  label2;
            private: System::Windows::Forms::StatusStrip^  statusStrip1;
            private: System::Windows::Forms::ToolStripStatusLabel^  toolStripStatusLabel1;



            private: System::Windows::Forms::Timer^  timer1;
            private: System::IO::Ports::SerialPort^  serialPort2;
            private: System::Windows::Forms::Timer^  timer2;
            private: System::Windows::Forms::ToolStripStatusLabel^  toolStripStatusLabel2;
            private: System::Windows::Forms::ToolStripStatusLabel^  toolStripStatusLabel3;
            private: System::Windows::Forms::ToolStripStatusLabel^  toolStripStatusLabel4;
            private: System::Windows::Forms::ToolStripStatusLabel^  toolStripStatusLabel5;
            private: System::Windows::Forms::SaveFileDialog^  saveFileDialog1;
            private: System::Windows::Forms::Button^  button9;


            private: System::ComponentModel::IContainer^  components;
            private: System::Windows::Forms::ToolStripStatusLabel^  toolStripStatusLabel6;

            private:
                        /// <summary>
                        /// Required designer variable.
                        /// </summary>


            private: System::Windows::Forms::ToolStripStatusLabel^  toolStripStatusLabel7;
            private: System::Windows::Forms::ToolStripStatusLabel^  toolStripStatusLabel10;
            private: System::Windows::Forms::ToolStripStatusLabel^  toolStripStatusLabel9;
            private: System::Windows::Forms::Button^  button10;
            private: System::Windows::Forms::Button^  button11;
            private: System::Windows::Forms::ToolStripStatusLabel^  toolStripStatusLabel8;
            private: System::Windows::Forms::Button^  button12;
            private: System::Windows::Forms::Button^  button13;
            private: System::Windows::Forms::Button^  button14;
            private: System::Windows::Forms::Button^  button15;
            private: System::Windows::Forms::Button^  button16;
            private: System::Windows::Forms::Button^  button17;
private: System::Windows::Forms::Panel^  panel3;
            private: System::Windows::Forms::Button^  button19;
            private: System::Windows::Forms::Button^  button18;
            private: System::Windows::Forms::NumericUpDown^  numericUpDown1;
            private: System::Windows::Forms::Label^  label3;
            private: System::Windows::Forms::Panel^  panel4;
            private: System::Windows::Forms::NumericUpDown^  numericUpDown3;
            private: System::Windows::Forms::Label^  label5;
            private: System::Windows::Forms::Button^  button20;
            private: System::Windows::Forms::Button^  button21;
            private: System::Windows::Forms::NumericUpDown^  numericUpDown2;
            private: System::Windows::Forms::Label^  label4;


StreamWriter^ w; // file stream used for log
System::String^ InjectionNo; // a way to remember last injection when injecting
//System::String^ OldInjectionNo;
System::String ^Flow; //= nullptr;
bool TimerBF;
bool ArduinoOn ; // a variable that aint working yet.
bool LampOn ;
bool AlreadyLampOn ;
bool FlowMarkOn;
bool AutoFlowSampling;
bool AutoActive;
bool LogCut;
bool InjectionNoRepeat;
Int64 TimeMemory;  //for the automated valve control for flowmeter..
Int64 TimeSampling;   //for the automated valve control for flowmeter..
Int64 TimeInterval;   //for the automated valve control for flowmeter..
// Int64 TimePause; // for the pausing wait out
Int64 TimeBF;  //for limiting the log to 1 per s...
private: System::Windows::Forms::Panel^  panel5;
private: System::Windows::Forms::NumericUpDown^  numericUpDown4;
private: System::Windows::Forms::Label^  label6;
private: System::Windows::Forms::Button^  button22;
```

```
private: System::Windows::Forms::Button^  button23;
private: System::Windows::Forms::NumericUpDown^  numericUpDown5;
private: System::Windows::Forms::Label^  label7;


private: System::Windows::Forms::ToolStripStatusLabel^  toolStripStatusLabel11;


static void TimeStamp(TextWriter^ w)
   {
   w→Write(DateTime::Now.ToLongTimeString()); //writes time and day (like Log of injection)
               w→Write(",");
               w→Write( DateTime::Now.Month.ToString());
               w→Write("/");
               w→Write(DateTime::Now.Day.ToString());
               w→Write("/");
               w→Write(DateTime::Now.Year.ToString());

      // Update the underlying file.
      w→Flush();
   }
static void Log(String^ logMessage,TextWriter^ w)
   {
                                    w→Write(",");
   w→Write(logMessage);
                  // Update the underlying file.
      w→Flush();
   }
                        // System::String ^SerialPacket(System::String ^signal, bool receives)
                        // fonction to do a custom write/read for communicating with Arduino
                        // input       System::String ^signal must be a single char, example "a" defined in Arduino code
                        //                                    bool receives: true or false: indicates if Arduino will reply with a string ending with a carrier
return
                        // Output  System::String of the Arduino answer, cut off its carrier return (ready to use on display)
                        //
System::String ^SerialPacket(System::String ^signal, bool receives)
{
               System::String ^Answer = nullptr;
               try {
               this→serialPort1→DiscardInBuffer();
                        serialPort1→Write(signal);
               if(receives== true)
               {

                        Answer=serialPort1→ReadLine();
                        if (Answer→Length>1)
                                 Answer= Answer→Remove(Answer→Length-1); // removes the carriage return
                        else
                                 Answer= "bugged";
                        }

   }
                        catch (TimeoutException ^) { return("Injecting");}
                        catch (InvalidOperationException ^) {
                                 return("error");}
                        catch ( IOException^ ) { ArduinoOn= false;

                                 return("Unpluged");
                        }
               return(Answer);
}
               //bool FlowMark()
                        // Opens communication ports for flowmark and flow meter will probably want integrer
                        // inputs nothing
                        // output true if flowmark is there
                        //
bool FlowMark()
{
               //MessageBox::Show("FlowMark found");
               array<String^>^ serialPorts = nullptr;
               bool NoConflict= true;
               if (ArduinoOn)
                          NoConflict= false;
               //this→serialPort1→PortName = L"PLUP"; // Invalid port definition (Defined COM1 by default)
               try
   {
      // Get a list of serial port names.
      serialPorts = this→serialPort2→GetPortNames();
   }
   catch (Win32Exception^ ex)
   {
     MessageBox::Show(ex→Message);
   }
               int j= 0;
```

```
            for each(String^ port in serialPorts)  // detects flowmeter
   {
            j++;
                        this→serialPort2→PortName = port; // important to not open COM1 or 2 messes up the other software
                           //  Possible comfict true→ false will invalidate only when Portname are the same, if false→ always true so changing name not
important..
                        if (( NoConflict && this→serialPort1→PortName != this→serialPort2→PortName)|| this→serialPort2→PortName != "COM1" ||
this→serialPort2→PortName != "COM2")
                        { // will not look at serialport1 portname (this is the arduino)
                        try
        {

                                    if (this→serialPort2→IsOpen)
                                                this→serialPort2→Close();
                                    this→serialPort2→BaudRate = 115200; // they changed the baudrate with the newer Flowmark jeez..
                                    this→serialPort2→Open(); // sets for an handshake
                                    //this→serialPort2→WriteTimeout = 500;
                                    this→serialPort2→ReadTimeout = TimeOutPerkin;  //waiting for any message from flowmeter
                                    this→serialPort2→ReadLine();
                                    this→serialPort2→DiscardInBuffer();
                                                //MessageBox::Show("FlowMark found");
                                                //this→serialPort2→DiscardInBuffer();
                                                return(true);
                                                //break;        //useless as would have return before..

        }
                                    catch (TimeoutException ^) {this→serialPort2→Close(); }// close the wrong port
                                    catch (InvalidOperationException ^) {}
                                    catch ( IOException^ ) {}
                                    catch ( UnauthorizedAccessException^ ) { }// no need for message MessageBox::Show(ex→Message);}//access
denied error?
                                    // all other ports would eventually make one of the above error, and will loop back. different logic then the arduino
detect..
                           // eventually a problem if something is sending at 57600 some data as well..
                        }
            }
            return (false);
}
                        //int StartUpSerial()
                        // Opens communication ports for Arduino
                        // input        nothing
                        // Output   bool = true if arduino is there
bool StartUpSerial()
{
            bool Arduino=false;
            array<String^>^ serialPorts = nullptr;
            //this→serialPort1→PortName = L"PLUP"; // Invalid port definition (Defined COM1 by default)
            try  // Get a list of serial port names.
            {       serialPorts = this→serialPort1→GetPortNames();
            }
   catch (Win32Exception^ ex) {  MessageBox::Show(ex→Message);  }
               // Define the last port as the good one ( just cause its the reality of the system..)

            int i= 0;

             for each(String^ port in serialPorts)  // detects Arduino board
             {
            //MessageBox::Show(port);
                        try
                        {
                         i++;  // com1 or com2 are real ports and can't be the usb port, avoids going there Access denied error if we do!)
              if (this→serialPort1→IsOpen)
                                                this→serialPort1→Close(); // close port if opens avoid confusion
                         this→serialPort1→PortName = port; //overwrites the port name everytime


                        if (this→serialPort1→PortName == "COM1" || this→serialPort1→PortName == "COM2" || this→serialPort1→PortName ==
this→serialPort2→PortName) // skips COM1 COM2 and a defined flowmeter port
                        {  // skips else
                        }
                        else
                        {
                                    this→serialPort1→BaudRate = 115200; //same as flowmeter now..
                                    this→serialPort1→Open(); // sets for an handshake
                                    this→serialPort1→WriteTimeout = 500;
                                    this→serialPort1→ReadTimeout = 500;
                                    this→serialPort1→DiscardInBuffer(); //cleans anything that could be in mem
                                    this→serialPort1→DiscardOutBuffer(); // cleaning less useful though.. should not have anything there
                                    SerialPacket("z", false); // send a single packet, doesn't look for answer
                                    if (this→serialPort1→ReadLine() == L"12345678\r")
                                    {
                                                Arduino=true;
                                                            this→serialPort1→WriteTimeout = TimeOutArduino;
                                                            this→serialPort1→ReadTimeout = TimeOutArduino;
```

```
                                                return(Arduino); // instead of break;
                                        }

        }

                }
                catch (TimeoutException ^) { this→serialPort1→Close();
                                }// close the wrong port
                catch (InvalidOperationException ^) {
                                 } //these shouldnt happen
                catch ( IOException^ ) {
                                }//these shouldnt happen
                catch ( UnauthorizedAccessException^) {}// no need now for special COM1 and COM2 MessageBox::Show(ex→Message);}//access denied
error?
                 }

                // will return false if it doesnt find anything
                return(Arduino);
}

#pragma region Windows Form Designer generated code
                        /// <summary>
                        /// Required method for Designer support - do not modify
                        /// the contents of this method with the code editor.
                        /// </summary>
                        void InitializeComponent(void)
                        {
                                this→components = (gcnew System::ComponentModel::Container());
                                System::ComponentModel::ComponentResourceManager^  resources = (gcnew
System::ComponentModel::ComponentResourceManager(Form1::typeid));
                                this→serialPort1 = (gcnew System::IO::Ports::SerialPort(this→components));
                                this→textBox2 = (gcnew System::Windows::Forms::Label());
                                this→button3 = (gcnew System::Windows::Forms::Button());
                                this→button4 = (gcnew System::Windows::Forms::Button());
                                this→button5 = (gcnew System::Windows::Forms::Button());
                                this→button6 = (gcnew System::Windows::Forms::Button());
                                this→toolTip1 = (gcnew System::Windows::Forms::ToolTip(this→components));
                                this→textBox3 = (gcnew System::Windows::Forms::Label());
                                this→button7 = (gcnew System::Windows::Forms::Button());
                                this→button8 = (gcnew System::Windows::Forms::Button());
                                this→button9 = (gcnew System::Windows::Forms::Button());
                                this→button10 = (gcnew System::Windows::Forms::Button());
                                this→button11 = (gcnew System::Windows::Forms::Button());
                                this→button12 = (gcnew System::Windows::Forms::Button());
                                this→button15 = (gcnew System::Windows::Forms::Button());
                                this→button16 = (gcnew System::Windows::Forms::Button());
                                this→button17 = (gcnew System::Windows::Forms::Button());
                                this→button13 = (gcnew System::Windows::Forms::Button());
                                this→button14 = (gcnew System::Windows::Forms::Button());
                                this→radioButton4 = (gcnew System::Windows::Forms::RadioButton());
                                this→radioButton3 = (gcnew System::Windows::Forms::RadioButton());
                                this→panel2 = (gcnew System::Windows::Forms::Panel());
                                this→radioButton1 = (gcnew System::Windows::Forms::RadioButton());
                                this→radioButton2 = (gcnew System::Windows::Forms::RadioButton());
                                this→panel1 = (gcnew System::Windows::Forms::Panel());
                                this→label2 = (gcnew System::Windows::Forms::Label());
                                this→statusStrip1 = (gcnew System::Windows::Forms::StatusStrip());
                                this→toolStripStatusLabel1 = (gcnew System::Windows::Forms::ToolStripStatusLabel());
                                this→toolStripStatusLabel10 = (gcnew System::Windows::Forms::ToolStripStatusLabel());
                                this→toolStripStatusLabel7 = (gcnew System::Windows::Forms::ToolStripStatusLabel());
                                this→toolStripStatusLabel11 = (gcnew System::Windows::Forms::ToolStripStatusLabel());
                                this→toolStripStatusLabel9 = (gcnew System::Windows::Forms::ToolStripStatusLabel());
                                this→toolStripStatusLabel2 = (gcnew System::Windows::Forms::ToolStripStatusLabel());
                                this→toolStripStatusLabel5 = (gcnew System::Windows::Forms::ToolStripStatusLabel());
                                this→toolStripStatusLabel3 = (gcnew System::Windows::Forms::ToolStripStatusLabel());
                                this→toolStripStatusLabel4 = (gcnew System::Windows::Forms::ToolStripStatusLabel());
                                this→toolStripStatusLabel6 = (gcnew System::Windows::Forms::ToolStripStatusLabel());
                                this→toolStripStatusLabel8 = (gcnew System::Windows::Forms::ToolStripStatusLabel());
                                this→timer1 = (gcnew System::Windows::Forms::Timer(this→components));
                                this→serialPort2 = (gcnew System::IO::Ports::SerialPort(this→components));
                                this→timer2 = (gcnew System::Windows::Forms::Timer(this→components));
                                this→saveFileDialog1 = (gcnew System::Windows::Forms::SaveFileDialog());
                                this→panel3 = (gcnew System::Windows::Forms::Panel());
                                this→button19 = (gcnew System::Windows::Forms::Button());
                                this→button18 = (gcnew System::Windows::Forms::Button());
                                this→numericUpDown1 = (gcnew System::Windows::Forms::NumericUpDown());
                                this→label3 = (gcnew System::Windows::Forms::Label());
                                this→panel4 = (gcnew System::Windows::Forms::Panel());
                                this→numericUpDown3 = (gcnew System::Windows::Forms::NumericUpDown());
                                this→label5 = (gcnew System::Windows::Forms::Label());
                                this→button20 = (gcnew System::Windows::Forms::Button());
                                this→button21 = (gcnew System::Windows::Forms::Button());
                                this→numericUpDown2 = (gcnew System::Windows::Forms::NumericUpDown());
                                this→label4 = (gcnew System::Windows::Forms::Label());
```

```
this→panel5 = (gcnew System::Windows::Forms::Panel());
this→numericUpDown4 = (gcnew System::Windows::Forms::NumericUpDown());
this→label6 = (gcnew System::Windows::Forms::Label());
this→button22 = (gcnew System::Windows::Forms::Button());
this→button23 = (gcnew System::Windows::Forms::Button());
this→numericUpDown5 = (gcnew System::Windows::Forms::NumericUpDown());
this→label7 = (gcnew System::Windows::Forms::Label());
this→panel2→SuspendLayout();
this→panel1→SuspendLayout();
this→statusStrip1→SuspendLayout();
this→panel3→SuspendLayout();
(cli::safe_cast<System::ComponentModel::ISupportInitialize^ >(this→numericUpDown1))→BeginInit();
this→panel4→SuspendLayout();
(cli::safe_cast<System::ComponentModel::ISupportInitialize^ >(this→numericUpDown3))→BeginInit();
(cli::safe_cast<System::ComponentModel::ISupportInitialize^ >(this→numericUpDown2))→BeginInit();
this→panel5→SuspendLayout();
(cli::safe_cast<System::ComponentModel::ISupportInitialize^ >(this→numericUpDown4))→BeginInit();
(cli::safe_cast<System::ComponentModel::ISupportInitialize^ >(this→numericUpDown5))→BeginInit();
this→SuspendLayout();
//
// textBox2
//
this→textBox2→Location = System::Drawing::Point(8, 104);
this→textBox2→Name = L"textBox2";
this→textBox2→Size = System::Drawing::Size(100, 20);
this→textBox2→TabIndex = 30;
this→textBox2→Text = L"Injection Interval (s)";
this→textBox2→TextAlign = System::Drawing::ContentAlignment::TopCenter;
this→textBox2→Visible = false;
//
// button3
//
this→button3→Location = System::Drawing::Point(12, 120);
this→button3→Name = L"button3";
this→button3→Size = System::Drawing::Size(26, 19);
this→button3→TabIndex = 8;
this→button3→Text = L"-";
this→toolTip1→SetToolTip(this→button3, L"-5");
this→button3→UseVisualStyleBackColor = true;
this→button3→Visible = false;
this→button3→Click += gcnew System::EventHandler(this, &Form1::button3_Click);
//
// button4
//
this→button4→Location = System::Drawing::Point(76, 120);
this→button4→Name = L"button4";
this→button4→Size = System::Drawing::Size(26, 20);
this→button4→TabIndex = 7;
this→button4→Text = L"+";
this→toolTip1→SetToolTip(this→button4, L"+5");
this→button4→UseVisualStyleBackColor = true;
this→button4→Visible = false;
this→button4→Click += gcnew System::EventHandler(this, &Form1::button4_Click);
//
// button5
//
this→button5→BackgroundImage = (cli::safe_cast<System::Drawing::Image^
>(resources→GetObject(L"button5.BackgroundImage")));
this→button5→BackgroundImageLayout = System::Windows::Forms::ImageLayout::Zoom;
this→button5→Enabled = false;
this→button5→Font = (gcnew System::Drawing::Font(L"Microsoft Sans Serif", 27.75F,
System::Drawing::FontStyle::Regular, System::Drawing::GraphicsUnit::Point,
                    static_cast<System::Byte>(0)));
this→button5→ForeColor = System::Drawing::Color::DeepPink;
this→button5→Location = System::Drawing::Point(178, 5);
this→button5→Name = L"button5";
this→button5→Size = System::Drawing::Size(220, 207);
this→button5→TabIndex = 10;
this→button5→Text = L"Start Flow";
this→button5→TextAlign = System::Drawing::ContentAlignment::BottomCenter;
this→toolTip1→SetToolTip(this→button5, L"Start experiment!!");
this→button5→UseVisualStyleBackColor = true;
this→button5→Click += gcnew System::EventHandler(this, &Form1::button5_Click);
//
// button6
//
this→button6→ForeColor = System::Drawing::Color::Crimson;
this→button6→Location = System::Drawing::Point(8, 177);
this→button6→Name = L"button6";
this→button6→Size = System::Drawing::Size(55, 35);
this→button6→TabIndex = 11;
this→button6→Text = L"BF Timing";
this→toolTip1→SetToolTip(this→button6, L"Edit the backflush timing.");
this→button6→UseVisualStyleBackColor = true;
```

```
this→button6→Visible = false;
this→button6→Click += gcnew System::EventHandler(this, &Form1::button6_Click);
//
// textBox3
//
this→textBox3→Location = System::Drawing::Point(8, 141);
this→textBox3→Name = L"textBox3";
this→textBox3→Size = System::Drawing::Size(100, 20);
this→textBox3→TabIndex = 29;
this→textBox3→Text = L"Number of Samples";
this→textBox3→TextAlign = System::Drawing::ContentAlignment::TopCenter;
this→toolTip1→SetToolTip(this→textBox3, L"Can not be edited while running.");
this→textBox3→Visible = false;
//
// button7
//
this→button7→Enabled = false;
this→button7→ForeColor = System::Drawing::Color::Crimson;
this→button7→Location = System::Drawing::Point(111, 167);
this→button7→Name = L"button7";
this→button7→Size = System::Drawing::Size(64, 20);
this→button7→TabIndex = 17;
this→button7→Text = L"Pause";
this→toolTip1→SetToolTip(this→button7, L"Pause Run; keep injection count.");
this→button7→UseVisualStyleBackColor = true;
this→button7→Click += gcnew System::EventHandler(this, &Form1::button7_Click);
//
// button8
//
this→button8→ForeColor = System::Drawing::Color::Crimson;
this→button8→Location = System::Drawing::Point(111, 189);
this→button8→Name = L"button8";
this→button8→Size = System::Drawing::Size(64, 23);
this→button8→TabIndex = 18;
this→button8→Text = L"Reset";
this→toolTip1→SetToolTip(this→button8, L"Reset Arduino Controller to original values.");
this→button8→UseVisualStyleBackColor = true;
this→button8→Click += gcnew System::EventHandler(this, &Form1::button8_Click);
//
// button9
//
this→button9→Location = System::Drawing::Point(111, 5);
this→button9→Name = L"button9";
this→button9→Size = System::Drawing::Size(64, 23);
this→button9→TabIndex = 22;
this→button9→Text = L"Start Log";
this→toolTip1→SetToolTip(this→button9, L"Record flow rate and injection data.");
this→button9→UseVisualStyleBackColor = true;
this→button9→Click += gcnew System::EventHandler(this, &Form1::button9_Click);
//
// button10
//
this→button10→Location = System::Drawing::Point(111, 129);
this→button10→Name = L"button10";
this→button10→Size = System::Drawing::Size(64, 36);
this→button10→TabIndex = 23;
this→button10→Text = L"Sample Toggle";
this→toolTip1→SetToolTip(this→button10, L"Switch between sample A and B. (current sample is displayed at
bottom left corner"
                L")");
this→button10→UseVisualStyleBackColor = true;
this→button10→Visible = false;
this→button10→Click += gcnew System::EventHandler(this, &Form1::button10_Click);
//
// button11
//
this→button11→Location = System::Drawing::Point(111, 29);
this→button11→Name = L"button11";
this→button11→Size = System::Drawing::Size(64, 50);
this→button11→TabIndex = 24;
this→button11→Text = L"Turn On FlowMeter Valve";
this→toolTip1→SetToolTip(this→button11, L"Use this to send flow to the Flowmeter (leaving digital flowmeter on
the eluant f"
                L"low for a long time period is damaging and willn destroy the unit over time).");
this→button11→UseVisualStyleBackColor = true;
this→button11→Click += gcnew System::EventHandler(this, &Form1::button11_Click);
//
// button12
//
this→button12→Location = System::Drawing::Point(8, 46);
this→button12→Name = L"button12";
this→button12→Size = System::Drawing::Size(100, 50);
this→button12→TabIndex = 25;
this→button12→Text = L"Turn On Tray Rotation";
```

```
this→toolTip1→SetToolTip(this→button12, L"Rotate Photo-reactor carousel.");
this→button12→UseVisualStyleBackColor = true;
this→button12→Click += gcnew System::EventHandler(this, &Form1::button12_Click);
//
// button15
//
this→button15→Location = System::Drawing::Point(62, 177);
this→button15→Name = L"button15";
this→button15→Size = System::Drawing::Size(46, 35);
this→button15→TabIndex = 28;
this→button15→Text = L"Shake Tray";
this→toolTip1→SetToolTip(this→button15, L"Lightly shake Photo-reactor carousel back and forth.");
this→button15→UseVisualStyleBackColor = true;
this→button15→Visible = false;
this→button15→Click += gcnew System::EventHandler(this, &Form1::button15_Click);
//
// button16
//
this→button16→Location = System::Drawing::Point(111, 78);
this→button16→Name = L"button16";
this→button16→Size = System::Drawing::Size(64, 50);
this→button16→TabIndex = 32;
this→button16→Text = L"Automatic Flow Rate Sampling";
this→toolTip1→SetToolTip(this→button16, L"Turn on and off Flowmeter valve at regular intervals");
this→button16→UseVisualStyleBackColor = true;
this→button16→Click += gcnew System::EventHandler(this, &Form1::button16_Click);
//
// button17
//
this→button17→Location = System::Drawing::Point(8, 48);
this→button17→Name = L"button17";
this→button17→Size = System::Drawing::Size(100, 50);
this→button17→TabIndex = 33;
this→button17→Text = L"Set Injection No";
this→toolTip1→SetToolTip(this→button17, L"Enter current injection number, useful for restarting an experiment");
this→button17→UseVisualStyleBackColor = true;
this→button17→Visible = false;
this→button17→Click += gcnew System::EventHandler(this, &Form1::button17_Click);
//
// button13
//
this→button13→Location = System::Drawing::Point(8, 102);
this→button13→Name = L"button13";
this→button13→Size = System::Drawing::Size(48, 50);
this→button13→TabIndex = 26;
this→button13→Text = L"Rotate CW 45°";
this→button13→UseVisualStyleBackColor = true;
this→button13→Click += gcnew System::EventHandler(this, &Form1::button13_Click);
//
// button14
//
this→button14→Location = System::Drawing::Point(60, 102);
this→button14→Name = L"button14";
this→button14→Size = System::Drawing::Size(48, 50);
this→button14→TabIndex = 27;
this→button14→Text = L"Rotate CCW 45°";
this→button14→UseVisualStyleBackColor = true;
this→button14→Click += gcnew System::EventHandler(this, &Form1::button14_Click);
//
// radioButton4
//
this→radioButton4→AutoSize = true;
this→radioButton4→Location = System::Drawing::Point(54, 3);
this→radioButton4→Name = L"radioButton4";
this→radioButton4→Size = System::Drawing::Size(31, 17);
this→radioButton4→TabIndex = 14;
this→radioButton4→Text = L"2";
this→radioButton4→UseVisualStyleBackColor = true;
this→radioButton4→Visible = false;
//
// radioButton3
//
this→radioButton3→AutoSize = true;
this→radioButton3→Checked = true;
this→radioButton3→Location = System::Drawing::Point(17, 3);
this→radioButton3→Name = L"radioButton3";
this→radioButton3→Size = System::Drawing::Size(31, 17);
this→radioButton3→TabIndex = 13;
this→radioButton3→TabStop = true;
this→radioButton3→Text = L"1";
this→radioButton3→UseVisualStyleBackColor = true;
this→radioButton3→Visible = false;
this→radioButton3→CheckedChanged += gcnew System::EventHandler(this,
&Form1::radioButton3_CheckedChanged);
```

```
                                        //
                                        // panel2
                                        //
                                        this→panel2→Controls→Add(this→radioButton3);
                                        this→panel2→Controls→Add(this→radioButton4);
                                        this→panel2→Location = System::Drawing::Point(8, 156);
                                        this→panel2→Name = L"panel2";
                                        this→panel2→Size = System::Drawing::Size(100, 23);
                                        this→panel2→TabIndex = 16;
                                        //
                                        // radioButton1
                                        //
                                        this→radioButton1→AutoSize = true;
                                        this→radioButton1→Checked = true;
                                        this→radioButton1→Location = System::Drawing::Point(0, 3);
                                        this→radioButton1→Name = L"radioButton1";
                                        this→radioButton1→Size = System::Drawing::Size(110, 17);
                                        this→radioButton1→TabIndex = 1;
                                        this→radioButton1→TabStop = true;
                                        this→radioButton1→Text = L"Headspace Mode";
                                        this→radioButton1→UseVisualStyleBackColor = true;
                                        this→radioButton1→CheckedChanged += gcnew System::EventHandler(this,
&Form1::radioButton1_CheckedChanged);
                                        //
                                        // radioButton2
                                        //
                                        this→radioButton2→AutoSize = true;
                                        this→radioButton2→Location = System::Drawing::Point(0, 20);
                                        this→radioButton2→Name = L"radioButton2";
                                        this→radioButton2→Size = System::Drawing::Size(77, 17);
                                        this→radioButton2→TabIndex = 2;
                                        this→radioButton2→Text = L"Flow Mode";
                                        this→radioButton2→UseVisualStyleBackColor = true;
                                        //
                                        // panel1
                                        //
                                        this→panel1→Controls→Add(this→radioButton2);
                                        this→panel1→Controls→Add(this→radioButton1);
                                        this→panel1→Location = System::Drawing::Point(8, 5);
                                        this→panel1→Name = L"panel1";
                                        this→panel1→Size = System::Drawing::Size(110, 40);
                                        this→panel1→TabIndex = 15;
                                        //
                                        // label2
                                        //
                                        this→label2→AutoSize = true;
                                        this→label2→Font = (gcnew System::Drawing::Font(L"Microsoft Sans Serif", 9.75F,
System::Drawing::FontStyle::Regular, System::Drawing::GraphicsUnit::Point,
                                                static_cast<System::Byte>(0)));
                                        this→label2→Location = System::Drawing::Point(41, 120);
                                        this→label2→Name = L"label2";
                                        this→label2→Size = System::Drawing::Size(29, 16);
                                        this→label2→TabIndex = 20;
                                        this→label2→Text = L"150";
                                        this→label2→TextAlign = System::Drawing::ContentAlignment::MiddleCenter;
                                        this→label2→Visible = false;
                                        //
                                        // statusStrip1
                                        //
                                        this→statusStrip1→Items→AddRange(gcnew cli::array< System::Windows::Forms::ToolStripItem^  >(11)
{this→toolStripStatusLabel1,
                                                this→toolStripStatusLabel10, this→toolStripStatusLabel7, this→toolStripStatusLabel11,
this→toolStripStatusLabel9, this→toolStripStatusLabel2,
                                                this→toolStripStatusLabel5, this→toolStripStatusLabel3, this→toolStripStatusLabel4,
this→toolStripStatusLabel6, this→toolStripStatusLabel8});
                                        this→statusStrip1→Location = System::Drawing::Point(0, 215);
                                        this→statusStrip1→Name = L"statusStrip1";
                                        this→statusStrip1→Size = System::Drawing::Size(398, 22);
                                        this→statusStrip1→SizingGrip = false;
                                        this→statusStrip1→TabIndex = 21;
                                        this→statusStrip1→Text = L"statusStrip1";
                                        //
                                        // toolStripStatusLabel1
                                        //
                                        this→toolStripStatusLabel1→Name = L"toolStripStatusLabel1";
                                        this→toolStripStatusLabel1→Size = System::Drawing::Size(13, 17);
                                        this→toolStripStatusLabel1→Text = L"0";
                                        this→toolStripStatusLabel1→Visible = false;
                                        //
                                        // toolStripStatusLabel10
                                        //
                                        this→toolStripStatusLabel10→Name = L"toolStripStatusLabel10";
                                        this→toolStripStatusLabel10→Size = System::Drawing::Size(50, 17);
                                        this→toolStripStatusLabel10→Text = L"Next Inj.";
```

```
this→toolStripStatusLabel10→Visible = false;
//
// toolStripStatusLabel7
//
this→toolStripStatusLabel7→Enabled = false;
this→toolStripStatusLabel7→Name = L"toolStripStatusLabel7";
this→toolStripStatusLabel7→Size = System::Drawing::Size(15, 17);
this→toolStripStatusLabel7→Text = L"A";
this→toolStripStatusLabel7→ToolTipText = L"Current channel flow that will be injected in the next cycle.";
//
// toolStripStatusLabel11
//
this→toolStripStatusLabel11→Name = L"toolStripStatusLabel11";
this→toolStripStatusLabel11→Size = System::Drawing::Size(17, 17);
this→toolStripStatusLabel11→Text = L"in";
this→toolStripStatusLabel11→Visible = false;
//
// toolStripStatusLabel9
//
this→toolStripStatusLabel9→Name = L"toolStripStatusLabel9";
this→toolStripStatusLabel9→Size = System::Drawing::Size(14, 17);
this→toolStripStatusLabel9→Text = L"X";
this→toolStripStatusLabel9→Visible = false;
//
// toolStripStatusLabel2
//
this→toolStripStatusLabel2→Name = L"toolStripStatusLabel2";
this→toolStripStatusLabel2→Size = System::Drawing::Size(12, 17);
this→toolStripStatusLabel2→Text = L"s";
this→toolStripStatusLabel2→TextAlign = System::Drawing::ContentAlignment::MiddleLeft;
this→toolStripStatusLabel2→Visible = false;
//
// toolStripStatusLabel5
//
this→toolStripStatusLabel5→Name = L"toolStripStatusLabel5";
this→toolStripStatusLabel5→Size = System::Drawing::Size(191, 17);
this→toolStripStatusLabel5→Spring = true;
this→toolStripStatusLabel5→TextAlign = System::Drawing::ContentAlignment::MiddleRight;
//
// toolStripStatusLabel3
//
this→toolStripStatusLabel3→Enabled = false;
this→toolStripStatusLabel3→Name = L"toolStripStatusLabel3";
this→toolStripStatusLabel3→Size = System::Drawing::Size(63, 17);
this→toolStripStatusLabel3→Text = L"Flowmeter";
this→toolStripStatusLabel3→TextAlign = System::Drawing::ContentAlignment::MiddleRight;
this→toolStripStatusLabel3→ToolTipText = L"If grey no flowmeter is detected";
//
// toolStripStatusLabel4
//
this→toolStripStatusLabel4→Enabled = false;
this→toolStripStatusLabel4→Name = L"toolStripStatusLabel4";
this→toolStripStatusLabel4→Size = System::Drawing::Size(50, 17);
this→toolStripStatusLabel4→Text = L"Arduino";
this→toolStripStatusLabel4→ToolTipText = L"If grey the Arduino is not detected";
//
// toolStripStatusLabel6
//
this→toolStripStatusLabel6→Enabled = false;
this→toolStripStatusLabel6→Name = L"toolStripStatusLabel6";
this→toolStripStatusLabel6→Size = System::Drawing::Size(27, 17);
this→toolStripStatusLabel6→Text = L"Log";
this→toolStripStatusLabel6→ToolTipText = L"If grey no logging is done";
//
// toolStripStatusLabel8
//
this→toolStripStatusLabel8→Enabled = false;
this→toolStripStatusLabel8→Name = L"toolStripStatusLabel8";
this→toolStripStatusLabel8→Size = System::Drawing::Size(37, 17);
this→toolStripStatusLabel8→Text = L"Lamp";
this→toolStripStatusLabel8→ToolTipText = L"If grey the lamp is off.";
//
// timer1
//
this→timer1→Interval = 1000;
this→timer1→Tick += gcnew System::EventHandler(this, &Form1::timer1_Tick);
//
// timer2
//
this→timer2→Interval = 600;
this→timer2→Tick += gcnew System::EventHandler(this, &Form1::timer2_Tick);
//
// saveFileDialog1
//
```

```
this→saveFileDialog1→DefaultExt = L"csv";
this→saveFileDialog1→FileName = L"flow_log.csv";
this→saveFileDialog1→Filter = L"CSV text file |*.csv";
this→saveFileDialog1→InitialDirectory = L"c:\\daniel";
this→saveFileDialog1→OverwritePrompt = false;
//
// panel3
//
this→panel3→BorderStyle = System::Windows::Forms::BorderStyle::Fixed3D;
this→panel3→Controls→Add(this→button19);
this→panel3→Controls→Add(this→button18);
this→panel3→Controls→Add(this→numericUpDown1);
this→panel3→Controls→Add(this→label3);
this→panel3→Location = System::Drawing::Point(204, 8);
this→panel3→Name = L"panel3";
this→panel3→Size = System::Drawing::Size(158, 37);
this→panel3→TabIndex = 34;
this→panel3→Visible = false;
//
// button19
//
this→button19→Location = System::Drawing::Point(103, 15);
this→button19→Name = L"button19";
this→button19→Size = System::Drawing::Size(50, 21);
this→button19→TabIndex = 3;
this→button19→Text = L"Cancel";
this→button19→UseVisualStyleBackColor = true;
this→button19→Click += gcnew System::EventHandler(this, &Form1::button19_Click);
//
// button18
//
this→button18→Location = System::Drawing::Point(67, 15);
this→button18→Name = L"button18";
this→button18→Size = System::Drawing::Size(30, 21);
this→button18→TabIndex = 2;
this→button18→Text = L"Ok";
this→button18→UseVisualStyleBackColor = true;
this→button18→Click += gcnew System::EventHandler(this, &Form1::button18_Click);
//
// numericUpDown1
//
this→numericUpDown1→Location = System::Drawing::Point(5, 17);
this→numericUpDown1→Maximum = System::Decimal(gcnew cli::array< System::Int32 >(4) {998, 0, 0, 0});
this→numericUpDown1→Name = L"numericUpDown1";
this→numericUpDown1→Size = System::Drawing::Size(56, 20);
this→numericUpDown1→TabIndex = 1;
//
// label3
//
this→label3→AutoSize = true;
this→label3→Location = System::Drawing::Point(3, 4);
this→label3→Name = L"label3";
this→label3→Size = System::Drawing::Size(115, 13);
this→label3→TabIndex = 0;
this→label3→Text = L"Enter Injection Number";
//
// panel4
//
this→panel4→BorderStyle = System::Windows::Forms::BorderStyle::Fixed3D;
this→panel4→Controls→Add(this→numericUpDown3);
this→panel4→Controls→Add(this→label5);
this→panel4→Controls→Add(this→button20);
this→panel4→Controls→Add(this→button21);
this→panel4→Controls→Add(this→numericUpDown2);
this→panel4→Controls→Add(this→label4);
this→panel4→Location = System::Drawing::Point(204, 47);
this→panel4→Name = L"panel4";
this→panel4→Size = System::Drawing::Size(158, 80);
this→panel4→TabIndex = 35;
this→panel4→Visible = false;
//
// numericUpDown3
//
this→numericUpDown3→Location = System::Drawing::Point(6, 55);
this→numericUpDown3→Maximum = System::Decimal(gcnew cli::array< System::Int32 >(4) {10000, 0, 0, 0});
this→numericUpDown3→Minimum = System::Decimal(gcnew cli::array< System::Int32 >(4) {1, 0, 0, 0});
this→numericUpDown3→Name = L"numericUpDown3";
this→numericUpDown3→Size = System::Drawing::Size(56, 20);
this→numericUpDown3→TabIndex = 5;
this→numericUpDown3→Value = System::Decimal(gcnew cli::array< System::Int32 >(4) {60, 0, 0, 0});
this→numericUpDown3→ValueChanged += gcnew System::EventHandler(this,
&Form1::numericUpDown3_ValueChanged);
//
// label5
```

```
                                        //
                                        this→label5→AutoSize = true;
                                        this→label5→Location = System::Drawing::Point(3, 39);
                                        this→label5→Name = L"label5";
                                        this→label5→Size = System::Drawing::Size(121, 13);
                                        this→label5→TabIndex = 4;
                                        this→label5→Text = L"Enter Interval Time (min)";
                                        //
                                        // button20
                                        //
                                        this→button20→Location = System::Drawing::Point(103, 52);
                                        this→button20→Name = L"button20";
                                        this→button20→Size = System::Drawing::Size(50, 21);
                                        this→button20→TabIndex = 3;
                                        this→button20→Text = L"Cancel";
                                        this→button20→UseVisualStyleBackColor = true;
                                        this→button20→Click += gcnew System::EventHandler(this, &Form1::button20_Click);
                                        //
                                        // button21
                                        //
                                        this→button21→Location = System::Drawing::Point(121, 20);
                                        this→button21→Name = L"button21";
                                        this→button21→Size = System::Drawing::Size(30, 21);
                                        this→button21→TabIndex = 2;
                                        this→button21→Text = L"Ok";
                                        this→button21→UseVisualStyleBackColor = true;
                                        this→button21→Click += gcnew System::EventHandler(this, &Form1::button21_Click);
                                        //
                                        // numericUpDown2
                                        //
                                        this→numericUpDown2→Location = System::Drawing::Point(5, 17);
                                        this→numericUpDown2→Maximum = System::Decimal(gcnew cli::array< System::Int32 >(4) {60, 0, 0, 0});
                                        this→numericUpDown2→Name = L"numericUpDown2";
                                        this→numericUpDown2→Size = System::Drawing::Size(56, 20);
                                        this→numericUpDown2→TabIndex = 1;
                                        this→numericUpDown2→Value = System::Decimal(gcnew cli::array< System::Int32 >(4) {4, 0, 0, 0});
                                        this→numericUpDown2→ValueChanged += gcnew System::EventHandler(this,
&Form1::numericUpDown2_ValueChanged);
                                        //
                                        // label4
                                        //
                                        this→label4→AutoSize = true;
                                        this→label4→Location = System::Drawing::Point(3, 4);
                                        this→label4→Name = L"label4";
                                        this→label4→Size = System::Drawing::Size(129, 13);
                                        this→label4→TabIndex = 0;
                                        this→label4→Text = L"Enter Sampling Time (min)";
                                        //
                                        // panel5
                                        //
                                        this→panel5→BorderStyle = System::Windows::Forms::BorderStyle::Fixed3D;
                                        this→panel5→Controls→Add(this→numericUpDown4);
                                        this→panel5→Controls→Add(this→label6);
                                        this→panel5→Controls→Add(this→button22);
                                        this→panel5→Controls→Add(this→button23);
                                        this→panel5→Controls→Add(this→numericUpDown5);
                                        this→panel5→Controls→Add(this→label7);
                                        this→panel5→Location = System::Drawing::Point(204, 129);
                                        this→panel5→Name = L"panel5";
                                        this→panel5→Size = System::Drawing::Size(158, 80);
                                        this→panel5→TabIndex = 36;
                                        this→panel5→Visible = false;
                                        //
                                        // numericUpDown4
                                        //
                                        this→numericUpDown4→Location = System::Drawing::Point(6, 55);
                                        this→numericUpDown4→Maximum = System::Decimal(gcnew cli::array< System::Int32 >(4) {10000, 0, 0, 0});
                                        this→numericUpDown4→Name = L"numericUpDown4";
                                        this→numericUpDown4→Size = System::Drawing::Size(56, 20);
                                        this→numericUpDown4→TabIndex = 5;
                                        this→numericUpDown4→Value = System::Decimal(gcnew cli::array< System::Int32 >(4) {70, 0, 0, 0});
                                        //
                                        // label6
                                        //
                                        this→label6→AutoSize = true;
                                        this→label6→Location = System::Drawing::Point(3, 39);
                                        this→label6→Name = L"label6";
                                        this→label6→Size = System::Drawing::Size(140, 13);
                                        this→label6→TabIndex = 4;
                                        this→label6→Text = L"Enter end of backflush (sec)";
                                        //
                                        // button22
                                        //
                                        this→button22→Location = System::Drawing::Point(103, 52);
```

```
this→button22→Name = L"button22";
this→button22→Size = System::Drawing::Size(50, 21);
this→button22→TabIndex = 3;
this→button22→Text = L"Cancel";
this→button22→UseVisualStyleBackColor = true;
this→button22→Click += gcnew System::EventHandler(this, &Form1::button22_Click);
//
// button23
//
this→button23→Location = System::Drawing::Point(121, 20);
this→button23→Name = L"button23";
this→button23→Size = System::Drawing::Size(30, 21);
this→button23→TabIndex = 2;
this→button23→Text = L"Ok";
this→button23→UseVisualStyleBackColor = true;
this→button23→Click += gcnew System::EventHandler(this, &Form1::button23_Click);
//
// numericUpDown5
//
this→numericUpDown5→Location = System::Drawing::Point(6, 22);
this→numericUpDown5→Maximum = System::Decimal(gcnew cli::array< System::Int32 >(4) {1000, 0, 0, 0});
this→numericUpDown5→Name = L"numericUpDown5";
this→numericUpDown5→Size = System::Drawing::Size(56, 20);
this→numericUpDown5→TabIndex = 1;
this→numericUpDown5→Value = System::Decimal(gcnew cli::array< System::Int32 >(4) {63, 0, 0, 0});
//
// label7
//
this→label7→AutoSize = true;
this→label7→Location = System::Drawing::Point(6, 4);
this→label7→Name = L"label7";
this→label7→Size = System::Drawing::Size(142, 13);
this→label7→TabIndex = 0;
this→label7→Text = L"Enter start of backflush (sec)";
//
// Form1
//
this→AutoScaleDimensions = System::Drawing::SizeF(6, 13);
this→AutoScaleMode = System::Windows::Forms::AutoScaleMode::Font;
this→ClientSize = System::Drawing::Size(398, 237);
this→Controls→Add(this→panel5);
this→Controls→Add(this→panel4);
this→Controls→Add(this→panel3);
this→Controls→Add(this→button16);
this→Controls→Add(this→button15);
this→Controls→Add(this→button14);
this→Controls→Add(this→button13);
this→Controls→Add(this→button11);
this→Controls→Add(this→button10);
this→Controls→Add(this→button7);
this→Controls→Add(this→button9);
this→Controls→Add(this→statusStrip1);
this→Controls→Add(this→label2);
this→Controls→Add(this→button8);
this→Controls→Add(this→textBox3);
this→Controls→Add(this→button6);
this→Controls→Add(this→button5);
this→Controls→Add(this→button3);
this→Controls→Add(this→button4);
this→Controls→Add(this→panel1);
this→Controls→Add(this→panel2);
this→Controls→Add(this→textBox2);
this→Controls→Add(this→button17);
this→Controls→Add(this→button12);
this→FormBorderStyle = System::Windows::Forms::FormBorderStyle::Fixed3D;
this→Icon = (cli::safe_cast<System::Drawing::Icon^ >(resources→GetObject(L"$this.Icon")));
this→MaximizeBox = false;
this→Name = L"Form1";
this→Text = L"Arduino Flow Interface  -  D. Chartrand 2011-13";
this→toolTip1→SetToolTip(this, L"Hi there! this bar can be used to drag around the window.. fun stuff..");
this→FormClosing += gcnew System::Windows::Forms::FormClosingEventHandler(this,
&Form1::Form1_FormClosing);
this→Load += gcnew System::EventHandler(this, &Form1::Form1_Load);
this→panel2→ResumeLayout(false);
this→panel2→PerformLayout();
this→panel1→ResumeLayout(false);
this→panel1→PerformLayout();
this→statusStrip1→ResumeLayout(false);
this→statusStrip1→PerformLayout();
this→panel3→ResumeLayout(false);
this→panel3→PerformLayout();
(cli::safe_cast<System::ComponentModel::ISupportInitialize^ >(this→numericUpDown1))→EndInit();
this→panel4→ResumeLayout(false);
this→panel4→PerformLayout();
```

```
                                    (cli::safe_cast<System::ComponentModel::ISupportInitialize^ >(this→numericUpDown3))→EndInit();
                                    (cli::safe_cast<System::ComponentModel::ISupportInitialize^ >(this→numericUpDown2))→EndInit();
                                    this→panel5→ResumeLayout(false);
                                    this→panel5→PerformLayout();
                                    (cli::safe_cast<System::ComponentModel::ISupportInitialize^ >(this→numericUpDown4))→EndInit();
                                    (cli::safe_cast<System::ComponentModel::ISupportInitialize^ >(this→numericUpDown5))→EndInit();
                                    this→ResumeLayout(false);
                                    this→PerformLayout();

                        }
#pragma endregion
// closing program are you sure warning
private: System::Void Form1_FormClosing(System::Object^ sender, System::Windows::Forms::FormClosingEventArgs^ e) {

            if(this→timer1→Enabled)
            {
                        if ( MessageBox::Show(
      "This will close the program, are you sure? \rPresent run wont be halted.\rProgram will not recognize current experiment running.",
      "Closing", MessageBoxButtons::YesNo,
      MessageBoxIcon::Question) == System::Windows::Forms::DialogResult::Yes )
                        {
                        if ( MessageBox::Show(
      "Final check: Are you sure you want to close the software with an ongoing experiment?\rIt is not a good idea you know.",
      "Closing", MessageBoxButtons::YesNo,
      MessageBoxIcon::Question) == System::Windows::Forms::DialogResult::Yes )
                                    e→Cancel = false;
                         else
                                    e→Cancel = true;
                        }
                        else
                        e→Cancel = true;
            }
            else
                        e→Cancel = false;
 }
// opening program, activate serial links and start timer2
private: System::Void Form1_Load(System::Object^ sender, System::EventArgs^ e) {
   //sets variable I couldnt initialise at the beginning..
            Flow= nullptr;
            TimerBF =false;
            AutoFlowSampling = false;
            AutoActive = false;
   ArduinoOn = false; // false!
            ArduinoOn = StartUpSerial();
            // ArduinoOn = true; // added to debug
            LampOn = false;
            AlreadyLampOn = false;
            TimeMemory = 0;
            LogCut= false;
            TimeInterval =0 ;
            TimeSampling =0 ;
            InjectionNoRepeat = true;
            if (ArduinoOn)
            {
                        this→toolStripStatusLabel4→Enabled = true;
                        InjectionNo = SerialPacket("n",true);
            }
            else
            {
                         MessageBox::Show("No Arduino detected!");
                        this→radioButton1→Enabled = false;  // disable all interface
                        this→radioButton2→Enabled = false;
                        this→button8→Enabled = false;
                        InjectionNo ="0";
            }
            FlowMarkOn = false;
            FlowMarkOn = FlowMark();
            if (FlowMarkOn)
                        this→toolStripStatusLabel3→Enabled = true;
            this→timer2→Enabled = true;
            MessageBox::Show("If software is laggy or non responsive and Flowmeter data not showing, turn off and on Flowmeter or turn off flowmeter
and restart interface.\rEvery 98th run an extra 5 minute is added to the injection interval to take into account GC loading time occuring after 98
injections.\rUnmatching injection number between GC and controller will create skiped runs.", "Information");
   // SerialPacket("e",true); // fetch numbers from arduino..   *removed because not storing this info anymore
            //this→label1→Text = SerialPacket("d",true);  * removed as button removed
            SerialPacket("g",true);
            this→label2→Text = SerialPacket("f",true);
            this→toolStripStatusLabel1→Text = SerialPacket("n",true);
            if(toolStripStatusLabel1→Text != L"Injecting")
                        InjectionNo = toolStripStatusLabel1→Text;
            else
                        this→toolStripStatusLabel1→Text= L""; // display nothing if error (or there is timeout),

            }
```

```
// timer 1 use to poll Arduino when running sample, reports data
private: System::Void timer1_Tick(System::Object^  sender, System::EventArgs^  e) {
		if (this→toolStripStatusLabel7→Enabled)
			this→toolStripStatusLabel7→Text= SerialPacket("x",true); // x for sampling sample

		//this→toolStripStatusLabel1→Visible= true; // timer visible
		this→toolStripStatusLabel2→Visible= true; // timer visible
		this→toolStripStatusLabel9→Visible= true; // timer visible
		this→toolStripStatusLabel10→Visible= true; // timer visible
		this→toolStripStatusLabel11→Visible= true; // timer visible
		this→toolStripStatusLabel1→Text = SerialPacket("n",true);
		if(toolStripStatusLabel1→Text != L"Injecting")
		{
			if (InjectionNo == toolStripStatusLabel1→Text)
				InjectionNoRepeat = true;
			else
				InjectionNoRepeat = false; // will only be false when a new number is there, this will correspond to a new injection
			InjectionNo = toolStripStatusLabel1→Text; //sets injectionNo if ok only do it even if it doesnt need to..

		}
		if(toolStripStatusLabel1→Text == L"Injecting") // removes the rest of the info
		{
			toolStripStatusLabel1→Text = InjectionNo; // will always keep the right injection no.
			this→toolStripStatusLabel2→Visible= false; // timer hide  not really useful but not a problem
			this→toolStripStatusLabel9→Visible= false; // timer hide
			this→toolStripStatusLabel10→Visible= false; // timer hide
		}
		else
			this→toolStripStatusLabel9→Text = SerialPacket("o",true);	//if Injecting wont log this!
		if (this→toolStripStatusLabel1→Text == L"Run Complete"
			|| this→button5→Text == L"Start Flow") //note Start Flow is a stop condition for the timer!
			//|| this→button5→Text == L"Pausing") // AutoStop condition for timer
		{
				this→toolStripStatusLabel1→Text = SerialPacket("n",true);
				this→toolStripStatusLabel11→Visible= false; // timer visible
				this→toolStripStatusLabel2→Visible= false; // timer visible
				this→toolStripStatusLabel9→Visible= false; // timer visible
				this→toolStripStatusLabel10→Visible= false; // timer visible
				this→button7→Enabled = false;

				if (this→toolStripStatusLabel1→Text == L"Run Complete")
				{
					this→button5→Text =L"Start Flow"; // this reset is done inside timer2 for pausing
					this→button5→Enabled = true;
				}
				this→timer1→Enabled = false; //stop timer
		}
}
// timer 2 use all the time, polls flowmeter; arduino for lamp on; logs data to file etc (this should be all individual functions..)
// ********************************************************************************************
private: System::Void timer2_Tick(System::Object^  sender, System::EventArgs^  e) {
			// this controls all the permanent timing: Lamp status, flowmeter etc
		// System::String ^Flow = nullptr;
		// **************lamp polling**********************
		System::String ^LampStatus = nullptr;
		LampStatus= SerialPacket("q",true);
		if( LampStatus == "ON") // sets LampOn flag if lamp is on
		{   // AlreadyLampOn flag if it is already on, used to trigger the log only once
			if (LampOn)
				AlreadyLampOn = true;
			LampOn= true;
			toolStripStatusLabel8→Enabled =true;
		}
		if( LampStatus == "OFF") // now if Lampstatus is nor ON or OFF (timeout exeption) it will keep previous status
		{
			if (!LampOn)
				AlreadyLampOn = false;
			LampOn= false;
			toolStripStatusLabel8→Enabled =false;
		}
		//********************* FLOW VALVE AUTOMATED STUFF ******************************
		if (AutoFlowSampling) //need the auto-sampling to be active this automation is controlled by the interface, not arduino
		{
			if(DateTime::Now.Ticks >TimeInterval) //runs only when interval is up
			{
				//turn on the valve
				while (SerialPacket("j",true) == L"Injecting") {} // repeat it if it returns injecting will freeze software if arduino
unpluged precisely here..
				AutoActive = true; //AutoFlowSampling
				// set the times
				TimeMemory= DateTime::Now.Ticks; // Sets the current time
				// reset sampling and  interval
				TimeSampling = TimeMemory +
System::Convert::ToInt64(this→numericUpDown2→Value)*TimeSpan::TicksPerMinute ; // sets the end of the sampling
```

```
                                TimeInterval = TimeMemory +
System::Convert::ToInt64(this→numericUpDown3→Value)*TimeSpan::TicksPerMinute ; // sets the reactivation
                        }
                        if ( DateTime::Now.Ticks >TimeSampling)
                        {
                                        //turn off the valve
                                while (SerialPacket("k",true) == L"Injecting") {} // repeat it if it returns injecting
                                AutoActive = false;
                        }
                }
                //**********  Arduino reactivation loop ****************************************
                if (!ArduinoOn)  // disable most of the interface if Arduino is unpluged
                {
                        //MessageBox::Show("Arduino unpluged!");
                        this→toolStripStatusLabel4→Enabled = false;
                        this→radioButton1→Enabled = false;  // disable most of the interface
                        this→radioButton2→Enabled = false;
                        this→button8→Enabled = false;
                        this→button11→Enabled = false;
                        this→button12→Enabled = false;
                        this→button13→Enabled = false;
                        this→button14→Enabled = false;
                        this→button15→Enabled = false;
                        this→button16→Enabled = false;
                    this→button17→Enabled = false;
                        this→radioButton3→Enabled = false;
                    this→radioButton4→Enabled = false;
                        this→textBox3→Enabled = false;
                        ArduinoOn = StartUpSerial(); //try to reconnect
                        if (ArduinoOn)  //very ugly reset of the interface
                        {               MessageBox::Show("Arduino Reactivated!");
                                        this→toolStripStatusLabel4→Enabled = true;
                                        this→radioButton1→Enabled = true;  // should reset interface to beginning (that should be a function..)
                                        this→radioButton2→Enabled = true;
                                        this→button17→Enabled = true;
                                        this→button16→Enabled = true;
                                        this→button8→Enabled = true;
                                        this→button11→Enabled = true;
                                        this→button12→Enabled = true;
                                        this→button13→Enabled = true;
                                        this→button14→Enabled = true;
                                        this→button15→Enabled = true;
                                        this→button15→ForeColor = System::Drawing::SystemColors::ControlText;
                                        this→button15→Visible = false;
                                        //this→label1→Visible = false;
                                        this→label2→Visible = false;
                                        this→button12→Visible = true;
                                        this→button13→Visible = true;
                                        this→button14→Visible = true;
                                        this→radioButton3→Checked = true;
//                                      this→textBox1→Visible = false;
                                        this→textBox2→Visible = false;
                                        this→textBox3→Visible = false;
//                                      this→button1→Visible = false;
//                                      this→button2→Visible = false;
                                        this→button3→Visible = false;
                                        this→button4→Visible = false;
                                        this→button5→Enabled = false;
                                        this→button10→Enabled = true;
                                        this→button12→ForeColor = System::Drawing::SystemColors::ControlText;
                                        this→button5→Text = L"Start Flow";
                                        this→button6→Visible = false;
                                        this→radioButton3→Visible = false;
                                        this→radioButton4→Visible = false;
                                        this→button7→Visible = false;
                                        this→button12→Text = L"Turn On Tray rotation";
                                        this→button11→ForeColor = System::Drawing::SystemColors::ControlText;
                                        this→button11→Text = L"Turn On FlowMeter Valve";
                                        this→radioButton3→Enabled = true;
                            this→radioButton4→Enabled = true;
                            this→textBox3→Enabled = true;
                                }
                }
                //**************** Flowmark Polling and reading**************************
                try  // flowmark constant monitoring to detect its status (might be a bug here..)
        {
                                                Flow= serialPort2→ReadLine(); //relies on failling this line to activate the flowmeter, very neat ;)
                                                Flow= Flow→Remove(0,1+Flow→IndexOf("@")); //removes everything before @ in output
                                                this→serialPort2→DiscardInBuffer();
                                                this→toolStripStatusLabel3→Enabled= true;
                                                //MessageBox::Show("FlowMark found");
                                                if (Flow→Length >1)
                                                {
                                                        Flow = Flow→Remove(Flow→Length-1);
```

```
                                                this→toolStripStatusLabel5→Text = Flow;
                                        }
                }
        catch (TimeoutException ^)
                {
                        // this is just a skiped beat happens often
                         this→toolStripStatusLabel5→Text = " ";// log it as nothing (and not as same as last)
                }
        catch (InvalidOperationException ^) // default exception occuring when not plugged in
                {
                        this→toolStripStatusLabel3→Enabled= false;
                        this→toolStripStatusLabel5→Text = ""; //standard error when not pluged in
                        if (FlowMark())
                                this→toolStripStatusLabel3→Enabled= true;
                }
        catch ( IOException^  )
                { // bigger problem, not likely
                        this→toolStripStatusLabel5→Text = "!";
                        //this→timer2→Enabled = false;
                        this→toolStripStatusLabel3→Enabled= false;
                        if (FlowMark())
                                this→toolStripStatusLabel3→Enabled= true;
                }
        //*****************************  DATA LOGGING*************************************************
                // should only log non-empty flow data and Special activity of run ( Run activity logon active run and log when log is open!
                // will not log under ranges  InjectionNo (will write injecting while Arduino is busy injecting..

         //  removes half the logs from flowmeter.. now roughtly one a second, instead of 2 per second

         if (LogCut)
         {
                        LogCut=false;
                        Flow ="";
         }
         else
                 LogCut=true;

         // Setting of the timer variable to hide backflush signal and also 20 sec of start of inj..
         //called only once per BF cycle 20 secs hard coding  //this was needed when flowmeter was logged actively to get good data.

         if((this→toolStripStatusLabel9→Text == "0" || this→toolStripStatusLabel9→Text == "BF") )
         {
                  TimerBF =true;
                  TimeBF = DateTime::Now.Ticks + 20*TimeSpan::TicksPerSecond ; //add 20 sec of equilibration (this was to avoid logging flows
that are not equilibrated, not useful anymore)
         }
         if ( DateTime::Now.Ticks > TimeBF)
                 TimerBF = false;
         // IF → all thing that causes a write is there.. lamp, injecting, and flow data. NOTE
         //  note BF stand for backflush → will not log flowdata while timeBF is on
         // Automatic flowmeter condition : AutoFlowSampling =true ==AutoActive = true
         //                        or  AutoFlowSampling =false ==AutoActive = false
         // main issue is it logs too much when lamp is on (when there is no flow, and too little when lamp is off)
         // now should log on and off correctly .. will log new injection no (after the arduino is responsive)
         if( ( !InjectionNoRepeat ||  ( LampOn  && !AlreadyLampOn )|| ( !LampOn  && AlreadyLampOn ) ||
                        (Flow != "" && Flow != "under range" && !TimerBF && AutoFlowSampling == AutoActive) )
                        && this→toolStripStatusLabel6→Enabled ) // obvious log only if log is on!
                {
                        TimeStamp(w);  //Time,Date
                        // "Time,Date,FlowMeter data, Sample, Current no of Inj, injection timer, lamp status \r\n"
                        // enter a empty flow log if it should not be writing a log for flow (because of no flow to measure)
                   if ((Flow != "" && Flow != "under range" && !TimerBF && AutoFlowSampling == AutoActive)  )
                                Log(this→toolStripStatusLabel5→Text, w); //,FlowMeter data
                        else
                                Log(" ", w);
                        // logs a space instead remove all useless data. Note will always log flow on manual (so can be used to monitor
anything..)

                        // sample correspond to the one being injecting, but it is the reverse of the flowsample..

                        Log(this→toolStripStatusLabel7→Text, w); // , Sample A or B
                        Log(this→toolStripStatusLabel1→Text, w); // ,  Current no of Inj
                        Log(this→toolStripStatusLabel9→Text, w); //injection timer
                        if (LampOn )
                                Log("ON", w);
                        else
                                Log("OFF", w);
                        w→WriteLine(""); //endline
                        w→Flush();
                }


                 // reset Pausing to Resume...
                 if (this→button5→Text == "Pausing")
```

```
                                {
                                        //MessageBox::Show(SerialPacket("L",true));
                                        if (SerialPacket("L",true) == "ok")
                                        {
                                                // this→timer1→Enabled = false; //stop timer will have been stoped when pausing is set
                                          this→button10→Enabled = true;
                                                this→button5→Text =L"Start Flow";
                                                this→button5→Enabled = true;
                                                this→radioButton3→Enabled = true;
                                                this→radioButton4→Enabled = true;
                                        }
                                }

                        }
// Selects between headspace and flow mode
private: System::Void radioButton1_CheckedChanged(System::Object^  sender, System::EventArgs^  e) {

  if(this→radioButton2→Checked == true && (this→button5→Text == L"Resume" || this→button5→Text == L"Start Flow" ||this→button5→Text ==
L"Run Complete"))
                {  // sets to flow experiment
    SerialPacket("b", false); //b for flow experiment wait state
                this→toolStripStatusLabel1→Visible= true;
                this→button12→ForeColor = System::Drawing::SystemColors::ControlText;
                this→button15→Visible = true;
                this→button17→Visible = true;
                this→button12→Visible = false;
                this→button13→Visible = false;
                this→button14→Visible = false;
                this→radioButton3→Enabled = true; //activate 1 or 2 if it was desactivated..
                this→radioButton4→Enabled = true;
                this→textBox3→Enabled = true;
//              this→textBox1→Visible = true;
//              this→label1→Visible = true;
                this→label2→Visible = true;
//              this→textBox1→Enabled = true;
                this→textBox2→Visible = true;
                this→textBox3→Visible = true;
//              this→button1→Visible = true;
//              this→button2→Visible = true;
                this→button3→Visible = true;
                this→button4→Visible = true;
                this→button5→Enabled = true;
                this→button6→Visible = true;
                this→toolStripStatusLabel7→Enabled =true;
                this→radioButton3→Visible = true;
                this→radioButton4→Visible = true;
                this→button7→Visible = true;
                this→button10→Visible = true;
                                        }
  else{  // condition to avoid shift while running
                if ( (this→button5→Text == L"Running") || (this→button5→Text == L"Pausing")  )
                 {
                                 MessageBox::Show(
        "Most stop or pause run before switching to headspace mode",
        "Halt Requested");
                    this→radioButton2→Checked = true;
                }
                else
                {  //set to headspace
                  SerialPacket("a", false); // a for headspace
                                this→button15→ForeColor = System::Drawing::SystemColors::ControlText;
                                this→button15→Visible = false;
                                this→button17→Visible = false;
//                              this→label1→Visible = false;
                                this→label2→Visible = false;
                                this→button12→Visible = true;
                                this→button13→Visible = true;
                                this→button14→Visible = true;
                                this→radioButton3→Checked = true;
//                              this→textBox1→Visible = false;
                                this→textBox2→Visible = false;
                                this→textBox3→Visible = false;
//                              this→button1→Visible = false;
//                              this→button2→Visible = false;
                                this→button3→Visible = false;
                                this→button4→Visible = false;
                                this→button5→Enabled = false;
                                this→button10→Enabled = true;

                                this→button5→Text = L"Start Flow";
                                this→button6→Visible = false;
                                this→radioButton3→Visible = false;
                                this→radioButton4→Visible = false;
                                this→button7→Visible = false;
```

```
                this→button10→Visible = false;
            }
 }

}
// select between single or dual mode
private: System::Void radioButton3_CheckedChanged(System::Object^  sender, System::EventArgs^  e) {
                if(this→radioButton4→Checked)
                        {
                        SerialPacket("i", false); // dual sample mode
                        // this→button10→Visible = true;
                        }
                else
                        {
                        SerialPacket("h", false); // single sample mode does not reset to A
                        // this→toolStripStatusLabel7→Text = L"A";
                         //this→toolStripStatusLabel7→Enabled = false;
                        // this→button10→Visible = false;
                        }
                }
// decrease inj max // not used anymore
private: System::Void button1_Click_1(System::Object^  sender, System::EventArgs^  e) {
//              this→label1→Text = SerialPacket("d",true); // d for decrease inj max
                }
// increase inj max // not used anymore
private: System::Void button2_Click(System::Object^  sender, System::EventArgs^  e) {
//              this→label1→Text = SerialPacket("e",true); // e for increase inj max
                }
// increase inj time
private: System::Void button3_Click(System::Object^  sender, System::EventArgs^  e) {

this→label2→Text = SerialPacket("g",true); // g for increase inj time
                }
// decrease inj time
private: System::Void button4_Click(System::Object^  sender, System::EventArgs^  e) {
this→label2→Text = SerialPacket("f",true); // f for decrease inj time
            }
// Start run button, start timer 1 NOTE could transfer everything to timer 2 with a condition instead
private: System::Void button5_Click(System::Object^  sender, System::EventArgs^  e) {
             // add artificial delay?  added a pausing state
    System::String ^BFstart = SerialPacket("W",true);
             System::String ^BFfinish = SerialPacket("Y",true);
            // System::String ^Message = "Current BF parameters are:\r Start = " + BFstart + " s\r Finish = " +  BFfinish + " s\r Are you sure you want to
start run with these parameters?";
             if ( MessageBox::Show(
      "Current BF parameters are:\r   Start = " + BFstart + " s\r   Finish = " +  BFfinish + " s\rAre you sure you want to start the run with these parameters?",
      "Start Run", MessageBoxButtons::YesNo,
      MessageBoxIcon::Question) == System::Windows::Forms::DialogResult::Yes )
              {
                        SerialPacket("c", false); // c for start run
                        this→radioButton3→Enabled = false; // locks the 1 or 2 samples
                        this→radioButton4→Enabled = false;
                        this→textBox3→Enabled = false;

                        this→timer1→Enabled = true;
                        this→button10→Enabled = false;
                         // locks control calls lock button!
                        //if (this→button6→Text == "Lock Controls")
                                //    button6_Click(sender, e);
                        this→button5→Enabled = false;
                        this→button5→Text = L"Running";
                        // this→button6→Text = L"Unlock Controls";
                        this→button7→Enabled = true;
                        if ( this→button9→Text == "Start Log") // trigger logging button if not started yet!!
                                                button9_Click(sender, e);
              }
            }
// BF TIMING CHANGE
private: System::Void button6_Click(System::Object^  sender, System::EventArgs^  e) {
              if  ( MessageBox::Show(
      "Are you sure you want to modify the Backflush interval?\rThis modifies the timing used to divert the flow of the sample from the GC.\rDefault values
are 60 to 90 sec, in current methods BF event of the GC occurs at 63 or 84 second",
      "Modifying Backflush interval", MessageBoxButtons::YesNo,
      MessageBoxIcon::Question) == System::Windows::Forms::DialogResult::Yes  )
                        {
                        this→panel5→Visible = true; // rest is done only when clicked on ok
                        this→button6→Enabled =false; //(cant reclick..
                        this→button5→Enabled = false; //disable start experiment windows while open
               }
   System::String ^TempBFtiming; //= nullptr;
            int Value=0;
            TempBFtiming = SerialPacket("W",true) ;// dispaly begining
                        switch (TempBFtiming→Length)
                        {
```

```
                                        case 1:
                                                Value= (TempBFtiming[0]-48);
                                                break;
                                        case 2:
                                                 Value= 10*(TempBFtiming[0]-48);
                                                 Value+= (TempBFtiming[1]-48);
                                                 break;
                                        case 3:
                                                Value= 100*(TempBFtiming[0]-48);
                                                Value+= 10*(TempBFtiming[1]-48);
                                                Value+= (TempBFtiming[2]-48);
                                                break;
                                }
                                this→numericUpDown5→Value = System::Decimal(gcnew cli::array< System::Int32 >(4) {Value, 0, 0, 0});
                        TempBFtiming = SerialPacket("Y",true) ;// display end
                                switch (TempBFtiming→Length)
                                {
                                        case 1:
                                                Value= (TempBFtiming[0]-48);
                                                break;
                                        case 2:
                                                 Value= 10*(TempBFtiming[0]-48);
                                                 Value+= (TempBFtiming[1]-48);
                                                 break;
                                        case 3:
                                                Value= 100*(TempBFtiming[0]-48);
                                                Value+= 10*(TempBFtiming[1]-48);
                                                Value+= (TempBFtiming[2]-48);
                                                break;
                                }
                                this→numericUpDown4→Value = System::Decimal(gcnew cli::array< System::Int32 >(4) {Value, 0, 0, 0});

                                //show the panel
                                        /* if (this→button6→Text == L"Unlock Controls")
                                {
                                this→radioButton1→Enabled = true;
                                this→button1→Enabled = true;
                                this→button2→Enabled = true;
                                //this→button3→Enabled = true;
                                //this→button4→Enabled = true;
                                this→textBox1→Enabled = true;
                                //this→textBox2→Enabled = true;
                                this→button17→Enabled = true;
                                this→button6→Text = L"Lock Controls";
                                if (this→button5→Text != L"Running")
                                        {  // Prevent a mess (changing number of samples)
                                        this→radioButton3→Enabled = true;
                                        this→radioButton4→Enabled = true;
                                        this→textBox3→Enabled = true;
                                        }
                                }
                         else
                                {
                           this→button6→Text = L"Unlock Controls";
                                 this→radioButton1→Enabled = false;
                                 this→radioButton3→Enabled = false;
                           this→radioButton4→Enabled = false;
                                 this→button1→Enabled = false; // locks control
                                 this→button2→Enabled = false;
                                 //this→button3→Enabled = false;
                                 //this→button4→Enabled = false;
                                 this→textBox1→Enabled = false;
                           //this→textBox2→Enabled = false;
                           this→textBox3→Enabled = false;
                                 this→button17→Enabled = false;
                                 }
                        */
}
// Pause button   → changed behavior of arduino to always do backflush while in flow mode -- delay before restarting any experiment
private: System::Void button7_Click(System::Object^  sender, System::EventArgs^  e) {

        if ( MessageBox::Show(
        "Are you sure that you would like to pause the experiment?\rNote: Arduino will wait for backflush before halting run.",
        "Halt Requested", MessageBoxButtons::YesNo,
        MessageBoxIcon::Question) == System::Windows::Forms::DialogResult::Yes )
                {
                                        SerialPacket("l",false);     // pauses run
                                        this→button7→Enabled = false;
                                        this→button5→Enabled = false;

                                        this→button17→Enabled = true;
                                        // change button to Pausing state
                                        this→button5→Text =L"Pausing"; // add a 75 sec delay before next start.. (changed to an Arduino verified event)
                                        //TimePause = DateTime::Now.Ticks + 75*TimeSpan::TicksPerSecond ;
```

```
                                        // Sets the current time
                        }
                }
// Reset button for Arduino microcontroller
private: System::Void button8_Click(System::Object^  sender, System::EventArgs^  e) {
                if ( (this→button5→Text == L"Running") || (this→button5→Text == L"Pausing")  )
                {
                        MessageBox::Show(
        "Most stop or pause run before switching to headspace mode",
        "Halt Requested");

                }
                else
                {
                        if ( MessageBox::Show(
        "This will halt experiment and reset the Arduino, are you sure?",
        "Reset Requested", MessageBoxButtons::YesNo,
        MessageBoxIcon::Question) == System::Windows::Forms::DialogResult::Yes )
                        {
                                //

                                SerialPacket("m",false);   // resets arduino
                                 this→timer1→Enabled = false; //stop timer
                                 this→button10→Enabled = true;
                                 this→button12→Visible = true;
                                this→button13→Visible = true;
                                this→button14→Visible = true;
                                 this→button10→Visible = false;
                                 this→button11→Text = L"Turn On FlowMeter Valve";
                                 this→button11→ForeColor = System::Drawing::SystemColors::ControlText;
                                 this→toolStripStatusLabel1→Visible= false; // timer visible
                                 this→toolStripStatusLabel2→Visible= false; // timer visible
                                 this→toolStripStatusLabel9→Visible= false; // timer visible
                                 this→toolStripStatusLabel10→Visible= false; // timer visible
                                this→button5→Text =L"Start Flow"; // reset to initial parameters
                        SerialPacket("e",true); // fetch numbers from arduino..
//                              this→label1→Text = SerialPacket("d",true);
                                SerialPacket("g",true);
                                this→label2→Text = SerialPacket("f",true);
                          this→radioButton1→Checked = true;
                                this→radioButton3→Checked = true;
                                this→radioButton1→Enabled = true;
//                              this→button1→Enabled = true;
//                              this→button2→Enabled = true;
                                this→button3→Enabled = true;
                                this→button4→Enabled = true;
//                              this→textBox1→Enabled = true;
                                this→textBox2→Enabled = true;
                                this→textBox3→Enabled = true;

                                this→radioButton3→Enabled = true;
                                this→radioButton4→Enabled = true;
                                this→button17→Enabled =true;
                                this→toolStripStatusLabel1→Text= L"0";

                        }
                }
}
// Start Log button, opens up the file and turn on logging
private: System::Void button9_Click(System::Object^  sender, System::EventArgs^  e) {
                        if (this→button9→Text == L"Start Log")
                        {
                                this→saveFileDialog1→ShowDialog();
                                if (saveFileDialog1→FileName != "flow_log.csv")  //this should change to include folder, if not been cancelled..
                                {
                                        w = File::AppendText(saveFileDialog1→FileName);
                                        w→WriteLine(FILEFORMAT);
                                        this→toolStripStatusLabel6→Enabled = true;
                                        this→button9→ForeColor = System::Drawing::Color::Crimson;
                                        //this→button9→ForeColor = System::Drawing::SystemColors::Highlight;
                                        this→button9→Text = L"Stop Log";
                                }
                                else
                                        MessageBox::Show("No file selected.");
                        }
                        else // Close file
                        {
                                w→Close();
                                this→button9→ForeColor = System::Drawing::SystemColors::ControlText;
                                this→toolStripStatusLabel6→Enabled = false;
                                this→button9→Text = L"Start Log";

                        }
                }
```

```
//  Switch sample from A to B or B to A
private: System::Void button10_Click(System::Object^  sender, System::EventArgs^  e)
                                {
                                this→toolStripStatusLabel7→Text = SerialPacket("p",true); // p for switching Sample A and B
                                }
// Turn on flow meter valve
private: System::Void button11_Click(System::Object^  sender, System::EventArgs^  e) {
                                if (this→button11→Text == L"Turn On FlowMeter Valve")
                                {
                                                if (SerialPacket("j",true) != L"Injecting") //error check for potential timeout of serial
                                                {
                                                                this→button11→Text = L"Turn Off FlowMeter Valve";
                                                                this→button11→ForeColor = System::Drawing::Color::Crimson;

                                                }
                                }
                                else
                                {
                                                if (SerialPacket("k",true) != L"Injecting")
                                                {
                                                                this→button11→ForeColor = System::Drawing::SystemColors::ControlText;
                                                                this→button11→Text = L"Turn On FlowMeter Valve";
                                                }
                                }


                                }
// start/stop stirring for headspace mode
private: System::Void button12_Click(System::Object^  sender, System::EventArgs^  e) {
                                if (SerialPacket("r",true) == L"ON")  // start stops stirring
                                {
                                                this→button12→Text = L"Turn Off Tray rotation"; // and block off manual control
                                                this→button13→Enabled = false;
                                                this→button14→Enabled = false;
                                                this→button12→ForeColor = System::Drawing::Color::Crimson;
                                                //TimeMemory= DateTime::Now.Ticks; //TimeOutFLowValve Timespan.TicksPerMinute
                                }
                                else
                                { // turn back on manual control
                                                 this→button12→ForeColor = System::Drawing::SystemColors::ControlText;
                                                this→button13→Enabled = true;
                                                this→button14→Enabled = true;
                                                this→button12→Text = L"Turn On Tray rotation";
                                }
                                }
// rotate X amount Clockwise carousel (headspace mode)
private: System::Void button14_Click(System::Object^  sender, System::EventArgs^  e) {
                                                SerialPacket("s",false) ; // turns the carousel CW
                                }
// rotate X amount Clockwise carousel (headspace mode)
private: System::Void button13_Click(System::Object^  sender, System::EventArgs^  e) {
                                                 SerialPacket("t",false) ; // turns the carousel CCW
                                }
// Shake carousel (flow mode)
private: System::Void button15_Click(System::Object^  sender, System::EventArgs^  e) {

                                if (SerialPacket("u",true) == L"ON") //shaking
                                 this→button15→ForeColor = System::Drawing::Color::Crimson;
                                else// turn back on manual control
                                 this→button15→ForeColor = System::Drawing::SystemColors::ControlText;

                                 }
// Set injection no activate windows
private: System::Void button17_Click(System::Object^  sender, System::EventArgs^  e) {
                                  // read current inj no and place it in the number updown
                                int Value=0;
                                switch (InjectionNo→Length)
                                {
                                                case 1:
                                                                Value= (InjectionNo[0]-48);
                                                                break;
                                                case 2:
                                                                 Value= 10*(InjectionNo[0]-48);
                                                                 Value+= (InjectionNo[1]-48);
                                                                 break;
                                                case 3:
                                                                Value= 100*(InjectionNo[0]-48);
                                                                Value+= 10*(InjectionNo[1]-48);
                                                                Value+= (InjectionNo[2]-48);
                                                                break;
                                }
                                this→numericUpDown1→Value = System::Decimal(gcnew cli::array< System::Int32 >(4) {Value, 0, 0, 0});
                                this→panel3→Visible =true; //show the panel
                                this→button5→Enabled =false; //disable button beneath avoid clicking errors
```

```
                        }
// Set injection no OK button
private: System::Void button18_Click(System::Object^  sender, System::EventArgs^  e) {
                                    System::String ^WaitOut;
                                    //send number to arduino.. convert number to string.. (same as BF timing, more robust)
                        //          InjectionNo= System::Convert::ToString( this→numericUpDown1→Value ); // converts
                                    //MessageBox::Show(InjectionNo);
                //  SerialPacket("v",false) ; //dd
                                    //  SerialPacket(InjectionNo,false) ;
                                    //  this→toolStripStatusLabel1→Text =InjectionNo;

                                     WaitOut = L"null";
                         // will loop to infinity if there is a mismatch not the best.. but ensure the command is passed
                        while(WaitOut != System::Convert::ToString( this→numericUpDown1→Value ))
                        {
                                    SerialPacket("v",false) ;// sets begining
                                    WaitOut= SerialPacket(System::Convert::ToString( this→numericUpDown1→Value ),true) ;
                        }
                        InjectionNo=WaitOut;
                        this→toolStripStatusLabel1→Text =InjectionNo;
                        this→panel3→Visible = false;
                        this→button5→Enabled =true; //reset button
this→toolStripStatusLabel1→Text = SerialPacket("n",true); // rereads from arduino
            if(toolStripStatusLabel1→Text != L"Injecting")
                        InjectionNo = toolStripStatusLabel1→Text;
            else
                        this→toolStripStatusLabel1→Text= L"";

                         }
// Set injection no CANCEL button
private: System::Void button19_Click(System::Object^  sender, System::EventArgs^  e) {
                                    this→panel3→Visible = false;
                                    this→button5→Enabled =true; //reset button to active
                         }
// Automatic flow valve switching (pops up menu in same window to keep me sane)
private: System::Void button16_Click(System::Object^  sender, System::EventArgs^  e) {
                        if (this→button16→Text == L"Automatic Flow Rate Sampling")
                        {
                                    this→panel4→Visible = true; // rest is done only when clicked on ok
                                    this→button5→Enabled =false;
                        }
                        else //reverts to its original state
                        {
                          this→button16→Text = L"Automatic Flow Rate Sampling";
                          this→button16→ForeColor = System::Drawing::SystemColors::ControlText;
                          this→button11→Enabled = true;
                          AutoFlowSampling = false;             //              activate something in the timer 2..
                          AutoActive = false;
                          if(AutoActive = true)
                                                while (SerialPacket("k",true) == L"Injecting") {}
                          AutoActive = false;
                        }
                         }
//Automatic flow valve  OK button
private: System::Void button21_Click(System::Object^  sender, System::EventArgs^  e) {
                          //if (SerialPacket("j",true) != L"Injecting") //error check for potential timeout of serial
                          this→button16→Text = L"Manual Flow Rate Sampling";
                          this→button16→ForeColor = System::Drawing::Color::Crimson;
                          this→button11→Enabled = false;
                          AutoFlowSampling =true;               //              activate something in the timer 2..

                          this→panel4→Visible = false;
                          this→button5→Enabled = true;
                         }
//Automatic flow valve  CANCEL button
private: System::Void button20_Click(System::Object^  sender, System::EventArgs^  e) {
                                    this→panel4→Visible = false;
                                    this→button5→Enabled = true;
                         }
private: System::Void numericUpDown2_ValueChanged(System::Object^  sender, System::EventArgs^  e) {
                         this→numericUpDown3→Minimum = this→numericUpDown2→Value;
                         }
private: System::Void numericUpDown3_ValueChanged(System::Object^  sender, System::EventArgs^  e) {
                                    this→numericUpDown2→Maximum = this→numericUpDown3→Value;
                         }
// backflush changing ok button NOTE change are immediate!!
private: System::Void button23_Click(System::Object^  sender, System::EventArgs^  e) {
                         System::String ^WaitOut;
                         WaitOut = L"null";
                         // will loop to infinity if there is a mismatch not the best.. but ensure the command is passed
                        while(WaitOut != System::Convert::ToString( this→numericUpDown5→Value ))
                        {
                                    SerialPacket("w",false) ;// sets begining
```

```
                                WaitOut= SerialPacket(System::Convert::ToString( this→numericUpDown5→Value ),true) ;
                        }
                         WaitOut = L"null";
                         // will loop to infinity if tehre is a mismatch not the best..
                        while(WaitOut != System::Convert::ToString( this→numericUpDown4→Value ))
                        {
                                 SerialPacket("y",false) ; // sets end
                                 WaitOut=SerialPacket(System::Convert::ToString( this→numericUpDown4→Value ),true) ;

                        }
                          this→panel5→Visible = false;
                          this→button6→Enabled =true;
                          this→button5→Enabled = true;

                         }
// backflush changing Cancel button
private: System::Void button22_Click(System::Object^  sender, System::EventArgs^  e) {
                                this→panel5→Visible = false;
                          this→button6→Enabled =true;
                          this→button5→Enabled = true;
                         }

};
}
```

5.S7.4. **Arduino Microcontroller – Code** (compiled with Arduino Uno compiler)

```
/*
University of montreal V1
 This project is to control a 480 Fixed gas analyzer

 Serial link is using Pin1 and pin2

 Ext GC Ready (inhibit while waiting) Pin3     OUTPUT
  GCStart                          Pin2     OUTPUT

Passing through a relay: pins can not be changed (shield module)

ValveSampleA                D0       pin 7    OUTPUT
ValveSampleB                D1       pin 6    OUTPUT pin 6 circuit not working anymore, changed to pin4 (D3-4)
ValveCarrier                D2       pin 5    OUTPUT
ValveFlow                   D3       pin 4    OUTPUT this is now taken out (valve unpluged) (switched to D1-6)

 * LCD RS pin to digital pin 12
 LCD RW  pin 15
 * LCD Enable pin to digital pin 13
 * LCD D4 pin to digital pin 11
 * LCD D5 pin to digital pin 10
 * LCD D6 pin to digital pin 9
 * LCD D7 pin to digital pin 8

 Photoresistor          Pin A0 or 14  analog input
 analogRead(lightPin) > 950 lamp is on
 created July 2011
 by Miles Snow (initial fixed timings for GC only and basic display)
 modified July-september 2011
 by Daniel Chartrand (interface, variable timings, valve control,
 stepper motor control, Light sensing)
 */

#define FASTADC 1  // improve speed for analog reading of photoresistor

// defines for setting and clearing register bits
#ifndef cbi
#define cbi(sfr, bit) (_SFR_BYTE(sfr) &= ~_BV(bit))
#endif
#ifndef sbi
#define sbi(sfr, bit) (_SFR_BYTE(sfr) |= _BV(bit))
#endif

#define PINS 4 //Number of steps or pins stepper uses (only 4 pin, half steps)
#define P1  16  // pin A2  will need to switch to 2 pin mode eventually to drive 2 motors
#define P2  17 //  pin A3
#define P3  18  // pin A4
#define P4  19  // pin A5
#define MAXSPEED 1500 //
// include the library code:
// Constant are used to assign pin configurations
//  Can not use pin 0 and 1 → serial link
#define  StartGCPin 2
#define  ExtReadyPin 3
#define  ValveSampleA 7
#define  ValveSampleB 4
#define  ValveCarrier 5
#define  ValveFlow 6
#define  lightPin  A0



#include <AccelStepper.h> // Copyright (C) 2009 Mike McCauley
//#include <LiquidCrystal.h>
#include <LiquidCrystalFast.h> // for faster LCD commands


#include <avr/wdt.h>

//****** fonctions for doing a live software reset
#define soft_reset()        \
do                          \
{                           \
   wdt_enable(WDTO_30MS);  \
   for(;;)                  \
   {                        \
   }                        \
} while(0)
// Function Prototype
void wdt_init(void) __attribute__((naked)) __attribute__((section(".init3")));
```

```
// Function Implementation
void wdt_init(void)
{
   MCUSR = 0;
   wdt_disable();
   return;
}

//***** end of functions for reset




// initialize the LCD library with the numbers of the interface pins
//LiquidCrystal lcd(7, 6, 5, 4, 3, 2); //will need to change once valve are in to:
LiquidCrystalFast lcd(12, 15, 13, 11, 10, 9, 8);


////////////////////////////////////  Stepper Motor variable ////////////////////////////////////////
AccelStepper stepper(PINS, P1, P3, P2, P4);
unsigned long MilliDelay=250;  // for display of rotation on LCD screen (delay for each rotation display)
unsigned long Millimemory=0;  // for display of rotation
boolean HeadSpaceWritten =false;
boolean StepperON =false;
//boolean NinetyNine = false; // using modulo instead directly in code to double up time for these case
unsigned long ExtraMillis = 300000; //for the 99th injection taking more time.. add 5 mins to the run
int Spin = 0; //for indication of rotation
int Speed = 500; // for step motor, maximum is 1080 (8 step)
int Forward =200; // position of step to move..  // for continuous rotoshaking
int Backward = -50;  // for continuous rotoshaking
int Shake = 200; // for shake only
int StepToDegree= 512; // value to have it be roughtly 45 degree..
boolean StepperShakeON =false; //sets the shaking mode
boolean Clockwise=true;  // for continuous rotoshaking
boolean CWDegree= false; //sets condition to move a small amount CW
boolean CCWDegree= false; //sets condition to move a small amount CCW

////////////////////////////////////// Sampling Sequence variable  ////////////////////////////////////////
unsigned long MinSampling= 130; // minimun value (to be adjusted to avoid any issues with valve switching → min set to time switch off BF  +60 sec
unsigned long SamplingTimeSeconds=150;      // Default Sampling frequency
unsigned long SamplingMemory = 0;
unsigned long FlowTime = 60;  //this represent the actual time the sample is passing through the GC sample loop (in second) used in adjusting the BF
int ResetDays=9; // message appear only when 9 day left (now valid if left on an never reseted..
int InjectionDelay=50; // the injection delay (in ms) used in the timing events to correct the interval to exactly the ammount written
int Delay=50;   // Delay used for the injection action
int MaxInj=999; // add a few extra in case instrument fails to inject (seen it happens) NOTE consistantly miss injection 99 198 etc..
int InjCount=0; // put here so can change if restart a run
unsigned long  BackFlushBegin= 60; //seconds (65 sec is the event in the run)  was 63 changeg tobe 1 //to 90→ good for injections of 2.5 min
unsigned long  BackFlushEnd= 90; // seconds, before we go back to our state normal state
//variables
boolean PauseDemand=false;
boolean LampOn=false;
boolean FlowMeter=false;
boolean BackFlushDone=false;
boolean BackFlushing=false;
boolean SampleA=true; // true if sample A runnin, false if sample B
boolean TwoSamples=false; // true if running 2 different samples back to back.
boolean Status=false; // true for on false for off (run terminated or paused)
boolean Headspace=true;  // change software mode to headspace (aka doing nothing)
boolean Sampling=false;                         // to determine if we run the sampling set
unsigned long DelayMillis=0;                      //delay time
unsigned long DelayMillisRemaining=0;           //remaining millis until the next sampling time
unsigned long OldDelayMillis=0;
// unsigned long InitialDelay=0;
int RollOver=0;  // in days, used to determine the end of time.
int Minutes=0; // temp variable used to write in minutes
int Seconds=0; //                                  and second
int Temp=0; // temp variable..
int val[3];

// int val=-1; // for serial communication, set it to nothing character;
// stepper declaration
////////////////////////// characters//////////////////////////////////////////////
byte lineA[8] = {
  0b00000,
  0b00000,
  0b00100,
  0b00100,
  0b00100,
  0b00100,
  0b00000,
  0b00000
};
```

```
byte lineB[8] = {
  0b00000,
  0b00000,
  0b00000,
  0b00010,
  0b00100,
  0b01000,
  0b00000,
  0b00000
};
byte lineC[8] = {
  0b00000,
  0b00000,
  0b00000,
  0b00000,
  0b01110,
  0b00000,
  0b00000,
  0b00000
};
byte lineD[8] = {
  0b00000,
  0b00000,
  0b00000,
  0b01000,
  0b00100,
  0b00010,
  0b00000,
  0b00000
};

byte Sun[8] = {
  0b00000,
  0b10101,
  0b01110,
  0b11111,
  0b01110,
  0b10101,
  0b00000,
  0b00000
};
byte Moon[8] = {
  0b00000,
  0b00111,
  0b01110,
  0b01110,
  0b01110,
  0b00111,
  0b00000,
  0b00000
};
////////////////////////////////// Setup function//////////////////////////////////////////

void setup() {
  #if FASTADC
  // set prescale to 16
  sbi(ADCSRA,ADPS2) ;
  cbi(ADCSRA,ADPS1) ;
  cbi(ADCSRA,ADPS0) ;
  #endif

    lcd.createChar(0,lineA);
    lcd.createChar(1,lineB);
    lcd.createChar(2,lineC);
    lcd.createChar(3,lineD);
    lcd.createChar(4,Sun);
    lcd.createChar(5,Moon);
  stepper.setMaxSpeed(MAXSPEED);
  stepper.setSpeed(Speed);
  wdt_init();  // Suposedely needed to avoid an infinite reset loop.. not tested.
  lcd.begin(16,2);  // set up the LCD's number of rows and columns: reversed
  Serial.begin(115200); // start serial communication high speed reduce delays
  pinMode(ExtReadyPin, OUTPUT);
  pinMode(StartGCPin, OUTPUT);
  // setting up the pins for valve (only when LCD will have been moved to its new pins)
  pinMode(ValveSampleA, OUTPUT);
  pinMode(ValveSampleB, OUTPUT);
  pinMode(ValveCarrier, OUTPUT);
  pinMode(ValveFlow, OUTPUT);

  //used to keep Analog pins clean (not use because they are use as digital pins

  analogReference(DEFAULT); // end of analog pin cleaning
  // default pins setting
```

```
  digitalWrite(StartGCPin,HIGH);   //Setup pins to negative logic
  digitalWrite(ExtReadyPin,LOW);   //GC configured by default to be in Headspace mode
  digitalWrite(ValveSampleA,LOW);  // Will be dependant on ON/OFF positions
  digitalWrite(ValveSampleB,LOW);  // A and B should be closed (flushing off the valve)
  digitalWrite(ValveCarrier,LOW);  // Should be on (carrier going to the GC by default)
  digitalWrite(ValveFlow,LOW);
   DelayMillis =SamplingTimeSeconds*1000;   //  msec/sec need to be changed later on as well
 // InitialDelay =InitialTimeSeconds*1000; //shorter time for first injection
 // DelayMillisRemaining=millis()+InitialDelay-InjectionDelay;
 // stepper.moveTo(0); // not moving by default..
}

void loop()
{
////////////////////// motor stepper control/////////////////////////////////////////
  if(CWDegree)  //moves the motor for a fixed distance
  {
    CWDegree = false;
    stepper.setCurrentPosition(0);
    if (Speed < 0) Speed = -Speed; // make it go in the right direction
    stepper.setSpeed(Speed);
    stepper.moveTo(StepToDegree);
  }
  if(CCWDegree)
  {
    CCWDegree = false;
    stepper.setCurrentPosition(0);
    if (Speed > 0) Speed = -Speed; // make it go in the right direction
    stepper.setSpeed(Speed);
    stepper.moveTo(-StepToDegree);
  }
  // condition for shaking
 if (stepper.currentPosition() == stepper.targetPosition() && StepperShakeON)
   {
    stepper.setCurrentPosition(0);

    if (Clockwise) // go back then else forward again
     {
       if (Speed > 0) Speed = -Speed;
       stepper.setSpeed(Speed); //invert direction
       stepper.moveTo(-Shake);
     }
    else
     {
       if (Speed < 0) Speed = -Speed;
      stepper.setSpeed(Speed); //invert direction
      stepper.moveTo(Shake);
     }
    Clockwise = !Clockwise ;
   }
   // condition for roto-shaking
  if (stepper.currentPosition() == stepper.targetPosition() && StepperON)
   {
    stepper.setCurrentPosition(0);

    if (Clockwise) // go back then else forward again
     {
       if (Speed > 0) Speed = -Speed;
       stepper.setSpeed(Speed); //invert direction
       stepper.moveTo(Backward);
     }
    else
     {
       if (Speed < 0) Speed = -Speed;
      stepper.setSpeed(Speed); //invert direction
      stepper.moveTo(Forward);
     }
    Clockwise = !Clockwise ;
   }
stepper.run();
 ////////////// condition for lamp on Photoresitor ////////////////////////////////////////////////////
 /*lcd.setCursor(0, 0);

       lcd.print(analogRead(lightPin));
       lcd.print("   ");
*/
if( analogRead(lightPin) > 400) //number chosen for light detection. (note UV light is weakly detected)
   LampOn=true;
 else
   LampOn=false;
  // interface section
 stepper.run();
  val[0] = Serial.read();      // read the serial port
stepper.run();
```

```
//*************************************************************************************************************
////////////////////////// Serial commands//////////////////////////////////////////////////////////////////

//*************************************************************************************************************
  if (val[0] !=-1)
  {
    stepper.run();
    switch (val[0]) {
      case 'a':// Headspace mode
        Status = false;
        Headspace= true;
        StepperShakeON = false;// (turns off shaking auto)
        digitalWrite(ExtReadyPin,LOW);
        digitalWrite(ValveSampleA,LOW);  // Will be dependant on ON/OFF positions
        digitalWrite(ValveSampleB,LOW);  // A and B should be closed (flushing off the valve)
        digitalWrite(ValveCarrier,LOW);
        break;
      case 'b': // flow mode (not ready, resets inj count)
        Status = false;
        Headspace= false;
        InjCount=0;
        StepperON = false; //turns off rotation
        digitalWrite(ExtReadyPin,HIGH);
        digitalWrite(ValveCarrier,HIGH); //stop carrier flow to GC, ready to start flow (not started)
        if (SampleA) // turns on or off the right valves (SAMPLE A data is good for monorun
          {
           digitalWrite(ValveSampleB,LOW);
           stepper.run();
           digitalWrite(ValveSampleA,HIGH);  // Sample A flow pass through GC
          }
          else   // will be a toggle button to adjust flows etc..
          {
           digitalWrite(ValveSampleA,LOW);
           stepper.run();
           digitalWrite(ValveSampleB,HIGH);  // Sample B flow pass through GC
          }
        break;
      case 'c': // flow mode (timer engaged)
        Status = true;
        Headspace= false;
        StepperON = false; //turns off rotation
         DelayMillisRemaining=millis()+5000;  // starts 5 sec after on.. for testing
        //DelayMillisRemaining=millis()+DelayMillis-InjectionDelay;     //removed initial setting of delay - 1 sec from delay of injection quite shorter then a
normal injection
        break;
      case 'd': // increase max inj (+25)
        MaxInj= MaxInj + 25;
        if (MaxInj >1010){ MaxInj= 1010;}
        Serial.println(MaxInj);
        break;
      case 'e': // decrease max inj (-25)

        if (MaxInj >25){ MaxInj= MaxInj - 25;}
        Serial.println(MaxInj);
        break;
      case 'f': // increase sampling time (+5)
        SamplingTimeSeconds = SamplingTimeSeconds + 5;
        //BackFlushEnd= SamplingTimeSeconds-FlowTime;   // adjust the length of the BF mode to the variable injection time This is not done anymore.. will
have to see
        DelayMillis =SamplingTimeSeconds*1000;   // sampling time is not called, delay millis is..
        Serial.println(SamplingTimeSeconds);
        break;
      case 'g': // decrease sampling time  (-5)
        if(SamplingTimeSeconds > MinSampling) //
        {
         SamplingTimeSeconds = SamplingTimeSeconds - 5;
         // BackFlushEnd= SamplingTimeSeconds-FlowTime; // seconds, before we go back to our state normal state this is valid as long as minimum is not too
low for method
          DelayMillis =SamplingTimeSeconds*1000;  // sampling time is not called, delay millis is..
        }
        Serial.println(SamplingTimeSeconds);
        break;
      case 'h': // one flow experiment Setting  (can now be done without stopping..)
        TwoSamples=false;
       // Status=false;
        //SampleA=true; //resets to sample A!!
        //InjCount=0;
        break;
      case 'i': // two flow experiment Setting this should
```

```
  TwoSamples=true;
  //Status=false;
  //InjCount=0;
  break;
 case 'j': // flowmeter on
  FlowMeter=true;
   Serial.println("ON");
  break;
 case 'k': // flowmeter off
  FlowMeter=false;
  Serial.println("OFF");
  break;
 case 'l': //halt experiment status false
  PauseDemand=true; // sends the pause condition (will only stop after BF)
  break;
 case 'L': //verify status of pause (only used after pausing.)
  if (PauseDemand) // still waiting for BF
    Serial.println("no");
  else //done
    Serial.println("ok");
  break;
 case 'm':   // reset Arduino board
  soft_reset();
  break;
 case 'n':  // polls count
  if (InjCount < MaxInj)
    Serial.println(InjCount);
  else
    Serial.println("Run Complete");
  break;
 case 'o':  // polls timer + BACKFLUSHING monitoring
  if (Status)
  {
    Serial.print( (InjectionDelay/1000+(DelayMillisRemaining-millis())/1000) ); //sends time all the time..
    if(BackFlushing)  // not the best, lose count..
      Serial.println(" (BF)");
    else
      Serial.println("");
  }
  else
    Serial.println(" ");
  break;
 case 'p': // Toggle between sample A and B (should be used only when not running)
 // if (TwoSamples) //protects against bad moves
   SampleA = !SampleA;
 if (SampleA) // turns on or off the right valves (SAMPLE A data is good for monorun
    {
     digitalWrite(ValveSampleA,HIGH);  // Sample A flow pass through GC
     digitalWrite(ValveSampleB,LOW);
      Serial.println("A");
    }
    else   // will be a toggle button to adjust flows etc..
    {
     digitalWrite(ValveSampleB,HIGH);  // Sample B flow pass through GC
     digitalWrite(ValveSampleA,LOW);
     Serial.println("B");
    }
  break;
 case 'q':  // polls lamp status
  if(LampOn)
    Serial.println("ON");
  else
    Serial.println("OFF");
  break;
 case 'r':  // Turn on and off the stepper
    StepperON = !StepperON;
    if (StepperON)
      Serial.println("ON");
    else
      Serial.println("OFF");
    break;
 case 's':  // Turn on stepper +45 degree
    StepperON= false;
    CWDegree = true;
    break;
 case 't':  //  Turn on stepper -45 degree
    StepperON= false;
    CCWDegree = true;
   break;
 case 'u':  // Turn on and off the stepper
    StepperShakeON = !StepperShakeON;
    if (StepperShakeON)
    {
     Speed= Speed/5;
```

```
        Serial.println("ON");
       }
       else
       {
        Speed= Speed*5;
        Serial.println("OFF");
       }
       break;
     case 'v':  // receive a new inj number from flow interface
       delayMicroseconds(1000); //need a small delay to wait for the other character coming in the serial port..
       stepper.run();  // must wait for all character to be out to know length, can be 1 to 3 (0 to 999)
       val[0] = 0;
       InjCount = 0;
       switch (Serial.available())
                        {
                case 1:
                                                val[0] = Serial.read()-48; //to convert back to a digit
                    InjCount+= val[0];
                                                break;
                                        case 2:
                      for (int i=0; i<2; i++) // write down the number sent along with v (ex v559)
                       {
                         val[i] = Serial.read()-48; //to convert back to a digit
                       }
                       InjCount+= val[0]*10;
                       InjCount+= val[1];
                       break;
                                        case 3:
                            for (int i=0; i<3; i++) // write down the number sent along with v (ex v559)
                       {
                         val[i] = Serial.read()-48; //to convert back to a digit
                       }
                       InjCount+= val[0]*100;
                       InjCount+= val[1]*10;
                       InjCount+= val[2];
                                                break;
                                }
        Serial.println(InjCount); // counter verification
        break;
       case 'w':  // receive a new BackFlushBegin= 63; //seconds (65 sec is the event in the run)
//BackFlushEnd= 70; // seconds, before we go back to our state normal state
       delayMicroseconds(1000); //need a small delay to wait for the other character coming in the serial port..
       stepper.run();  // must wait for all character to be out to know length, can be 1 to 3 (0 to 999)
       val[0] = 0;
       BackFlushBegin = 0;
       switch (Serial.available())
                        {
                case 1:
                                                val[0] = Serial.read()-48; //to convert back to a digit
                    BackFlushBegin+= val[0];
                                                break;
                                        case 2:
                      for (int i=0; i<2; i++) // write down the number sent along with v (ex v559)
                       {
                         val[i] = Serial.read()-48; //to convert back to a digit
                       }
                       BackFlushBegin+= val[0]*10;
                       BackFlushBegin+= val[1];
                       break;
                                        case 3:
                            for (int i=0; i<3; i++) // write down the number sent along with v (ex v559)
                       {
                         val[i] = Serial.read()-48; //to convert back to a digit
                       }
                       BackFlushBegin+= val[0]*100;
                       BackFlushBegin+= val[1]*10;
                       BackFlushBegin+= val[2];
                                                break;
                                }
       case 'W':   // emits BackFlushBegin
         Serial.println(BackFlushBegin);
         break;
       case 'x':   // return sample (A or B)
        if (SampleA)
         Serial.println("A");
        else
          Serial.println("B");
        break;
         case 'y':  // receive a new  BackFlushEnd= 70; // seconds, before we go back to our state normal state
       delayMicroseconds(1000); //need a small delay to wait for the other character coming in the serial port..
       stepper.run();  // must wait for all character to be out to know length, can be 1 to 3 (0 to 999)
       val[0] = 0;
       BackFlushEnd = 0;
       switch (Serial.available())
```

```
                    {
                case 1:
                                                val[0] = Serial.read()-48; //to convert back to a digit
                    BackFlushEnd+= val[0];
                                                break;
                                        case 2:
                    for (int i=0; i<2; i++) // write down the number sent along with v (ex v559)
                     {
                       val[i] = Serial.read()-48; //to convert back to a digit
                     }
                     BackFlushEnd+= val[0]*10;
                     BackFlushEnd+= val[1];
                     break;
                                        case 3:
                           for (int i=0; i<3; i++) // write down the number sent along with v (ex v559)
                     {
                       val[i] = Serial.read()-48; //to convert back to a digit
                     }
                     BackFlushEnd+= val[0]*100;
                     BackFlushEnd+= val[1]*10;
                     BackFlushEnd+= val[2];
                                                break;
            }
      case 'Y':   // emits backflushend
        Serial.println(BackFlushEnd);
        break;

         break;
      case 'z':   // handshake
        Serial.println(12345678);
        break;
    }
    Serial.flush(); //removes any extra commands at the end so can still read the buffer for more data
    val[0] = -1;          // reset value so match with cleared buffer
  }
//*************************************************************************************************************
 //   ********** GC and Valve control logic section**********
 // flowmeter part for now just turning valve on and off..
 //*************************************************************************************************************
 stepper.run();
  if (FlowMeter)
    digitalWrite(ValveFlow,HIGH);
  else
    digitalWrite(ValveFlow,LOW);
stepper.run();
// Sets the injection event
  if(InjCount < MaxInj && Status)
  {
     if(millis() >= DelayMillisRemaining)    //sampling loop to move valve and start sampling
     {
     Sampling=true;  //turn on sampling set
     }
  }
  else
  {
    Status=false; // ends Injection, display waiting.
  }
 stepper.run();

/************************************** Pause condition (waits for backflush) *****************************/
if(PauseDemand == true && millis()>(BackFlushEnd*1000+OldDelayMillis) )
{
  PauseDemand = false;
  Status = false;
}


//*************************************************************************************************************
//                                      Backflushing  conditions and operation
//*************************************************************************************************************

 // Backflushing flagging Verify all conditions are true for backflush → note will backflush the lst run
 if (!Headspace && OldDelayMillis!=0 && millis()>(BackFlushBegin*1000+OldDelayMillis) && millis()<(BackFlushEnd*1000+OldDelayMillis))
   BackFlushing=true;
 else
   BackFlushing=false;
// backflush Action
  stepper.run();
  if (!Headspace) // only do backflushing when in flow mode, do it even on stoped run. (this is not working on a pause it failed to BF.)
  {
    if(BackFlushing)
    {
      if(!BackFlushDone)
      {
```

```
      digitalWrite(ValveSampleA,LOW);  // TURN s both valve off (does not care about sample)
      digitalWrite(ValveSampleB,LOW);
      stepper.run();
      BackFlushDone= true;
     }
   }
   else
   {
    stepper.run();
    BackFlushDone= false;
    if (SampleA ) // removes the backflush protection important to reset back to the right sample
        {
         digitalWrite(ValveSampleA,HIGH);  // Sample A flow pass through GC
         stepper.run();
        }
    else
        {
         digitalWrite(ValveSampleB,HIGH);  // Sample B flow pass through GC
         stepper.run();
        }
   }
 }
//*************************************************************************************************************
//                                        INJECTION TIME!!
//*************************************************************************************************************
if (Sampling && Status)
  {
    Sampling=false; // resets the condition immediately
    InjCount=InjCount+1;  // increment injection count variable for display and for the 99th skiped inejection
    digitalWrite(ExtReadyPin,LOW);  //let GC become ready
    lcd.setCursor(0, 1);
     stepper.run();
    lcd.print("   READYING     ");
     stepper.run();
    delay(Delay);
   stepper.run();  //delay to ensure GC is ready that second is taken out of DelayMillisRemaining to make it exact
    digitalWrite (StartGCPin,LOW);  //Start the GC
    lcd.setCursor(0, 1);
     stepper.run();
    lcd.print("   INJECTING    ");
    OldDelayMillis= DelayMillisRemaining; // stores start of timer
    if (InjCount % 98 == 0) //The GC need more time for 99th run!! (double injection delay)
      {
       DelayMillisRemaining=millis()+DelayMillis+ExtraMillis-InjectionDelay;
       lcd.setCursor(0, 1);
       lcd.print("  adding 5 min ");
      }
    else
       DelayMillisRemaining=millis()+DelayMillis-InjectionDelay;     //resetting of delay - injection delay
    delay(Delay);  //wait
    stepper.run();
    digitalWrite (StartGCPin,HIGH);  //Return the GC
    // delay(1000);  //wait
    // lcd.clear();
    digitalWrite(ExtReadyPin,HIGH);  //prevent from GC become ready .

    if (TwoSamples) // switch sample for next run and switch valves
     {
      SampleA = !SampleA; // sets the new current sample (the one that is flushing the system, not the one eluting in GC..
      if (SampleA)
      {
       digitalWrite(ValveSampleB,LOW);
       stepper.run();
       delay (10); //
       stepper.run();
       digitalWrite(ValveSampleA,HIGH);  // Sample A flow pass through GC

      }
      else   // will be a toggle button to adjust flows etc..
      {
       digitalWrite(ValveSampleA,LOW);
       stepper.run();
       delay (10);
       stepper.run();
       digitalWrite(ValveSampleB,HIGH);  // Sample B flow pass through GC

      }
     }
}

//*************************************************************************************************************
  //   **********LCD display section***********
//*************************************************************************************************************
  stepper.run();
```

```
RollOver= (4294967295-millis())/1000/60/60/24; // RollOver in days is not pertinent without a control switch, will leave it there as it is a likely upgrade
//lcd.clear();  // cause flickering at high refresh
if (!Sampling)
{
 stepper.run();
 if((RollOver-ResetDays) <= 0) // Rollover message appearing only when there is ResetDays left (instead of frequency and inj)
 {
  stepper.run();
  lcd.setCursor(0, 0);
  lcd.print("!RESET IN ");
  lcd.print(RollOver);
  if (RollOver <2)
  {lcd.print(" DAY !");}
  else {lcd.print(" DAYS!");}

 }
 else
 {
  stepper.run();
  if(!Headspace)
  {
   if (HeadSpaceWritten) // true means it need to refresh the upper screen
   {
    lcd.setCursor(0, 0);
    //lcd.print(analogRead(lightPin));
    lcd.print("Freq ");
    stepper.run();
    lcd.setCursor(7, 0);
    lcd.print(":");
    lcd.setCursor(10, 0);
    lcd.print(" ");
    lcd.setCursor(13, 0);
    lcd.print("Inj");
    stepper.run();
   }
   if (SamplingTimeSeconds !=SamplingMemory || HeadSpaceWritten)
   {
    SamplingMemory = SamplingTimeSeconds;
    lcd.setCursor(5, 0);
    Temp=SamplingTimeSeconds/60;
    if(SamplingTimeSeconds/60 < 10)
    {
     lcd.print('0');
    }
    stepper.run();
    lcd.print(SamplingTimeSeconds/60);
    stepper.run();
    lcd.setCursor(8, 0);
    if((SamplingTimeSeconds-(Temp*60)) < 10)
    {
     lcd.print('0');
    }
    stepper.run();
    lcd.print(SamplingTimeSeconds-(Temp*60));
   }
   HeadSpaceWritten = false;
   stepper.run();
   if(Status) // display remaining time
   {

       stepper.run();
       lcd.setCursor(0, 1);

       lcd.print("Left");
       lcd.setCursor(5, 1);
       Minutes = ((InjectionDelay+DelayMillisRemaining-millis())/1000)/60; // convert millis to minutes, scrapping the decimals
       Seconds= ((InjectionDelay+DelayMillisRemaining-millis())/1000)-60*Minutes; // comvert millis to seconds, substracting the minutes
       stepper.run();
       if (Minutes < 10)
       {
          lcd.print('0');
       }
       stepper.run();
       lcd.print(Minutes);
       stepper.run();
       lcd.print(":");
       if(Seconds < 10)
       {
         lcd.print('0');
       }
       stepper.run();
       lcd.print(Seconds);
       lcd.setCursor(11, 1);
       stepper.run();
```

```
      //if (TwoSamples)  //change message to show witch sample is flowing
          if (SampleA)
           lcd.print("A ");
          else
           lcd.print("B ");
      //   else  lcd.print("  ");
       stepper.run();
       lcd.setCursor(12, 1);
       if(InjCount < 1000)
         { stepper.run();
          lcd.print(" ");
         }
         if(InjCount < 100)
         {  stepper.run();
          lcd.print(" ");
         }
         if(InjCount < 10)
         {  stepper.run();
          lcd.print(" ");
         }
         stepper.run();
         lcd.print(InjCount);
 if (BackFlushing)
   {
    stepper.run();
     lcd.setCursor(4, 1);
     lcd.print("B");
     stepper.run();
    lcd.setCursor(10, 1);
    lcd.print("F");
   }
  else
   {
      stepper.run();
    lcd.setCursor(4, 1);
    lcd.print(" ");
    stepper.run();
    lcd.setCursor(10, 1);
    lcd.print(" ");
   }
  }

  else
  {
   lcd.setCursor(0, 1);
   stepper.run();
   //if (TwoSamples)//change message to show witch sample is flowing
    if (SampleA)
      lcd.print("Sample A ");
    else
      lcd.print("Sample B ");
  /* else
    {stepper.run();
      if (LampOn)
        lcd.print("WAITING  ");
        else
          lcd.print("Waiting  ");
    }*/
   lcd.setCursor(9, 1);
   stepper.run();
   if (LampOn)
         lcd.print("MAX");
         else
   lcd.print("Max");
   lcd.setCursor(12, 1);
    if(MaxInj < 1000)
      {stepper.run();
       lcd.print(" ");
      }
      if(MaxInj < 100)
      {stepper.run();
       lcd.print(" ");
      }
      if(MaxInj < 10)
      {stepper.run();
       lcd.print(" ");
      }
      stepper.run();
      lcd.print(MaxInj);
  }
}
else
{
 stepper.run();
```

```
    if (!HeadSpaceWritten)
    {
     HeadSpaceWritten = true;
     stepper.run();
     lcd.setCursor(0, 0);
     stepper.run();
     lcd.print  ("Headspace       ");
      stepper.run();
       lcd.print("Auto-Sampler    ");
       lcd.setCursor(11, 0);
       lcd.write(Spin);
    }
   }
     lcd.setCursor(12, 0);
     if (LampOn) //display detectection of light
            lcd.write(4); //sun
     else   lcd.write(5);  // moon
     stepper.run();
    //Animation of motion
      if (stepper.currentPosition() < stepper.targetPosition())
       {
        lcd.setCursor(11, 0);
        stepper.run();
        if (Millimemory < millis())
        {
         Millimemory= millis()+MilliDelay;
         if (Spin < 3) Spin = Spin+1;
         else Spin = 0;
         lcd.write(Spin);
        stepper.run();
        }
       }
      if (stepper.currentPosition() > stepper.targetPosition())
       {
        lcd.setCursor(11, 0);
        stepper.run();
        if (Millimemory < millis())
        {
         Millimemory= millis()+MilliDelay;
         if (Spin > 0) Spin = Spin-1;
         else Spin = 3;
         lcd.write(Spin);
        stepper.run();
        }
       }
      }
    }
}   //turn off current sampling set moved from Logic section to avoid ugly screen refreshes
```